

**Investigation Of Several Critical
Issues In Screen Mesh Heat Pipe
Manufacturing And Operation**

**Andreas Engelhardt, MEng (Hons),
Dipl. Ing. (FH)**

Thesis submitted to



**The University of
Nottingham**

for the Degree of Doctor of Philosophy

February 2010

Abstract PhD Thesis Andreas Engelhardt

The PhD thesis with the title “Investigation of several critical issues in screen mesh heat pipe manufacturing and operation” presented hereafter describes work carried out in four main areas. Initially the relevant literature is reviewed and presented, followed by the presentation of theoretical work regarding screen mesh heat pipe fill calculations, heat pipe processing and an investigation into the capillary or lifting height for screen mesh heat pipes. Further, the possibility of tailoring screen mesh heat pipes towards certain applications was investigated and it was found that further work is required in this area to allow a conclusive judgement whether a coarser or finer wick at the wall provides a distinguish advantage over two wraps of a medium coarse type. Within this approach a calculation method for the determination of the optimum working fluid fill of a screen mesh heat pipe based on geometrical parameters of the wick was developed and successfully implemented for the production of the later tested samples.

The investigation into the effects of bending on the heat pipe performance, both using single phase flow CFD as well as experimentation, was performed using five different geometrical cases, each with five samples. These were tested in order to minimise the effects of sample variation. The test cases investigated contained the deformation angles of 0° (straight), 45° , 90° , 135° and 180° . During all test cases the orientation of the samples was kept constant at 0° to minimise additional influences like the effects of gravity on the reduction of available power handling capability. The test results show in deviation from CFD results that screen mesh heat pipe performance is

significantly affected when bends are introduced and the reduction in power handling capability can be up to nearly 50% of a straight heat pipe value.

Finally this thesis advances into the field of water heat pipe freeze thaw and the possibility of screen mesh heat pipes with changed shapes to withstand multiple freeze thaw cycles. It was found that correctly engineered screen mesh copper water heat pipes can be used in applications where they are subjected to multiple freeze thaw cycles. The fluid charge for water heat pipes subjected to these conditions needs to be adjusted in such a way, that accumulation of working fluid in certain areas, regardless of orientation or process variation during filling, is avoided.

ACKNOWLEDGEMENTS

The author would like to take the opportunity to thank Xudong Zhao of the School of Built Environment at the University of Nottingham and David Mullen of Thermacore Europe for their continuous support and offering of advice when required over the entire duration of this PhD.

Further thanks have to go to Saffa Riffat of the School of Built Environment at the University of Nottingham and Kevin Lynn of Thermacore Europe for their understanding and their support during the period of the work conducted.

Since most of the experimental work was carried out at the sponsoring company, Thermacore Europe, an additional large thank you has to go to all the co-workers there for their support and help. But a special thank you has to go to Ian Davies for the production of the test samples and advice when required. Without his knowledge and skills the production of test samples with certain characteristics would have been more time consuming and less successful than it was.

Last but not least the author would like to thank the EPSRC (Engineering and Physical Sciences Research Council), which made this PhD thesis possible through their financial support under the Grant number EP/P501733/1.

COPYWRITER DECLARATION

I declare that this thesis is the result of my own work and has not, whether in the same or a different form, been presented to this or any other university in support of an application for any degree other than that of which I am now a candidate.

TABLE OF CONTENTS

Abstract	i
Acknowledgements	iii
Copyright Declaration	iv
Nomenclature	xi
List of Figures	xv
List of Tables	xxiii
CHAPTER 1 – INTRODUCTION	1
1.1 BACKGROUND	1
1.2 DESCRIPTION OF THE RESEARCH	4
1.3 WORK INVOLVED IN THE RESEARCH.....	7
CHAPTER 2 - LITERATURE REVIEW HEAT PIPE TECHNOLOGY	11
2.1 HEAT PIPE CONSTRUCTION	12
2.1.1 Container Materials	12
2.1.2 Working Fluids	20
2.1.3 Performance Limits Of Heat Pipes	24
2.1.4 Types Of Heat Pipes	26
2.2 HEAT PIPE APPLICATIONS	36
2.2.1 Typical Heat Pipe Applications	36

2.2.2	Detail Focused Investigation Of Heat Pipe Behaviour (Start-Up; Freeze- Thaw)	40
2.3	MATHEMATICAL MODELLING OF HEAT PIPES	44
2.3.1	General Approaches To Heat Pipe Performance Modelling	44
2.3.2	Heat Pipe Modelling Using Commercial CFD Codes ...	52
2.3.3	Modelling Of Multiphase Flow Using Commercial CFD Codes	54
2.3.4	Numerical Investigation Of The Effects Of Bends And Shape-Changes In Related Areas	57
2.4	EXPERIMENTAL TECHNIQUES WITH FOCUS ON HEAT PIPES.....	61
2.4.1	Test Rig Design	61
2.4.2	Temperature Measurement Techniques	66
2.4.3	Previous Experimental Work On The Subject Of Bending	67
2.5	LATEST TECHNOLOGY DEVELOPMENTS IN THE HEAT PIPE AREA	68
2.6	SCOPE OF THE WORK OF THIS THESIS AND ITS NOVEL ASPECTS TO THE SCIENTIFIC COMMUNITY	70
2.7	AREAS OF FURTHER RESEARCH REQUIRED	73
 CHAPTER 3 – INVESTIGATIONS OF HEAT PIPE FILLING AND VENTING TECHNIQUES		75

3.1	INTRODUCTION	75
3.2	MESH HEAT PIPE FILL CALCULATIONS	77
	3.2.1 Weight Of Water Required For Generating Saturated Steam Within The Vapour Space	80
	3.2.2 Mathematical Foundations Of The Porosity Calculation For Screen Meshes Used As Heat Pipe Wicks	83
	3.2.3 Development And Implementation Of VB Based Screen Mesh Wick Heat Pipe Fill Calculation Software	88
3.3	ANALYTICAL INVESTIGATION OF THE CAPILLARY OR LIFTING HEIGHT FOR DIFFERENT WICK STRUCTURES	94
3.4	VENTING OR PROCESSING OF HEAT PIPES.....	100
	3.4.1 Venting Techniques	100
	3.4.2 Venting Technique Applied To The Heat Pipes Used For This Study	105
	3.4.3 Most Common Venting Failure Modes	107
3.5	SUMMARY AND CONCLUSIONS	113
 CHAPTER 4 – INVESTIGATION OF THE USE OF DISSIMILAR SCREEN MESHES AS HEAT PIPE WICKS		
		115
4.1	INTRODUCTION	116
4.2	DISSIMILAR SCREEN MESH WICK HEAT PIPE INVESTIGATIONS	117

4.2.1	Design And Manufacturing Considerations For Dissimilar Mesh Wick Heat Pipes	117
4.2.2	Experimental Results And Analysis Of Dissimilar Mesh Wick Heat Pipe Investigations.....	121
4.3	CONCLUSIONS	129

CHAPTER 5 – BENDING OF SCREEN WICK HEAT PIPES .
..... 130

5.1	FLOW SIMULATION THROUGH PIPE BENDS USING CFD SOFTWARE	131
5.1.1	Introduction Into Separate Phase Modelling Theory ...	132
5.1.2	Separate Phase Modelling	134
5.1.3	Calculation Of Flow Parameters	135
5.1.3.1	<i>Liquid Film Height Calculation</i>	135
5.1.3.2	<i>Reynolds Number Calculation</i>	137
5.1.4	Theory Used For Obtaining The CFD Settings	141
5.1.4.1	<i>Flow Models and Boundary Conditions used</i>	145
5.1.4.2	<i>Settings as per Heat Pipe Theory disregarding Validity of Mathematical Models for certain Flow Conditions</i>	145
5.1.5	CFD Results And Result Plots	150
5.1.5.1	<i>Results And Plots From Runs Of Annular Flow Per Heat Pipe Theory</i>	150
5.1.5.2	<i>Results And Plots From Runs Of Full Pipe Flow At Flow Velocity From Heat Pipe Theory.</i>	152

5.1.6	Creating The Link Between The Pressure Results From The CFD Model And The Experimental Results	155
5.2	TEST RIG DESIGN FOR BENT HEAT PIPES	161
5.2.1	Purpose Of The Test Rig And Introduction To The Principle	161
5.2.2	Instrumentation Used	162
5.2.3	Water Side And Cold Plates	164
5.2.4	Test Side And Heater Blocks	166
5.2.5	Adaptability For Different Heat Pipe Diameters And Shapes	168
5.3	EXPERIMENTAL TRIALS WITH BENT HEAT PIPES	169
5.3.1	Experimental Methodology	170
5.3.2	Figures Of Experimental Procedure For One Single Heat Pipe	172
5.3.3	Failure Mode Analysis	185
5.3.4	Analysis Of The Thermal Load Transmitted By The Heat Pipes	186
5.3.5	Comparison Of The CFD Simulation Results To Experimental Results	190
5.4	DEVELOPMENT OF A MATHEMATICAL APPROXIMATION FOR PERFORMANCE LOSSES DUE TO THE BEND ANGLE	192

5.5	CONCLUSIONS	194
CHAPTER 6 – FREEZE - THAW BEHAVIOUR		
INVESTIGATION OF HEAT PIPES		
6.1	INTRODUCTION	198
6.2	FROZEN START-UP MODELS OF HEAT PIPES	199
6.3	PREVIOUS PRACTICAL WORK	202
6.4	PRACTICAL INVESTIGATIONS OF FREEZE-THAW EFFECTS ON SCREEN WICK WATER HEAT PIPES	204
6.5	CONCLUSIONS	217
 CHAPTER 7 – CONCLUSIONS & FURTHER WORK		
REQUIRED		
7.1	CONCLUSIONS	220
7.2	FURTHER WORK REQUIRED	226
 REFERENCES		
PAPERS PUBLISHED BY AUTHOR		
APPENDICES		
Appendix 1 – Data Table for Temperature Dependence of Fill		
Calculations		
Appendix 2 – Result Plots obtained from the CFD Runs		
Appendix 3 - Thermocouple Fabrication and Calibration		
Appendix 4 – Graphs of the Experimental Measurements and Analysis ..		
.....		
		269

NOMENCLATURE

Symbol:

a, b	Geometrical constants	[m]
A	Area of wick	[m ²]
A' _w	Cross Sectional Area of the Working Fluid in the Wick	[m ²]
c	Clearance	[m]
C	Specific Heat Capacity per unit length of pipe wall	[J/(m*K)]
c _p	Specific heat capacity	[J/(kg*K)]
d	Screen wire diameter	[m]
d _h	Hydraulic diameter	[m]
d _i	Here: vapour core diameter of Pipe	[m]
d _o	Internal diameter of pipe	[m]
DNF	Does Not Function	
H	Capillary or Lifting Height	[m]
h _{fg}	Latent heat of Evaporation	[J/kg]
g	Gravity constant	[m/s ²]
K	Permeability	[m ²]
l _{eff}	Heat pipe effective length	[m]
<i>m</i>	Mass flow rate	[kg/s]
M _S	Mass of Screen Wire Sample	[kg]
N	Number of Screen Openings per unit length	[1/m]
Q	Heat Load (Power)	[W]

r_1	Maximum aperture, warp wires	[m]
r_2	Maximum aperture, shoot wires	[m]
r_c	Capillary Radius	[m]
Re	Reynolds number	
r_v	Vapour Core Radius	[m]
r_w	Internal Radius of the Pipe	[m]
R_w	Radius of curvature, warp wire	[m]
R_s	Radius of curvature, shoot wire	[m]
S	Crimping Factor of Screen, dimensionless	
s, w	Indexes used as subscripts for Shoot and Warp Wire	
T_{mel}	Melting Temperature of the Working Fluid	[K]
T_∞	Initial or ambient Temperature of the Working Fluid	[K]
u_l	Velocity of liquid within the wick	[m/s]
V	Volume of Wick	[m ³]
V_s	Volume of Screen Wire	[m ³]
w	Screen opening (Aperture)	[m]

Greek Symbols:

α	Gap of the single screen layer, dimensionless	
γ	Liquid Air Surface Tension	[N/m]
δ_l	Thickness of Screen	[m]
ΔP_c	Capillary Pressure within the heat pipe wick	[bar or Pa]
ΔP_l	Differential Pressure in liquid phase	[bar or Pa]
ΔP_v	Differential Pressure in vapour phase	[bar or Pa]
ΔT	Temperature difference	[K]
ε	Surface roughness (Fig. 5.4 only)	[m]
ε	Porosity, dimensionless	
ε_l	Porosity, dimensionless	
θ	Contact Angle Working Fluid	[°]
Θ	Bend Angle in the Heat Pipe	[° or rad]
μ_l	Dynamic viscosity of liquid	[kg/(m*s)]
ν	Kinematic viscosity	[m ² /s]
ν_g	Specific volume of vapour	[m ³ /kg]
π	Pi	
ϕ_1	Geometrical Angle used for Warp Wires	[rad]
ϕ_2	Geometrical Angle used for Shoot Wires	[rad]
ϕ_w'	Additional Angle used for Warp Wire	[rad]

ϕ_s'	Additional Angle used for Shoot Wire	[rad]
Φ	Geometrical Angle used for Shot and Warp Wires	[rad]
ρ_l	Liquid density	[kg/m ³]
ρ_s	Density of Screen Wire	[kg/m ³]
	8800 kg/ m ³ for Phosphor Bronze (ISO 4783-1, 1989)	
ρ_v	Vapour density	[kg/m ³]
σ	Surface tension	[N/m]

LIST OF FIGURES

Figure 1.1: Picture showing internal construction of a screen mesh heat pipe	3
Figure 2.1: Useful Temperature Range of Working Fluids (Reay & Kew, 2006)	22
Figure 2.2: Internal Structure of a Grooved Heat Pipe (Thermacore, 2008)	27
Figure 2.3: Screen Mesh as used for wicks inside Heat Pipes (Thermacore, 2008)	27
Figure 2.4: View into Sintered Heat Pipe (Thermacore, 2008)	28
Figure 2.5: Loop Heat Pipe Schematic (Maydanik, 2006)	29
Figure 2.6: Capillary Pumped Loop (CPL) Schematic (Hoang, 1997)	30
Figure 2.7: View of a Vapour Chamber (Flat Plate Heat Pipe) (Thermacore, 2008)	32
Figure 2.8: Schematic of a Loop Thermosyphon (LTS) (McGlen, 2007) ...	34
Figure 2.9: Schematic of a Variable Conductance Heat Pipe (Sarraf, Bonner & Colahan, 2006)	35
Figure 2.10: Heat Pipe Resistance Model (Peterson, 1994, p.147)	46
Figure 2.11: Analytical model of Zhu and Vafai (1999)	49
Figure 2.12: Network model of Zuo and Faghri (1998)	51

Figure 2.13: Schematic of the SINDA/FLUINT node model (C&R Technologies, 2008)	52
Figure 2.14: Schematic of different Two-Phase patterns (Lun, Calay & Holdo, 1996)	56
Figure 2.15: Schematic of different heat input methods (Faghri, 1995)	62
Figure 2.16: Schematic of different heat output methods (Faghri, 1995)	63
Figure 2.17: Brief Schematic of a typical Test Rig (Reay & Kew, 2006)	63
Figure 2.18: Schematic of the Test Rig used by Kempers, Ewing and Ching (2006)	64
Figure 2.19: Schematic of the Test Rig used by Maziuk et al. (2001)	65
Figure 2.20: Schematic of the Test Rig used by Murer et al. (2005)	66
Figure 3.1: Average Percentage Overfill	78
Figure 3.2: Steam (red) and Liquid (blue) Density vs. Temperature (Wikipedia, 2008)	81
Figure 3.3: Pressure inside a heat pipe during venting	83
Figure 3.4: Layout of the Calculation Software	89
Figure 3.5: Screen Mesh Wick Heat Pipe Fill Calculation Software Flowchart	92
Figure 3.6: Fill for various Screen Mesh Heat Pipe Configurations	94
Figure 3.7: Definition of screen mesh parameters (ISO 4783-2, 1989)	95

Figure 3.8: Scheme of a Heat Pipe containing a Source of Contamination .	108
Figure 3.9: Scheme of a Heat Pipe containing Non Condensable Gas	109
Figure 3.10: Scheme of a dried out Heat Pipe	110
Figure 3.11: Scheme of a Heat Pipe with excess Working Fluid	111
Figure 3.12: Scheme of a good Heat Pipe	112
Figure 4.1: Scheme of the Screen Mesh used in Heat Pipes (ISO 4783-1, 1989)	115
Figure 4.2: Wick with vapour leaving freely (150 Mesh with $q = 52 \text{ kW/m}^2$) (Brautsch & Kew, 2002)	119
Figure 4.3: Wick with vapour collecting in patches and depleting the wick of working fluid in the top right corner (150 Mesh with $q = 137 \text{ kW/m}^2$) (Brautsch & Kew, 2002)	120
Figure 4.4: Close-up of a bursting vapour bubble (150 Mesh with $q = 137 \text{ kW/m}^2$) (Brautsch & Kew, 2002)	120
Figure 4.5: Wick with dried out Areas on the top right side (150 Mesh with $q = 152 \text{ kW/m}^2$) (Brautsch & Kew, 2002)	120
Figure 4.6: Entire Test Rig Setup	123
Figure 4.7: Schematic of Test Rig including Instrumentation used	123
Figure 4.8: Thermal load transmitted per sample and wick structure	125
Figure 4.9: Average thermal load transmitted per wick structure	126

Figure 4.10: ΔT Results for all Heat Pipe samples including limit	129
Figure 5.1: Scheme of Liquid Film Height (Fu & Klausner, 1997)	136
Figure 5.2: Error in dependence of the Reynolds number (Romeo, Royo & Monzó, 2002)	140
Figure 5.3: Comparison of the models including and excluding interfacial effects (Zhu & Vafai, 1999)	142
Figure 5.4: Definition of Surface Roughness Height (Engineer’s Edge, 2006)	143
Figure 5.5: Mesh quality and Prism Layer number	144
Figure 5.6: Meshing models and Physics models used	146
Figure 5.7: Differential Pressure inside the Pipe including the Error bars . .	151
Figure 5.8: Total Deviation from Straight Pipe Value	151
Figure 5.9: Differential Pressure inside the Pipe including the Error bars . .	153
Figure 5.10: Total Deviation from Straight Pipe Value	154
Figure 5.11: Entire Test Rig Setup	162
Figure 5.12: Scheme of Test Rig Setup including data- logging and controls	162
Figure 5.13: Cold Plate used	165
Figure 5.14: Function Scheme Cold Plate	165
Figure 5.15: Cold Plate Arrangement	165

Figure 5.16: Embedded Thermocouples	165
Figure 5.17: Filter, Bypass & Needle Valve	165
Figure 5.18: Test Chamber and Insulation	166
Figure 5.19: Heater Block	166
Figure 5.20: Heater Block Assembly	167
Figure 5.21: Adiabatic Section and Thermocouple Positions	167
Figure 5.22: 8mm Adaptor Block	168
Figure 5.23: Hinge Arrangement	169
Figure 5.24: 70W Run Straight Heat Pipe 3 Raw Data	172
Figure 5.25: 70W Run Straight Heat Pipe 3 Analysed Data	172
Figure 5.26: 80W Run Straight Heat Pipe 3 Raw Data	173
Figure 5.27: 80W Run Straight Heat Pipe 3 Analysed Data	173
Figure 5.28: 90W Run Straight Heat Pipe 3 Raw Data	173
Figure 5.29: 90W Run Straight Heat Pipe 3 Analysed Data	173
Figure 5.30: 100W Run Straight Heat Pipe 3 Raw Data	174
Figure 5.31: 100W Run Straight Heat Pipe 3 Analysed Data	174
Figure 5.32: 90WRamp Up Run Straight Heat Pipe 3 Raw Data	174
Figure 5.33: 90WRamp Up Run Straight Heat Pipe 3 Analysed Data	174

Figure 5.34:100W Run Straight Heat Pipe 3 Raw Data with Phenomena Explained	177
Figure 5.35:100W Run Straight Heat Pipe 3 Analysed Data	177
Figure 5.36:92W Ramp Up Run Straight Heat Pipe 3 Raw Data	178
Figure 5.37:92W Ramp Up Run Straight Heat Pipe 3 Analysed Data	178
Figure 5.38:50W Run 1 90° Heat Pipe 1 Analysed Data	179
Figure 5.39:50W Run 2 90° Heat Pipe 1 Analysed Data	179
Figure 5.40: 60W Run 200 Mesh at the Wall Heat Pipe Analysed Data . . .	180
Figure 5.41: 70W Run 200 Mesh at the Wall Heat Pipe Analysed Data . . .	181
Figure 5.42: 60W Run Heat Pipe 4 45° Bend Analysed Data	182
Figure 5.43:70W Run 200 Run Heat Pipe 4 45° Bend Analysed Data	182
Figure 5.44:80W Run Heat Pipe 4 45° Bend Analysed Data	182
Figure 5.45: 90W Run Heat Pipe 4 45° Bend Analysed Data	183
Figure 5.46: Thermal Performance transmitted in Watts averaged per Bend Angle	188
Figure 5.47: Reduction in Thermal Performance in Watt averaged per Bend Angle	189

Figure 5.48: Reduction in Thermal Performance in Percent averaged per Bend Angle	189
Figure 5.49: Pressure Degradation in % from Straight Heat Pipe obtained through Experimental Analysis	190
Figure 5.50: Comparison Pressure Deviation from Straight Heat Pipe CFD Runs and Experiments	191
Figure 5.51: Remaining Thermal Performance in Percent vs. Bend Angle .	193
Figure 6.1: Heat Pipe Failure during operational Freeze Thaw Cycling (Cheung, 2004)	203
Figure 6.2: Heat Pipe with good Mesh Distribution	205
Figure 6.3: Heat Pipe with two Bubbles in the Mesh wick due to Freeze Thaw Cycling	204
Figure 6.4: Heat Pipe with very slight Wick distortion due to Freeze Thaw Cycling	204
Figure 6.5: Heat Pipe Sample with Wick distortion due to Freeze Thaw Cycling	207
Figure 6.6: Heat Pipe with very slight Wick distortion due to Freeze Thaw Cycling	207
Figure 6.7: Heat Pipe Sample with Wick distortion due to Freeze Thaw Cycling	208

Figure 6.8: Heat Pipe Sample with Wick distortion due to Freeze Thaw	
Cycling	208
Figure 6.9: Heat Pipe Sample with Wick distortion due to Freeze Thaw	
Cycling	209
Figure 6.10: Heat Pipe Sample with Wick distortion due to Freeze Thaw	
Cycling	209
Figure 6.11: Picture of the Test Rig and Instrumentation used for the	
Thermal Testing	212
Figure 6.12: Schematic of the Test Rig and Instrumentation used for the	
Thermal Testing	212
Figure 6.13: Heat Pipe Fill vs. Bulging Trend Graph	216

LIST OF TABLES

Table 2.1: Compatibility Matrix Working Fluids- Materials [22]	21
Table 3.1: Calculated Porosity, Effective Pore Radius and Lifting Height [last two m]	98
Table 4.1: ΔT Results for all Heat Pipe samples including Standard Deviation	127
Table 5.1: Models and Boundary Conditions used for CFD investigation . .	147
Table 5.2: Pressure values for annular flow as given by the CFD Software .	150
Table 5.3: Pressure values for full flow as given by the CFD Software . . .	153
Table 5.4: Set of Experiments conducted	170
Table 5.5: Monitored Channels	175
Table 5.6: Failure Modes and Heat Fluxes per Heat Pipe tested	185
Table 5.7: Thermal Load in Watt transmitted per Heat Pipe and averaged per Bend Angle.	186
Table 5.8: Reduction in Thermal Performance in Watt and Percents	187
Table 5.9: Capillary Pressure Comparison Results	191
Table 6.1: Geometrical Data Compared to Fill Information of 16 Heat Pipe Samples	215

CHAPTER 1 – INTRODUCTION

1.1 BACKGROUND

“A heat pipe is an evaporative- condensation device for transferring heat in which latent heat of vaporization is exploited to transport heat over long distances with a corresponding small temperature gradient. The heat transport is realized by means of evaporating a liquid in the heat inlet region (called the evaporator) and subsequently condensing the vapour in a heat rejection region (called the condenser). Closed circulation of the working fluid is maintained by capillary action and/ or bulk forces. The heat pipe was originally invented by Gaugler of the General Motors Corporation in 1944, but did not truly garner any significant attention within the heat transfer community until the space program resurrected the concept in the early 1960’s. Early development of terrestrial applications of heat pipes proceeded slowly; however due to the high cost of energy, the industrial community has begun to appreciate the significance of heat pipes in energy savings and design improvements in various applications. Most recently, with heat density of electronic components continually increasing, there is a growing interest in using heat pipes for transferring and spreading heat in conjunction with cooling these components.

A simple constant conductance heat pipe consists of a sealed case lined with an annular porous wicking material. The wick is filled with a working fluid in the liquid state. A heat load is placed in contact with the casing at the evaporator end. Heat is transferred radially through the case and into the wick. This causes the liquid to evaporate, transferring mass from the wick to the

vapour core. This addition of mass in the vapour core increases the pressure of the vapour at the evaporator end of the pipe, thus creating a pressure differential that drives vapour flow to the condenser end of the heat pipe. Heat is removed via a suitable heat sink attached to the outside of the casing at the condenser end of the heat pipe. This causes the vapour to condense, replacing previously evaporated liquid mass to the wick. In absence of bulk forces (gravity, centrifugal, etc) in the axial direction, capillary forces “pump” the liquid axially through the wick, feeding liquid back to the evaporator. An advantage of a heat pipe over other conventional methods to transfer heat such as a finned heat sink, is that a heat pipe can have an extremely high thermal conductance in steady state operation. Hence, a heat pipe can transfer a high amount of heat over a relatively long length with a comparatively small temperature differential. Heat pipes with liquid metal working fluids can have a thermal conductance of a thousand or even tens of thousands times greater than the best solid metal conductors, silver or copper. Heat pipes, that utilize water as the working fluid, can have a thermal conductance tens of times greater than the best metallic conductors. This is because the heat transfer in a heat pipe utilizes the phase change of the working fluid, where a high amount of heat can be transferred with very little temperature difference between the source and the sink.

There are generally at least five physical phenomena that will limit, and in some cases catastrophically limit, a heat pipe’s ability to transfer heat. They are commonly known as the sonic limit, the capillary limit, the viscous limit, the entrainment limit and the boiling limit.”

These descriptions have been found in a journal paper of Williams and Harris (2005) and very well describe the heat pipe itself; the functional principles of it and the motivation behind its application. Within the following chapters of this thesis the oldest of the three conventional heat pipe types, which are sintered, screen mesh wick and grooved heat pipes, is investigated. Screen mesh wick heat pipes utilize a single or multiple layers of woven wire cloth inside the heat pipe container as the wick structure providing capillary forces to return the working fluid to the evaporation section in absence of gravitational support. For all the work presented the most common, and the one with the highest heat transfer capabilities within the low temperature region, working fluid is used, which is water.

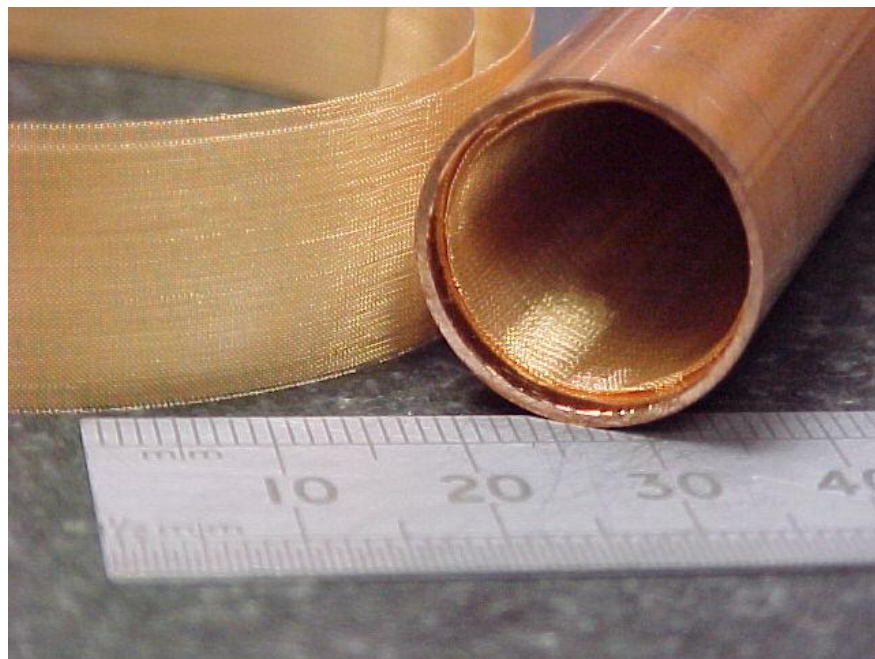


Figure 1.1: Picture showing internal construction of a screen mesh heat pipe

Screen mesh wick heat pipes are not only one of the oldest heat pipe types, but also one which is lacking a distinctive use for real life applications and are subject to common misconceptions that they cannot be used for anti-gravitational operations or are unable to withstand freeze-thaw. These

misconceptions are tried to be removed during the work presented within this thesis on the basis of scientific evidence found in existing literature sources as well as own analysis and experimentation.

The following questions have arisen and require solving for a deeper understanding of screen mesh wick heat pipes:

- Can the fluid charge/ fill level for a screen mesh wick heat pipe be analytically determined based on screen mesh wick geometry?
- How can the filling and venting/ charging processes be improved in order to reduce production variation?
- What are the limitations of screen mesh heat pipes in terms of capillary/ lifting height and can they be used for anti-gravitational operation?
- Can screen mesh wicks be tailored for certain application conditions; for example high heat fluxes or low ΔT s along the heat pipes by implementing different screen mesh types?
- Are screen mesh heat pipes affected by bends and if so how severe are the effects on overall performance?
- How are screen mesh wicks affected by multiple freeze thaw cycles and if they are affected, what are the mechanisms inside the heat pipes which cause failure?

1.2 DESCRIPTION OF THE RESEARCH

Despite the time which has passed since heat pipe technology was first developed, and the fact that most of the phenomena around heat pipes are scientifically described, there are still many areas, and in particular, when it

comes to application specific and manufacturing considerations, which are not fully scientifically described and require further attention to obtain a deeper understanding of screen mesh heat pipe applications. The following areas addressed present novel and additional factors to the common knowledge of screen mesh wick heat pipes:

Venting/ Charging Processes And Screen Mesh Wick Fill Calculations

One area which is addressed would be the fluid charge for screen mesh heat pipes. Whilst reviewing existing literature as well as preliminary test results, it was found that the calculation of the amount of working fluid for screen mesh heat pipes as well as failure modes during the venting or charging process (despite their paramount importance on the overall heat pipe performance) have largely been neglected. This work was seen as too significant in terms of the impact on the aim to investigate the effects of bends on screen mesh wick heat pipes to remain unsolved. Therefore, as a first step a calculation software has been developed which allows the calculation of the fluid charge for screen mesh heat pipes whilst being able to compensate for venting losses and cater for different venting temperatures which influence the amount of fluid charge required inside the heat pipe. However the software did not only compensate for losses and process temperature differences, it also allowed the calculation of the fluid charge for each heat pipe type based on the screen wick parameters. It indicated that significant improvements could be made over previous methods using tables and the amount of experimentation and time for proving certain fill levels has been reduced to a great degree, as well as improving the first time process yield. Based on the new calculation software

the design process for screen mesh wick heat pipes could be accelerated and made more precise.

Investigations of Performance Issues based on Screen Mesh Wick Geometries

Most people within the heat pipe community still believe that screen mesh heat pipes cannot be used for applications where gravitational support or at least horizontal operation can be ensured. An investigation into a mathematical model for the capillary or lifting height is presented and from there it can be shown that screen mesh heat pipes can be used for applications that do not depend on the gravitational support. The mathematical model also indicates the actual limitations of the screen mesh wick heat pipe. Apart from the experimental validation, additional literature resources have been used as a background source to discuss novel aspects to the statement and support the two different opinions prior to conducting the practical experimentations.

Bent Heat Pipe Performance Trials

The developed fill calculation software was used for the manufacturing of the bending test samples. These samples were then used to conduct research into the field of heat pipe bending. Whilst bends occur in most industrial heat pipe applications, they have been neglected by the scientific community. Only one source (Quick Cool Heat Transfer GmbH, 2008) was found stating that bends in heat pipes do have negative effects on performance. In order to investigate the effects of bends on the overall heat pipe performance, detailed experimentation investigating multiple bend angles has been carried out. Based on the results, an equation for the performance losses has been derived and can now be used to assess the performance losses of heat pipes of a

similar type but with different bend angles. The use of this performance reduction equation, whilst linked to the straight heat pipe performance allows adjustments to heat pipe designs accordingly and avoids the risk of prototype failure in the application. This does not only help to reduce costs during the development process of heat pipe based cooling solutions, but it further reduces the time for the development of such solutions.

Multiple Freeze Thaw Cycling of Screen Mesh Heat Pipes

Furthermore, the developed software also gave the capability of solving freeze thaw issues of screen mesh wick heat pipes where destructive mechanisms linked to excess working fluid caused the heat pipe container to change its shape and created a risk of losing the vacuum inside the heat pipe through mechanical breakage. For the visualisation of the freeze thaw related phenomena, X-ray imaging technology was used and presented a novel way of showing the phenomena occurring inside the heat pipes. Being able to resolve these issues and avoid these phenomena allows the successful application of screen mesh heat pipes into areas which previously would have required a different type of heat pipe or technology altogether.

1.3 WORK INVOLVED IN THE RESEARCH

Work presented within this thesis contains five different technical parts, of which some are broken down into two or more sub-sections:

Part 1: The first part contains a review of existing research presented in literature. This review is presented in Chapter 2 and contains numerous topics related to heat pipes. Different types of heat pipes are presented as well as the

components required to construct heat pipes in general, their performance limits, mathematical models to describe them and techniques to simulate heat pipes using different numerical techniques. Further typical applications and their behaviour during start-up from conditions below zero degrees Celsius are described. All of these aspects were used as a foundation for the research presented and used as a point to evolve new approaches from.

Part 2: The second part of this work is presented in Chapter 3, where manufacturing issues around the production of high quality heat pipes are discussed. A high quality of heat pipe is required in order to be able to investigate certain parameters of the heat pipes rather than comparing manufacturing variations. Therefore, in the first section of this part, existing literature resources have been carefully reviewed with the aim to be able to obtain a mathematical model for the calculation of the required fill or working fluid charge depending on the screen mesh wick geometry. Once this model was established, existing data about fluid charges for different heat pipe diameters and length has been reviewed and compared with the new calculation software. As a second section of this part, venting techniques for heat pipes are presented and the most suitable one for the production of the test samples is identified. Further failure modes during the heat pipe venting or charging process, which have the most significant impact on heat pipe performance, have been analysed with their effects on the performance of the finished heat pipe and visually presented in order to be able to avoid these during the manufacturing of the heat pipe test samples.

Part 3: The third part of this work is introduced in Chapter 4, which is broken down into two sub-sections evolving around design parameters for screen mesh heat pipes. As a first section of this part a mathematical model for the calculation of the capillary or lifting height based on the screen mesh wick geometry is derived and then analysed with respects of available screen mesh wick types and their ability to be operated without gravitational support for the working fluid. The second sub section of this part presents an approach to use screen mesh wick properties to tailor particular screen mesh wick heat pipes towards certain applications like a low ΔT along the heat pipe length or their ability to handle high heat fluxes at the evaporator end. This work involved the use of different screen mesh types within the same heat pipe as well as different locations for these wick types within the heat pipe towards the container wall and was practically investigated using experimental techniques.

Part 4: The forth part of this work is presented in Chapter 5 of this thesis, where as a first sub section the difference in pressure drop for a single phase flow in a tube was investigated using commercially available CFD packages. These results were then linked to potential heat pipe heat transfer limitations due to the capillary limit which is seen as the main limit when heat pipes are bent. Moving on from there the construction of a dedicated test rig for horizontal heat pipe tests of the type described in Chapter 3 was presented as a second sub section and carefully discussed including all the components and instrumentation involved. This test rig was then used to obtain the test results which were analysed within the third subsection. Since no suitable correlation between the pressure drop work and the experimental results was found, a

second order mathematical equation to describe the performance degradation has been developed and is presented.

Part 5: The fifth part of this research contains work around the freeze thaw behaviour of screen wick heat pipes and how the screen wick is affected by multiple freeze thaw cycles. This can be found in Chapter 6, where an in depth investigation of the behaviour of screen mesh wick heat pipes when subjected to multiple non-operational freeze thaw cycles has been launched. This work was aimed to resolve the issue of destructive mechanisms not allowing the screen mesh heat pipes to withstand these cycles without showing geometrical distortions of the container and used X-ray techniques as well as thermal cycling and geometrical measurements to prove that these problems can be overcome. A link to work presented earlier during the fill calculations has been established and proved to be the solution to this additional task.

Finally within Chapter 7 of this work, the results of all the technical parts were critically discussed and the novelty and the benefits obtained from the results of this research are presented in a summarised form. Additionally, areas where further in depth research would be beneficial are introduced.

All the work carried out within this thesis has been aimed to give the screen mesh wick heat pipe its position amongst other wick structures and more advanced heat pipe types they deserve. It will be shown that screen mesh wick heat pipes still have despite their technological age, spare potential which could be used to give them unique advantages when applied correctly for certain applications.

CHAPTER 2 - LITERATURE REVIEW HEAT PIPE TECHNOLOGY

INTRODUCTION TO HEAT PIPE TECHNOLOGY:

What is a heat pipe? A heat pipe is a two phase device which allows heat to be transported over a certain length with very little temperature difference, at great speed, and is often referred to as superconductor (Shankara Narayanan, 2005). It consists of three main sections, the evaporator section, the adiabatic section and the condenser section. A heat pipe's basic functional principles are the evaporation of the working fluid in the evaporator, the transport of the working fluid as vapour along the adiabatic section with little temperature loss and the condensation of the working fluid at the condenser section. In order to be able to complete the two phase cycle, the liquid return to the evaporator section is provided by a wick structure within the heat pipe. In order to have a heat pipe fulfilling its designated job without problems over many years, particular interest needs to be paid to the three components in a heat pipe, such as container material, wick structure and working fluid, in order to find the most suitable combination for a required application without having any material compatibility issues. Within the following chapter a brief overview of heat pipe construction, heat pipe performance limits as well as typical and more specific heat pipe applications will be provided. This work has been conducted as part of a PhD thesis and is aimed to provide an overview leading towards the chapters which deal with the investigation of novel approaches to existing problems and offering new combinations or view points on problems not fully addressed previously.

2.1 HEAT PIPE CONSTRUCTION

2.1.1 Container Materials

The container is the envelop which forms the heat pipe once it has been evacuated and sealed. Container materials can be of different types, metals, glass, plastic, even ceramics and many others (Groll et al., 1998). Due to their high thermal conductance and the possibility to reliably seal them and change their shape, metals, and in particular copper, are the most common container materials.

A very comprehensive overview about heat pipes used for cooling electronic components especially with regards of material selection and possible material combinations has been given by Groll et al. (1998) and was seen as a good starting point for this literature review.

This paper states that typical wall materials are carbon steel, stainless steel, and copper as well as their alloys. It confirms what was already said in the introduction of this chapter that copper is the most common wall material for low temperature heat pipes. The main advantage of copper is its compatibility with water and other low temperature working fluids as well as having a high thermal conductivity. The main advantages of aluminium are its low density and therefore low weight and its compatibility with ammonia which makes it the standard heat pipe for satellite thermal control. A further advantage is the possibility to manufacture various profiles of very complex shapes by extrusion (Groll et al., 1998).

Reay and Kew (2006) provide a statement about the function of the container which is to isolate the working fluid from the outside environment. Therefore it is emphasised that it has to be leak-proof as well as maintain the pressure differential across its wall and to enable the transfer of heat to take place into and away from the working fluid. According to them, the most common three container materials used are copper, aluminium and stainless steel. Copper is eminently the preferred choice for electronics cooling applications with working temperatures in the range between 0°C and 200°C. When commercially available tube is used, the oxygen-free high-conductivity type should be preferred. Aluminium is the next common container material but by far less often used in commercial heat pipe applications. The main area of use is by the aerospace industry with its more rigorous weight constraints and is generally used in alloy form. These alloys are then either drawn to suit the applications requirements or extruded into a suitable shape, to incorporate a grooved wick for example. Stainless steel is the third common container material but as with aluminium cannot be used with water as a working fluid due to gas generation problems. On the other hand, stainless steel is compatible with many other working fluids and can be, in many cases, the only suitable container material. These cases include the use of liquid metals such as mercury, sodium and potassium. Reay and Kew (2006) are amongst the few who present a use for mild steel as a container material utilizing organic working fluids.

Recent advances in materials for heat pipe container materials can be found in conference proceedings or journals such as “Applied Thermal Engineering” or many others. Most new materials investigated are aiming to either enhance the

temperature range of heat pipes, or save weight and costs in comparison to other known container materials.

Hwang et al. (2007) proposed the use of titanium as a container material for a heat pipe with water as the working fluid. The main reason for the use of titanium was its higher structural strength, and therefore, its capability to operate the water heat pipe at higher temperatures than a copper version, without risking the container rupturing due to the vapour pressure. Doing so still enables the benefits of good heat transfer properties of water as a working fluid.

Very recent industrial research at Thermacore Inc. through Rosenfeld (2006) investigates the use of magnesium and magnesium alloys as container material for heat pipes. The use of these materials is seen beneficial due to low density and high structural strength of the material, which makes it particularly interesting for the aerospace industry as well as consumer products such as laptop computers. The major challenges with the use of magnesium and its alloys are the sealing processes, and to find suitable combinations of container materials, wick structures and working fluid which will give these heat pipes the desired lifetime of up to 25 years. Once this is successfully resolved magnesium offers weight savings up to 35% by replacing aluminium within grooved heat pipe applications.

Wicks

A wick is the material inside a heat pipe which forms the capillary structure in order to provide liquid return to the evaporation section. Along with the container material it is also exposed to the working fluid and therefore compatibility between wall and wick, as well as wick and working fluid, needs

to be ensured. Throughout the literature three main categories of wicks can be found, screen mesh heat pipes, sintered powder heat pipes and grooved heat pipes. Whilst there are other sub categories of wicks these can be more or less related to one of the three main categories.

Groll et al. (1998) states that a wick structure for conventional heat pipes as investigated in this study and mostly implemented in electronics cooling applications can be made out of sintered metal powders, screens and wire meshes. In more advanced wicks, woven fibre glass or carbon fibres can also be employed into the heat pipe.

Analysing the three main books on the topic of heat pipes authored by Faghri (1995), Peterson (1994) and Reay and Kew (2006), they contain information about wicks but only one will be presented.

Reay and Kew (2006) probably provide the most comprehensive section on the wick selection and are the only ones which specify materials for screen wicks. They state that meshes and twills are the most common wick form, which can be manufactured from a range of materials including stainless steel, nickel, copper and aluminium as well as alloys of the above. Further, metal foams and felts can be used as well. Within their work they provide very detailed information about different pore radii for different mesh types. In total, they divide the wicks into five categories including a sixth sub category which is derived from the first five categories. The five categories are meshes, sintered wicks, grooved wicks, concentric annulus wicks and sintered metal fibres whilst the sixth sub category is the arterial wick. This category also contains the monogrooved heat pipe.

More recent research has been conducted by various authors and has been published in various technical journals such as “Applied Thermal Engineering”, “Experimental Thermal and Fluid Sciences”, “International Journal of Heat and Mass Transfer” and many more. This review has been focused on the two categories of wicks used for electronics thermal management applications which are sintered wicks and screen mesh wicks.

Sintered Wicks:

Leong, Liu and Lu (1997) did a very detailed metallurgical analysis of sintered copper wicks to be used in heat pipes. Within their paper they state the main advantage of sintered copper wicks to be the existence of smaller pores when compared to wire mesh and the better controllability of porosity and pore size to optimize heat pipe performance. Within their experiments they compared a constant sphere size copper powder when sintered at different temperatures and durations in the sinter oven. One of their main findings was that the sintering temperature, whether it is 800°C or 1000°C has less of an effect on the overall porosity of the wick than the sintering time which when extended can lower the porosity quite significantly. The sintering temperature on the other hand does significantly influence the pore size distribution in the wick. Only at the lower temperature of 800°C are there significant numbers of pores below the size of 0.35µm, whilst this is not seen at the higher temperature. Finally they confirm the achievable range of heat fluxes for high performance sintered heat pipes to be between 50 and 100 W/cm².

Another interesting approach in order to raise the achievable heat flux in a sintered wick has been undertaken by Semenic et al. (2008), who promote the

use of biporous wicks in order to remove high heat fluxes. With their wick, which consists of clusters of sintered material of finer pores within the cluster, they manage to achieve heat fluxes up to 494 W/cm^2 , which is almost 2.5 times what is believed to be the critical heat flux limit for sintered heat pipes. The approach of Hwang et al. (2007) is similar to the one mentioned above but points into a different direction, rather than changing the structure of the wick, in their approach the shape of the wick has been changed and extensive research on the optimum shape of the wick has been conducted. In general, they are mimicking the shape of a grooved heat pipe through a sintered structure within a plain tube which forms the grooves. This approach has the advantage that it provides extra capillary forces through the stacks which form the grooves for the working fluid to return to the evaporator and still have low resistance against vaporisation in the evaporation section. For their wick they used titanium as material whilst the other papers presented used copper powder. The approach of Mwaba, Huang and Gu (2006) presented under the screen mesh wick section following, also uses copper powder as part of their composite wicks.

Screen Mesh Wicks:

Canti et al. (1998) provide an overview of stainless steel as a wick material for a heat pipe as well as provide a good definition for having a wick inside a heat pipe, which states, that heat pipe design and manufacturing requires the knowledge of the thermal hydraulics of the wick. They present work on stainless steel, which is not the most common material for either sintered wicks or mesh wicks. This review is merely focused on the screen mesh part of their work. Through using very simple apparatus they provide a detailed

analysis of the properties, like the capillary height/ head, permeability and the heat fluxes possible. An interesting part of their work is that they actually achieve heat fluxes between 55 and 70 W/cm² for a composite wick, made out of a combination between sintered and mesh wicks, which is by some degree higher what is assumed to be the critical heat flux for screen meshes. Further their paper presents the mathematical foundations for further work and descriptions around screen mesh wicks which are utilized in later sections of this thesis.

Kozai, Imura and Ikeda (1991) have also presented very interesting fundamental research around screen meshes. Their work shows how to obtain the porosity of a certain screen mesh directly from using its geometrical data like wire diameter, aperture and crimping factor. They provide a correlation between their experimental work and their analytical work showing a very small difference of around 3%, as well as providing information on how to treat multilayer screen wicks which are commonly used in heat pipes with regards of overall porosity. This is of paramount importance for carrying out work on fill/ fluid charge calculations of heat pipes.

Kempers, Ewing and Ching (2006) have worked on the problems of fluid loading as well as investigating the effects of different numbers of wick layers within the screen mesh heat pipe. Their most significant findings were that the overall thermal resistance of the heat pipe does not increase in a linear way with an increasing number of mesh layers, but almost reaches a stable state once three layers are implemented. But, the number of mesh layers has a positive effect on the other side on the maximum overall thermal resistance prior to failure of the heat pipe. The next phenomenon they investigated was

the amount of working fluid required. Their results coincide with what has been stated by Peterson (1994). They found that the heat pipes with less fluid load had a lower overall thermal resistance but a reduced maximum heat transfer rate as well. The ideal heat pipe has a saturate wick and no excess working fluid whilst the heat pipes with excess working fluid have in nearly all orientations, apart from the vertical one, a higher maximum heat transfer rate but also a higher overall thermal resistance.

The work of Brautsch and Kew (2002) directly investigating the heat transfer capabilities of the wick is very interesting as the work compares the heat transfer capabilities of each wick type investigated. The wick types investigated coincides very nicely with wick geometries available for uses in heat pipes as well, and are 50 mesh, 100 mesh, 150 mesh and 200 mesh. Within the work conducted and presented as part of this thesis, all three, 100 mesh, 150 mesh and 200 mesh have been used and therefore there is a great relevance of their work to this work. Their work clearly indicates that for the transmission of high heat fluxes a great amount of evaporation surface needs to be provided, and therefore, the finer meshes with higher numbers are capable of handling higher heat fluxes, which can even be increased further by providing more than one layer of wick.

The final study to be mentioned with regards of screen mesh heat pipes is the one of Mwaba, Huang and Gu (2006). Firstly their definition of heat pipes needs to be mentioned, which states that in its conventional form, a heat pipe consists of a sealed tube that is partially filled with a working fluid. A wick, saturated with a working fluid, lines the inner sides of the tube. Within their study, they have investigated three different wick types, first a coarse screen

mesh type of 100 copper mesh, secondly a fine sintered copper wick and third a combination between the two where the sintered wick is used in the evaporator, whilst the screen is used in the adiabatic section as well as the condensation section. Their conclusions are that the combined wick performs best of all three and can enhance the performance of the heat pipe up to a factor of two when all the other conditions like heat load and cooling conditions are kept the same. Their combined wick combines a high surface area for evaporation in the evaporation section with a low thermal resistance in the condenser section.

2.1.2 Working Fluids

The working fluid is the medium inside a heat pipe which gets evaporated, transports the heat and condenses at the condenser section prior to being returned either through gravitational or capillary forces to the evaporation section. Its latent heat of evaporation as well as other thermodynamic properties has a paramount influence on the heat pipe's overall performance.

Table VI List of subjects		
Fluid	Compatible	Incompatible
Freon 11	Aluminium	
Freon 22	Aluminium	
Freon 113	Aluminium	
Ammonia	Aluminium (+ alloys) Stainless steel Nickel	Copper
Acetone	Aluminium (+ alloys) Copper (+ alloys) Stainless steel Nickel	
Methanol	Copper (+ alloys) Stainless steel Nickel	Aluminium
Ethanol	Copper (+ alloys) Stainless steel Nickel	Aluminium
Water	Copper (+ alloys) Stainless steel Nickel Titanium	Aluminium (Inconel)

Table 2.1: Compatibility Matrix Working Fluids- Materials (Groll et al., 1998)

Apart from compatibility issues with the container material and the wick, the working fluid is also of paramount importance when the classification due to the operating temperature of the heat pipe needs to be conducted. An overview of working temperature ranges for working fluid is provided in Figure 2.1 below which is providing information based on information of Reay and Kew (2006) and is presented in a similar manner and coincides with information provided by Groll et al. (1998).

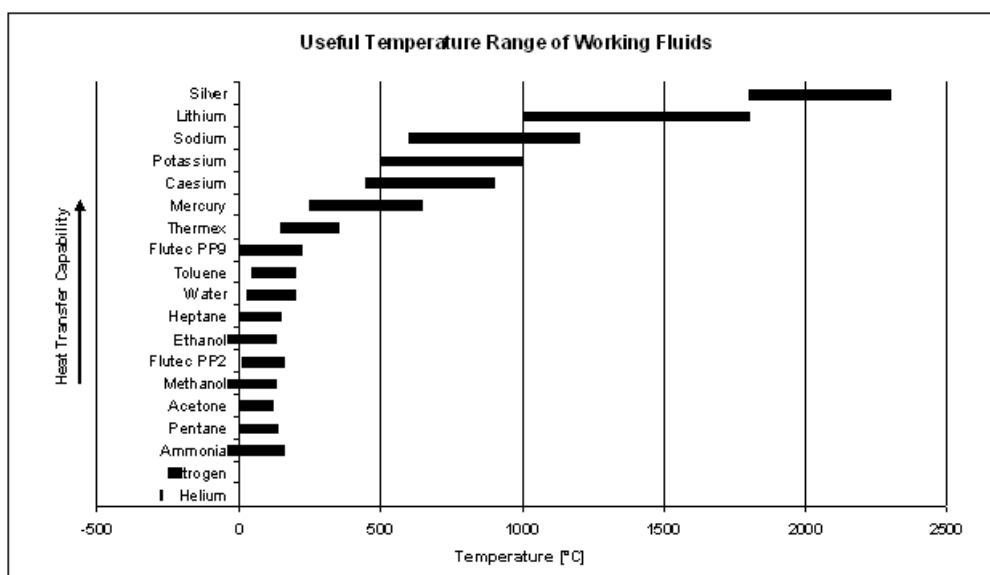


Figure 2.1: Useful Temperature Range of Working Fluids (Reay & Kew, 2006)

In general, heat pipes can be classified into the following 4 categories depending on their operational range: Cryogenic heat pipes; low temperature heat pipes; medium temperature and high temperature heat pipes. The total number of categories is totally depending on which author of the three leading books about heat pipes, Reay and Kew (previously Reay and Dunn) (2006), Faghri (1995) and Peterson (1994) is followed and may vary between three to four depending on the author.

The review of operational ranges presented is the one of Faghri (1995), who provided the most detailed information on temperature ranges and promotes the use of four different categories for heat pipe classification: First there is the cryogenic heat pipe which has a useful temperature range between -270°C and -75°C . This type of heat pipe uses either helium or argon, oxygen and krypton as working fluid and is capable only of transporting minimal amounts of heat due to the small heat of vaporisation.

The second category according to him is the low temperature category which has a temperature range between -75°C and 275°C and is the category into which most electronics cooling and heat pipe applications generally fall. This category houses the most common working fluids, like water, ammonia, acetone, the Freons along with ethanol and methanol. The use of these category boundaries coincides as well with the statements of Sarraf and Anderson (2007) which use water as a working fluid with titanium and Monel as container materials within the same temperature range.

The third category proposed by Faghri (1995) contains the medium temperature heat pipe with an operational range between 275°C and 475°C . Heat pipes within this category are already liquid metal heat pipes using sulphur and mercury as working fluids. Mercury is an attractive working fluid due to its high thermal conductivity but is rarely used in applications due to wetting problems with the wick and the fact that it is a toxic heavy metal.

The fourth category announced by Faghri (1995), the high temperature heat pipe contains the liquid metal heat pipes with an operational range between 475°C and 2725°C . Heat pipes within this category use sodium, lithium, silver and potassium and their compounds as working fluids and offer therefore much higher heat transport rates than heat pipes of the other temperature ranges (Faghri, 1995).

More recently research has been conducted on mixtures of water with either ethanol or methanol in order to increase the heat transport properties of the alcohol without the possibility of separating the combination by distillation again. These mixtures are called azeotropic mixtures and are merely aimed at applications where freezing of the working fluid as well as thermal

performance with weight restrictions such as onboard of satellites are problematic (Savino, Abe & Fortezza, 2008; Savino et al., 2009 and di Francescantonio, Savino and Abe, 2008). This research has been conducted very recently and has not been introduced into heat pipes on a wider scale yet. Therefore it is not explained further in this review.

2.1.3 Performance Limits Of Heat Pipes

The main performance limits of heat pipes are very well described and could justify a full scale review themselves. Since the main focus of this PhD thesis is aimed to a different area, only a short descriptive section is dedicated to the performance limits of heat pipes. Due to the extent of work presented; only the three main books on heat pipes are reviewed with regards of that topic. It has to be mentioned that the dry-out limit and the entrainment limits are seen most critical to the work presented at a later stage.

A book to be mentioned out of the three reviewed is the one of Faghri (1995), which provides the most comprehensive review on the topic. In total eight different limitations are described, which are the capillary limitation; the boiling limitation; the sonic limitation; the entrainment limitation; the viscous limitation; the condenser limitation; the continuum flow limitation and the frozen start-up limitation.

A very brief description is provided onto each limitation and more details can be found in the source itself whilst only the brief ones are cited here.

1. Capillary Limitation: “For a given capillary wick structure and working fluid combination, the pumping ability of the capillary structure to provide the

circulation for a given working medium is limited. This limit is usually called the capillary or hydrodynamic limit.”

2. Boiling Limitation: “If the radial heat flux or the heat pipe wall temperature becomes excessively high, boiling of the working fluid in the wick may severely affect the circulation of the working fluid and lead to the boiling limit.”

3. Sonic Limitation: “For some heat pipes, especially those operating with liquid metal working fluids, the vapour velocity may reach sonic or supersonic values during the start-up or steady state operation. This choked working condition is called the sonic limit.”

4. Entrainment Limitation: “When the vapour velocity in the heat pipe is sufficiently high, the shear force existing at the liquid-vapour interface may tear the liquid from the wick surface and entrain it into the vapour flow stream. This phenomenon reduces the condensate return to the evaporator and limits the heat transport capability.”

5. Viscous Limit: “When the viscous forces dominate the vapour flow, as for a liquid-metal heat pipe, the vapour pressure at the condenser end may reduce to zero. Under this condition the heat transport of the heat pipe may be limited. A heat pipe operating at temperatures below its normal operating range can encounter this limit, which is also known as the vapour pressure limit.”

6. Condenser Limitation: “The maximum heat rate capable of being transported by a heat pipe may be limited by the cooling ability of the condenser. The presence of non-condensable gases can reduce the effectiveness of the condenser.”

7. Continuum Flow Limitation: “For small heat pipes, such as micro heat pipes and for heat pipes with very low operating temperatures, the vapour flow in the heat pipe may be in the free molecular or rarefied condition. The heat transport capability under this condition is limited because the continuum vapour state has not been reached.”

8. Frozen Start-Up Limitation: “During the start-up process from frozen state, vapour from the evaporation zone may be refrozen in the adiabatic or condensation zones. This may deplete the working fluid from the evaporation zone and cause dry out of the evaporator.

A more detailed review on that limitation will be provided in section 2.2.2 of this literature review and therefore no more details are provided here.

2.1.4 Types Of Heat Pipes

The first three types of heat pipes are already described in greater detail in section 2.1 under wick structures. Therefore the focus here will be on the unique application of these three heat pipes and the section on advanced heat pipe types will provide further details of those heat pipe types which are not investigated further at a later stage for this PhD thesis.

1. Grooved Heat Pipes:

Grooved Heat Pipes are primarily used for space applications. The advantages of these devices have been pointed out by Hoa, Demolder and Alexandre (2003). They state: “Most of heat pipes for space applications have axial grooves and are made of extruded aluminium 6063. The common working

fluid is ammonia as its operational temperature is well suited to space applications (-40, 80°C). Axially grooved heat pipes offer relatively simple industrial fabrication and greater reliability than other wick designs, such as artery heat pipes.”

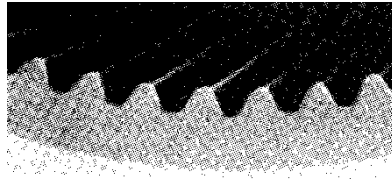


Figure 2.2: Internal Structure of a Grooved Heat Pipe (Thermacore, 2008)

2. Mesh Wick Heat Pipes

Screen mesh heat pipes are one of the older types and have been in the market place since the mid 1960's when heat pipes were mentioned by Cotter, Grover and Erickson (1964). They can be used in various applications but lack a distinctive market.



Figure 2.3: Screen Mesh as used for wicks inside Heat Pipes (Thermacore, 2008)

3. Sintered Heat Pipes

Sintered heat pipes have the highest proportion amongst all heat pipes manufactured. They can be found in all sorts of electronic cooling applications including laptops, personal computers and many more.



Figure 2.4: View into Sintered Heat Pipe (Thermacore, 2008)

4. Advanced Heat Pipe Types: Loop Heat Pipes; Capillary Pumped Loops; Vapour Chambers, Thermosyphons; Loop Thermosyphons and Variable Conductance Heat Pipes:

Loop Heat Pipes:

When it comes to the topic of loop heat pipes, one name has to be mentioned and that is the one of Yury Maydanik. He provides a very comprehensive review on the topic of loop heat pipes in his paper “Loop Heat Pipes” (Maydanik, 2006) as well as the typical applications for loop heat pipes. He describes a loop heat pipe the following way: “Loop heat pipes (LHPs) are two-phase heat-transfer devices with capillary pumping of a working fluid. They possess all the main advantages of conventional heat pipes, but owing to the original design and special properties of the capillary structure are capable of transferring heat efficiency for distances up to several meters at any orientation in the gravity field, or to several tens of meters in a horizontal position. Besides, the LHP conception allows a wide variety of different design embodiments, which essentially extends the sphere of functional possibilities and practical application of these devices.”

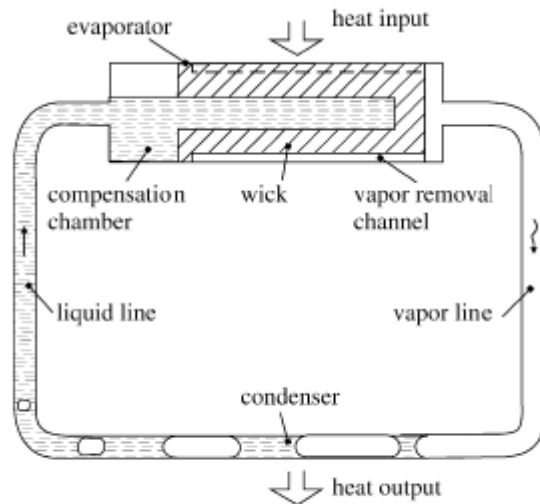


Fig. 1. Principal scheme of an LHP.

Figure 2.5: Loop Heat Pipe Schematic (Maydanik, 2006)

Due to the loop heat pipes ability to overcome gravitational effects and their high cost, he describes their main application in space technology. Another interesting application is proposed in the paper of Pastukhov and Maydanik (2006). They describe the use of miniature loop heat pipes for the cooling of personal computers (PCs). The main advantage is seen in the superior power handling ability of the loop heat pipe in comparison to normal heat pipes. Therefore they are capable of transporting the higher power provided by modern CPUs within the same space envelop.

Further work on Loop Heat Pipes has been presented by Zan et al. (2004), where particular interest is paid to the sintered evaporator wick and the material used for creating it. They investigated both, different porosities of the dendritic nickel powder as well as two different manufacturing methods for sintering the wick. Based on these and the experimental results of trials run for four different porosities, it was found that there is an optimum composition of the wick to maintain maximum power handling at a minimum overall thermal resistance.

Capillary Pumped Loops:

Capillary pumped loops (CPL) are very similar to loop heat pipes but still different in a multiple of ways. According to Faghri (1995), the CPLs were invented five years earlier than the LHPs, in the United States in 1966 versus the LHP in 1971 in Russia. They consist of the same components, an evaporator, a condenser, transport lines, in case of the CPL, a sub-cooler to liquefy the working fluid and avoid bubbles prior to entering the evaporator and a liquid-vapour reservoir.

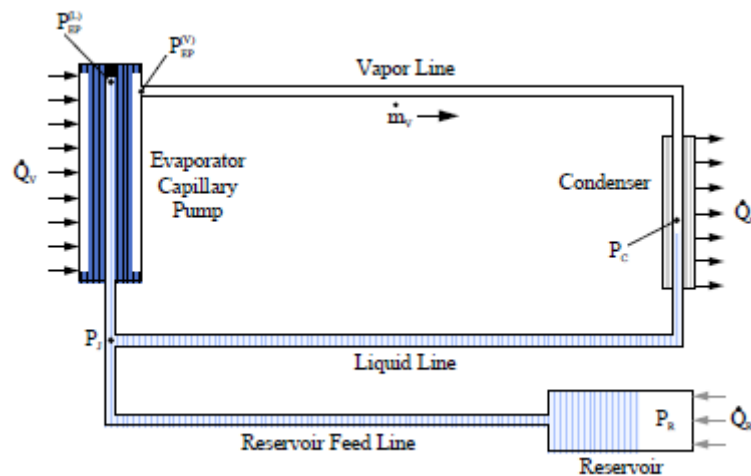


Figure 2.6: Capillary Pumped Loop (CPL) Schematic (Hoang, 1997)

The major difference between a LHP and a CPL is the location of the reservoir. In a LHP, the reservoir is part of the evaporator (compensation cavity), whilst the CPL has a separate component, which is a two-phase accumulator. The temperature of the reservoir is controlled through electrical heaters and changing conditions anywhere in the loop will cause either liquid to move in or out of the reservoir until the loop has reached stable conditions again. The main applications are similar to the ones of LHP's, including spacecraft, space stations and satellites as well as electronic cooling.

Chen and Lin (2001) have investigated the possibility of using CPL's for the cooling of electronic components such as CPUs in personal computers and notebooks. They positively describe the ability of using CPL's for the proposed application even though their tested power levels are not up to the ones recently seen for the application and are below the ones proposed by Pastukhov and Maydanik (2006).

According to Faghri (1995), CPL's are structurally more complex than LHP's but offer the ability to transport higher amounts of heat over long distances which gives them a slight advantage over LHP's.

Vapour Chambers and Flat Plate Heat Pipes:

Vapour chambers and flat plate heat pipes are very popular in electronics cooling application, since their flat shape allows components to be directly attached to them without having to have special connector plates. The main difference between vapour chambers and flat plate heat pipes is seen as their fabrication. Flat plate heat pipes can be stamped from originally round material, whilst the vapour chambers are formed through a welding or brazing operation and originally consist of a separate evaporator and condenser where only the evaporator has a wick structure.

Groll et al. (1998) proposed various uses of flat plate heat pipes which range from the direct attachment of flat heat pipes directly to the back of printing wiring boards. These applications can be extended to avionics applications as well.

Faghri (1995) provides the following description for a flat plate heat pipe: "The flat-plate heat pipe is capillary driven and has a rectangular shape with a

small aspect ratio. Additional wick blocks between evaporator and condenser aid in condensate return, especially when the condenser is below the evaporator in a gravity field. If the condenser is above the evaporator, there is no need to have a wick in the condenser section, since the working fluid will drip back to the evaporator.”



Figure 2.7: View of a Vapour Chamber (Flat Plate Heat Pipe) (Thermacore, 2008)

Further it was stated, that “a wick is needed over the evaporator section, however, in order to uniformly distribute the liquid over the entire surface so that dry-out is prevented. The flat-plate heat pipe is an excellent candidate for use in electronics cooling applications. Small semiconductors or transistor packages can be mounted in arrays onto the flat heat pipe for cooling and/ or temperature flattening.”

More practical work with regards to vapour chambers can be found in a paper of Haddad, Boukhanouf and Buffone (2006), where a small vapour chamber of 40x40mm is experimentally investigated. Within the work, different wick structures inside the vapour chamber, screen mesh and sintered powder are compared and it was found that for vapour chambers, sintered wicks are the

superior choice over screen mesh due to the higher heat flux handling capabilities and the lack of sensitivity to gravitational orientation.

Thermosyphons and Loop Thermosyphons:

Thermosyphons and Loop Thermosyphons are a simplified version of their heat pipe equivalents and therefore require gravitational aid for the liquid to return to the condenser.

A description of a two-phase closed thermosyphon can be found in the book of Faghri (1995) and the following one is given: “A two-phase thermosyphon is a gravity-assisted wickless heat pipe. The condenser section is located above the evaporator so that the condensate is returned by gravity. The sonic and vapour pressure limits are constraints of the thermosyphon as with capillary driven heat pipes. The entrainment limit is more profound in the thermosyphon than in capillary driven heat pipes due to the free liquid surface. The counterpart of the entrainment limit in thermosyphons is called flooding, which is the most severe limitation in the operation of these systems.”

Loop Thermosyphons are very similar to the loop heat pipes and a description can be found in the work of McGlen (2007).

A loop thermosyphon consists of two large chambers which act as the evaporator and the condenser and are connected by two liquid lines. The functional principle is based on the vapour generated through the evaporation of the working fluid in the evaporator, travelling up the vapour line, prior to condensing in the condensation chamber and returned to the evaporator down the liquid line with the help of gravity. The main advantage is seen as that the liquid does not have to overcome the pressure drop of the vapour and hence an increased return flow rate can be achieved. Further, in comparison to a

standard heat pipe, the LTS's larger area in the evaporator section allows higher heat inputs and the condenser section offers a lower dT due to the lack of a wick there.

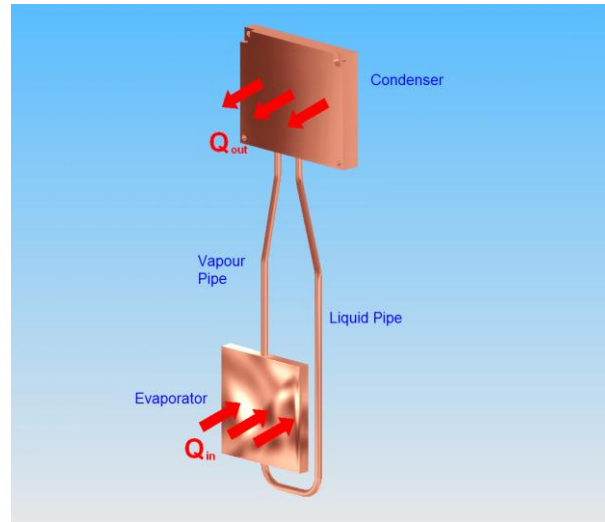


Figure 2.8: Schematic of a Loop Thermosyphon (LTS) (McGlen, 2007)

Joudi and Witwit (2000) conducted some very interesting work where they worked on numerous topics, gravity assisted heat pipes, which are effectively thermosyphons and thermosyphons with partially wicked evaporators as well as heat pipes with separators, internal tubes separating the liquid and vapour phase, were also investigated. Within their investigation, they investigated both, different fill levels as well as multiple orientations. The interesting remark to be made is that they can see notable reductions in the heat pipe wall temperatures at the same external conditions whilst having a 35% increase in the heat transfer coefficient. There has been very little work trying to combine both types, the thermosyphon and the screen wick heat pipe, in order to tailor the thermal solution towards a particular application. Their work is very similar to the approach of the author trying to tailor screen wick heat pipes towards particular applications which can be found in chapter 4 of this thesis.

Variable Conductance Heat Pipes:

Variable conductance heat pipes are heat pipes capable of maintaining the temperatures at a heat source or electrical component attached to them. Since they are not the key part of this work but worthwhile mentioning only the very good brief description of Sauciuc, Akbarzadeh and Johnson (1996) is provided. They state that most important feature of a variable conductance heat pipe is the NCG pressure and working fluid composition to enable temperature control of a hot source. The length of the condensing section or heat transfer in general starts when the saturated partial vapour pressure equals the NCG pressure inside the heat pipe. The NCG is carried to the condenser section by the working fluid vapour where it is becoming trapped.

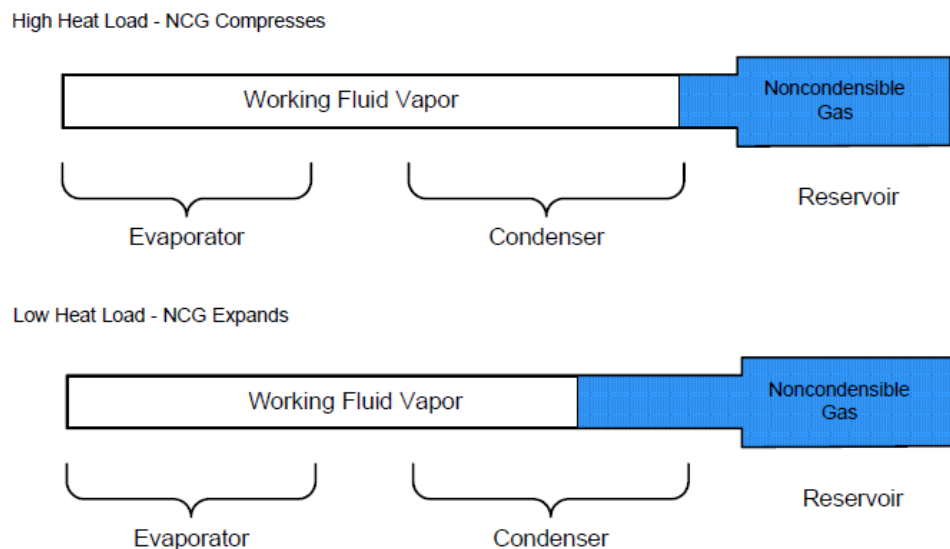


Figure 3 VCHP Operation

Figure 2.9: Schematic of a Variable Conductance Heat Pipe (Sarraf, Bonner & Colahan, 2006)

The condenser length is varied during operation with the increase in vapour temperature and corresponding larger increase of operating pressure. Therefore, when designed properly, the heat source temperature can remain

constant whilst the heat transfer rates vary during the operation of Variable Conductance Heat Pipes.

2.2 HEAT PIPE APPLICATIONS

2.2.1 Typical Heat Pipe Applications

Heat Pipes have been employed in various applications apart from the typical electronics cooling ones. They can be found in various other applications like solar collectors, drill bits, medical applications and military applications as well as various other ones. The number and area of heat pipe applications extends on a daily basis.

All three major books on the topic of heat pipes have sections about the applications of heat pipes in them as well as quite a few review journal papers deal with that topic. For length reasons, only a few major ones will be quoted here.

Faghri (1995) provides a chapter in his book about heat pipe applications which is divided into the areas of applications as well as groups. In total three groups are mentioned which contain i) separation of heat source and sink; ii) temperature equalisation and iii) temperature control.

The first area mentioned is the area of aerospace, containing both conventional aerospace applications as well as space craft. For spacecraft heat pipes are used for satellite thermal control as well as isothermalisation of the effects of solar radiation from the sun around the structure. In conventional aerospace applications the use is described as heat pipe laser mirrors where heat pipes

are used to overcome the effects of distortion through overheating and extend the lifetime of these mirrors.

The second area is the area of heat exchangers where the use of heat pipe heat exchangers is described as cheaper due to reduced size as well as being more efficient due to a higher grade of isothermalisation in comparison to conventional tubular heat exchangers. Furthermore, three groups of heat pipe heat exchangers are provided, which are described as gas-gas, gas-liquid and liquid-liquid heat exchanger units. The first group finds the widest usage amongst the three types.

The third area of applications is the one of electrical and electronic equipment cooling. Applications described here range from cooling of hot spots where cables cross other hot pipes, to the increase of the life of bearings in electrical motors and electrical components. Due to the use of heat pipes these can be operated for longer because of the reduce temperatures they are facing. This area includes the application in computers such as laptops and desktop PCs as described by Kim et al. (2003).

The fourth area is also one where heat pipes or their predecessors were first used at the middle of the 19th century and contains ovens and furnaces. Heat pipes and thermosyphons were used to transport heat from a separate fire box into the baking chamber offering up to 25% fuel savings at a higher temperature. More recent applications of heat pipes in that area are high temperature furnaces and calibration furnaces for temperature measurement equipment.

The fifth area described are production tools and contain primarily injection moulding tools where heat pipes are used to spread the heat across the tool as

well as cool the die and prevent it from overheating, as well as cool the cast material.

The sixth area mentioned is medicine and human body temperature control, where heat pipes are used for surgical instruments as well as for clothing and blankets which are used to either cool large regions of the body or prevent extremities from under cooling.

The seventh area proposed for heat pipe applications is transportation systems and de-icing where heat pipes and waste energy, either from a natural source, like the ground or sea, or an external source like a ships engine, are used to melt snow and ice on pavements, airfield runways, roads, bridges, handrails on ships and other seaborne and land bound structures which are suffering from icing problems.

As an eighth area of heat pipe applications, engines and the automotive industry are proposed. This mainly includes Stirling engines with incorporated heat pipes as well as automotive brake discs and pads, where heat pipes are used to reduce the thermal stresses within these components.

An area which is described in ninth place is Permafrost stabilisation and the case mentioned, in particular the Trans Alaska pipeline and her “Cryo-Anchors” have been described by Reay and Kew (2006) as well.

The tenth area of applications is solar systems, in which inclined banks of heat pipes or thermosyphons collect solar energy and either transport it into water storage tanks or convert it into heat which is used to heat up internal spaces.

The eleventh and final area is the one of manufacturing where liquid metal heat pipes can be used to increase the dipping frequency and decrease the

waste during the manufacturing of glass bottles by isothermalising the steel piston used to make the billets which are later blown into bottle shape.

An interesting paper describing rather unusual heat pipe application was written by Vasiliev (1998) and deals with heat pipe applications in the former Soviet Union. Within the paper the usage of flexible heat pipes (FHP) for heating of greenhouses and railway points as well as cooling electric cables is described. Further a solar cooker based on a long thick heat pipe is mentioned, which provides a hot plate to cook on within a building. In terms of residential heating, a system named BETA, was developed and is based on heat pipes and an electric heat ceramic storage block. In this system, a control valve is used to start the release of the stored energy through the heat pipe and allows precise control of the ambient temperature. In terms of medical applications, an apparatus was described, which allows the cooling of cavities within the human body through heat pipes and peltier elements.

Zhang and Zhuang (1998) present a similar approach for heat pipe applications in China and emphasise on the use of heat pipes in industrial process applications. They are amongst very few who work on carbon steel water heat pipes which are not widely used due to corrosion issues, but in their case, they report successes for heat pipe heat exchangers.

Many other applications have been described in great detail as well but are very similar to applications described earlier in this section and are therefore not mentioned in greater detail, which does not reflect any critics of the descriptions provided.

2.2.2 Detail Focused Investigation Of Heat Pipe Behaviour (Start-Up; Freeze- Thaw)

One of the most interesting parts of heat pipe operation is the start up and the start-up from frozen state, when non liquid metal working fluids are used. Further, the behaviour of the heat pipe container during frozen state, whether it is suffering from any influences of the working fluid directly or if the working fluid is gathered in frozen state in a different location than the evaporator which will prevent the heat pipe from working are well worth investigating. Unfortunately the topic of frozen start-up and heat pipe freeze thaw are not very well investigated and only very few publication are available.

Successfully starting up a heat pipe can prove to be not straight forward, the two-phase cycle needs to be successfully started and that can depend on various factors like orientation and length of the heat pipe, the system mass the heat pipe is integrated in, ambient conditions etc.

This coincides with the statement provided by Reay and Kew (2006), which is that “heat pipe start-up behaviour is difficult to predict and may vary considerably depending upon many factors.” Further, the start-up conditions are described in great detail and it is stated that vapour must travel at a relatively high velocity from the evaporator to the condenser with a large pressure drop along the vapour space. The temperature gradient along the wall is determined by the vapour pressure drop, therefore the temperature at the evaporator is much higher than at the condenser during start-up. Once the heat input has reached a certain level, the temperature front will move and the pipe

will behave near isothermal. This process and the duration of the transient period are determined by the wick structure and the working fluid used.

The book that particular deals with start-up of heat pipes is the one of Faghri (1995). He states that most heat pipe design parameters deal with the heat pipe's steady state operation and the related temperature rather than start-up from ambient. Depending on the heat pipe type, this can be either higher or lower than the operational temperature. If the heat input during start-up is happening too fast, the evaporation section can be overheated and cause damage to the heat pipe. Faghri (1995) proposes a start up procedure where the entire heat pipe is taken to its operational temperature. This can either be an increase or a decrease of temperature depending on the heat pipe type. Then the power should slowly be ramped up from zero to operational whilst maintaining a uniform temperature along the pipe. Due to the fact that this condition cannot always be maintained in reality, where the power input happens suddenly, he describes an additional three real start up scenarios, which are uniform start-up; gas loaded start-up and frozen start-up. Uniform start-up is happening when the heat pipe has a uniform axial temperature and the working fluid in the wick is in a liquid state with the vapour at continuum state. A practical example would be the start-up of a copper-water heat pipe started from an above 0°C ambient to its higher operating temperature without any problem. The next one would be the gas-loaded heat pipe start-up, which is very similar to what Peterson (1994) describes as frontal start-up with NCG present. The working fluid is in the wick and the vapour space is filled with the gas. Once the evaporation is started, the working fluid vapour drives the gas to the condenser end of the heat pipe. Since the gas is blocking the

condenser, this phenomenon can be seen on the axial temperature gradient along the pipe. Once sufficient heat is inserted to build up a vapour pressure which is higher than the gas pressure, the NCG is driven further to the end of condenser with reduction of its effect. Once the pressure is high enough to ensure normal operation, it can be seen by the temperature along the pipe where the sudden drop of temperature gets moved further along the pipe till it reaches the condenser end. The final mode of start-up is the frozen start-up. Here the working fluid within the wick structure is frozen and the vapour space is evacuated of any working fluid vapour. This is referred to be a mode of frontal start-up and is normal for liquid metal heat pipes. The principles of frozen start-up are described as following: First heat is conducted through the container material into the wick structure, which raises the temperature in the evaporator section only. This first changes the phase of the working fluid into liquid and then evaporates it. This vapour then travels and condenses in the adiabatic section where the temperature gets raised. This cycle gets repeated until the condenser region is reached and the temperature gradient along the pipe is uniform and the start-up process is completed. If a large temperature gradient is seen during start-up the sonic limit is reached during frozen start-up.

The start-up of heat pipes which are classified as low temperature from frozen state has been investigated by some researchers but still not a great number. Certainly Faghri (1995) has provided a great deal of work and is one of the few who actually provide some advice on how to investigate the start-up of a heat pipe prior to conducting experiments. He proposes a frozen start-up limit (FSL):

$$\text{FSL} = \frac{\varepsilon_1 \rho_l A'_w h_{fg}}{C^*(T_{\text{mel}} - T_\infty)} \geq 1 \text{ (Eq. 2.1)}$$

This equation requires the porosity of the wick, the density of the working fluid, the area of the wick, which is covered by the working fluid, the latent heat of evaporation of the working fluid, the heat capacity per unit length, the melting temperature and the initial ambient temperature. If this condition is fulfilled, the heat pipe should start up successfully. But if this limit is seen, then more working fluid is evaporated than can be returned by the wick structure. A possible reason for that is that the working fluid is totally frozen in the adiabatic and condenser section whilst the evaporator is overheating due to the lack of working fluid and actually drying out.

A very interesting phenomenon is described by Vukovic and Watkins (1999), where heat pipes under operational conditions were freeze thaw cycled. In order to simulate conditions as to be seen, by for example telecommunication base stations, which can have a heat pipe based cooling solution, fully thermally loaded finned assemblies were used. It was seen that the working fluid can freeze and the heat pipe will cease operation. Then a large temperature gradient occurs which will overheat the components attached. That phenomenon is called suction- freezing and was envisaged by other researchers like Cheung (2004) as well. In order to overcome the phenomenon of suction freezing, he proposed the usage of electrical heaters to keep the condenser section above the freezing point of the working fluid.

Some researchers like Tournier and El-Genk (1996) describe the frozen start-up of liquid metal heat pipes. The temperature range they claim the frozen start-up is happening is at 290K, which is equal to around 17°C. The working

fluid is a solid state at that temperature and it is at solid state as well when it gets filled into the heat pipe prior to charging/ venting of the heat pipe. Therefore it can not really be compared with the frozen start-up of low temperature heat pipes, for example with water as working fluid, where the working fluid has changed phase from its initial liquid state to a solid frozen state due to the reduction in ambient temperature.

2.3 MATHEMATICAL MODELLING OF HEAT PIPES

Heat Pipe modelling in CFD can be undertaken to different degrees. But so far, the two phase models are not seen accurate enough to be considered for industrial applications. Further the computational power requirements will increase dramatically when the two-phase simulations are used in general.

2.3.1 General Approaches To Heat Pipe Performance Modelling

Heat pipe performance can be simulated with a multitude of options.

First, the type of model has to be determined, this could either be a steady state model which requires fairly little computational efforts, to the more complex and less accurate transient start-up models. Generally Models can range from 1D and 2D to the most complex 3D models. Sections about different modelling approaches can be found in two of the three main books on the topic of heat pipes.

Peterson (1994) dedicated an entire chapter in his book to the performance modelling of heat pipes, for both, steady state conditions and transient

conditions. For steady state conditions he promotes two different approaches, one is for the heat pipe performance limits depending on temperature whilst the other is based on the heat pipe thermal resistance. The performance limit approach means that each performance limit will be calculated separately starting with the capillary limit. Once the capillary limit is determined iteratively as a function of the operating temperature, the other limits like viscous, sonic, entrainment and boiling limitations have to be calculated. These are dependent on operating temperatures as well. Once all limitations are calculated, the heat pipe performance map can be drawn and the maximum power handling capability at a certain orientation and operating temperature can be found. The second approach, through a heat pipes thermal resistance, is a network approach, where various resistances around the heat pipe are determined in order to be able to calculate the overall temperature gradient between heat source and heat sink. Therefore the various separate resistances, like radial resistance of the pipe wall at the evaporator; resistance of the liquid-wick at the evaporator etc. will be determined alone. There are nine resistances in total for the heat pipe itself plus possibly more when a thermal system with evaporator plate and condenser attached to a heat pipe are to be considered. These resistances can be found in figure 2.6 below.

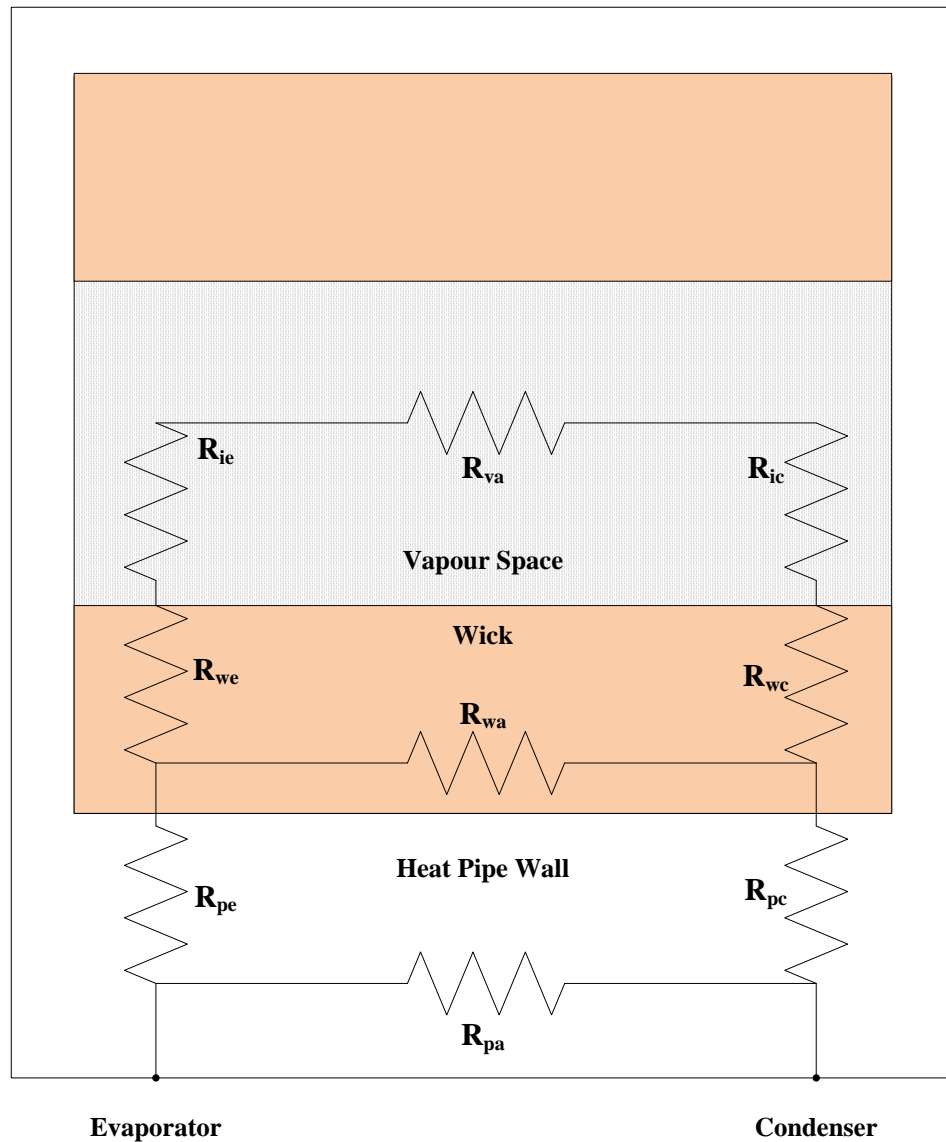


Figure 2.10: Heat Pipe Resistance Model (Peterson, 1994, p.147)

Nine Resistances as per Figure 2.6 above:

1. $R_{p,e}$: Radial resistance of the pipe wall at the evaporator
2. $R_{v,e}$: Resistance of the liquid-wick combination at the evaporator
3. $R_{i,e}$: Resistance of the liquid-vapour interface at the evaporator
4. $R_{v,a}$: Resistance of the adiabatic vapour section
5. $R_{p,a}$: Axial Resistance of the heat pipe wall

6. $R_{w,a}$: Axial Resistance of the liquid- wick combination
7. $R_{i,c}$: Resistance of the liquid-vapour interface at the condenser
8. $R_{v,c}$: Resistance of the liquid-wick combination at the condenser
9. $R_{p,c}$: Radial resistance of the pipe wall at the condenser

Once these are all obtained, they will be summed up and give the total temperature gradient between heat source and heat sink. This has to be seen in conjunction with the performance map of a heat pipe in order to find its suitability for a certain application. The thermal resistance network approach is applied mostly when heat pipes are used for cooling electronic components. Transient modelling is only touched very briefly in his book and it is mentioned that heat pipes can be modelled using a lumped capacitance method when analysing an entire thermal system. Further, particular interest needs to be paid to the situation when the heat pipe and system are subjected to freeze thaw etc.

Faghri (1995) presents the most comprehensive analysis on modelling of heat pipes. He has dedicated two separate chapters in his book, one very long one to steady state condition modelling of various orders and a slightly shorter one on transient conditions including the transient start- up from frozen state. Further special modelling attempts for non standard heat pipes can be found in the relevant chapters dealing with each type. Since transient start-up is not the focus point of this investigation and the frozen start-up is described at an earlier stage in this review, the main described focus here will be on steady state modelling. The modelling effort for steady state is based around the attempt to determine the maximum heat capacity transmittable through a heat pipe. In order to be able to do so, it is necessary to know the heat pipe's liquid

and vapour pressure losses in each separate segment. Within the heat pipe the thermal fluid phenomena occurring can be divided into three different categories, which are the vapour flow in the core region, the liquid flow in the wick and the interaction between the liquid and vapour flows. Faghri (1995) further states that most research of analytical and numerical nature has been conducted around the vapour core because the liquid flow is hard to describe with an exact theoretical model due to the presence of different wick structures. The attraction to work on the vapour core can be seen because of the differences in geometry and boundary conditions for each different type of non conventional heat pipes whilst the phenomena related to the liquid return in the wick and the boundary conditions at the liquid vapour interface are seen to be similar. In order to be able to predict effects related to the wick structure and the interface between liquid and vapour in a heat pipe accurately, both need to be based on some empirical data obtained through experimentation.

Zhu and Vafai (1999) present a two dimensional analytical model for low temperature cylindrical heat pipes. Their solution method contains a closed form solution which incorporates liquid and vapour interfacial hydrodynamic coupling and non Darcian transport through the porous wick. Further their model allowed them to predict the pressure distributions, vapour and liquid velocities as well as steady state wall and vapour temperatures that could be obtained for given heat input in the evaporator region and a known convective boundary condition in the condenser region. Reviewing work of other researchers, Zhu and Vafai (1999) found that most numerical models dealing with overall heat pipe operation, when they are dealing with both, liquid and vapour flow, made the coupling of the liquid and vapour interface through

applying either the Laplace- Young equation or the momentum jump condition. Both neglect interfacial drag caused by velocity and shear stress at the liquid-vapour interface and assume a non-slip condition. This was the starting point for their mathematical modelling and they developed their model as seen in Figure 2.3 below based on the following assumptions for the functional principle of a heat pipe: The heat entering the heat pipe in the evaporator section causes vaporisation and therefore subsequent pressurization of the working fluid. This makes the vapour flow to the condenser section and causes the vapour to condense. During the condensation the latent heat is released. In their analysis, the flow regimes for liquid and vapour were considered to be steady, incompressible and laminar. For the wick, isotropic behaviour was assumed as well as full saturation of the cavities with working fluid. Both phases in the model, liquid and vapour, are coupled with each other at the liquid-vapour interface. The rates of vapour injection and suction are assumed to be uniform at the liquid-vapour interface.

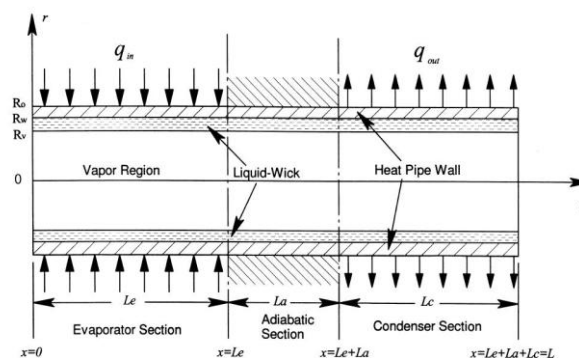


Fig. 1. Schematic of the heat pipe and the coordinate system used in the analysis.

Figure 2.11: Analytical model of Zhu and Vafai (1999)

They see their work as the first comprehensive closed solution, which provides information about the vapour and liquid flow as well as operating temperatures and maximum heat removal rate.

Generally they found good agreement between their analytical model and numerical as well as experimental results. Therefore they see their closed form analytical solution as a quick and accurate prediction method for low temperature operation. Further they found that the interfacial effects on the boundary between the liquid and vapour phase are very small and can therefore be neglected.

Zuo and Faghri (1998) present a thermal network model which was aimed to be a simplified engineering model of the heat pipe and therefore reduce the required computing resources. In order to be able to do so, the thermodynamic cycle approach was used to analyse the working fluid and its circulation within the heat pipe. This model was extended to transient heat pipe analysis and within the network there were various components with different thermal resistances and dynamic responses as to be seen in Figure 2.4 below. These were represented in a simplified form through first order, linear, ordinary differential equations.

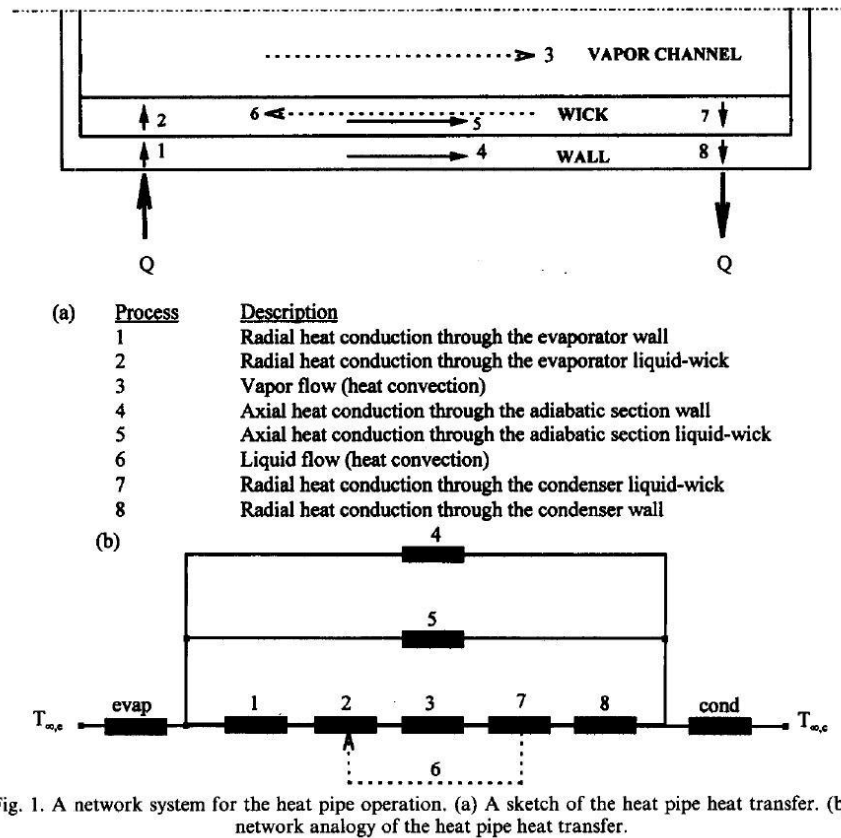


Figure 2.12: Network model of Zuo and Faghri (1998)

In order to be able to compare the accuracy with experimental data present, they used a screen mesh heat pipe with two layers of 150 mesh wick and an outside diameter of 19.1mm. They started their experiments when the heat pipe was at equilibrium with the ambient. Then they applied uniform heat fluxes to the evaporator side and convective cooling to the condenser side. Doing so, they found that their model slightly over-predicted the vapour temperature in a heat pipe, especially during the early transient stages. They explained these over-predictions through the lack of heat losses to the ambient in their model and also that the model does not consider any heat capacities such as insulation layers and cooling water jackets. This has produced slightly faster heat pipe transients than measured but the overall the largest deviation between measurements and prediction was not bigger than 5%.

2.3.2 Heat Pipe Modelling Using Commercial CFD Codes

One approach on how to model a heat pipe was undertaken by C&R Technologies (2008), where a 1D heat pipe model consisting of different wall and vapour nodes is proposed. This model is implemented into their software SINDA/ FLUINT and a scheme of their model can be found in Figure 2.5 below.

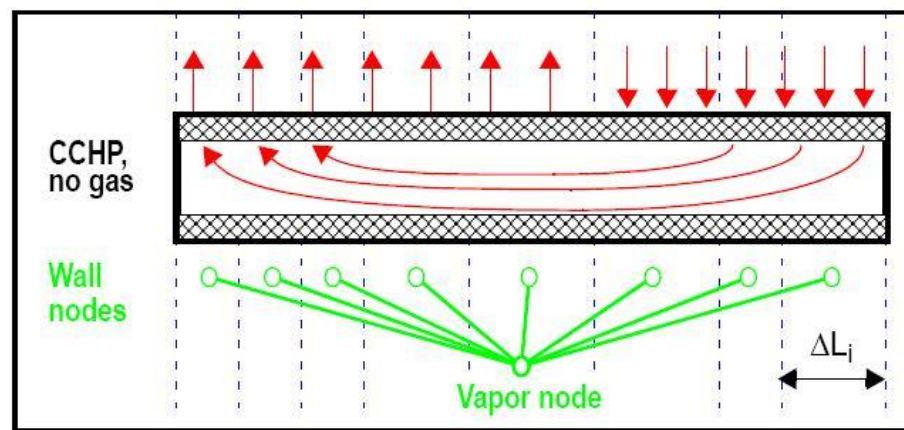


Figure 2.13: Schematic of the SINDA/FLUINT node model (C&R Technologies, 2008)

The key components of their model can be seen as the vapour nodes to which the wall nodes are attached via linear conductance and resistances. The vapour nodes represent the saturation conditions in the heat pipe whilst the wall nodes represent the wall, wick and liquid vapour interface. In some cases the wick and the wall can be neglected for the “wall” nodes. But their model requires some data input from the heat pipe vendor like the power length coefficient at a certain temperature and tilt angle. This means that the maximum heat pipe performance is not totally determined using their method as the method is not entirely empirical.

However, the more conventional approach of modelling heat pipes, which was advised not to be used for heat pipe modelling, can still be valid and worth

using for many applications where complex two phase solutions are not required. But there are tight restraints and more input parameters required than just to undertake a general approach. It has to be ensured that the heat pipes used for the applications are actually meeting the assumptions made during the modelling of the thermal system such as that they can handle the power subjected to in the application. This is only possible for heat pipe manufacturers or when the actual performance limitations of the heat pipes used are very well known. In these cases it is possible to use a high thermal conductivity for a heat pipe but this requires that each heat pipe is meeting the assumed thermal conductivity i.e. is 100% tested to a certain limit prior to being used for any products. This measured temperature gradient along the pipe/ heat pipe ΔT limit can then be used to calculate the overall heat pipe thermal conductivity for that orientation and this can be used as a single high conductivity cylinder in a CFD model. This method is only valid if the heat pipes are tested in the same orientation as they will be used in the final application, otherwise the model might represent either a too high or too low thermal conductivity. All other interfaces around the cylinder need to be modelled as they are in the real application. A weak point of this method is that for any heat pipes performing better than the heat pipe performance limit, the advantage will not be represented by the CFD model. In reality, if the maximum allowable ΔT limit for a heat pipes is used for the calculation of the thermal conductivity, the vast majority of all heat pipes produced may exceed the performance assumed in the CFD model, depending on the process capabilities of the heat pipe manufacturer.

2.3.3 Modelling Of Multiphase Flow Using Commercial CFD

Codes

A comparison of different two phase models is provided by Banjeree et al. (2002). But, generally they state that the modelling of two phase problems with fluids comprising water or gasoline, as in their case for a fuel tank filler pipe as the liquid phase and air vapour for the gas phase, poses several challenges for the CFD engineer. The models available for the governing equations contain the volume-of-fluid (VOF) model, the cavitation model and the algebraic slip model. All three models are available in Fluent, the CFD software used for their analysis for multiphase simulations. Further they state that the choice of a certain model is dependent on several factors but also often guided by experience of the particular CFD engineer. For their study the VOF model was chosen for the presented simulations and this model is designed for tracking the interface between the immiscible fluids. In the model, a single set of momentum equations is shared by the fluids and the volume fraction of each fluid in each computational cell in the domain is tracked during the solution. Apart from the direct choice of the two phase model, they put further emphasis onto the correct choice of the turbulent model used for the simulation. Within Fluent, they described four different models to be available. These models are the standard $k-\epsilon$ model; its variant the RNG (renormalisation group) $k-\epsilon$ model; the Reynolds stress model (RSM) and the large eddy simulation (LES) model. Each model has its own advantages. The $k-\epsilon$ model is described as the most widely used model, whilst the RNG $k-\epsilon$ model has an improved accuracy for rapidly strained flows and

seems to be better for predicting flows with swirl. The RSM model solves individually all the terms of the Reynolds stress tensor, but the additional required computational time could not be justified since the differences between the RNG k- ϵ model and the RSM models were less than 5% for the two direct comparison cases. The LES model was not supported in Fluent for the multi phase option and could therefore not been investigated.

Sussman, Smereka and Osher (1994) worked on a level set approach for incompressible two-phase flow. They have considered the interface between the two fluids as sharp and described it as the zero level set of a smooth function. The medium they used was water and air for their simulation where water is not treated as a perfect gas. Even though they are not treating water as a perfect gas, they solve the equations for both, water and air as perfect gas, and found that that approximation has proved to be very good for cases where the fluid velocities are much smaller than the speed of sound in that medium. Finally they propose the use of a second order accurate algorithm for tracking the interface of two incompressible fluids, where the interface remains sharp due to the high density ratio of the two fluids of 1000.

Lun, Calay and Holdo (1996) have presented a fairly general approach to two-phase modelling in CFD. They state that two phase flows can be found in a wide range of industrial applications and natural situations.

As a general description, two phase flow is seen as the interacting flow of two phases where the interface between the phases is influenced by their motion. The complexity of these flows made experimental and analytical investigations the only options. Only recently, with the broader availability of computational resources of sufficient speed, has computational analysis been

made an attractive alternative to the building of large scale prototypes and expensive test rigs. When using CFD, the quality of mesh is important for the modelling of two- phase flow in horizontal pipelines which means that additional computing power is required. But even with sufficient computational power available, the accuracy of the simulations may vary dramatically, depending on the modelling input parameters like grid or mesh density for the numerical solution method. If these parameters are chosen incorrectly, this might help to solve the solution in a smooth way but guide to physically inaccurate results. During previous experimentations it was found that two-phase flow can take many different forms at the interface between the two phases. Especially in horizontal and inclined pipes, where gravity causes an asymmetric distribution of the phases, the flow patterns get more complex. Figure 2.6 below describes several different flow patterns which can occur in pipes. Particular interest has to be paid to flow pattern f) which is very similar to the flow pattern in a thermosyphon or heat pipe.

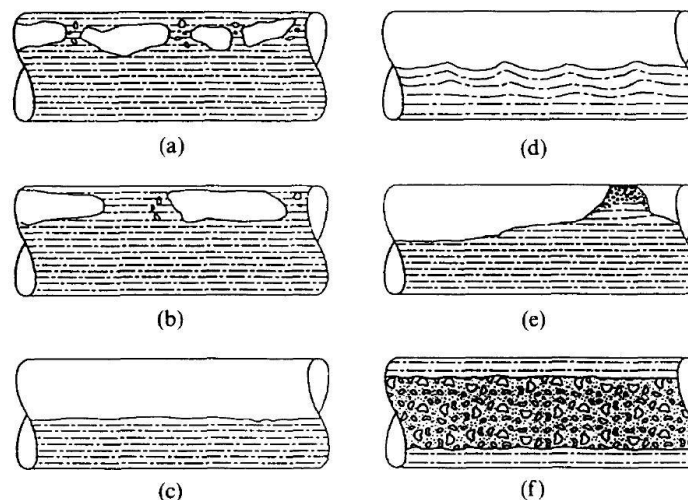


Fig. 1. Classification of flow patterns: (a) bubble flow — at high liquid velocity bubbles tend to flow in the upper part of the pipe; (b) plug flow — asymmetric nose bullet shaped bubbles occur; (c) stratified flow — liquid flows along the bottom of the pipe and the gas along the top; (d) wavy flow — at increased gas velocity, stratified layers turn into waves; (e) slug flow — further increase in gas velocity causes waves to touch the top of the pipe and liquid is carried by the gas; (f) annular flow — at very high gas flow rate the slug becomes penetrated with a gas core and the flow becomes annular.

Figure 2.14: Schematic of different Two-Phase patterns (Lun, Calay & Holdo, 1996)

2.3.4 Numerical Investigation Of The Effects Of Bends And Shape-Changes In Related Areas

The effects of bends are not only to be considered when investigating the effects of bends within heat pipes but there are many other areas where bends can influence the flow characteristics of fluids. These fluids can either be liquids or gases or even a combination of both so the flow is two phase as in a heat pipe. In the following pages a brief overview will be given about literature found on these investigations.

Supa-Amornkul, Steward and Lister (2005) present a comparison between simulations and experimental results of a water- air mixture. Their study was started when corrosion was found in feeder pipes of reactors which were filled with an air water mixture of a temperature below 55°C. As their research sample, a 73° bend in a 5.9cm diameter pipe filled with water in a turbulent flow regime was investigated. Later this was expanded to two phase flow with air voids between 5 and 50%. For the single phase flow it was found that Fluent, the CFD software used, was able to predict the single phase flow and pressure drop accurately. Later the two phase model was used. This model solves both sets of transport equations, for the liquid phase and the vapour phase, separately and both phases are treated as homogenous. Once these equations were solved, they were coupled through pressure and interface exchange coefficients. It was found that this CFD model predicts the pressure drop less accurate than the single phase model and requires further development work to raise accuracy. The higher rate of voidage in the two phase flow combined with curved pipe geometry will guide towards an

inhomogeneous phase distribution, flow reversal, flooding and secondary flow. Further it was stated the evolution of bubbles in two phase flow is not considered in the CFD model which might be the case of finding less accuracy in the pressure drop and flow results.

Banerjee et al. (2002) investigated the two phase flow in an automotive fuel tank filler pipe numerically as well as experimentally. For their experiments they used an air water mixture running through a glass pipe of the shape of the filler tube investigated. This setup allowed them to visualize the problems occurring within the flow and especially after bends. One thing noticed was that they are amongst very few who are actually presenting results for three-dimensional bends. Most people concentrate on just two-dimensional bends which are following the axis of the co-ordinate system, this means that the pipe is either horizontally or vertically orientated. Generally they found a good correlation between their simulations and their experiments. Even so, the design rules for fuel filler pipes state that the radii of curvature should be large for bends to minimise the flow losses in them, they found that swirl occurred. This was found in both the simulations as well as the experiments. In the simulations section it was stated that due to the swirl being introduced in out-of-plane bends, the misalignment of the flow along the grid can increase numerical diffusion. During their experiments it was found that swirls introduced in one bend can be enhanced after another later bend, but this is depending on the flow rate as well. It was found swirls can be so strong that they enhance air entrainment which is often referred to as dynamic seal.

Spedding and Benard (2007) investigated the two phase air-water flow through a vertical to horizontal 90° bend with an inner diameter of 26mm, and

also review work of others on the topic of single and two phase flow and pressure drop predictions in pipe bends. Generally they found that the calculation of the pressure drop in elbows with two phase flow is more complicated than within single phase flow. Unlike single phase flow the orientation of the bend plane plays a role, and the method of calculating the straight pipes frictional losses can not be used. It was found that the two phase bend pressure drop is independent of the pipe diameter itself but highly dependent on the ratio between the bend radius and the pipe diameter. This is similar to what can be found for single phase flow. For some flow regimes they found that the inflow can even be partially choked by the elbow and this leads towards a build up of pressure and liquid in the vertical riser, but this can be seen unique to the orientation of their experimental setup.

Harris and Goldschmidt (1999) have investigated the external heat transfer coefficient in 180° U-shaped bends. They have investigated a geometry which is commonly found in tubular or serpentine heat exchangers and their investigated tube diameter ranges from 12.5 to 44.5 mm. All their experiments were carried out in the horizontal plane, which means that the air flow on the outside of the tube is running parallel to the bend plane. It was found that the Nusselt number for the u-bend was about four times higher than for straight pipes of identical diameter and that the external heat transfer coefficient for bent pipes was considerably increased. Further a strong dependence of the performance enhancement on the curvature ratio was discovered and the optimum value for this relation was found to be 0.23. This means that their ideal bend radius is about 4.3 times the pipe radius.

Barletta and Rossi di Schio (2001) have investigated stadium shaped ducts as applied for liquid-gas heat exchangers. This shape can be found in flattened heat pipes as well. The authors of that study state that some authors reporting on similar cases have found conditions in non- circular cross sections of either elliptical or stadium shape, where the losses in the flow on the gas side are reduced whilst the heat exchanging surface on the gas side is increased. The flow regime they investigated was always laminar and they investigated three different wall boundary conditions, uniform wall temperature distribution, axially uniform wall heat flux distribution with peripherally uniform wall temperature distribution and finally axially and peripherally uniform wall heat flux distribution. These cases were investigated with FlexPDE and PDEase 2D, two different software types used to solve partial differential equations. With all software versions, it was found that for any given value of β , which is the ratio between the heights of the duct to the widths of the duct, a stadium shape gives an increased Nusselt number in comparison to a normal round shape.

Ismail and Zanardi (1996) developed a general analytical numerical heat pipe model which could be used with two different co-ordinate systems and cater for both, circular shapes and rectangular shapes of heat pipe container cross sections. That model is based on two dimensional equations and would still not be suitable for being modified for the investigation of bends. But the approach of postulating certain assumptions prior to the setup of the model has been used for CFD models described in later sections of this work.

2.4 EXPERIMENTAL TECHNIQUES WITH FOCUS ON HEAT PIPES

While reviewing the literature it was found that most heat pipe test rigs are more or less of the same design and are only modified and improved in different areas. These improvements are mostly the areas where people want to carry out their particular research, but the overall layout does only deviate slightly and was therefore seen applicable for the practical studies at a later part of the PhD. Following the sub- topics this will be reviewed in greater detail.

2.4.1 Test Rig Design

Test rigs can be seen as consisting of two different large component groups, the test rig itself and the instrumentation. Both groups could become the main focus of the experiment but generally the test rig itself is the main focus. For heat pipe testing the test rig consists of a heater attached to the heat pipe and a condenser. The condenser can either be natural convection through fins or forced convection through fins with forced airflow or liquid cold plates. With liquid cold plates it is fairly easy to determine the experimental error through the flow rate, electrical power supplied and the temperature difference between the inlet and outlet water temperature. Therefore, as it can be seen from the following referenced books and papers, this seem to have become the most favoured option amongst heat pipe researchers.

Starting with the evaporator side, Faghri (1995) provides with Figure 2.7 a very comprehensive guide about different heater block designs. According to him, there are six different types: a) A heater wire which needs to be cemented in place after being wrapped around the pipe; b) heater tape or c) a heater rod, which are as well wrapped around the pipe. Some more flexibility in terms of Watt density is offered by d) the flexible etched foil heater. Cartridge heaters, as proposed in e) require mechanical attachment in terms of heater blocks, but, can provide through their multiplication quite a high heat load. Only where very high heat fluxes are required, the usage of Eddy current heaters (f) is promoted as they are very cost intensive.

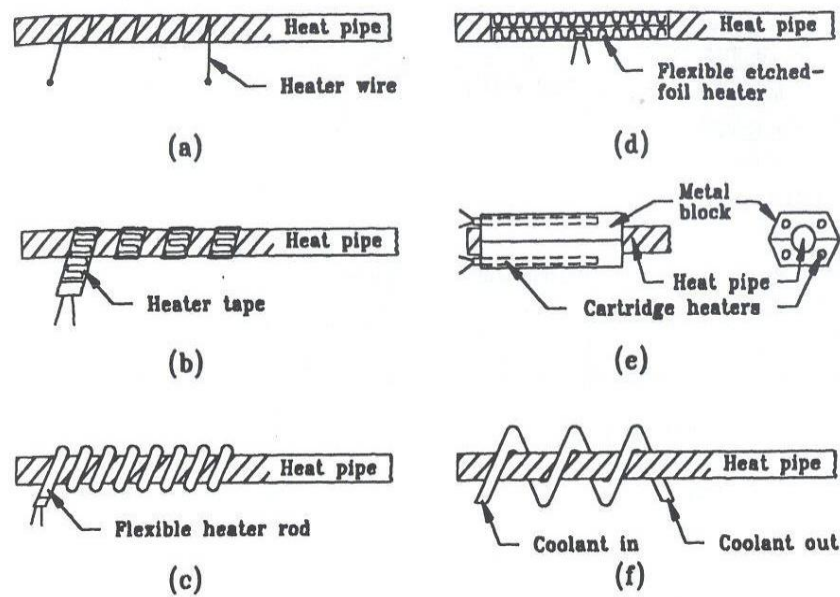


Figure 14.5: Heat input methods: (a) Heater wire; (b) Heater tape; (c) Heater rod; (d) Flexible etched-foil heater; (e) Heater block with cartridge heaters; (f) Eddy-current heating (RF).

Figure 2.15: Schematic of different heat input methods (Faghri, 1995)

For the condenser side, Faghri (1995) provides six different types as well which are: Open bath (a); direct fluid contact (b); tube calorimeter (c); fins, either forced or natural convection (d); spray evaporative cooling (e), which is

very advanced and not easy to realise for a simple and quick test setup and finally a gas gap calorimeter as used for high temperature heat pipes.

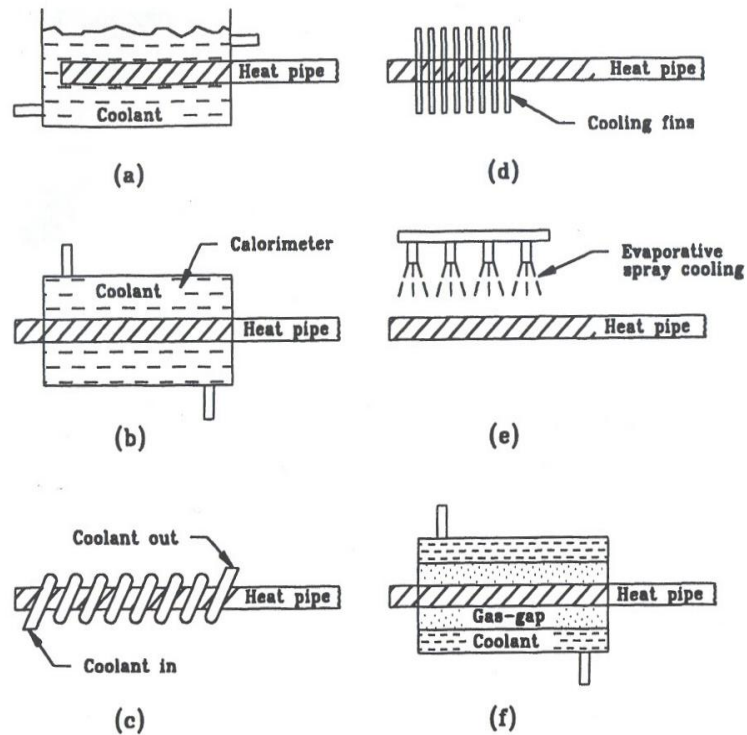


Figure 14.6: Heat output methods: (a) Open bath; (b) Direct fluid contact calorimeter; (c) Tube calorimeter; (d) Fins; (e) Evaporative spray cooling; (f) Gas-gap calorimeter (high-temperature heat pipes).

Figure 2.16: Schematic of different heat output methods (Faghri, 1995)

Reay and Kew (2006) shows in their book as seen in Figure 2.9 a typical brief test setup with very minor experimentation but the main principles including thermocouple positions can be seen.

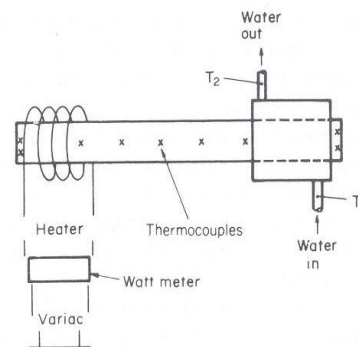


Fig. 5.22 Heat pipe performance test rig.

Figure 2.17: Brief schematic of a typical Test Rig (Reay & Kew, 2006)

Figure 2.10 below shows the test setup as used by Kempers, Ewing and Ching (2006). As a unique point the full instrumentation set is shown as well in great detail. This includes the water loop with flow meter, chiller and temperature measuring and logging equipment in that loop. Further the separate temperature measurement and logging equipment for the pipe temperature itself are shown and finally the heater circuit including the power measurement equipment.

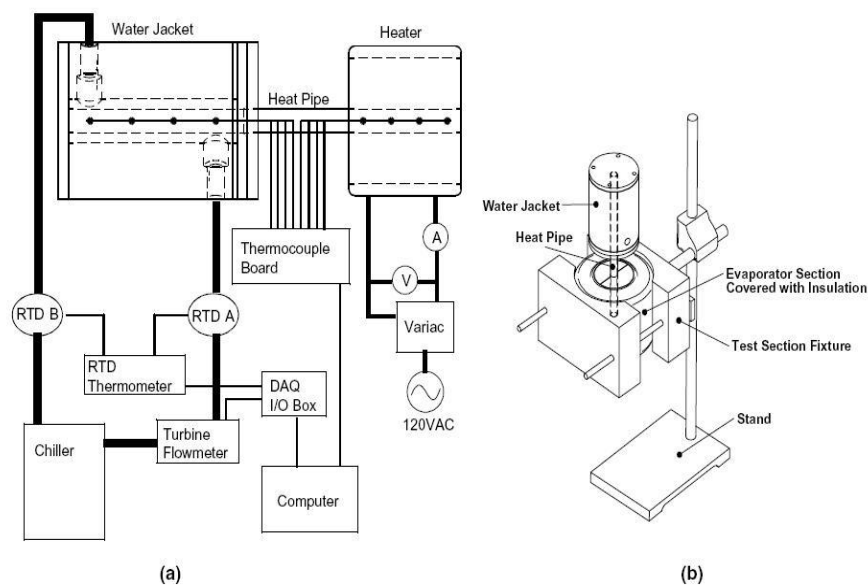


Fig. 1. Heat pipe test facility: (a) schematic of facility layout and (b) schematic of heat pipe fixture.

Figure 2.18: Schematic of the test rig used by Kempers, Ewing and Ching (2006)

Below in Figure 2.11 a very similar setup used by Maziuk et al. (2001) can be found. Apart from the similar instrumentation used and a similar heater and condenser setup, a unique point found on that rig is a platform which allows the testing of heat pipes under a changed orientation. This platform is indicated in Figure 2.11 No. 3 and this allows the rotation of the test rig by full 180°. Both vertical orientations, evaporator above condenser and condenser above evaporator can be tested.

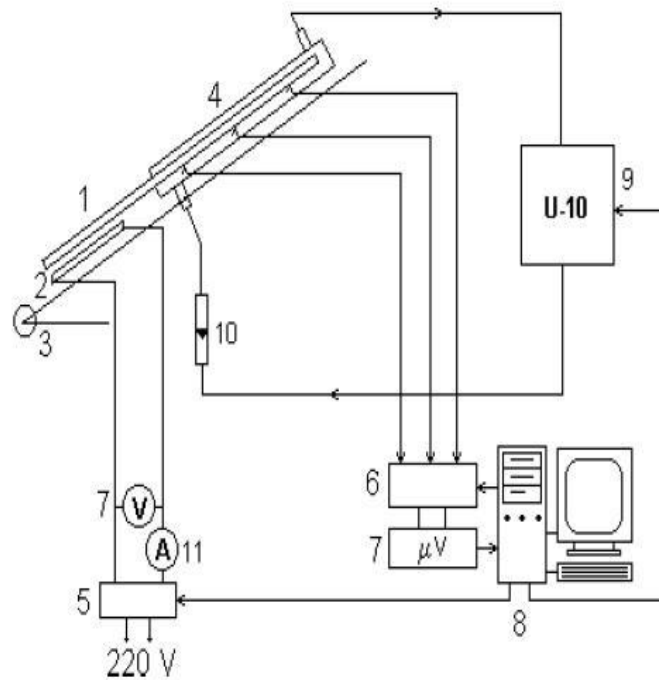


Figure 2.19: Schematic of the Test Rig used by Maziuk et al. (2001)

A particular focus on the test rig's main or core part is shown in Figure 2.12 below. This setup was used by Murer et al. (2005) and shows in a very detailed way even the smallest components like thermal interface materials and the exact locations of thermocouples. Unique is the usage of adaptor blocks, highlighted in Copper colour on the heater and condenser side, which allow the attachment of different shapes and diameters to the existing heater and cold plates. This allows the testing of the three different diameters of the round miniature heat pipes (2, 3 and 4mm) as well as the use of a flat shape miniature heat pipe with a greater width. Therefore this rig design will not be the most responsive one but offers a great amount of flexibility.

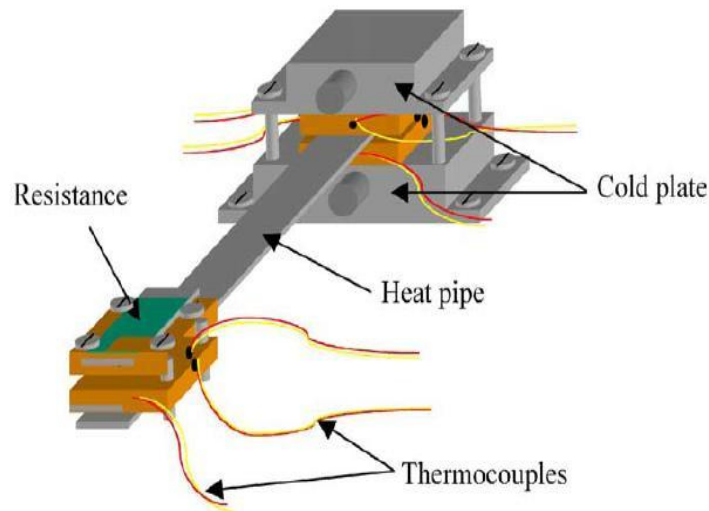


Fig. 2. Experimental setup.

Figure 2.20: Schematic of the Test Rig used by Murer et al. (2005)

Most of the experimental results and test rig designs described above were used for steady state experimentation. Legierski, Wiecek and de Mey (2006) present an approach using two controlled temperature water baths to investigate the transient characteristics of heat pipe. This is a rather unusual approach but seems reasonable to be able to determine the heat pipes effective thermal conductivity during start-up of the heat pipe.

2.4.2 Temperature Measurement Techniques

There are three main temperature measurement techniques used generally for obtaining temperatures in the normal range. First there are wire thermocouples of different types, and suitable for different temperature ranges, and secondly there are RTD's, which are resistance thermal detectors and provide greater accuracy than normal wire thermocouples. The last group is infrared thermography, which is a very powerful tool to visualize heat transfer, especially for natural convection assemblies like finned heat pipes.

Faghri (1995) presents advice on how to measure heat pipe wall temperatures and what will have to be considered when attaching a thermocouple to a surface. The chosen thermocouple diameter should not be too large so that the thermocouple is acting as a heat sink itself and good contact to the measured surface is mandatory. Further, if the thermocouples are permanently attached through epoxy or a strap, mechanical or thermally resistant tape like Kapton, calibration is required prior to attachment to the heat pipe. Only when the thermocouple is welded to the heat pipes, is calibration not required, as the weld changes the bead resistance.

2.4.3 Previous Experimental Work On The Subject Of Bending

During the search of the literature, hardly any information and references on bending of heat pipes was found. Any information found was contradictory. First there is information found on a heat pipe producer's website. Noren Inc. (2008) claims that bending does not have any effects on the heat pipe performance if it is done with quite elaborate factory tooling, and that even the shape of the bends and the amount of them will not change that fact. But here they lack to prove that statement through test results. Cheung (2004) has found out that heat pipes can be bent moderately when required for the application. There, two 90° angle bends were introduced into the pipe and no degradation in performance or conductance was found. It was noticed that the bend radius was chosen in accordance with the industrial standard of three times the diameter and that the power of max. 1W was probably too low to realize any degradation in performance. Finally there was Quick Cool (2008)

in Germany who promoted that bends, even if carried out to a high standard with a required tool will cause degradation in performance of up to 30%. Further they recommend that the bend angle should not exceed 120° in total. Again, no test data is supplied to back up any of these statements even though they sound reasonable logical.

2.5 LATEST TECHNOLOGY DEVELOPMENTS IN THE HEAT PIPE AREA

Even within a well proven technology like a heat pipe there are still plenty of non investigated areas which would require further research. The motivation for doing this research might be very different, and recently with raising energy and material prices, a huge drive is on either energy conservation or renewable and alternative energy, in general, as well as minimising the usage of material. So, each unique application or market has their own needs to drive further research. In the following section a more detailed review of the driving forces will be provided.

Driving Forces For New Technology Developments On Heat Pipes

The particular driving forces on heat pipe development are highly dependent on the certain markets or areas where heat pipes are used. For example there is the energy conservation area where heat pipes are used to either conserve existing energy or transport waste process energy from the place where it is produced to a place where it can be re-used. This has become particularly

more attractive recently, when energy prices have risen quite dramatically. Work on that subject was presented very recently at various international conferences on the topic of heat pipes. One example to be mention in that area is the work presented by Pereira (2008) where the usage of heat pipes for industrial processes is suggested and particular interest was pointed towards the energy sector like oil and gas refineries.

Another sector to be mentioned is the one of renewable/ sustainable energy. Apart from the well known application for heat pipes as solar collectors, some new uses to reduce energy costs were proposed with emphasises on the reduced cost due to the heat pipe. Aleksandravicius (2008) proposed the usage of ground source heat pumps in order to reduce the total costs of energy for heating the house by 75% for the same period of time.

The consumer products market containing mobile computer devices currently drives the technological development for different reasons, but primarily to reduce cost. A further drive is to produce notebook and laptop products thinner and therefore reduce the height of the heat pipe solution. This has to be done in the existing low cost envelop and also not to compromise the thermal performance of the product. As stated by Mongia (2007), further factors like the skin temperature on the outside of the casing have to be considered as well and the thermal challenge of cooling the chips has to coincide with human comfort factors like a relatively low casing temperature.

The final market which is always driving heat pipe technology in terms of reducing weight whilst increasing the performance are military and space applications. That market is different from the others since the quality of the solution and the fact that it fulfils the requirements as perfectly as possible is

the priority whilst costs are only of secondary importance. Here the ambient conditions and tight weight constraints push the development of new lighter container materials, different heat pipe types which perform better than existing ones and working fluid which can meet contradicting ambient temperature ranges. The military market is less challenging than the space one but still a big enough driver to revise existing technologies and either improve them or come up with new uses for them.

2.6 SCOPE OF THE WORK OF THIS THESIS AND ITS NOVEL ASPECTS TO THE SCIENTIFIC COMMUNITY

The work presented in this PhD thesis was undertaken in order to investigate and tackle a multitude of issues. One issue was to reduce the process variation during the charging process in order to be able to investigate the effects of bends in heat pipes.

The main focus of the work presented in this thesis was initially focussed on the performance changes due to these bends but broadened to the manufacturing process very soon, due to the linkage between the phenomena of performance handling and production accuracy. Generally bends are application specific requirements and therefore worth investigating in order to gain a more in depth knowledge about them. So far, only a minor industrial reference was found (Quick Cool Heat Transfer GmbH, 2008), which states that heat pipe bending requires particular attention and that bending angles of more than 120° should not be realised. Further it was stated that even minor bends introduced into the heat pipe, even when done correctly, can influence

the performance of heat pipes of up to 30%. Apart from this single reference, no further ones have been found on the topic of bending and flattening of heat pipes.

In order to be able to investigate the effects of bends on heat pipe performance and minimise existing production variations, the fill and charging/ venting operations need to be optimised. Fill calculations for certain wick structures have only been described very briefly and require a more detailed investigation as the performance of a heat pipe can be highly influenced by the amount of working fluid present in the pipe as well as the degree of evacuation of air and non condensable gas. From previous experiments it became clear that the accuracy of fill and also quality of vent have a very big influence on the overall performance as well as the start-up performance of a heat pipe and therefore require a high degree of attention prior to investigation of any other phenomena on heat pipes. This was then taken as a starting point for the theoretical work and a more detailed insight of these areas is presented at a later stage together with the conclusions drawn from these investigations. Based on the theoretical value of the fill calculated, the experimental samples were then produced to the highest manufacturing standard possible and tested. These tests have proved to be successful and clear correlations in performance for different bending angles at a radius close to the tightest achievable one could be seen. Even so the fill used was contradicting that mentioned in well known literature (Faghri, 1995; Peterson, 1994 and Reay&Kew, 2006) about heat pipes. In general it was seen during heat pipe experiments that leaving the standard procedure and not adhering to common prediction not only helped to investigate the effects required but also very clearly showed that further

optimisation on performance can be achieved. In order to be able to improve the performance of a heat pipe, the direction of optimisation needs to be known. A heat pipe can be either optimised for performance or low thermal resistance and only very few heat pipes will fulfil both criteria at the same time. Different screen mesh wicks were investigated theoretically and experimentally and brought to a new non described use. This use is opposing that mentioned by Reay and Kew (2006) in their book about how to use coarse and fine wicks within the same heat pipe and new theoretical considerations are proposed for further considerations and investigation within the scientific community.

Carrying out additional work on freeze thaw phenomena of screen wick heat pipes have created an extra emphasis on the importance of having the correct amount of working fluid inside the heat pipe and to have a repeatable charging / venting process. Further it will be proven that there is a direct link between the amount of working fluid inside the heat pipe and its likelihood of being affected by freeze- thaw phenomena.

Despite the fact that all the work presented in this thesis was carried out on screen wick heat pipes, the importance of correct amounts of working fluids and the choice of a reliable venting method apply to any kind of heat pipe, not just screen mesh heat pipes and/ or heat pipes subjected to bending or flattening. For that reason the outcome of the work presented in this thesis is seen beneficial for a broad range of heat pipe applications.

2.7 AREAS OF FURTHER RESEARCH REQUIRED

There are still various areas related closely to the area investigated in this thesis where further research is required. One aspect would be on the development of new lighter materials which are not as widely used and therefore not subject to high world market fluctuations in price. Research in that area for example has been carried out by Rosenfeld (2006) at Thermacore Inc. on Magnesium heat pipes. There the compatibility of the container material with various wick structures and working fluids has been investigated. Further research in the area of materials for example is being conducted by Intel Inc, where aluminium as a container material is investigated. All research does not only contain the material to be used for the heat pipe (container) itself and their compatibility with wick structures and working fluid itself but also the related manufacturing processes. Each material has its own characteristics and therefore requires its specialised manufacturing processes in order to allow a successful break through into the mass market. But new materials research is not only limited to metals, alternative materials from the plastics sector and composites are investigated for the usage as container materials as well. Unfortunately, this research is at very early stages and therefore referenceable publications are rare.

Some new approaches to experimental techniques have been presented by Vasiliev Jr. et al. (2008). There, the entire test rig has been placed inside a vacuum chamber in order to have the heat losses towards the ambient kept to an absolute minimum. An advanced condenser design has been presented as well which could be used for R&D type experiments.

But even in the field of conventional heat pipes, further research is required. Currently there are various fields where big improvements can be made to the pipe performance and therefore would benefit the application industries. Areas of improvements would be calculations of fill/ fluid charge for various wick structures, investigations on bending of heat pipes and the effects on wick structures and container materials. This would help the application industries to minimise the usage of materials and improve on the design time as well as reduce the amount of practical experimentations required in order to provide an optimised product design. There is a high demand on that topic with raw material prices high at the present point of time.

Further work on optimising the wick structure has been presented as well by Vasiliev Jr. et al. (2008), where characteristics from very specialised high heat flux heat pipe wicks have tried to be mimicked in low cost parts by using a binding/ separating agent which evaporate during the sintering process and allows the production of grooves which will help to reduce the thermal resistance along the heat pipe. There is an opportunity to improve heat pipe performance and save mass on the wick but this technology needs further development in terms of manufacturability. Life tests also have to be conducted in order to determine whether the agent has any effects on the pipe in terms of contamination and the occurrence of NCG inside the pipe which could reduce performance.

CHAPTER 3 – INVESTIGATIONS OF HEAT PIPE FILLING AND VENTING TECHNIQUES

Within this chapter, theoretical investigations leading towards the finalized design of the tested heat pipes and the results thereof are presented in Chapter 5. This chapter contains three major sub-sections, the first section starts with some preliminary work carried out, which identifies areas of improvement within the manufacturing process for heat pipes and in particular the screen mesh heat pipe fill calculations. The second sub section continues work from the first sub-section by expanding it into a theoretical investigation of the possibility of using screen mesh heat pipes without gravitational support for the liquid return and the possibility of predicting the actual capillary or lifting height based on the screen mesh wick geometry. The third sub-section then focuses on venting techniques and the most common errors occurring during the venting process and was seen as essential for the production of high quality test samples used for the experimentation presented in the later chapters of this thesis.

3.1 INTRODUCTION

Despite their paramount influence on the performance of heat pipes, both fill calculations and venting techniques are rarely quantified in work investigating heat pipe performance. It seems that the heat pipes to be tested were introduced with no background information about the fill levels, unless the work was specific to the investigation of different fluid charges. Reviewing

existing literature about this topic, different techniques are used and information is very limited about how to determine the fill and statements are made that heat pipe manufacturers are spending considerable amounts of time on determining the fill for each wick structure (Peterson, 1994) but no more useful details appear to exist. Information on venting and subsequent failures during venting or information on process yield is even rarer than information on heat pipe fill.

Based on that lack of information about fills, addressing this issue was seen as very beneficiary for the experimental investigation presented at a later stage in this thesis. Therefore, some time was spent developing a numerical calculator rather than rely on empirically determined fill levels. There are two different ways of determining the optimum fluid charge for heat pipes, both of which are very similar and both require some experimentation at the end to prove the developed fill. The major difference between the two methods is the amount of experimentation required. The first method would be to produce large amounts of heat pipes, split them into equally sized batches and then fill and vent them with different amounts of working fluid. The amount of working fluid needs to be increased in equal small steps and then tested until the heat pipe batch with the lowest dT and most consistent performance for a certain power level is found. The second method would be a more analytical way where the porosity of the wick structure is determined analytically and then a fill calculated to saturate the openings in the wick plus the vapour space with vaporised working fluid. This will still require some experimentation running trials with 90%, 95%, 100%, 105% and 110% fill in order to avoid mathematical inaccuracies. The amount of experimentation in this method is

considerably less and the main advantage is that a change in wick structure can be catered for relatively easily, rather than having to start from a blank sheet every time again. In the next section of this chapter an approach to develop a calculator following the second approach for screen wick heat pipes will be described in greater detail and some reasons why the first approach is seen as inappropriate.

3.2 MESH HEAT PIPE FILL CALCULATIONS

Previous work carried out for the sponsoring company Thermacore Europe lead into this theoretical investigation. During this work it was determined that the different pipes of a single batch were exhibiting a lot of variation. Even testing of the same heat pipe showed differing performances after starting the test again with the same start conditions. This was due to different thermal contact areas in the collars of the rig and highlighted that further attention would be needed in order to investigate a single parameter, for example, the effects of bending of the heat pipes which is one subject of this PhD thesis. The uncovered facts were than the starting point of further investigations to resolve these matters.

An area where more attention was needed in order to determine accurate fluid charges was the fill of screen mesh heat pipes and manual filling process used at Thermacore Europe. The fill for screen mesh heat pipes was determined using tables produced some time ago within Thermacore Europe and has been used ever since. This method was seen as very inaccurate especially when the number of wraps of the internal wick structure and the mesh count of the wick

itself were changed. This guided to a different free volume available in the wick and was not taken into consideration within the previous fill calculations. The venting temperature, which has an influence on the amount of water required for saturation of the vapour space with working liquid, was also not taken into account. Based on these findings, every heat pipe length outside of the tabled ones and a different wire mesh wick count used as a wick structure in order to achieve a different performance was leading towards an even more inaccurate fill due to interpolation errors. Starting from these facts the tables (Thermacore, 2008) were analysed in order to gather information about the percentage of water applied to the available free volume in the wick. It was determined that there was no analysable trend after averaging out the percentage of overfill per pipe diameter and then showing the percentage of overfill over the pipe diameter. The results of this work are presented in Figure 3.1 below:

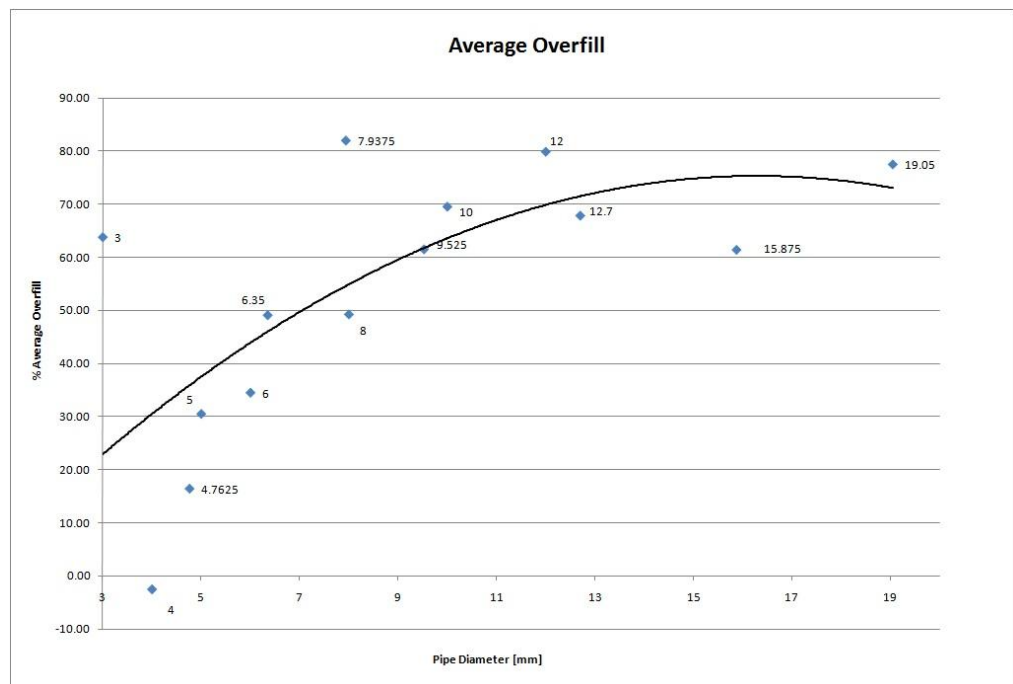


Figure 3.1: Average Percentage Overfill (Thermacore, 2008)

These results guided towards a much more theoretical analysis of the wick structure in terms of free volumes and ways to work out how much working liquid can be held by certain wick structures and how it was the appropriate way to calculate it. A review of literature shows that Reay and Kew (2006) recommend that further work needs to be undertaken in this particular area.

The approach of filling pipes with a certain fluid charge and calculate it as described by Reay and Kew (2006) comes with a major disadvantage as the performance is dependent upon the power level and can therefore not be seen appropriate for industrial heat pipe production. The major problem is that the heat pipe performance is dependent upon not only on the power level, but also on the orientation. Therefore the fill should enable a stable operating condition for the heat pipe in all operation conditions, rather than give a much more optimized performance in one orientation. Taking it further from this approach a fill saturating the wick was seen to be a good starting point. Due to the high inaccuracy within the overflow values as well as the manual venting process and due to the fact that heat pipes operate over a wide filling range, the saturation of the available cavities in the wick as well as creating saturated steam within the vapour space was seen sufficient. Additional water is not seen as beneficial from a thermal point of view as it could increase the temperature gradient along the heat pipe.

3.2.1 Weight Of Water Required For Generating Saturated Steam Within The Vapour Space

In order to be able to saturate the wick as well as the vapour space in a heat pipe, the venting temperature should be higher than the operational temperature. This is due to the fact that the amount of water which can be diluted as saturated steam into a certain amount of air is dependent upon temperature and can vary by quite a significant amount. Therefore at least saturation of wick, as well as having sufficient water molecules to generate saturated steam in the vapour space should be targeted at the maximum operational temperature and the amount of excess liquid should be kept as low as possible.

Figure 3.2 below shows the amount of water possible to be diluted as vapour in the gaseous phase in the heat pipe as a function of temperature and density g/m^3 (Wikipedia, 2008). The data on this graph is supported by a reference in a book which reports that the specific volume, is an inversion of the specific density for both phases, the liquid phase as well as the vapour phase (Lucas, 2000). In the reference table, which can be found in Appendix A-2, v' displays the specific volume for the liquid phase whilst v'' displays the specific volume for the vapour phase. Inverting the actual value from the table for a certain temperature will generate the amount of liquid substituted into the air at that temperature.

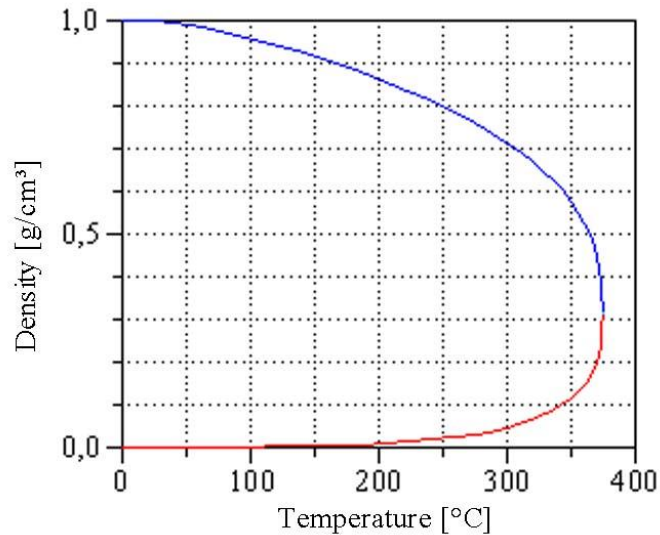


Figure 3.2: Steam (red) and Liquid (blue) Density vs. Temperature (Wikipedia, 2008)

On the graph the red line shows the density of the vapour phase, whilst the blue line shows the density for the liquid water at equilibrium conditions. Both lines merge at the critical temperature of 374.1°C. When closing in to the critical temperature the difference between both densities decreases to equilibrium at the critical temperature.

From this graph it can be clearly seen that the density of the vapour rises significantly above the 200°C mark. This coincides with the fact that the pressure due to the much higher saturation pressure within the heat pipe rises dramatically. Due to the limited mechanical strength of the pipe wall it was seen as appropriate from a Health and Safety point of view to limit the calculation software to a maximum temperature of 200°C. For heat transfer reason, the walls of the container of a heat pipe are designed to be as thin as possible and therefore have as low a thermal resistance as possible. During venting at a higher temperature, the pressure inside a pipe can overcome the structural strength and lead to a burst of the pipe wall. Therefore it was seen as appropriate together with other precautions during the venting process to keep

this risk low. Figure 3.3 below shows the pressure build up within a heat pipe demonstrating all the elements involved in the total pressure. A heat pipe during the venting process is a sealed container with air trapped inside it. This air is expanding at constant volume (isochoric), but there is also the water introduced which vaporises and can achieve a pressure up to the saturation pressure. Since heat pipe filling and charging is aimed at saturation of the wick and the vapour space, it has to be ensured that this state is reached. Both lines as well as the original ambient pressure are shown. It has to be mentioned that an extension of the temperature is guiding to a very high increase in the scale of the y-axis and pressures above 200bar can be reached at the temperature of 374.1°C.

Figure 3.3 below shows the saturation pressure for steam (P_{vapor}), the ambient pressure, the air pressure for isochoric expansion of trapped volumes (P_{air}) and then the total pressure, which is a superposition of the saturation and the isochoric expansion pressure and is represented through the purple line.

The isochoric expansion pressure is calculated using equation 3.1 below:

$$P_2 = P_{\text{ambient}} * \frac{T_2}{T_{\text{ambient}}} \text{ (Eq. 3.1)}$$

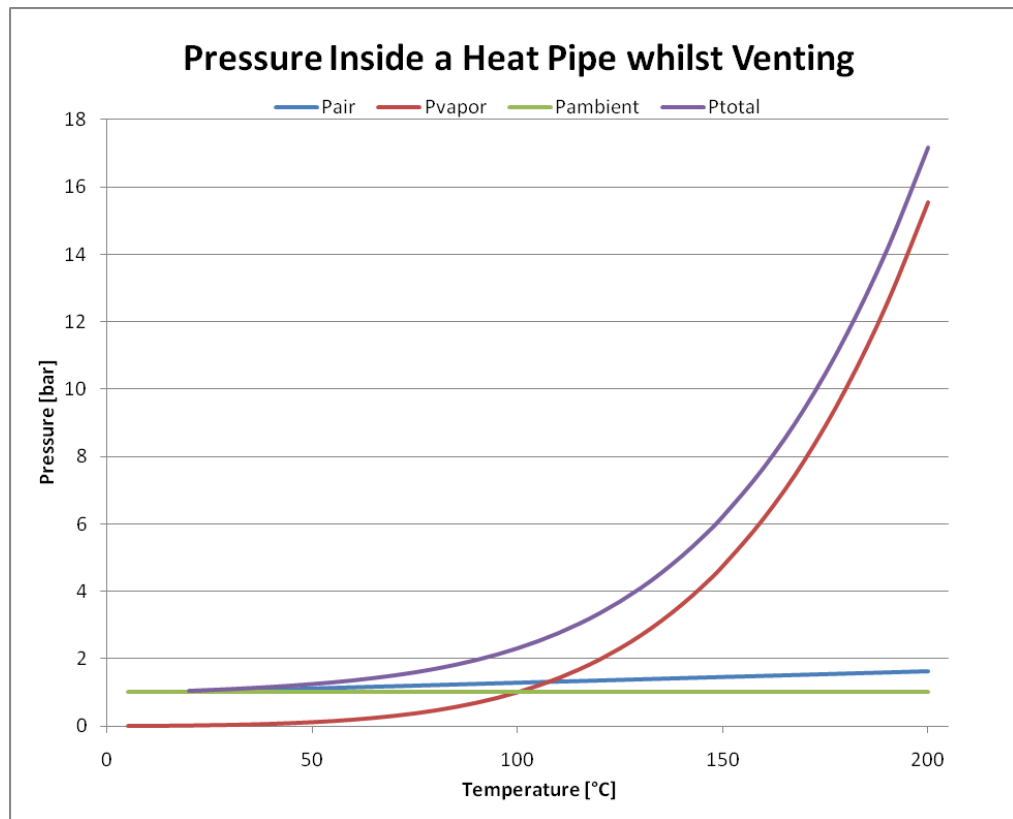


Figure 3.3: Pressure inside a heat pipe during venting

Once the results of the calculation of the amount of water molecules to saturate the vapour space have been achieved, the next step is to calculate the volume of water required to saturate the wick. Again this volume is temperature dependant and it has to be taken into consideration that the density of water at a temperature between 20 and 25°C when it is injected into the heat pipe is different from the one at venting temperature and has to be compensated for.

3.2.2 Mathematical Foundations Of The Porosity Calculation For Screen Meshes Used As Heat Pipe Wicks

The most critical part of the heat pipe fill calculation for a screen mesh wick heat pipe is the calculation of the screen porosity, as this represents the largest

proportion of the working fluid contained within the wick's cavities. Apart from the two experimental methods described by Kozai, Imura and Ikeda (1991) and Canti et al. (1998) the calculation of the screen porosity is the only other logical method to obtain porosity for a certain screen type.

Experimentally there are two methods which allow the evaluation of the screen in use. One is based on the void volume of the screen and the immersion of a certain amount of screen into a measurement cylinder filled with either water or ethyl alcohol. From the volume displaced by the immersion the volume of screen wires V_s can be determined. Subtracting this volume from 1 after divided it by the theoretical volume of a plate with the same thickness and size as the screen immersed gives the porosity (Kozai, Imura & Ikeda, 1991; Canti et al., 1998).

The second method is based on mass measurements of the mass of the screen wires on electronic scales. Therefore, a sample of a certain size will be applied to the scales and later divided by the volume of a plate of the same material at the same thickness than the screen multiplied by the density of that material. Subtracting that figure from 1 gives the porosity as well:

$$\varepsilon_i = 1 - \frac{V_s}{V} = 1 - \frac{M_s}{(\rho_s V)} \quad (\text{Eq. 3.2})$$

Both methods are well known but come with a number of disadvantages and therefore a third method is seen as more appropriate as it is entirely mathematical and delivers results within +- 3% from the other two. This is seen as sufficient when considering the process inaccuracies of the venting process. The major disadvantages of the two experimental methods are that they are based on readings obtained from manual instruments like micrometers or measuring microscopes which come with an error and

therefore that error carries through to the final calculation. Further inaccuracies can incur when the reading of the volume of the immersed screen is taken and the weight of the screen on the scales is obtained. This is due to inaccuracies of the human eye as well as the possibility that the scales are effected by a lack of level arrangements.

Further, whenever a new mesh type with different wire diameters or mesh numbers is used, new experiments have to be conducted, which is a lengthy and costly procedure. Therefore and with contemplation that all results for the porosity are within a 3% range of each other (Kozai, Imura & Ikeda, 1991) the numerical method described below is seen as the most appropriate.

For this method first a couple of parameters need to be obtained, generally from the source of the screen wick like the mesh supplier or distributor. These are the wire diameter as well as the mesh number, which could be calculated following a route described in the International Standard ISO 4783-2 (1989) but are generally available when screen mesh is purchased.

First the clearance c has to be calculated via the following formula (Eq. 3.3):

$$c = \delta_1 - 2 * d \text{ (Eq. 3.3)}$$

Considering that the total thickness of a wick layer is nominal $2.2 * d$ (Eq. 3.4) this works out to be $0.2 * d$.

$$\delta_1 = 2.2 * d \text{ (Eq. 3.4)}$$

Now the aperture (number of openings per unit length) of the screen wick is required. There are two possible methods, which will guide to the same results: First the mesh number (for example 150) is the number of openings per inch, so this one can be converted mathematically into openings per meter and gives the required aperture which is then used in a number of equations.

This, like the wire diameter, is a unique characteristic of the wick and available at the point of purchasing the wick. The second approach is described in ISO 4373-2 (1989) and shows how to experimentally/mathematically obtain this number (Eq. 3.5).

$$N = \frac{1}{w+d} \text{ (Eq. 3.5)}$$

For this calculation it was seen as more appropriate to use the mesh number and then convert it but both ways have been checked and the difference is negligible. Once this value is determined the warp and the shoot angles can be calculated following equations 3.6 and 3.7:

$$\phi_w = 2 * \tan^{-1} \left\{ \frac{d+c}{w+d} \right\} \text{ (Eq. 3.6)}$$

$$\phi_s = 2 * \tan^{-1} \left\{ \frac{d-c}{w+d} \right\} \text{ (Eq. 3.7)}$$

These two angles, which are received as a rad value are then implemented into the calculation for the radius of curvature for the warp and shoot wire (Eq. 3.8 and Eq. 3.9). These are then needed to calculate the crimping factors for the shoot and warp wire.

$$R_w = (w+d) / (2 * \sin \phi_w) \text{ (Eq. 3.8)}$$

$$R_s = (w+d) / (2 * \sin \phi_s) \text{ (Eq. 3.9)}$$

After obtaining these two radii the crimping factors for the two wires can be obtained directly from the following two linear equations (Eq. 3.10 and Eq. 3.11).

$$S_w = \frac{2 * R_w \phi_w}{(w+d)} \text{ (Eq. 3.10)}$$

$$S_s = \frac{2 * R_s \phi_s}{(w+d)} \text{ (Eq. 3.11)}$$

These two crimping factors are then combined into one general crimping factor for the screen mesh disregarding the weaving technique of having a shoot and a warp wire (Eq. 3.12).

$$S_m = \frac{(S_w + S_s)}{2} \text{ (Eq. 3.12)}$$

At this stage it has to be mentioned that it can be seen as clearly advantageous of the work of Kozai, Imura and Ikeda (1991) to provide empirical data as well as more in depth explanations of factors and parameters used and involved in comparison to the work of Mwaba, Huang and Gu (2006) which promotes a simpler model for obtaining the porosity of screen wicks. This model can be found in Equation 3.13 but is not used for these calculations as the use of the model of Kozai, Imura and Ikeda (1991) is seen as superior.

$$\varepsilon_i = 1 - \frac{\pi * N * d * S}{4} \text{ (Eq. 3.13)}$$

The main difference between both models, as can be seen later in equation 3.15, is the addition of the term for the dimensionless gap of the single layer screen into the denominator of Equation 3.15. This term is defined in equation 3.14 and its existence was confirmed when a supplier of screen meshes within the United Kingdom specified the thickness of its weave as 2.2*d nominal rather than 2*d nominal as assumed by Mwaba, Huang and Gu (2006). Further, it was assured that this factor is closely monitored and recorded as part of their production quality control and therefore seen as valid. The extra 0.2*d is taken up by the clearance c as well as the dimensionless gap α , which justifies the existence of the extra thickness of the wick.

$$\alpha = \frac{c}{2 * d} \text{ (Eq. 3.14)}$$

Once all the parameters are calculated the porosity can be determined using the method of Kozai, Imura and Ikeda (1991) through the derivation of the following equation (Eq. 3.15).

$$\varepsilon_i = 1 - \frac{\pi * N * d * S_m}{\{4(1 + \alpha)\}} \text{ (Eq. 3.15)}$$

This porosity is then directly looked up through a software function for that particular type of screen rather than being calculated directly. This will be described in greater detail in the next paragraph.

3.2.3 Development And Implementation Of VB Based Screen Mesh Wick Heat Pipe Fill Calculation Software

As mentioned earlier, the heat pipe fill calculations are temperature dependent and superimpose the amount of water required to saturate the wick and the vapour space with water molecules at a certain temperature. Figure 3.4 shows the layout of the input screen of the calculation software and indicates the required input parameters as well as the values looked up from datasets behind the calculation software. They will be explained in greater detail later on, first in written form explaining the details and then in form of a flow chart in Figure 3.5.

<u>Inputs</u>				<u>Legend:</u>		
Pipe Length	230 mm					Input Required
Diameter	12.7 mm					Automatically Calculated Value
t Wall	0.5 mm					
No of Wraps	2					Final Calculated Value
Mesh No	250		(100; 150; 200; 250)			
Wire Diameter	0.04 mm					
Venting Temp.	200 °C		(in 10°C Steps from 100°C-200°C max)			
<u>Fill</u>						
Saturation of Wick	1.01 cc					
Saturation of Vapour S.	0.17 cc		@20°C Ambient Temperature			
Vent losses	0 cc		Ask for Engineering Consultation prior to make changes to this line!			
<u>Total Fill</u>	1.18 cc		© A.Engelhardt, 2008			

Figure 3.4: Layout of the Calculation Software

The first input required is the length of pipe. This will be used at a later stage to determine the volume of the wick to be saturated as well as the volume of the vapour space. Due to the fact that the length of the pipe is significantly longer than double the wall thickness of the wick which could be used at the end form of the heat pipes, the amount of wick possibly located within the end form is neglected.

The next two inputs are the outside diameter and the wall thickness of the heat pipe. These two parameters are used to determine the internal pipe diameter which is the outside diameter of the wick. Further, the number of wraps is used to ultimately determine the vapour space diameter, but first the wick thickness which is then used to determine the wick volume combined with the length of the pipe. Using the drop down box to select the Mesh No is used to look up the relevant wire diameter. This wire diameter is then automatically introduced into the box below and used together with a factor of 2.2 to determine the thickness of the wick layer. The factor of 2.2 was given by the supplier of the wick and is regularly checked during the manufacture of the wick in order to maintain a constant thickness weave. It has to be considered that the factor of 2.2 is only valid for the type of plain weave as shown in

figure 3.7 below, which is the most common one used in heat pipes. For other types as show in the International Standard ISO 4783-2 (1989) and other references like manufacturers' data this factor has to be obtained separately and implemented prior to calculating the thickness of the wick layer and the resulting overall thickness of the wick.

The overall thickness of the wick layers when multiplied by the number of wraps will then give the thickness of the wick and once the area of the circular ring being occupied by the wick inside the heat pipe is calculated, multiplying this by the length will give towards the total volume of the wick. The use of the drop down boxes has only been programmed for ease of use for the wicks shown as they are widely available and are considered as “standard wicks”, but it could be expanded to be a more generic type. The limited amount of “standard wicks” also allows for the porosity to be looked up from a table rather than be calculated directly and this will save valuable computational resources.

Further, the thickness of the wick is used to determine the diameter of the vapour space which will then be used to determine the volume of the vapour space. From the law of mass conservation, which says that the product of density and volume remains constant unless there is mass transfer out of the system, it can be derived that the volume shown as a result in the calculation software is required for saturation of the vapour space with water molecules and is obtained from dividing the density for the higher temperature by the one for the lower and multiplying it by the volume determined for the higher temperature.

The other calculated parameter is the amount of working fluid required for saturation of the wick. This amount is obtained by multiplying the volume of the wick with its porosity. The calculation of the porosity has been described in greater detail in an earlier section and the value will not change unless physical parameters of the wick are changed, e.g. wire diameter or mesh number. Therefore a look up function has been seen as sufficient for the calculation software. In order to avoid a heat pipe which has too little fluid charge during operation, it is of significant importance that the heat pipe is vented at a temperature higher than the planned operating temperature. Depending on the difference between the venting and operating temperature, this approach might even almost be sufficient to give the 10 to 20% of overfill Peterson (1994) is suggesting.

A flow chart detailing the equations and order of these used to determine the required amount of working fluid for a screen mesh wick heat pipe with a certain wick structure including the saturation of the vapour space can be found below in Figure 3.5:

Calculation Flow Chart Screen Mesh Heat Pipe Fill Calculation Software

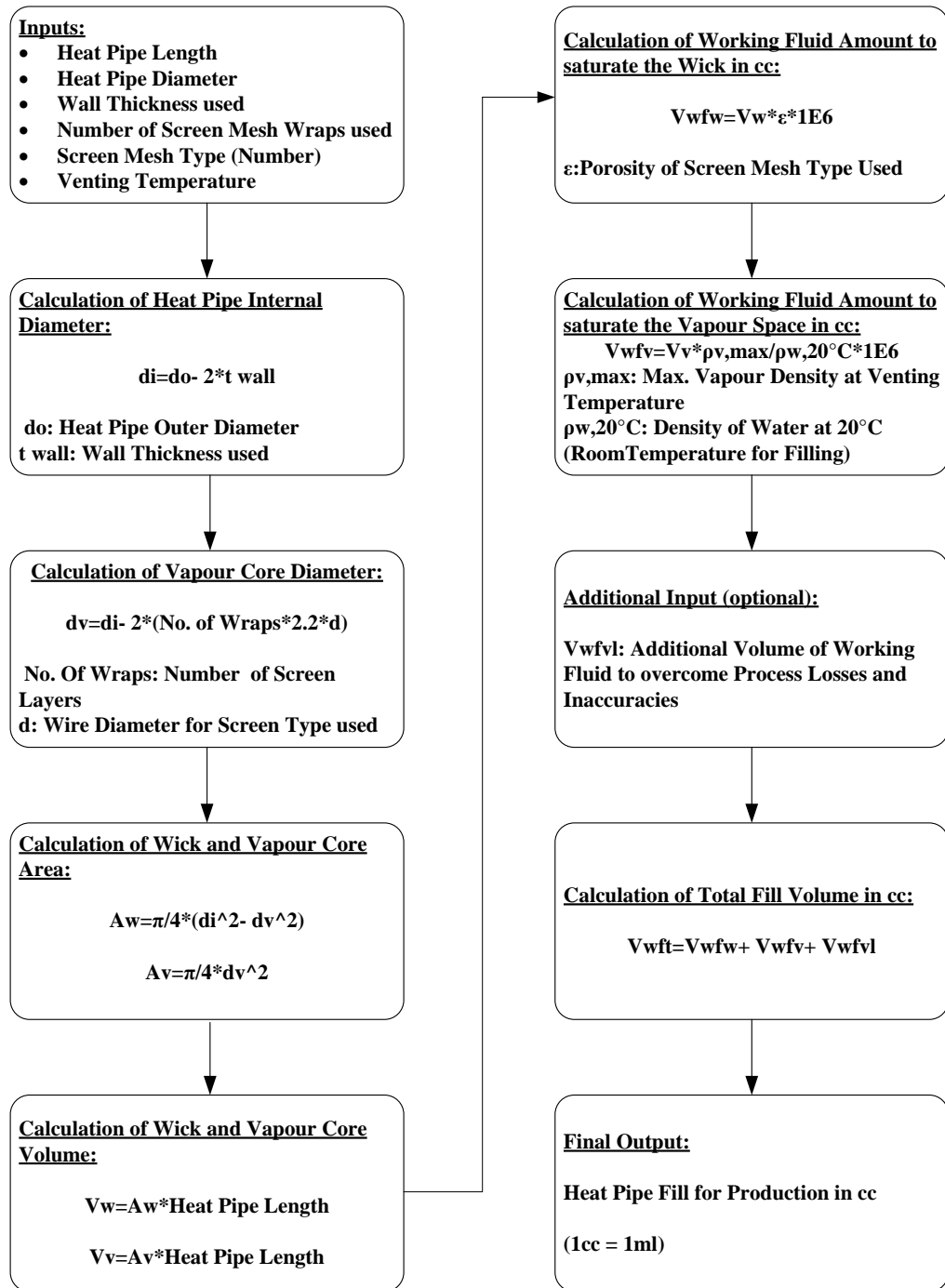


Figure 3.5: Screen Mesh Wick Heat Pipe Fill Calculation Software Flowchart

One thing which has not been taken into consideration is the effect of intermeshing between the relevant numbers of mesh layers (Reay&Kew, 2006). Any gaps between layers of wick could add up as an extra capillary

space, but is a unique feature of each pipe and are therefore hard to be taken into account using theoretical fill calculations. One way proposed by Reay and Kew (2006) is to measure the actual thickness of the wick. This is not seen as an appropriate way for medium to large batch size manufacturing. There are various reasons for this, first it is not possible to measure the thickness of the wick and neither appropriate to change the fill prior to filling each pipe. Secondly this method assumes a similar thickness of the gap around the circumference of the wick which cannot actually be realised. Chapter 6 of this PhD thesis work will show some X-Ray pictures to prove this statement and show the distribution of the wick around the container wall. Finally the measurement and the venting operation are subject to errors as well as process variations which have a bigger effect than the adjustment volume of the fill and therefore the approach is seen as inappropriate for industrial applications. Figure 3.6 shows a diagram, where heat pipes with a length of 230mm, such as used for the later experimentation as presented in chapters 4 and 5 were used to calculate the fill depending on the screen mesh wick type used inside. For all of these pipes two wraps of screen mesh was used and for the lower three diameters, 0.5mm wall thickness was used, whilst for the largest diameter of 19.05mm 0.8mm was used to use container material diameters, which are available in reality. Once the diameter, wall thickness and number of wraps was chosen, the fill for each of the four wick structures/ screen mesh types included in the calculation software was calculated and plotted. From the lines it can be clearly seen that the coarser wicks with lower numbers have a significantly high fluid charge than the finer wicks where the overall thickness of the wick is less due to the thinner wire used.

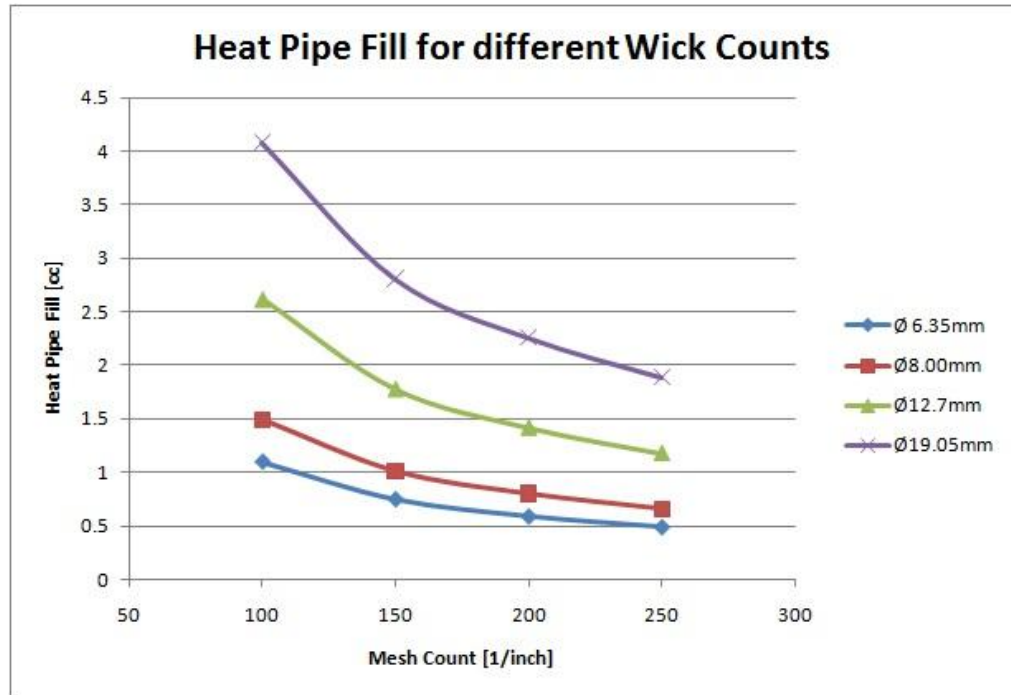


Figure 3.6: Fill for various Screen Mesh Heat Pipe Configurations

3.3 ANALYTICAL INVESTIGATION INTO THE CAPILLARY OR LIFTING HEIGHT FOR DIFFERENT WICK STRUCTURES

For screen wick heat pipes the same basic design considerations apply as for any other heat pipe type. Primarily the compatibility between the container material, wick material and the working fluid has to be ensured in order to avoid out-gasing (the production of non-condensable gases inside the heat pipe due to material incompatibility), and the loss of the vacuum seal. A very comprehensive guide on the selection of material working fluid combinations can be found in Groll et al. (1998). The operational limits of heat pipes as presented by Garner (1996) and are valid for each of the three different wick structures. Zaghdoudi, Tantolin and Godet (2004) provide a more recent overview of heat pipe applications in the electronics cooling industry. They give the impression that the lifting height of the mesh heat pipe is inherently

less than that of sintered heat pipes. However, this is only true when relatively coarse meshes are used.

The work in this section explores the relationship of mesh size to lifting height and shows that the lifting height can be significantly increased with the use of finer meshes. There are various screen mesh types which can be used as a wick for a heat pipe. The main screen mesh wick characteristics are the mesh number and the wire diameter. But screen mesh wicks are limited by the capabilities of manufacturing techniques, and the finest achievable mesh available has a mesh number of 625, which means 625 openings per inch. The type of mesh limits the achievable porosity to around 0.6- 0.7 and the minimum pore radius to around 40 μm (Williams & Harris, 2005).

Based on the wire diameter and the mesh number, the aperture (opening width) can be obtained either by information from the manufacturer or by calculation.

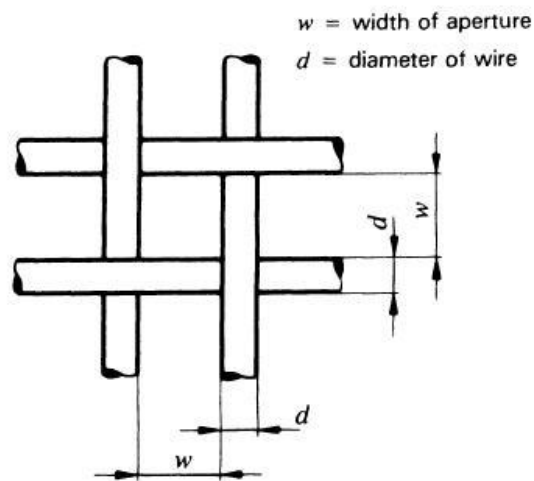


Figure 3.7: Definition of screen mesh parameters (ISO 4783-2, 1989)

Work presented in section 3.2 within this chapter can be expanded to obtain an equation for the capillary or lifting height and this approach is presented within this section. Within equations 3.8 and 3.9 the mathematical foundations for the calculations of the radii of curvature for the warp and shoot wire are presented. These radii can then be used to calculate an additional angle for both the warp and shoot wire between the vertical and the radius for the particular wire at the position of half the wire diameter on the other type of wire:

$$\phi_w' = 2 * \sin^{-1} \{d / (2 * R_w)\} \text{ (Eq. 3.16)}$$

$$\phi_s' = 2 * \sin^{-1} \{d / (2 * R_s)\} \text{ (Eq. 3.17)}$$

Once obtained, these angles can then be used to determine additional geometrical offsets required to determine the next calculation steps, which are the angles between two warp or shoot wires on the top and bottom side of the screen wick and the horizontal:

$$a = d / 2 + R_w * (1 - \cos \phi_w') \text{ (Eq. 3.18)}$$

$$b = 3 * d / 2 - R_s * (1 - \cos \phi_s') \text{ (Eq. 3.19)}$$

Once these offsets are obtained, the angles between the warp or shoot wires and the horizontal can be calculated whereas θ_1 is the angle for two warp wires and the horizontal and θ_2 respectively for two shoot wires and the horizontal:

$$\theta_1 = \tan^{-1} \{(\delta_1 / 2 - a) / [(w + d) / 2]\} \text{ (Eq. 3.20)}$$

$$\theta_2 = \tan^{-1} \{(b - \delta_1 / 2) / [(w + d) / 2]\} \text{ (Eq. 3.21)}$$

These angles are then used to be able to determine the radius of a circle which could be fitted in between two adjacent warp or shoot wires on the top and

bottom side of the wick. Again, the index 1 is used for the warp wires whilst the index two is reserved for the shoot wires:

$$r_1 = \frac{(w+d)}{2 * \cos \theta_1} - \frac{d}{2} \text{ (Eq. 3.22)}$$

$$r_2 = \frac{(w+d)}{2 * \cos \theta_2} - \frac{d}{2} \text{ (Eq. 3.23)}$$

These two radii finally enable the calculation of the average capillary radius or the effective pore radius as Imura, Kozai and Ikeda (1994) are referring to, which is a unique characteristic for each screen mesh type, using the relationship below:

$$r_c = \frac{2 * r_1 * r_2}{(r_1 + r_2)} \text{ (Eq. 3.24)}$$

From the average pore radius, the lifting or capillary height for a certain wick/working fluid combination can be obtained. The derivation of the equation above is based on the assumption of constant wick properties along the heat pipe in an ideal case with no voids between wick and wall.

Equation 3.25 below shows how the lifting or capillary height can be obtained from the average capillary radius whilst Table 3.1 shows a comparison of results for the lifting / capillary height for six different wick types; four different screen meshes and two different sinter powder types, which are available at Thermacore Europe. In all six cases, water was used as working fluid. Other working fluids could be used, but would only offset the results obtained for water.

$$H = \frac{2 * \gamma * \cos \theta}{r_c * \rho_l * g} \text{ (Eq. 3.25)}$$

Within this equation, H is the capillary or lifting height, whilst γ is the surface tension [N/m], which is a unique characteristic for each working fluid at certain temperatures. Furthermore, the contact angle θ [rad] differs for each working fluid, whilst r_c , the effective capillary radius[m] is a unique characteristic of the wick type used and the way to obtain the radius for screen wicks is described above. The gravitational support g [m/s²] can be assumed as constant for this equation, whilst the working fluid density ρ_l [kg/m³] is dependent upon application conditions like the operating temperature and the type of working fluid used. Using the equations presented above, as well as proprietary information (Thermacore Inc., 2008) for the two different sintered powders the table 3.1 below shows the results. These are valid for heat pipes of any diameter with these wick structures and could be expanded for and porous material used as a wick structure inside a heat pipe as long as a capillary radius can be obtained.

Mesh Type	Screen Mesh				Sintered Powder	
	100 Mesh	150 Mesh	200 Mesh	250 Mesh	Powder Type 1	Powder Type 2
Calculated Porosity	0.690	0.709	0.690	0.691	n.a.	n.a.
Effective Pore Radius	7.93E-05	5.46E-05	3.96E-05	3.19E-05	n.a.	n.a.
Lifting/ Capillary Height	0.171	0.248	0.342	0.425	0.499	0.560

Table 3.1: Calculated Porosity, Effective Pore Radius and Lifting Height [last two m] (Thermacore Inc., 2008)

From the last row of Table 3.1, it can be seen that screen mesh wicks provide a lifting height and therefore can work without gravitational support. These results do not only correlate very well with the experience of the author, where screen mesh heat pipes of a higher mesh number were the only solution to transport a certain quantity of heat within a small space, but also with work presented by Reay and Kew (2006).

A corrected statement therefore has to be: “Screen mesh heat pipes work against gravity as long as the pipe is reasonably short and its vertical length/height when tilted is below the lifting/ capillary height for the particular mesh deployed.”

The main advantage which makes screen mesh wick heat pipes attractive is their ability to handle higher power levels when the same container diameter is used. This advantage is obtained from the larger vapour space available due to the thinner wick within the screen mesh wick heat pipe compared to a sintered heat pipe. But screen mesh wick heat pipes can only be used when the heat fluxes at the evaporator and condenser length kept below the critical values for the wick type used. For standard sintered heat pipes the heat flux limit is typically around $50\text{W}/\text{cm}^2$ whilst with more specialised design approaches combining special powder types with a particular shape of wick structure, heat fluxes up to $250\text{W}/\text{cm}^2$ can be achieved. For grooved heat pipes the heat flux limit is relatively low due to less surface area available for evaporation (around $5\text{W}/\text{cm}^2$). Screen mesh wicks can typically handle between 10 and $15\text{W}/\text{cm}^2$ so the evaporator and condenser design needs to allow the use of this type of heat pipe (Zaghdoudi, Tantolin & Godet, 2004; Peterson, 1994).

3.4 VENTING OR PROCESSING OF HEAT PIPES

Venting or processing is the process in which the working fluid is introduced into the heat pipe and the vacuum is then generated prior to sealing the heat pipe container and finishing the transition from a copper tube to a heat pipe. The accuracy of the vent itself, apart from the amount of working fluid introduced into the heat pipe has a very significant influence on the performance and the characteristics of the heat pipe and therefore needs to be considered very carefully. Common errors or shortfalls during the manufacturing and venting process are described at a later stage of this section and also graphically represented.

3.4.1 Venting Techniques

When the venting process of a heatpipe is carried out manually, it is highly inaccurate and one of the major reasons for introducing variations in the heat pipe performance of a batch. This is due to the different ways the heat pipes are vented on a production run. The pipes are heated beyond evaporation temperature of the working fluid at the top of the pipe after the required amount of fill has been introduced into the pipe using a syringe and a needle. The opening is then sealed using a brass pin. There are two pin sizes regularly used for heat pipes, so the opening of the pin hole varies between 0.9mm and 1.2mm. Depending upon the time the pin is removed from the pipe, the amount of water escaping in a vaporized state varies. In order to overcome this production inaccuracy, an approach to calculate the pressure inside the pipe

and from there being able to get information on the escaping water was undertaken. This will guide towards a more accurate fill calculation, as well as identifying a compensation factor to overcome the venting losses.

The major problem for calculating the losses during the venting process is the two-phase phase change during the venting process. From theory, the process is an isochoric process, but due to the phase change, the pressure built up before the removal of the pin is always higher than in a pure isochoric process. This has to be considered because in the next calculation the exact relationship between the quantity of water and the quantity of air is required in order to predict the pressure inside the pipe and from there being able to predict the amount of water escaping. The removal of the pin will allow the hot trapped air in the pipe to be pushed out by the vapour and therefore, once cooled, create the vacuum inside the pipe which is required for heat pipe operation. The ratio of dispensed water and trapped air is a characteristic of a single pipe, therefore a general rule is hard to achieve as the pressure inside the pipe varies with size, length and wick structure which influences the available vapour space whilst the pure isochoric approach of treating the fluid as an ideal gas would be a linear function of initial pressure, and the temperatures at starting and pin removal conditions. The isochoric part of the overall pressure is not seen critical during production, as a high risk of mechanical distortions can be seen on short thick pipes, whilst the isochoric pressure rise would only be one bar above ambient and therefore not sufficient to mechanically expand the pipe. This feature can be used to mechanically create a good thermal interface whilst embedding the pipes into cavities, but during the venting process it is

an unwanted side effect, which needs further theoretical investigation to be resolved.

Once the internal pressure is calculated the outflow from a pressure vessel can be calculated taking nozzle shape and internal pressure into account. From the calculated outflow speed, the mass flow rate out of the venting hole can be determined and from there the amount of escaping liquid through the venting hole over a set period of time can be obtained. This work has proved to be hard to carry out due to the fact that the outflow speed of the vapour is close or above the critical speed of sound and therefore even if the critical pressure ratio is implemented directly, mathematical inaccuracies during calculation and checking of results guide towards a vapour speed which is higher than the critical one. Therefore a closer investigation of this phenomenon is suggested to be undertaken later. From experiments carried out at Thermacore Europe, it has been proven that typical vent losses on venting technique 2, as described in a later section of this chapter for small pipes in the 6 to 8mm diameter range and 150 to 250mm length are in an order of magnitude of 0.1-0.15cc and can therefore be manually added into the calculation software to counteract the loss of working fluid.

There are four venting techniques which are commonly used to produce heat pipes.

Some of the techniques seem to be laboratory based whilst others can be modified to suit industrial scales and needs of through-put whilst still offering the required fill and geometrical accuracies. Another criterion not to be neglected is the temperature range of the working fluid. Generally low to

moderate temperature range working fluids like water, ammonia and methanol are easier to handle and more commonly used in industrial heat pipe applications. Therefore, in later sections of this chapter only low temperature venting techniques will be dealt with. The four venting techniques are (Peterson, 1994):

1. Use of an evacuation and back-filling technique
2. Use of a liquid fill and vapour generation technique
3. Use of a solid fill and sublimation technique, and
4. Charging using a supercritical vapour technique

These venting techniques coincide with techniques presented by Faghri (1995), but due to the greater extent of work presented here, the focus in the following section will be on the work of Peterson (1994).

Depending on the amount of automation required, not all the venting techniques offer much of flexibility and therefore can not be seen as applicable for small to medium batch sizes of pipes to be produced. For low to medium temperature heat pipes used in electronic cooling, the two most common techniques are the evacuation and back-filling technique and the liquid fill and vapour generation technique. Both techniques are compatible with the more standard working fluids like water, methanol and ammonia, whilst ammonia due to its low boiling point hardly needs any additional heat input with the liquid fill and vapour generation technique.

The evacuation and back filling technique consist of a vacuum pump as well as a set of valves. The vacuum pump is used to generate a vacuum down to a pressure of 1.3332237×10^{-7} bar (Reay & Kew, 2006). Once this pressure is achieved the valves towards the pump are shut and the valves towards the

container with the working fluid are opened. A controlled amount of working fluid is injected into the heat pipe. Then the valves towards the heat pipe are shut and the unit is heated up to desired venting temperature. Then the valve towards the heat pipe is opened again and any air or gases left in the heat pipe is forced out into the venting system. This step is similar to the liquid and vapour generating technique and is essential because the vacuum achieved by the pump is not strong enough to get rid off all the air in the system. Any air remaining in the heat pipe will act as a non condensable gas and can shorten the active pipe length due to a gas pocket in the condenser section which can not be used for active heat transfer into any sort of heat sink.

The liquid fill and vapour generation technique will be described in greater detail in section 3.4.2 of this chapter where the charging of the heat pipes used for this PhD thesis work is described.

A solid fill and sublimation technique is applicable for heat pipes where the working fluid is solid at room temperature, e.g. liquid metal heat pipes. This technique is similar to the liquid fill and vapour generation technique. The working fluid is heated up to its evaporation temperature and the air or Non Condensable Gases (NCG) are removed from the inside of the heat pipe container by the pressure of the vapour from the working fluid.

The fourth process is the most complicated and is described in Peterson's work (1994). This technique certainly requires the highest amount of equipment and automation. The process is based on the evacuation of a high pressure chamber down to a certain pressure and then a controllable amount of working fluid is injected into the chamber. This amount has to be sufficient to saturate the vacuum in the entire chamber at a temperature higher than the

critical temperature of the working fluid. The entire chamber has to be taken to a temperature higher than the critical temperature of the working fluid. Another alternative is to allow repetitive injections of working fluid amounts less than the saturation amount in the chamber and therefore give a better control on how much working fluid is applied. This technique relies mostly on the precise control of the temperature of the pressure vessel and quantity of working fluid applied after the initial evacuation. It is seen that this gives a good control for every heat pipe within the batch.

3.4.2 Venting Technique Applied To The Heat Pipes Used For This Study

The heat pipes to be tested for this study were produced using the liquid fill and vapour generation technique. This technique can be used to produce pipes as well as to achieve what is referred by Peterson (1994) as “burping the pipe”, a final attempt to get rid of traces of Non Condensable Gas (NCG), where the heated heat pipe is opened for a short period of time to the ambient in order to force any NCG out of the pipe.

Since the samples used for this PhD are relatively small, the technique was adapted to deal with the reduced size. Therefore, a brass pin was used rather than a fill tube which requires crimping, opening etc, whilst a pin can be released from the hole during the venting process and applied back in before being soldered in place.

The venting of a heat pipe starts with the injection of the correct amount of working fluid determined as described earlier in this chapter into the pipe and

the sealing of it through either a pin used to fill the hole or a crimp of the fill tube. The pipe is then inserted into a venting rig which contains a heating element and an insert with the same diameter to the heatpipe to be vented. This rig is set then to a controlled temperature between 100°C and 200°C for water as a working fluid for safety reasons. Another important parameter is the insertion depth of the pipe into the rig as this determines the amount of heat directly transferred into the pipe. There are two different methods widely used to evaluate the temperature of the top end of the heat pipe. One uses thermocouples and therefore allows the temperature to be read at the top end of the heat pipe directly. This temperature has to be higher than the evaporation temperature of the working fluid and lower than the temperature of the venting rig in order to give a pressure gradient along the pipe and make sure that the NCG's are collected at the top end of the pipe and being forced out of the system by the vaporised working fluid. This method, as well as the second one relies on the fact that the point where the pipe is opened is the highest point.

The second method is more practical and less scientific and can only be applied to working fluids which have no major hazardous effects to the surrounding. For this method a small amount of working fluid is applied to the outside of the container at the point where it is vented. Once this amount of working fluid on the outside of the top end of the pipe has reached its boiling temperature, it starts to evaporate and the person processing the pipe knows that the correct venting temperature has been achieved and NCG's are ready to be forced out of the pipe. This also indicates that the working fluid within the pipe has already reached its boiling point beforehand and is available as

vapour in the pipe. Therefore, at this point the pipe is opened and the NCG's are let out. The heat pipe is now sealed and after mechanical preparations, like removal of excess pin length, is now ready to be used for tests, applications, etc.

3.4.3 Most Common Venting Failure Modes

During the Venting or Processing of a Heat Pipe there are various reasons which can cause a heat pipe to incorrectly function. There are four main failure modes as well as combinations of these four failure modes which can cause a heat pipe not to perform as designed. All these venting failure modes have been anticipated during initial work for this thesis and it was found that very little consideration was given to them by the scientific community as hardly any work dealing with issues during the venting process has been presented.

In this work the main four failure modes are illustrated below in Figures 3.8 to 3.11 with a description of how these failure modes can be identified during heat pipe testing. Finally an illustration of a heat pipe vented to a desired condition on the venting rig is shown as a comparison in Figure 3.12.

1. Contamination:

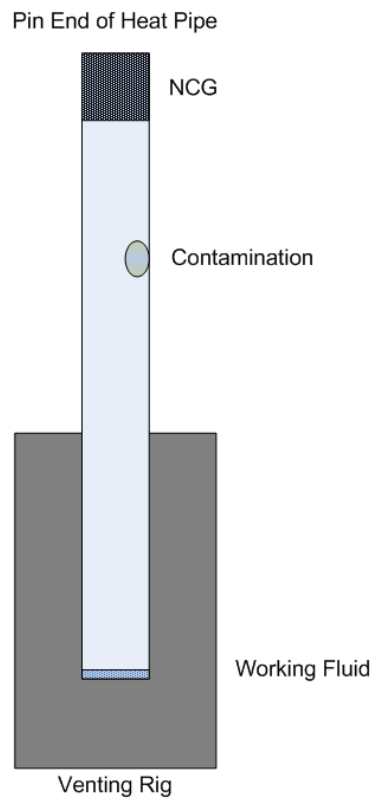


Figure 3.8: Scheme of a Heat Pipe containing a Source of Contamination

Contamination inside a heat pipe can be anything which will create or assist to create the formation of Non-Condensable-Gas (NCG), or will limit the performance of the heat pipe by other means. NCG's are normally caused by chemical impurities left inside a heat pipe, like greases, etc, which will then form gas during heat pipe operations and therefore shorten the active length of the condenser. NCG's can also be formed through the oxidization of metals other than the container material. This can be either metals mistakenly left over during the manufacturing process like snapped drill bits or can occur through a non-suitable working fluid/ wick and container combination. The NCG's collect during the operation of the heat pipe in the condenser section due to the lower pressure at this end and shorten its active length.

A Heat Pipe like this will show up during testing with having a high ΔT between the evaporator and the condenser and will not handle the power very well.

2. Dry out with NCG left

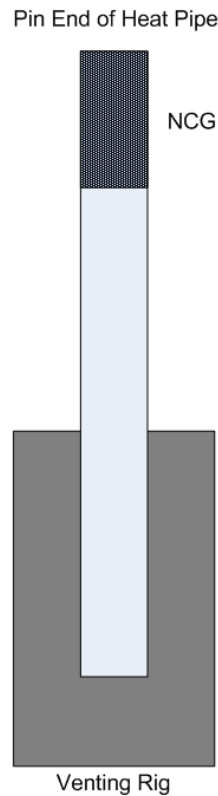


Figure 3.9: Scheme of a Heat Pipe containing Non Condensable Gas

Dry out with NCG left occurs if the working fluid charge to start the venting/processing is very low and insufficient to force the NCG's out of the pipe whilst the pipe is opened to the ambient. This failure mode is the most catastrophic one and will result in a "dead" or non-operational heat pipe. This pipe will not even perform in a simple water test and will not warm up from top to bottom. Therefore, this failure mode is the easiest to identify. Furthermore, the pipe will show a very high ΔT on a power test on a test rig and the temperatures of the heat input rig components will carry on rising until the steady state temperature is reached. This will take longer than a standard

time for pipe testing. Conduction through the pipe wall is in this situation the only heat transport mechanism available. The NCG's left in the pipe will shorten the condenser length up to an extent where there is no active condenser length. Therefore, there is no circulation of the working fluid and no operation of the heat pipe results from it. This phenomenon was reported by Peterson (1994) as well and he provided information that any NCG's remaining in the heat pipe are collected in the condenser section.

3. Dry- Out

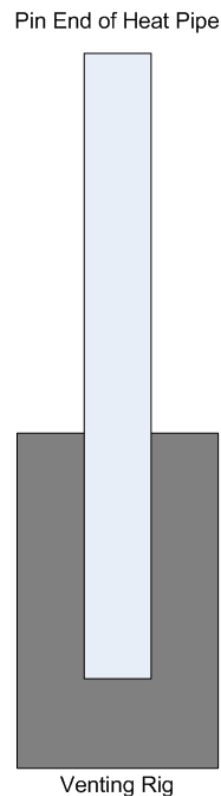


Figure 3.10: Scheme of a dried out Heat Pipe

The second dry-out scenario occurs when there is just enough working fluid molecules in the pipe to force out the NCG's but does not have sufficient molecules left inside the pipe to handle all the power.

During tests, these pipes will perform very well at lower power input levels with a low ΔT and stable operation at various inclination angles. At higher power input levels, close to the design power, these pipes will start to show a rising ΔT and eventually dry out. This dry out will cause components attached to it, like heater blocks, to overheat and the heat pipes will not be able to handle any power and will stop operating. However, the heat pipes will be able to operate again after a complete cool down period.

4. Excess Fluid Charge

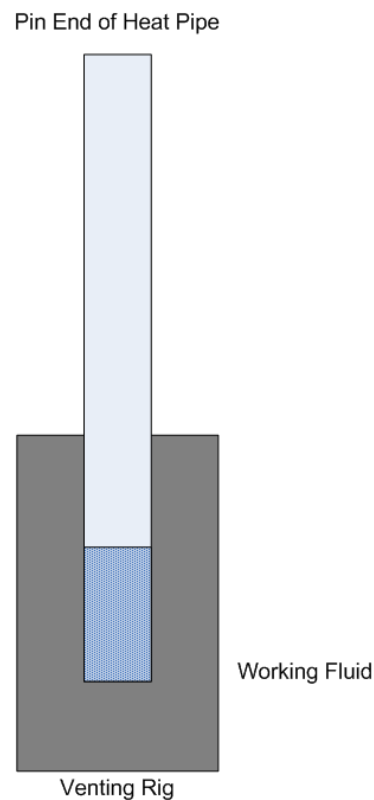


Figure 3.11: Scheme of a Heat Pipe with excess Working Fluid

An excess fluid charge occurs when the fill volume of the Heat Pipe was not calculated correctly or there were less losses of the working fluid during the venting process than anticipated. Also, the introduction of extra working fluid

due to inaccurate dispensing equipment or operator error during the charging process will have the same effect as a high calculated fill volume. Upon testing, the heat pipe will be capable of carrying the power as designed, but it will have a high ΔT . When aligned at an angle, the pipe will show a high ΔT and might even have erratic temperature behaviour at the evaporator section if the pipe wall temperature is measured directly. Overall this scenario is less critical than a drying out pipe, but still far away from a good performing pipe.

5. Ideal State

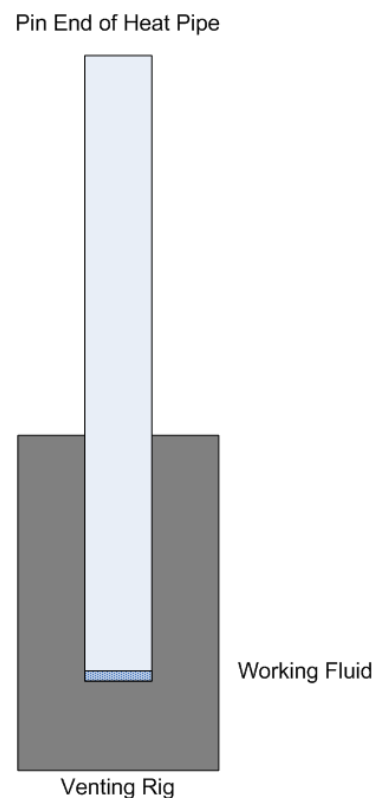


Figure 3.12: Scheme of a good Heat Pipe

The ideal state for a heat pipe filled normally shows a little bit of excess water at the bottom of the pipe, but not too significant. This follows the guidelines as proposed by Peterson (1994) to introduce between 10 and 20% overcharge, although it is believed that this figure is too high for certain applications

where the pipes are subject to freeze/ thaw cycles, as well as shape changes and angle inclinations. It can clearly be seen that there is no contamination or any NCG's left in the pipe. It is believed that this pipe which has full saturation of the wick will perform well on the test rig and in applications.

3.5 SUMMARY AND CONCLUSIONS

Three different subjects were investigated within this chapter and are presented above. Firstly the theory behind a calculation software for calculating the fill for screen wick heat pipes based on geometrical wick properties and venting temperature has been presented. The geometrical properties of the screen wick are directly used to calculate the porosity of screen mesh wick using equation 3.15 and combining that with the number of wraps used and the venting temperature leads towards the required fluid charge. This approach is seen as being quite novel as this has not been presented in a similar form before and so has not been used before for larger production batches of heat pipes and comparison with previous methods. Both the material presented above and other work which has not been presented in this section, indicates an accuracy of 7% between the theoretically determinate fill and the experimentally concluded fill. That accuracy is seen as a vast improvement and helps considerably to reduce the amount of experimentation required to produce well performing heat pipes with significantly reduced development time. Continuing this work has led within the second sub-section towards the possibility of calculating the capillary or lifting height for a particular screen mesh wick type and its ability to be used for operations

against gravity. That approach is based on the calculation of the capillary radius (Eq. 3.24) and proposes that screen mesh wick heat pipes can be used against gravity. From these results presented in Table 3.1 and practical experience of the author it was concluded that screen mesh heat pipes can be used for anti- gravitational operation as long as the heat pipe is not utilized to a greater vertical length than its capillary or lifting height. Furthermore, these calculations can be used to prevent the detrimental effects of “puddling”, the collection of working fluid at the bottom of heat pipes operated with gravity, on the ΔT observed during operation of the heat pipe.

Within the third sub-section, the most common errors during the venting process, which is one of the most influential processes with regards to heat pipe performance, have been described. This information is new to the scientific community as most heat pipes just seem to appear from an “unknown source” and the process variation effects on the performance of heat pipes, even within the same batch, have either not been presented before or are not considered at all due to the relatively small batch sizes that have been investigated previously. This work can be used to explain the occurrence of certain failure modes described in literature. Only the existence of these failure modes has been described previously, but not the reasons why they occur and how they are caused by the manufacturing process. From this point of view it was extremely valid to undertake this work in order to be able to produce heat pipes of the highest quality to then be subsequently investigated with regards to the effects of bending upon heat pipes.

CHAPTER 4 – INVESTIGATION OF THE USE OF DISSIMILAR SCREEN MESHES AS HEAT PIPE WICKS

This chapter reviews existing literature with respect to a single important parameter of screen mesh wick heat pipes, the mesh count or number of openings and tries to link changes to this parameter and mixing of different layers of screen mesh wick to advantages in performance for certain industrial applications, such as the ability to manufacture heat pipes with screen mesh wicks with a particular low ΔT across the wick structure or to overcome maximal operational angles for the application.

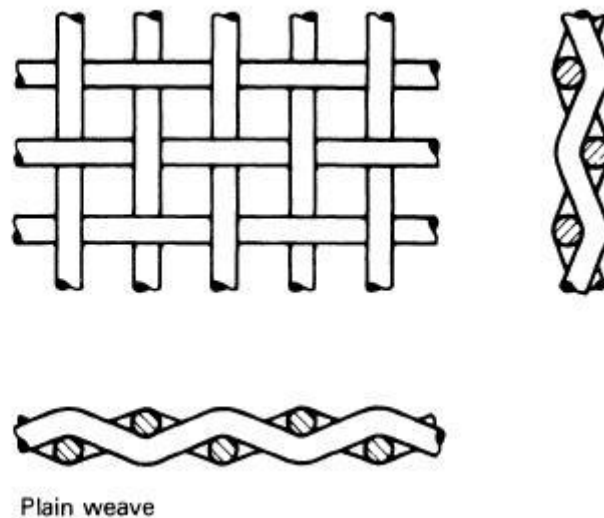


Figure 4.1: Scheme of the Screen Mesh used in Heat Pipes (ISO 4783-1, 1989)

Equation 4.1 below shows a relationship between the Mesh number per inch and the wire diameter and aperture of the screen used (Brautsch & Kew, 2002):

$$N = \frac{1}{w + d} \text{ (Eq. 4.1)}$$

Based on this definition, the use of dissimilar screen mesh types for multiple layers of the wick was investigated. This work includes a review of existing work on dissimilar screen mesh wick heat pipes, which is quite rare, followed by a discussion of screen mesh parameters vital for the function of heat pipes. These parameters are then compared with a statement found in literature advising on the use of a certain combination of layers of screen mesh. Finally the author's own experimental results are used to validate or disprove the content of the statement where the position of the finer screen mesh towards the vapour space is promoted (Reay & Kew, 2006). From the results of the experimentation it is also shown that the use of dissimilar screens meshes inside heat pipes is not totally free of manufacturing barriers and that this part needs consideration as well.

4.1 INTRODUCTION

Screen mesh is one of the oldest types wick structure used within heat pipes and has been used since 1964 when Cotter, Grover and Erickson (1964) first published articles about heat pipes as they are known today. However, with today's requirements of higher power handling and reduced space available, screen mesh heat pipes are becoming a more attractive option for certain demanding applications. Work presented here will show an investigation of whether it is possible to engineer screen mesh wick heat pipes towards any application by using a different composition of the screen wick itself or use multiple layers of different types of screen wicks.

4.2 DISSIMILAR SCREEN MESH WICK HEAT PIPE INVESTIGATIONS

This section of work can be seen as an expansion of the work presented in chapter 3 and goes more into the detail of screen wick theory. Investigations will review published work as well as own experimentation and determine whether it is possible to tailor make heat pipes with screen mesh wicks to meet the demands of certain applications like low ΔT along the heat pipes rather than produce general “all-round” heat pipes suitable for most applications.

4.2.1 Design And Manufacturing Considerations For Dissimilar Mesh Wick Heat Pipes

The point starting for this work was a paragraph in Reay and Kew’s book (2006), which deals with the usage of dissimilar meshes within heat pipes. In the book it is stated “In instances where two mesh sizes may be used in the heat pipe say two layers of 200 mesh and one layer of 100 mesh, the liquid-vapour layer must always be in the 200 mesh to achieve maximum capillary rise. It is therefore advisable to wrap the 200 mesh over the end of the 100 mesh as shown in Figure 5.9. It is possible to locate the fine mesh against the wall, where it will suppress boiling.”

The above statement has provoked various comments and discussions from others involved in the heat pipe industry, these comments sometimes varied significantly. Some agreed with the statement in the book whilst others were to dispute it. Those disputing the statement stated two main objections against having the finer mesh towards the liquid vapour interface. The finer mesh certainly reduces the entrainment forces acting on the liquid returning to the

evaporation section of the heat pipe, however, there were concerns over the statement. Firstly, the finer wick structure at the wall will positively support the evaporation of the working fluid by providing a greater heated surface area. Secondly, having the coarser mesh towards the liquid vapour interface is seen to present less resistance to the evaporated working fluid vapour leaving the wick structure due to the larger pore size and it offers better alignment of fine wick to the wall due to the higher spring force provided for pressing the wick against the wall due to the thicker wire diameter utilised. The likelihood of vapour being trapped within the wick was reported as a major cause for heat pipe failure and premature dry-out of the evaporator section, preventing the liquid from returning into the evaporator, by Williams and Harris (2005) investigating step-graded metal felt as wicks for heat pipes. Furthermore, they have identified two limits to be critical to heat pipe operation, both of which are directly linked to the wick. These limits are the capillary limit, which is the ability of the wick to return the working fluid to the evaporator section and the boiling limit, which is the wick's ability to evaporate working fluid and allow the two-phase heat transfer to happen. The second limit is influenced by the wick's pore size allowing the working fluid vapour to leave and the amount of evaporation surface provided to reach its vaporisation temperature.

Brautsch and Kew (2002) present very interesting work on the two limits mentioned by Harris and Williams (2005) and confirm their findings in a more detailed way for heat pipe screen mesh wicks even using the same mesh numbers as during the experimentation presented in a later section of this work. They investigate the boiling and the wicking/ capillary limit as the main limitations for screen mesh wicks and state that local dry-out is encouraged by

trapped vapour bubbles within the wick and this leads to a decrease in the achievable heat transfer coefficient. This issue is caused by the reduced available cross section of the wick and thus reduces the amount of returning working fluid whilst at the same time increasing the pressure drop through the wick structure. The finer the top structure, the more likely they found it to be an obstacle for the bubbles to leave and therefore act as a vapour trap.

Additionally, they also confirmed that a fine wick structure applied to the wall of a heat pipe enhances the heat transfer coefficient in comparison to the bare surface. Depending on the temperature, the enhancement for a fine mesh is greater than a coarser one, but the configuration is then more likely to suffer from burnout or local dry-out. Interestingly, for the work presented here is their use of high speed video equipment in conjunction with a dedicated evaporation test rig visualising the evaporation process within screen mesh wicks. Some examples of the visualisation at different heat fluxes are presented in the Figures 4.2 – 4.5 below. The lighter the area of the investigated screen wick behind the coarse carrier wick is, the less liquid is contained within the wick, where the picture is white and shiny, it indicates the wick is depleted of working fluid, whilst the grey shows vapour and the darker patches are working fluid in its liquid phase. The exit of a vapour out of the wick through bursting bubbles can be seen in Figure 4.4.

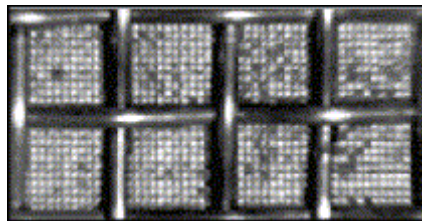


Figure 4.2: Wick with vapour leaving freely (150 Mesh with $q = 52\text{kW/m}^2$) (Brautsch & Kew,

2002)

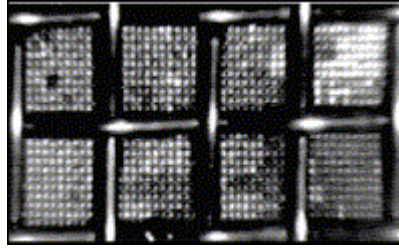


Figure 4.3: Wick with vapour collecting in patches and depleting the wick of working fluid in the top right corner (150 Mesh with $q = 137\text{kW/m}^2$) (Brautsch & Kew, 2002)

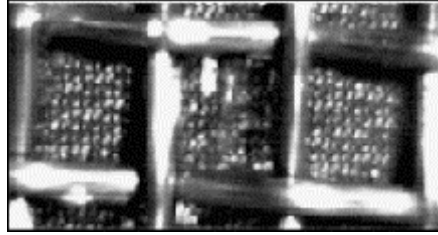


Figure 4.4: Close-up of a bursting vapour bubble (150 Mesh with $q = 137\text{kW/m}^2$) (Brautsch & Kew, 2002)

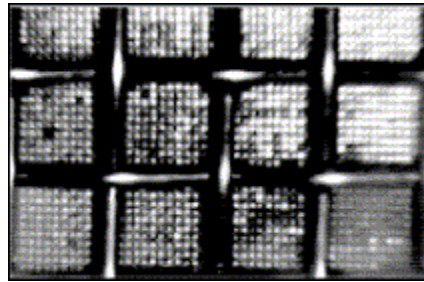


Figure 4.5: Wick with dried out Areas on the top right side (150 Mesh with $q = 152\text{kW/m}^2$) (Brautsch & Kew, 2002)

Based on all the findings from literature presented above it was concluded that the only way to resolve the various differences would be to build some sample heat pipes of each design and then test them. Based on work presented by Kempers, Ewing and Ching (2006) stating that a higher number of mesh layers does not in all cases support the heat transfer rate and general manufacturing experience, two layers of mesh were chosen for the test sample. Further calculation software developed by the author as part of previous work, has been utilized to determine the theoretical optimum fill, and was used to

determine the fill for each design. The fill of each heat pipe was calculated to ensure that the wick is saturated with working fluid. This method has been based on work presented by Imura et al. (1988) and Imura, Kozai and Ikeda (1994) but no provisions were made for over- charging as suggested by Peterson (1994) by 10 to 20%. The main aim of this research was to determine the influence of the wick and optimum thermal performance rather than aim for high yield production heat pipes. All four papers, Kozai, Imura and Ikeda (1991), Imura et al. (1988), Imura, Kozai and Ikeda (1994) and Kempers, Ewing and Ching (2006) state, that they have found very little evidence of negative effect of intermeshing between different layers of screen wicks. That assumption was used for the fill calculations for these heat pipes as well as the assumption that intermeshing is unique to each heat pipe and therefore cannot be considered in theoretical calculations. When carrying out the calculations with these parameters, it was found that the difference in fill between having the 100 mesh wick at the wall and at the liquid vapour interface was minor and only in the range of one thousand of a cc. That value is below the known processing parameters for filling accuracy and venting of around 0.05cc and therefore both sets of heat pipes were produced using the working fluid fill.

4.2.2 Experimental Results And Analysis Of Dissimilar Mesh Wick

Heat Pipe Investigations

The results presented below were obtained using a water cooled test rig with two heater blocks and cold plates of the same design as shown in Figure 4.7 and a schematic indicating the instrumentation used in Figure 4.8. The heater blocks and cold plates were transferring heat into and out of the heat pipe at

the top and bottom face in the horizontal orientation. In order to minimise the number of variables for all the experiments, the heat pipe orientation was kept constant at an angle of 0° (0° tilt angle). On the condenser end of the heat pipe a Lytron RC006 recirculating chiller was used to supply the two cold plates of 1.5" x 2" with a uniform cooling water flow of 25°C inlet temperature and a flow rate of 0.0011/s. The thermal load was introduced into the heat pipe using four electrical DC heater cartridges with a total capacity of 200W. These cartridges were equally spread within the two copper heater blocks in order to maintain an even heat flux at an acceptable level into the heat pipe. The electrical power was monitored using a calibrated power meter whilst the water flow was monitored using a contactless magnetic flow meter which is directly logged via the same software which is used to log the temperatures. Further details of the test rig used as well as some pictures and design considerations can be found at a later stage of this thesis in Chapter 5, where the results of the primary experiments are presented.

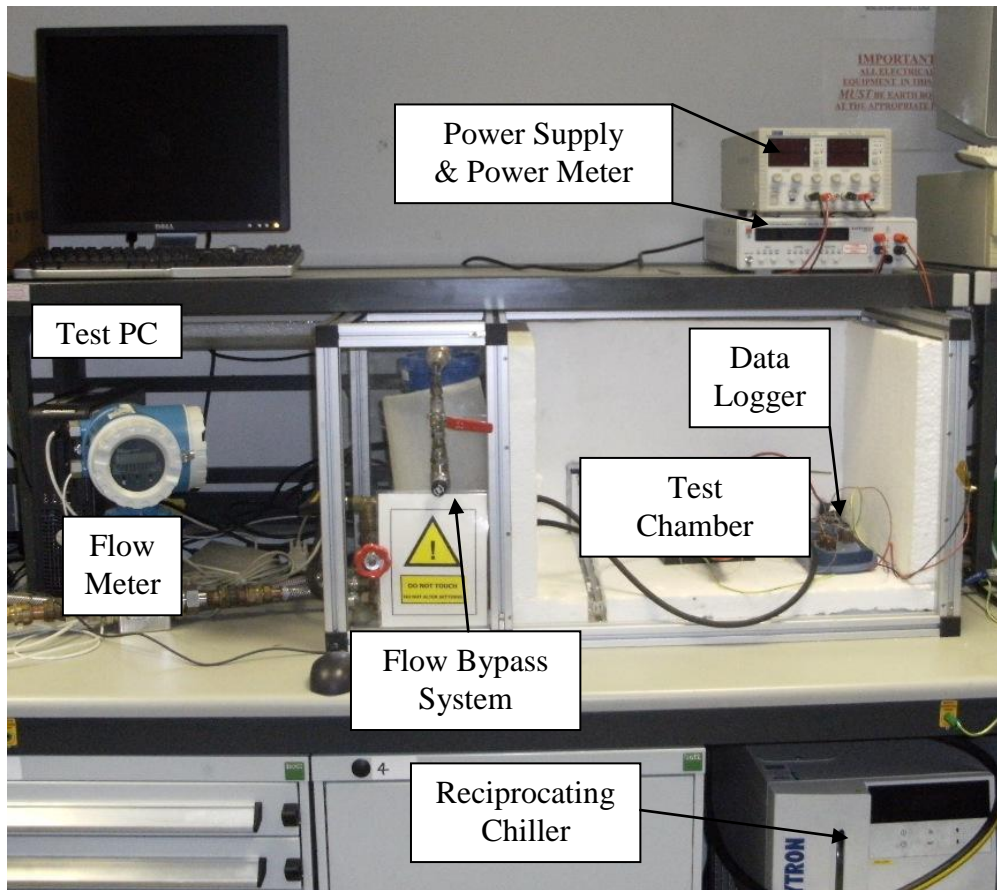


Figure 4.6: Entire Test Rig Setup

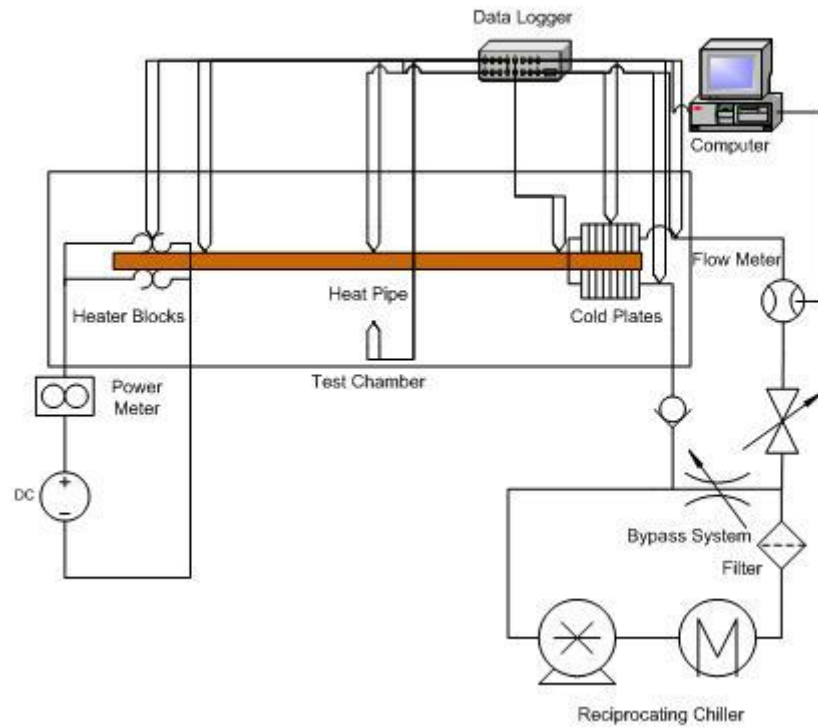


Figure 4.7: Schematic of Test Rig including Instrumentation used

In total eight different temperatures on the heat pipe external surfaces as well as heater and condenser block and inlet and outlet water temperature were monitored. These temperatures were the water in and outlet temperatures, the test chamber ambient temperature, the heater and condenser diameter specific adaptor block temperatures and the temperature on the heat pipe itself right in front of the heater adaptor block, in front of condenser adaptor block and at the heat pipe middle. Wherever in this work references to a ΔT of the heat pipe are made, the temperature difference between the heat pipe temperature right in front of the heater adaptor block and right in front of the condenser block is considered. All heat pipes tested have been subjected to a single pass test where the test conditions bar the heat load were maintained constant. The tests took place in an insulated test chamber as shown without the front and top insulation in Figure 4.6 and the incoming water temperature was maintained at 25°C whilst the outgoing water temperature was measured and used for the calculation of the heat load as described below. In order to be independent from production variations, a batch size of 5 was tested for each design as a single pass test per heat pipe. The results presented in Figures 4.8 are the thermal loads actually transferred by the heat pipes into the water and are calculated using the energy equation (Faghri, 1995):

$$Q = \dot{m} * c_p * \Delta T \text{ (Eq.4.18)}$$

All the results presented are clear of any heat losses to the ambient and losses across interfaces. Therefore, the thermal load results are lower than the values for the electrical loads applied to the heater cartridges. The results presented in Figure 4.9 show the average values per heat pipe type obtained from the individual results presented in Figure 4.8.

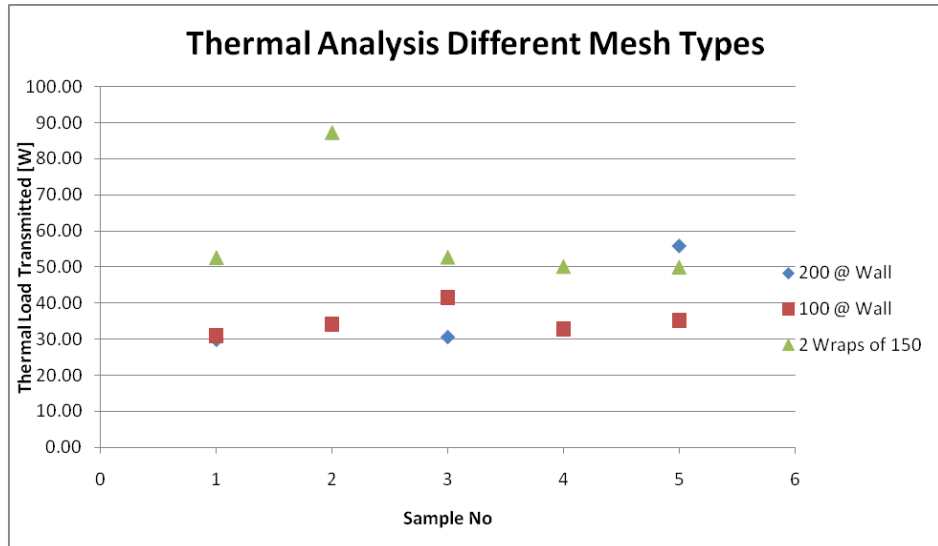


Figure 4.8: Thermal load transmitted per sample and wick structure

From the results presented in Figure 4.8 above it can be seen that the conventional two layers of 150 screen mesh wick heat pipes have, apart from one exceptionally good pipe, a very consistent performance over the entire batch size, whilst the other two designs appear to be more susceptible to process variations. The sample 2 with 2 wraps of 150 Mesh seemed to be performing significantly better than the other samples of that particular design. The recorded transmitted thermal load is about 70% higher than the average obtained from the rest of the results for that design and has therefore a significant influence on the average thermal load value for that design. This fact cannot be neglected and makes that design type look particularly attractive whilst in reality this may not be constantly maintainable for larger batch sizes of that heat pipe type.

Both dissimilar screen mesh wick combination heat pipe types would need some more process refinements to achieve their performance consistently. For the 200 screen mesh wick at the wall design, only three heat pipes out of the batch of five could be tested and judged using conventional criteria whilst heat

pipes 2 and 4 appeared to have Non-Condensable Gas (NCG) present. This has resulted in a ΔT along the adiabatic section of around 10- 12°C and was lowered towards 7°C for higher power levels when the dry-out of the evaporator section occurred. The reduction of ΔT with rising power levels was seen as being linked to the extension of the condenser length where the NCG is compressed by the rising vapour pressure and therefore more thermal load can be transferred out of the pipe at a risen power level.

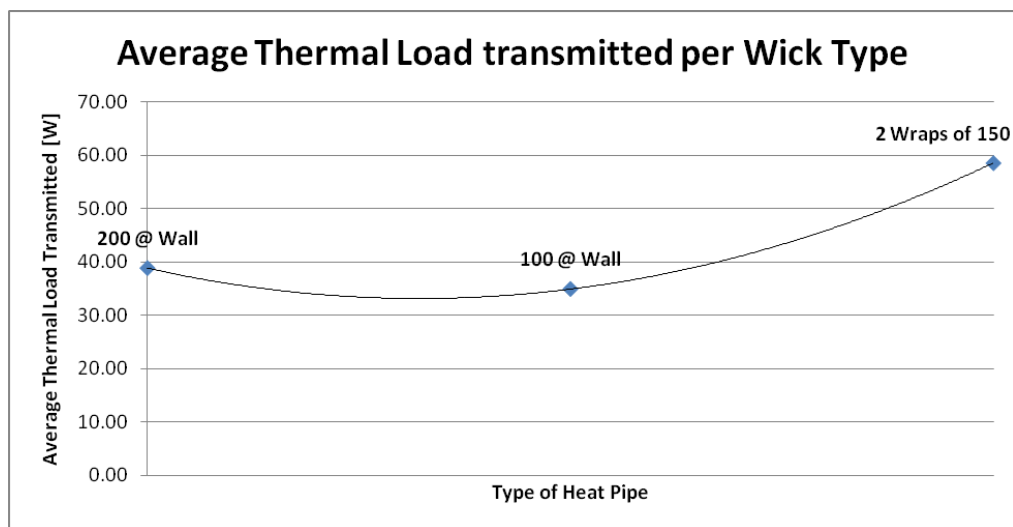


Figure 4.9: Average thermal load transmitted per wick structure

From Figure 4.9 above, it can be seen that the 200 screen mesh wick at the wall combination offers a marginally superior performance over the 100 mesh at the wall combination but both are still below the performance of the well established two layers of 150 screen mesh wick heat pipes. The reason for that is seen due to the fact that heat pipes with two layers of the same screen mesh have been produced in volumes of several hundred thousand to millions, whilst the combination of two different screen wicks is still in its infant stage and has not left the area of R&D applications yet. Furthermore, a statement by Imura, Kozai and Ikeda (1994), states that the effects of intermeshing between

two screen layers has to be proved for heat pipes with two different screen mesh layers inside.

The results presented above do not emphasise the fact that all the working heat pipes with 200 screen mesh wick at the wall had a significantly lower ΔT between the evaporator and condenser section and would therefore present an advantage over the 100 screen mesh wick at the wall.

The results of the experimental analysis with respect to ΔT can be found in table 4.1 below, which represents the analysis of the runs at a power level which has been successfully completed as a stabilized run (1h duration) by all heat pipe samples. For all of the 100 Mesh at the Wall samples the power levels for these runs were lower by one 10W increment than for the heat pipe with two wraps of 150 Mesh and the 200 Mesh at the Wall samples bar one containing NCG.

Heat Pipe ΔT	150 Mesh	200 @ Wall	100 @ Wall
Sample 1 [°C]	0.25	2.52	5.58
Sample 2 [°C]	0.32	7.38	5.80
Sample 3 [°C]	2.12	4.82	12.96
Sample 4 [°C]	0.78	9.9	10.78
Sample 5 [°C]	0.15	2.10	6.28
Average [°C]	0.72	5.34	8.28
STD [°C]	0.82	3.30	3.38

Table 4.1: ΔT Results for all Heat Pipe samples including Standard Deviation

The results of table 4.1 can be found in graphical form below as figure 4.10. It has to be pointed out that all samples with dissimilar wick inside have a higher ΔT than the conventional benchmark samples with two wraps of 150 Mesh, however non- NCG samples (1; 3; 5) of the 200 Mesh at the Wall type have a lower ΔT than the 100 Mesh at the Wall type. Further it can be clearly seen that these samples of the 200 Mesh at the Wall type as well as all conventional benchmark samples remain below the 5°C limit used for the experimental

analysis in chapter 5; whilst all samples of the 100 Mesh at the wall have ΔT values above this limit.

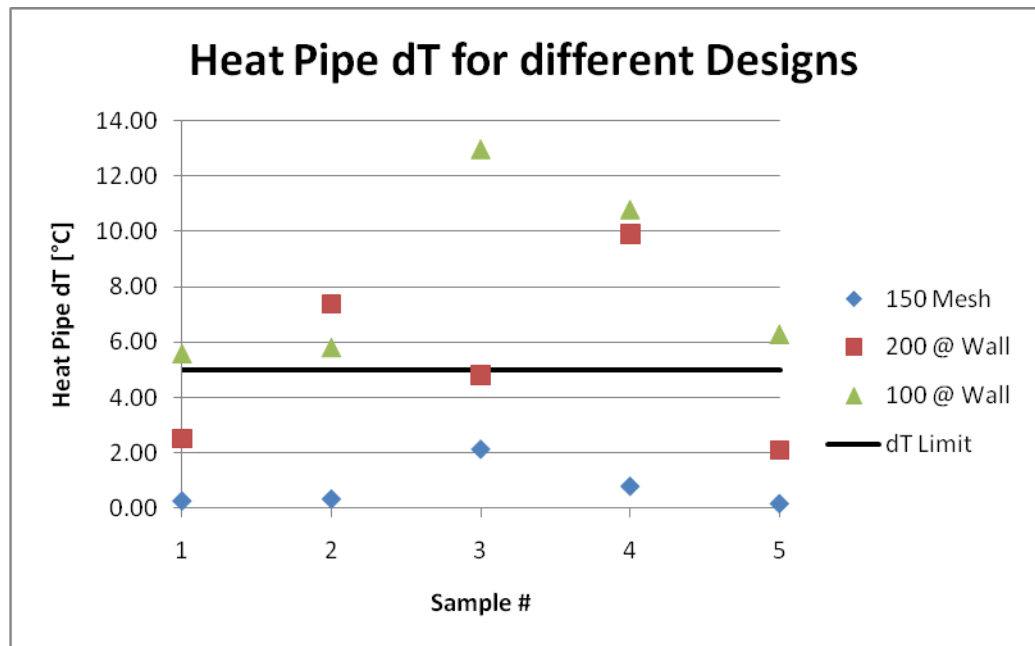


Figure 4.10: ΔT Results for all Heat Pipe samples including limit

The reasons for this trend and the fact that the 200 Mesh at the Wall samples are performing better than their 100 Mesh at the Wall counter parts are relatively hard to prove as the amount of produced and correctly working heat pipes of the 200 Mesh at the Wall design was low, whilst the failure rate out of that batch was very high at 40%. Further the failure modes of all the heat pipes tested were different and could not be compared directly. For more definitive proof, additional process and fill optimisation tests as well as experimentation is required to clearly outline the advantages of having the finer wick aligned on the wall. The additional direct comparisons of results of experiments for heat pipes with two layers of the 100 screen mesh wick and 200 screen mesh wick would complete this work and might be presented at a later stage in a different format.

4.3 CONCLUSIONS

In this chapter, different combinations of screen mesh wick types were experimentally compared and some potential for screen mesh wicks with higher mesh numbers was found. Based on these findings and additional work optimising the fill and manufacturing processes the possibility of tailoring screen wick heat pipes towards certain industrial applications is envisaged.

However, there has to be a significant amount of additional work to be undertaken, before dissimilar screen mesh heat pipes can reach the same maturity as “normal” screen mesh heat pipes with layers of the same mesh inside. This can be seen through the fact that, despite all the theoretical considerations presented within this chapter, the performance in terms of power handling for both types of dissimilar screen wicks was very close together and no significant conclusions can be drawn from that yet. Further it has to be considered, that only three of the 200 Mesh at the wall samples could be used for the analysis of the test results as the other two had shown the presence of NCG and no definite failure power level could be determined. Therefore these results are seen as a bit weaker than for the batch of five heat pipes with the 100 Mesh at the wall. Despite the drawn back and lack of distinctive results at this very early stage, it should not be concluded that screen mesh wick heat pipes with dissimilar mesh wicks inside do not have potential but it should be aimed to prove their potential through continuation of this work.

CHAPTER 5 – BENDING OF SCREEN WICK HEAT PIPES

Within this chapter theoretical investigations guiding towards the finalized design of the heat pipes tested, and the results obtained during the experimentation, will be presented. This chapter contains four major sub-sections, the first one starts with some preliminary work carried out to identify the setup parameters for the CFD runs and theoretical investigation on the effects of bending on heat pipe performance, whilst the second sub section is focused on the design of the test rig used to obtain the test results presented in analysed form within the third sub section of this chapter. Within the first section, various approaches on how to numerically capture the effects of bending on the reduction of heat pipe performance are described. The second section describes the design process of the test rig used for the experimentation in great detail. The third section contains a detailed analysis of the experimental results including failure modes seen during the experimentation, plus the trends of performance reduction obtained from the experimental runs. Further these results were compared to the CFD results obtained in the first sub section. The fourth sub section is presenting an approach to utilize the experimental results to develop an equation to predict the performance of bent heat pipes.

The conclusions will describe why a numerical approach alone will never fully capture the phenomena that can occur within a heat pipe which has been subjected to bending, and in particular when the wick structure is a screen mesh.

5.1 FLOW SIMULATION THROUGH PIPE BENDS USING CFD SOFTWARE

This section presents an approach to simulate the effects of bends in heat pipes. This work was undertaken after other approaches using different commercial codes as well as self-programmed codes failed. All the undertaken approaches failed to prove the capability of providing the required accuracy. A number of different pipe geometries were investigated using the same settings and models as used by the commercial CFD software. In total, five different geometries were investigated. They were a straight pipe and pipes with bend angles of 45°, 90°, 135° and 180°.

A commercially available CFD software named Star-CCM+ from cd-adapco, a competitor of FLUENT, was used to carry out the investigation. This software had to face the same challenges that other software like Fluent and ICEPAK also struggled to compute. Star-CCM+ has its origin in the automotive and oil and gas as well as offshore industry and offers in comparison to FLUENT enhanced meshing and CAD geometry import capabilities. The initial shape of the flow body (water film) investigated was modelled using a CAD software called SolidWorks and then introduced into Star-CCM+ via STEP CAD files, which could then be directly imported and converted into solvable flow domains.

The main challenge was not the geometrical shape, but more the very thin thickness of the water layer used in heat pipes. In order to be able to compute

the solution, theoretical assumptions simplifying the geometry had to be undertaken. These followed well known heat pipe theory and will be described in greater detail in the following sections of the chapter.

Through the progression of this chapter it will be outlined why CFD on a thin film layer is very complicated and the results have to be reviewed carefully. The various reasons why this is the case will be shown clearly.

Multiple CFD runs with various geometries and different model settings, as well as different flow speeds, have been conducted in order to present a rounded work package and validate the various models. It was found difficult to model all the flow conditions to include all the required settings. In this report only selected cases are presented, along with the theoretical part of work carried out regardless of whether it was finally implemented into the CFD software or not. This is included as it provided vital information required for understanding the flow regime within a heat pipe.

5.1.1 Introduction Into Separate Phase Modelling Theory

In order to investigate the influence of bends on the performance of heat pipes, a separate phase modelling approach was taken as currently there is no mathematical model available representing the countercurrent liquid –vapour interaction accurately.

It was assumed that the bend will occur in the adiabatic section of the pipe so no heat transfer with the external environment occurs. Deriving from first principles, the liquid film height was calculated for a certain operating

condition, and from there further calculations of the flow conditions like the Reynolds number, Fanning friction Factor were taken. Attempts were then conducted to accurately convert the results into an equivalent surface roughness to represent an interface wall for the CFD model.

This was then used to calculate the power handling performance using the results obtained from commercial CFD code based on the Star-CCM+ solver engine from cd-adapco. The newly obtained results were then used to compare the actual heat pipe limits with the mathematical model presented by Riffat et al. (2004). This model allows the prediction of the operational limits in a steady state condition, whilst transient start-ups of the investigated heat pipes are much more complicated. From these limits a performance degradation trend was hoped to be achieved.

For reasons of simplicity plain copper tube with no wick was modelled to easily obtain a trend reflecting the effect of bends in a heat pipe. An attempt was made to replicate the vapour- water interface using a wall including a friction factor, which had to be determined before being used. This did not prove to be successful since both roughness heights combined were found to be greater than the actual film thickness obtained. This was due to inaccuracies in the mathematical models used. Therefore a slip wall approach was then undertaken. A separate phase modelling approach is a fairly common technique used by the chemical industry but does not appear to have been applied to this particular area of research.

5.1.2 Separate Phase Modelling

Separate Phase modelling is a widely used approach to investigate certain areas of interest in fluid flow as well as utilizing the limited capabilities of today's CFD code on Two Phase Flow, especially if it is in countercurrent. The most common approach to solve the thermo-hydraulics of single phase, and especially the more complicated two-phase, flow models is separate phase modelling. Typical characteristics of two-phase flow models are that they treat the flow as steady, with a simplified geometry of the investigated flow structure. They also use the conservation of mass, momentum and energy to predict the thermodynamic properties of the flow.

The attractiveness of this type of model is their broad applicability as well as being able to be used with 1-D models as well as 2-D models (Fu & Klausner, 1997). Further to this the 1D- model approach has been known for some time and was introduced by Hewitt and Hall-Taylor (1970 cited in Fu & Klausner, 1997), who widely discussed the ability of these models.

The approach taken for this work was one of separated flow 1-D models for the vapour core and liquid film and then coupled through closure relations applied to the liquid vapour interface. This was attempted and shown as a wall in the CFD model.

In many cases of previous works the interface between the liquid and the vapour of air are treated as hydraulically smooth which means that they are considered not to add any additional friction to the flow. It will be shown later in this work why this had to be adapted, as had been done by fellow researchers.

The ultimate aim of the work carried out was to develop a simple easy-to-use tool to predict the performance, and performance degradation, of heat pipes under various operating conditions as well as being subjected to shape changes.

5.1.3 Calculation Of Flow Parameters

5.1.3.1 *Liquid Film Height Calculation*

In order to predict the liquid height/ film thickness in the adiabatic section, where the bends are assumed to take place, it was assumed that the heat input in the evaporator section is only through the wall of the tube. Following well established models the assumptions were made that the liquid film thickness is uniform around the wall as well as the flow is steady. Further, no change of thermodynamic properties, like extra evaporation within the adiabatic section and a uniform radial pressure, are assumed.

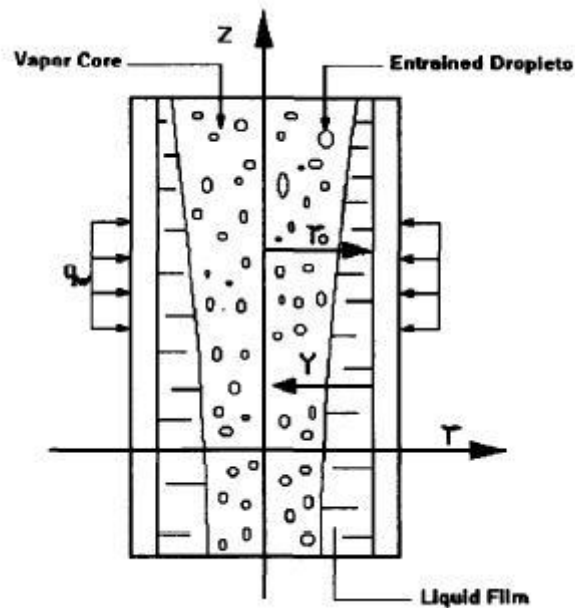


Figure 5.1: Scheme of Liquid Film Height (Fu & Klausner, 1997)

The starting point for this calculation was the Conservation of Energy equation which states that $Q_l = Q_v$. From there, the Continuity equation was introduced to this which states $\rho_1 * A_1 * u_1 = \rho_2 * A_2 * u_2$ (Hewitt, Shires & Bott, 1994). In order to be able to resolve this equation, further assumptions were required in absence of known operating conditions for the heat pipe. Therefore, it was assumed for simplicity reasons that the velocity of the vapour is equal to the velocity of the liquid, $u_l = u_g$. This supports the closed loop system theory for a heat pipe and allows the use of the separate phase modelling theory, which was used to determine the pressure drop difference due to a change of geometry.

Introducing these two statements into the continuity equation, plus applying it to the two fluids involved in the problem investigated, guides towards the derivation of equation 5.1 shown below.

$$d_i = d_o * \sqrt{\frac{\rho_l}{(\rho_l + \rho_v)}} \quad (\text{Eq. 5.1})$$

In order to be able to obtain accurate data for the previous equation, the equation 5.2 below has to be applied to data from the reference books (Houghton & Brock, 1975; Rogers & Mayhem, 1995).

$$\rho_v = \frac{1}{v_g} \quad (\text{Eq. 5.2})$$

Applying these two equations guides towards a liquid film height, which is dependent on the temperature of the surrounding wall. Therefore it is shown that the liquid film height for a given diameter of tubing is dependent on the wall temperature and that the flow regime is largely depending on that input, as well as the assumed velocity in the pipe. It was proved that this liquid film height is below the peak height of the surface roughnesses and can therefore not be used for numerical computation. Instead, the wick thickness where the working fluid returns was intended to be used for computation of the pressure required to overcome the bend. This will be described in greater detail in section 5.1.4 of this chapter.

5.1.3.2 Reynolds Number Calculation

The dimensionless Reynolds number used in fluid mechanics is an indicator for the flow regime applicable to a certain set of conditions in pipe flow. Being one of the most important dimensionless numbers used in fluid flows, it provides a criterion to determine dynamic similitude of different flows. Unequal flows of different liquids can have the same Reynolds numbers,

whilst the liquid velocity and the pipe diameter are different, but the behaviour is judged dynamically similar.

The Reynolds number is physically the ratio of inertial forces to viscous forces and therefore consequently quantifies the relative contribution of these two types of forces to a certain flow regime. Inertial forces in pipe flow are represented by mean fluid velocity multiplied by density of fluid whilst the viscous forces are incorporated through the ratio dynamic fluid velocity divided by the hydraulic diameter. As heat pipes are most commonly round and the hydraulic diameter for that geometry is equal to round pipe diameter, this was used. Further considerations need to be taken into account for other shapes like stadium shaped pipes.

There are three main flow regimes occurring within pipes: For very low Reynolds numbers, which are smaller than 2300, the flow is laminar. Laminar flow is characterized through smooth, constant fluid motion. At this flow regime, viscous forces are the dominant ones. The more common flow regime in pipes potentially used as evacuated containers such as heat pipes, is the turbulent flow regime. This is considered for Reynolds numbers bigger than 3000 where inertial forces dominate the flow. Within this flow all sorts of flow fluctuations like vortices and random eddies can occur. This flow regime can be completely described mathematically. The most complicated flow to describe scientifically is the transient flow for Reynolds number regions between 2300 and 4000. The exact transition can only be determined through experiments of the flow conditions for each particular case. In order to avoid

that sort of problem the Reynolds number range between 2300 and 4000 where the flow is neither fully laminar nor fully turbulent is generally avoided when designing a system. For circular pipes as often used for heat pipe applications the transition is around 2300. At this point the flow is dependent on the pipe diameter as well as the mean velocity in the pipe. Deriving of this equation will guide towards the equation (Eq. 5.3) used below for calculating the Reynolds number for the application simulated.

The Calculation of Reynolds number is a straight forward calculation following the equation proposed by Osborne Reynolds (1883):

$$\text{Re} = \frac{\rho_l * u_l * d_h}{\mu_l} \text{ (Eq. 5.3)}$$

In order to use the available data for the two liquids involved in the simulation, the properties of water and air were assumed in order to simulate the vapour. Where properties like kinematic and dynamic viscosity are not both available at the same time, the missing parameter can be calculated using the following equation:

$$\mu_l = \rho_l * \nu_l \text{ (Eq. 5.4)}$$

The density of the working fluid as a temperature dependent variable is obtained from the following reference data books (Houghton & Brock, 1975; Rogers & Mayhem, 1995). The tables of Rogers and Mayhem (1995) are widely used in any thermodynamic area and were applied as source for the base material data for that very reason. As the average velocity was seen as an unknown value, which can vary from very low values up to sonic velocity for the vapour flow, a velocity was chosen which places both flows into the area

of turbulent flow. In order to keep the thermodynamic cycle working and to justify the assumption that the separated flow modelling the vapour velocity was equal to the velocity of the water travelling into a countercurrent direction.

For the calculation of the Reynolds numbers of the flow an average surface roughness for drawn Copper tubing, which is widely used as container material for heat pipes, was assumed to be 0.0015mm (Anon, 2005). As shown by Romeo, Royo and Monzó (2002), this might introduce an error into the calculation, but this error seems to be negligible in consideration of the accuracy of currently available CFD codes.

Further percentages of the error introduced can be found in Fig. 5.2 below.

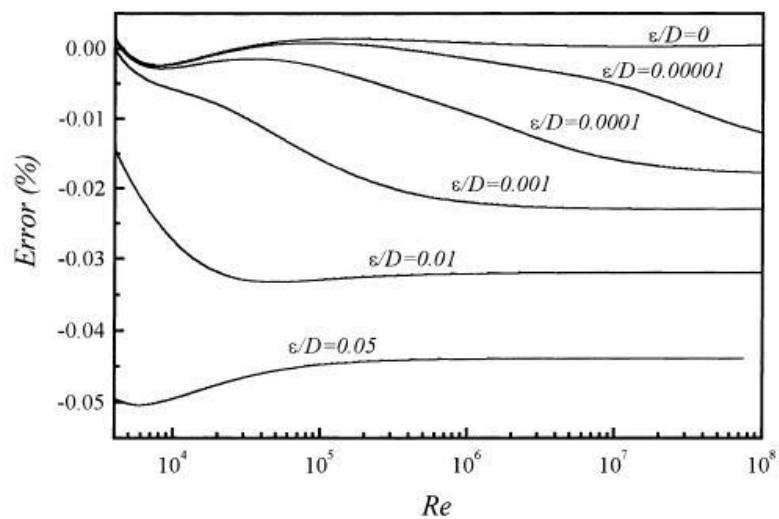


Figure 5.2: Error in dependence of the Reynolds number (Romeo, Royo & Monzó, 2002)

It can be seen clearly from this figure that the introduced error is less than 0.1% and so small that it will not have a significant influence on the overall error occurring when carrying out this numerical iteration. Due to different definitions of the different parameters, it has proved to be impossible to finally convert the equivalent surface roughness of Romeo, Royo and Monzó (2002)

into an equivalent surface roughness as per definition of Figure 5.4 of this chapter, where it is a geometrical value of the boundary of the fluid passing along it.

5.1.4 Theory Used For Obtaining The CFD Settings

In order to be able to obtain the CFD boundary settings for Star – CCM+, the following theoretical approach was undertaken to gain the values used as inputs:

1. The maximum axial velocity in the adiabatic section, where the bend is, was obtained following a method proposed by Zhu and Vafai (1999). The use of this method has guided towards the following equation:

$$u_l(x) = \frac{Q}{\rho_l * \pi * h_{fg} * (r_w^2 - r_v^2)} \text{ (Eq. 5.5)}$$

This equation was derived by implementing equation (9) and (23) into equation (21) of the work of Zhu and Vafai (1999). In order to be able to solve the equation, the maximum transmittable power Q was obtained through the use of Thermacore priority software and has worked out to be 176 W for a pipe of the same geometry and orientation. Implementing this as well as all the other parameters leads towards a maximum axial liquid velocity of 0.0122m/s. In order to deal best with the settings in the CFD software this was converted into a mass flow rate of 0.000179kg/s, which was set as a boundary condition in the mass flow inlet face for the first case with annular flow.

For second case with full flow the same liquid velocity was used but due to the changed geometry it has guided towards a new mass flow rate of 0.001241kg/s. For all cases, the interfacial effects between liquid and vapour have been neglected.

From Figure 5.3 it can be seen that the accuracy of that assumption is seen appropriate for settings implemented into CFD code:

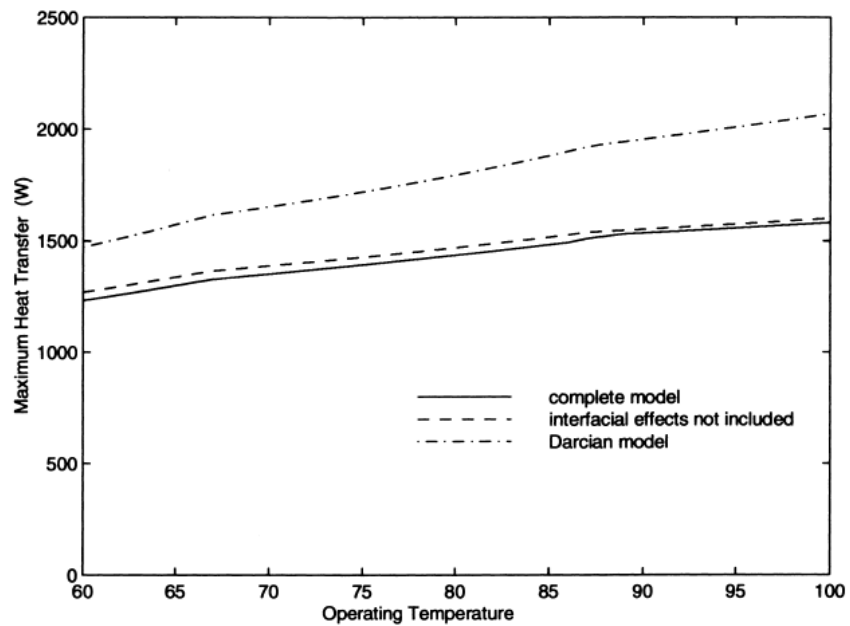


Figure 5.3: Comparison of the models including and excluding interfacial effects
(Zhu & Vafai, 1999)

Following these results the internal wall boundary has been set to be a friction-less slip wall and has no significant influence on the flow, apart from guiding the liquid along the geometry. This setting is a standard within CFD code like Star- CCM+ for investigating pressure drops within geometries.

2. The outlet is set to be a pressure outlet and the pressure at the outlet was set to be 0.2501bar. This is equal to the saturation pressure for

65°C temperature. Assuming a perfect vacuum in the pipe this is the minimum pressure in a fully operational pipe at that temperature. Therefore this assumption can be seen as perfectly valid following the theory of heat pipes.

3. The external wall is set to be a rough wall with a surface roughness of 0.0015mm which is a common value for drawn copper pipe as used for heat pipe container material. The surface roughness was obtained from an engineering web source for drawn copper pipe (Anon, 2005). In this application a constant surface roughness as per definition of Engineer's Edge (2006), flat along the length of the wall, is assumed.

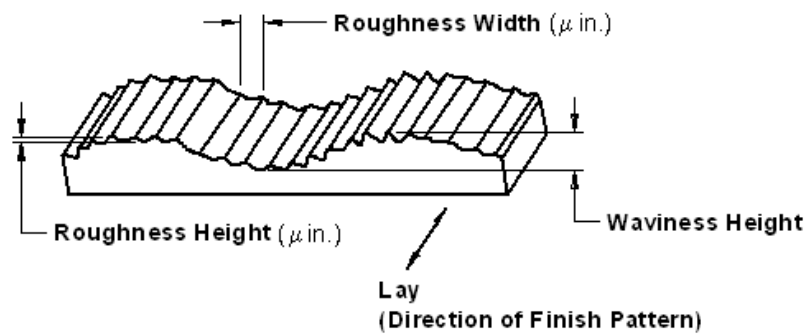


Figure 5.4: Definition of Surface Roughness Height (Engineer's Edge, 2006)

The effects of different surface roughness have been investigated by Romeo, Royo and Monzó (2002) but this investigation was only conducted on straight pipe samples with a full flow regime rather than only a thin layer of water along the wall. Therefore, their approach cannot really be seen representative for heat pipe applications.

4. In order to take the different evaporation and condensation rates along the evaporator and condenser length into account, the theory of the effective length was used. This means that only half of the evaporator and half of the condenser length will be added to the adiabatic length of the heat pipe. This theory is widely used in heat pipe applications (Reay & Kew, 2006) and was used in this application in order to get rid of the very sharp edged triangular feature as shown in Figure 5.1 at the evaporator and condenser end of the pipe. This allowed a far more solid and solvable geometry for the CFD software before meshing. It also guided towards a far better grid, as it limited the number of cell types down in that area towards rectangular ones which can be much easier solved than others. Figure 5.5 shows the achieved grid as well as the prism layers.

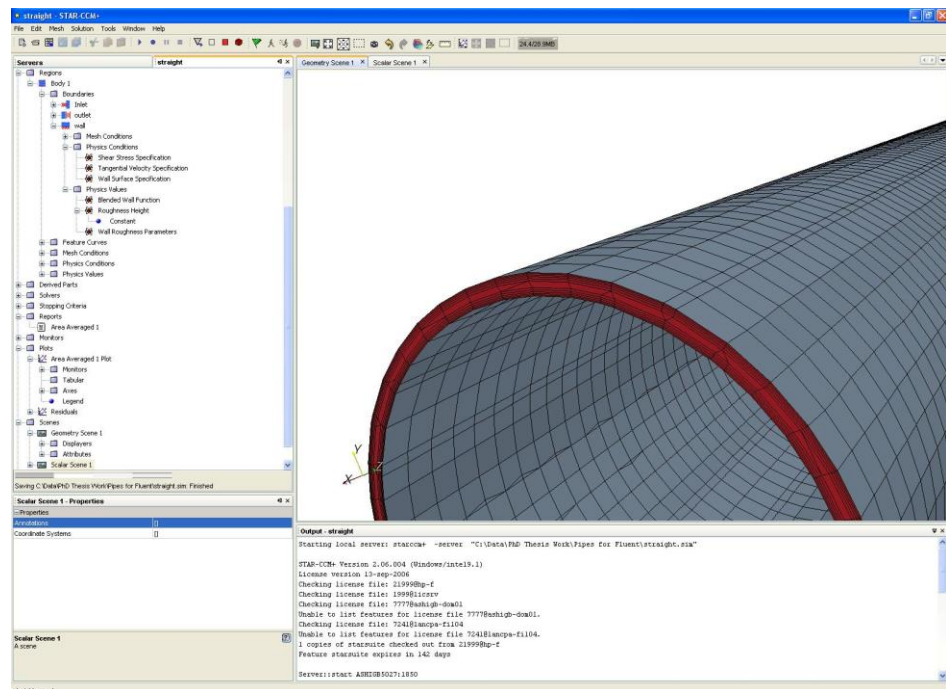


Figure 5.5: Mesh quality and Prism Layer number

5.1.4.1 Flow Models and Boundary Conditions used

In order to obtain meaningful results multiple runs with different settings were performed. These varied from the theoretical settings in order to overcome the lack of mathematical models of dealing with the real time situation in the heat pipes.

5.1.4.2 Settings as per Heat Pipe Theory disregarding Validity of Mathematical Models for certain Flow Conditions

For the simulations carried out, all different geometries replicating the bent heat pipes were investigated using the same settings and models in the CFD software, allowing a direct comparison of the results and show the performance difference due to the bends. The only variation between the different simulation cases was the freshly imported CAD geometry. This was introduced into the CFD software via STEP files.

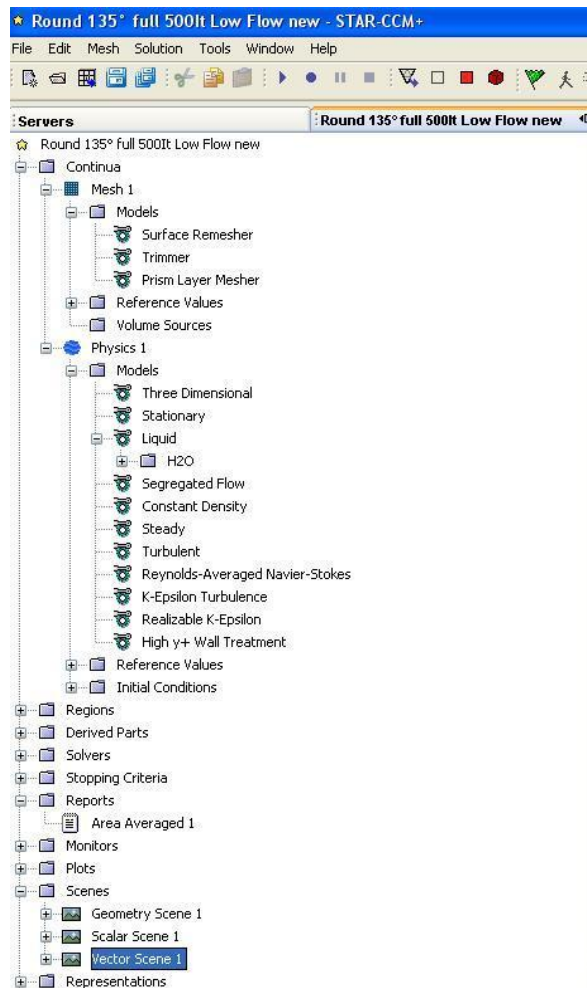


Figure 5.6: Meshing models and Physics models used

Figure 5.6 shows the actual models used for the simulation, both the Physics models specifying the fluid used for the simulation, as well as the meshing models, used to create the grid. The grid generated is shown in Figure 5.5, whilst all the settings used can be found in a table format below as table 5.1.

Common CFD Settings used for both Flow Types

Meshing Models:	
	Surface Remesher Trimmer Prism Layer Mesher (Setting 5 Prism layers at T=0.1mm max)
Physics Models:	
	Three Dimensional Stationary (instead of moving Coordinate System) Liquid (H2O) as per Working Fluid in Heat Pipe Samples Segregated Flow Constant Density Steady (instead of Transient) Turbulent Reynolds- Averaged Navier- Stokes K-Epsilon Turbulence Realizable K-Epsilon High y+ Wall Treatment
Boundary Conditions:	
Inlet:	
	Inlet Temperature set at 65°C Constant Mass Flow set to reflect Mass Flow Rates for: Annular Flow: 0.00018kg/s; Full Flow: 0.00124kg/s Inlet Pressure is the obtained Parameter
Outlet:	
	Pressure Set to be 25010Pa (Saturation Pressure at 65°C)
Outside Wall:	
	Surface Roughness: 0.0015mm (for Drawn Copper Tube) Wall Temperature to be set at 65°C
Inside Wall:	Annular Flow only
	Set to be a frictionless "Slip Wall" used for Fluid Guidance

Table 5.1: Models and Boundary Conditions used for CFD investigation

Table 5.1 above lists all the models and boundary conditions used to obtain the results for the two different flow types run and presented at a later stage of this chapter. The meshing models used were the Trimmer type in order to improve and make the imported CAD geometry more handlable. The Surface Remesher was used to improve the initially generated surface mesh before the volume mesh was generated. The Prism Layer Mesher was an essential tool to be used for this simulation due to this part geometry.

As the emphasises of this investigation was on the effects of the bends onto pipe performance, it was seen vital to have a high number of prism layers in order to be able to get accurate results of the pressure required in the inlet section. This pressure was required in order to overcome the effects of the wall surface roughness, as well as the effects of the bend itself. Even if the flow is laminar, a turbulent model has to be used in order to be able to set up a wall surface roughness, as the laminar model does not allow any wall roughness to be set up. From the available models the k- ϵ turbulence model was chosen. In accordance with the work of Lacasse, Turgeon and Pelletier (2004), this model is capable of delivering adequate results as long as the geometry is not too complicated.

Even with geometry to be seen relatively simple, due to the bends, a Three-dimensional model had to be used. A large proportion of the remaining Physics models guided towards themselves with regards of the conditions within the heat pipe to be investigated. As the most common working fluid used for heat pipes is water, the liquid investigated representing the working fluid had to be water. Per heat pipe theory, no heat transfer takes place in the adiabatic section, where the bends are located. Therefore the use of a constant

density model with changing geometries replicating the bent heat pipes was seen adequate for these simulations. As per separate phase modelling theory, it was entirely focussed on the liquid phase (water flow along the heat pipe wall) and circulation as occurring inside a heat pipe was represented through the constant mass flow rate into and out of the control volume (geometry used). Further the choice of the k- ϵ turbulence model has led itself towards more settings in the software which were exclusive defaults for the model used. Assumptions made previously have been used in the same way as CFD analysis of flows in pipes has been conducted by Fu and Klausner (1997). The main difference was the geometry and diameter of the pipe. Most applications previous investigated are from the field of chemical engineering. Therefore the pipe diameters investigated as well as the flow regimes can not be directly linked to heat pipe applications since in chemical engineering pipe diameter are rather large and flow regimes are mostly turbulent .

In order to improve the run time and the accuracy, this model setup followed and approach by Löhner et al. (2006), where it was emphasised to use the steady state solver as well as reduce the pressure iterations. As the inlet pressure required for overcoming the wall resistance was the criteria investigate, this step towards run time reduction of the model has not been undertaken. But already the use of a steady state solvers, as well as different other setups reduced the runtime of the model down to about 45min. This can be seen as adequate for a model with a similar mesh count used on a standard PC (Cd-adapco, 2007). A further reduction of the runtime was achieved though a reduction of iterations from 1000 down to 500. This was seen adequate as the model converges, depending on the geometry, between 80 and

100 iteration steps. Therefore 500 iterations will give sufficient time to let the model fully reach steady state as well as achieve the engineering values like pressure, to be solved satisfactorily.

Star-CCM+ 2.06 offers a multiphase solver but as the accuracy of the single-phase solver already reaches the limits for a very thin featured object like the one investigated. The use of a multiphase model would have only added towards the results inaccuracies. Added to this there are no accurate predictions of the interfacial friction factors available. Therefore the use of that model has not been seen beneficial and therefore not performed.

5.1.5 CFD Results And Result Plots

5.1.5.1 Results And Plots From Runs Of Annular Flow Per Heat Pipe Theory

Results from Initial Runs in Accordance to Heat Pipe Theory:

Plots for the pressure distribution and velocity of the fluid can be found in appendix A of this thesis whilst the numerical results for the annular flow are presented in the Table 5.2 below:

Analysis of Initial Runs:

Pressure at Outlet P_s 25010 Pa

Bend Angle	Pressure required at Pipe Inlet		dP		Deviation	
0° (0)	25744.07	Pa	734.07	Pa	0.00	%
45° ($\pi/4$)	25732.97	Pa	722.97	Pa	1.51	%
90° ($\pi/2$)	25732.2	Pa	722.2	Pa	1.62	%
135° ($3\pi/4$)	25719.84	Pa	709.84	Pa	3.30	%
180° (π)	25728.15	Pa	718.15	Pa	2.17	%

Table 5.2: Pressure Values as given by the CFD Software

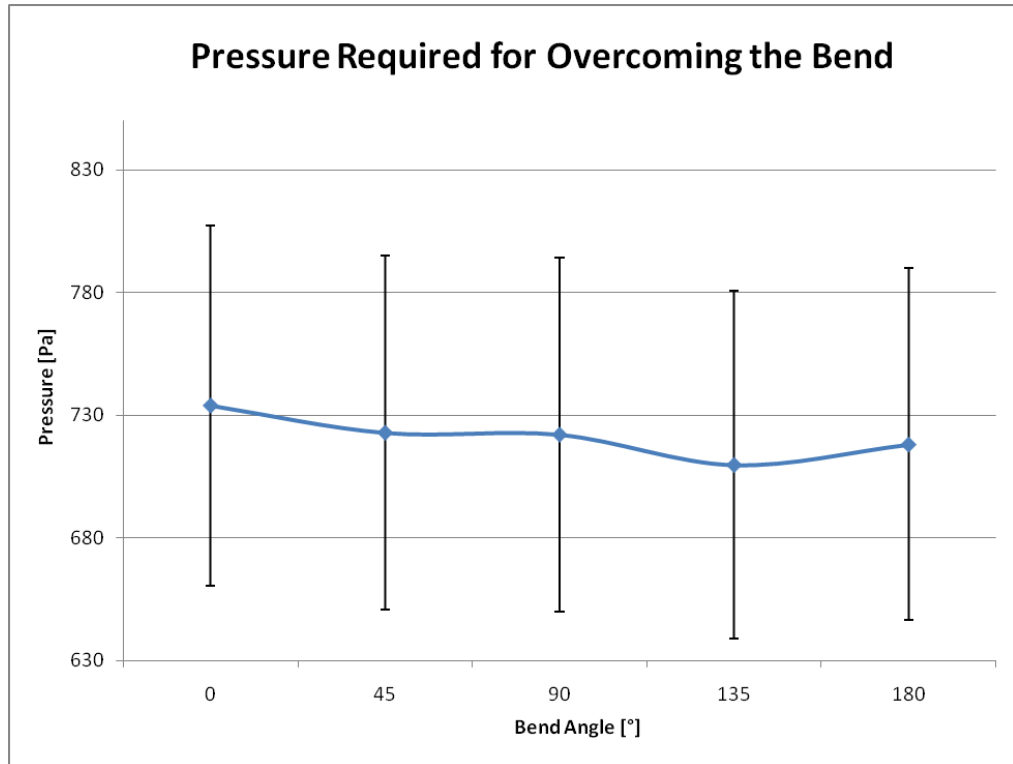


Figure 5.7: Differential Pressure inside the Pipe including the Error bars

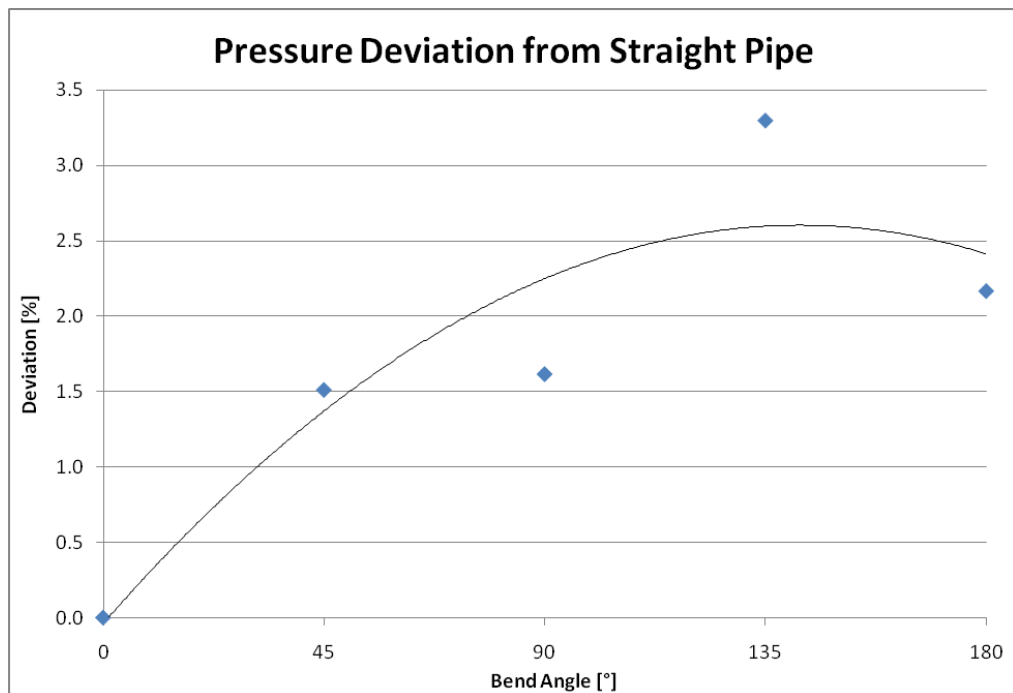


Figure 5.8: Total Deviation from Straight Pipe Value

This analysis and the later one were performed in a way that the deviation within the pipe was assumed to be added to the pressure available on the outlet end of the pipe. This is equal to the saturation pressure for water vapour at the

set temperature of 65°C. For analysis purposes, the value of 0.2501bar or 25010Pa was subtracted after the results of the simulation were obtained. The internal resistance value for the straight pipe was then taken as a 100% benchmark value. All results for bent pipes were then compared to the value of the straight heat pipe and the absolute deviation was obtained. A significant outcome from this was that all the results for the bent pipes were lower than the result for the straight pipe. Numerous re-iterative runs even with new models have been conducted and have proved that result. Therefore it was assumed that the initial geometry cannot be investigated using current CFD software. In order to obtain meaningful results, an approach investigating a full pipe flow with the same liquid velocity was undertaken. These results can be seen in the next section of this report.

5.1.5.2 Results And Plots From Runs Of Full Pipe Flow At Flow Velocity From Heat Pipe Theory

The runs presented are performed with a flow velocity which is obtained from the heat pipe theory but the flow rate is adapted to cater for the larger cross section area that the water is going through. Therefore the mass flow rate was adapted adequately to maintain a velocity of 0.0122m/s and the increased open area of the liquid. Plots for the pressure distribution and velocity of the fluid can be found in appendix A of this thesis whilst the numerical results for the annular flow are presented in the table 5.3 below:

Analysis of Runs with Full Pipe Flow and Flow Velocity from Heat Pipe Theory:

Pressure at Outlet P_s 25010 Pa

Bend Angle	Pressure required at Pipe Inlet	dP	Deviation
0° (0)	25014.16 Pa	4.16 Pa	0.00 %
45° ($\pi/4$)	25014.24 Pa	4.24 Pa	1.92 %
90° ($\pi/2$)	25014.36 Pa	4.36 Pa	4.81 %
135° ($3\pi/4$)	25014.43 Pa	4.43 Pa	6.49 %
180° (π)	25014.5 Pa	4.5 Pa	8.17 %

Table 5.3: Pressure Values as given by the CFD Software

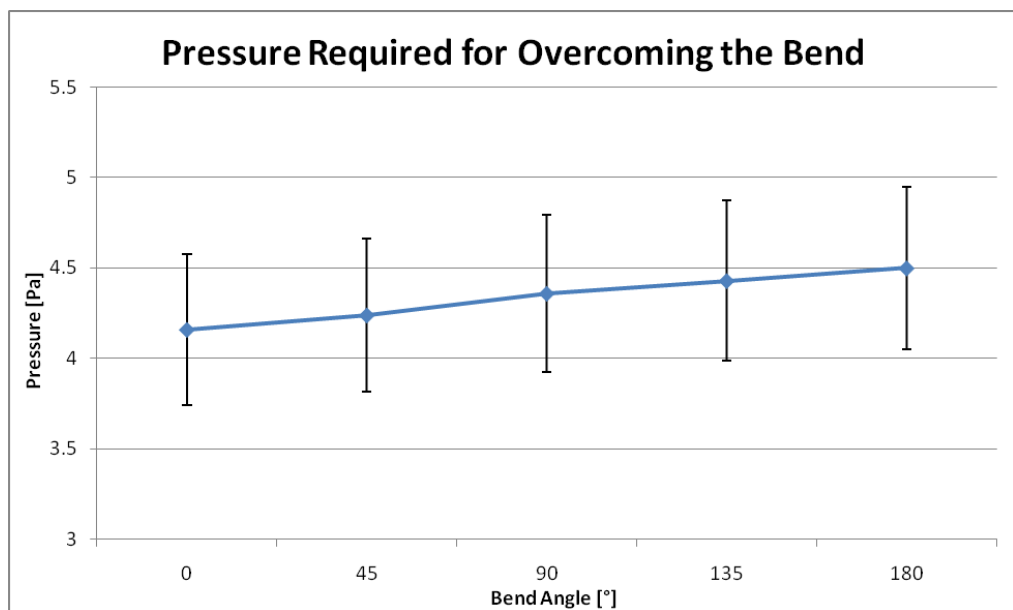


Figure 5.9: Differential Pressure inside the Pipe including the Error bars

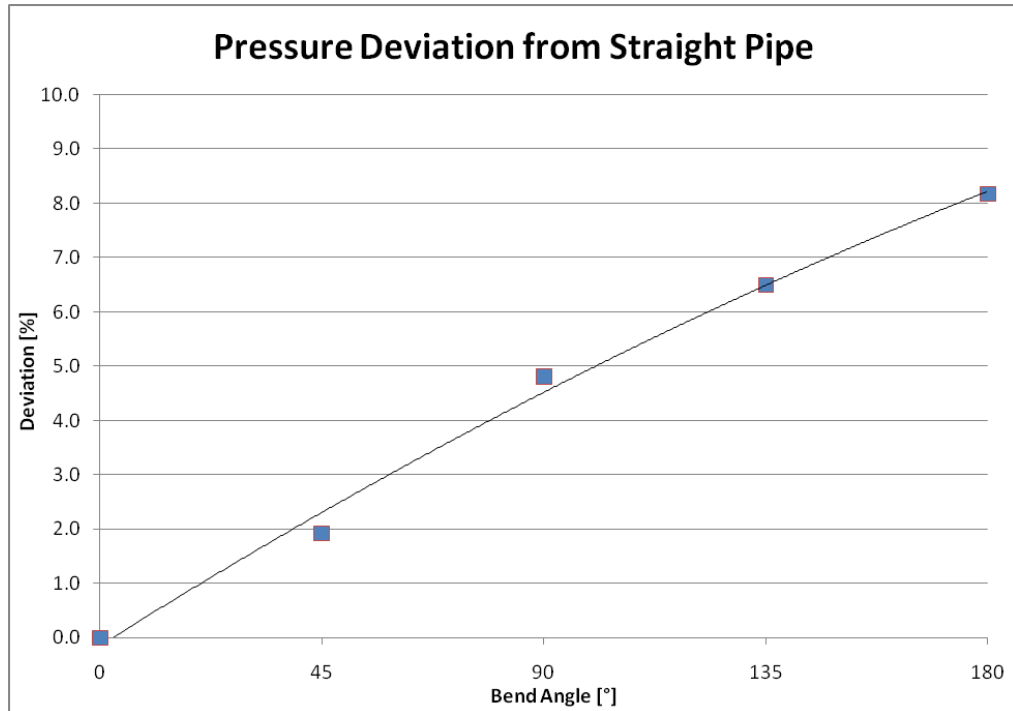


Figure 5.10: Total Deviation from Straight Pipe Value

This analysis shown in Fig. 5.10 indicates that the effects of bends in heat pipes can be investigated using commercial CFD and separate phase modelling but also shows that the performance deviation from a normal round pipe due to changed geometry is very minor. It is in total a deviation of a maximum of 0.34 Pa from a straight pipe to a 180° bent pipe. The results presented in figure 5.9 oppose in a direct way the results presented in figure 5.7, which are seen as unrealistic and conflictive to well known hydraulics theory where bends or elbows increase the pressure drop of the system and should be avoided. Therefore it can only be concluded that the results presented in figure 5.7 suffer from the lack of the ability of current CFD software to cope with the simulation of thin liquid films and can therefore be seen as error loaded. Based on that, the full flow case was used to investigate the effects of bends on the overall pressure required.

Figure 5.9 clearly indicates through the use of 10% error bars that the pressure changes, due to shape changes of the geometry investigated, are minor in comparison to the total achievable accuracy of CFD (Shao & Riffat, 1995).

In reality these effects might be much bigger due to effects described later in the conclusions.

5.1.6 Creating The Link Between The Pressure Results From The CFD Model And The Experimental Results

The key to comparison of the simulation results with the experimental results is the link in between them. In order to create this link and validate the separate phase modelling theory applied for the CFD runs presented above, the heat pipe theory needs to be fulfilled. The key parameter seen responsible for the degradation of the performance in a heat pipe due to bends is the capillary limit or more specially the capillary pressure. The capillary pressure allows the working fluid to return to the evaporator and be available for further evaporation. A reduction in capillary pressure due to a bend would result in less liquid in the evaporator and therefore reduce directly the maximum transmittable power.

Starting this work on the theoretical side guides towards a minimum condition, which needs to be fulfilled in all cases to allow the heat pipe to function, that is the capillary pressure condition (Reay & Kew, 2006):

$$\Delta P_c \max \geq \Delta P_l + \Delta P_v + \Delta P_g \text{ (Eq. 5.6)}$$

Applying the test conditions of 0° operational angle for the experiments allows the following simplification of Equation 5.6:

$$\Delta P_c \max \geq \Delta P_l + \Delta P_v \text{ (Eq. 5.7)}$$

This simplification is seen suitable for both, the CFD runs and the experiments where the conditions were always horizontal. Therefore the wick inside the heat pipe did not have to overcome any gravitational heads. In the horizontal orientation of the heat pipes tested the screen mesh wick only needed to overcome the liquid resistance in the wick and the resistance of the vapour pressure preventing the liquid from returning to the evaporator.

In order to establish the maximum condition rather than the real condition, heat pipe theory has been consulted once more. Starting from equation 5.7 above, the maximum available capillary pressure needs to be known in order to be compared to the liquid pressure and vapour pressure produced. Peterson (1994) states the maximum condition for the capillary pressure to be obtained when the contact angle is zero, this guides towards the following equation:

$$\Delta P_c \max = \frac{2\sigma}{r_c} \text{ (Eq. 5.8)}$$

The value for the surface tension can be obtained from the National Physics laboratory for air to water and are available in the nomenclature. Instead of using the description for the capillary radius provided with the equation, the later and more accurate description for the capillary radius of Kozai, Imura and Ikeda (1991), which has been already used in chapter 3 of this thesis, is used. This guides towards a maximum available capillary pressure for the used wick structure and water as a working fluid at 60°C of 2423.19Pa.

For the liquid pressure drop ΔP_l a form of Darcy's law can be used in accordance to the heat pipe book of Reay and Kew (2006):

$$\Delta P_l = \frac{\mu_l l_{eff} \dot{m}}{\rho_l K A} \text{ (Eq. 5.9)}$$

Equation 5.9 above is seen valid for homogeneous wicks such as screen mesh wicks and is linked to fluid parameters such as the dynamic viscosity, the mass flow rate and the density of the working fluid. These fluid parameters are temperature dependent, but for comparison between CFD results and experimental results a constant temperature of 60°C was chosen to obtain the values, and that assumption was maintained throughout the analysis. The mass flow rate was chosen to be the same as in the separate phase flow model. This was used to obtain the pressure difference in order to be able to have a direct link or chance of comparison between experiments and CFD runs, rather than relating back to the heat pipe theory. Further, there is only one additional parameter, which is the permeability K, required in Equation 5.9 above, which can be obtained from the empirically analysed data presented in chapter 3 of this thesis. The permeability K is defined (Faghri, 1995; Peterson, 1994) as:

$$K = \frac{d^2 * \varepsilon^3}{122(1-\varepsilon)^2} \text{ (Eq. 5.10)}$$

Both, the wire diameter of the screen wick used and the way the porosity of the screen wick is calculated have been presented earlier leaving only additional constants to be added into the equation.

Using the mass flow rate of 0.000179kg/s for the annular flow case guides towards a maximum capillary pressure of 4891.83Pa. For the full flow case the mass flow rate is 0.001241kg/s leads to a maximum available capillary pressure of 33920.31Pa. Since the second value is obtained for a simplified model to increase accuracy of CFD software, this condition cannot be seen as realistic in terms of heat pipe theory and is therefore discarded.

A further description of the liquid pressure inside the wick dependent on the heat load (power) transmitted can be found at equation 2.30 in Reay and Kew's book (2006), which states:

$$\Delta P_l = \frac{8\mu_l Q_{eff}}{\pi(r_w^2 - r_v^2)\epsilon r_c^2 \rho_l h_{fg}} \text{ (Eq. 5.11)}$$

All parameters within the equation are either known or their derivations have been earlier described. In comparison to Equation 5.10, this equation is depending on the transmittable power rather than the mass flow rate inside the heat pipe. Through the link shown in the equation towards the transmittable power, it can be used in two different ways. One is to gain from the flow/pressure drop CFD analysis, a maximum transmittable power for that heat pipe configuration, and the second would be to obtain the liquid pressure inside the pipe from analysis of experimental results. Due to the assumptions made, despite their better logical correlation, the full flow results have not proved to be realistic and do not coincide with the heat pipe theory. Their sole purpose was for increased computational accuracy. However, the pressure drops along the heat pipe wall are unrealistically low with a range increasing from 4.1 to 4.5 Pa obtained through the CFD software. This indicates a transmittable power around 0.75 W, which is not realistic.

Since the calculated differential pressure inside the wick and the maximum available pressure drop are know, only the vapour pressure drop needs to be known in order to be able to quantify if Equation 5.7 is fulfilled. For the vapour pressure Faghri (1995) provides the following expression for the total vapour pressure drop occurring using a “generalised similarity closed-form approximation”:

$$\Delta P_v = \frac{8Q_a \mu_v}{\pi \rho_v h_{fg} r_v^4} * l_{eff} \text{ (Eq. 5.12)}$$

Using values for the vapour constants assuming full saturation from Rogers and Mayhem (1995) guides towards a vapour pressure of less than 1 Pa for all the experimental cases described at a later stage. Therefore the vapour pressure drop was seen negligible to the overall result for this investigation and the condition from equation 5.7 seems to be fulfilled at any point of the experiments conducted.

Deriving the equation towards heat load leads to the following equation:

$$Q = \frac{\Delta P_l \pi (r_w^2 - r_v^2) \epsilon r_c^2 \rho_l h_{fg}}{8 \mu_l l_{eff}} \text{ (Eq. 5.13)}$$

Using the equation above in combination with the pressure results for the differential pressure obtained from the annular flow run, which range from 709 to 734Pa guide towards a maximum transmittable power of 122W. That correlates approximately with the maximum thermal power transmitted within the experiments of 87.34W for the straight sample 2.

Unfortunately, these equations are all one dimensional and do not allow to compensate or cater for any bends etc. Therefore, only direct correlation could be made between the results of the equations and the experimental results for the straight heat pipe cases.

Both methods described either relied on an assumed input or empirical or experimentally obtained results.

Using the equation stated by Reay and Kew (2006) presented above for the pressure drop gives good correlation for the straight heat pipe case between the thermal power transmitted by the heat pipe, and the pressure drop obtained

for the annular run. The accuracy is within 33% of each other. It was not seen appropriate to compare the results of any other cases apart from the straight heat pipe as the equation used for the pressure drop does not have any provisions for bend angles. Overall the correlation between the CFD results for the straight case with annular flow and the experimental results for the same pipe geometry differ by a factor of 2. That factor could be reduced by lowering the flow rate or velocity and introducing an appropriate porosity into the CFD model. Further, the accuracy of the CFD correlation could be improved if scaling along a non straight axis were possible in the CFD package used, as more cells along the perimeter could be introduced.

5.2 TEST RIG DESIGN FOR BENT HEAT PIPES

5.2.1 Purpose Of The Test Rig And Introduction To The Principle

A test rig specially designed for the characterization of heat pipes and testing of bent and/ or flattened heat pipes was commissioned and can be found in Figure 5.11 below. The test rig contained a number of DC cartridge heaters evenly distributed through the top and bottom heater block capable of providing 200W of heat on the heat input side. On the cooler side two standard Thermacore Porous Metal cold-plates were provided to remove the heat. These cold plates are normally used for CPU cooling and therefore are capable of removing 75W each. Their size is 1.5” x 2”. The coolant flow was provided by a re-circulating chiller combined with an electro-magnetic flow meter as well as a bypass system to compensate for excess liquid to be pumped through the cold plates. This was necessary as a too high pressure drop through the system would stop the chiller from working. Further a paper cartridge filter was implemented in the system to collect any occurring particles in a set location and prevent the cold plates from becoming clogged up. Two thermocouples, one in the inlet stream and one in the outlet stream of the cold plates were put in place in order to get the energy balance controlled and to obtain a failure rate between heat input and output.

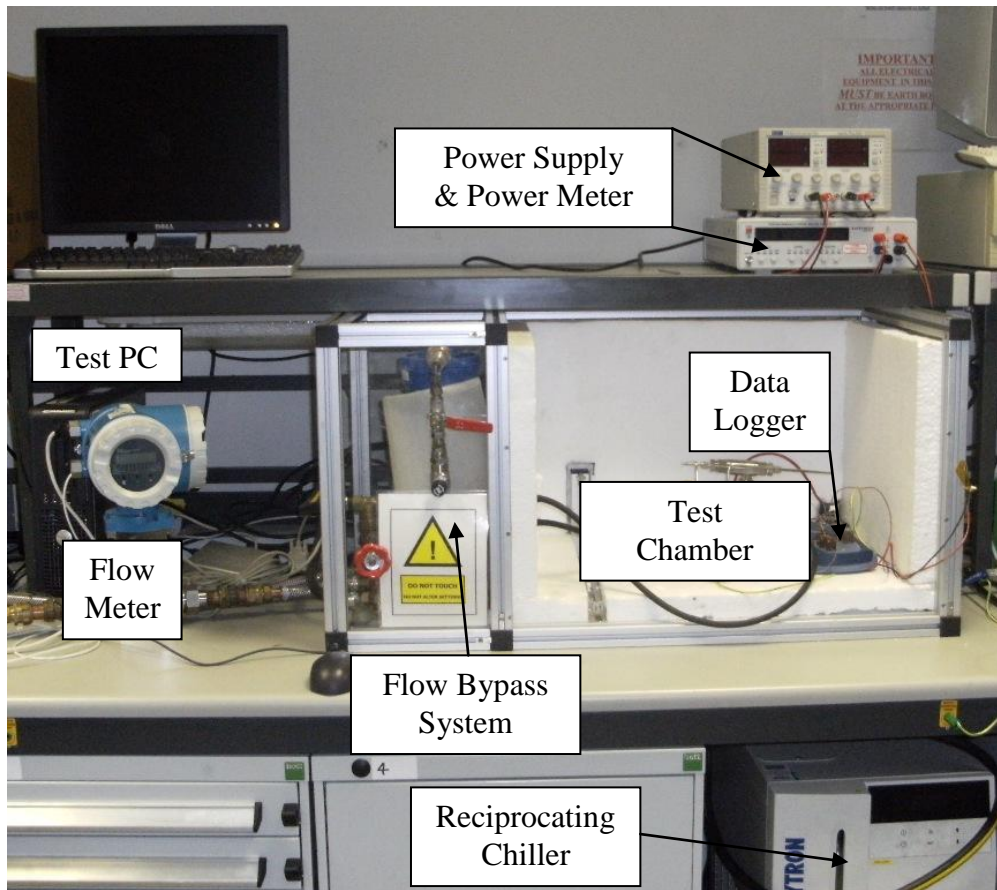


Figure 5.11: Entire Test Rig Setup

5.2.2 Instrumentation Used

Test Rig Scheme PhD Test Rig

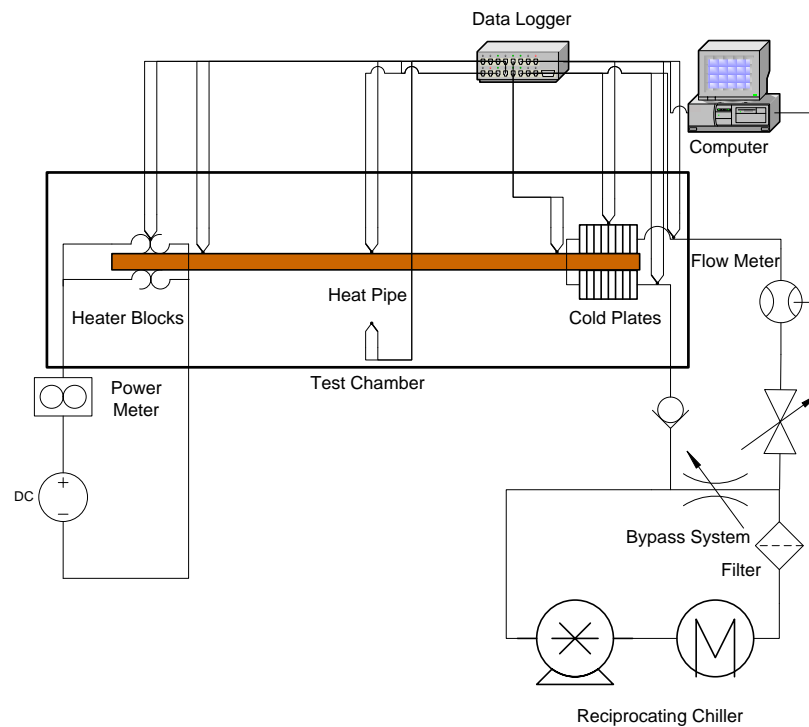


Figure 5.12: Scheme of Test Rig Setup including data- logging and controls

Figure 5.12 shows a schematic test rig setup including the instrumentation, data logging equipment, thermocouple positions as well as controls applied.

The data logging of the temperatures on the rig is performed by one single eight channel USB data logger (Pico TC-08 USB) onto a PC dedicated for this experiment. The initial data including the separate signal from the flow meter is transferred into Microsoft Excel for further post processing and analysis. The data logging logs temperature readings directly whilst the flow meter input is in micro-volts which is re-converted into a volumetric flow rate by the data logging software.

The heat input is conducted via a DC power supply being capable of transmitting 200 W and the power level is controlled in addition to the numerical displays on the instrument itself, via a Power meter, which can also be fed into the PC via a serial cable. The control level allows monitoring at two decimal places which can be seen as accurately enough. The flow rate is automatically recorded during the test duration via a serial input after the signal has been transformed into a readable format of micro-volts via a data converter. The flow rate will be determined by the pressure drop through the cold plates and therefore a pressure drop free flow meter as the electromagnetic one used is seen to be beneficial.

For heat pipe performance monitoring as well as obtaining temperature readings of ambient and water inlet and outlet temperatures T-type thermocouples are used as standard sensor probes. These are manufactured on site and calibrated using thermocouple calibration equipment. For the temperature range monitored, T-type thermocouples with a maximum measuring junction temperature of 300°C are seen to be sufficiently accurate

and offer less deviation than other thermocouples. T-type thermocouples only have a tolerance of $\pm 0.5^{\circ}\text{C}$ whilst the accuracy of K-type thermocouples is three times as low with a tolerance of $\pm 1.5^{\circ}\text{C}$. There are no standard thermocouples available offering a greater accuracy apart from Platinum resistance ones which are seen as too expensive for this purpose.

5.2.3 Water Side And Cold Plates

The water side of the test rig consists of a recirculating chiller providing coolant flow through an electro-magnetic flow meter (Promag 30A) into two porous metal cold plates which are a standard Thermacore product designed for CPU cooling capable of removing 75W each. The cold plate itself is shown in Figure 5.13 below, whilst Figure 5.14 visualises the function principle and inner structure of the cold plate. At a later stage, within Figure 5.15 below, the arrangement within the rig, containing the two cold plates and their surrounding insulation and mounting blocks are shown.

Further the system is equipped with a bypass system allowing excess water to get into the return stream and therefore keeping the systems pressure on the inlet side at a lower level and preventing the chiller from operating the overpressure/ blocked- system switch. Ultimately the achievable flow rate of the given system is determined by the pressure drop through the cold plates. The flow through the cold plates can be controlled in a very accurate manner through a needle valve directly inserted in the inlet pipe upstream from the paper filter prior to the cold plates. The exact flow arrangement has been shown in the Figure 5.17.



Figure 5.13: Cold plate used

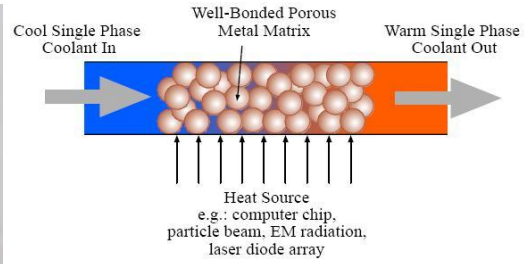


Figure 5.14: Function Scheme Cold Plate

The temperature of the inlet and outlet stream is measured through two thermo-couples, one embedded directly into each liquid stream. The arrangement of the flow thermocouples is shown in Figure 5.16 below. Due to the operating temperature range of the cooling system and the capabilities of the chiller as well as the absence of any materials like Aluminium, which would require corrosion protection, pure DI water is used. This also allows a higher heat transport capacity than a coolant containing additives. The water flow is run through a paper cartridge filter in order to protect the pump and the cold plates from damage or pollution from randomly occurring debris particles and dirt left in the system.

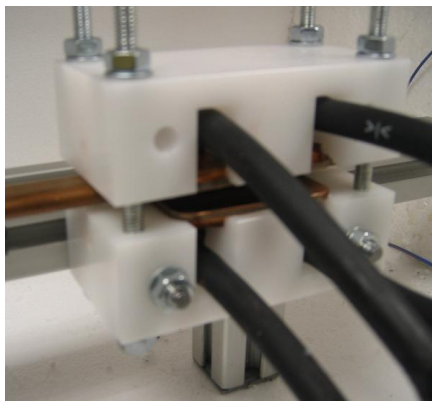


Figure 5.15: Cold Plate Arrangement



Figure 5.16: Embedded Thermocouples



Figure 5.17: Filter, Bypass & Needle Valve

5.2.4 Test Side And Heater Blocks

The testing of the various heat pipes takes place in a test chamber which is isolated by 2” polystyrene foam. This test chamber is shown in Figure 5.18 below. For clarity purposes the front cover as well as the insulation were removed. Further woollen insulation and Rockwool is used to cover the pipe itself and minimize heat losses to the environment.



Figure 5.18: Test Chamber and Insulation

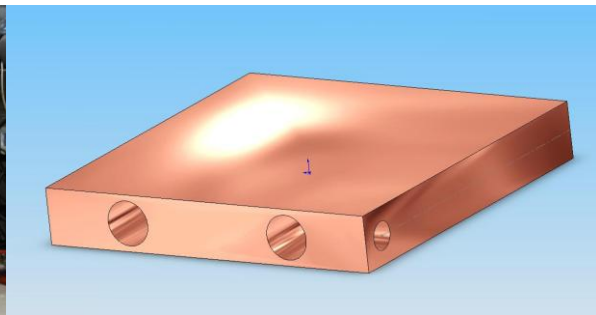


Figure 5.19: Heater Block

The heat input is performed via two copper blocks as shown in Figure 5.19 above containing in total, four heater cartridges. These DC heater cartridges are evenly distributed through both heater blocks, which are both the same design for cost purposes. In total, 200W of power can be introduced, which is more than sufficient for the heat pipe sizes to be tested. Each heater cartridge has a length of 1.5” and a diameter of ¼” and is capable of delivering 50W. The heater blocks have a size of 2” square and a thickness of 8mm. In order to secure good thermal contact between the heater blocks and the heater cartridges, thermal grease is applied around the heater cartridges. The same thermal grease is applied on the pipe/ heater block interfaces. For safety reasons as well as to prevent electrical noise visible on the thermocouple readings, both heater blocks are earthed separately.

For the mounting brackets, a general purpose engineering plastic called Delrin was used. The heater block covered in Delrin, is shown in Figure 5.20 below. The material was chosen due to its thermal properties as it does not act as a thermal conductor, so heat transfer into the test sample is ensured. The use of a metal like Aluminium would act as a heat sink and is therefore not appropriate. Delrin is widely available and provides good machining capabilities and has become first choice due to the properties mentioned before. Unfortunately, Delrin is only capable of withstanding maximum temperatures between 150°C and 180°C. Therefore during the experiments, the temperature of the heater block close to the pipe had to be limited to 120°C. This lower threshold was required as the additional interface between the pipe adapter and the heater block can raise the temperature at the block very close to its limits and cause fatal test rig damage.

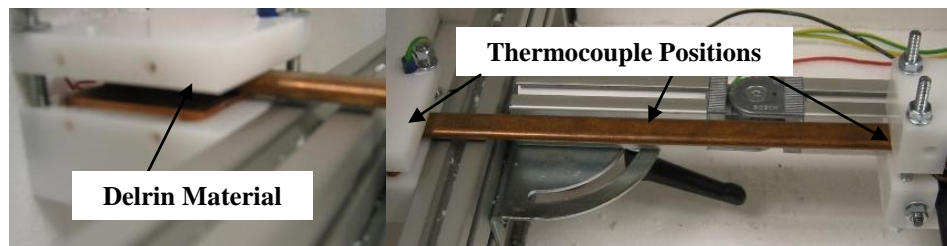


Figure 5.20: Heater Block Assembly

Figure 5.21: Adiabatic Section and Thermocouple Positions

Along the adiabatic length of the tested heat pipe, T-type thermocouples are attached using Kapton tape. Indications of the positions can be found in Figure 5.21 above. This allows a very flexible thermocouple adjustment and provides good contact of the thermocouple tip with the pipe outer wall which is used as the point of temperature measurement.

5.2.5 Adaptability For Different Heat Pipe Diameters And Shapes

In order to be able to use the test rig for testing round as well as flattened stadium shaped heat pipes without major mechanical modifications, some adaptor blocks for round pipes were made. Their design as well as the location of the thermocouple in the heater and condenser block is shown in the Figure 5.22 below. Due to the higher thermal mass, the test duration for a round pipe had to be increased to fulfil the stability criterion as well as achieve the same operating conditions. For monitoring purposes, 2mm holes allowing thermocouples to be greased in are implemented in the blocks. Introducing thermocouples in these holes will give accurate feedback about the block temperature. Extra time had to be added to the test duration until these two temperatures have reached the same values as the respective block and cold plate values. The blocks are produced using standard 12mm square copper C101 bar and the centre hole has a diameter of 8mm in order to accommodate the 8mm heat pipes solely focused on for this PhD.

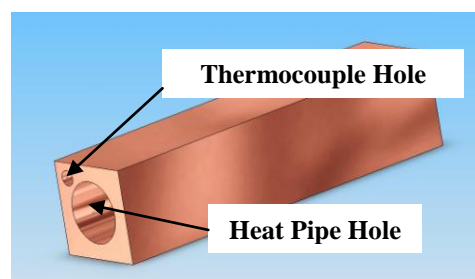


Figure 5.22: 8mm Adaptor Block

Inside the test chamber a Bosch Rexroth strut profile system was used to allow multiple shape adjustments. The heater and the chiller blocks can be moved along the profile. Further, there are two more possibilities of adjusting the test angles within the rig in order to accommodate the different heat pipe

geometries. This arrangement is shown in Figure 5.23 below. There is a large hinge allowing the entire arm to be articulated as well as a small hinge allowing the length of the arm to be bent further. This will give a great deal of flexibility and multiple heat pipe designs can be tested with a very little amount of physical modification on the test rig required. The proposed designs included in the experimentation list are all suitable to be used in the test chamber.

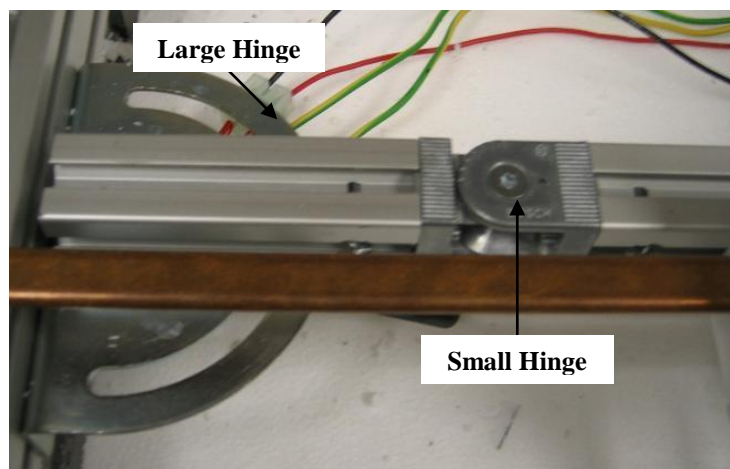


Figure 5.23: Hinge Arrangement

5.3 EXPERIMENTAL TRIALS WITH BENT HEAT PIPES

The previously described trials were carried out with a set of 5 heat pipes per shape in order to minimize the effects of production variations. All heat pipes tested have a wall thickness of 0.5mm and the length of the heat pipes is 235mm. As a wick structure two wraps of 150 Mesh count Phosphor Bronze screen wire mesh with a wire diameter of 0.063mm were applied to all heat pipes. The fill volume per heat pipe is fixed to 0.57cc for a diameter of 8mm using the fill calculation software developed and described in chapter 3 of this thesis. The pulley diameter used for bending the heat pipes into the different

geometric shapes was kept constant at the minimum advisable bend radius of three times the diameter of the heat pipes. During all experiments, the orientation of the test rig was kept constant at 0° and no further orientation angles were tested. Adding different orientational angles can be performed at a later stage outside of the work presented here.

For the given condition the maximum transmittable power Q_{max} of the heat pipe is measured. Changes in the power levels transmittable are seen as a measurement of performance degradation due to the shape changes.

Heat Pipe Shape	Heat Pipe Diameter
Round pipe straight	8mm
Round Pipe 45° Bend	8mm
Round Pipe 90° Bend	8mm
Round Pipe 135° Bend	8mm
Round Pipe 180° Bend	8mm

Table 5.4: Set of Experiments conducted

5.3.1 Experimental Methodology

Within this section the methodology of the experiments carried out as described above is shown, and the raw data obtained is systematically analysed and presented. First the methodology of the tests is presented and at the latter stage the obtained results are thoroughly analysed and presented in an understandable manner.

The following methodology was applied to obtain the results presented in this section of the thesis: First the power was ramped up to a dry out stage in 10W steps. For each of these 10W levels a run time of 3600seconds was used. Once severe dry out up to the critical heater block temperature, was occurring within runs, where further power input would damage the test rig, the power was

switched off and the rig allowed to cool down to its starting conditions. Once these starting conditions were achieved, the power was switched on at the lower stable power level where the 10W increment test had been run for its entire duration successfully before. For example, if a heat pipe was drying out at 80W, but has successfully withstood the 70W test without any signs of performance loss, the ramp up test was started at 70W and then run for 10 minutes in order to double check the conditions observed in previous tests. After 10 minutes or 600 seconds, the power was ramped up to the next level in 2W increments. The 2W increment was chosen because of electrical mains instability of up to about 0.6W. It was seen as unsuitable to choose a smaller ramp up increment as the uncertainties would cater for more than 50% of the next power level. So after 600 seconds the power was ramped up to 72Watts and left at that level to stabilise for 600 seconds. After the second segment of 600 seconds, assuming that there were no anomalies envisaged, the power was ramped up to the next 2W increment. This procedure was repeated until the heat pipe on test showed signs of dry out or other performance limiting failures were observed. If issues were found, it was decided on an individual test basis to extend the previous 600 seconds segment by another 600 seconds. This was carried out in order to eliminate any possibility of dry out occurring during the later stage of the test, and pass by unnoticed. If the heat pipe had reached the next higher 10W increment without drying out, during the ramp up runs, the power level of the previous 1 hour or 3600 seconds run was assumed as the dry out power level. Within the following Figures 5.24 – 5.33, one set of a typical test with multiple runs is presented. Afterwards, only the values of the dry out power/ load will be reported, unless the graphs show

some anomalies or phenomena which were considered worthwhile. In that case more detailed explanation differing from the dry-out phenomenon explained previously is presented.

5.3.2 Figures Of Experimental Procedure For One Single Heat Pipe

The following Figures 5.24 – 5.33 represent the test runs of the Straight Pipe 3, and is used as an example to describe the experimental procedure. The other results produced have similar curves and their addition would add no value.

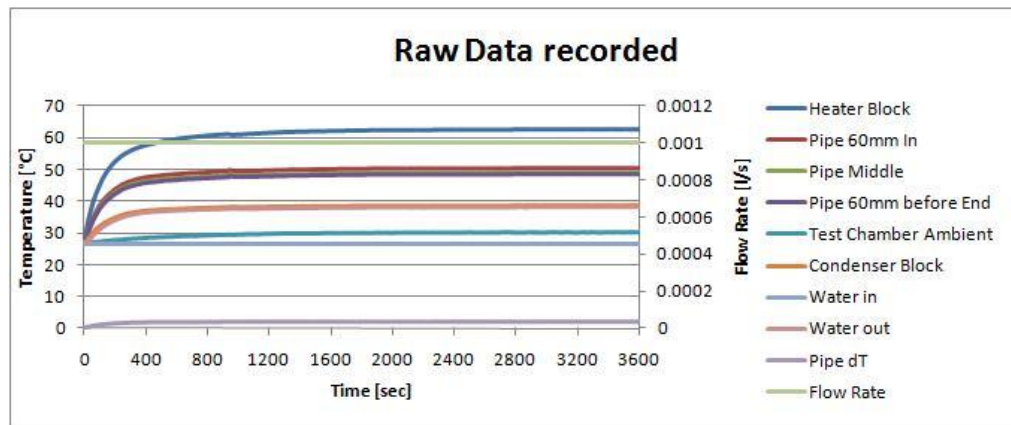


Figure 5.24: 70W Run Straight Heat Pipe 3 Raw Data

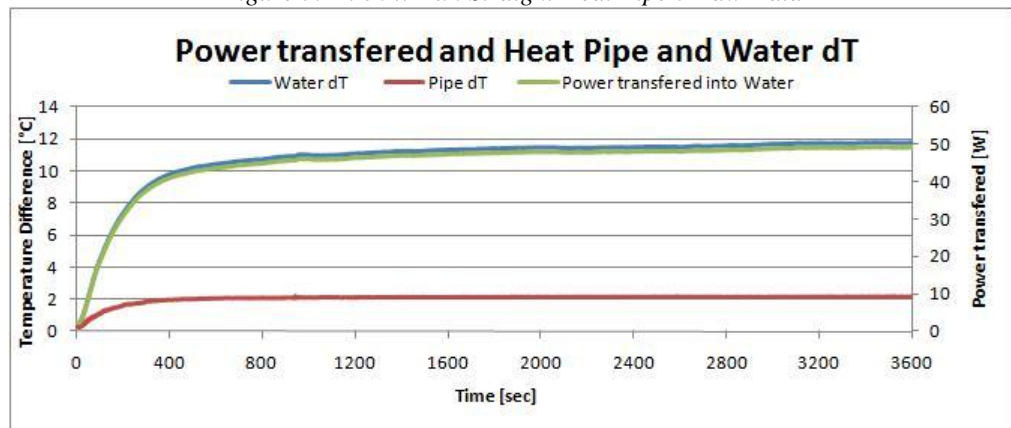


Figure 5.25: 70W Run Straight Heat Pipe 3 Analysed Data

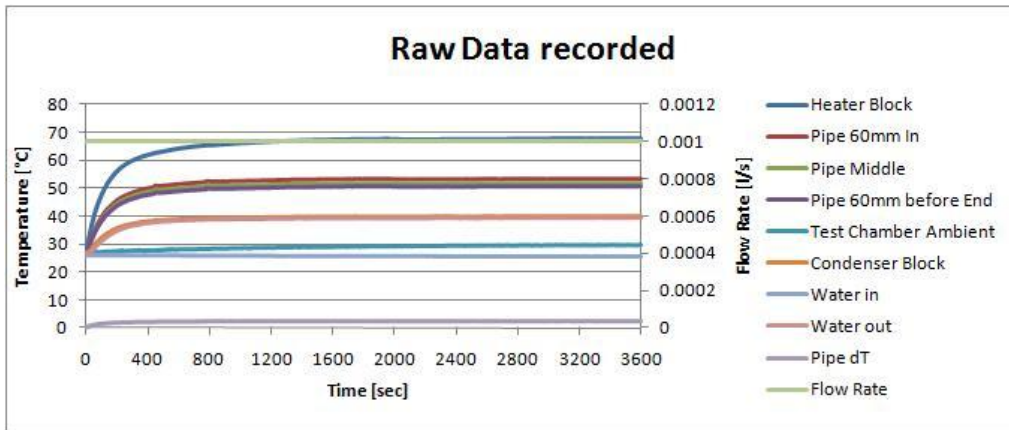


Figure 5.26: 80W Run Straight Heat Pipe 3 Raw Data

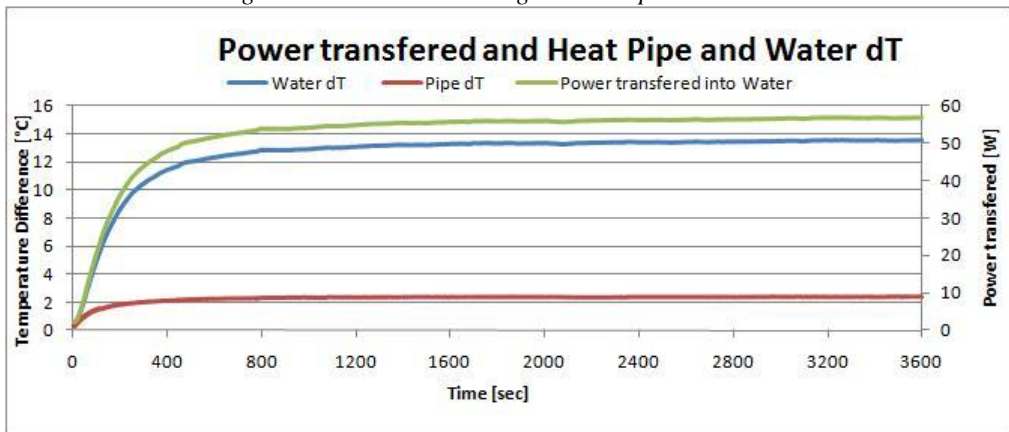


Figure 5.27: 80W Run Straight Heat Pipe 3 Analysed Data

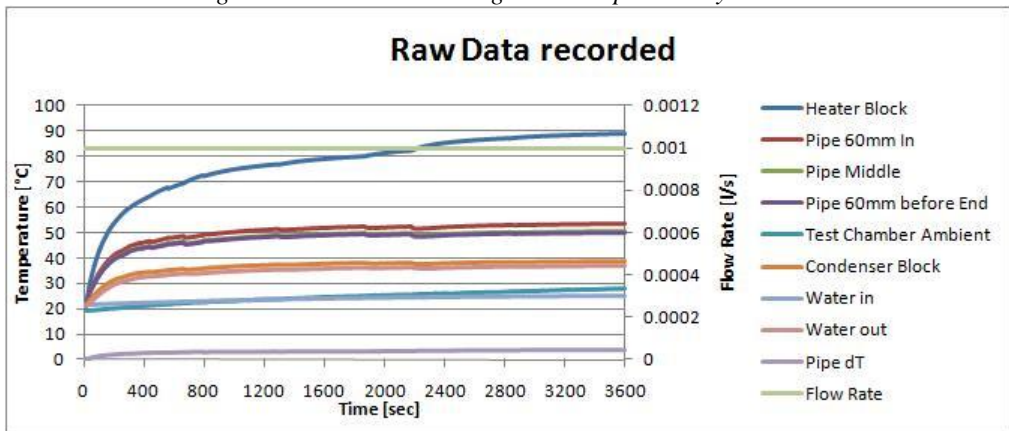


Figure 5.28: 90W Run Straight Heat Pipe 3 Raw Data

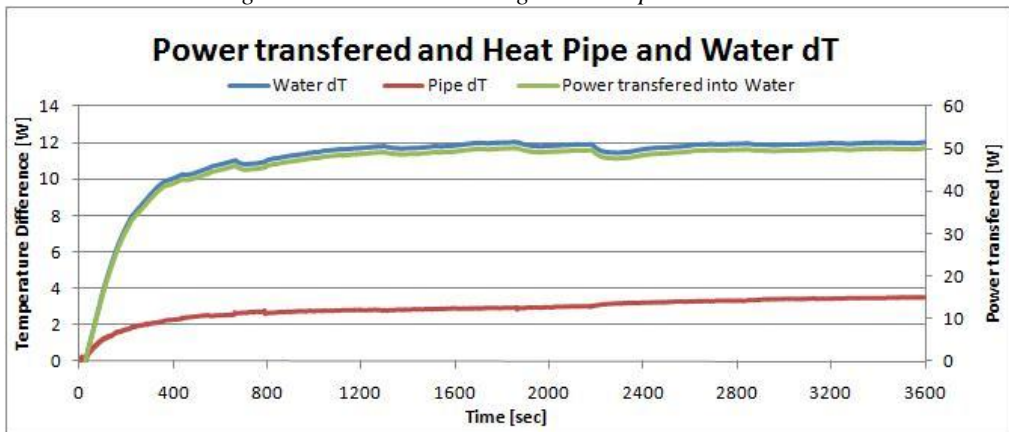


Figure 5.29: 90W Run Straight Heat Pipe 3 Analysed Data

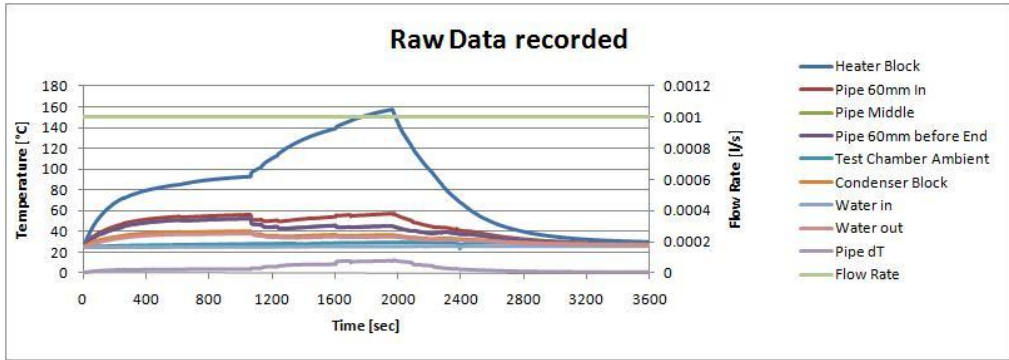


Figure 5.30: 100W Run Straight Heat Pipe 3 Raw Data

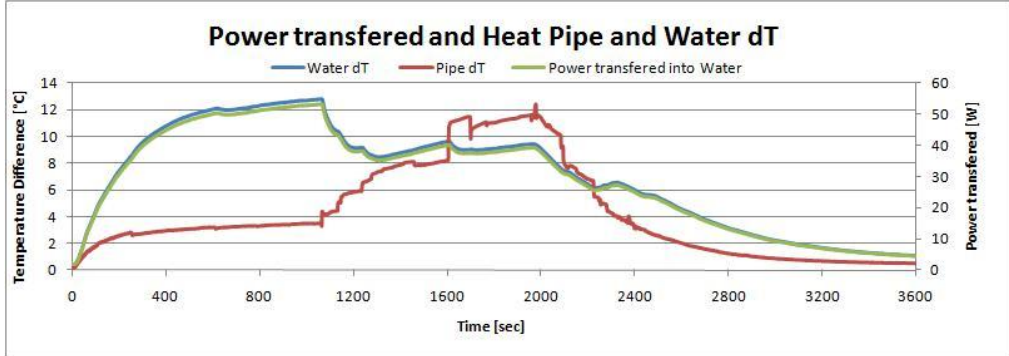


Figure 5.31: 100W Run Straight Heat Pipe 3 Analysed Data

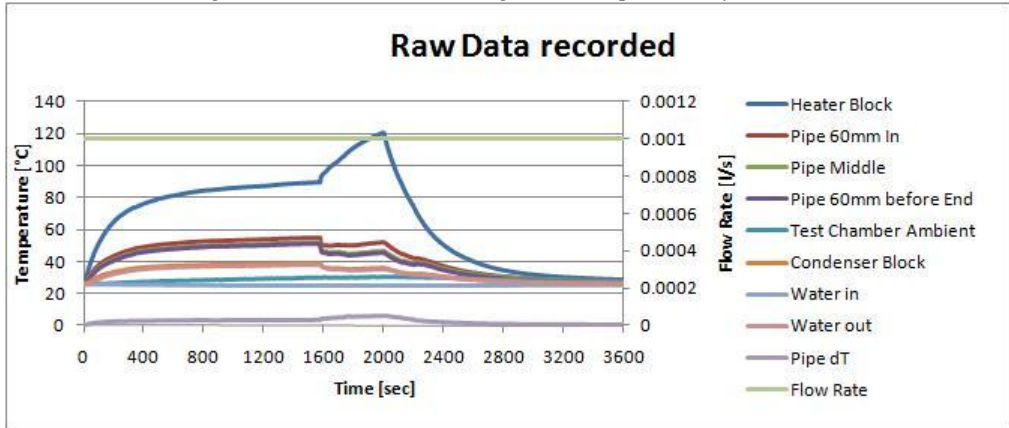


Figure 5.32: 90WRamp Up Run Straight Heat Pipe 3 Raw Data

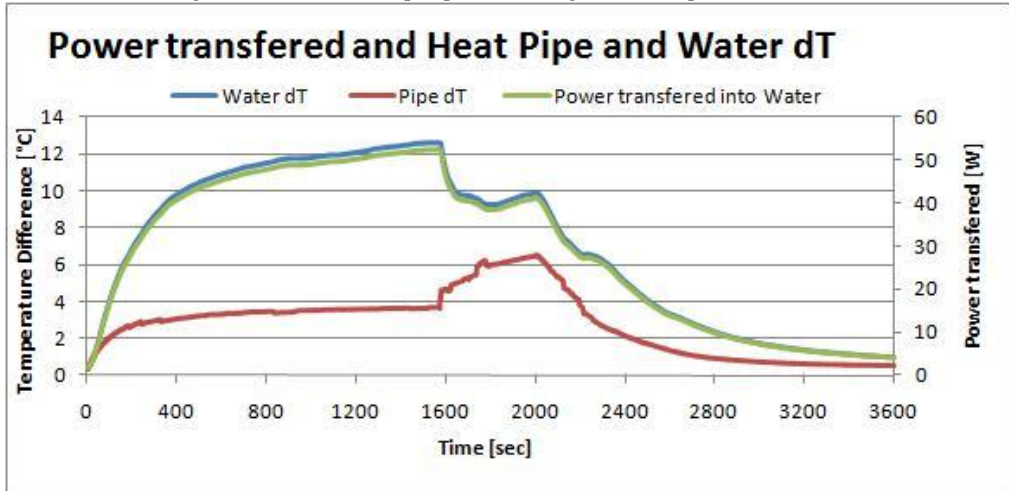


Figure 5.33: 90WRamp Up Run Straight Heat Pipe 3 Analysed Data

Above a full set of test results for one heat pipe can be found. The figures with the even numbers present the raw test data as recorded and contain the results for all nine channels, one flow rate and eight temperatures, which are:

<u>Channel:</u>	<u>Logged Parameter:</u>	<u>Comments:</u>
Channel 1	Heater Block Temperature	To be maintained below 120°C to prevent permanent test rig damage
Channel 2	Pipe 60mm In	Temperature on the heat pipe in front of the heater block
Channel 3	Pipe Middle	Temperature on the heat pipe in the middle
Channel 4	Pipe 60mm from End	Temperature on the heat pipe in front of the condenser block
Channel 5	Test Chamber Ambient	Chamber temperature close to the test sample but underneath the insulation blanket
Channel 6	Condenser Block	Condenser block temperature
Channel 7	Water In	Water temperature when entering the cold plates
Channel 8	Water Out	Water temperature when leaving the cold plates and returning to the chiller
Calculated Parameter	Heat Pipe ΔT	Difference between Channel 2 and Channel 5, indicating heat pipe performance
Channel 9	Flow Rate	Coolant Flow measured separately

Table 5.5: Monitored Channels

The odd figures represent the analysed data, particularly the water ΔT which is the difference between the water inlet and water outlet temperature, and the heat pipe ΔT . Taking the water ΔT and the flow rate plus the values for the flow rate, the power transmitted by the heat pipe itself transported into the water can be determined using the following equation (Faghri, 1995):

$$Q = \dot{m} * c_p * \Delta T \text{ (Eq. 5.14)}$$

The flow rate had to be converted from a volumetric flow rate as provided from the flow meter and logged by a data logger into a mass flow rate, which could then be used in the equation above. For the equation above, the flow

rate was converted by using the constant density for water at 25°C, 997.1 kg/m³ and the cp of 4181 J/(kgK) was used for 25°C water temperature. This approach was undertaken due to the very minor deviation between the cp and water density values for 25°C and 35°C and interpolation on an individual case was not seen necessary. It obviously has to be considered that the power transmitted into the water is slightly lower than the electrical power applied to the heater cartridges. The total deviation contains a number of accountable experimental errors, which are heat losses in the interfaces between heater cartridges and heater plate, the heater plates into the pipe specific heater block and from there into the pipe itself, heat radiated off the free heater surfaces, which are required in order to accommodate all the different heat pipes. On the condenser end, there are two cold plates used instead of the heater plates but the design is similar. Therefore similar errors are seen at the condenser end. As there are similar errors on both ends, the overall deviation between the electrical power of the system and the thermal power transmitted could be considered significant.

During the following section below the detailed phenomena within the particular data set is explained in greater detail.

First the dry out phenomenon will be described using straight heat pipe number 3, which is presented above and in particular the 100W run.

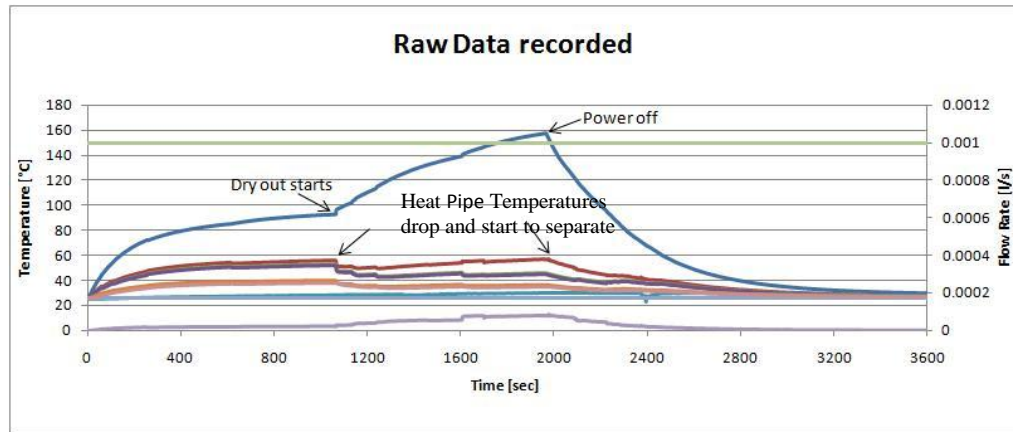


Figure 5.34: 100W Run Straight Heat Pipe 3 Raw Data with Phenomena explained

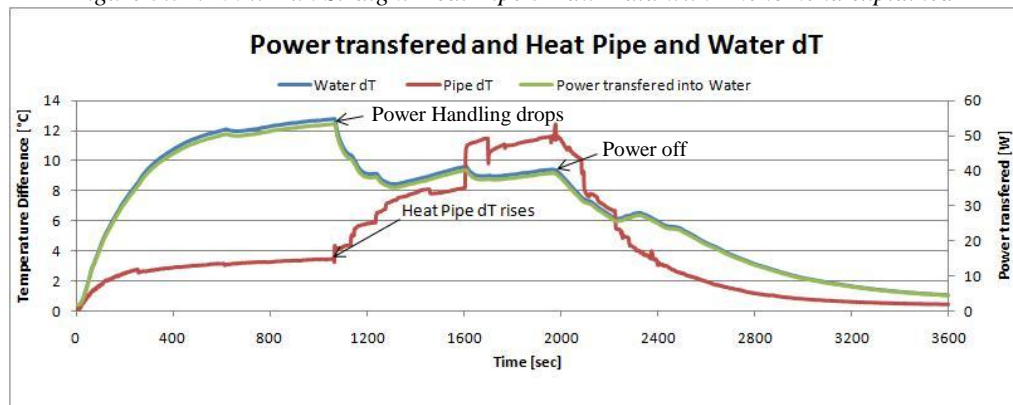


Figure 5.35: 100W Run Straight Heat Pipe 3 Analysed Data

It can be clearly seen from Figure 5.35 that the significant rise of temperature of the heater block is linked to the dry out of the heat pipe. Both of them occur at the same time and are the starting point of the significant rise of the heat pipe ΔT as well. The power handling capability drops at exactly the same point of time when the heater block temperature runs away. This is seen as a temporary failure of operation of the heat pipe and is presented through Figure 5.36, where the heater block temperature is shown, and Figure 5.37 where the analysed power through the water is presented. The following heat pipe ramp up run, to determine the 2W increment at which the dry-out occurs, is presented below. The phenomenon observed is similar to the 100W run where the heat pipe dried out and is presented above. Therefore only the new phenomena observed are described.

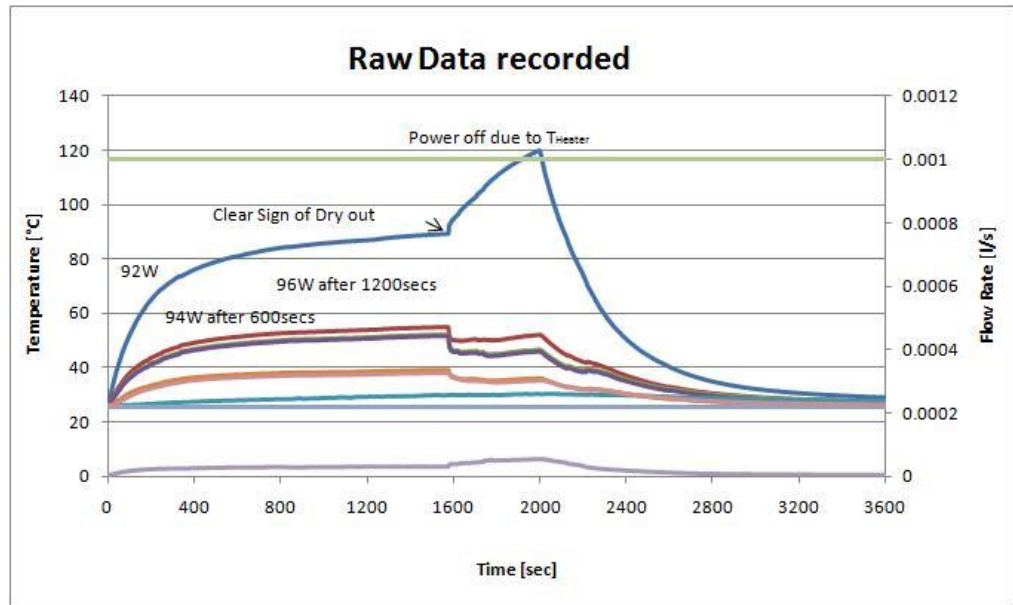


Figure 5.36: 92W Ramp Up Run Straight Heat Pipe 3 Raw Data

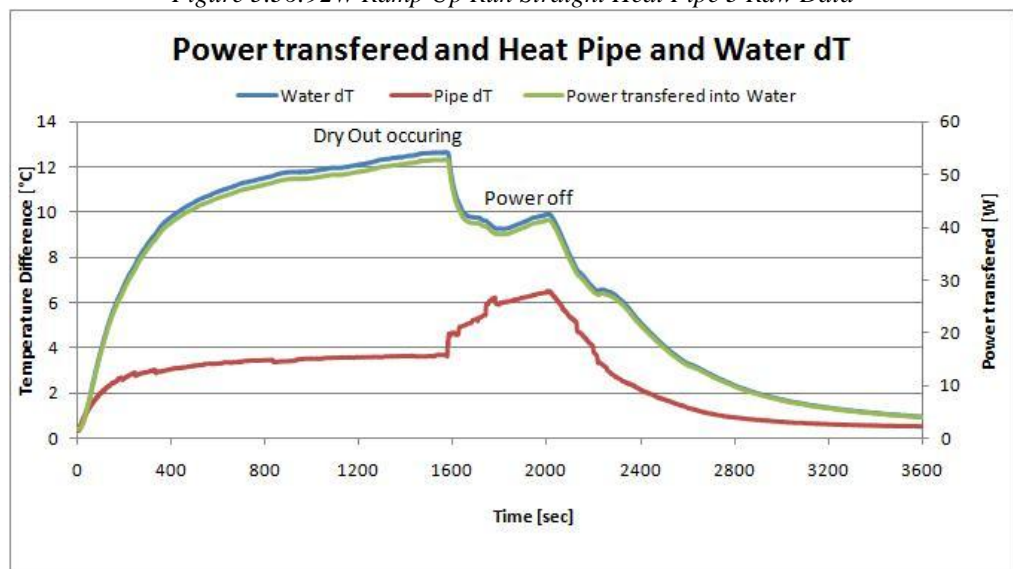


Figure 5.37: 92W Ramp Up Run Straight Heat Pipe 3 Analysed Data

The colours of the series on these graphs are exactly the same as the ones for the full runs presented previously. The next interesting phenomenon observed was the one of either an out-gassing heat pipe or a heat pipe containing NCG (Non Condensable Gas). Figures 5.38 and 5.39 show the performance of that heat pipe reducing with each run. The power level of the run, the heat pipe had successfully finished, was assumed as the limit. Further investigations could not be conducted as the heat pipe seemed to have lost its mechanical integrity

and could not add any value to the investigation of the effects of bends within the adiabatic section of heat pipe.

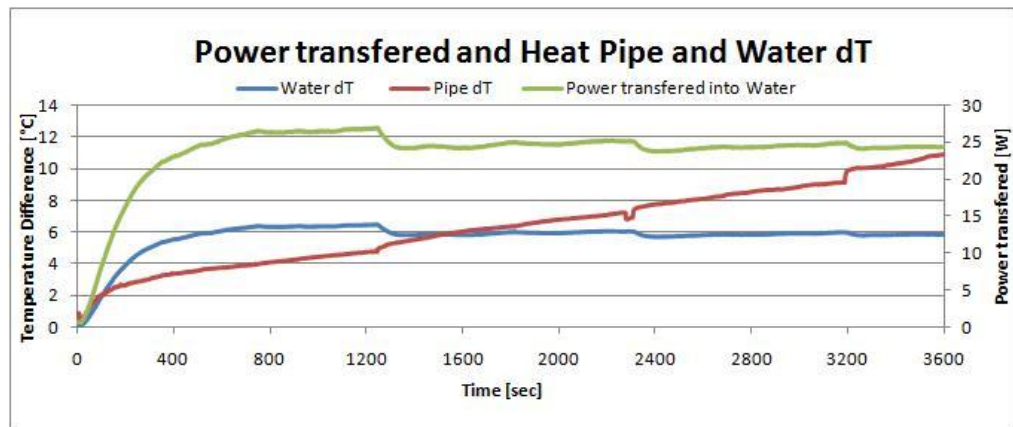


Figure 5.38: 50W Run 1 90° Heat Pipe 1 Analysed Data

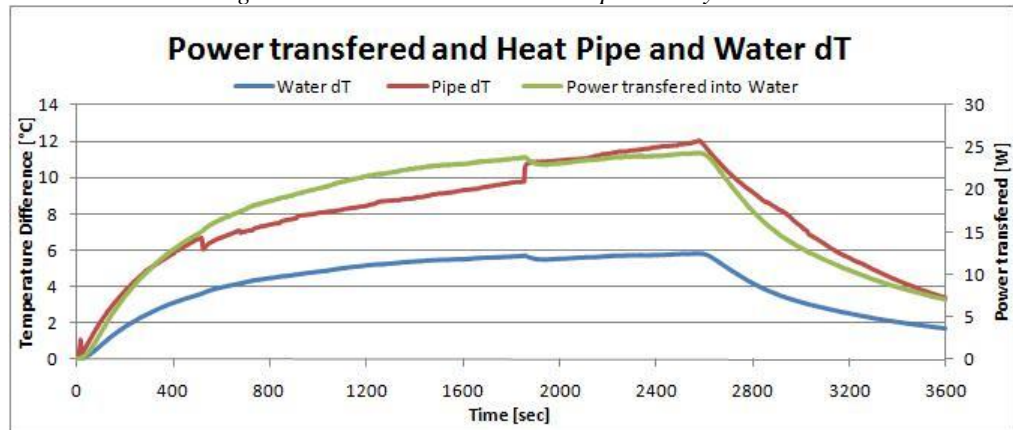


Figure 5.39: 50W Run 2 90° Heat Pipe 1 Analysed Data

It should be noted that with each of the two runs under exactly the same conditions, the heat pipe performance had deteriorated and the characteristics had been changed. A very slow deterioration in performance over repeated runs can be an indication for a slow loose of the vacuum inside the heat pipe. One cause for a slow loose of vacuum could be the presence of micro cracks, which allow portions of air to penetrate into the heat pipe envelope with time and working fluid vapour to escape during each run and therefore the performance reduces gradually until total failure. The escape of working fluid is called “outgasing”, but for this study the heat pipe was considered damaged and no further investigation into the root cause of the damage were launched.

Indications for the phenomenon of “outgasing” can be seen on the graphs above, during the first run (Fig 5.38), the power handling capability dropped at around 1300 seconds from 27W to round about 25W. At the same time the ΔT rose above the 5°C limit. During the second run presented in Figure 5.39, the 5°C limit was already passed at 300 seconds and the power handling capability is significantly slower than during the previous run presented in Figure 5.38. It was observed that the maximum value of round about 25W was only reached at a very late stage during the test when the heater block temperature was at a temperature level where the power had to be switched off to prevent the rig from overheating.

The next interesting phenomenon noted was the presence of NCG. This phenomenon can be found when the heat pipe ΔT reduces from a high level down to a lower level within a raising power level transmitted through the pipe. The higher internal pressure reduces the length of the NCG cylinder in the condenser section of the pipe and the active length of the condenser is increased, reducing the heat flux within that region and therefore the ΔT of the heat pipe. This can be seen in the Figures 5.40 and 5.41 below.

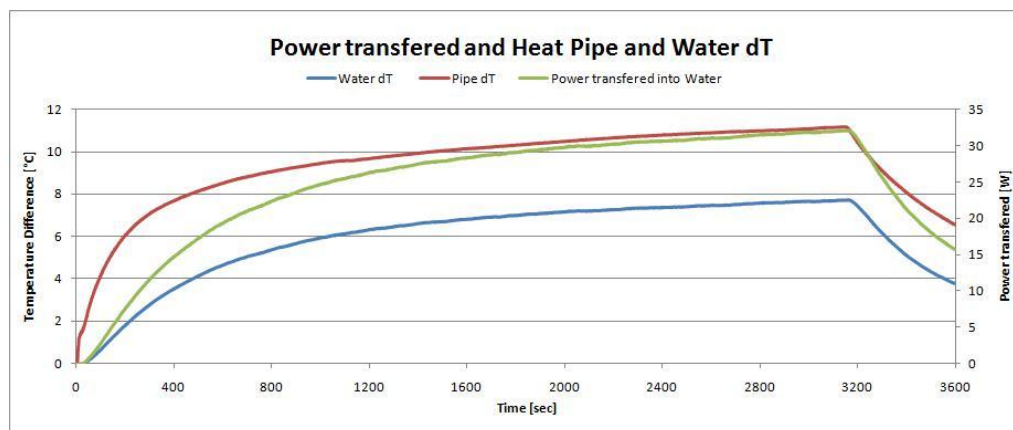


Figure 5.40: 60W Run 200 Mesh at the Wall Heat Pipe Analysed Data

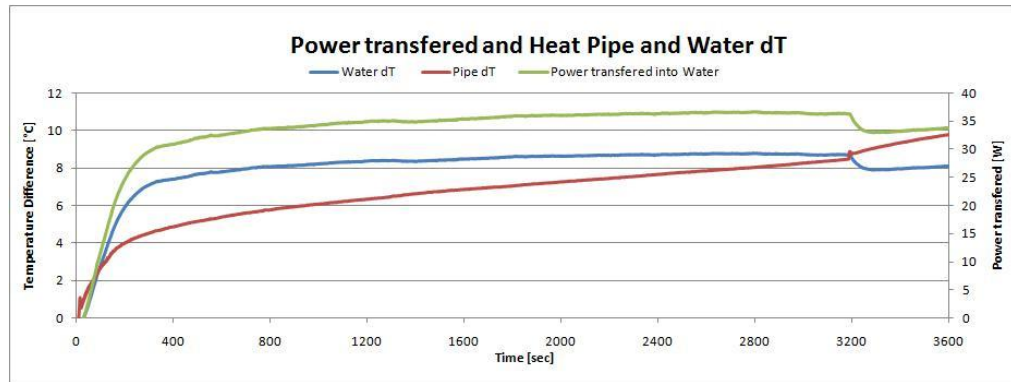


Figure 5.41: 70W Run 200 Mesh at the Wall Heat Pipe Analysed Data

From the two graphs (Figures 5.40 and 5.41) above it can be clearly seen that despite the fact that the power level is higher during the second run, the heat pipe ΔT , which is the red line, is significantly lower and stays below the 10°C marker. During the first run the heat pipe ΔT is above the 10°C marker whilst the water temperature rise is lower than during the second run with 70W. The most logical explanation, as mentioned above, is the change of internal pressure and therefore reduced length of the NCG cylinder within the condenser area.

The next phenomenon observed was related to the entrainment limit and described below as well as in the section where the table of the failure modes of each test set is presented. The following four graphs (Figure 5.42- 5.45) taken from runs at different power levels for the same heat pipe (45° Bend Heat Pipe 4) describe in greater detail why it is believed that this particular limit is observed. Other heat pipes with bent angles beyond 45° , but certainly not all heat pipes tested, show the same symptoms but are less distinctive than for the case presented. For this reason this case was chosen to be presented.

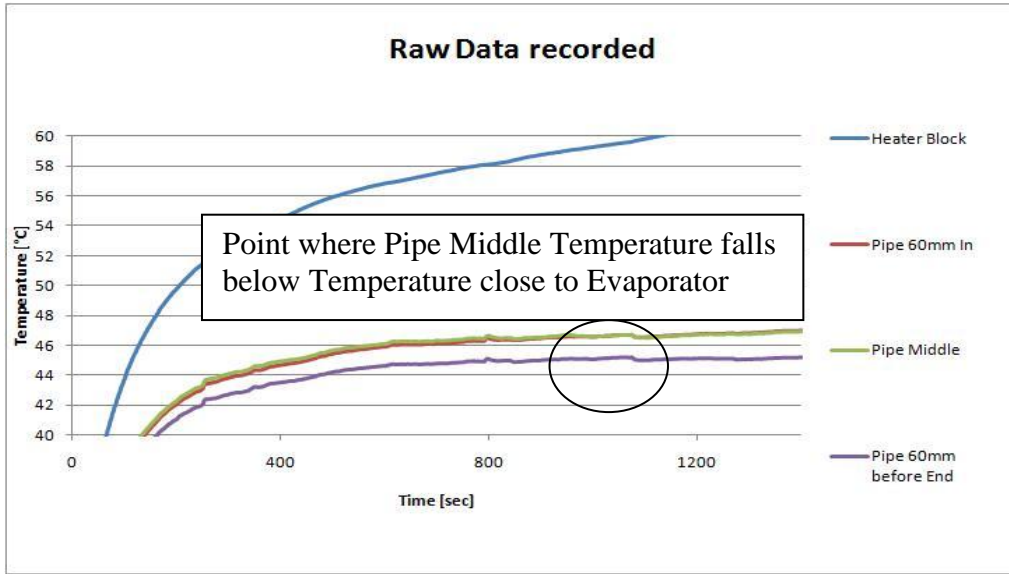


Figure 5.42:60W Run Heat Pipe 4 45° Bend Analysed Data

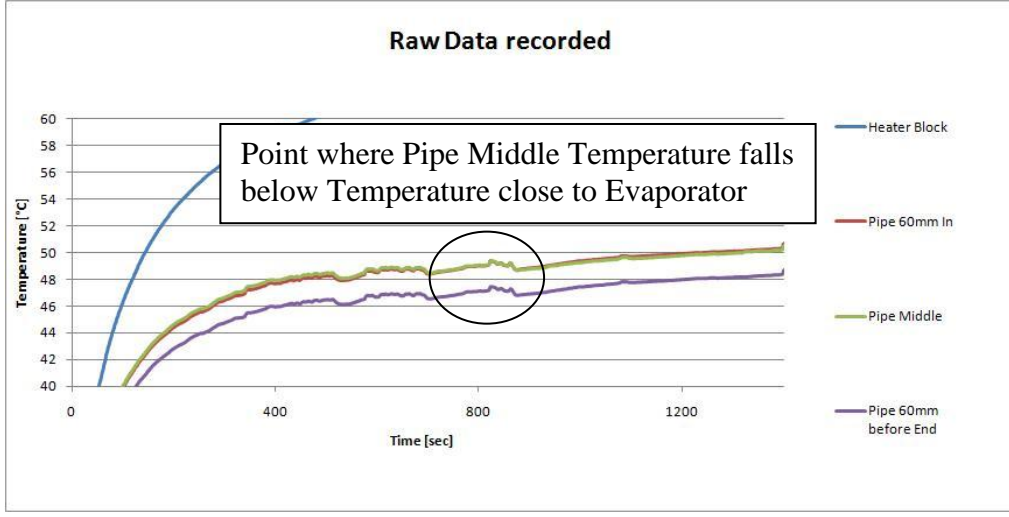


Figure 5.43:70W Run 200 Run Heat Pipe 4 45° Bend Analysed Data

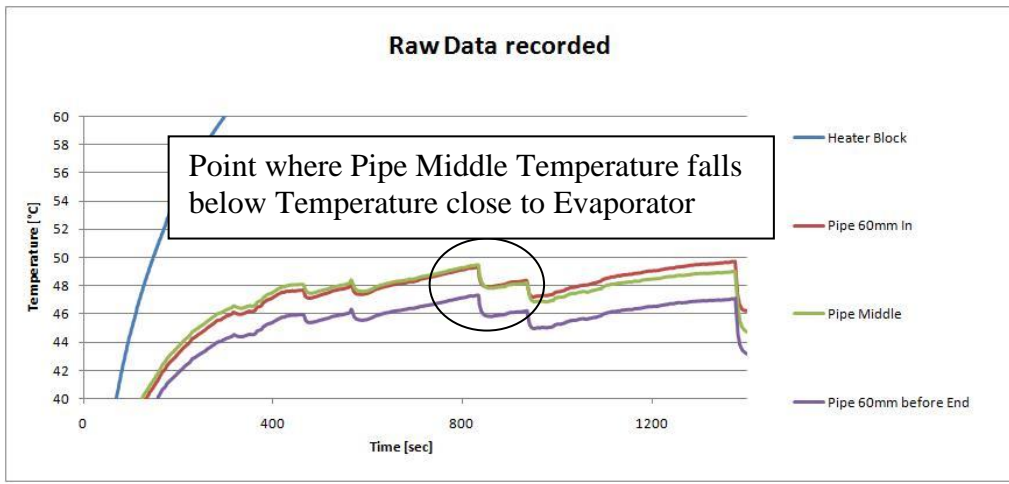


Figure 5.44:80W Run Heat Pipe 4 45° Bend Analysed Data

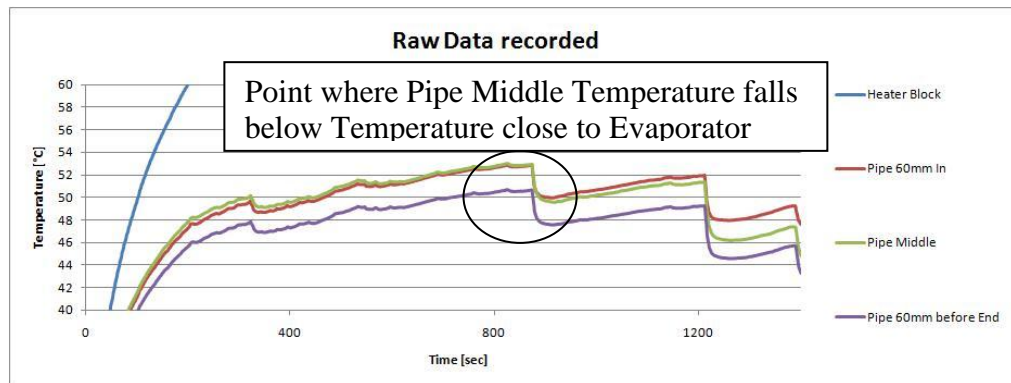


Figure 5.45: 90W Run Heat Pipe 4 45° Bend Analysed Data

The figures 5.42 to 5.45 above clearly indicate the same phenomenon on all of them independent of the power level introduced into the heat pipe. The power introduced into the system was varied in 10W increments from 60W up to 90W. All four graphs clearly indicate the point where the temperature in the middle of the bend in the adiabatic section sinks below the temperature taken directly on the heat pipe in front of the heater block. This reverts back into logical order of the temperatures according to traditional conduction understanding, as the test progressed. It is believed that the middle temperature is raised due to entrainment phenomenon where the working fluid vapour is subjected to friction against the wick within the heat pipe. This can cause performance reductions when very high vapour velocities are present within the heat pipe or when the geometry of the heat pipe is changed. In case of changed geometries, vapour velocities of lower magnitude can produce the same phenomenon. At a point during the test runs, the temperature conducted through the copper of the heat pipe container was observed to be the same as the one in the middle of the adiabatic section. This instant rise of the temperature is seen as linked to the working fluid vapour travelling past the point of the bend, and cause local heating of the wick and the container wall.

At later stages of the test the temperature close to the heater, represented through the pink line on the graph, rises and passes above the temperature in the middle of the adiabatic section. The temperature in the middle of the adiabatic section, represented through the light green line, in Figures 5.44 and 5.45 can clearly be seen to close in on the purple line representing the temperature close to the condenser block. The closing together of both lines at one point in the test is seen as linked to the entrainment limit rather than the presence of NCG within the heat pipe. NCG would still have a negative effect on the ΔT of the heat pipe at lower power levels, which could not be found within these tests.

Due to the amount of data available and due to the absence of phenomena which would justify presenting further graphs, only the absolute results in terms of power handling capabilities, as well as the deviation from the power handling capability, in both W and % are presented as tables and graphs. Where appropriate, an entire series has been presented as a graph but mostly it is referred to as an average value per geometrical design. This method has been chosen to ensure that the results are not solely dependent on a single heat pipe and its process and performance variation. For every case, apart from the dissimilar mesh investigation, the results were averaged out over the entire batch size of five units.

5.3.3 Failure Mode Analysis

8mm

		Straight (0)	45° ($\pi/4$)	90° ($\pi/2$)	135° ($3\pi/4$)	180° (π)
Sample	1	DT / DO	DO	EN / DT	DO / DT	DT & DO
Heat flux [W/cm²]		6.58	5.49	3.38	4.40	3.28
Sample	2	Rig Limit	DO	DO / DT	DT	DO & DT
Heat flux [W/cm²]		10.92	4.37	4.87	3.28	2.77
Sample	3	DO	DO	DT / DO	DT	DT
Heat flux [W/cm²]		6.59	4.68	3.75	3.14	3.99
Sample	4	DO	EN	DT	DO / DT	DT & DO
Heat flux [W/cm²]		6.27	5.39	2.69	2.78	2.79
Sample	5	DO	DO / DT	DT / DO	DO & DT	DT / DO
Heat flux [W/cm²]		6.24	6.35	3.50	2.48	2.79
Average Heat Flux [W/cm²]		7.32	5.26	3.64	3.21	3.11

Table 5.6: Failure Modes and Heat Fluxes per Heat Pipe tested

Table 5.6 above shows the failure modes which are related to each individual pipe tested. The following failure modes were used for the table above:

DT: Heat Pipe ΔT has exceeded 5°C and therefore the test was stopped.

DO: Dry-out of the Heat Pipe occurred and the heater block temperature ran away. The test was abandoned at that stage to prevent the test rig from permanent damage.

EN: The heat pipe had reached its entrainment limit and the vapour flow had slowed down. This can be seen when the three heat pipe temperatures cross from their normal order with the one closest to the heater being the highest, to the middle temperature taking over that position. The symptoms for that limit are very similar to dry-out, apart from the phenomenon mentioned above.

Rig Limit: The power supply used was capable of providing 200W at a certain Voltage and Current combination. When connected to the heater cartridges within the rig, this limit dropped to a maximum of 129W and was only achieved for one case.

Further, the heat fluxes, at which the failure modes occurred, are included in the table. It can be seen that in all cases the heat fluxes remain below the limit of 15W/cm² for screen mesh wicks as proposed by Reay and Kew (2006) and Zaghoudi; Tantolin and Godet (2004). This can be seen as an indication that the dry out phenomena envisaged are related to return of the working fluid rather than critical heat flux at the heat input area.

5.3.4 Analysis Of The Thermal Load Transmitted By The Heat Pipes

Maximum Power	Straight (0)	45° ($\pi/4$)	90° ($\pi/2$)	135° ($3\pi/4$)	180° (π)
Sample 1 [W]	52.61	43.94	27.01	35.23	26.26
Sample 2 [W]	87.34	34.98	38.94	26.22	22.14
Sample 3 [W]	52.74	37.44	30.02	25.10	31.89
Sample 4 [W]	50.15	43.11	21.51	22.22	21.76
Sample 5 [W]	49.94	50.82	27.97	19.80	22.35
Average [W]	58.56	42.06	29.09	25.71	24.88
St. Dev. [\pm W]	16.14	6.18	6.34	5.88	4.32

Table 5.7: Thermal Load in Watt transmitted per Heat Pipe and averaged per Bend Angle

Table 5.7 above presents the thermal loads which were transported into the water of the chiller at the dry out point and raised the water temperature within the cold plates above the set temperature of 25°C for the water inlet temperature. These values were numerically obtained by using Equation 5.13

presented above and were influenced by all errors and heat losses occurring within the system. It can be noted that for the Straight heat pipes and the heat pipes with the 90° bends and 135° bends that each set had one pipe with a significantly higher performance. In the case of the straight pipes, the heat pipe with the highest power handling capability was sample 2, for the 90° bend it was the heat pipe sample 2 again and for the 135° set it was sample 1. These are seen as the heat pipes with the performance close to the theoretical performance limit whilst the other heat pipes are subject to normal production variation. The variation seen is still one of the reasons mass produced heat pipes are 100% sample tested.

The standard deviation for each heat pipe geometry investigated can be found in the last row of table 5.7 above. The standard deviation varies from 4.3°C for the 180° case to 16.1 for the 0° (Straight) heat pipe case. The values outside the average value for each case plus or minus the standard deviation are highlighted through orange cells. Particularly for sample 2 of the straight heat pipe the result is about 70% higher than the average obtained from the rest of the results for that design and has therefore a significant influence on the average thermal load value for that design. Reducing this value towards 50W would not only reduce the standard deviation by a factor of 10, it would also lower the average value by about 10%.

Bend Angle [°/ (rad)]	Thermal Load [W]	% Qmax	Reduction in Qmax [%]	Reduction in Qmax [W]
0/ (0)	58.56	100.00	0.00	0.00
45/ ($\pi/4$)	42.06	71.82	28.18	16.50
90/ ($\pi/2$)	29.09	49.68	50.32	29.47
135/ ($3\pi/4$)	25.71	43.91	56.09	32.84
180/ (π)	24.88	42.49	57.51	33.68

Table 5.8: Reduction in Thermal Performance in Percents and Watt

Table 5.8 above shows the average reduction in performance against the performance of a straight heat pipe set in percent as well as in Watt. Column 1 presents the bend angle, column 2 presents the average transmitted thermal load, column 3 presents the performance in percent of Q_{max} , and column 4 presents the reduction in percent from the straight case whilst column 5 presents the reduction in performance in Watts from the straight case. The data presented above was used to generate Figures 5.46, 5.47 and 5.48. They are based on the more accurate measurement of the properties within the water circuit of the chiller and are therefore independent from the electrical input parameters. The electrical parameters are subject to mains fluctuation and were not recorded electronically, but the data was taken manually. The data presented above was 100 percent recorded or calculated and therefore independent of human error.

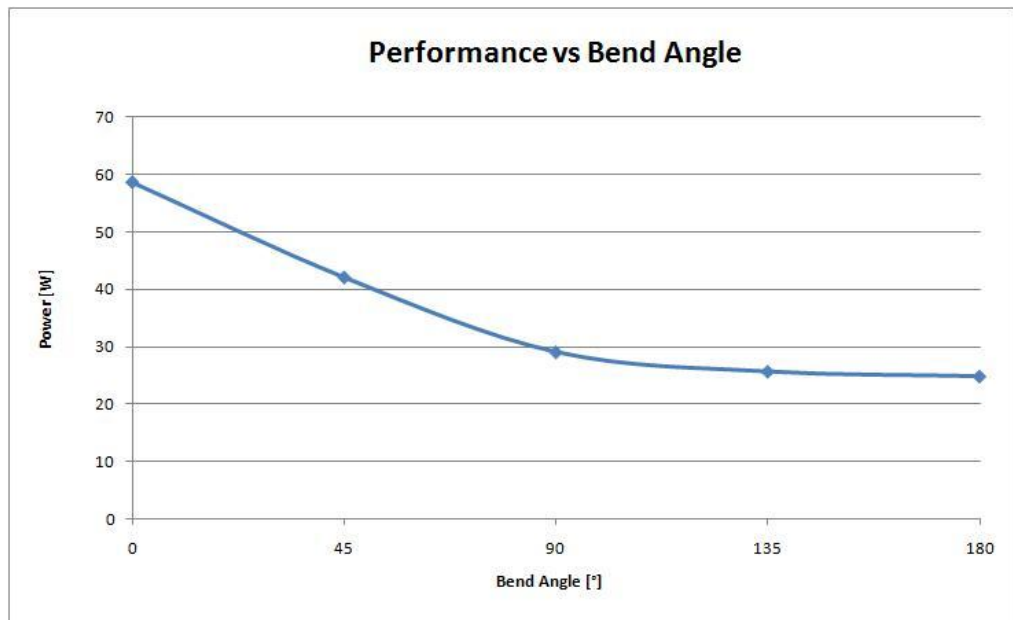


Figure 5.46: Thermal Performance transmitted in Watts averaged per Bend Angle

Figure 5.46 above shows the thermal load transmitted by the heat pipes into the water. The thermal performance transmitted into the water of the chiller starts with 58Watts for the straight pipe configuration and ends with about

25Watt transmitted for the horse shoe shaped pipe with a 180° bend. The figure clearly indicates that the heat pipe performance is reduced. Within the next two figures the analysis of reduction in thermal performance is presented. Firstly the reduction in Watts is presented whilst the second figure shows the reduction in percent from the straight performance. Again it can be seen that bends with angles greater than 90° do not much further reduce the performance handling capabilities of the heat pipes.

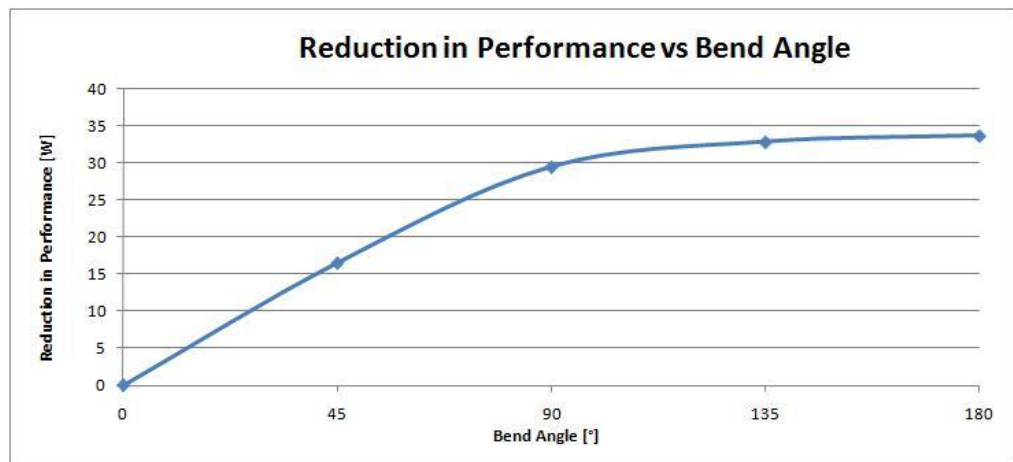


Figure 5.47: Reduction in Thermal Performance in Watt averaged per Bend Angle

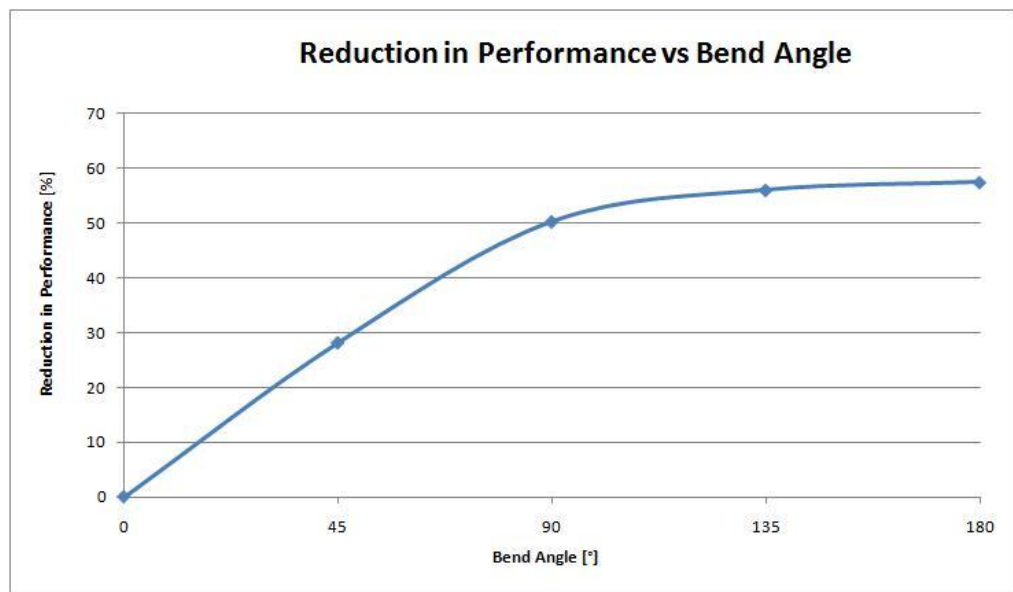


Figure 5.48: Reduction in Thermal Performance in Percent averaged per Bend Angle

5.3.5 Comparison Of The CFD Simulation Results To Experimental Results

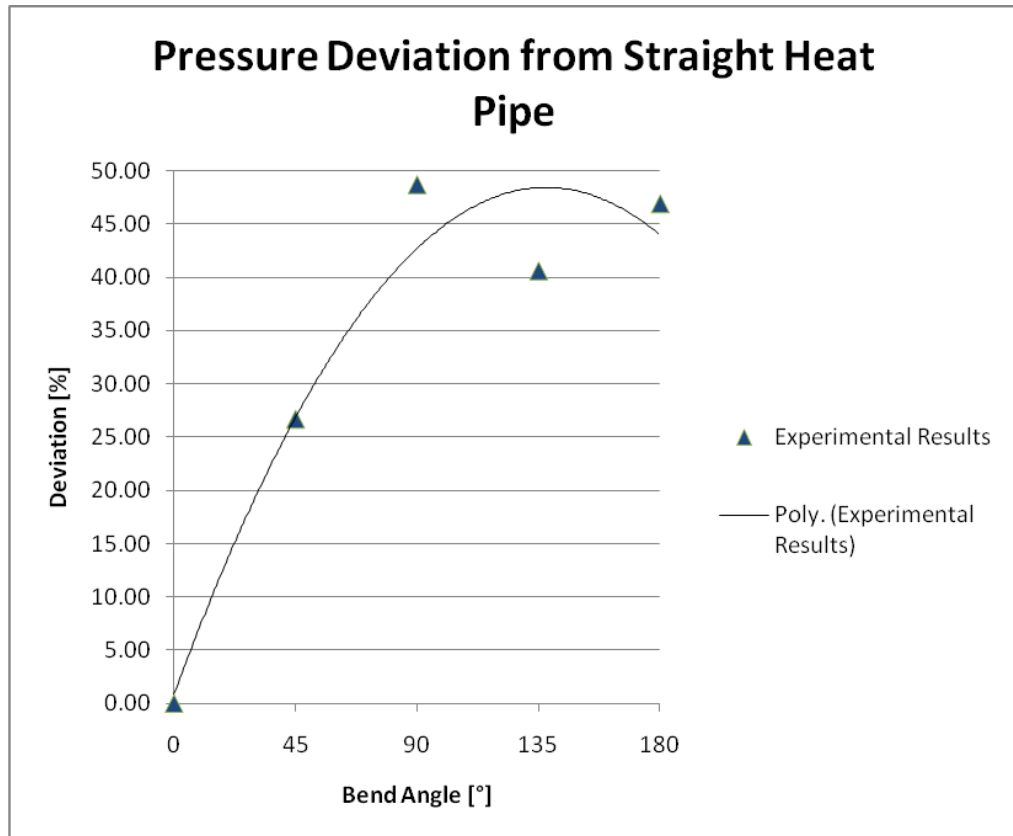


Figure 5.49: Pressure Degradation in % from Straight Heat Pipe obtained through Experimental Analysis

Figure 5.49 shows the results of the analysis of the experimental results towards pressure deviation from the straight heat pipe value. In order to be able to obtain this deviation, the experimental results have been analysed towards the heat pipe middle temperature at the failure point. These results were then averaged over the total batch size of five samples and for the obtained average, the saturation pressure was looked up from a reference table (Rogers & Mayhem, 1995). Once the saturation pressure per invested geometry was obtained, it was compared towards the value for the straight heat pipe and the deviation from it was calculated. Table 5.9 below presents

the absolute results for the deviation in this case as well as the pressure deviation results obtained from the CFD analysis carried out and presented earlier in this chapter.

Pressure Deviation Analysis

Temperature assumed for CFD: 65 °C
 Corresponding Saturation Pressure: 25010 Pa

Bend Angle [°/ rad]	Annular Flow CFD [Pa]	Deviation [%]	Full Flow CFD [Pa]	Deviation [%]	Experiment. Results [Pa]	Deviation [%]
0/ 0	25744.07	0.00	25014.16	0.00	14717	0.00
45/ $\pi/4$	25732.97	1.51	25014.24	1.92	10791.12	26.68
90/ $\pi/2$	25732.2	1.62	25014.36	4.81	7551.56	48.69
135/ $3\pi/4$	25719.84	3.30	25014.43	6.49	8743.34	40.59
180/ π	25728.15	2.17	25014.5	8.17	7816.4	46.89

Table 5.9: Capillary Pressure Comparison Results

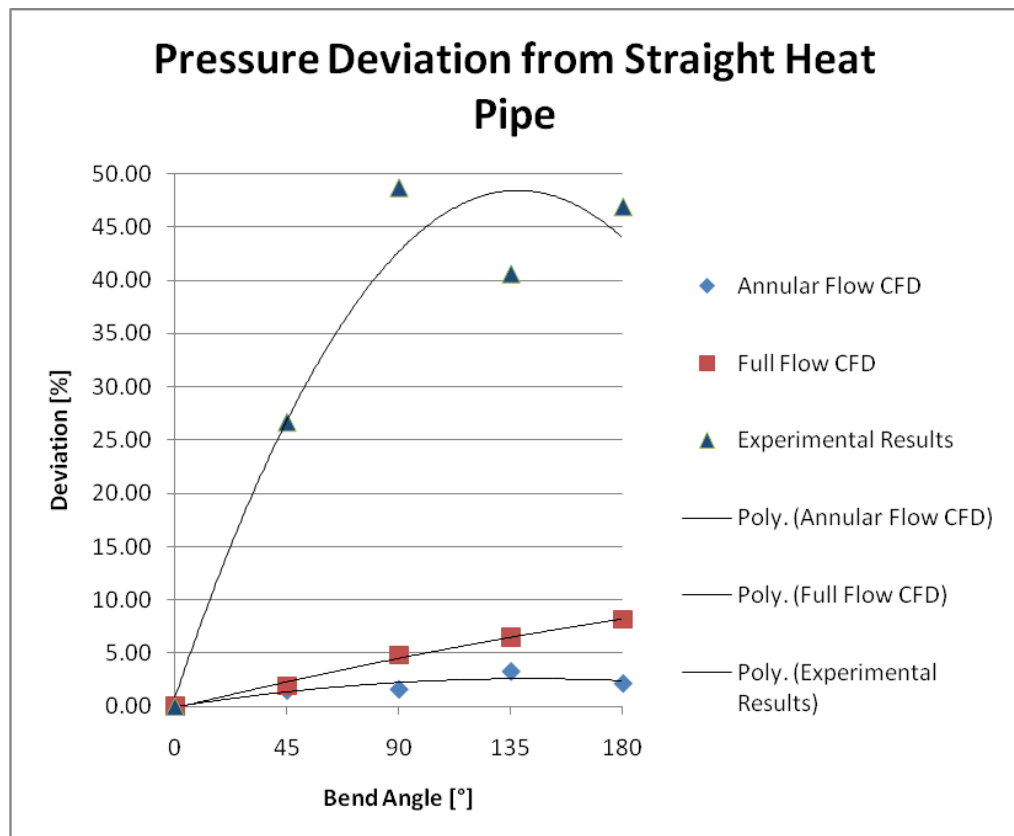


Figure 5.50: Comparison Pressure Deviation from Straight Heat Pipe CFD Runs and Experiments

Figure 5.50 shows the comparison of the pressure deviations from the straight heat pipe geometry for each investigated geometry in percent due to the wall friction for the CFD cases with full flow, annular flow as well as the analysed experimental results. The experimental results are the average values for each geometrical set as described earlier.

The deviation between the simulated performance reduction in percent and the experimentally obtained performance reduction is of the magnitude of a factor of 5, so it can be seen clearly that there are other factors influencing the performance handling capability other than only the friction caused by the working fluid passing along the wall at the bend in the heat pipe. There are more reasons that can cause performance reduction than only single phase flow. This was simulated as a starting point for the investigation of bending phenomena. In reality there is the liquid vapour interface which has to be investigated with the respect of the area of the bend.

Since no real correlation could be found between the two different CFD settings used and the experimental results, an equation was developed to predict the performance of heat pipes of a similar design with bend angles anywhere between the tested ones. This approach is shown in section 5.4 below.

5.4 DEVELOPMENT OF A MATHEMATICAL APPROXIMATION FOR PERFORMANCE LOSSES DUE TO THE BEND ANGLE

Based on the average data for the bend angles experimentally tested and presented, the following second order polygon has been found to match the

graph. The use of that equation allows the estimation of performance losses for other bending angles apart from the ones tested.

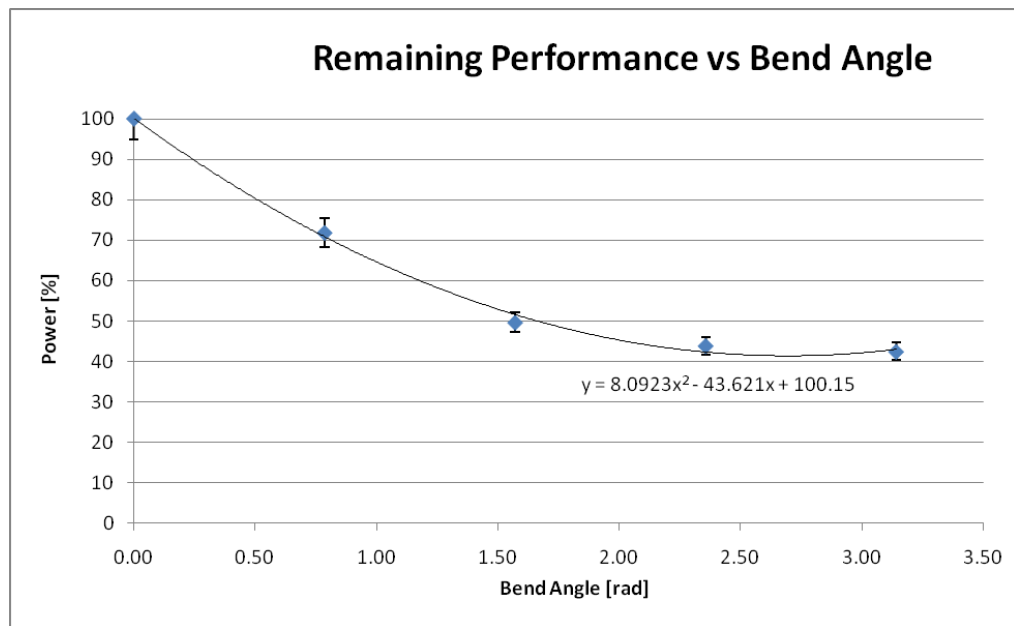


Figure 5.51: Remaining Thermal Performance in Percent vs. Bend Angle

From Figure 5.51 above and the trend line presented the following second order equation can be developed to link the performance of a straight heat pipe of the mesh wick structure investigated to the performance of a heat pipe of the same wick structure and geometry with a bend in the middle of any angle between 0 and $\pi(180^\circ)$:

$$Q_{Bent} = \frac{(8.0923 * \Theta^2 - 43.621\Theta + 100.15)}{100} * Q_{Straight} \quad (\text{Eq. 5.15})$$

Within that equation Θ is the value of the bend angle in rad and the outcome is a performance figure based on the maximum straight performance of that heat pipe. This approach should allow an easy to use approximation for the performance of a bent heat pipe and gives, as it can be seen from the error bars applied to the graph, a correlation within 5%. That value is seen reasonable for an initial development.

5.5 CONCLUSIONS

Work presented in this chapter compares two different approaches to the investigation of the effect of bends within heat pipes. One was a theoretical approach using CFD software and empirical equations to describe the effects of bends within heat pipes whilst the second one was a practical approach where experimentation with different heat pipe geometries was carried out. It is known that performance changes occur through bending of heat pipes but the total influence of shape changes has not been closely investigated so far. One reason is that commercially available CFD code as well as self written ones do not provide the required accuracy or are not solvable on normal PCs. This is due to the very small thickness of the water layers within heat pipes, as well as the difficulty of replicating actual geometries as used in heat pipes used for general applications. Neither do they follow the guidelines as proposed by Shao and Riffat (1995) for modelling inlet length etc. It is also known that there are large discrepancies in the accuracy of the numerical solutions when changing geometry. Shao and Riffat proposed an accuracy of around 10% for bends on HVAC ducting, whilst the worst total deviation in this case is only around 10% from the straight pipe case for full flow and around 3.2% for the annular flow case. Experimental results indicate a totally different outcome as can be seen in Figures 5.49, 5.50 and 5.51 where a clear reduction in performance for bent heat pipes, and in particular for greater bend angles over 90° , is reduced by a magnitude of up to more than 50% and is therefore far more severe than predicted by any CFD models.

It is believed that the performance changes on test samples are more related to conditions unique to each pipe like the overlapping conditions of the wick inside the pipe, and where two cavities of the wick are on top of each other, or where a cavity and a wire are overlaid. This will influence the capillary forces provided by the wick and therefore a decrease of this limit may make it the ultimate one for that particular pipe. This will be more related to production variation within the pipe making process. Further the radius of the bend has an influence on the integrity and smoothness of the wall, too tight a bend will guide towards a bowing and wrinkling effect of the container material at the inner radius of the bend and therefore the wick will be separated from the wall. This will have an effect on the capillary force caused by that effect. A similar effect can be seen on sintered heat pipes where the wick follows the wrinkling of the wall and therefore has an influence on the pore shape as well as the liquid-vapour interface.

The simulation approach has proved that the effects of bends on the performance of heat pipes are hard to investigate theoretically as most of the factors influencing the heat pipe performance are difficult to describe theoretically and are likely to differ from heat pipe to heat pipe. It is seen that the only way of investigating the effects of bends in heat pipes is the use of practical experimentation with a suitable number of heat pipes. These results will then guide towards a more conclusive picture about the real effects of bends and can be used for the proposal of a power law such as equation 5.15. This equation can then be used as an indication for the performance changes of heat pipes of similar geometrical constraints within future applications.

In addition to the reasons presented above there is the possibility that the heat pipe wick becomes mechanically distorted within the bend itself and negatively influence the liquid return to the evaporator end of the heat pipe. This is a condition which can occur to both sintered and screen mesh wick heat pipe but this has a higher influence in the non bound two material wick-wall combination within the screen mesh wick heat pipe where a gap between the wire mesh and the wall can be formed. This gap, depending onto its location around the circumference of the wick can have a negative effect on the liquid return to the evaporator end of the heat pipe and lead to reduced power handling capabilities, plus the likelihood of earlier dry-out of the heat pipe. So far there are no real time fluid flow models which deal with all aspects of the two phase circle occurring in a heat pipe, even if the heat pipe were simulated in all details including evaporation, condensation, vapour flow and liquid return through the porous material in the wick. As far as the author of this thesis is concerned, such models do not consider any phenomena as seen in practical applications such as collapsing pores within the bend area due to the bends in sintered pipes, or separation from the wall for screen mesh heat pipes. From an equivalent porosity point of view the screen mesh is seen as more uniform than the sintered wick which is subject to variation in the grain size and grain size distribution of the copper powder used. Screen mesh heat pipes are seen to be more affected by bends. If such a model were available, at the current time it would require a vast amount of computational power to solve and such a model would still require manual inputs for the refined porosity in the region of the bend. This reduction in porosity would still need to be based on experimental results. Therefore it is seen that investigating the

effects of bending is neither an easy task numerically or empirically, but the performance losses need to be considered when designing heat pipe based cooling solutions. One outcome of this study is that heat pipes, even when manufactured to the highest standard possible, suffer from the effects of bends within them. The severity of the deterioration is dependent on multiple factors, these are the operating conditions such as operating temperatures influencing the vapour speed within the heat pipe, the wick structure used within the heat pipe, the bend radius used to create the geometry, as well as the number of bends. From the reasons presented above, it is clear that to design a heat pipe system with numerous bends and have it operating in very close proximity of one of its performance limits calculated for straight heat pipes, and not considering any deviation in performance due to bends introduced is not desirable. Due to the spread in performance in production batches, as well as inaccuracy in the models predicting these performance limits, there is a very high likelihood that such a system will not meet the set expectations of the designing engineer using straight heat pipe parameters.

CHAPTER 6 – FREEZE - THAW BEHAVIOUR INVESTIGATION OF HEAT PIPES

The sixth chapter of this thesis contains work regarding the investigation of copper water screen mesh heat pipe behaviour when subjected to freeze- thaw cycles which can occur in automotive and airborne applications, as well as in other harsh environments. In addition, the effects the low ambient temperature can have on function and performance of the heat pipes is also documented.

6.1 INTRODUCTION

Freeze Thaw behaviour of heat pipes is an area where very little work has been reported, whilst it is an area which gets more important to be considered with heat pipes entering new market segments like the automotive or aerospace market. In addition to in these markets, the telecommunications market with its outdoor applications and water heat pipes will be frequently subjected to temperatures below the freezing point of the working fluid due to either ambient temperature below 0°C or high altitudes where the temperatures are lower.

Work reported so far dealt with the start up of heat pipes where the working fluid is frozen in the wick and its relevant phenomena. A tremendous amount of work was reported on the development of start-up simulation models whilst only very few reported experimental results or practical investigations. Three people mentioned in this context are Ochterbeck and Peterson who have published three articles and a chapter in a book. Third, Faghri conducted some further work including the development of a mathematical model. Initially

frozen start-up models of heat pipes are reviewed in this chapter, whilst at a later stage will be concentrated on reviewing more of the practical work.

It has to be separated at the very beginning of this work the difference between the two most common mesh types, sinter and screen mesh, since both types have different failure behaviours. This is due to the different mechanical properties of the wicks having different restrains. Sintered wicks are a lot less susceptible to wick separation off the wall and therefore their changes are solely due to excess water accumulating in certain regions and forming the container material back to round shapes. Neither in reports of other work or in practical experience has it been found that the force provided by the frozen water was strong enough to either overcome the resistance of sintered powder grains towards each other or between the sinter powder and the wall, assuming that the sintering process has been performed in a suitable and professional manner. This will be shown in greater detail in section 6.3 of this chapter. Section 6.4 then takes the theoretical work and links it to own investigations with regards to a particular screen mesh heat pipe design where a flattened section was subjected to bulging or geometrical distortion during thermal storage cycling.

6.2 FROZEN START-UP MODELS OF HEAT PIPES

Amongst numerous start-up models for transient start-up of heat pipes, models for frozen start-up are a rather rare exception since work on this topic is limited to very few people. This PhD thesis work is concentrated on more common working fluids like water and methanol, which does not freeze during

normal operation, liquid metal start-up is only mentioned as an aside and not further investigated since liquid metal is already at a solid state during normal ambient temperatures.

Chapters on frozen start-up behaviour can be found in both books dealing with heat pipes, Peterson's (1994) and Faghri's (1995) whilst Faghri has further publications dealing with modelling of heat pipes during frozen start-up (Jang et al., 1989; Faghri, 1992).

Peterson describes in great detail work previously conducted and also indicates three types of freezing that can occur in a heat pipe: suction freezing, freezing blowby and diffusion freezeout. The third phenomenon, diffusion freezeout, requires the presence of NCG (Non Condensable Gas) and is therefore not further described as it is not applicable to normal copper water heat pipes. The first phenomenon is what Cheung (2004) envisaged and is described in section 3 of this chapter. Further it is described by Peterson where the heat pipe will eventually start working even with the water frozen out in the condenser section, however this used a large gradient along the pipe in the magnitude of around 100°C between evaporator and condenser. Here conduction through the heat pipe container was the mechanism which eventually caused the working fluid in the condenser section to thaw. This cannot be seen as an appropriate start up by any means for technical applications as most components to be cooled by heat pipes are not able to withstand that temperature. Depending on the length of the heat pipe, this can be a very time consuming start-up condition to solely rely on conduction through the pipe wall.

The second phenomenon freezing blowby was investigated by Ochterbeck and Peterson (1992, 1995) and is described in great detail as well in a later section of this chapter.

The work of Amir Faghri in his book (Faghri, 1995) seems to be the most comprehensive one on the topic of frozen start up and mathematical modelling of that phenomenon and the only one which gives a very practical explanation in the shape of a Frozen Start-Up Limit on how to deal with start-up of low temperature heat pipes. Further work was published by him as well as together with others previously (Jang et al., 1989; Faghri, 1992) and backs his work in the book. His definition of the Frozen Start-Up Limit (FSL) can be used as an indication whether any problems during the start-up of a heat pipe are likely to occur and if further precautions are required. The derivation is described in great detail in Chapter 5 of his book (Faghri, 1995) but here only the final equation can be found below (Eq. 6.1):

$$FSL = \frac{\varepsilon_l \rho_l A'_w h_{fg}}{C^* (T_{mel} - T_\infty)} \geq 1 \text{ (Eq. 6.1)}$$

For uniformity reasons the nomenclature of this equation was changed so that the porosity of the wick remains in all cases mentioned within this work ε_l rather than staying with Faghri's nomenclature. The term A'_w is the cross sectional area of the working fluid in the wick, which is unequal to the wick cross sectional area. Even with a fully saturated wick, these values cannot be equal as working fluid and wick material share the same space.

The Frozen Start-Up Limit was then tested against certain test samples where data was available and this criterion was always satisfied when a heat pipe had been started up successfully.

6.3 PREVIOUS PRACTICAL WORK

The main focus of this work is on screen mesh heat pipes but sintered heat pipes have been briefly investigated theoretically as well. It became quickly obvious that there are contradicting opinions about freeze thaw behaviour of sintered heat pipes. Zaghoudi, Tantolin and Godet (2004) state that sintered heat pipes only have sufficient fluid charge to saturate the wick and therefore can be subjected to freeze thaw cycling without any degradation of performance. This statement is theoretically true but as stated by Peterson (1994) heat pipes can have a 10- 20% overfill in order to ensure their performance. For batch produced heat pipes it has to be ensured that these pipes, subjected to process accuracies, maintain at least the required minimum fill rather than being underfilled. Therefore there is a chance that the pipes contain excess liquid which can support effects as reported by Cheung (2004). Here a failure mode due to a forced temperature gradient along the pipe was seen. This has caused the water within the relatively long pipe (305mm) in comparison to the thin diameter of 4mm to be frozen in the condenser section and caused the container to rupture and loose its vacuum. This failure can be seen in Figure 6.1 which also presents thermal conductance measurements in between cycles.

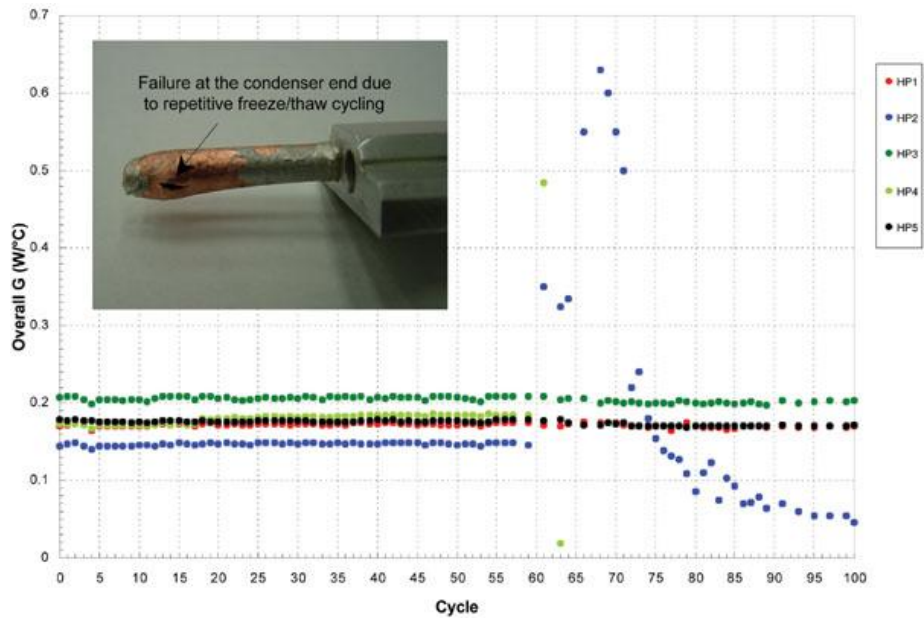


Figure 6.1: Heat Pipe Failure during operational Freeze Thaw Cycling (Cheung, 2004)

The major concern with pure freeze thaw cycling is that the heat pipe during these tests is actually operational and therefore forces its working fluid to accumulate at the cold end and freeze there. In this test a dry out of the evaporator end is ultimately achieved and the heat pipe stopped operating due to the lack of working fluid in the evaporator section whilst the condenser section is frozen and fails due to a burst container. Overall the failure mode is more related to work performed by Ochterbeck and Peterson (1991, 1992 & 1995). Already during the introduction of an article by Ochterbeck and Peterson (1991) it is stated that “If enough liquid is transported into the condenser region, depletion of liquid in the evaporator wicking structure and dryout can result.” Further the paper states that the depletion of available working fluid inventory by mass freezeout in the frozen or freezing condenser region. This is the phenomenon Cheung (2004) has envisaged in Figure 6.1 where vapour freeze out in the condenser region happened and there for caused the container to rupture.

Ochterbeck and Peterson's investigation of the Freeze Blowby phenomenon (1992, 1995) clearly allows visualisation of the blockage of the vapour path with solid frozen working fluid and also shows the effects of start-up behaviour. However, the sheer scale of this experiment (2m length) will not show certain phenomena like screen wicks moving away from the wall etc. Therefore its overall validity for start-up investigation for normal scale heat pipes (Round shape with a diameter up to 25.4mm and a length up to 1000mm) is doubted. These experiments should be performed on a smaller scale closer to the actual investigation sample.

6.4 PRACTICAL INVESTIGATIONS OF FREEZE-THAW EFFECTS ON SCREEN WICK WATER HEAT PIPES

In this section the physical effects of repetitive freeze- thaw cycling on screen mesh heat pipes is described. X-Ray images of heat pipes which have been subjected to freeze thaw thermal cycling in an orientation where any excess liquid collects in the bottom section of the evaporator are included. The heat pipe cross section is D-shaped which means that it has been flattened from its round shape with a diameter of 6.35mm (1/4") down to 4.25mm nominal for application related reasons. The heat pipe has an overall length of 153mm with 93mm being flattened down to 4.25mm where the heat input is and 52mm remaining round at the original diameter of 6.35mm. The remaining length is the transitional area. Within the heat pipe a 200mesh screen wick has been utilized to ensure the working fluid return to the evaporator section in all operations. All the heat pipes, X-Ray images and thermal results are presented

of within this chapter, have undergone the same test routine. First they were thermally tested at a fixed power level to ensure their function and were found to be working to a ΔT of less than 6°C between evaporator and condenser and then assembled into a mechanical structure, which was then subjected to a HALT/ HASS qualification for the electronics attached to the mechanical structure. This procedure is described in greater detail at a later stage in this chapter. After this test, bulging was found on most heat pipes and an investigation into the root causes of this phenomenon was launched. During these tests the orientation was kept constant at 90° towards the horizontal, which is a worst case scenario for heat pipes.

At that orientation, bulges in the area of the flattening were found in numbers of one or two up to a height gain of 1.6mm above the nominal height. It was found that excess liquid gathered in that area has caused this and therefore an approach of fill optimisation and fill calculations improvements had to be undertaken in order to overcome this problem. The X-ray images taken after the thermal cycling clearly indicate the failure modes and a good distributed wick is shown for comparison as well.

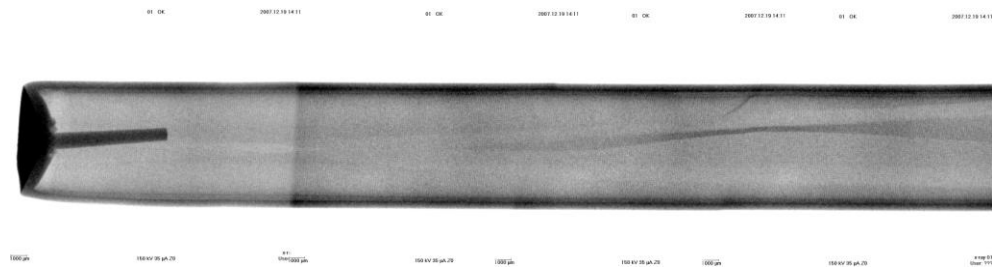
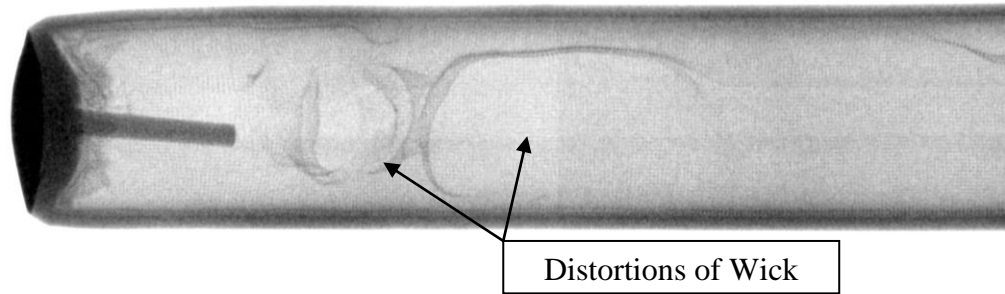


Figure 6.2: Heat Pipe with good Mesh Distribution



2000 μm

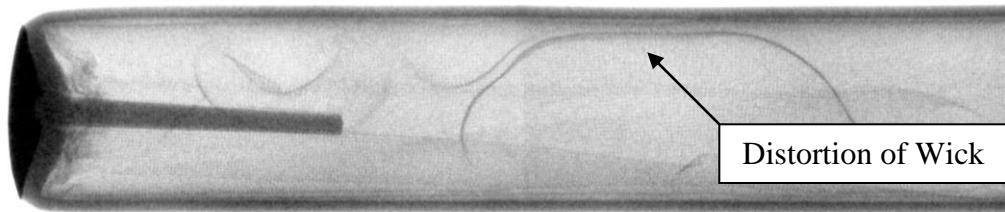
120 kV 40 μA Z0

2000 μm

120 kV 40 μA Z0

X-ray 01
User: ???

Figure 6.3: Heat Pipe with two Bubbles in the Mesh wick due to Freeze Thaw Cycling



2000 μm

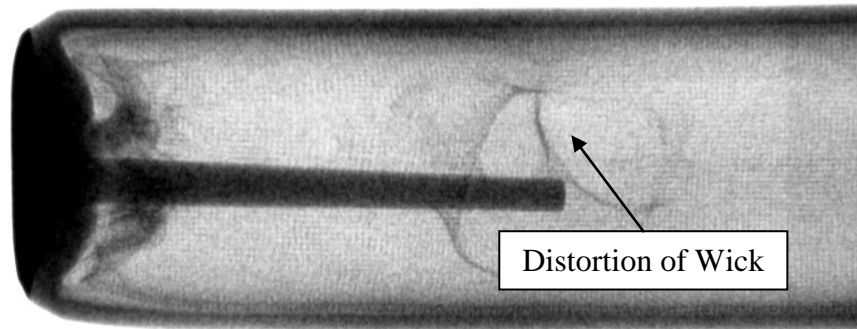
120 kV 40 μA Z0

2000 μm

120 kV 40 μA Z0

X-ray 01
User: ???

Figure 6.4: Heat Pipe with very slight Wick distortion due to Freeze Thaw Cycling

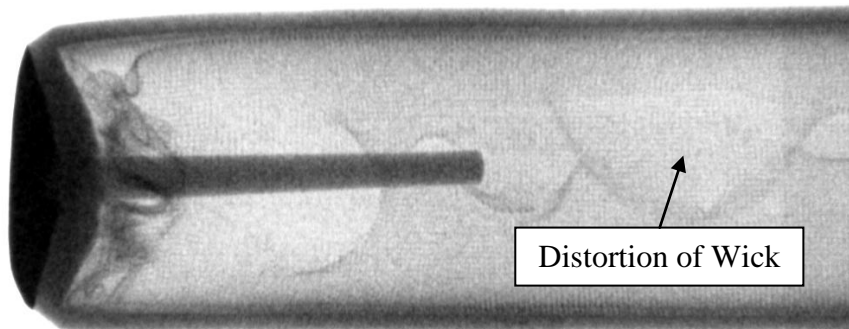


2000 μm

120 kV 40 μA Z0

x-ray 01
User: ???

Figure 6.5: Heat Pipe Sample with Wick distortion due to Freeze Thaw Cycling



2000 μm

120 kV 40 μA Z0

x-ray 01
User: ???

Figure 6.6: Heat Pipe with very slight Wick distortion due to Freeze Thaw Cycling

01 OK

2007.12.21 10:16

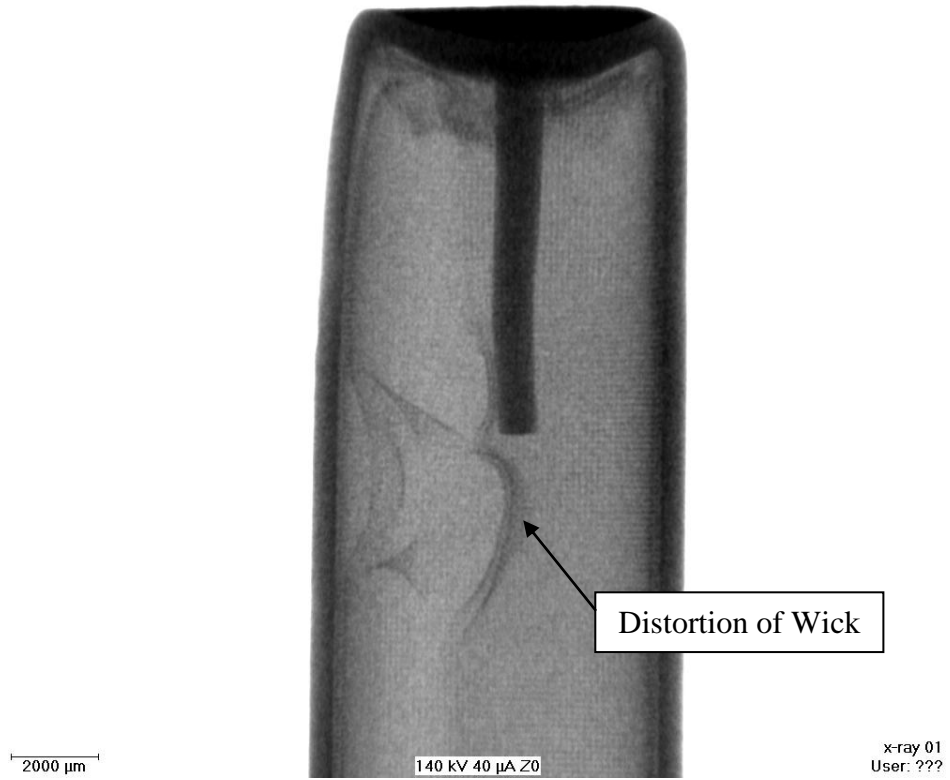


Figure 6.7: Heat Pipe Sample with Wick distortion due to Freeze Thaw Cycling

01 OK

2007.12.21 10:16

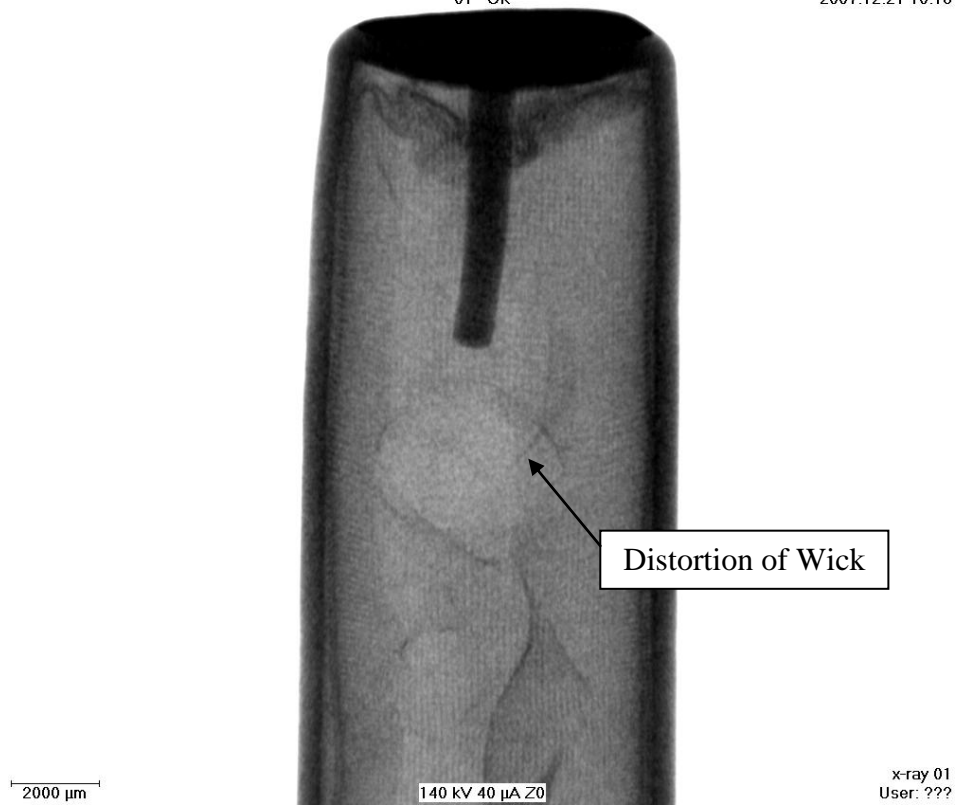


Figure 6.8: Heat Pipe Sample with Wick distortion due to Freeze Thaw Cycling

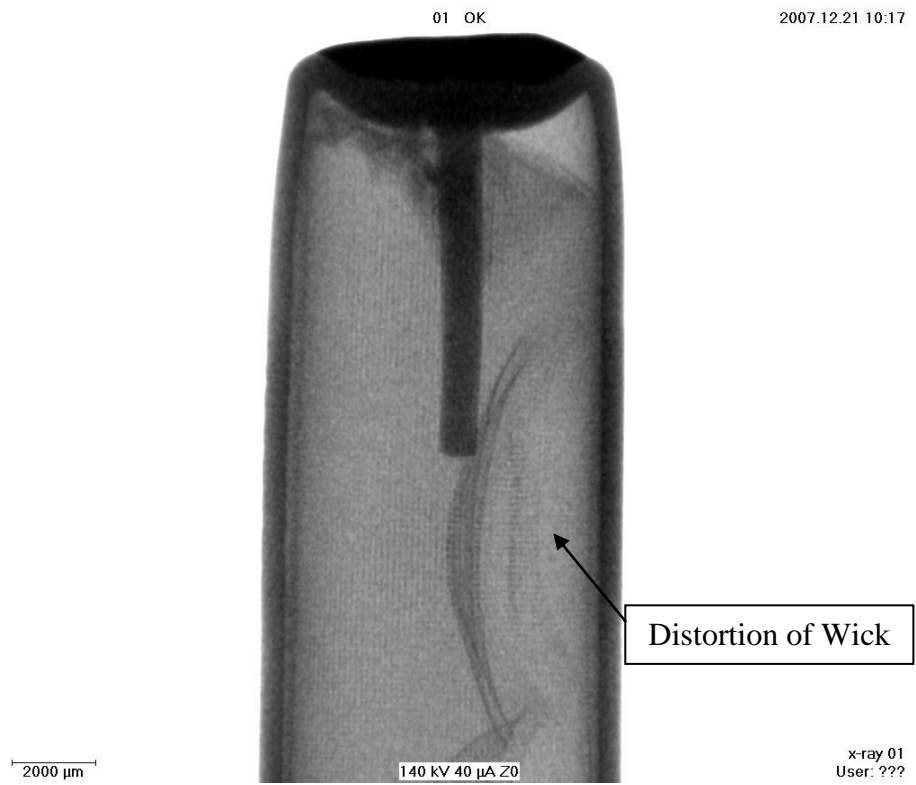


Figure 6.9: Heat Pipe Sample with Wick distortion due to Freeze Thaw Cycling

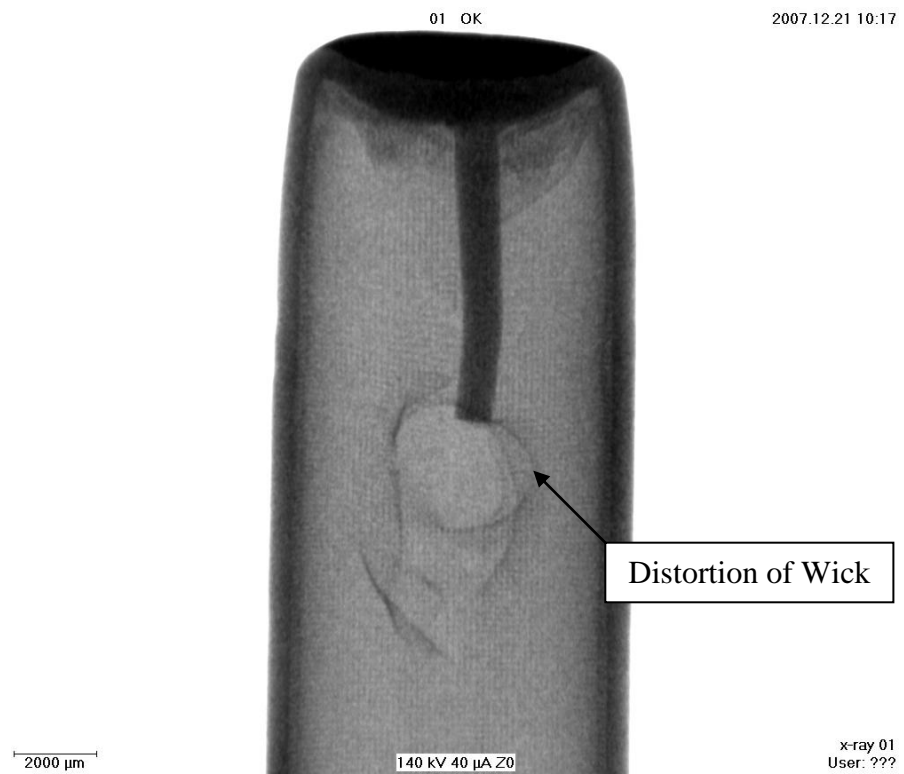


Figure 6.10: Heat Pipe Sample with Wick distortion due to Freeze Thaw Cycling

Figure 6.2 above shows a merged image out of three different x-ray shots along the length of the pipe and displays a wick as it should be in a screen mesh heat pipe produced to a good quality standard. Figure 6.3 and 6.4 show merged images out of three x-rays along the length of heat pipes where distortions of the wick due to repetitive freeze thaw cycling are visible. The pipes in Figure 6.3 and 6.4 as well as the pipes in Figures 6.5 to 6.10 were subject to 300 freeze thaw cycles between -20°C and $+20^{\circ}\text{C}$ in an upright position (90° towards the horizontal) and all show significant distortions of the wick in regions where mechanical deformation of the flattened container took place. Figure 6.3 shows two positions where the wick is removed from the wall due to water collecting between the wall and screen mesh and the expansion of the water due to freezing has caused the mesh to move as well. The pipe from Figure 6.3 shows two bulges, whilst the pipe of figure 6.4 only shows one bulge a long way up the pipe.

The Figures 6.5 to 6.10 belong to heat pipes which were previously implemented into a mechanical structure containing 16 heat pipes in total combined in four separated fin stacks and underwent a reverse engineering exercise after a mechanical deformation due to freeze thaw cycling was found. They are only exemplary for the sixteen pipes in total which were x-rayed and then retested thermally after removal from the mechanical structure. But all of these figures show a characteristic distortion of the wick where mechanical deformation of the D-shape has happened. Therefore it can be concluded that the freezing water at the bottom of the heat pipe is removing the wick from the wall. Once that phenomenon is started it gradually increases as the progressing cavity supports the problem through being filled by water. This water then

freezes during the next freeze cycle and the wick is moved further away from the wall. In extreme cases a total blockage of the vapour path can occur and the formation of a secondary bulge is possible. Yet this problem was supported by the fact that the heat pipes were not operational during these tests and the tests more related to storage conditions. Operating the heat pipes would have positively prevented the growing of the bulges and removal of the wick from the wall as it would have redistributed the working fluid inside the wick and prevented its accumulation in areas where the wick is already misaligned from the wall. Once all the X-Ray images were taken of the heat pipes within the mechanical structure, they were removed and subjected to an additional thermal function test with a fixed heat load prior to a destructive test where the amount of working fluid within the heat pipe was determined. The results of these tests as well as geometrical measurements are presented within the next section of this chapter.

Description of Experimental Procedure:

After removal of the pipes from the mechanical structure these pipes have been power tested in a horizontal orientation and the ΔT value of the pipe between the evaporator and condenser for a fixed power level of 16.5W was reported. In order to be able to conduct these tests, a purposefully designed and built test rig with two separate test stations has been used for conducting the single pass test. A picture of the test rig can be found in Fig. 6.11 below whilst the schematic diagram of the test rig and the instrumentation used can be found in Fig. 6.12, both below.



Figure 6.11: Picture of the Test Rig and Instrumentation used for the Thermal Testing

**Test Rig Scheme Two Station
Heat Pipe Tester**

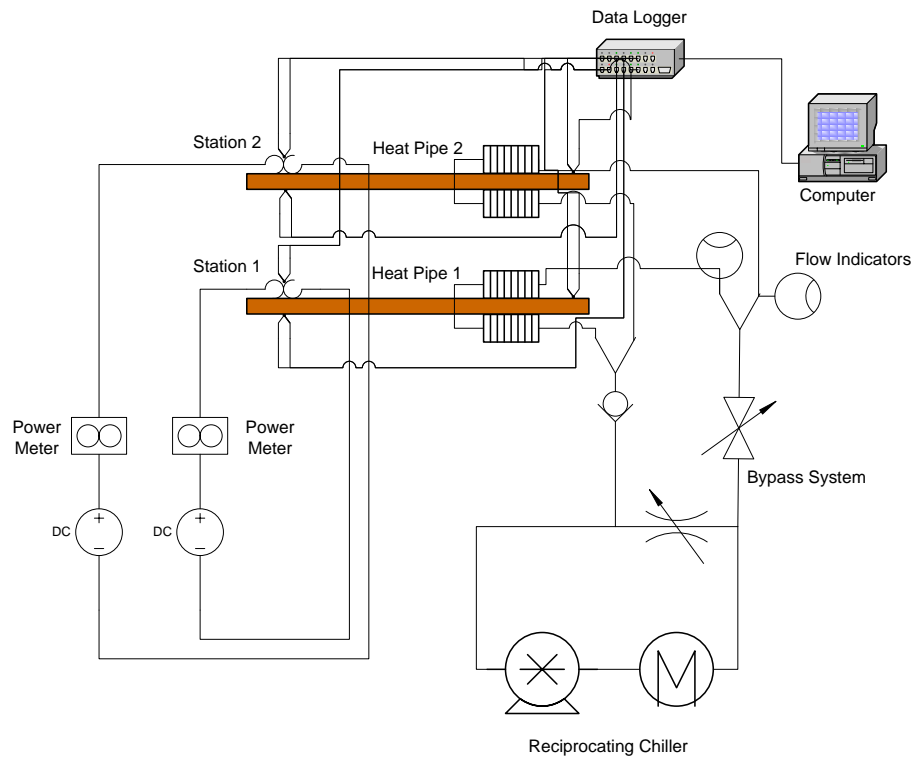


Figure 6.12: Schematic of the Test Rig and Instrumentation used for the Thermal Testing

For the tests, the thermal results can be found in the last column of Table 6.1 below, the heat load of the components was simulated using two DC heater cartridges capable of providing a maximum heat load of 25W each which were independently connected to a dual channel power supply. For the tests conducted a TTI CPX 200 power supply was used. The power level was set to 16.5W which was 110% of the system heat load per heat pipe and the power per heat pipe was independently monitored through two calibrated HAMEG power meters allowing the power to be set to two decimal places.

The cooling of the heat load introduced into the heat pipes is performed through a Lytron recirculating chiller with a set water temperature of 6°C and the flow is evenly distributed to two pairs of purposefully designed cold plates through adjustable gauge style flow indicators. The cold plates contain half circular grooves for the heat pipes round ends to rest in and to optimize thermal contact between the cold plates and the heat pipes. The flow indicators used for matching each of the cold plate pairs flow consist of a calibrated float and have their own adjuster valve to match each other's flow rate. Further the coolant circle consisted of a bypass system consisting of three valves, one one-way valve in the return path of the coolant from the cold plates and one shut off valve in the coolant feeding side to be able to close the liquid loop in the case of a leak within the test side of the rig. Finally there was an adjuster valve connecting both paths and allowing adjustment of the flow rate through the test rig and to minimize the pressure drop the chiller has to cope with to a sustainable level. A sketch of the bypass system layout can be found in the bottom right half of the test rig schematic shown in Figure 6.12 above.

The data logging of the measured temperatures was done at a sampling rate of 1 sample per second over the entire test duration of 300 seconds using an 8 channel Pico TC08-USB data logger connected to a standard PC. In total three thermocouples were used per test station, leaving the data logger with two unused connector places. The layout of both test stations was exactly the same; one thermocouple was placed within the heater block as a pure monitoring device to ensure the functionality of the interface between the heater block and the heat pipe and to prevent the rig from overheating whilst the other two were placed directly on the heat pipe. The heat input in the evaporator region was realized solely from the top of the heat pipe in order to mimic the application as close as possible. The evaporator thermocouple was embedded into a Delrin block which is a good thermal insulator and therefore seen as suitable to prevent the thermocouple mount or mechanical stop from acting as a heat sink itself. Its location was in the middle of the evaporator section, which had a length of 38.5mm from the flattened end of the heat pipe. The condenser thermocouple was of a split wire type where the temperature is measured at the point where the Constantan wire of the T-type thermocouple is touching the copper container of the heat pipes. The two wires of that thermocouple were located on a leaf spring at the very end of the heat pipe past the cold plate pairs. That location was chosen as it is the most stringent test method for a heat pipe detecting even traces of NCG (Non-Condensable Gas) in the heat pipe and would result in a thermal failure of the heat pipe. The ΔT reported in the final column of Table 6.1 below was obtained from deducting the condenser temperature from the evaporator temperature as a single point measurement at the end of the 300seconds test interval.

After the thermal tests have been carried out the heat pipes samples were labelled and weighed on high precision scales and afterwards the pipe containers were mechanically opened without removing any material and the pipe was subjected to a temperature of 120°C for duration of 2h. This is proved to be sufficient to cause all the working fluid in the container to evaporate and remove to the ambient of the oven. Afterwards the heat pipe samples were weight again and through the weight difference the fill volume at the filling temperature of 20°C was determined.

One thing to be mentioned is the fact that the distorted wick did not cause sufficient problems within the heat pipe structure to stop it from functioning. Only one pipe failed due to mechanical damage during removal from its surrounding mechanical structure.

Table 6.1 below shows the combined data of the destructive reverse engineering exercise as well as previous thermal tests the 16 heat pipe samples have under gone as well as geometrical measurements taken after removal.

	Point 1 w [mm]	Point 1 h[mm]	Weight 2[g]	Weight dry [g]	Fill [cc]	ΔT [° C]
Sample 8	7.76	4.2	14.52	14.05	0.476	5.63
Sample 14	7.62	4.29	14.56	14.08	0.486	5.19
Sample 6	7.67	4.35	14.64	14.09	0.557	3.27
Sample 5	7.7	4.51	14.78	14.05	0.739	3.14
Sample 15	7.64	4.57	14.61	14.06	0.557	7.14
Sample 4	7.6	4.62	14.6	13.94	0.668	DNF
Sample 11	7.46	5.15	14.76	14.05	0.718	5.01
Sample 2	7.36	5.19	14.14	13.46	0.688	4.93
Sample 13	7.35	5.27	14.2	13.48	0.729	7.23
Sample 3	7.46	5.28	14.84	14.07	0.779	7.17
Sample 1	7.22	5.36	14.19	13.49	0.708	4.75
Sample 10	7.3	5.36	14.84	14.07	0.779	5.57
Sample 7	7.34	5.38	14.88	14.09	0.799	8.61
Sample 9	7.09	5.44	14.17	13.43	0.749	10.94
Sample 16	7.17	5.7	14.8	14.03	0.779	10.59
Sample 12	7.16	5.79	14.81	14.02	0.799	7.55

Table 6.1: Geometrical Data Compared to Fill Information of 16 Heat Pipe Samples

The test results obtained were higher than the original failure limit of 6°C for that test rig but the deviation of the performance was not seen as solely related to the reduction in performance due to freeze thaw cycling but also to the fact that the heat pipes had been mechanically removed from a structure and therefore the interface surfaces were not as smooth as it would be representative from a thermal point of view.

In the table the data is sorted by the amount of mechanical distortion in the D-section of the pipe which is in the column 3 of the table and is a height of 4.25mm nominal. A direct link between that data and the amount of overfill can be concluded since the data clearly shows the trend that the higher the fill the higher the amount of bulging/ mechanical distortion is likely to happen in that area. This trend is shown in Figure 6.13.

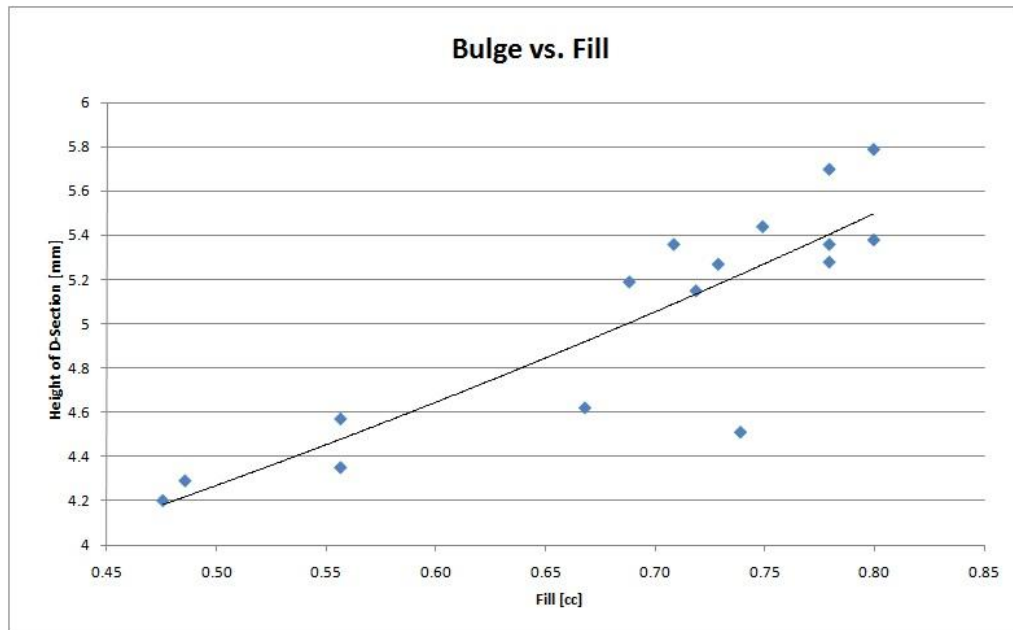


Figure 6.13: Bulging Trend vs. Heat Pipe Fill Graph

Even though the graph shows some anomalies, the trend can be clearly found that with a higher fill the risk of a bulge is increasing. It has to be considered that these pipes were in a mechanical structure as well and the data obtained is

entirely empirical and is subject to measurement errors and instruments accuracies as well as other restrains which were not closer investigated in this study.

Comparing this fill data with a fill calculated for these pipes by a software program calculating the heat pipe fill for screen wick heat pipes developed for this PhD thesis work has shown that the pipes where overfilled between 25% and 110%. This excess working fluid will form a free water column at the bottom of the heat pipe and therefore cause distortion of the heat pipe container during freezing.

It has to be pointed out that this failure mode is purely due to storage thermal cycling of the heat pipe and the failure mode being very similar is not directly linked to operational suction freezing mentioned by Peterson (1994) and envisaged by Cheung (2004). It is mostly related to excess working fluid not entirely contained in the wick.

6.5 CONCLUSIONS

When water heat pipes are exposed to lower temperatures than the freezing point of their working fluid, special attention has to be paid to a great amount of details. For example the orientation is of vast importance as it will determine where excess working fluid within the heat pipe is collecting. If the fact that any working fluid not contained in the wick coincides with an area where a shape change of the heat pipe has taken place, permanent distortions are possible up to the pipe trying to regain its original round shape or the container material ruptures. For this repetitive thermal cycling down to low

temperatures has to take place in an orientation with parts of the heat pipe facing downwards and the excess water column needs to be severe enough to leave the region where the pipe end is formed. No distortion takes places near the endform due to the fact that the endform itself hardens the pipe material and therefore helps to prevent further shape changes. Both mesh types investigated, sinter and screen mesh are subject to shape changes due to freezing if there is excess water available but the mechanisms working are very different. Within a screen mesh heat pipe it is possible that the wick is removed from the wall due to water trapped in between wall and wick, whilst in a sintered wick pipe the walls are moved outwards due to the expansion of the water column formed in the vapour space. Investigations have proved that these effects do in general not fatally reduce the thermal performance of a heat pipe and even a mechanically distorted heat pipe can carry the required power assuming that the heat transfer interfaces are still intact. This statement is seen valid for the tests described above where the heat pipes were subjected to one single set power level for an application type and not been tested to their failure power. If the test accuracy with regards to interfaces and repeatability would be high enough and the test scheme would be to measure fatal failure, it might have been found that the bulges and the wick distortions inside the heat pipe would have been severe enough to cause a reduction in the returning liquid inside the heat pipe and therefore reduce the power handling capability of the distorted heat pipes.

Further the use of X-Ray images has proved a very valuable tool to investigate the distortion of screen wick or any other anomalies within the screen wick which affect the heat pipe performance. The use of X-Ray technology for wick

investigations has not been reported to be used very often for the investigation of heat pipes despite its proven tremendous value.

CHAPTER 7 – CONCLUSIONS AND FURTHER WORK REQUIRED

Within this chapter the work presented previously in this thesis is reviewed and the most significant findings are summarised. Further areas are identified where additional work would be required or is seen as beneficial to the understanding of the subject are identified.

7.1 CONCLUSIONS:

The theoretical part of this work started by reviewing existing literature with relevance to the topic of screen mesh wick heat pipes and additional aspects to their performance and operation; for example the effects of bending but also the use of advanced wick structures and the effects of freeze- thaw behaviour. Whilst conducting that review, which is presented in chapter 2 of this thesis, it was found that only very little work had been presented on the subject of bending of heat pipes, in fact only one minor industrial reference was found. Therefore the work presented in this thesis can be seen as a starting point to gain more detailed knowledge of the effects of bending heat pipes to match applications needs and provide topics for further research in narrower areas. But the review was not limited to the effects of bending heat pipes; it also presented a general overview of heat pipe construction and the materials used for heat pipes, types of heat pipes available and their application ranges. Furthermore, the limitations of heat pipes are explained in detail and more specialised heat pipe types like loop heat pipes, capillary pumped loops and vapour chambers plus many others are described. Beyond the heat pipe types, suitable material combinations for successful lasting heat pipe operation and

working fluids for a wider range of temperatures than the low temperature heat pipes with water as the working fluid investigated in the later chapters of this thesis were introduced.

The third chapter started from some preliminary work where significant process and performance variations were identified and seen unsuitable for a scientific investigation of certain aspects of heat pipe operation. Based on these identified variations, the manufacturing processes involved in the production of heat pipes were reviewed and the area of filling and venting was identified through initial experimentation to be one of the key sources of performance variation. Firstly, it was found that for screen mesh wick heat pipes which were to be used as the core heat pipes for the investigations, no suitable calculation software for the fill was available. From that shortfall, literature was reviewed again and suitable mathematical models were found. Previous fill calculations seemed to have been done on a rather experimental basis where tables were consulted to determine the amount of working fluid required. That method was seen as problematic as it was not easy to determine the fill for different screen mesh types than the ones the tables were based on or for heat pipes with different amounts of layers of screen mesh. The tables did not consider the screen geometry such as wire diameter and opening width and therefore additional experimentation was always required. But not only were existing mathematical models used, this work was then extended and the temperature dependence of the amount of working fluid required to be able to have sufficient water molecules in the vapour space to create saturated steam was introduced. From there process improvements were identified and implemented. The fill calculation software was not only used for the heat

pipes experimentally investigated in chapters 4 and 5 but was employed to solve the problems envisaged during the freeze- thaw work presented in chapter 6 as well. During other occasions the calculation software has proved valuable by being able to theoretically determine the fill with an accuracy of 7% of the experimentally determined optimum fill amount and therefore significantly reduces the quantity of required experimentation.

The second part of the work presented within chapter 3 was conducted in order to be able to realise the ability of the screen mesh wick heat pipe of having a higher power handling capability when the same container diameter is used as would be used for a sintered heat pipe. So far a common misconception that screen mesh heat pipes cannot be used for anti-gravitational operation and working fluid would collect at the bottom. Therefore, it was seen as invaluable to have an in-depth knowledge of the boundaries of anti-gravitational operation. Literature was reviewed and mathematical models leading towards an expression for the capillary or lifting height for different screen mesh wick types were presented. The theoretical work clearly shows that screen mesh wick heat pipes do have capillary or lifting height performance and can therefore be used for anti-gravitational operation without any problems as long as their capillary or lifting height is not exceeded.

Within the third part of chapter 3 the most common failure modes during heat pipe venting were graphically illustrated and described in detail. Furthermore, it was proposed that the heat pipe venting or charging temperature on heat pipes with an optimised fill should always be higher than the continuous operating temperature to ensure that there are always sufficient water

molecules available to create saturated steam in the vapour space rather than to overcharge the heat pipes by a fixed percentage of the working fluid.

Work based around screen mesh geometries and their usability for heat pipe wicks was extended into chapter 4. Within that chapter the use of different types of screen mesh wicks within the same heat pipe and the effects, the different types of screen mesh wicks used either towards the vapour space or the heat pipe wall have on the overall heat pipe performance, is presented. Based on a statement from Reay and Kew (2006), the work was carried out as serious objections against that statement were raised. It was aimed to validate the statement that a finer wick towards the vapour space would be beneficial for the overall heat pipe performance. A review of the literature available on the subject of capillary or wicking and boiling limits for screen mesh wicks confirmed the issues, experimentation carried out during this PhD study did not quite manage to do the same. The improvement seen with the coarser wick towards the vapour space, combined with the higher failure rate of that design over the finer wick towards the vapour space was too marginal to conclude with confidence that this combination is superior. The doubts were further confirmed by the fact that both designs fell short of the performance of the well established two layer of the same screen mesh wicked heat pipe. In order to be able to definitely prove or disprove the statement from literature, additional work would be required and could prove beneficial to obtain new valuable screen mesh wicked heat pipes tailored for certain applications.

In chapter 5, the effects of bending on screen mesh wick heat pipe performance are investigated. Firstly, investigation were carried out using CFD software, but unfortunately the accuracy of the CFD software available

made it difficult to have confidence in the results and the results differed significantly from the experimental results. At the current stage, even with techniques like separate phase modelling, CFD software and available mathematical models fall short of being useful in investigating two-phase phenomena occurring inside a heat pipe when combined with a shape change like a bend at the microscopic level. It is seen that each model is too inaccurate to make results obtained for the combination of the multiple models meaningful. 1 and 2D models can accurately predict the performance of heat pipes but cannot be used to investigate the effects of 3D bends.

During a later section of that chapter the design of a test rig used for the heat pipe experimentation is described. This design has proved to be suitable and accurate enough for the experimental work that was conducted.

Finally, experimentation was been carried out with five different sets of heat pipes with bend angles of 0° , 45° , 90° , 135° and 180° and a batch size of five heat pipes per set. The tests for each heat pipe were carried out under equal conditions and the power level introduced to each heat pipe was the only parameter varied. The results were averaged per design in order determine the performance achievable for a certain design rather than relying on a single heat pipe performance. Depending on the geometrical shape the process variation varied in intensity, but a clear trend for the effects of the bends could be developed. The trend indicates that the performance of screen mesh wick heat pipes is reduced significantly when bent, but once the bend angle has reached 90° , the performance reduction for higher bend angles is almost negligible. Up to a bend of 90° the performance is reduced significantly to around 50% of the straight heat pipe performance.

A second order equation based on the experimental results has been developed and is able to calculate the expected performance of heat pipes of the same design and length but with bend angles other than the ones experimentally investigated. Based on the calculated straight heat pipe performance, the performance of the heat pipe design with the bend angle can be determined and considered for more accurate application designs.

Chapter 6 presents work investigating the effects of freeze- thaw on heat pipes and in particular multiple freeze- thaw cycling. Starting with an application specific problem the root cause of the problem was linked to the fill and amount of working fluid within the heat pipes. That link could further proven as the problem became more apparent during orientations where the heat pipes were vertical and excess working fluid was allowed to accumulate in the bottom of the heat pipes where the normal shape changed. That excess working fluid caused the container material to bulge and remain plastically deformed. Since this phenomenon was a growing one and the bulges became more severe with each cycle, there was concern that the freezing of working fluid, in this case water, would be able to rupture the container material and therefore cause the heat pipe to cease operation. Finding a solution to this problem was therefore vital to ensure that the heat pipes remained suitable for this particular application. During the investigation of the already deformed heat pipes, X-ray imaging technology has proved to be an invaluable tool to visualise the effects inside the heat pipe and the fact that it is a non-destruction test was of great value. The visualisation confirmed that working fluid was trapped in pockets of the wick and therefore was able to expand locally and cause the container material to move outwards. So far very little further use of

X-ray technology to investigate heat pipes as an entire assembly has been reported. After identifying the root cause of this issue, the elimination was rather straight forward and offered the first proof for the value of the calculation software developed and presented in chapter 3 of this thesis. The calculation software was successfully used to determine a fill which accurately coincided with experimentally obtained results. Through a suitable fill, which was considerably less than at the beginning of the investigation, the problem could be eliminated. Copper water screen mesh wick heat pipes proved to be able to withstand temperatures below the freezing point of water without any geometrical deformation of the heat pipe container.

7.2 FURTHER WORK REQUIRED:

Within this thesis, work was predominantly focussed on screen mesh heat pipes and parameters associated with their wick structure. Therefore, an expansion of the work presented in this thesis can be undertaken in different directions, either to broaden the work and expand it to cover other wick structures like sintered heat pipes and grooved heat pipes or going into more detail and improving manufacturing processes and conducting further experimentation with different screen mesh types and multiple combinations of different screen mesh layers within a heat pipe.

Starting in a chronological order to review where additional work would be beneficial, it was found that very little work is reported into the investigation of bending and shape changes of heat pipes. Both theoretical investigations and practical experimentation into bending and shape changes of heat pipes

are not existent. It would have been beneficial to have a comparison of work presented by others as a benchmark, but since there is none, the work presented in this thesis will fill that gap and be available to others as a benchmark.

From the manufacturing aspect it was found that that process parameters like the fill for screen mesh heat pipes were partially described mathematically, but the work is very fragmented and therefore hard to collect and combine in a useful manner. Based on this experience, a review paper with emphasis on the manufacturing processes and process parameters would be seen beneficial as in order to create a link between academia and the heat pipe manufacturing industry. That link seems to be non-existent at the present moment as most information concerns experimental results on entire heat pipes and does not investigate certain wick structures or fill parameters. The heat pipes used for tests appear to just appear and very little consideration or explanation on the manufacturing process is provided.

Within chapter 4 the aim was to advance the use of screen mesh wicks for heat pipes and whilst doing so it was found that the work is not totally free of obstacles. Additional experimental work with different screen mesh wicks and different screen wick compositions within the same heat pipes would round up the overall results. In particular testing a batch of heat pipes with two layers of a rather coarse 100 screen mesh as a wick and a similar batch of heat pipes with two layers of the finer 200 screen mesh would be beneficial, not only would it give additional data to compare, but also to judge the manufacturing issues envisaged during the work with dissimilar meshes. Furthermore this

would allow a benchmark of the accuracy of the calculation software developed in an earlier part of this thesis.

Once these results are obtained for the horizontal heat pipe orientation they could then be expanded to include vertical heat pipe orientation. This work would then be used to validate the empirical findings presented in the first part of that chapter.

Work presented in chapter 5 of this thesis comprises of a number of different tasks. One task attempted to use commercial available CFD software to investigate the effects of bends on the pressure drop of a thin film flow like the liquid return in a heat pipe. During the use of the software it was found that at the present moment the commercially available CFD software is not able to provide accurate pressure drop results and a review of the results for the entire set of bend angles was found to be incorrect. The main problem was the amount of mesh cells required. Due to the thin feature and the 3D geometry, a very large number of cells were required and this caused problems to be run on a standard CFD PC. One solution to the problem would be the scaling function along a heat pipe axis rather one of the three coordinate axis or improved mathematical models for thin features. With currently available software, the model had to be amended to such a high degree it was no longer an accurate representation of the conditions within a heat pipe.

On the experimental side of the presented work there are two main parts, into which the work could be expanded, the first would be to broaden the work to additional wick structures or different geometries. So far, work presented in this thesis has been limited to screen mesh wick heat pipes whilst the most common heat pipe in terms of quantities produced worldwide is the heat pipe

with a sintered wick structure. Therefore expanding the work to sintered heat pipes would be the next logical step in order to obtain a full picture of the effects of bending on heat pipe performance. Sintered heat pipe wicks are seen as less susceptible to the effects of bending as the wick is in permanent contact with the container wall and if certain parameters like correct sintering temperature and minimum bend angle are considered, the wick should not separate from the wall. Therefore the liquid return should be less affected than in a screen wick heat pipe and the effects should be less severe. Further the work of the production optimisation for sintered heat pipes is seen as being easier as the heat pipe type is a lot more common and therefore the parameters to be considered like porosity and pore size within the wick structure are better described mathematically.

Additionally, to the work suggested above, the experimentation and theoretical work could be expanded to investigate the effects of flattening heat pipes and how the performance will change. This would then guide towards understanding all the shape changes which could be carried on a heat pipe in real life applications and allow the prediction of potential performance losses for both shape changes occurring alone as well as combined. Having an indication of these performance losses available would be well appreciated by the industries applying heat pipes to their products. As a second part, the work could be expanded to different diameters of screen mesh wick heat pipes and different types of screen wicks in order to validate the expression found for the performance losses due to bends. Using different types of screen wicks might guide towards a different set of results which would either require a new expression or an offset for the existing expression.

For the work carried out in chapter 6, it would be beneficial to define a method of testing which could accommodate the existence of bulges in the heat transfer surface or have a means to test heat pipes incorporating bulges allowing the comparison of prior results and past bulging and not having to re-flatten the heat pipes prior to the tests. Furthermore, it would have been beneficial to have the initial results of the heat pipes tested prior to the freeze-thaw cycling, but this was not available in this case. These results would then allow the assessment of performance degradation due to the screen mesh wicks being locally removed from the wall and therefore reducing the available heat transfer surface and influencing the liquid return to the evaporator.

REFERENCES

Aleksandravicius, T. A., (2008). Investigation of the Results of a Heat Pump in a real House. *Proceedings of the 7th Minsk International Seminar "Heat Pipes, Heat Pumps, Refrigerators, Power Sources"*, Minsk, Belarus.

Amili, P. and Yortsos, Y. C., (2004). Stability of heat pipes in vapour-dominated systems. *Int. J. Heat Mass Transfer*, Vol.47, pp. 1223-1246.

Anon., (2005). Major loss in Ducts, Tubes and Pipes. *Engineering Toolbox*, http://www.engineeringtoolbox.com/major-loss-ducts-tubes-d_459.html, (Accessed 20 October 2006).

Banerjee, R.; et al., (2002). Features of Automotive Gas Tank Filler Pipe Two-Phase Flow: Experiments and Computational Fluid Dynamics Simulations. *Journal of Engineering for Gas Turbines and Power, Transactions of the ASME*, Vol. 124, pp. 412-420.

Barletta, A. and Rossi di Schio, E., (2001). Analysis of the Effects of Viscous Dissipation for Laminar Flow in Stadium Shaped Ducts. *Int. Comm. Heat Mass Transfer*, Vol.28, pp. 449-459.

Brautsch, A. and Kew, P., (2002). Examination and visualisation of heat transfer processes during evaporation in capillary porous structures, *Appl. Thermal Eng.*, Vol. 22, pp. 815-824.

C&R Technologies, (2008). How to model a Heat Pipe. <http://www.crtech.com>, (Accessed 22 September 2008)

Canti, G.; et al., (1998). Thermal hydraulic characterisation of stainless steel wicks for heat pipe applications. *Rev. Gén. Therm.*, Vol. 37, pp. 5-16.

Canti, G.; et al., (2002). Thermal hydraulic characterisation of a heat pipe with extracapillary circulation. *Int. J. Therm. Sci.*, Vol. 41, pp. 115-123.

CD-adapco, (2007). Star-CCM+/Design v.2.06 Training Handbook, London.

Chen, P.C. and Lin, W. K., (2001). The application of capillary pumped loop for cooling of electronic components. *Appl. Thermal Eng.*, Vol. 21, pp. 1739-1754.

Cheung, K., (2004). Qualification of Copper Water Heat Pipes for Space Applications. US Naval Research Laboratory, <http://www.nrl.navy.mil/content.php?P=04REVIEW153>, (Accessed 20 February 2008).

Cole, J.S.; Donnelly, G.F. and Spedding, P.L., (2004). Friction Factors in Two Phase Horizontal Pipe Flow. *Int. Comm. Mass. Transfer*, Vol. 31, pp. 909-917.

Cotter, T.P.; Grover, G.M., and Erickson, G.F., (1964). Structures of very high thermal conductance. *Journal of Applied Physics*, Vol. 35, pp. 1990-1991.

di Francescantonio, N.; Savino, R. and Abe, Y., (2008). New alcohol solutions for heat pipes: Marangoni effect and heat transfer enhancement. *Int. J. Heat Mass Transfer*, Vol. 51, pp. 6199-6207.

Engineer's Edge, (2006). Def. Roughness Height: URL: http://www.engineersedge.com/surface_finish.htm, (Accessed 4 October 2006)

European Cooperation for Accreditation of Laboratories, (1997). *EAL-G31: Calibration of Thermocouples*.

Faghri, A., (1992). Frozen start-up behaviour of low-temperature heat pipes. *Int. J. Heat Mass Transfer*, Vol. 35, pp. 1681-1694.

Faghri, A., (1995). *Heat Pipe Science and Technology*. 1st Edition, Taylor and Francis Group, Oxon.

Fu, F. and Klausner, J.F., (1997). A separated Flow model for predicting two-phase pressure drop and evaporative heat transfer for vertical annular flow. *Int. J. Heat and Fluid Flow*, Vol. 18, pp. 541-549.

Garner, S.D., (1996). Heat Pipes for Electronics Cooling Applications. *Electronics Cooling*, Vol. 2. <http://electronics-cooling.com>. (Accessed 12 December 2007).

Groll, M.; et al., (1998). Thermal control of electronic equipment by heat pipes. *Rev. Gén. Therm.*, Vol. 37, pp. 323-352.

Haddad, A.; Boukhanouf, R. and Buffone, C., (2006). Testing of vapour chamber used in electronics cooling. *Proceedings of the 9th International Conference on Advanced Computational and Experimental Measurements in Heat and Mass Transfer*, The New Forrest, United Kingdom.

Harris, D.K. and Goldschmidt, V.W., (1999). An empirical investigation into the external heat transfer of a U-bend in cross-flow. *Int. J. Heat Mass Transfer*, Vol.42, pp. 1957-1968.

Hewitt, G.F.; Shires, G.L. and Bott, T.R., (1994). *Process Heat Transfer*. 1st Edition, CRC Press, London.

Hoa, C.; Demolder, B. and Alexandre, A., (2003). Roadmap for developing heat pipes for ALCATEL SPACE's satellites. *Appl. Thermal Eng.*, Vol. 23, pp. 1099-1108.

Hoang, T. T., (1997), Development of an Advanced Capillary Pumped Loop. *Proceedings of the 27th International Conference on Environmental Systems*, Lake Tahoe, USA

Houghton, E.L. and Brock, A.E., (2001). *Tables for Compressible Flow*. 3rd Edition, Butterworth Heinemann, Oxford.

Hwang, G.S.; et al., (2007). Modulated wick heat pipe. *Int. J. Heat Mass Transfer*, Vol.50, pp. 1420-1434.

Imura, H., et al., (1988). Heat-Transfer Characteristics of Screen-Wick Heat Pipes. *JSME International Journal*, Vol.31, pp. 88-97.

Imura, H.; Kozai, H. and Ikeda, Y., (1994). The effective Pore Radius of Screen Wicks. *Heat Transfer Engineering*, Vol.15, pp. 24-32.

International Standard ISO 4783-1:1989. *Choice of aperture size and wire diameter combinations for industrial wire screens and woven wire cloth – Part 1: General*. ISO, London.

International Standard ISO 4783-2:1989. *Choice of aperture size and wire diameter combinations for industrial wire screens and woven wire cloth – Part 2: Preferred combinations for woven wire cloth*. ISO, London.

Ismail, K. A. R. and Zanardi, M. A., (1996). A steady-state model for heat pipes of circular or rectangular cross-sections. *Appl. Thermal Eng.*, Vol.16, pp. 753-767.

Jang, J. H.; et al., (1989). Mathematical Modelling and Analysis of Heat Pipe Start-Up from the Frozen State. NASA Contractor Report 185132.

Joudi, K. A. and Witwit, A. M., (2000). Improvements of gravity assisted wickless heat pipes. *Energy Conversion & Management*, Vol.41, pp. 2041-2061.

JEDEC Publications, (2006). *JEP140: Beaded Thermocouple Temperature Measurements of Semiconductor Package*.

Kempers, R.; Ewing, D. and Ching, C.Y., (2006). Effects of number of mesh layers and loading on the performance of screen mesh wick heat pipes. *Appl. Thermal Eng.*, Vol. 26, pp. 589-505.

Kim, K S.; et al., (2003). Heat pipe cooling technology for desktop PC CPU. *Appl. Thermal Eng.*, Vol. 23, pp. 1137-1144.

Kozai, H.; Imura, H. and Ikeda, Y., (1991). The Permeability of Screen Wicks. *JSME International Journal*, Vol. 34, pp. 212- 219.

Lacasse, D.; Turgeon, E. and Pelletier, D., (2004). On the judicious use of the $k-\epsilon$ model, wall functions and adaptivity. *Int. J. Therm. Sci.*, Vol. 43, pp. 925-938.

Legierski, J.; Wiecek, B. and de Mey, G., (2006). Measurements and simulations of transient characteristics of heat pipes. *Microelectronics Reliability*, Vol.46, pp. 109–115.

Leong, K.C.; Liu, C.Y. and Lu, G.Q., (1997). Characterisation of Sintered Copper Wicks used in Heat Pipes. *Journal of Porous Materials*, Vol. 4, pp. 303-308.

Löhner, R.; et al., (2006). Improving the speed and accuracy of projection-type incompressible flow solvers. *Comput. Methods Appl. Mech. Engrg.*, Vol. 195, pp. 3087-3109.

Lu, G. and Wang, J., (2008). Experimental investigation on heat transfer characteristics of water flow in a narrow annulus. *Appl. Therm. Eng.*, Vol. 28, pp. 8-13.

Lucas, K., (2000). *Thermodynamik - Die Grundgesetze der Energie- und Stoffumwandlung*. (in German), 2nd Edition, Springer, Berlin.

Lun, I.; Calay, R. K. and Holdo, A. E., (1996). Modelling Two-Phase Flows using CFD. *Applied Energy*, Vol.53, pp. 299-314.

Ma, H. B.; Peterson, G. P. and Peng, X.F., (1996). Experimental Investigation of countercurrent Liquid-Vapour Interactions and their Effect on the Friction Factor. *Experimental Thermal and Fluid Science*, Vol. 12, pp.25-32.

Maydanik, Y.F., (2006). Loop Heat Pipes. *Appl. Thermal Eng.*, Vol. 25, pp. 635-657.

Maziuk, V.; et al., (2001). Miniature heat-pipe thermal performance prediction tool – software development. *Appl. Thermal Eng.*, Vol. 21, pp. 559-571.

McGlen, R. J., (2007). Advanced Thermal Management Techniques for High Power Electronic Devices. PhD thesis, University of Newcastle upon Tyne.

McKeon, B.J.; Zagarola, M.V. and Smits, A.J., (2005). A new Friction Factor Relationship for fully developed Pipe Flow. *J. Fluid. Mech.*, Vol. 538, pp. 429-443.

Moffat, R. J., (1997). Notes on using Thermocouples. *Electronics Cooling*, Vol. 3. www.electronics-cooling.com, (Accessed 19 November 2007).

Mongia, R. K., (2007). Heat Pipe in Future Mobile Platforms. *Proceedings of the 14th International Heat Pipe Conference*, Florianopolis, Brazil

Moon, S. H.; et al., (2004). Experimental study on the thermal performance of micro-heat pipe with the cross-section of polygon. *Microelectronics Reliability*, Vol.44, pp. 315-321.

Murer, S.; et al., (2005). Experimental and numerical analysis of the transient response of a miniature heat pipe. *Appl. Thermal Eng.*, Vol. 25, pp. 2566-2577.

Mwaba, M.; Huang, X. and Gu, J., (2006). Influence of wick characteristics on heat pipe performance. *Int. J. Energy Research*, Vol. 30, pp. 489-499.

Noren Products Inc., (2008). Guide to Designing. <http://www.norenproducts.com>, (Accessed 22 September 2008).

Ochterbeck, J.M. and Peterson, G.P., (1991). Visualisation of the Freeze/Thaw Characteristics of a Copper/ Water Heat Pipe: Effects of Non-Condensable Gas Charge. *AIAA Paper 91-1402*.

Ochterbeck, J.M. and Peterson, G.P., (1992). Experimental Investigation of Freezing Blowby on a Copper/ Water Heat Pipe”, *AIAA Paper 92-2909*.

Ochterbeck, J.M. and Peterson, G.P., (1995). Investigation of the Freezing Blowby Phenomenon in Heat Pipes. *Journal of Thermophysics and Heat Transfer*, Vol. 9, pp. 314-321.

Pastukhov, V.G. and Maydanik, Y.F., (2006). Low-noise cooling system for PC on the base of loop heat pipes. *Appl. Thermal Eng.*, Vol. 27, pp. 894-901.

Pereira, C. A., (2008). Back to Earth and real big business: Heat Pipes from Satellites and Microchips to Industry. *Proceedings of the 7th Minsk International Seminar “Heat Pipes, Heat Pumps, Refrigerators, Power Sources”*, Minsk, Belarus.

Peterson, G. P., (1994). *An Introduction to Heat Pipes: Modelling, Testing and Applications*. 1st Edition, John Wiley & Sons, Inc., New York.

Peterson, G.P. and Ma, H.B., (1996). Analysis of Counter-current Liquid-Vapour Interactions and the Effect on the Liquid Friction Factor. *Experimental Thermal and Fluid Science*, Vol. 12, pp.13-24.

Pico Technology, (2007). *Thermocouple Application Note*. www.picotech.com, (Accessed 20 November 2007).

Quick Cool Heat Transfer GmbH, (2008). Einbauhinweise Heat Pipes. (In German), <http://www.quick-cool.de/index.html> , (Accessed 17 October 2008).

Reay, D. and Kew, P., (2006). *Heat Pipes*, 5th Edition, Elsevier, London.

Reynolds, O., (1883). An experimental investigation of the circumstances which determine whether the motion of water shall be direct or sinuous, and of the law of resistance in parallel channels. *Philosophical Transactions of the Royal Society*, Vol. 174, pp. 935–982

Riffat, S.B.; et al., (2004). Development of a simplified heat pipe numerical model and case study/experimental validation using a long ‘wicked’ heat pipe. *Int. J. Energy Res*, Vol. 28, pp.1293-1311.

Rogers, C.F.C. and Mayhem, Y.R., (1995). *SI Units*. 5th Edition, Blackwell Publishing, Oxford.

Romeo, E.; Royo, C. and Monzó, A., (2002). Improved explicit equations for estimation of the friction factor in rough and smooth pipes. *J. Chem. Eng.*, Vol. 86, pp. 369-374.

Rosenfeld, J., (2006). Ultra-Lightweight Magnesium Heat Pipes for Spacecraft Thermal Management. Internal Documentation, Thermacore Inc.

Sarraf, D. B.; Bonner, R. W. and Colahan, D., (2006), Passive Thermal Management for a Fuel Cell Reforming Process. *Proceedings of the 4th International Energy Conversion Engineering Conference*, San Diego, USA

Sarraf, D.B. and Anderson, W.G., (2007). Heat Pipes for High Temperature Thermal Management, *Proceedings of IPACK2007*, ASME InterPACK'07, Vancouver, Canada.

Sauciuc, I.; Akbarzadeh, A. and Johnson, P., (1996). Temperature control using variable conductance closed two-phase heat pipe. *Int. Comm. Mass. Transfer*, Vol. 23, pp. 427-433.

Savino, R.; Abe, Y. and Fortezza, R., (2008). Comparative study of heat pipes with different working fluids under normal gravity and microgravity conditions. *Acta Astronautica*, Vol. 63, pp. 24-34.

Savino, R.; et al., (2009). Marangoni heat pipe: An experiment on board MIOsat Italian microsatellite. *Acta Astronautica*, Vol. 65, pp. 1582-1592.

Semenic, T.; Lin, Y.Y., Catton, I. and Sarraf, D.B., (2008). Use of biporous wicks to remove high heat fluxes. *Appl. Thermal Eng.*, Vol. 28, pp. 278-283.

Shankara Narayanan, K.R., (2005). What is a Heat Pipe? *Cheresources.com*, www.cheresources.com, (Accessed 17 November 2005)

Shao, L. and Riffat, S.B., (1995). Accuracy of CFD for Predicting Pressure Losses in HVAC Duct Fittings. *Applied Energy*, Vol. 51, pp. 233-248.

Spedding, P.L. and Benard, E., (2007). Gas-liquid two phase flow through a vertical 90° elbow bends. *Experimental Thermal and Fluid Sciences*, Vol. 31, pp. 761-769.

Spiga, M. and Dall'Olio, R., (1995). Friction Factor and Nusselt Number in Flat Tubes with round Edges. *Int. J. Heat and Fluid Flow*, Vol. 16, pp. 307-310.

Suman, B.; De, S. and DasGupta, S., (2005). A model of the capillary limit of a micro heat pipe and prediction of the dry-out length. *Int. J. Heat and Fluid Flow*, Vol. 26, pp. 495-505.

Supa-Amornkul, S.; Steward, F. R. and Lister, D. H., (2005). Modelling Two-Phase Flow in Pipe Bends. *Journal of Pressure Vessel Technology, Transactions of the ASME*, Vol. 127, pp. 204-209.

Sussman, M.; Smereka, P. and Osher, S., (1994). A Level Set Approach for Computing Solutions to Incompressible Two-Phase Flow. *Journal of Computational Physics*, Vol. 114, pp. 146-159.

Thermacore Inc., (2008). *Internal Process Documentation*. Lancaster, USA

Tournier, J.M. and El-Genk, M.S., (1996). A vapour flow model for analysis of liquid metal heat pipes from frozen state. *Int. J. Heat Mass Transfer*, Vol.39, pp. 3767- 3780.

Vasiliev, L.L., (1998). State-of-the-Art on Heat Pipes Technology in the former Soviet Union. *Appl. Thermal Eng.*, Vol. 18, pp. 507-551.

Vasiliev, L. Jr.; et al., (2008). An Advanced Miniature Copper Heat Pipes Development for Cooling systems of mobile PC platforms. *Proceedings of the 7th Minsk International Seminar "Heat Pipes, Heat Pumps, Refrigerators, Power Sources"*, Minsk, Belarus

Vukovic, M. and Watkins, J., (1999). Reliability Characterization of Copper/Water heat pipe below 0°C. *Advances in Electronic Packaging*, ASME, Vol. 26, pp. 1979-1987.

Wikipedia, (2008). <http://de.wikipedia.org/wiki/Dampfdruck> (in German) (Accessed 5 February 2008).

Williams, R. R. and Harris, D. K., (2005). The heat transfer limit of step-graded metal felt heat pipe wicks. *Int. J. Heat Mass Transfer*, Vol.48, pp. 293-305.

Wongwises, S., (1998). Interfacial Friction Factors in counter-current stratified Two-Phase Flow in a nearly-horizontal circular Pipe. *Int. Comm. Mass. Transfer*, Vol. 25, pp. 369-377.

Yao, G.F. and Ghiaasiaan, S.M., (1996). Wall friction in annular dispersed two-phase flow. *Nuclear Engineering and Design*, Vol.163, pp.149-161.

Zaghdoudi, M.C.; Tantolin, C. and Godet, C., (2004). Use of Heat Pipe Cooling Systems in the Electronics Industry”, *Electronics Cooling*, Vol. 10. <http://electronics-cooling.com>, (Accessed 14 February 2008).

Zan, K. J.; et al., (2004). Analysis of the parameters of the sintered loop heat pipe. *Heat Transfer- Asian Research*, Vol.33, pp. 515-526.

Zhang, H. and Zhuang, J., (1998). Research, development and industrial application of heat pipe technology in China. *Appl. Thermal Eng.*, Vol. 23, pp. 1067-1083.

Zhu, N. and Vafai, K., (1999). Analysis of cylindrical heat pipes incorporating the effects of liquid-vapour coupling and non-Darcian transport- a closed form solution. *Int. J. Heat Mass Transfer*, Vol.42, pp. 3405-3418.

Zuo, Z. J. and Faghri, A., (1998). A network thermodynamic analysis of the heat pipe. *Int. J. Heat Mass Transfer*, Vol.41, pp. 1473-1484.

LIST OF PUBLICATIONS ANDREAS ENGELHARDT

1. Engelhardt, A., Buffone, C., Riffat, S. and Zhao, X., Experimental study of a novel thermoelectric/ heat-pipe assembly for probe cooling of the surface analysing machine, Proceedings of the 14th International Heat Pipe Conference, Florianopolis, Brazil, April 2007
2. Engelhardt, A., Passive Heat Sinks Designed to Out-perform Active Solutions, Bodo's Power, www.bodospower.com, April 2008
3. Engelhardt, A., Lynn, K.V., Riffat, S. and Zhao, X., Theoretical and experimental study of a copper-water screen mesh heat pipe for an airborne application with particular Focus on the effects of multiple freeze thaw cycles, Proceedings of the 8th Minsk International Seminar "Heat Pipes, Heat Pumps, Power Sources and Refrigeration", Minsk, Belarus, September 2008
4. Engelhardt, A., Pushing the Boundaries of Heat Pipe Operation, Electronics Cooling Magazine, www.electronics-cooling.com, November 2008
5. Engelhardt, A., Poehl, M., Mitic, G., Broadbent, J., Riffat, S. and Zhao, X., Water-methanol based heat pipe array for automotive application, Submitted to *Appl. Thermal Engineering* for Correction, February 2009

APPENDICES

The appendices for this thesis contain four parts, first a table from a book which was used as the basis for the temperature dependant fluid charge/ fill level calculation is reproduced. The second part presents the images for the flow characteristics like velocity vectors and pressure distributions for the cases investigated using CFD software. The results were presented earlier but this gives the chance to observe how these results were obtained. As a third part, the results of the thermocouple calibration for the thermocouples used for the experiments are presented to allow accessing the quality of the thermocouples used. Finally as a fourth part the additional graphs for the bending and additional heat pipe experiments are presented as analysed and recorded.

Appendix 1 – Data Table for Temperature Dependence of Fill Calculations

Due to the relevance of the data presented by Lucas [45] as Table A1.1 “Properties of Water and Steam – Saturation Phase – Temperature Table” for the fill calculation work presented in chapter 3 of this thesis, the most relevant data is reproduced and shown here. Additional data can be found within the original source but has had little used during the work presented and is therefore not reproduced.

Within the following table A1.1, v' represents the specific volume of the liquid phase for water. The specific volume is the inverse of the density for the fluid in a certain phase. The second half of the third column, v'' , represents the specific volume of water vapour in the saturated state. That is the state where the maximum possible amount of water molecules is held by the vapour and that is the state to be aimed for to achieve in a heat pipe at a certain temperature and therefore these values are used for the look-up function within the heat pipe fill calculation software developed.

t	p	Spec. Volume	
		v'	v''
°C	kPa	m ³ /kg	
0.01	0.6113	0.001	206.14
5	0.8721	0.001	147.12
10	1.2276	0.001	106.38
15	1.7051	0.001	77.93
20	2.339	0.001	57.79
25	3.169	0.001	43.36
30	4.246	0.001	32.89
35	5.628	0.00101	25.22
40	7.384	0.00101	19.52
45	9.593	0.00101	15.26
50	12.349	0.00101	12.03
55	15.758	0.00102	9.568
60	19.94	0.00102	7.671
65	25.03	0.00102	6.197
70	31.19	0.00102	5.042
75	38.58	0.00103	4.131
80	47.39	0.00103	3.407
85	57.83	0.00103	2.828
90	70.14	0.00104	2.361
95	84.55	0.00104	1.982
100	0.10135	0.00104	1.6729
105	0.12082	0.00105	1.4194
110	0.14327	0.00105	1.2102
115	0.16906	0.00106	1.0366
120	0.19853	0.00106	0.8919
125	0.2321	0.00107	0.7706
130	0.2701	0.00107	0.6685
135	0.313	0.00108	0.5822
140	0.3613	0.00108	0.5089
145	0.4154	0.00109	0.4463
150	0.4758	0.00109	0.3928
155	0.5431	0.0011	0.3468
160	0.6178	0.0011	0.3071
165	0.7005	0.00111	0.2727
170	0.7917	0.00111	0.2428

t	p	Spec. Volume	
		v'	v''
°C	kPa	m ³ /kg	
175	0.892	0.00112	0.2168
180	1.0021	0.00113	0.19405
185	1.1227	0.00113	0.17409
190	1.2544	0.00114	0.15654
195	1.3978	0.00115	0.14105
200	1.5538	0.00116	0.12736
205	1.723	0.00116	0.11521
210	19062	0.00117	0.10441
215	2.104	0.00118	0.09479
220	2.318	0.00119	0.08619
225	2.548	0.0012	0.07849
230	2.795	0.00121	0.07158
235	3.06	0.00122	0.06537
240	3.344	0.00123	0.05976
245	3.648	0.00124	0.05471
250	3.947	0.00125	0.05013
255	4.319	0.00126	0.04598
260	4.688	0.00128	0.04221
265	5.081	0.00129	0.03877
270	5.499	0.0013	0.03564
275	5.942	0.00132	0.03279
280	6.412	0.00133	0.03017
285	6.909	0.00135	0.02777
290	1.436	0.00137	0.02557
295	7.993	0.00138	0.02354
300	8.581	0.0014	0.02167
350	9.202	0.00143	0.01995
310	9.856	0.00145	0.01835
315	10.547	0.00147	0.01687
320	11.274	0.0015	0.01549
330	12.845	0.00156	0.013
340	14.586	0.00164	0.0108
350	16.513	0.00174	0.00881
360	18.651	0.00189	0.00695
370	21.03	0.00221	0.00493
374.14	22.09	0.00316	0.00316

Appendix 2 – Result Plots obtained from the CFD Runs

Within the second part of the appendices the result plots from the CFD runs are presented. Within the part there are two sections representing different CFD models run. First a model investigating the effects of bends within heat pipes when subjected to an annular single phase flow using separate flow modelling techniques is presented with all five bending cases.

The second part contains the result plots for a full flow where the flow rate was adapted to cater for the increased space available. The flow velocity entering the pipes at the front end was maintained at the same level as during the annular flow cases. For both of the two sections, five cases with bend angles starting from 0° (Straight) and continuing with 45°, 90°, 135° and finally 180° were simulated.

A2.1 Annular Flow Cases

A2.1.1 Straight Pipe

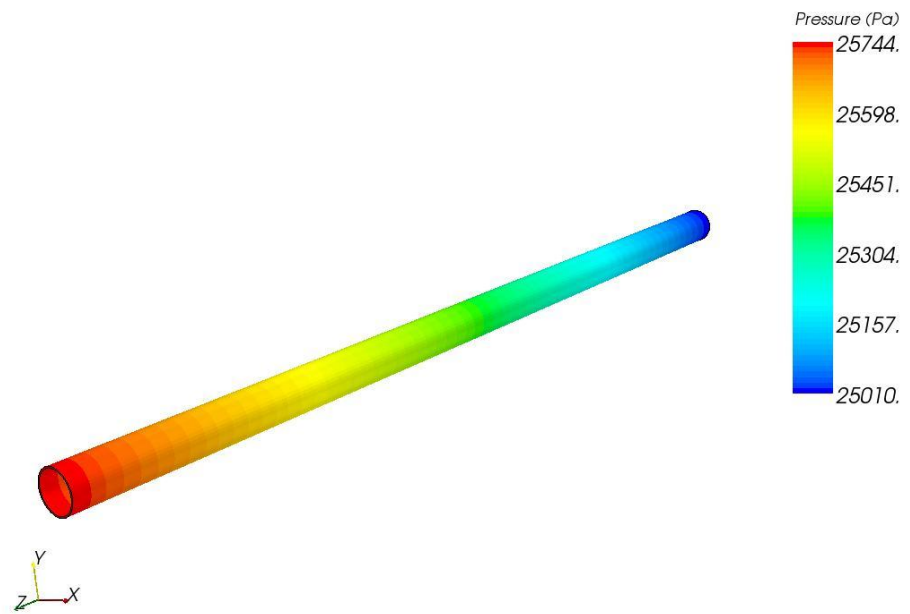


Figure A2-1: Pressure Distribution for Straight Pipe

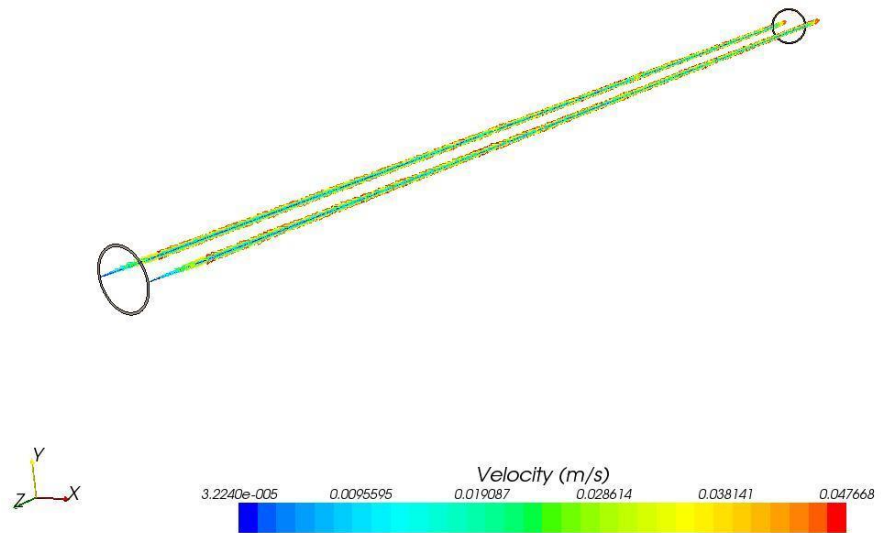


Figure A2-2: Velocity Vectors for Straight Pipe

A2.1.2 Pipe with 45° Bend

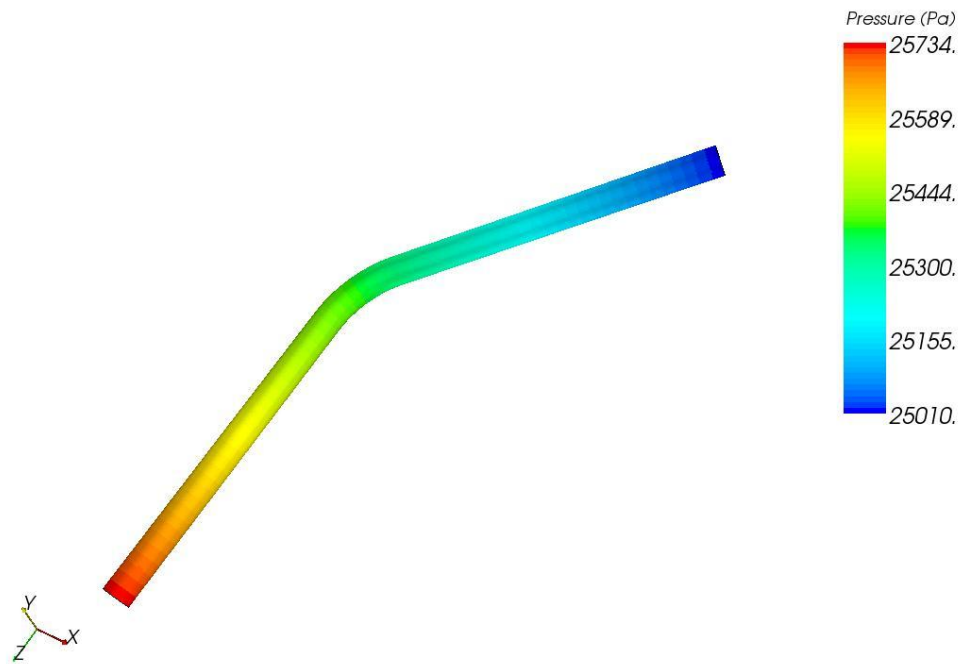


Figure A2-3: Pressure Distribution for Pipe with 45° Bend

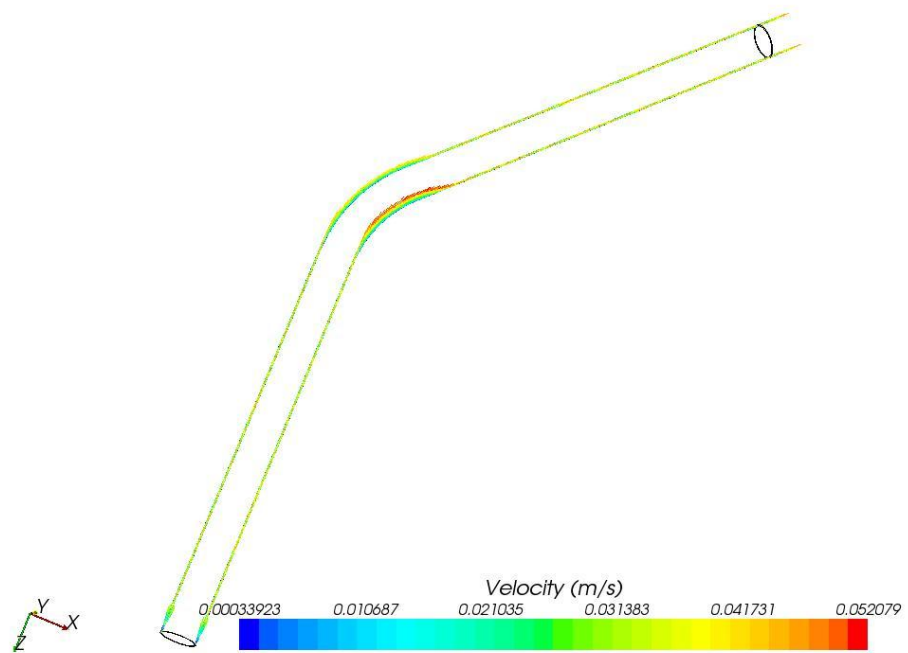


Figure A2-4: Velocity Vectors for Pipe with 45° Bend

A2.1.3 Pipe with 90° Bend

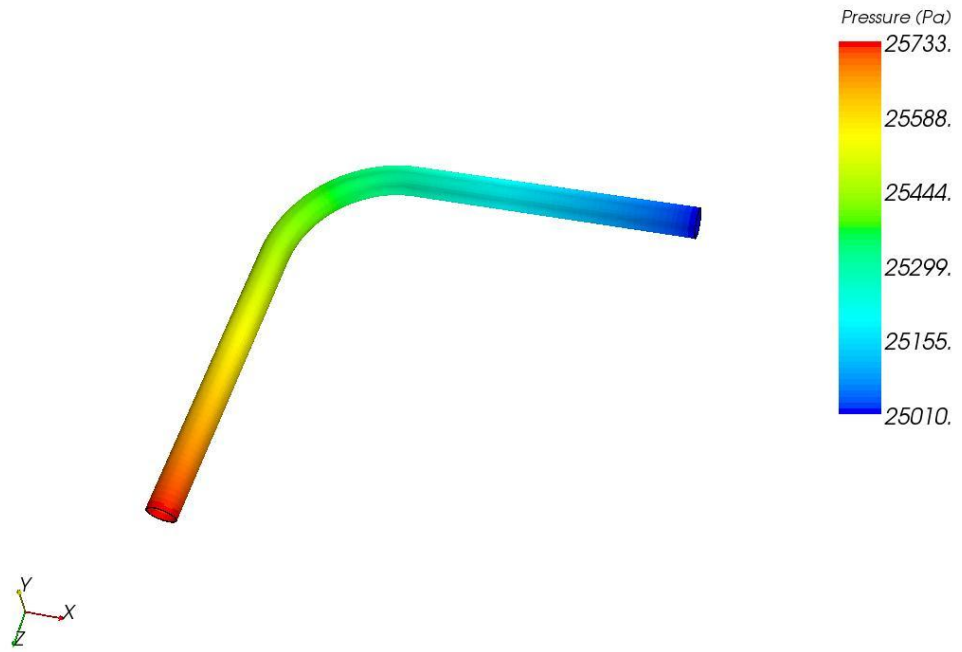


Figure A2-5: Pressure Distribution for Pipe with 90° Bend

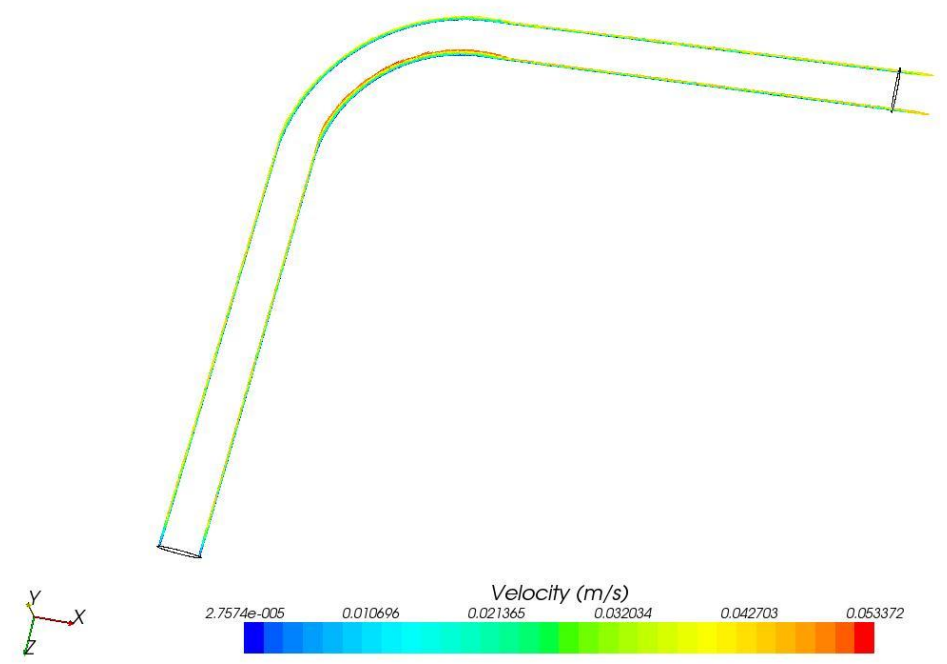


Figure A2-6: Velocity Vectors for Pipe with 90° Bend

A2.1.4 Pipe with 135° Bend

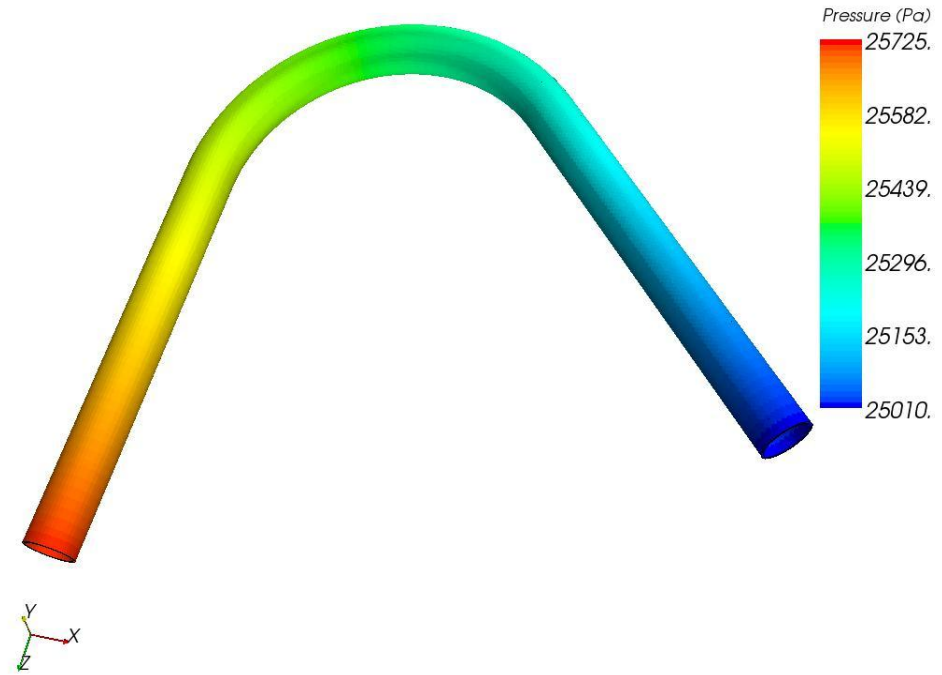


Figure A2-7: Pressure Distribution for Pipe with 135° Bend

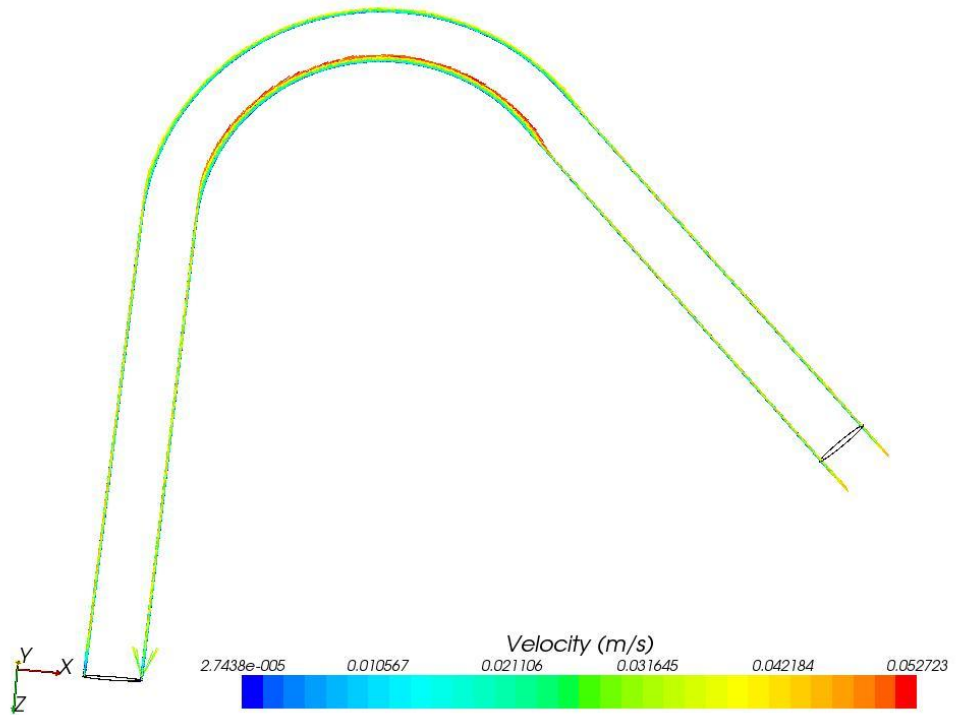


Figure A2-8: Velocity Vectors for Pipe with 135° Bend

A2.1.4 Pipe with 180° Bend

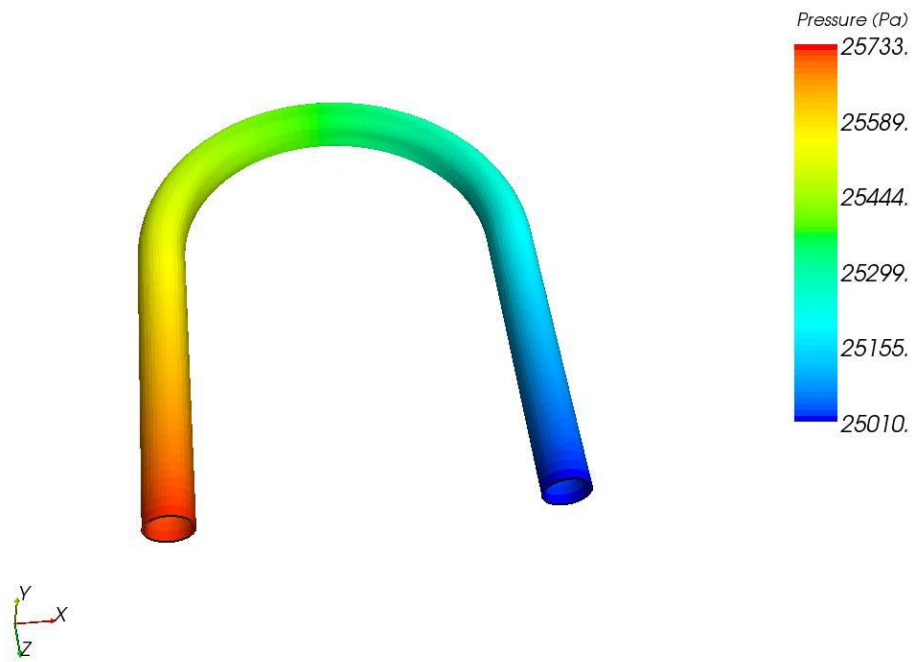


Figure A2-9: Pressure Distribution for Pipe with 180° Bend

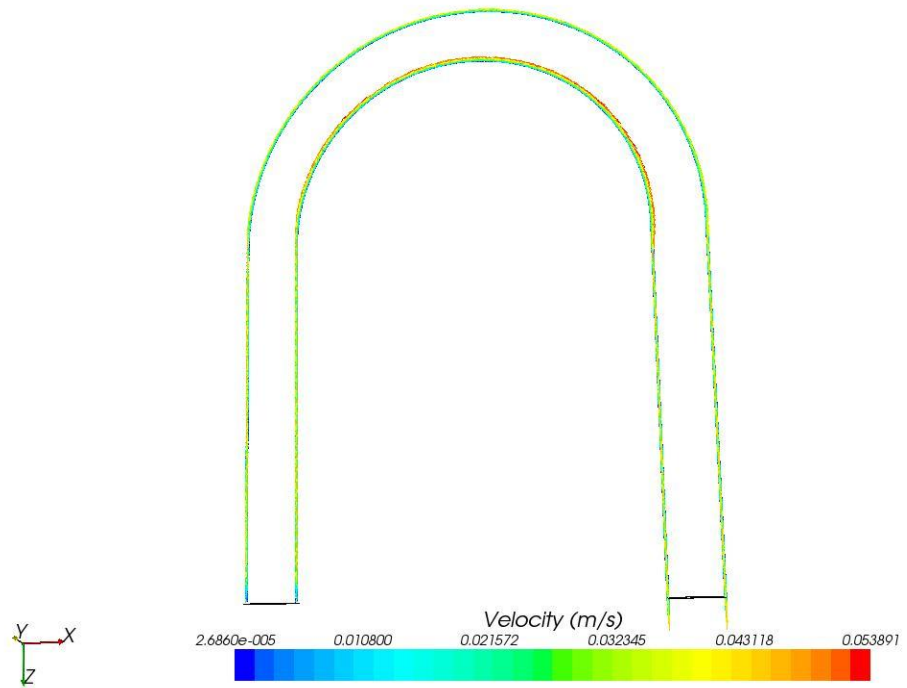


Figure A2-10: Velocity Vectors for Pipe with 180° Bend

A2.2 Full Flow Cases with Flow Velocity from Heat Pipe Theory

A2.2.1 Straight Pipe with Full Pipe Flow and Flow Velocity from Heat Pipe Theory

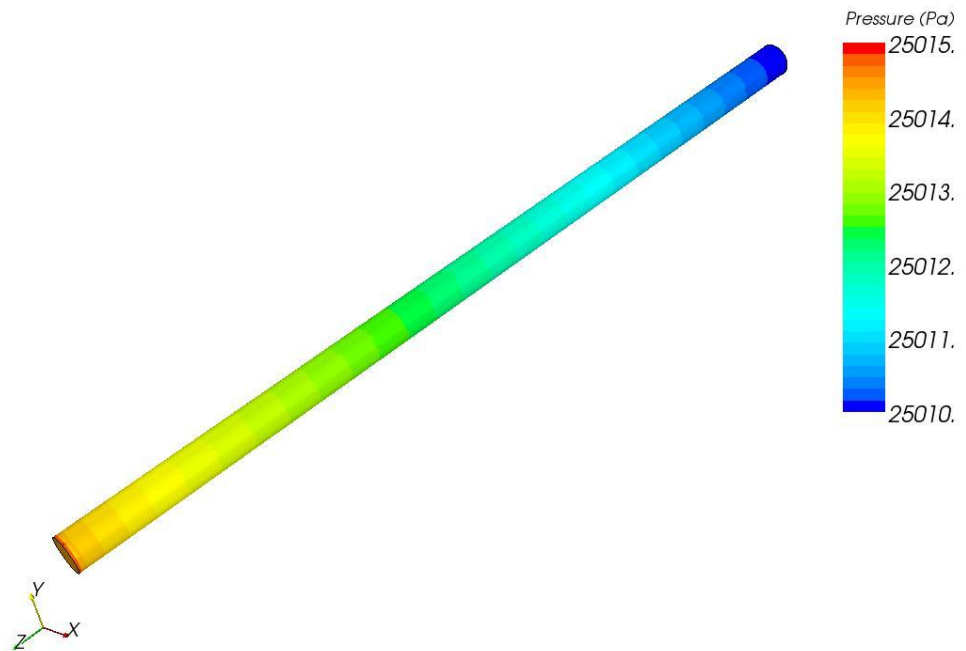


Figure A2-11: Pressure Distribution for Straight Pipe

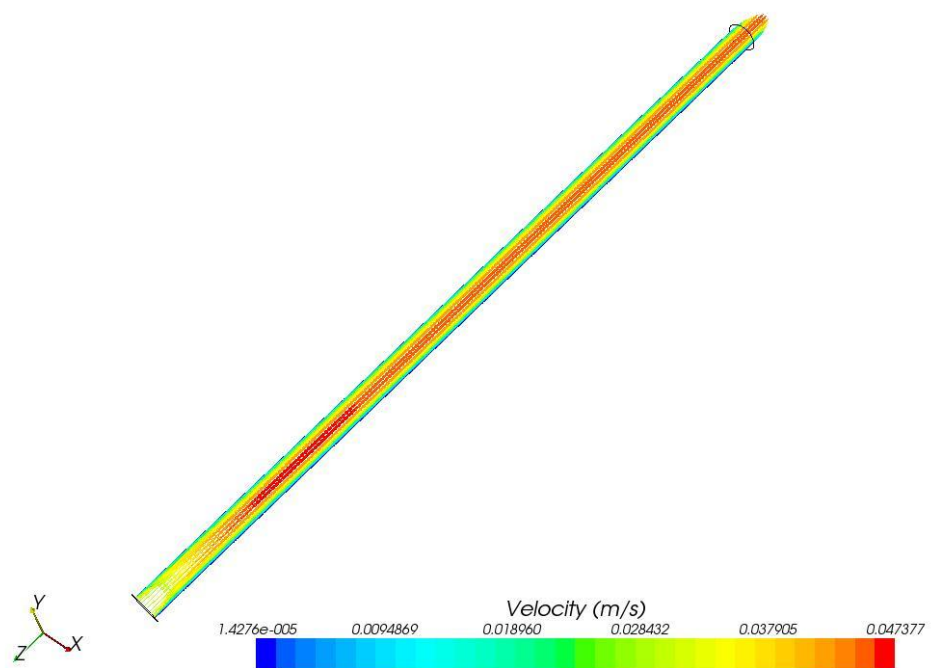


Figure A2-12: Velocity Vectors for Straight Pipe

A2.2.2 Pipe with 45° Bend and Full Pipe Flow and Flow Velocity from Heat Pipe Theory

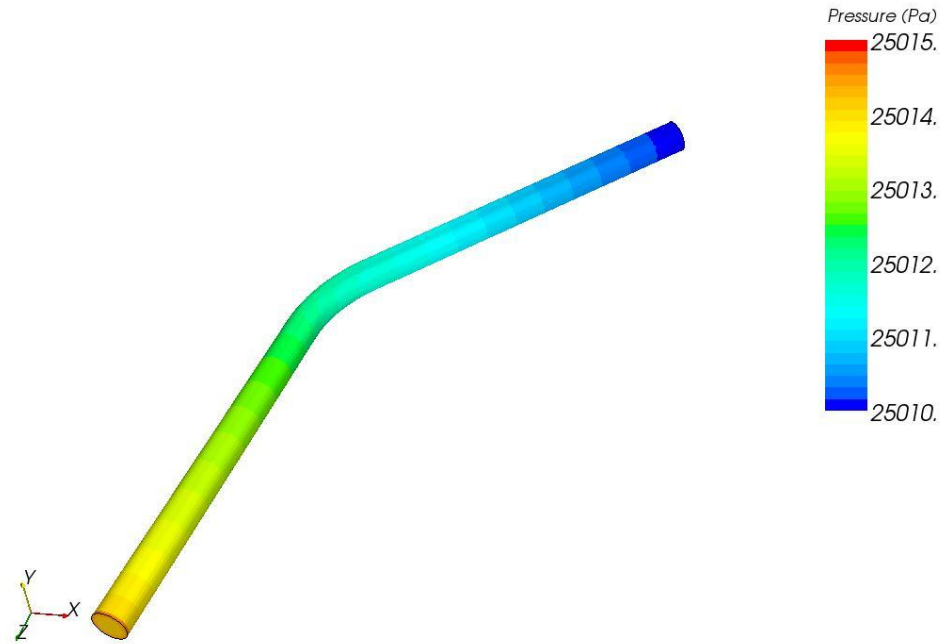


Figure A2-13: Pressure Distribution for Pipe with 45° Bend

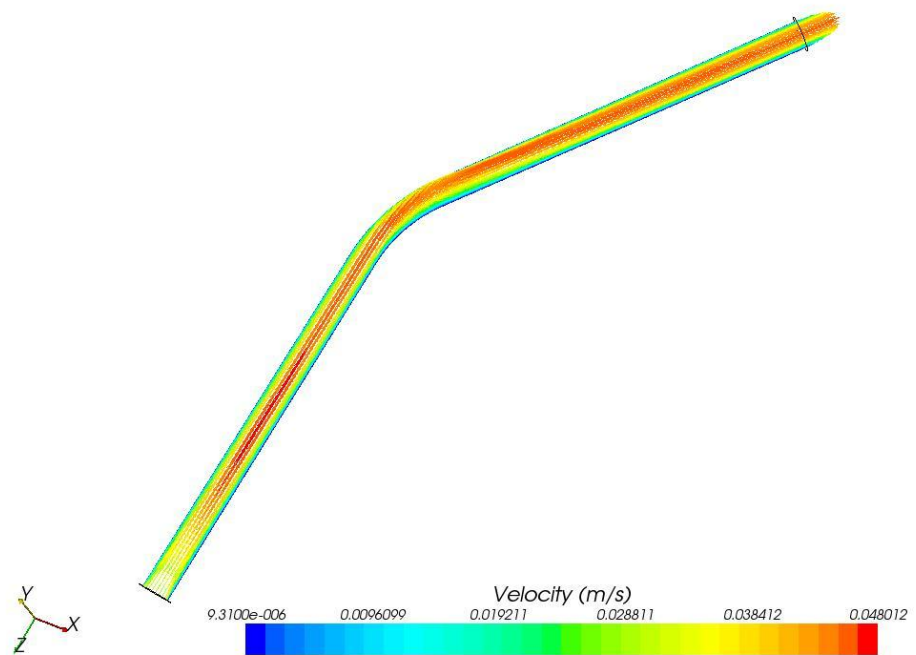


Figure A2-14: Velocity Vectors for Pipe with 45° Bend

A2.2.3 Pipe with 90° Bend and Full Pipe Flow and Flow Velocity from Heat Pipe Theory

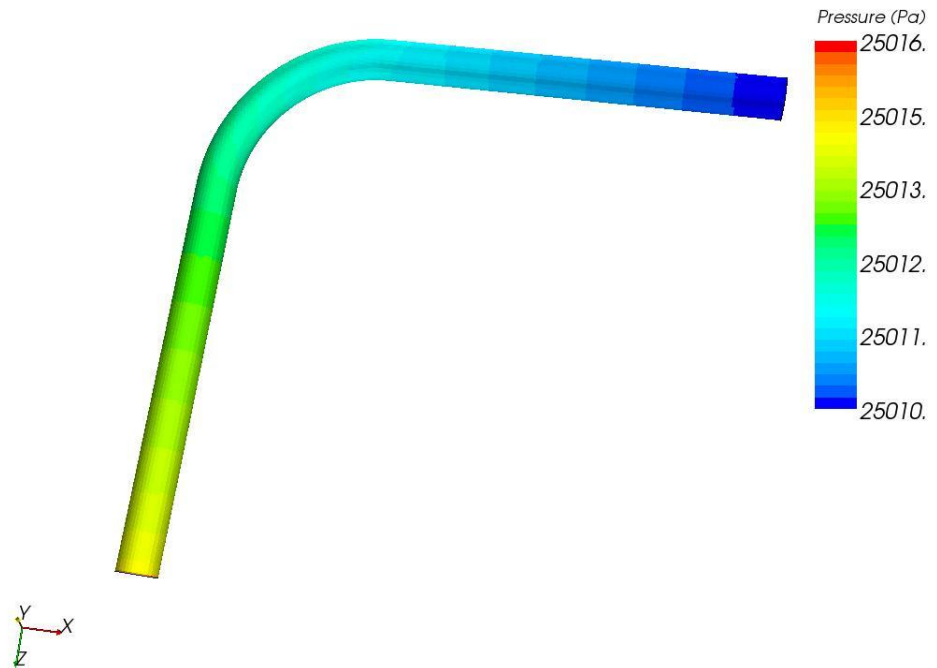


Figure A2-15: Pressure Distribution for Pipe with 90° Bend

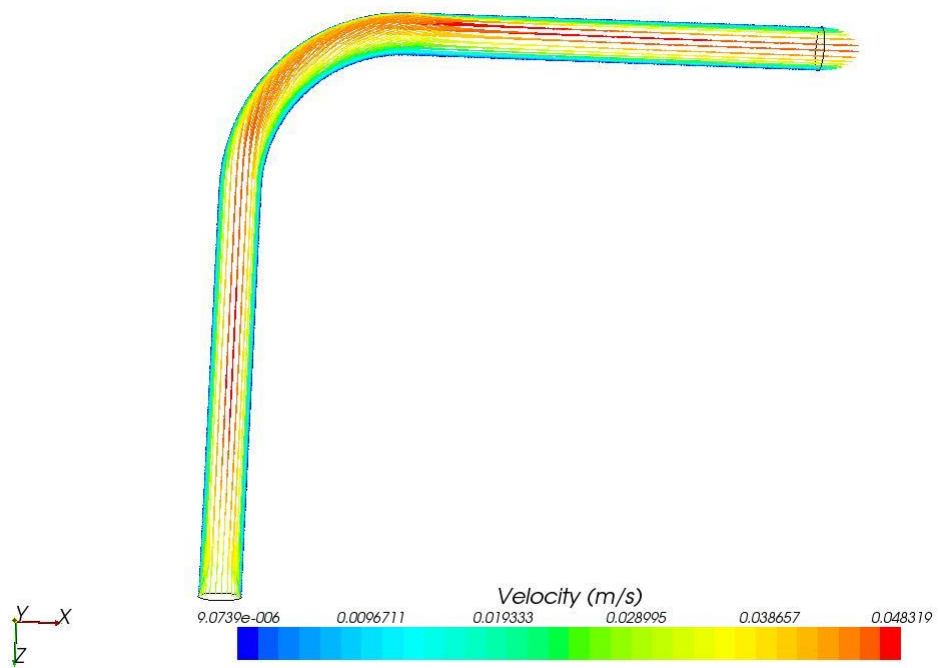


Figure A2-16: Velocity Vectors for Pipe with 90° Bend

A2.2.4 Pipe with 135° Bend and Full Pipe Flow and Flow Velocity from Heat Pipe Theory

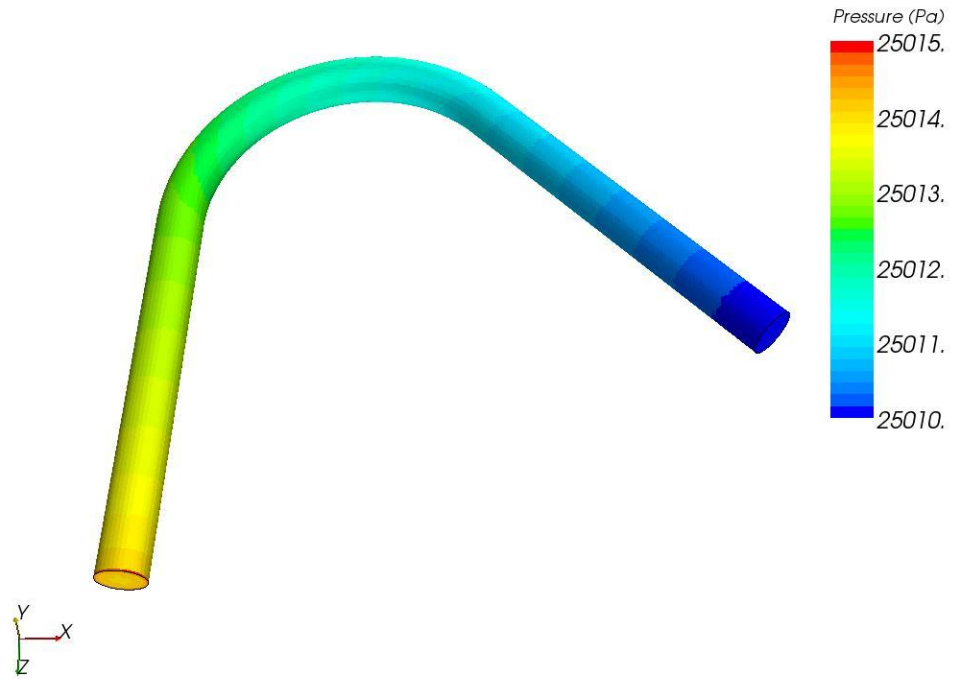


Figure A2-17: Pressure Distribution for Pipe with 135° Bend

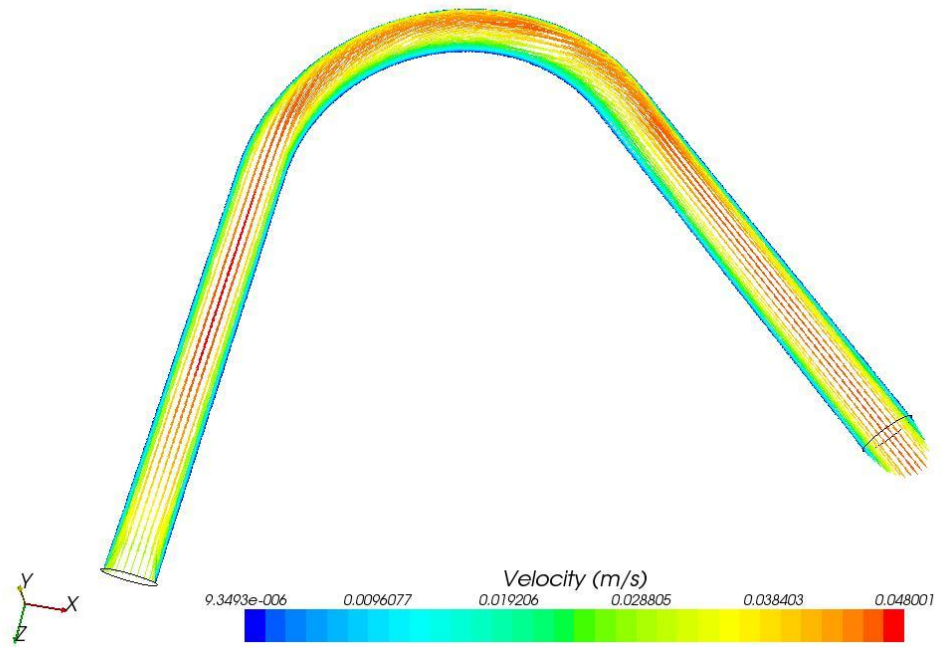


Figure A2-18: Velocity Vectors for Pipe with 135° Bend

A2.2.5 Pipe with 180° Bend and Full Pipe Flow and Flow Velocity from Heat Pipe Theory

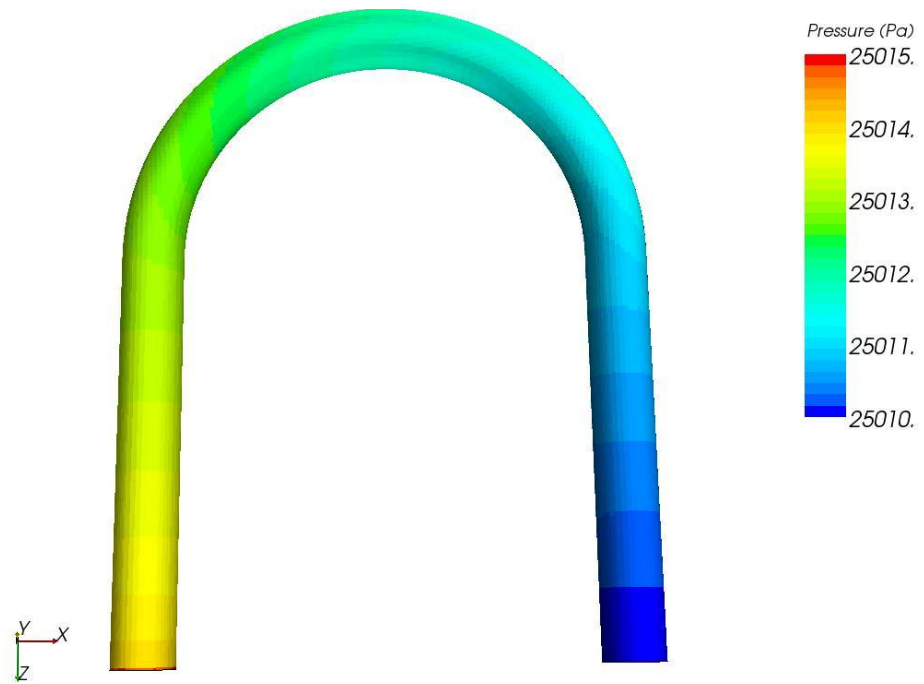


Figure A2-19: Pressure Distribution for Pipe with 180° Bend

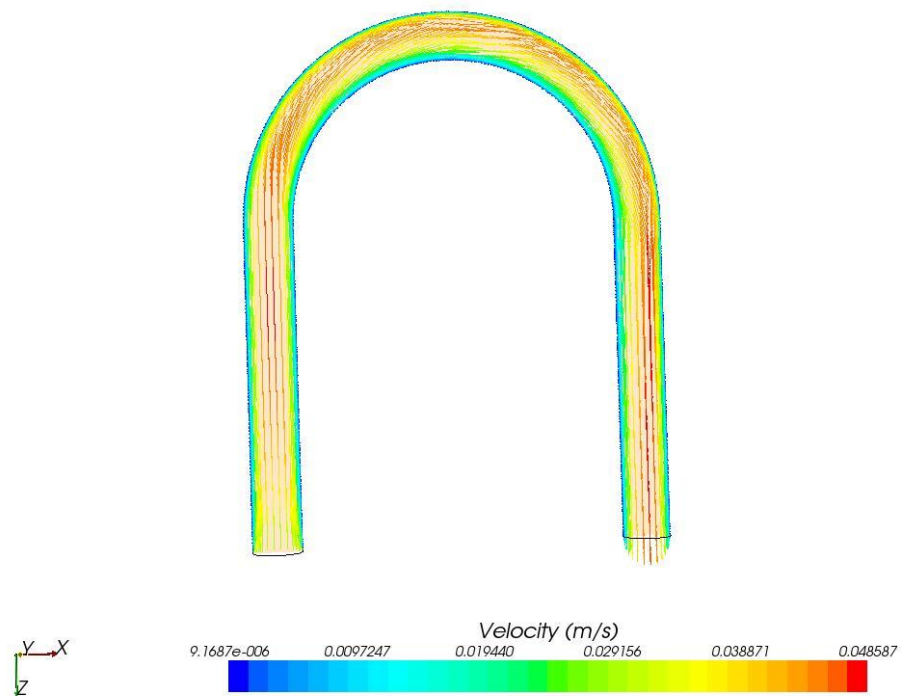


Figure A2-20: Velocity Vectors for Pipe with 180° Bend

Appendix 3 - Thermocouple Fabrication and Calibration

Thermocouples are the most widely used temperature sensor in test and development work. Therefore some time will be spend during the following sub-section to explain their function and what precautions were undertaken to ensure their accuracy for the experiments carried out for this study. During the experimentation carried, T-type thermocouples were used due to the suitability of temperature range and highest accuracy amongst the different thermocouple types.

A3 – 1: Definition of a Thermocouple

A temperature measurement sensor that that consists of two dissimilar metals intimately joined together in a bead at one end (a junction) that produces a small thermoelectric voltage, corresponding to a temperature, when the junction is heated (JEDEC Publications, 2006).

The physical effects thermocouples are relying on is the Seebeck effect. This effect was named after the Estonian physician Thomas Seebeck who accidentally discovered in 1822 that in a junction between two metals a voltage is generated which is a function of temperature (Pico Technology, 2007). This was than used for wire thermocouples which became increasingly popular with the availability of electronic instruments and data logging equipment and ever since the wire thermocouple is the most common thermometric tool in component thermometry. Thermocouples are relatively

inexpensive, have a fast response time and are well supported by electronic instrumentation and computing infrastructure. They are interchangeable, have standard connectors and can measure a wide range of temperatures (JEDEC Publications, 2006). Data logging equipment supporting channels from four up to 60 channels is available. The thermocouples' thermal effects on the apparent temperature of the test point are minimized when:

- a) The thermocouple is fabricated with fine wire
- b) The junction of the metallic couple or “bead” is small
- c) The junction is in good thermal contact with or is well coupled to the surface to be measured
- d) The attached medium is not too thick
- e) The attached medium has an emissivity not significantly different from the one of the surface being measured
- f) The wire lie flat against the surface of interest, for a distance of $>20\times$ the diameter of the wire (JEDEC Publications, 2006).

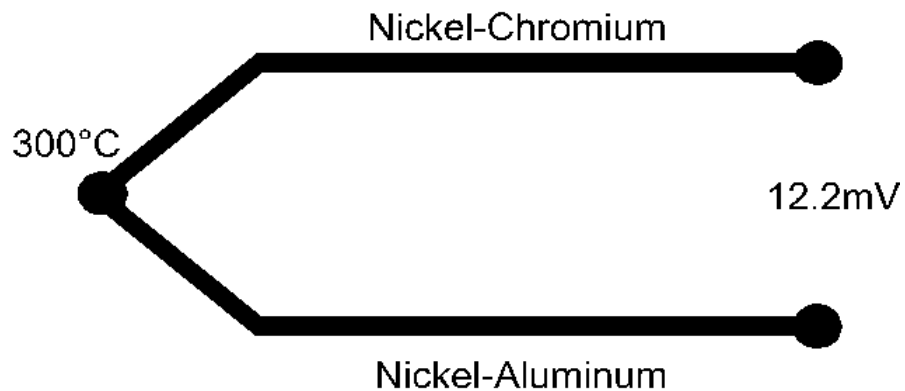


Figure A3 -1: Scheme of a Wire Thermocouple (K-type) (Pico Technology, 2007)

Type K (chromel-alumel) or Type T (copper-constantan) thermocouple materials are generally used for peak temperature ranges from 200°C to 400°C

and in either oxidizing or neutral atmosphere. Three grades of wire are available in each type based on calibration accuracy: Precision, Standard and Lead wire. The calibration of Precision grade thermocouple is the highest one available and guaranteed within $\pm 3.8\%$ or $1^{\circ}\text{C}(2^{\circ}\text{F})$, whichever is largest (Moffat, 1997). Considering the low cost and little difference between grades precision grade was used for this experimentation.

A3 – 2: Thermocouple Fabrication

Three techniques are the most common ones for fabricating thermocouples from thermocouple wire supplied on a reel:

1. The simplest method of generating a thermocouple junction is simply by twisting or crimping the two wires together at one end. Unfortunately this is also the method which has the least defined junction as it is hard to predict on which of the twists the temperature is measured.
2. The second way is by simply soldering the two different metals of the wire together as the solder will not affect the reading.
3. The third way which is used for the fabrication of most commercially made thermocouples is by welding the ends together. This welding process can be done in two ways, either through the use of a finer oxygen – hydrogen welding torch or more widely used is a capacitive discharge micro spot welding thermocouple welder. The main advantages of that technique are that it forms the wire into a

homogenous bead as well as does not limit its performance to the melting point of the solder used (JEDEC Publications, 2006).

The thermocouple response time is proportional to the surface area of the active junction to the diameter of the round of which the thermocouple is formed. A spherical or ball-shaped thermocouple junction has the smallest ratio. Response time of round wire thermocouples are typically in the range of milliseconds to seconds, dependent on the thermocouple gauge and attachment technique, with finer wire and more refined attachment having the faster response time (JEDEC Publications, 2006).

Poor joining techniques could result in monitoring errors and/ or performance instabilities. Therefore the resistance of the thermocouple assembly should be measured before using and must be compatible with the measuring device input specifications since thermocouple wire can change resistance at high temperature and thus induce error in measurement (JEDEC Publications, 2006)

For the fabrication of the thermocouples used for this experimentation a thermocouple welder was used and can be seen on Figure A3-2 below. This welder was of a Labfacility L60+ type and allows adjustments of power as well as current level. The quality of the welds was inspected only visually.



Figure A3-2: Thermocouple Welder inc manufactured TC

A3 – 3: Thermocouple Calibration

Thermocouple calibration is an important measure to improve accuracy of temperature measurements. According to the well recognized European standard EAL-G31, effective measurements and calibrations are possible only if the hot and cold junction are maintained in isothermal regions and at a depth sufficient to overcome heat losses (or gains), thereby ensuring that each junction actually reaches the temperature of its environment (European Cooperation for Accreditation of Laboratories, 1997).

Further this standard text advises that with time and use, degradation of the thermocouple and its calibration is inevitable and, in the long term, therefore a

scheme of regular checks and eventual replacement should be established and maintained.

The following advice was given with regards to the direct calibration: Every thermocouple which shall be calibrated should be homogenous. Further heat treatment/ annealing of a thermocouple should be seen as a kind of 'adjustment' (European Cooperation for Accreditation of Laboratories, 1997).

In terms of direct calibration, thermocouples are calibrated by measurement either at a series of fixed point temperatures, e.g. melting/ freezing points or, by comparison with reference/ standard thermometers, in thermally stabilized baths or furnaces suitable for the calibration, or by a combination of techniques, e.g. comparisons and fixed-point temperatures (European Cooperation for Accreditation of Laboratories, 1997).

A thermally stabilised bath or furnace suitable for calibration is one in which the spatial temperature profiling using two or more standard thermometers at usually the midpoint and both ends of the working temperature range and within the working volume has been shown to be within required limits (European Cooperation for Accreditation of Laboratories, 1997).

Temperature gradients within thermally stabilized baths or furnaces can be reduced or minimised by the insertion of a metal equalising block drilled with thermowells to receive the standard and test instruments. Such a block is not always necessary for example in multi-zone controlled furnaces and without a block, stabilisation may be achieved more quickly (European Cooperation for

Accreditation of Laboratories, 1997).

For the calibration of the six thermocouples used in direct contact with the pipe as well as for measuring the temperature within the test chamber in close proximity to the test sample a commercially made thermocouple calibrator using a metal equalizing block was used. This calibrator was manufactured by ISOTECH and was of an ISOCAL-6 Venus^{Plus} 2140 type. A metal equalising block was used to avoid temperature gradients within the calibration chamber. A picture of the thermocouple calibrator whilst being used in the lab can be seen below in Fig. A3-3.



Figure A3-3: Thermocouple Calibrator inc TCs

For this PhD experimentation a four point calibration up to a 100°C was run. The monitored temperature points are 25°C, 50°C, 75°C and 100°C. This was seen sufficient since the simulation of performance was done for a set temperature of 65°C. Tests at much higher temperatures than 100°C can not be performed because it will guide towards melting of the insulation/ carrier around the heater blocks which are made out a thermo plastic. The obtained

results for deviations between readings of the logger and the reference thermocouple/ temperature from the calibrations were used as inputs for the table look up functions within the Pico software used for the data logging of the temperatures. Results of the calibration can be found below.

A3-3.1 Results of the Calibration Runs:

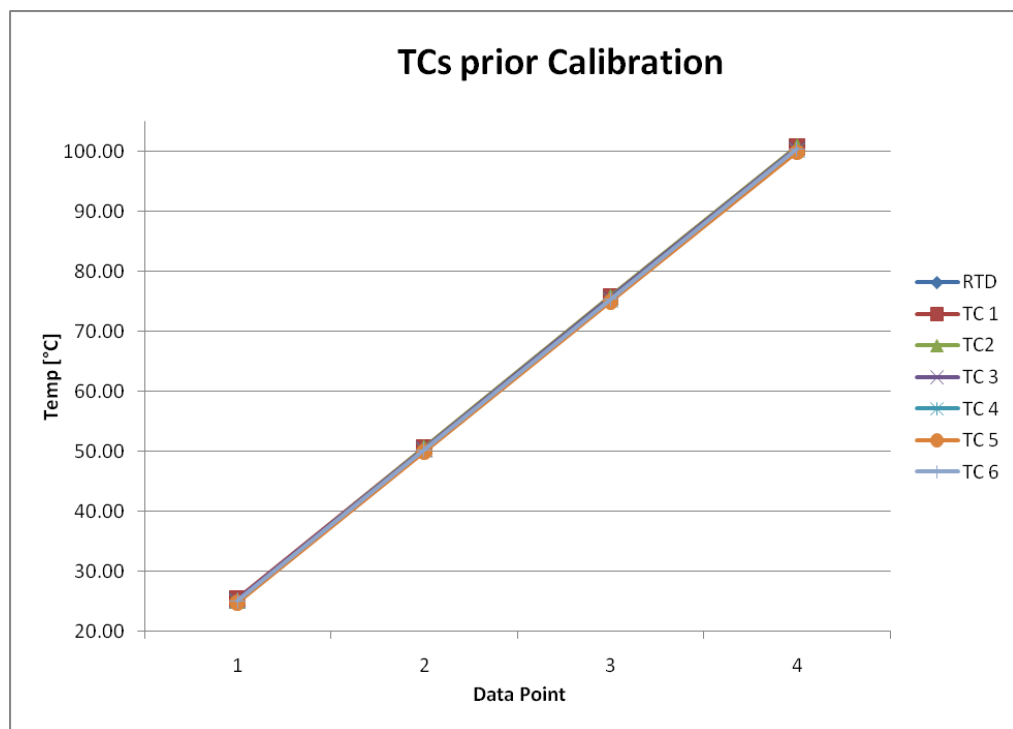


Figure A3-4: Thermocouple Readings prior to Calibration

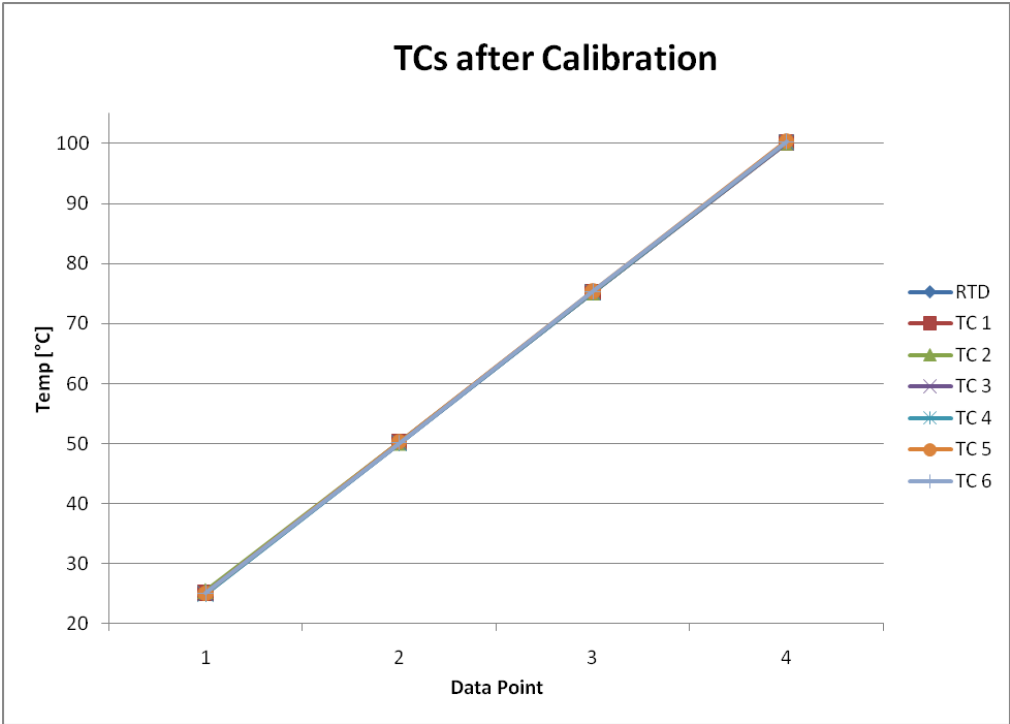


Figure A3-5: Thermocouple Readings after Calibration

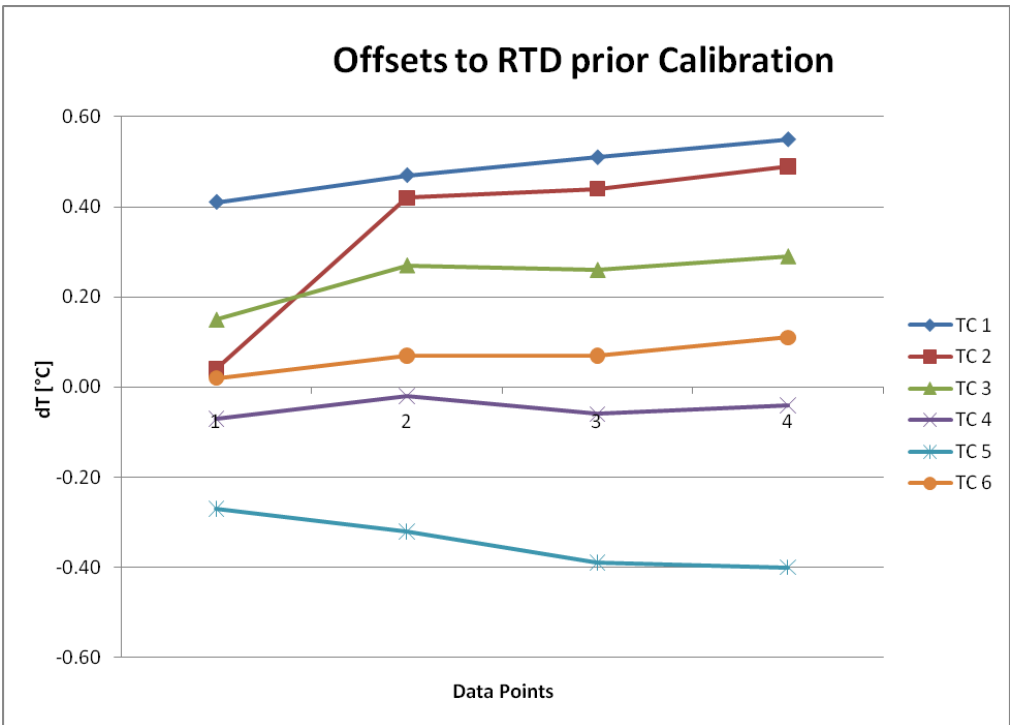


Figure A3-6: Offsets prior to Calibration

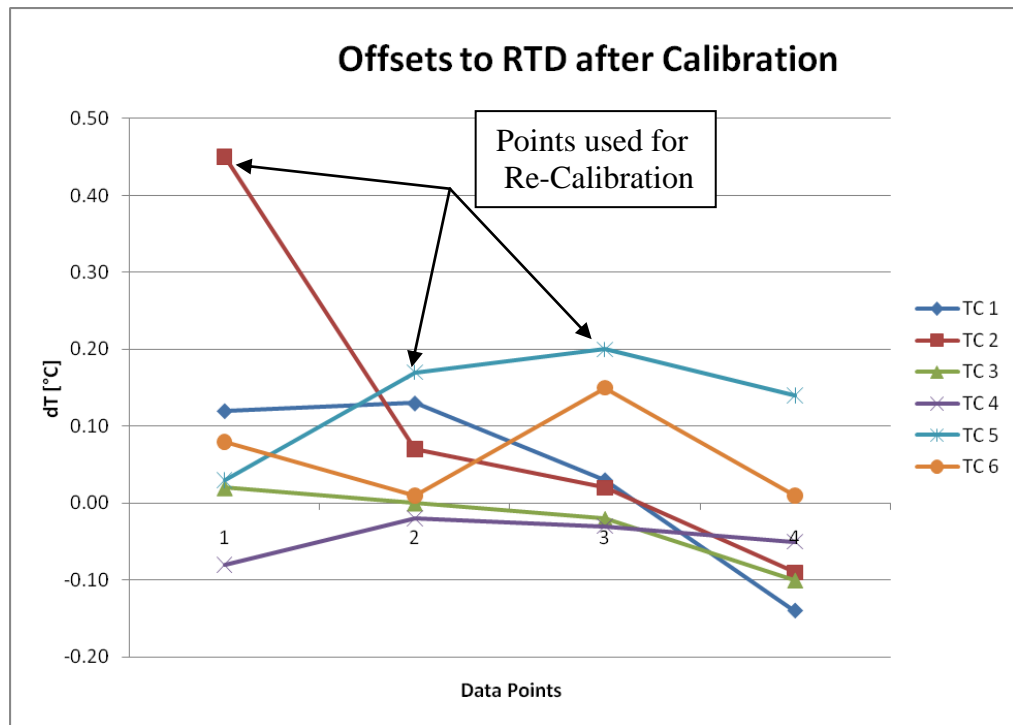


Figure A3-7: Offsets after Calibration

For values above 0.15°C nominal offsets marked in yellow the new gained results were introduced in the look-up table and no further verifications undertaken. This approach was seen accurate enough and in this case it was obtained to get down the accuracy of the thermocouple wire down to around one third of the precision grade thermocouple wire with 0.5°C. Therefore this accuracy is seen as a good result and good enough for experimentation using thermocouples. Furthermore only three out of the 24 data points required this step whilst after calibration every other data point was below that threshold or better. The total values of the offsets prior to and after calibration can be found in table A3-1 and A3-2 below.

RUN 1	TC 1	TC 2	TC 3	TC 4	TC 5	TC 6
25° C	0.41	0.04	0.15	-0.07	-0.27	0.02
50° C	0.47	0.42	0.27	-0.02	-0.32	0.07
75° C	0.51	0.44	0.26	-0.06	-0.39	0.07
100° C	0.55	0.49	0.29	-0.04	-0.40	0.11

Table A2-1: Offsets prior to Calibration

RUN 2	TC 1	TC 2	TC 3	TC 4	TC 5	TC 6
25° C	0.12	0.45	0.02	-0.08	0.03	0.08
50° C	0.13	0.07	0.00	-0.02	0.17	0.01
75° C	0.03	0.02	-0.02	-0.03	0.20	0.15
100° C	-0.14	-0.09	-0.10	-0.05	0.14	0.01

Table A3-2: Offsets past first Calibration Run

References:

European Cooperation for Accreditation of Laboratories, 1997. *EAL-G31: Calibration of Thermocouples*.

JEDEC Publications, 2006. *JEP140: Beaded Thermocouple Temperature Measurements of Semiconductor Package*.

Moffat, R. J., 1997. Notes on using Thermocouples. *Electronics Cooling*, Vol. 3. www.electronics-cooling.com, (Accessed 19 November 2007).

Pico Technology, 2007. *Thermocouple Application Note*. www.picotech.com, (Accessed 20 November 2007).

Appendix 4 – Graphs of the Experimental Measurements and Analysis

Within the fourth section of this appendix, the additional experimental results, which have not previously been shown within the main body of this PhD thesis, are presented. First the analysed results, only presenting the heat pipe ΔT as well as the water ΔT (red and blue line, both $^{\circ}\text{C}$) and the heat load transferred into the water (W) over time are shown for each test run. Then as a second graph per test run, the original recording, which are the eight temperatures measured and described earlier in chapter 5 of this thesis, as well as the flow rate recorded in l/s over time, are shown. If certain graphs are not presented in this appendix, they have been used to indicate certain phenomena within the main body of the thesis and are therefore not replicated within the appendix and no additional comments are added to the graphs presented. The order of the runs is presented as recorded, the 10W increment runs first and then the ramp-up runs establishing the failure within the nearest 2 W increment are shown at the end of the test results set.

A4-1 Straight Heat Pipes:

Heat Pipe 1:

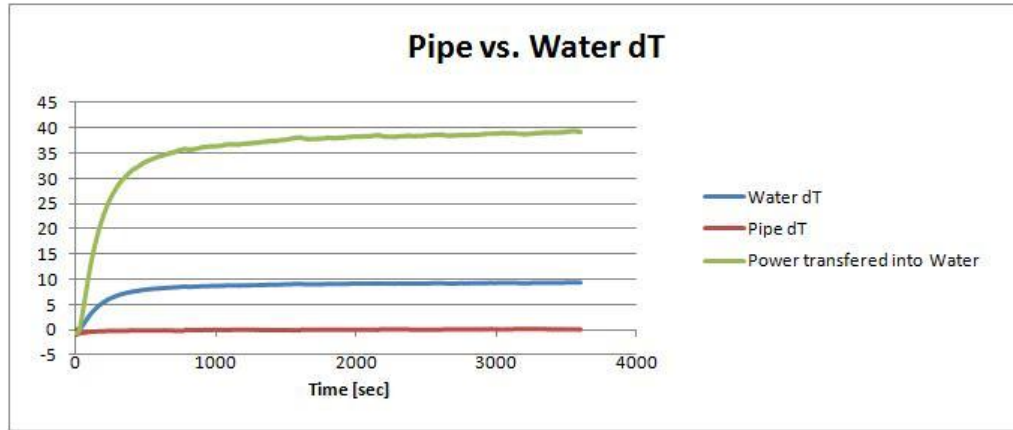


Figure A4-1: Analysed Results Heat Pipe 1 60W Run

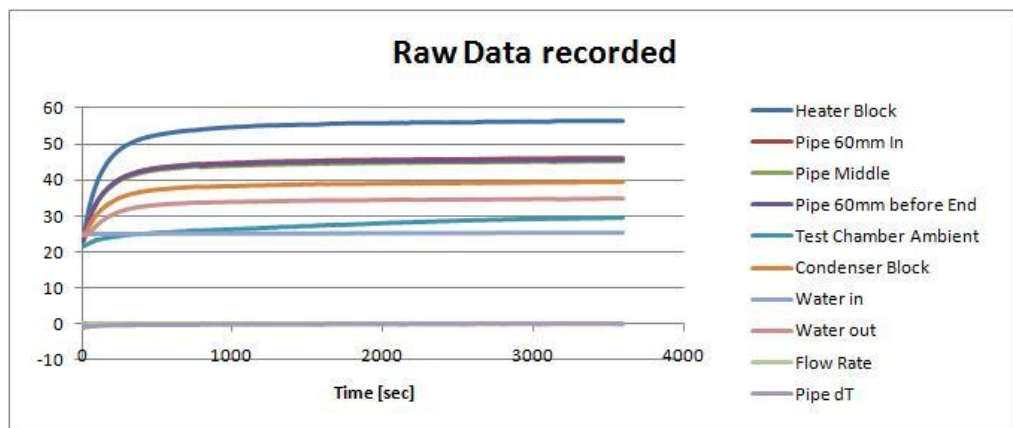


Figure A4-2: Recorded Results Heat Pipe 1 60W Run

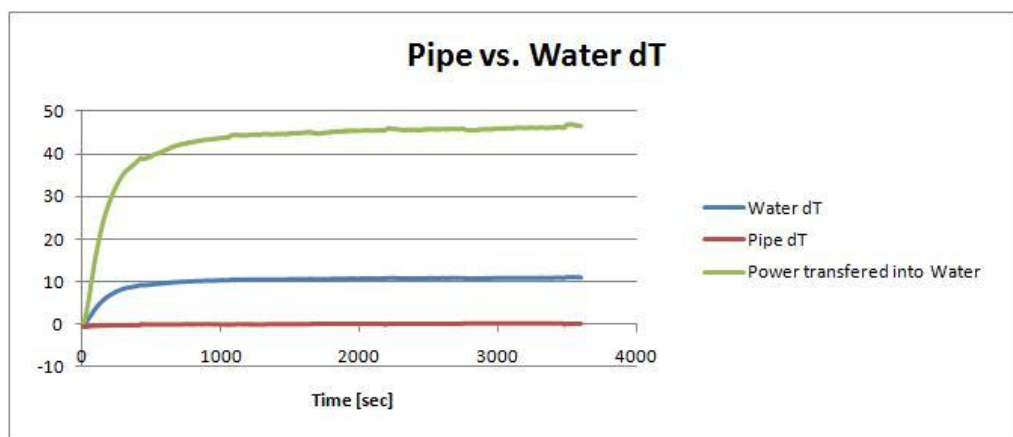


Figure A4-3: Analysed Results Heat Pipe 1 70W Run

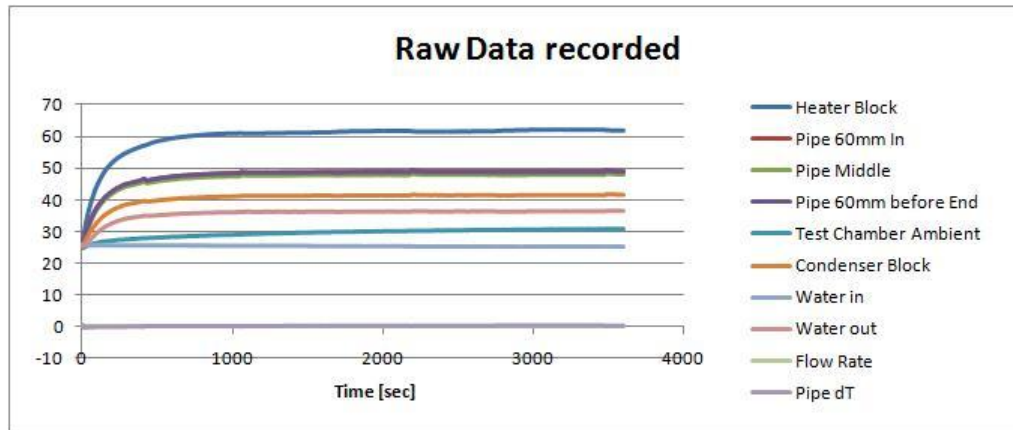


Figure A4-4: Recorded Results Heat Pipe 1 70W Run

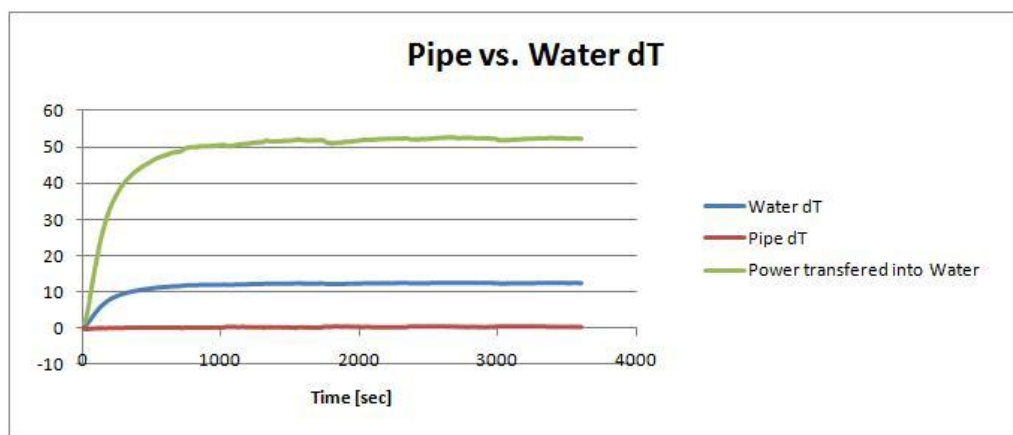


Figure A4-5: Analysed Results Heat Pipe 1 80W Run

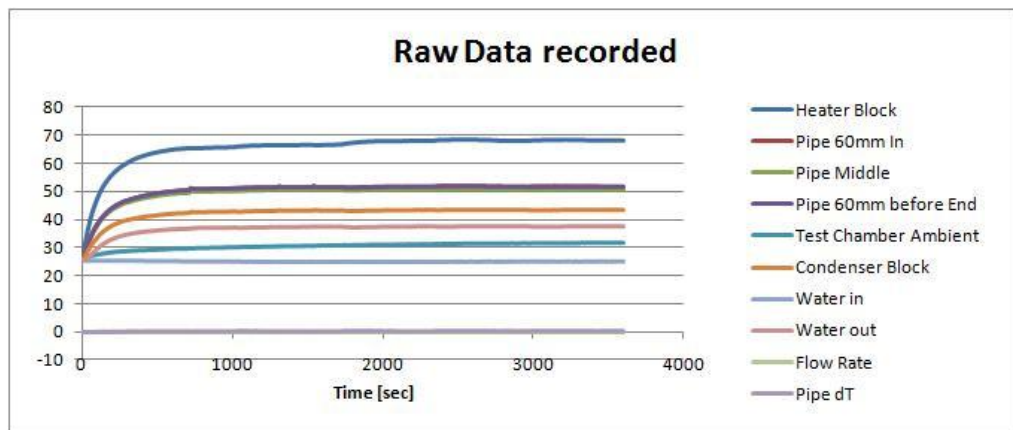


Figure A4-6: Recorded Results Heat Pipe 1 80W Run

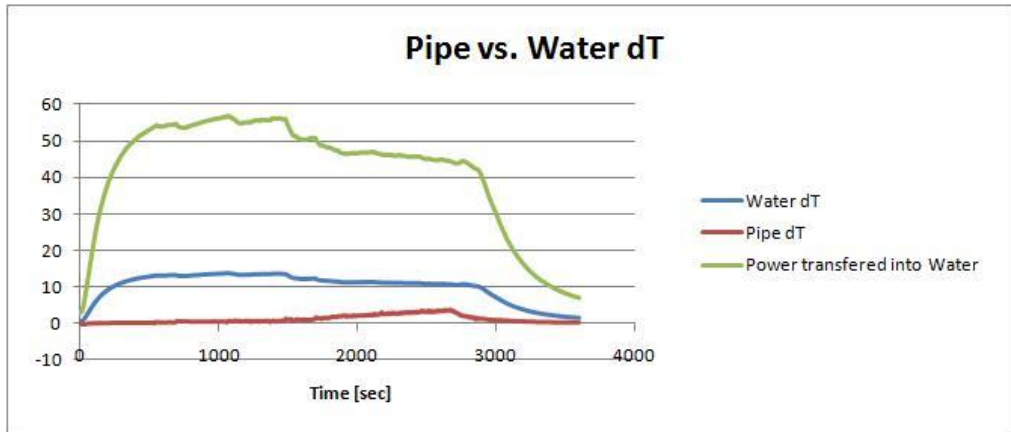


Figure A4-7: Analysed Results Heat Pipe 1 90W Run

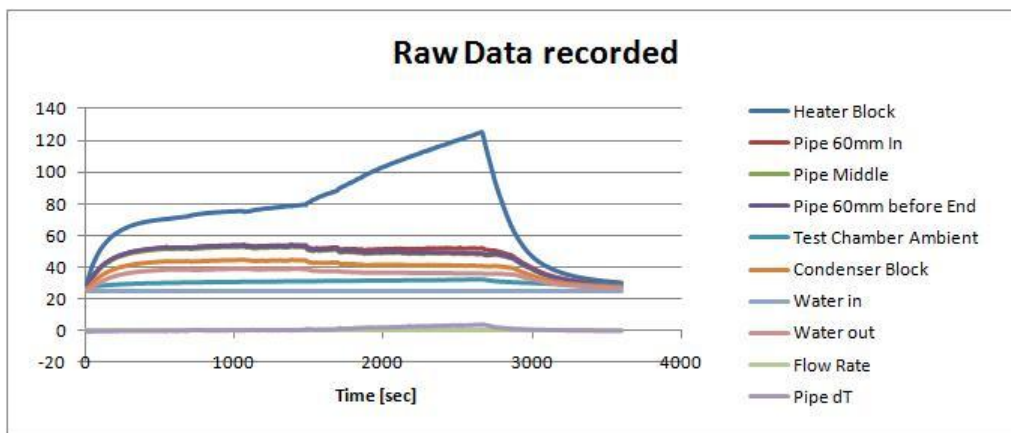


Figure A4-8: Recorded Results Heat Pipe 1 90W Run

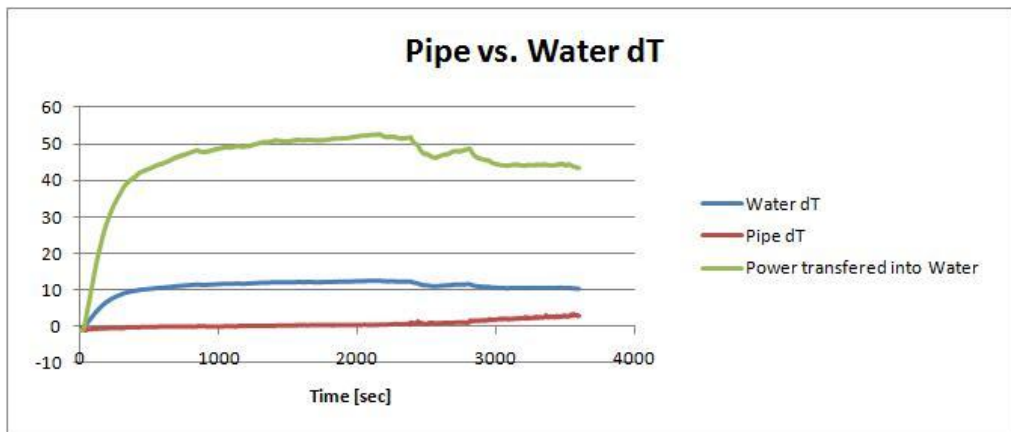


Figure A4-9: Analysed Results Heat Pipe 1 80W Ramp-Up Run

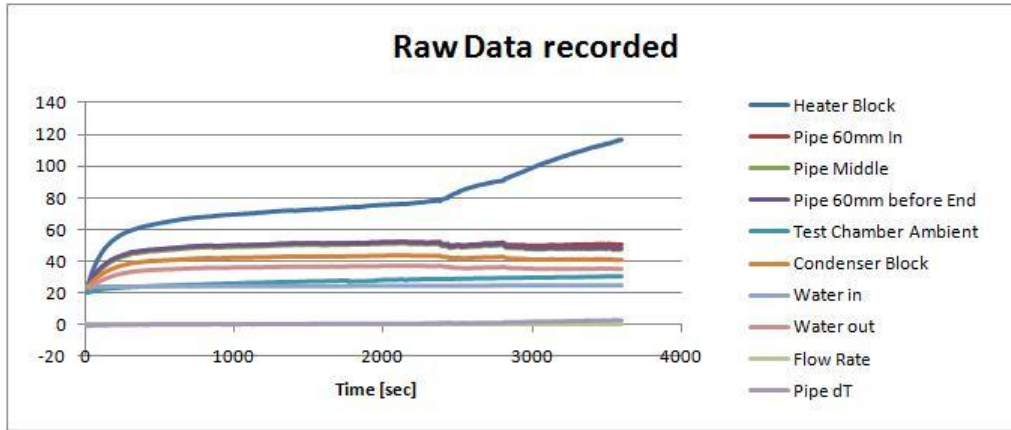


Figure A4-10: Recorded Results Heat Pipe 1 80W Ramp-Up Run

Heat Pipe 2:

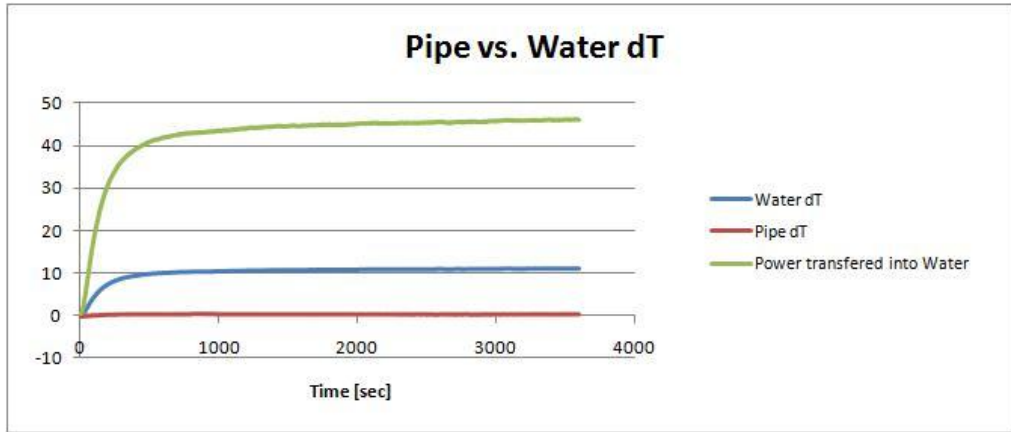


Figure A4-11: Analysed Results Heat Pipe 2 70W Run

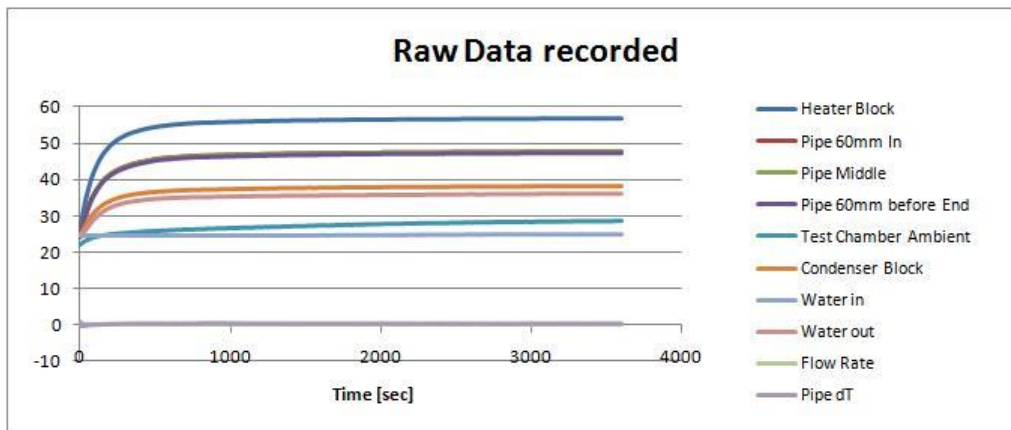


Figure A4-12: Recorded Results Heat Pipe 2 70W Run

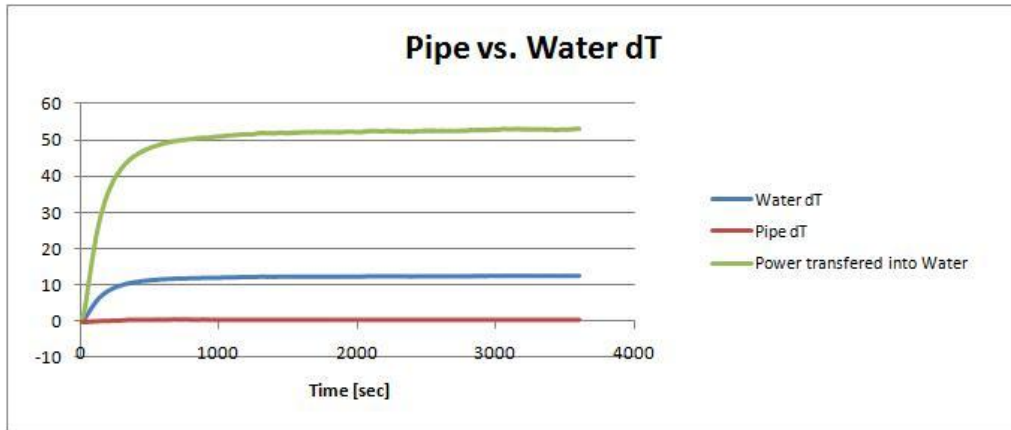


Figure A4-13: Analysed Results Heat Pipe 2 80W Run

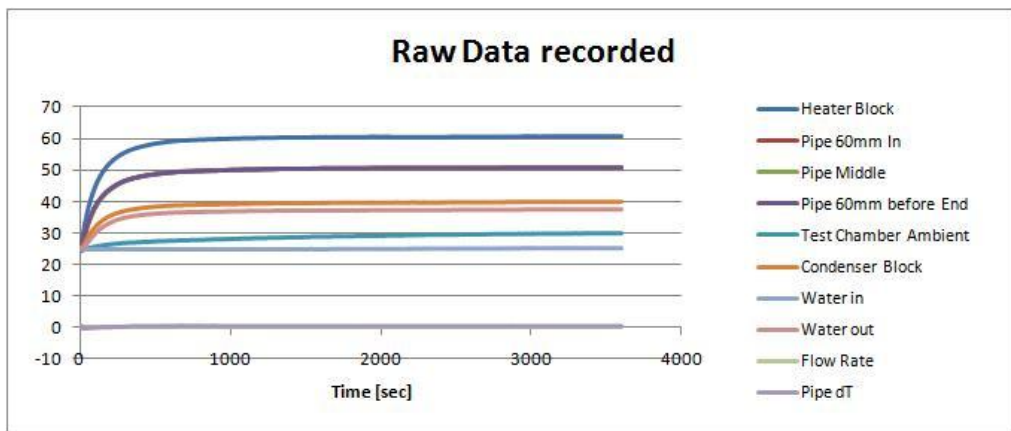


Figure A4-14: Recorded Results Heat Pipe 2 80W Run

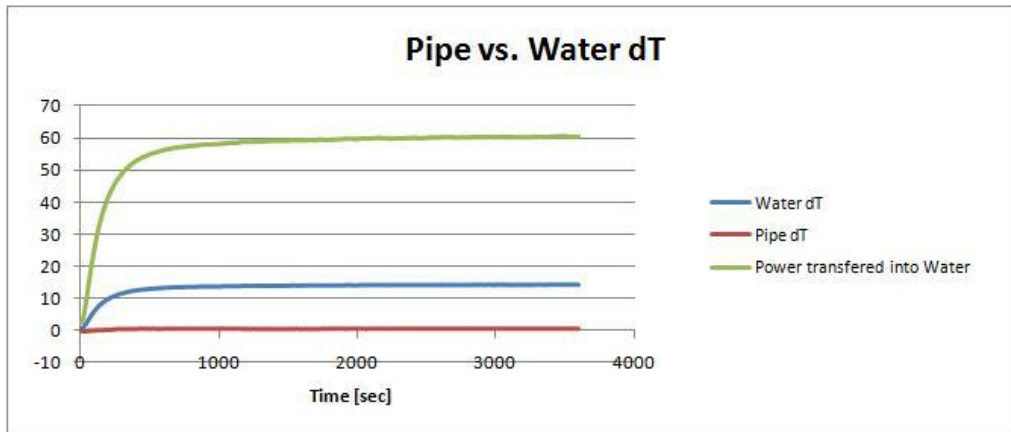


Figure A4-15: Analysed Results Heat Pipe 2 90W Run

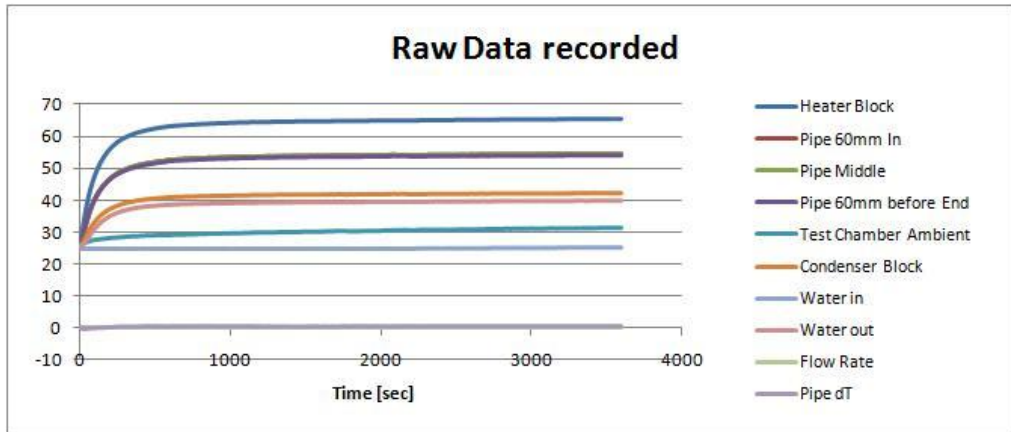


Figure A4-16: Recorded Results Heat Pipe 2 90W Run

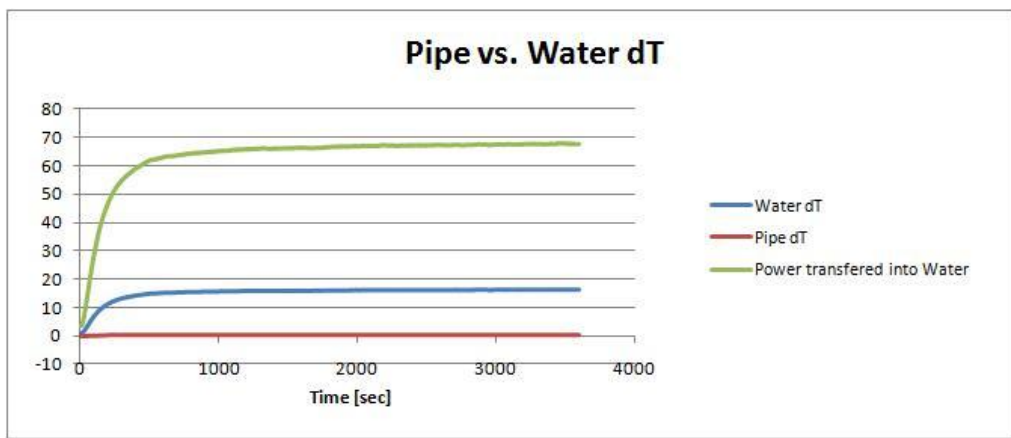


Figure A4-17: Analysed Results Heat Pipe 2 100W Run

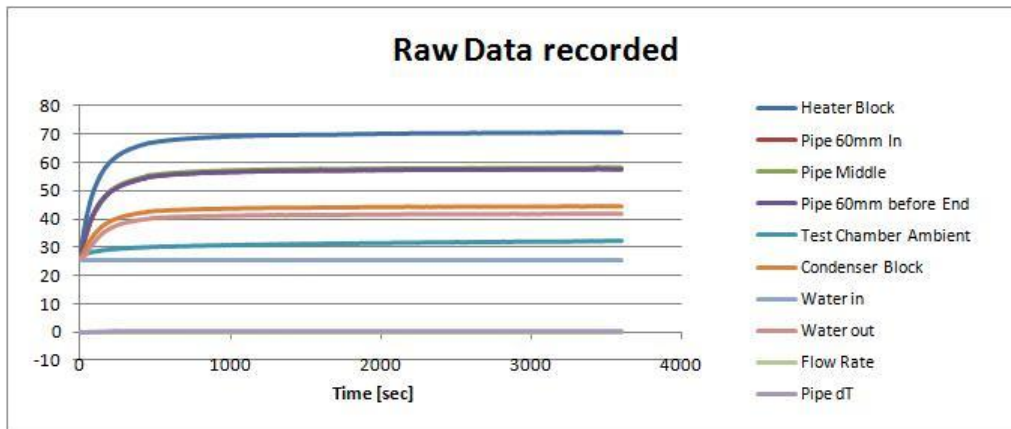


Figure A4-18: Recorded Results Heat Pipe 2 100W Run

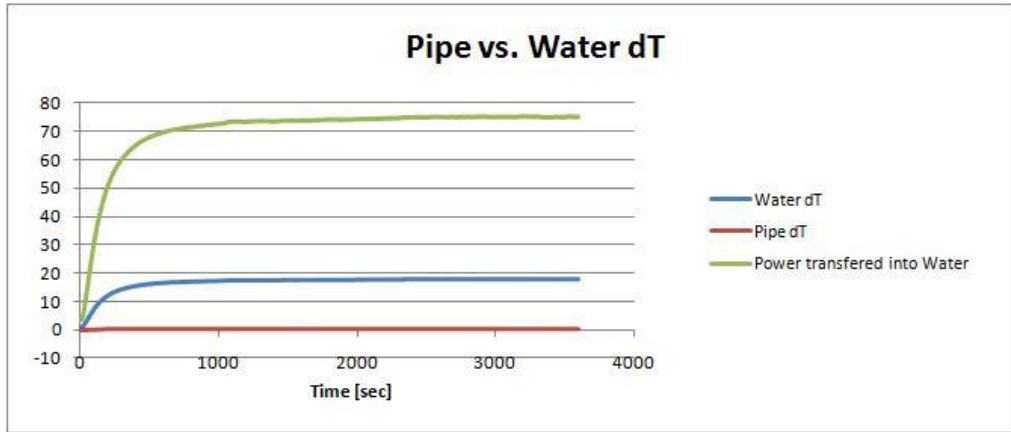


Figure A4-19: Analysed Results Heat Pipe 2 110W Run

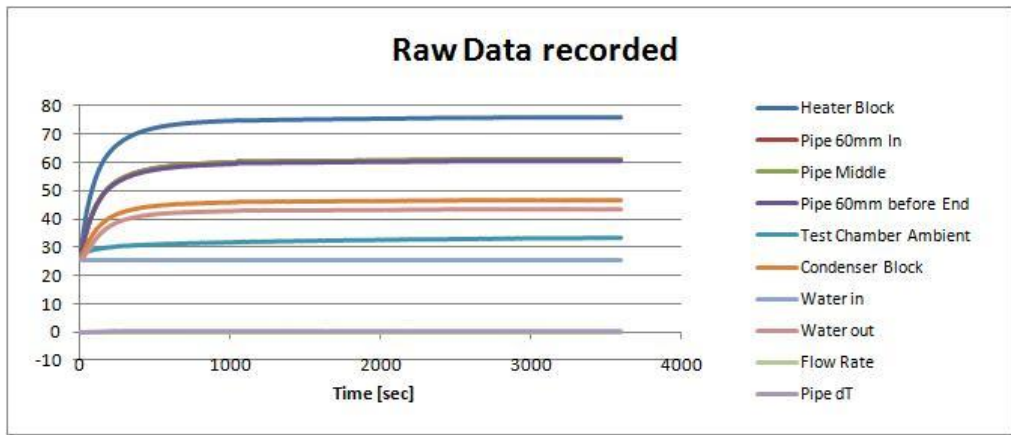


Figure A4-20: Recorded Results Heat Pipe 2 110W Run

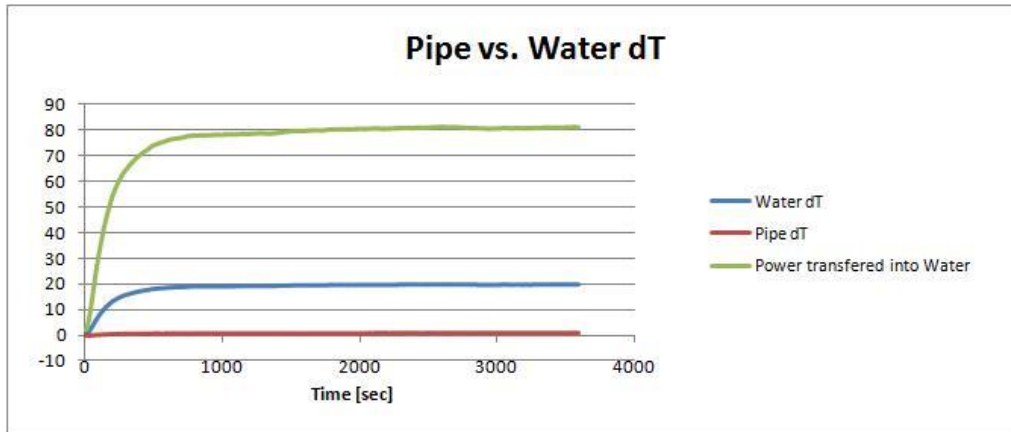


Figure A4-21: Analysed Results Heat Pipe 2 120W Run

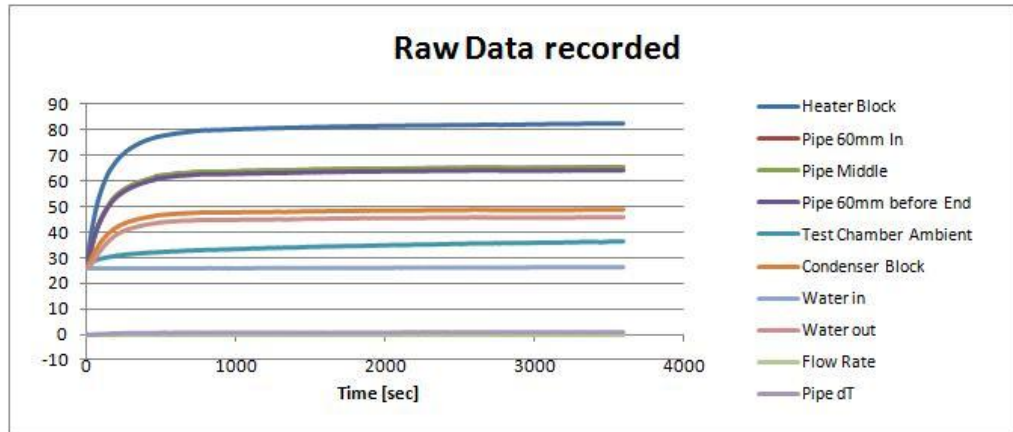


Figure A4-22: Recorded Results Heat Pipe 2 120W Run

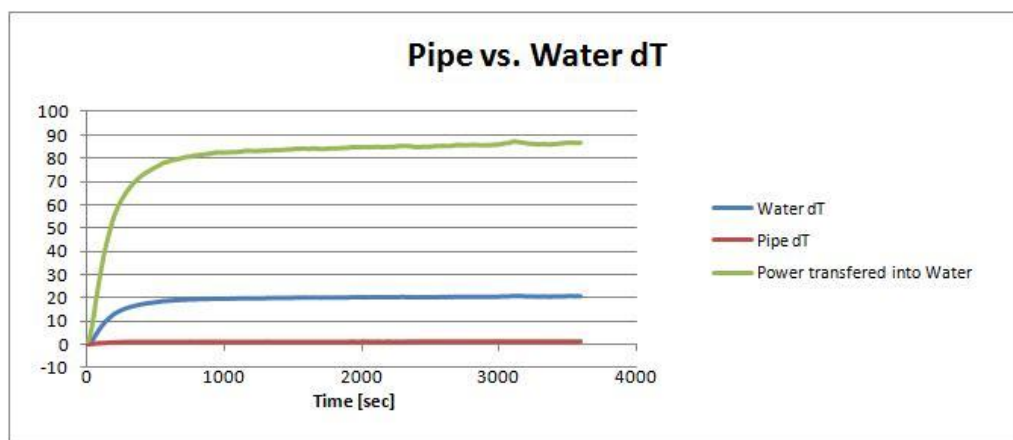


Figure A4-23: Analysed Results Heat Pipe 2 130W Run

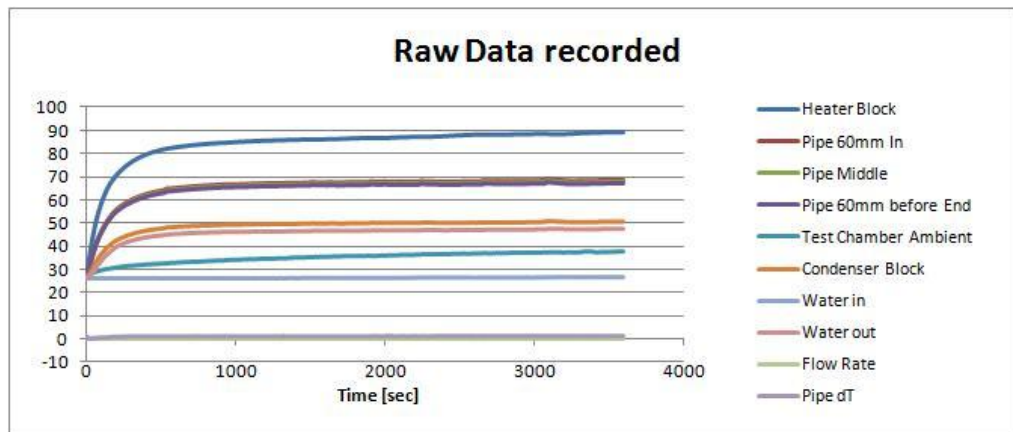


Figure A4-24: Recorded Results Heat Pipe 2 130W Run

Heat Pipe 3:

The results for the straight heat pipe 3 are presented and described within chapter 5 of this PhD thesis.

Heat Pipe 4:

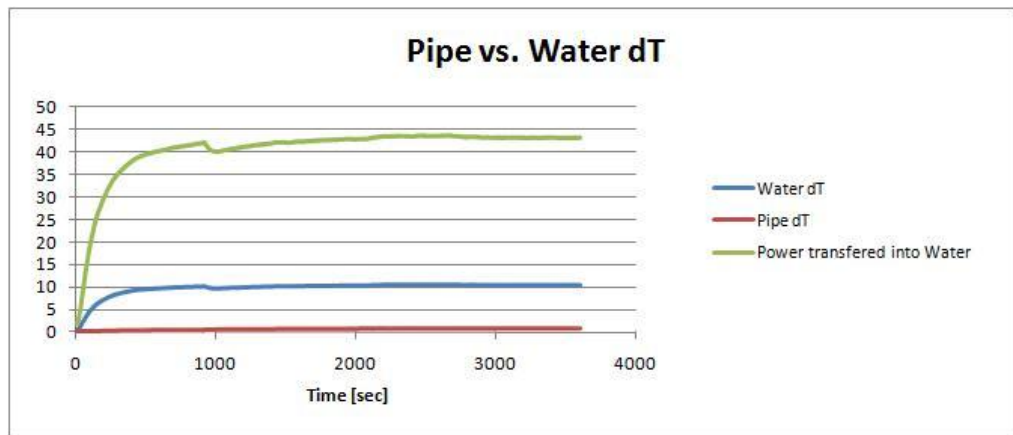


Figure A4-25: Analysed Results Heat Pipe 4 70W Run

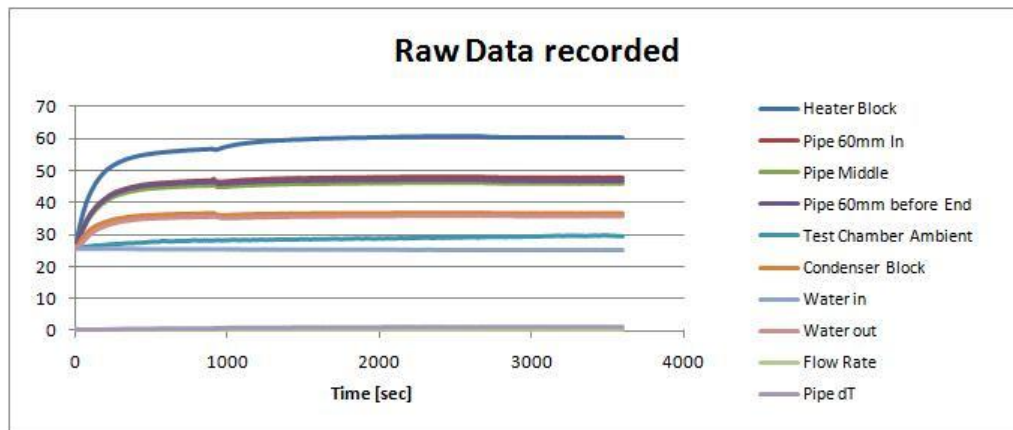


Figure A4-26: Recorded Results Heat Pipe 4 70W Run

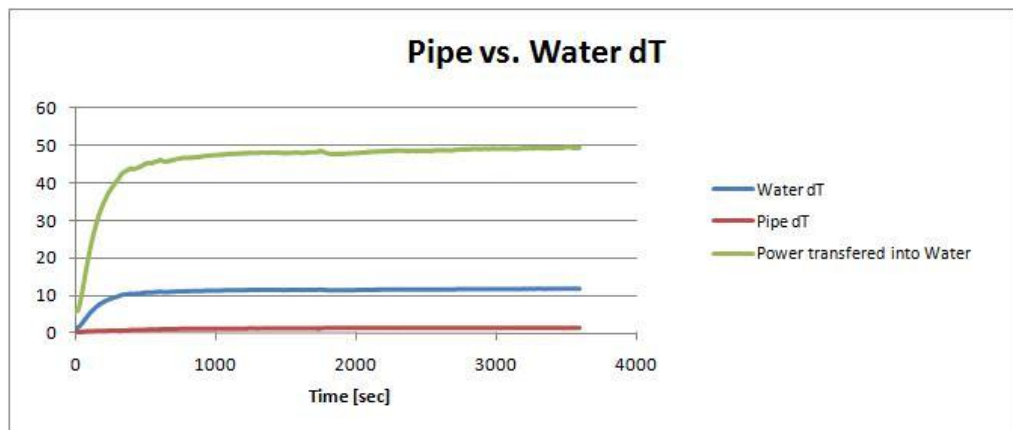


Figure A4-27: Analysed Results Heat Pipe 4 80W Run

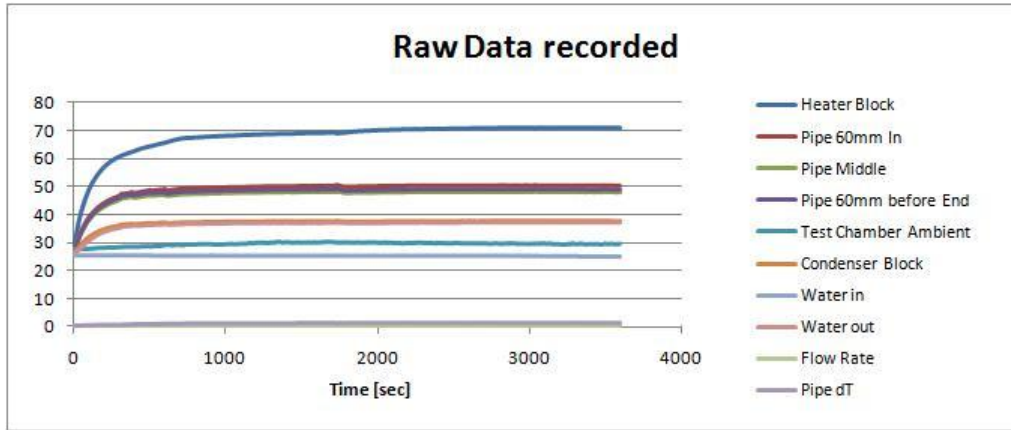


Figure A4-28: Recorded Results Heat Pipe 4 80W Run

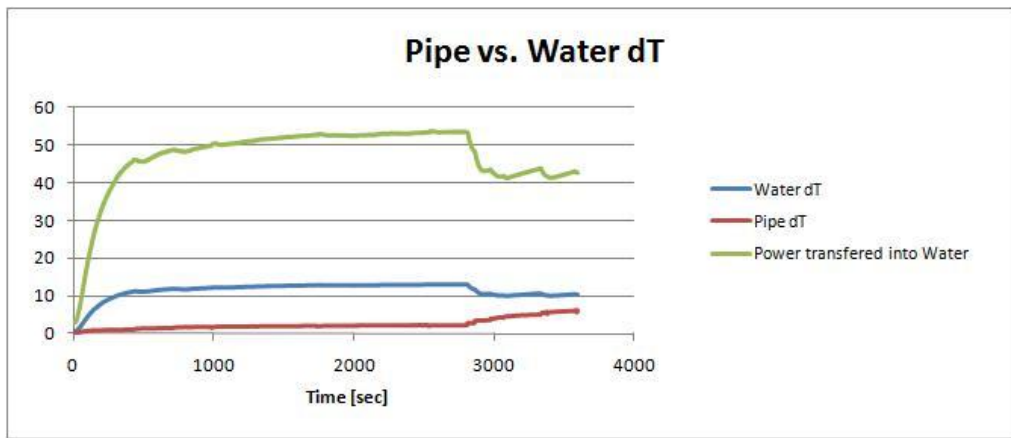


Figure A4-29: Analysed Results Heat Pipe 4 90W Run

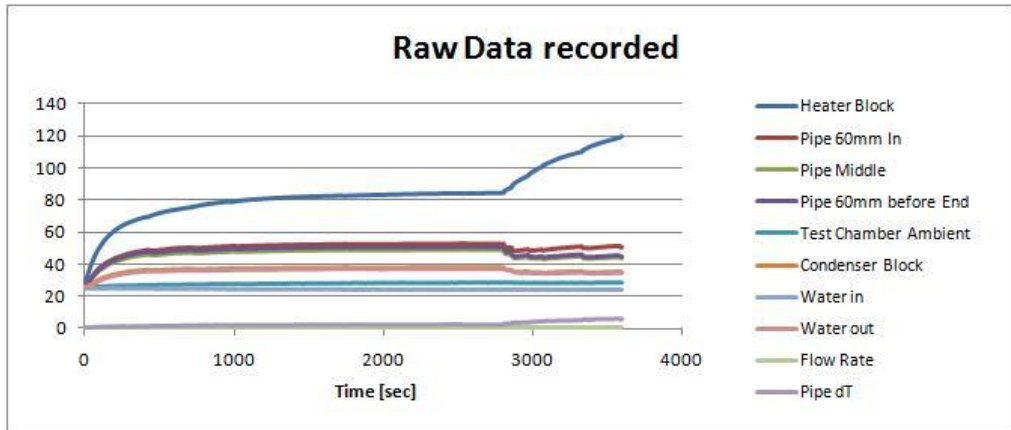


Figure A4-30: Recorded Results Heat Pipe 4 90W Run

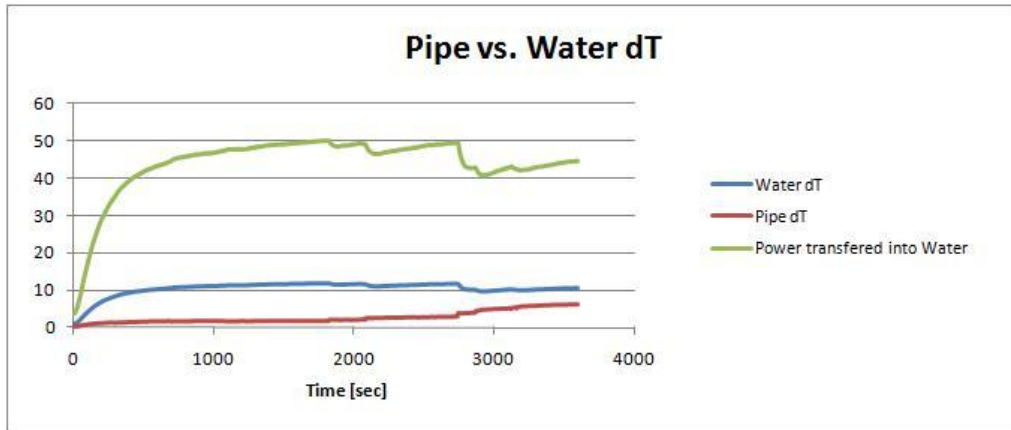


Figure A4-31: Analysed Results Heat Pipe 4 80W Ramp-Up Run

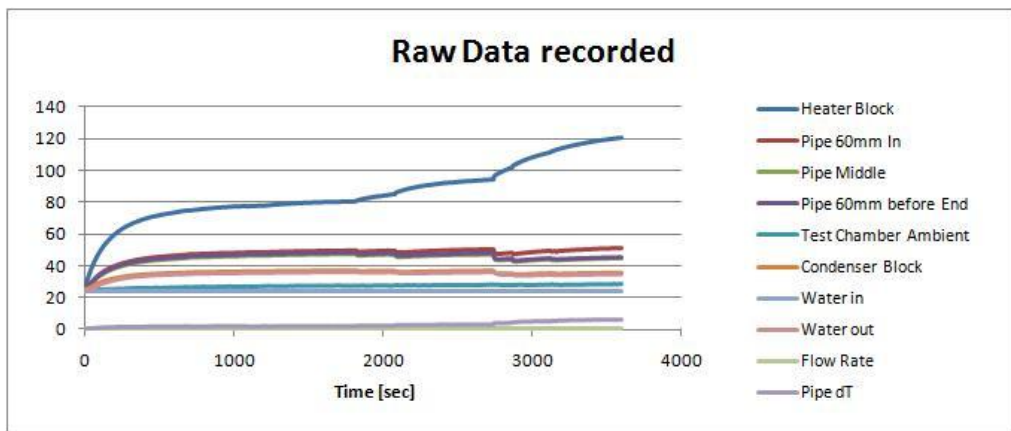


Figure A4-32: Recorded Results Heat Pipe 4 80W Ramp-Up Run

Heat Pipe 5:

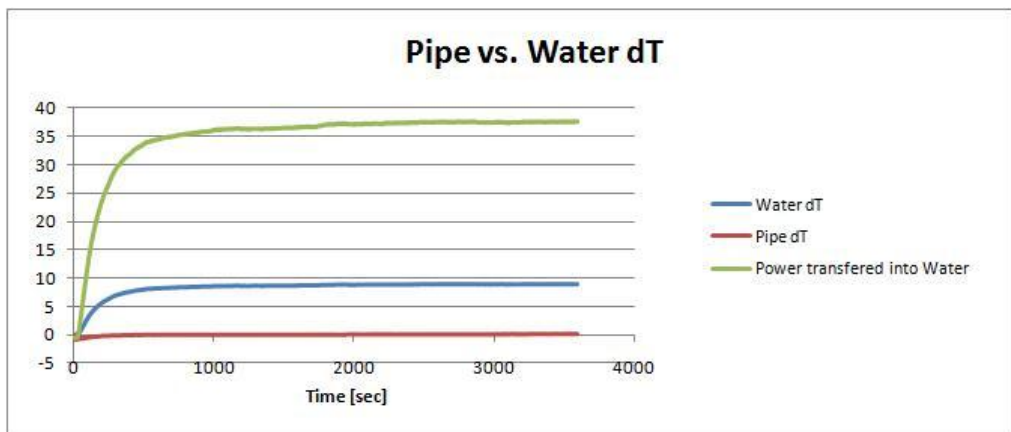


Figure A4-33: Analysed Results Heat Pipe 5 70W Run

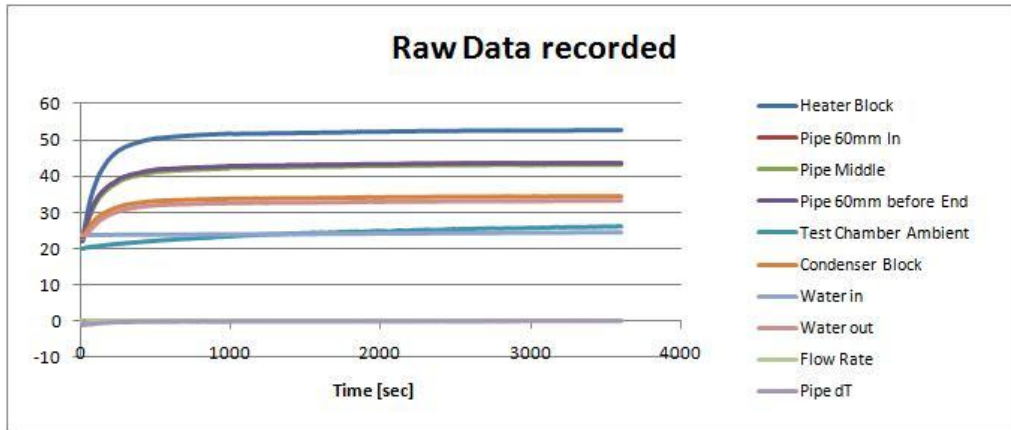


Figure A4-34: Recorded Results Heat Pipe 5 70W Run

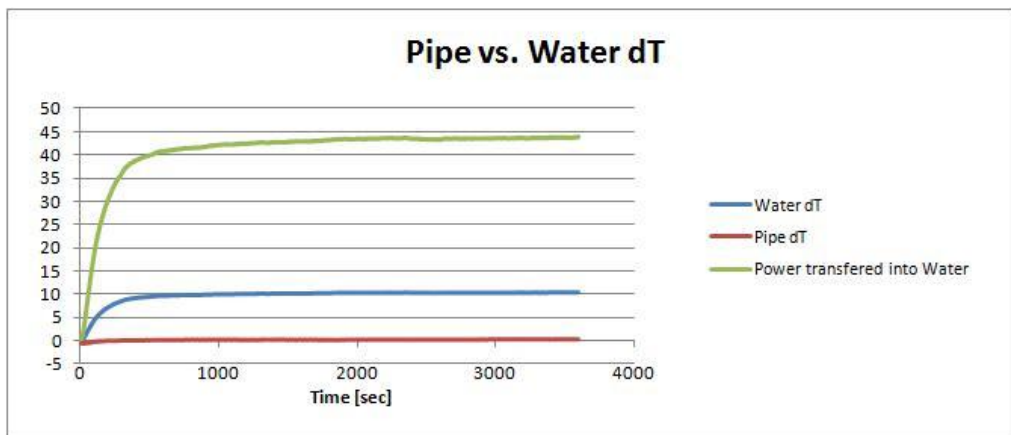


Figure A4-35: Analysed Results Heat Pipe 5 80W Run

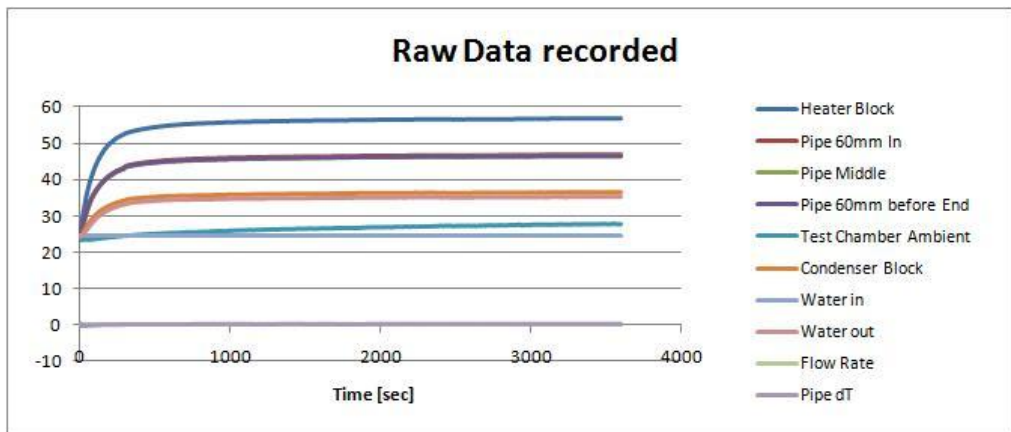


Figure A4-36: Recorded Results Heat Pipe 5 80W Run

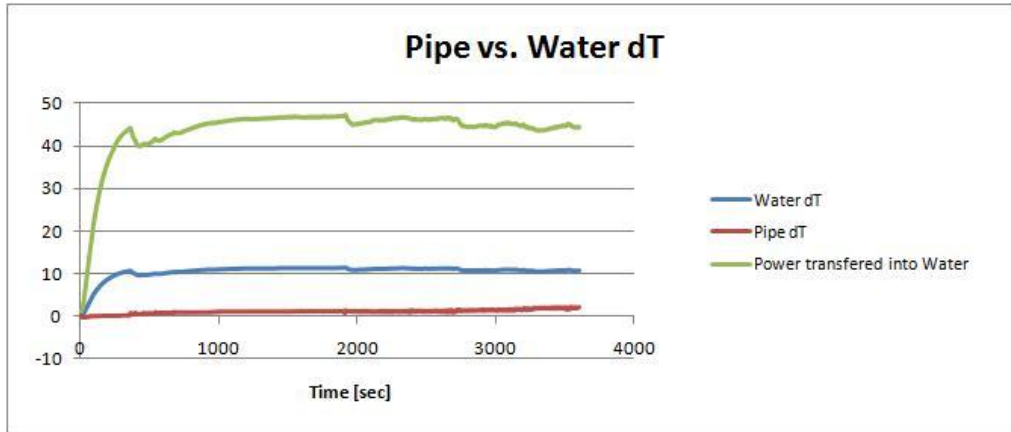


Figure A4-37: Analysed Results Heat Pipe 5 90W Run

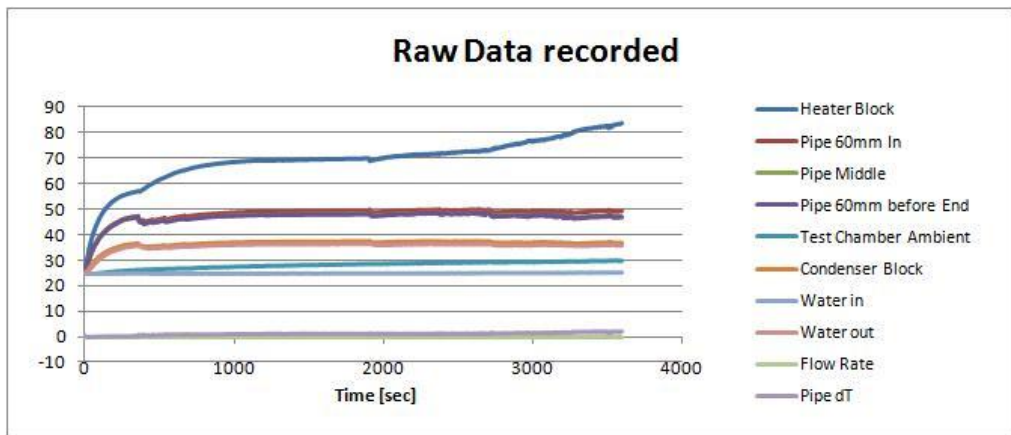


Figure A4-38: Recorded Results Heat Pipe 5 90W Run

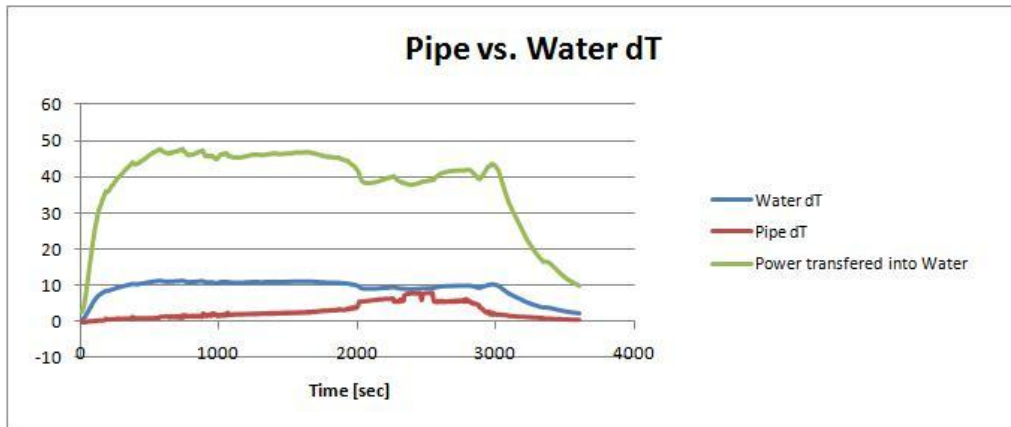


Figure A4-39: Analysed Results Heat Pipe 5 100W Run

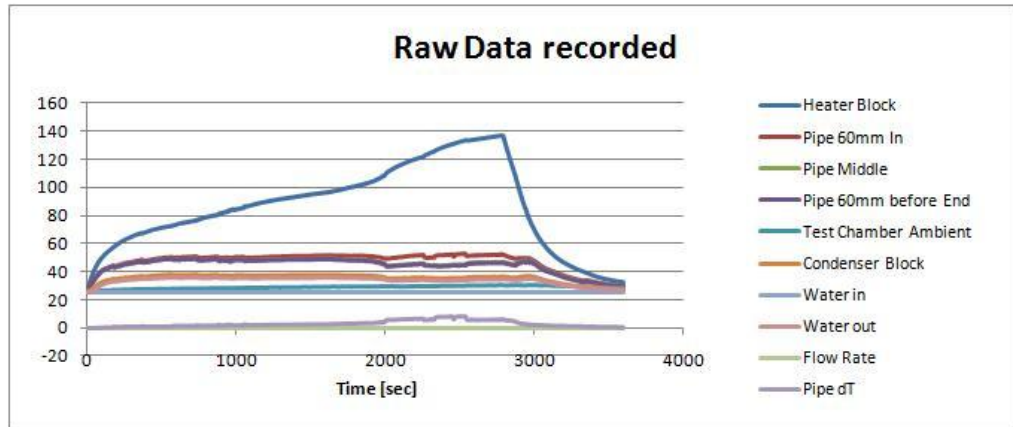


Figure A4-40: Recorded Results Heat Pipe 5 100W Run

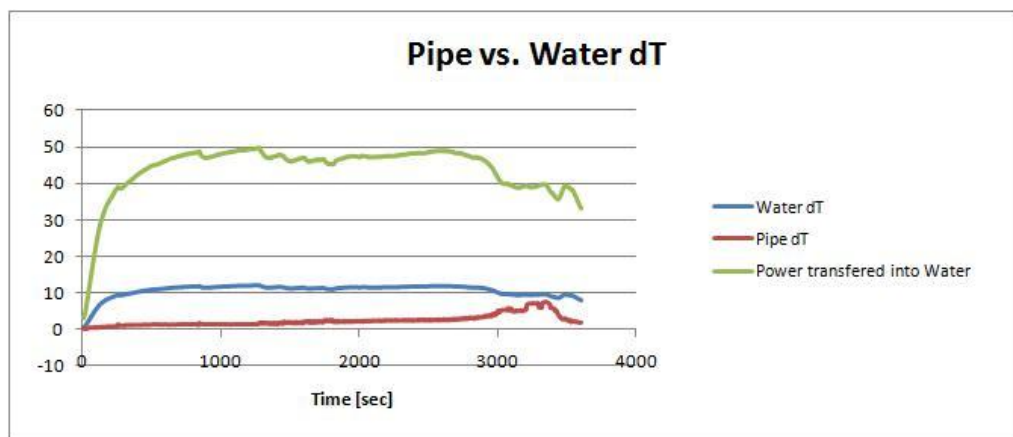


Figure A4-41: Analysed Results Heat Pipe 5 90W Ramp-Up Run

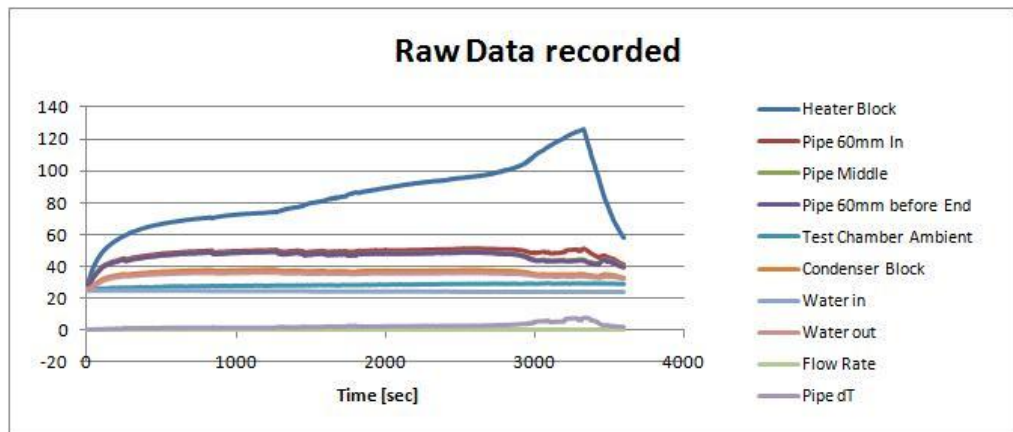


Figure A4-42: Recorded Results Heat Pipe 5 90W Ramp-Up Run

A4-2 45° Bent Heat Pipes:

Heat Pipe 1:

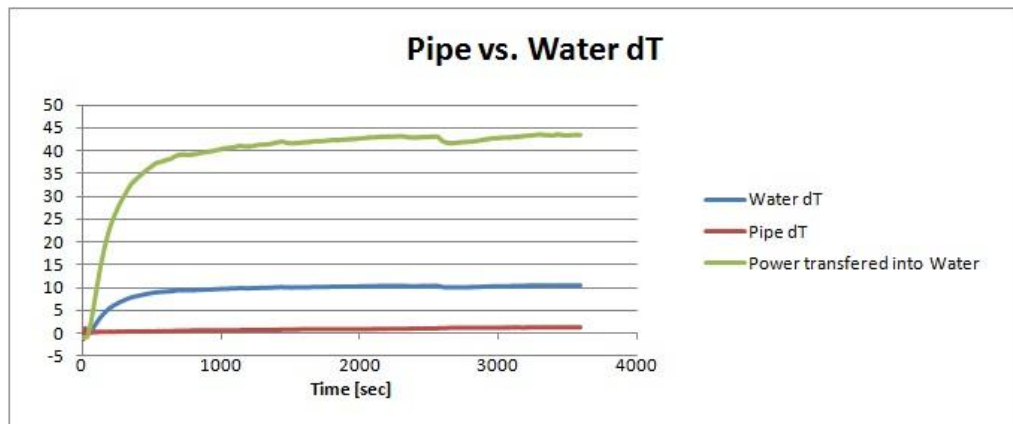


Figure A4-43: Analysed Results Heat Pipe 1 60W Run

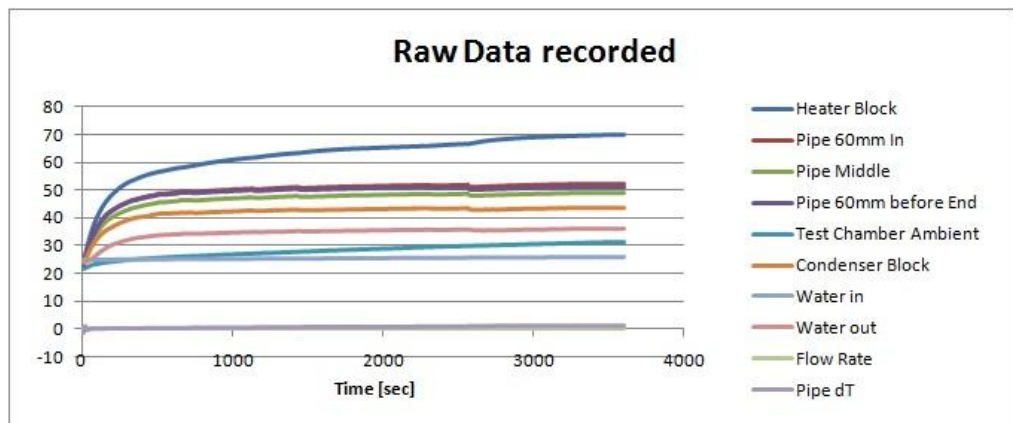


Figure A4-44: Recorded Results Heat Pipe 1 60W Run

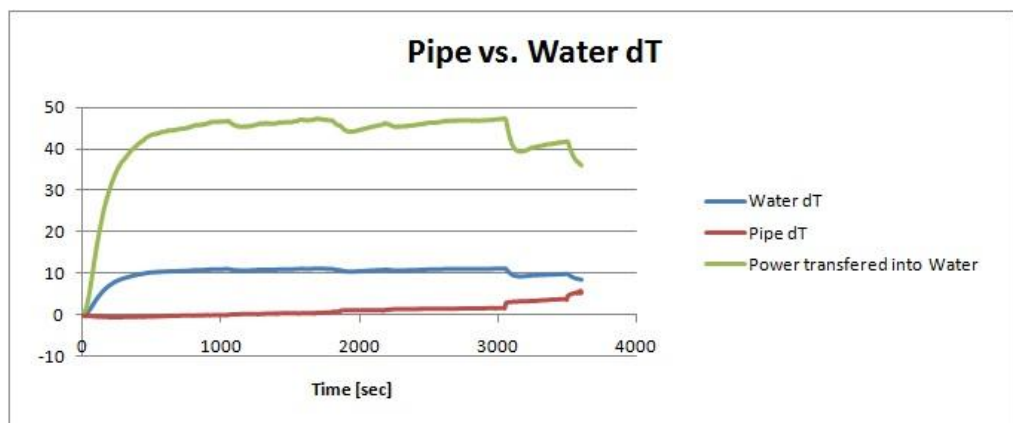


Figure A4-45: Analysed Results Heat Pipe 1 70W Run

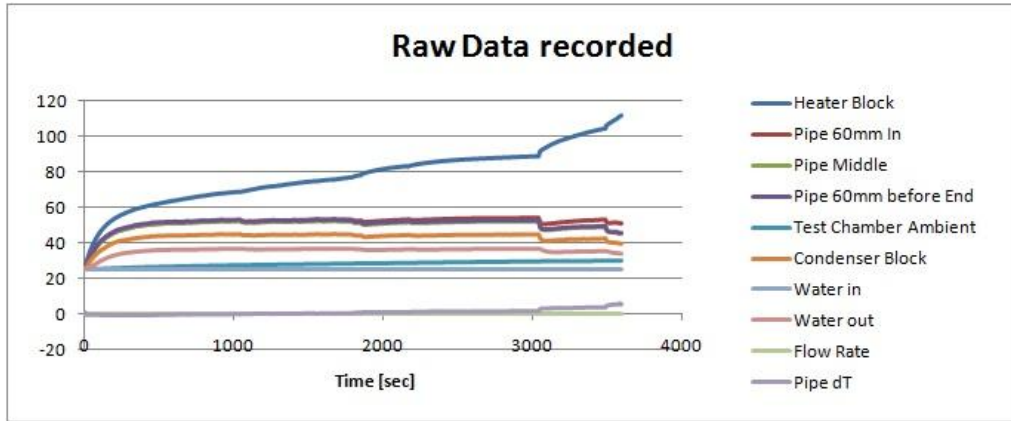


Figure A4-46: Recorded Results Heat Pipe 1 70W Run

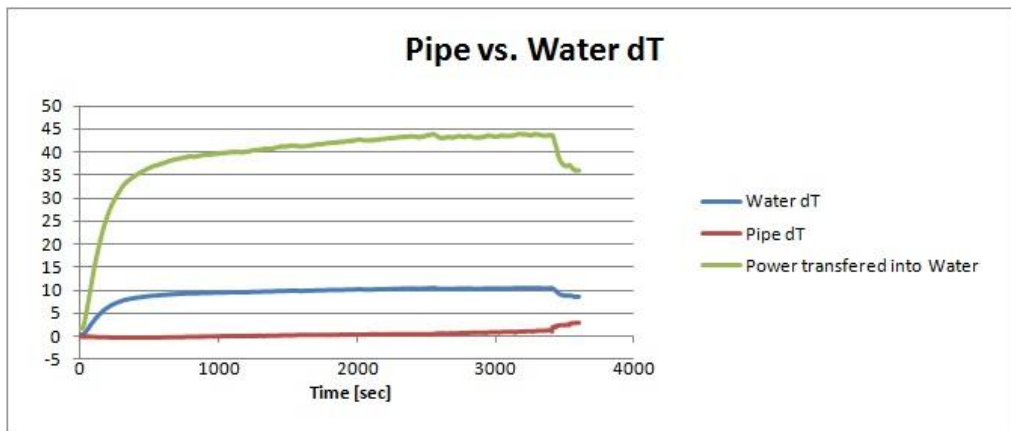


Figure A4-47: Analysed Results Heat Pipe 1 60W Ramp-Up Run

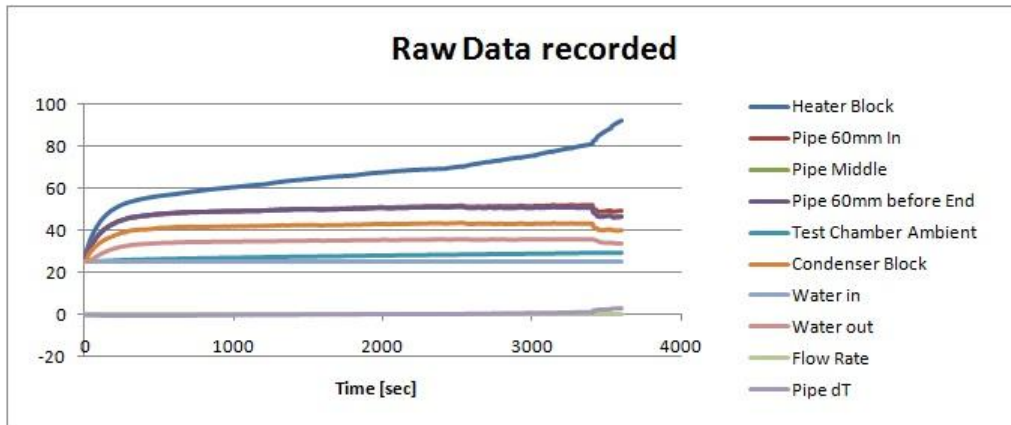


Figure A4-48: Recorded Results Heat Pipe 1 60W Ramp-Up Run

Heat Pipe 2:

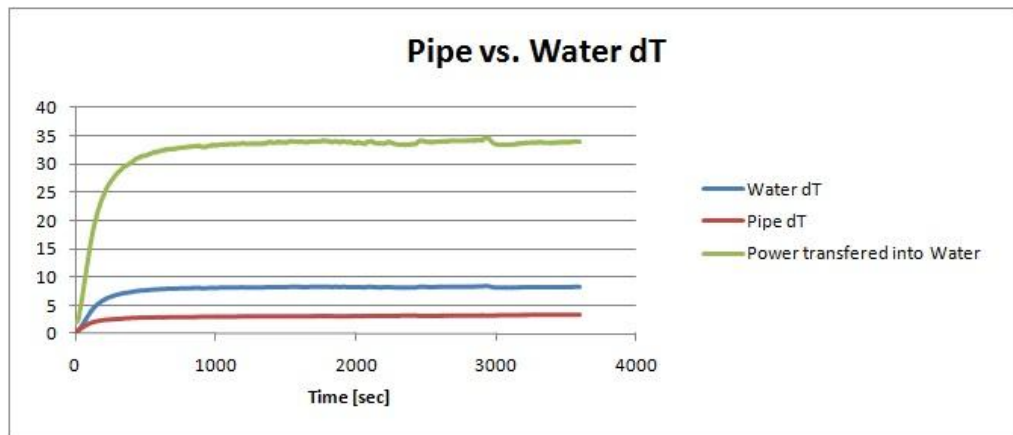


Figure A4-49: Analysed Results Heat Pipe 2 50W Run

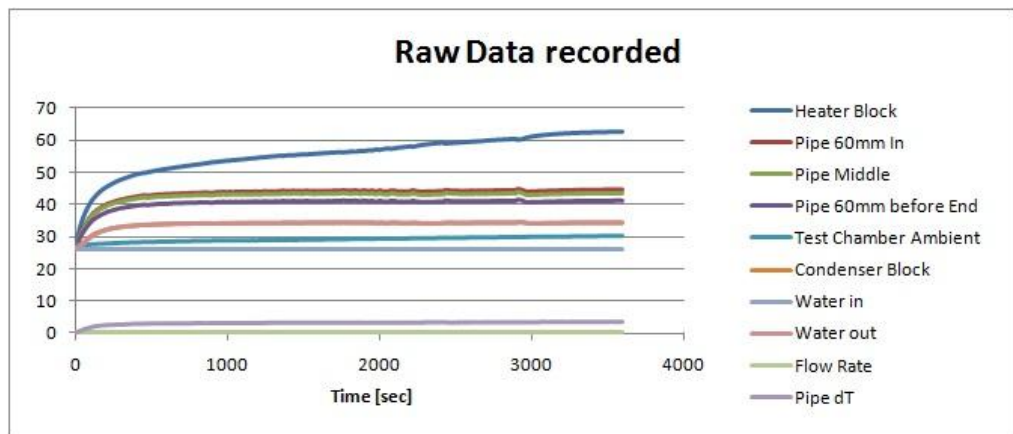


Figure A4-50: Recorded Results Heat Pipe 2 50W Run

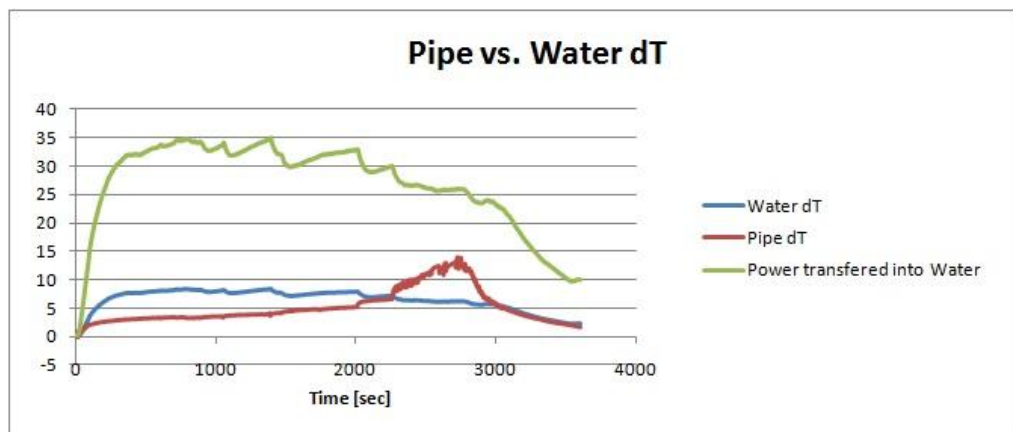


Figure A4-51: Analysed Results Heat Pipe 2 60W Run

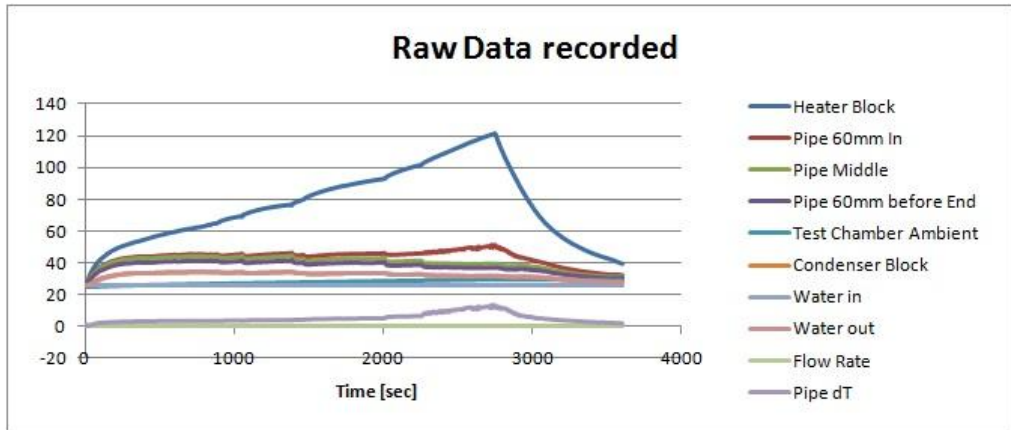


Figure A4-52: Recorded Results Heat Pipe 2 60W Run

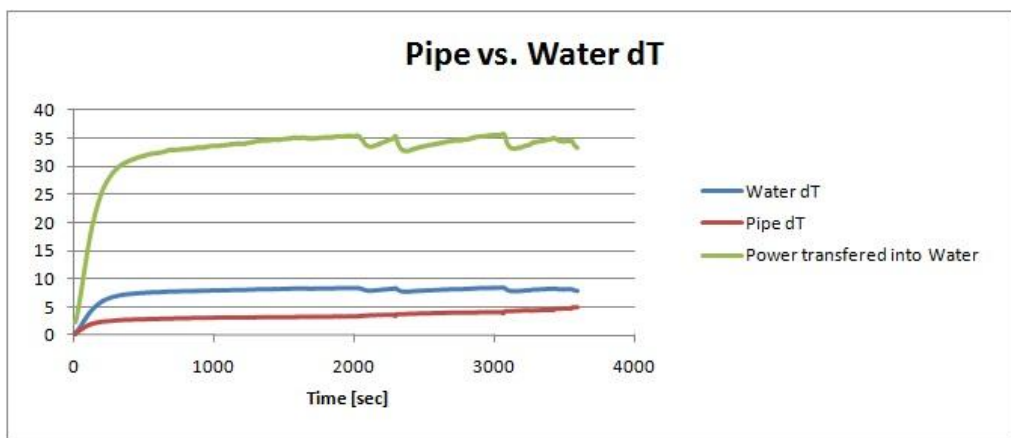


Figure A4-53: Analysed Results Heat Pipe 2 50W Ramp-Up Run

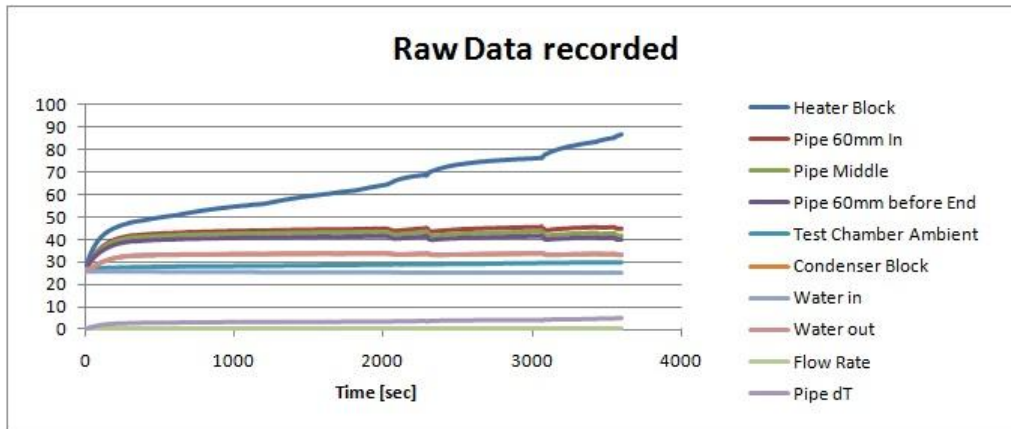


Figure A4-54: Recorded Results Heat Pipe 2 50W Ramp-Up Run

Heat Pipe 3:

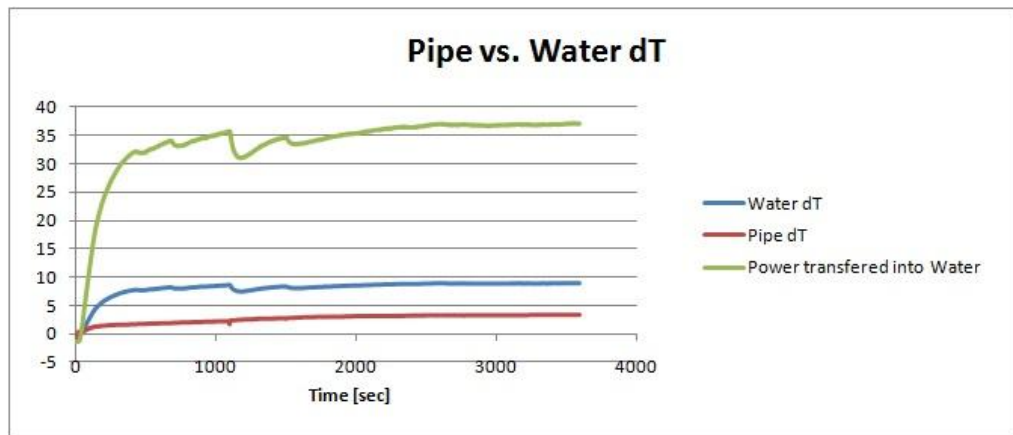


Figure A4-55: Analysed Results Heat Pipe 3 60W Run

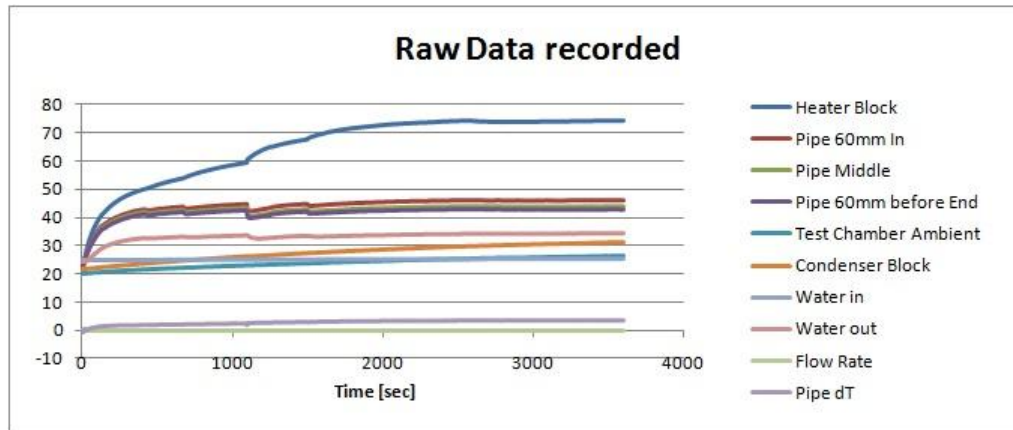


Figure A4-56: Recorded Results Heat Pipe 3 60W Run

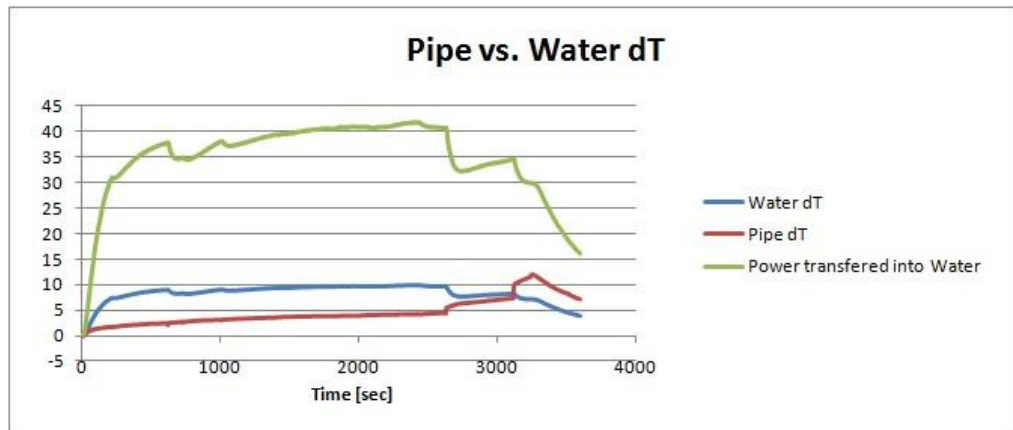


Figure A4-57: Analysed Results Heat Pipe 3 70W Run

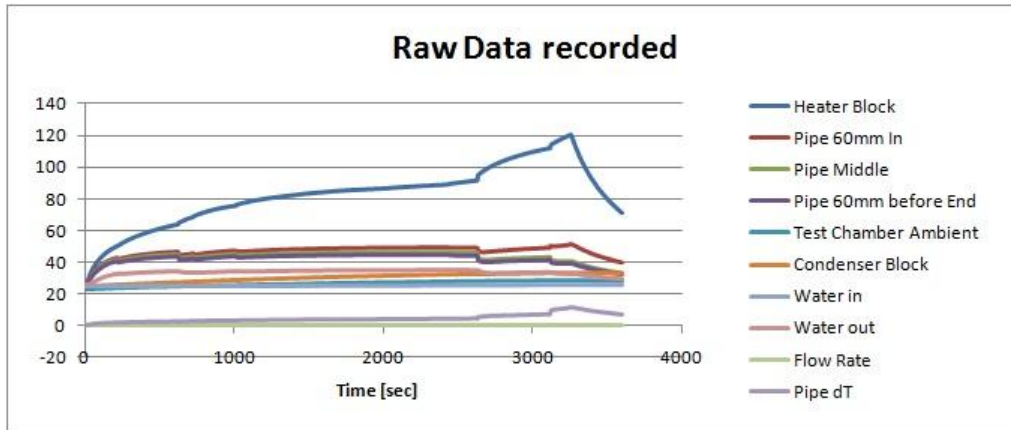


Figure A4-58: Recorded Results Heat Pipe 3 70W Run

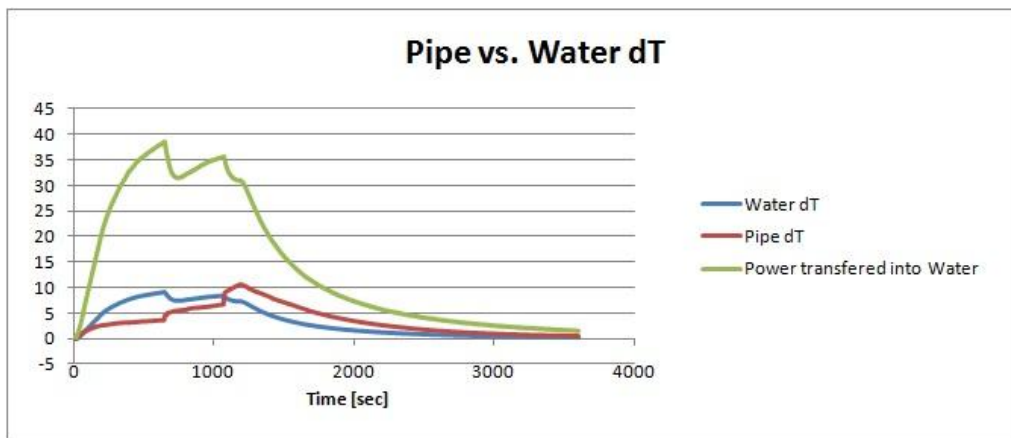


Figure A4-59: Analysed Results Heat Pipe 3 80W Run

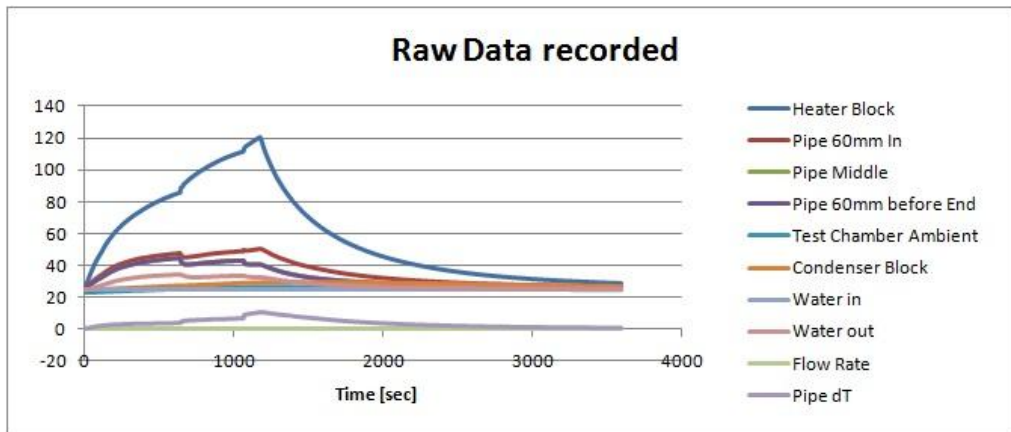


Figure A4-60: Recorded Results Heat Pipe 3 80W Run

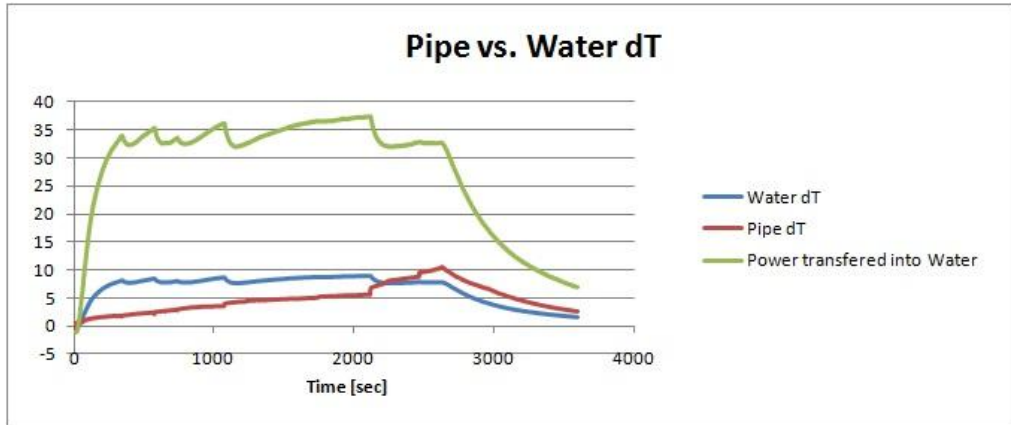


Figure A4-61: Analysed Results Heat Pipe 3 70W Ramp-Up Run

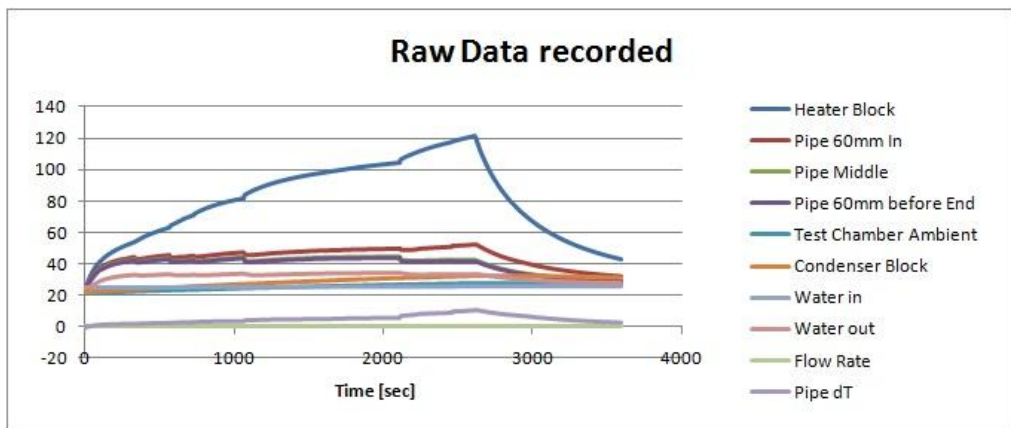


Figure A4-62: Recorded Results Heat Pipe 3 70W Ramp-Up Run

Heat Pipe 4:

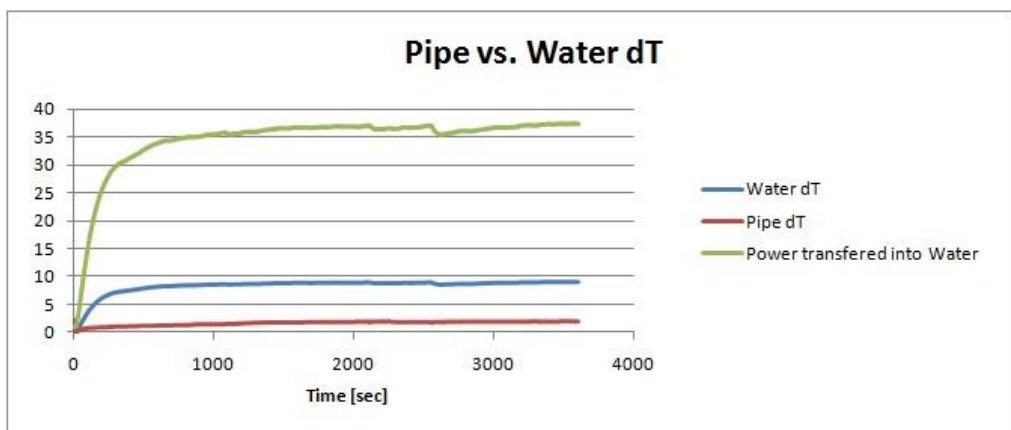


Figure A4-63: Analysed Results Heat Pipe 4 60W Run

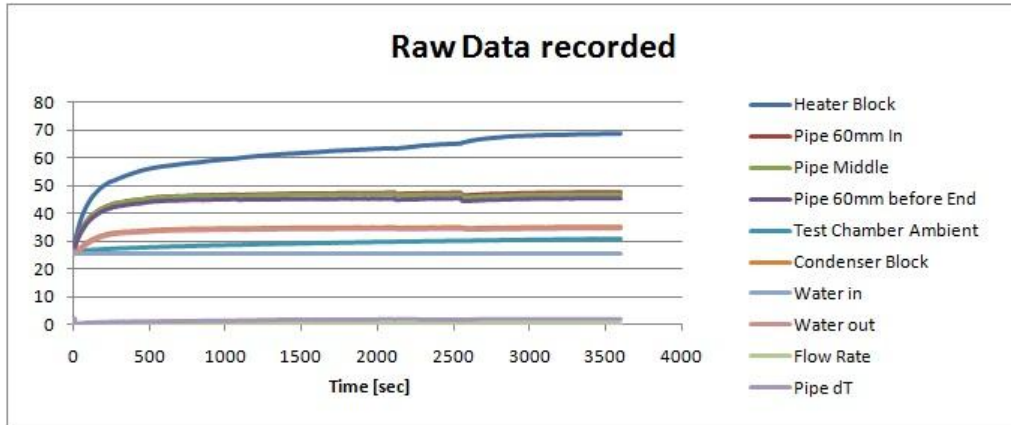


Figure A4-64: Recorded Results Heat Pipe 4 60W Run

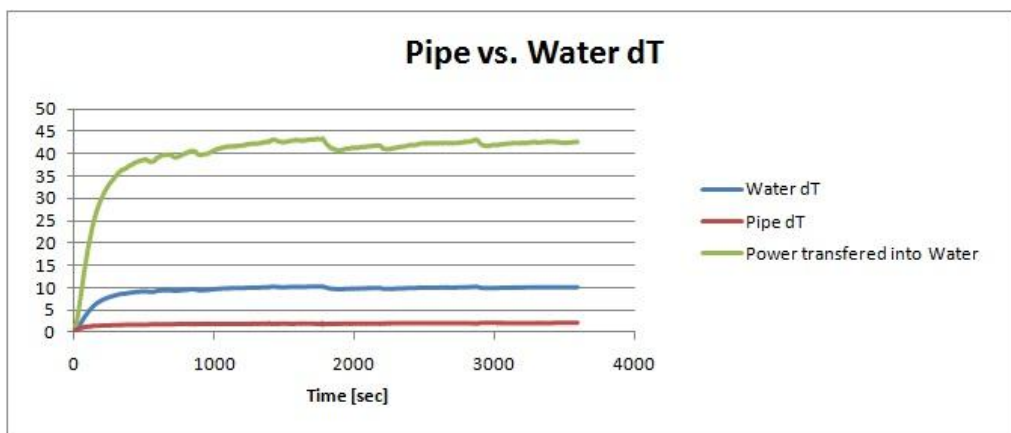


Figure A4-65: Analysed Results Heat Pipe 4 70W Run

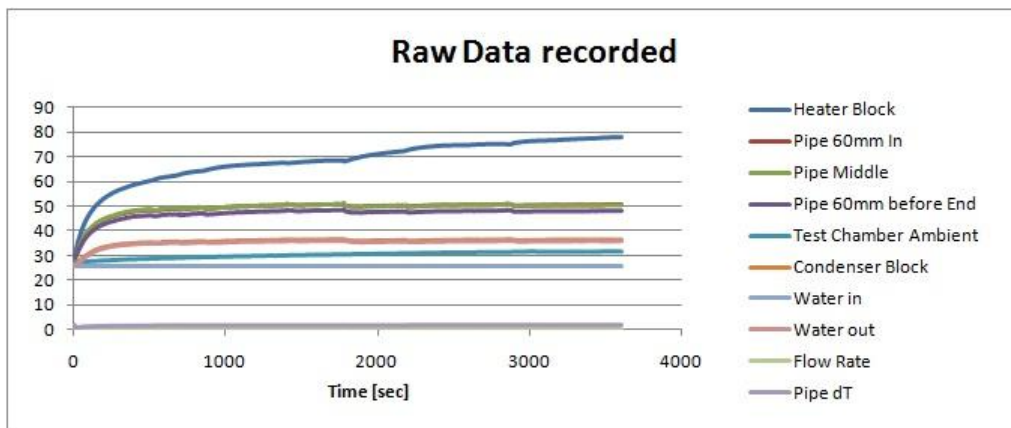


Figure A4-66: Recorded Results Heat Pipe 4 70W Run

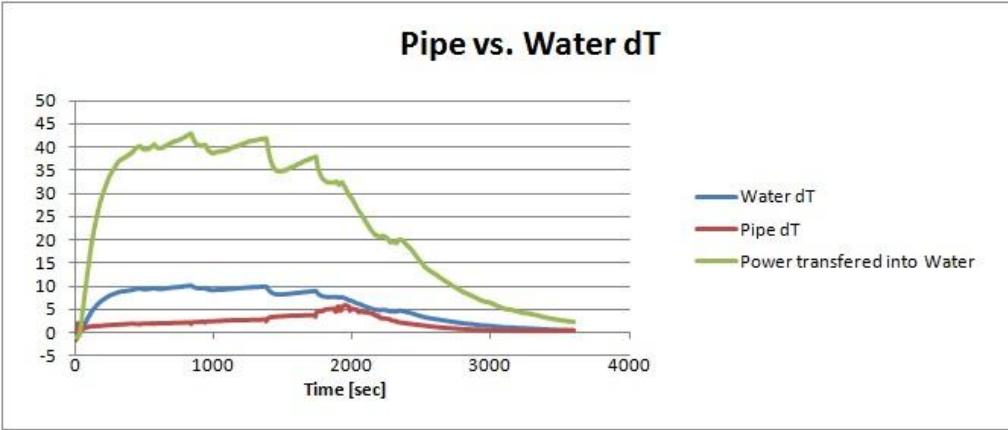


Figure A4-67: Analysed Results Heat Pipe 4 80W Run

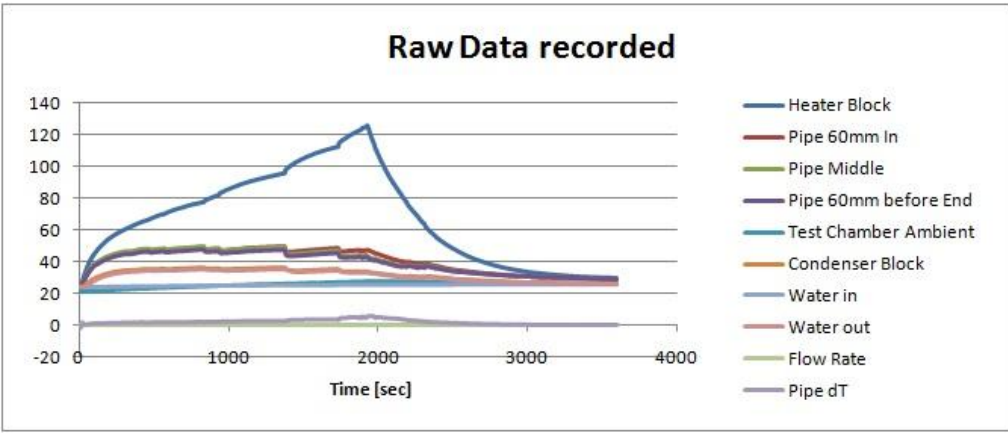


Figure A4-68: Recorded Results Heat Pipe 4 80W Run

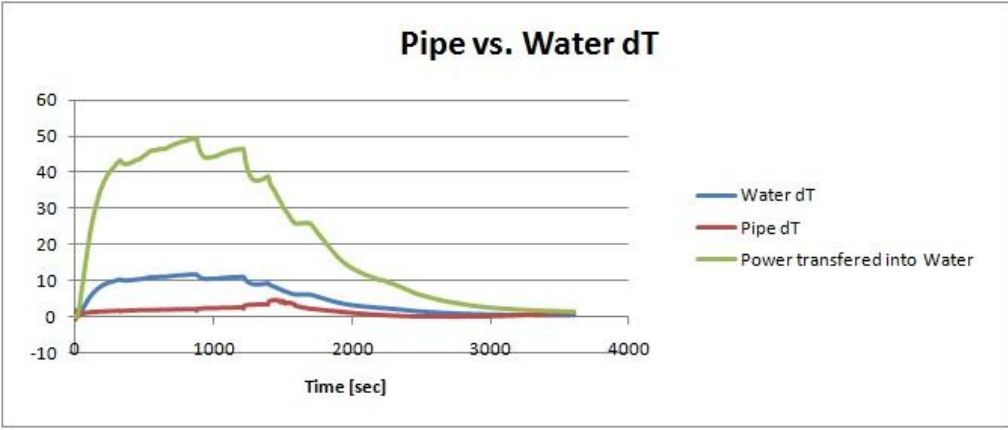


Figure A4-69: Analysed Results Heat Pipe 4 90W Run

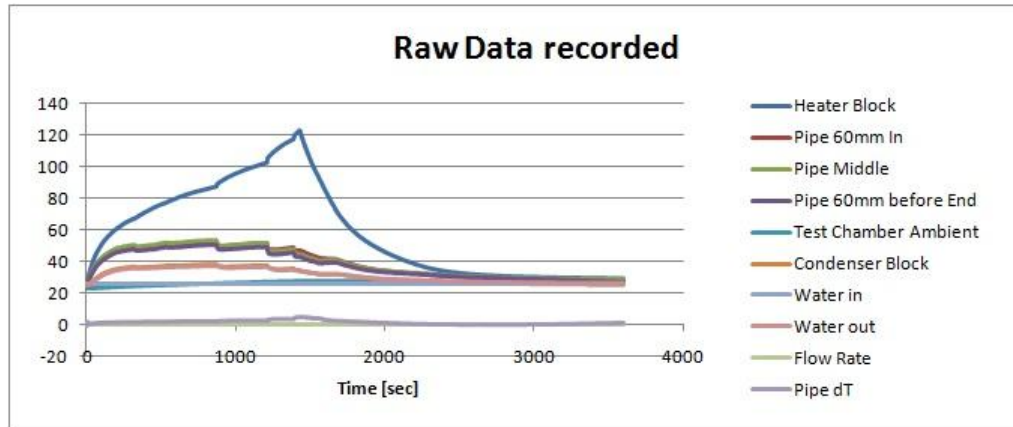


Figure A4-70: Recorded Results Heat Pipe 4 90W Run

Heat Pipe 5:

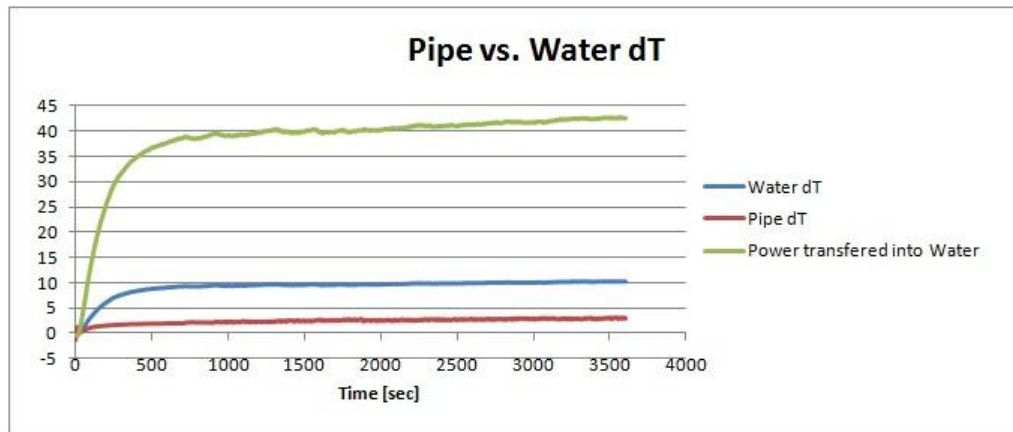


Figure A4-71: Analysed Results Heat Pipe 5 60W Run

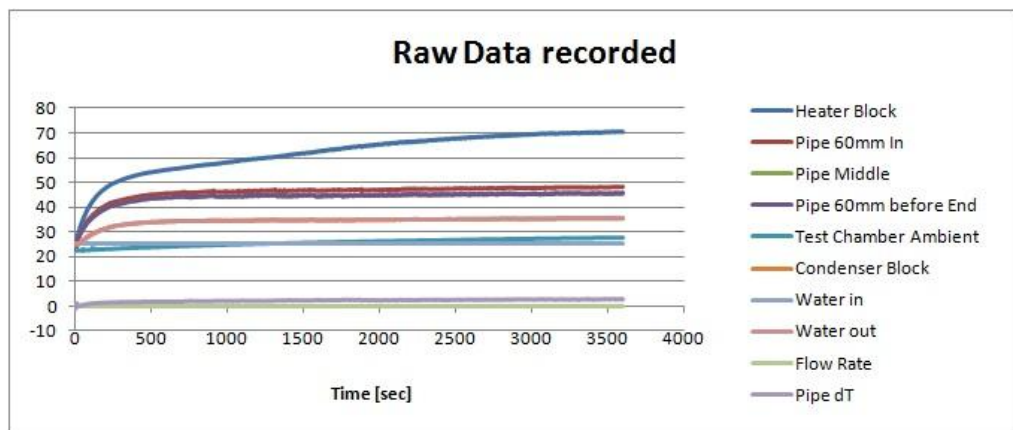


Figure A4-72: Recorded Results Heat Pipe 5 60W Run

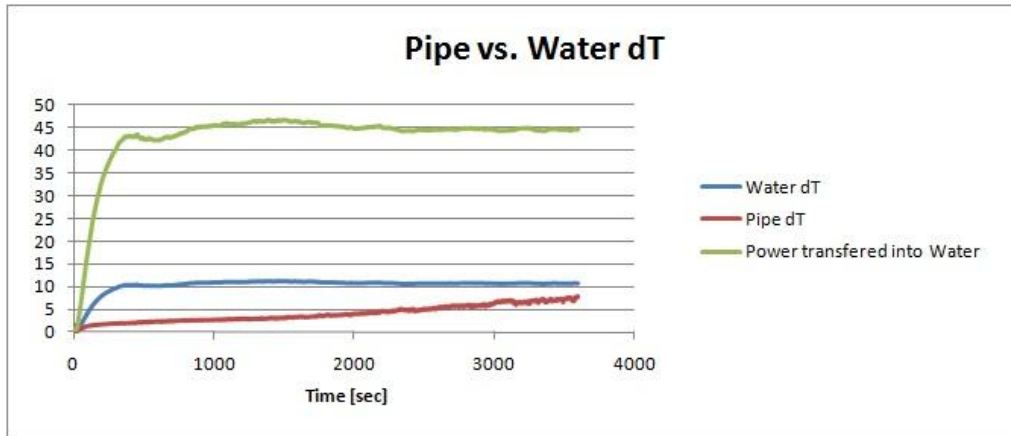


Figure A4-73: Analysed Results Heat Pipe 5 70W Run

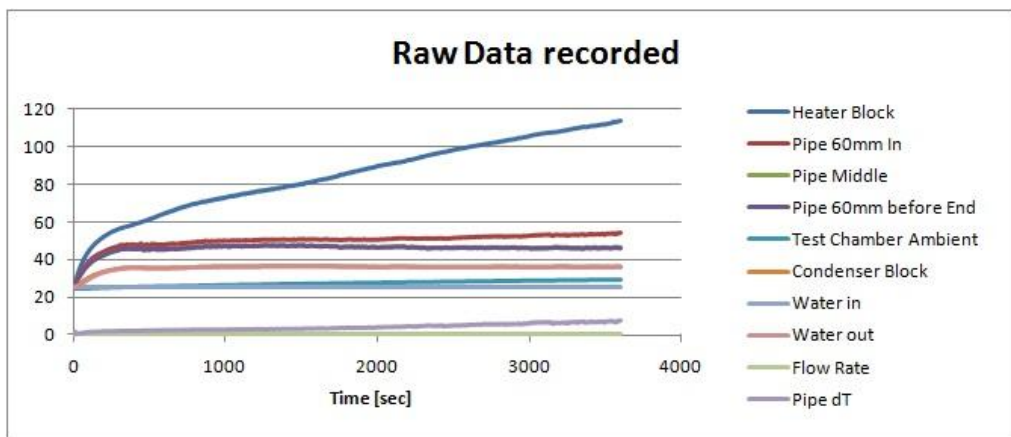


Figure A4-74: Recorded Results Heat Pipe 5 70W Run

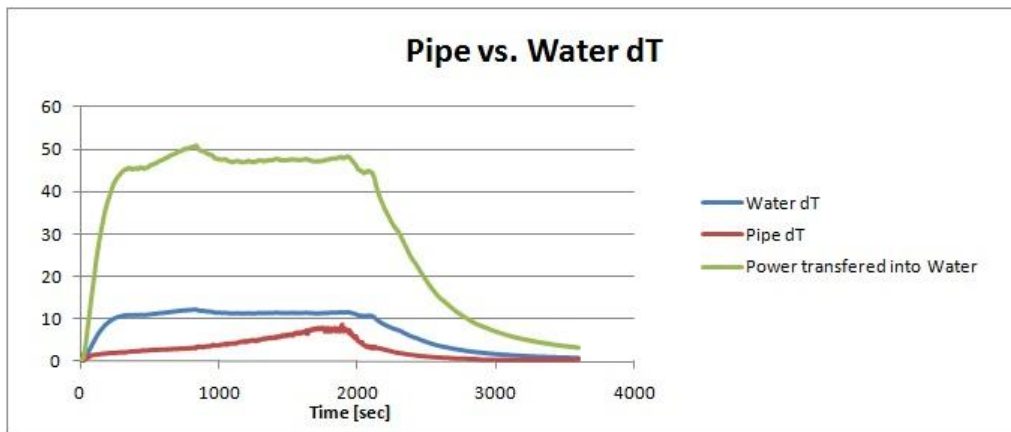


Figure A4-75: Analysed Results Heat Pipe 5 80W Run

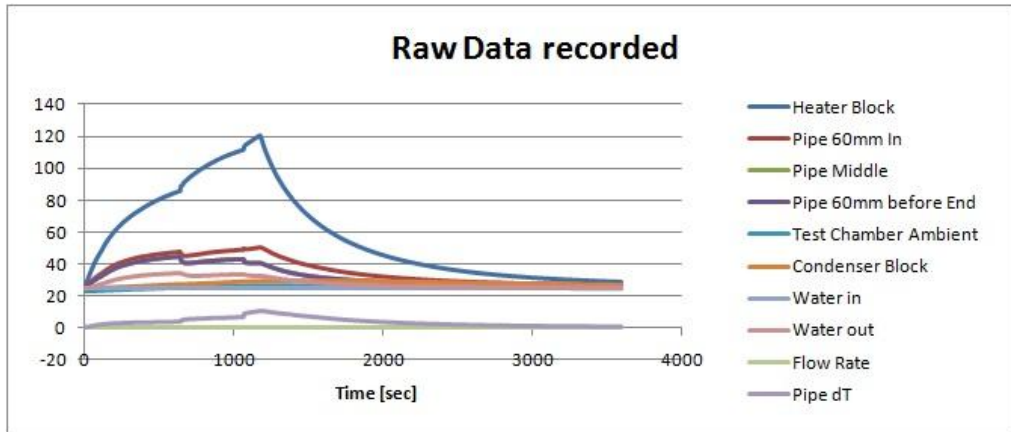


Figure A4-76: Recorded Results Heat Pipe 5 80W Run

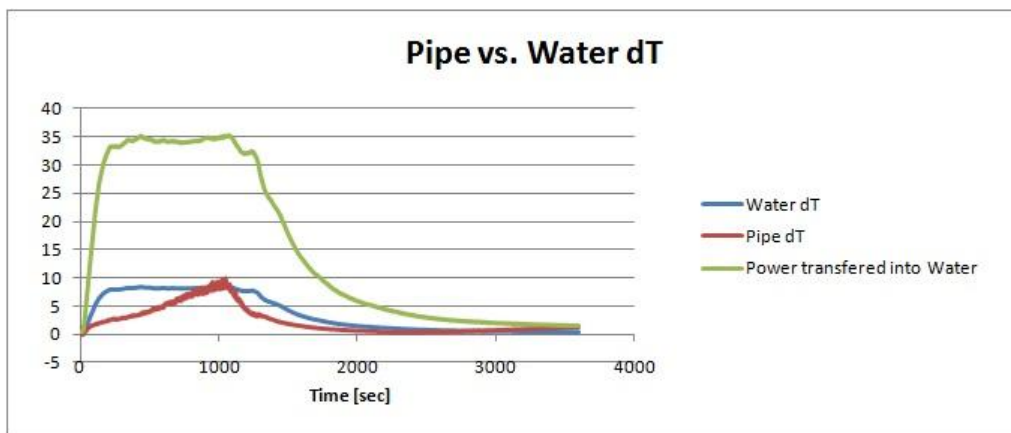


Figure A4-77: Analysed Results Heat Pipe 5 90W Run

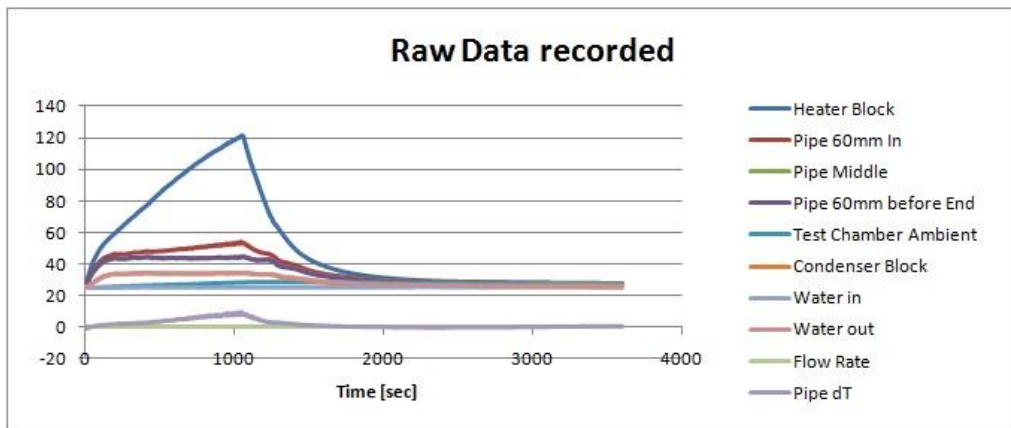


Figure A4-78: Recorded Results Heat Pipe 5 90W Run

A4-3 90° Bent Heat Pipes:

Heat Pipe 1:

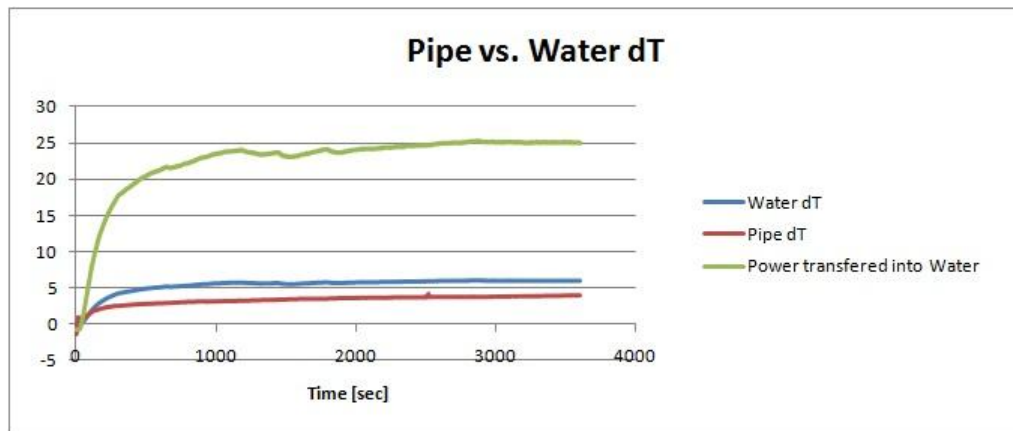


Figure A4-79: Analysed Results Heat Pipe 1 40W Run

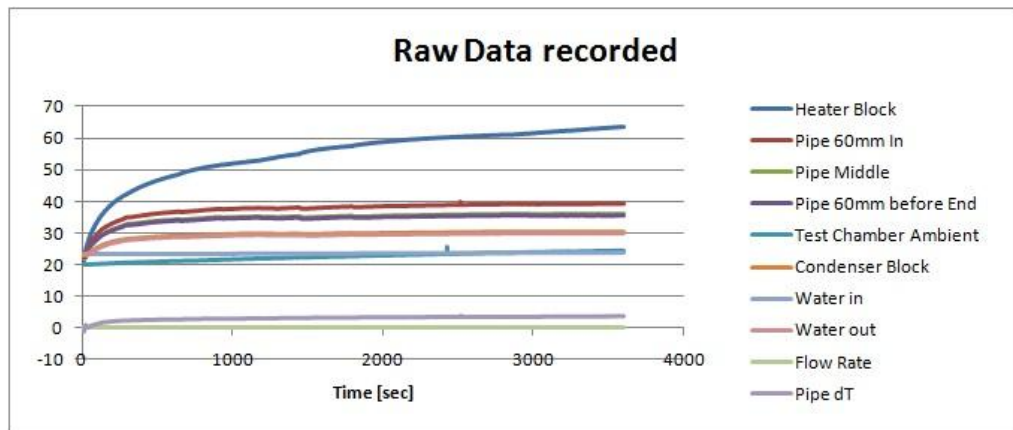


Figure A4-80: Recorded Results Heat Pipe 1 40W Run

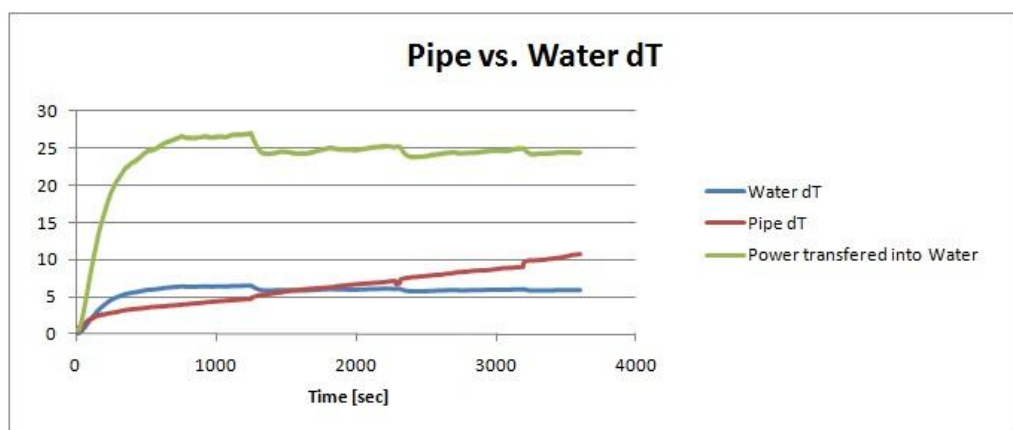


Figure A4-81: Analysed Results Heat Pipe 1 50W Run 1

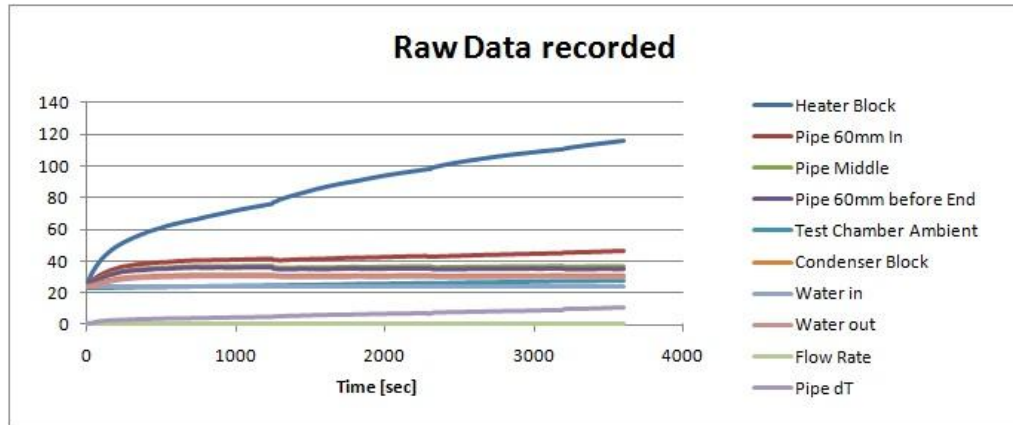


Figure A4-82: Recorded Results Heat Pipe 1 50W Run 1

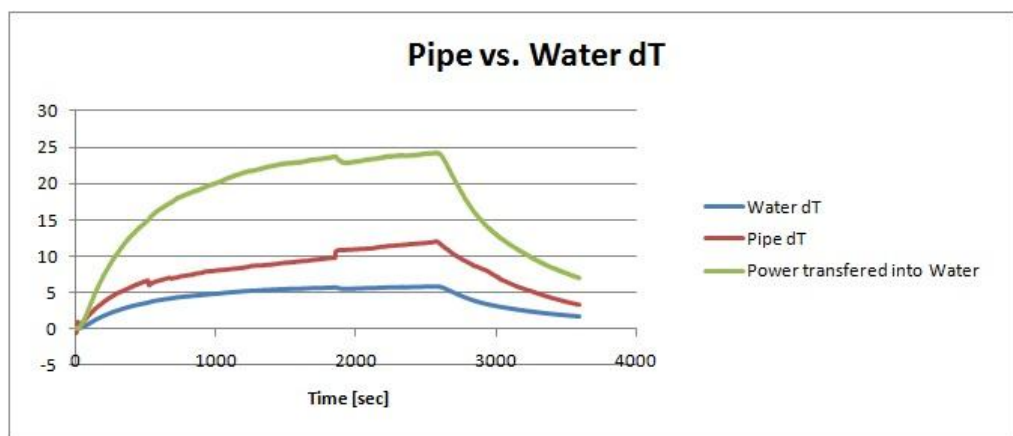


Figure A4-83: Analysed Results Heat Pipe 1 50W Run 2

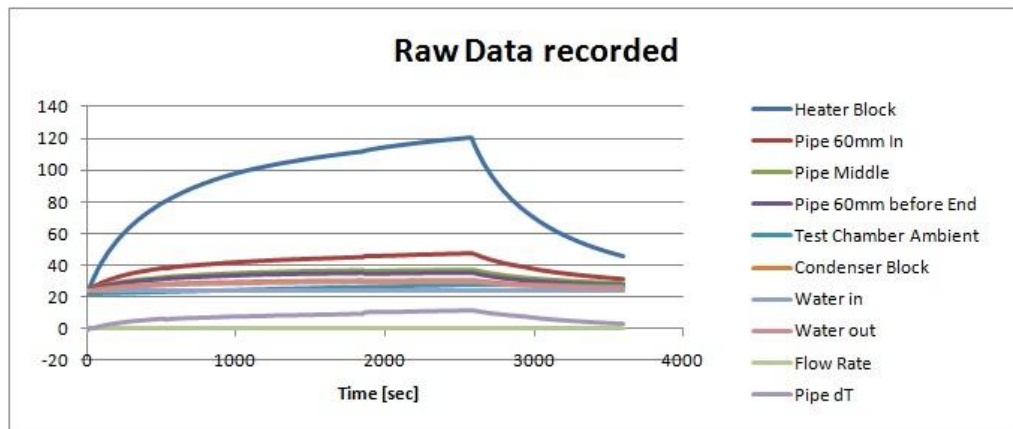


Figure A4-84: Recorded Results Heat Pipe 1 50W Run 2

Heat Pipe 2:

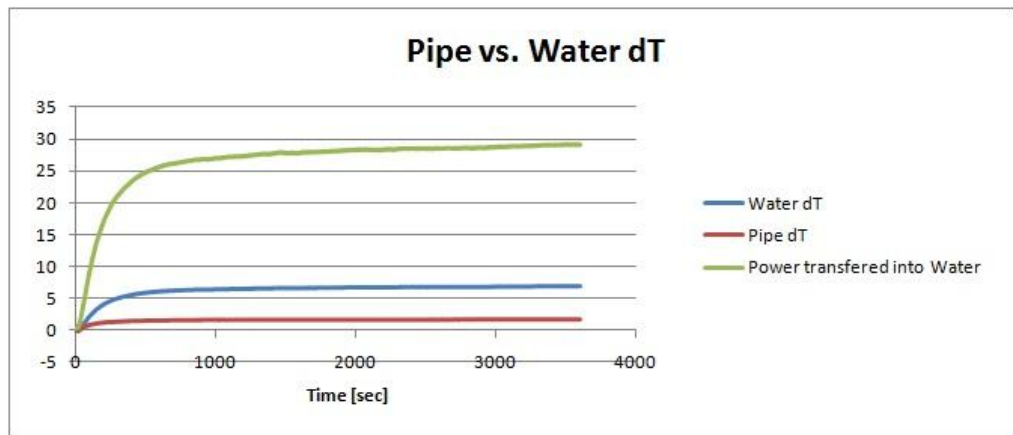


Figure A4-85: Analysed Results Heat Pipe 2 40W Run

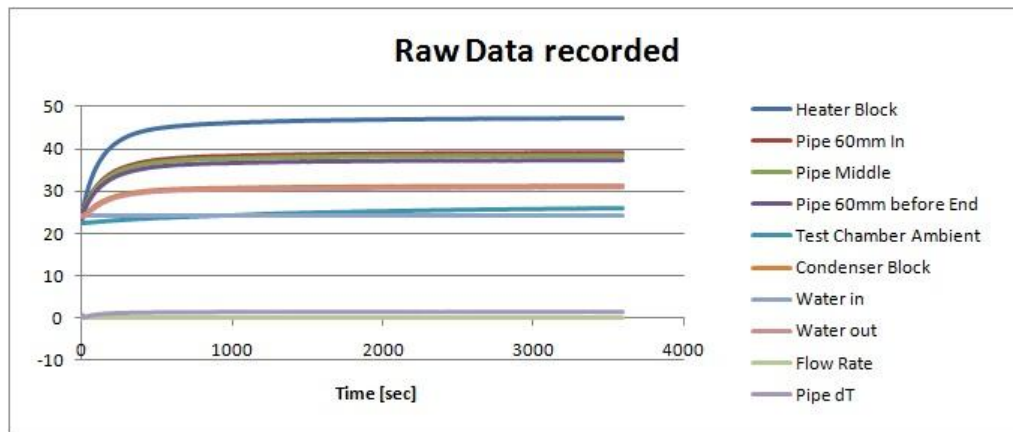


Figure A4-86: Recorded Results Heat Pipe 2 40W Run

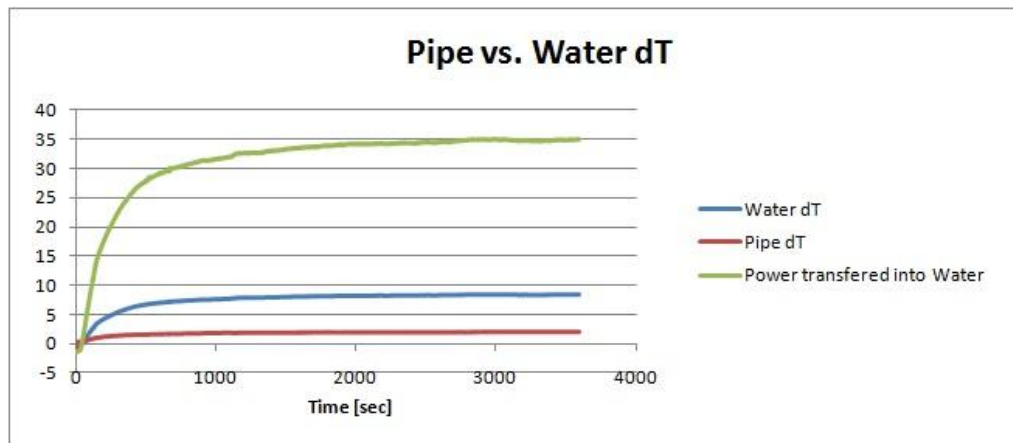


Figure A4-87: Analysed Results Heat Pipe 2 50W Run

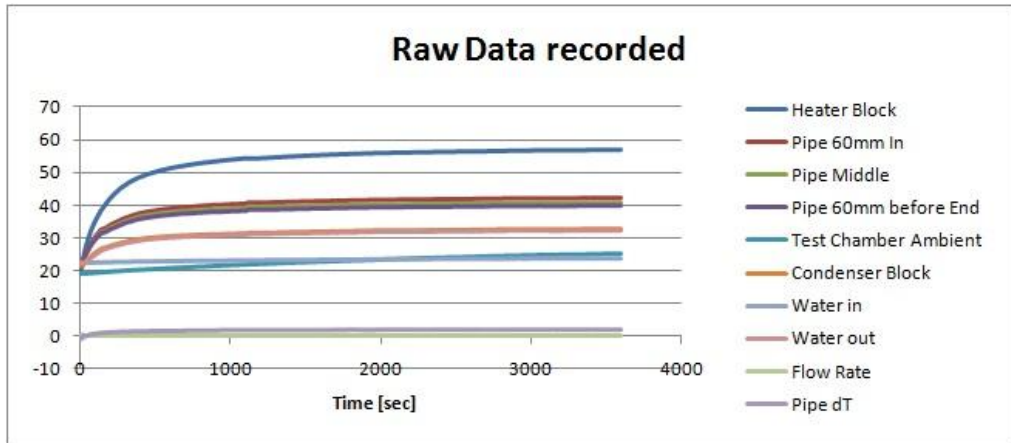


Figure A4-88: Recorded Results Heat Pipe 2 50W Run

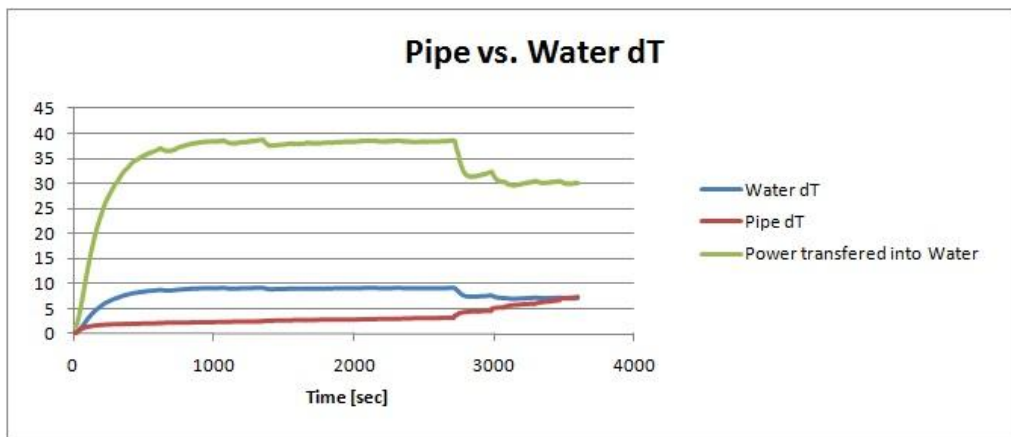


Figure A4-89: Analysed Results Heat Pipe 2 60W Run

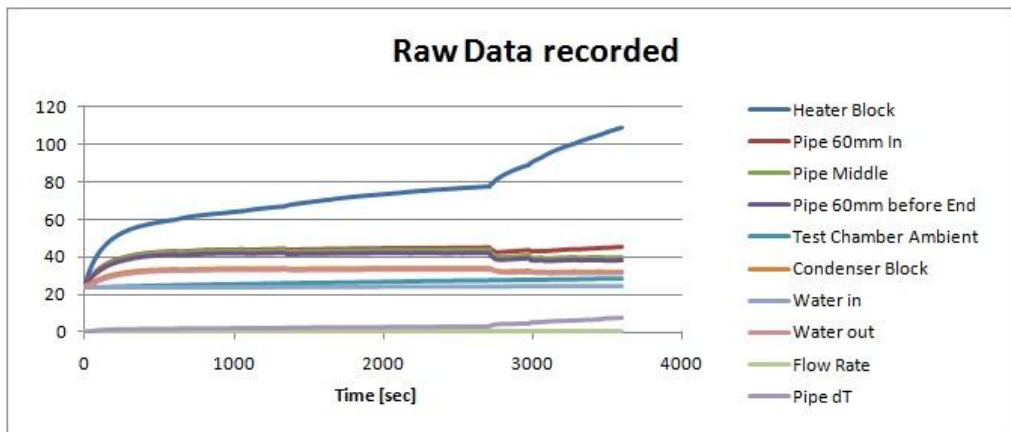


Figure A4-90: Recorded Results Heat Pipe 2 60W Run

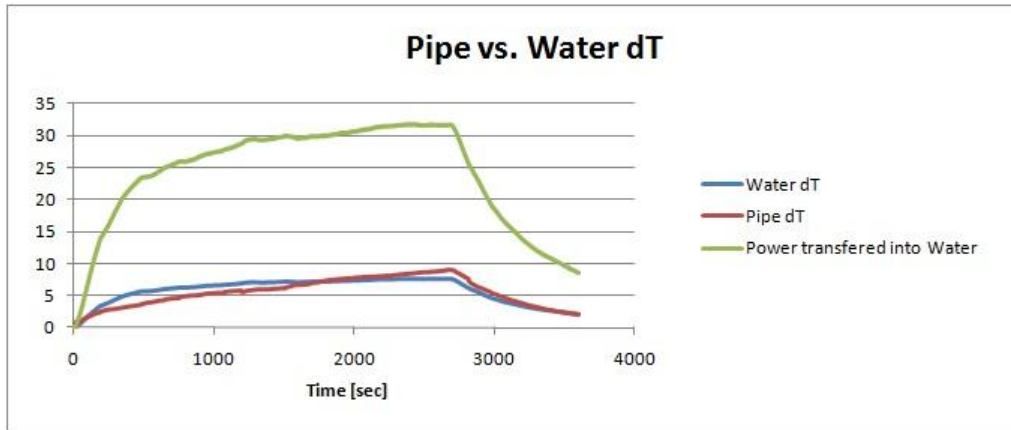


Figure A4-91: Analysed Results Heat Pipe 2 58W Ramp-Up Run

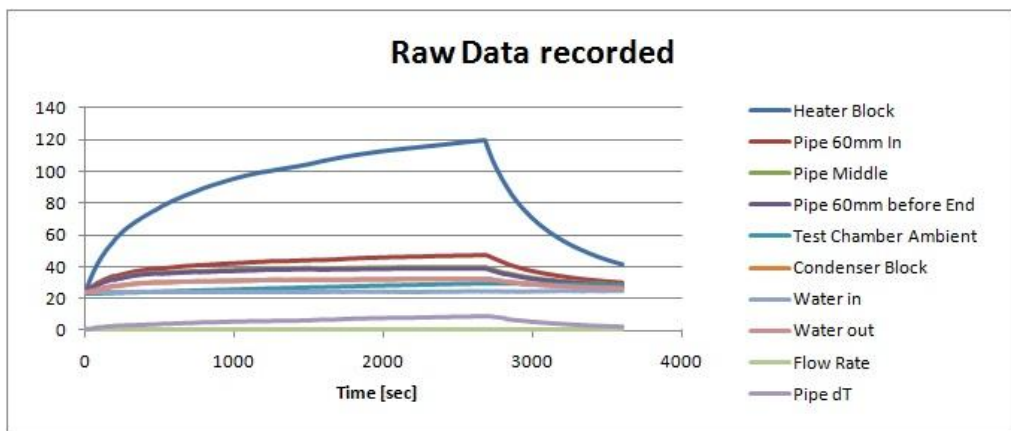


Figure A4-92: Recorded Results Heat Pipe 2 58W Ramp-Up Run

Heat Pipe 3:

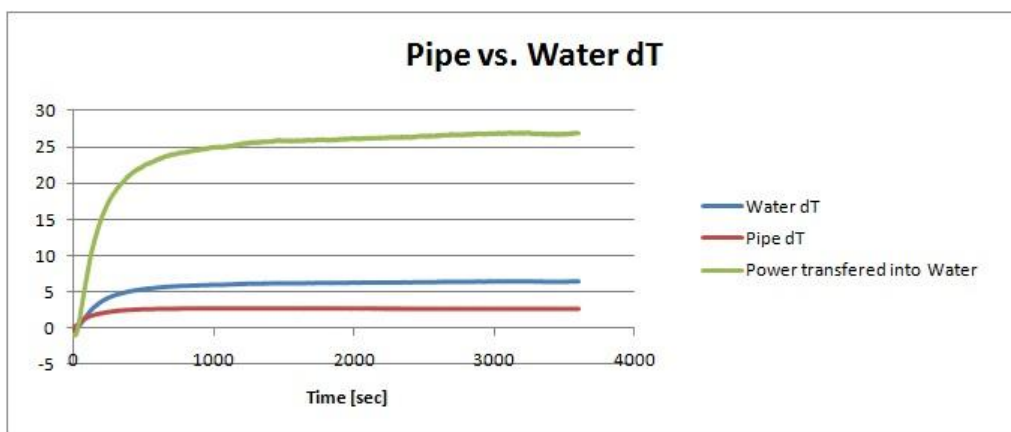


Figure A4-93: Analysed Results Heat Pipe 3 40W Run

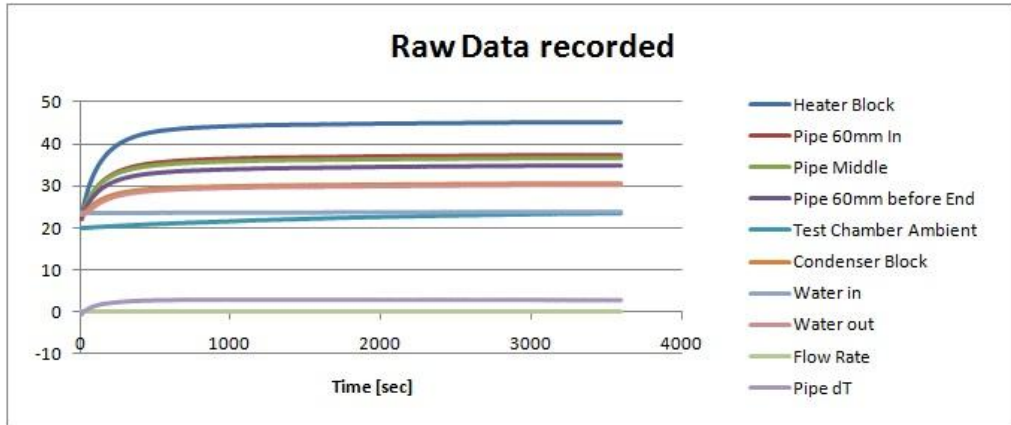


Figure A4-94: Recorded Results Heat Pipe 3 40W Run

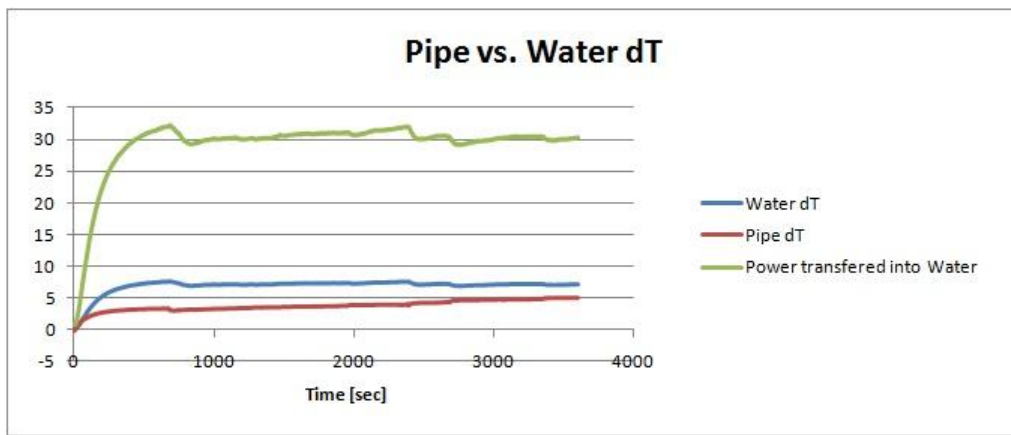


Figure A4-95: Analysed Results Heat Pipe 3 50W Run

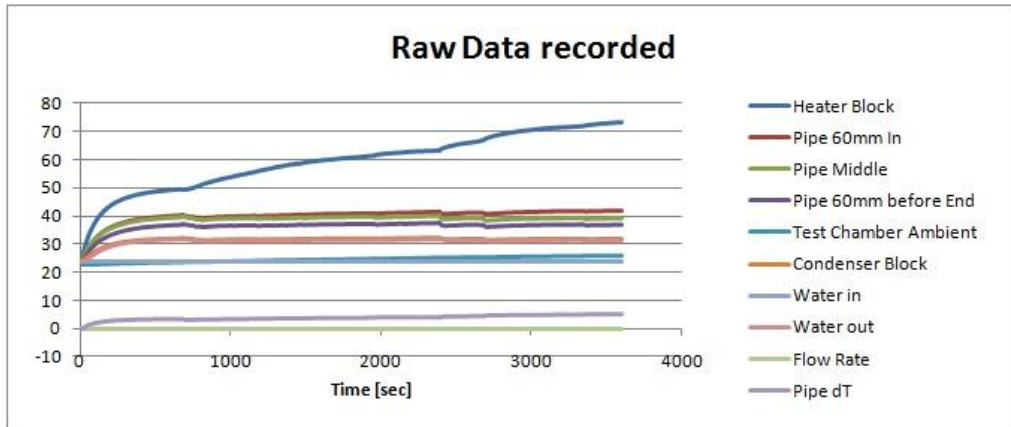


Figure A4-96: Recorded Results Heat Pipe 3 50W Run

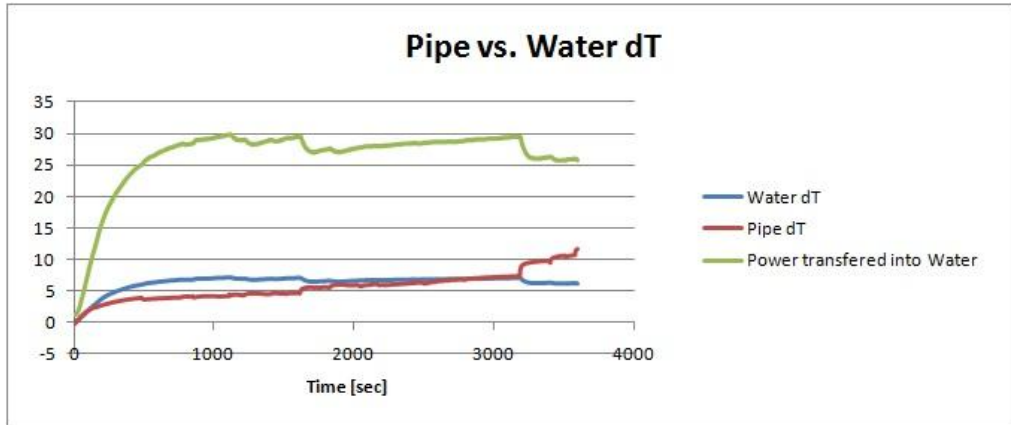


Figure A4-97: Analysed Results Heat Pipe 3 50W Ramp-Up Run

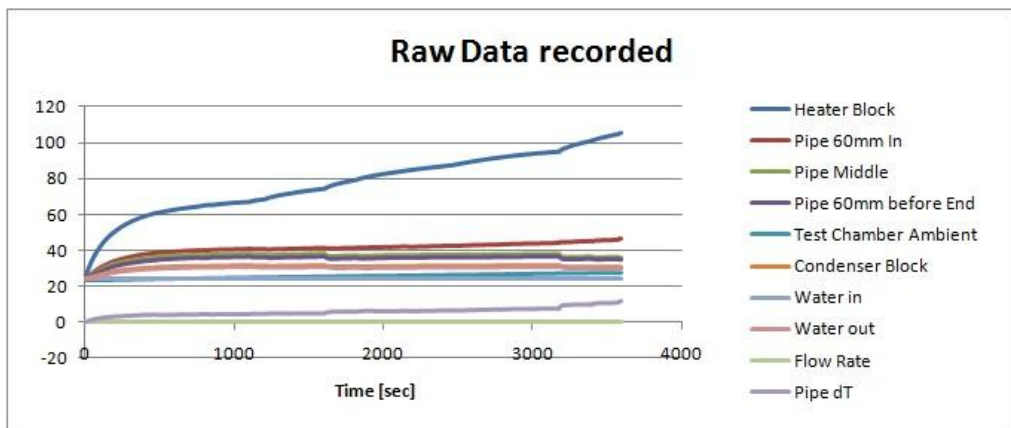


Figure A4-98: Recorded Results Heat Pipe 3 50W Ramp-Up Run

Heat Pipe 4:

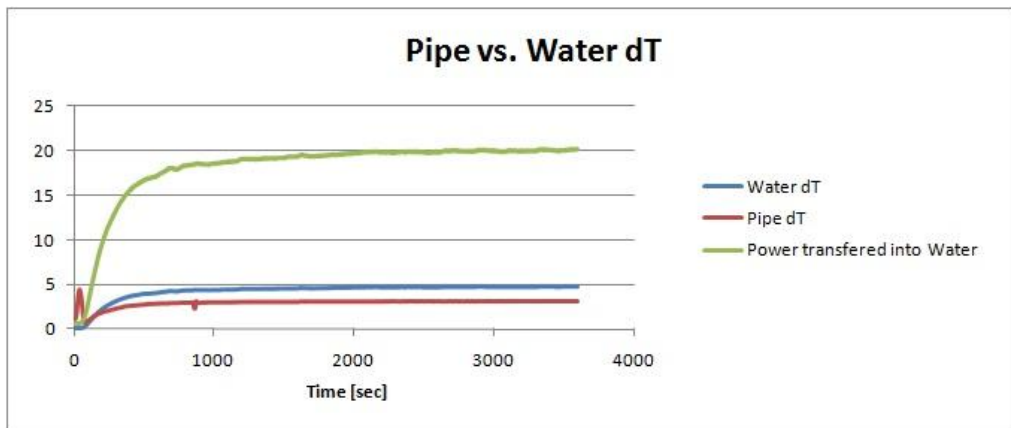


Figure A4-99: Analysed Results Heat Pipe 4 30W Run

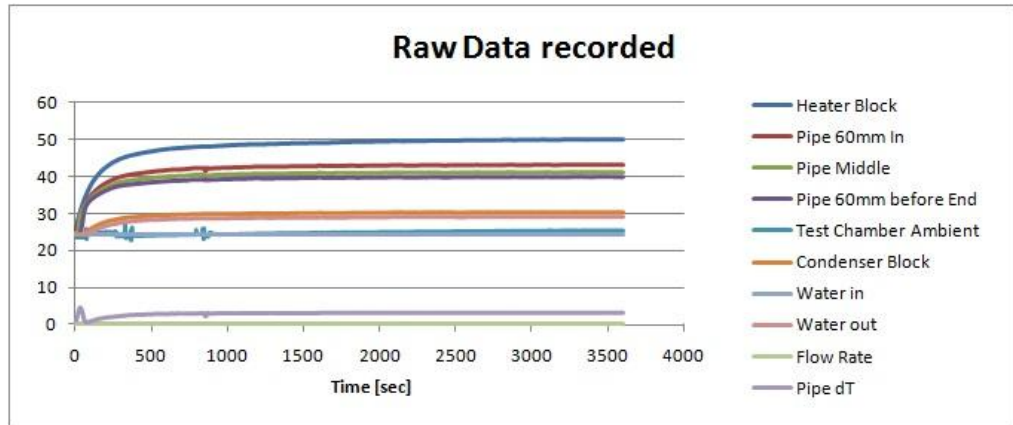


Figure A4-100: Recorded Results Heat Pipe 4 30W Run

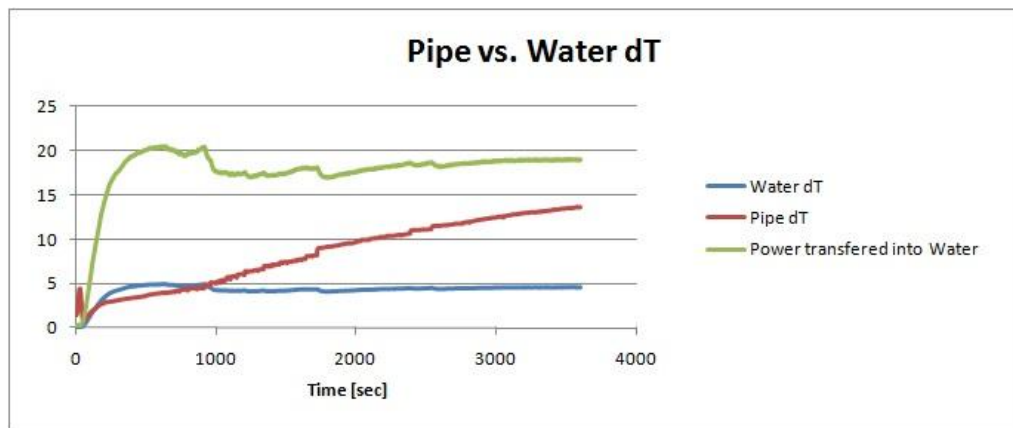


Figure A4-101: Analysed Results Heat Pipe 4 40W Run

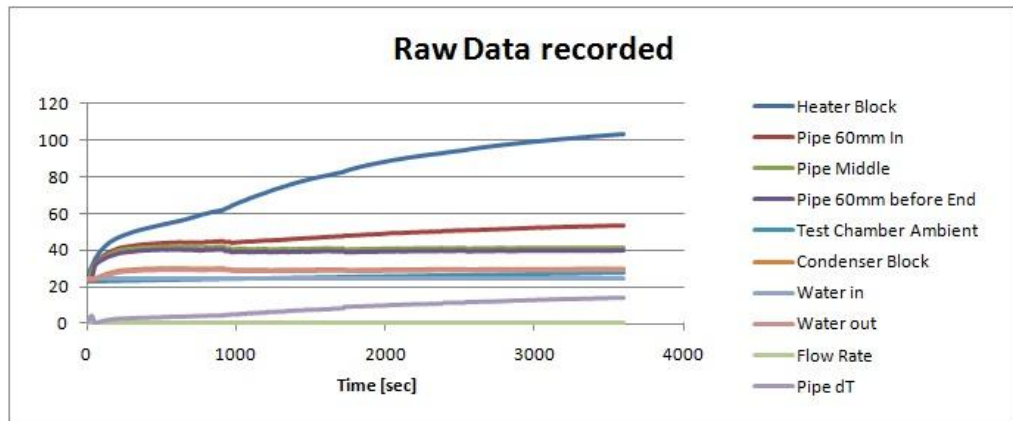


Figure A4-102: Recorded Results Heat Pipe 4 40W Run

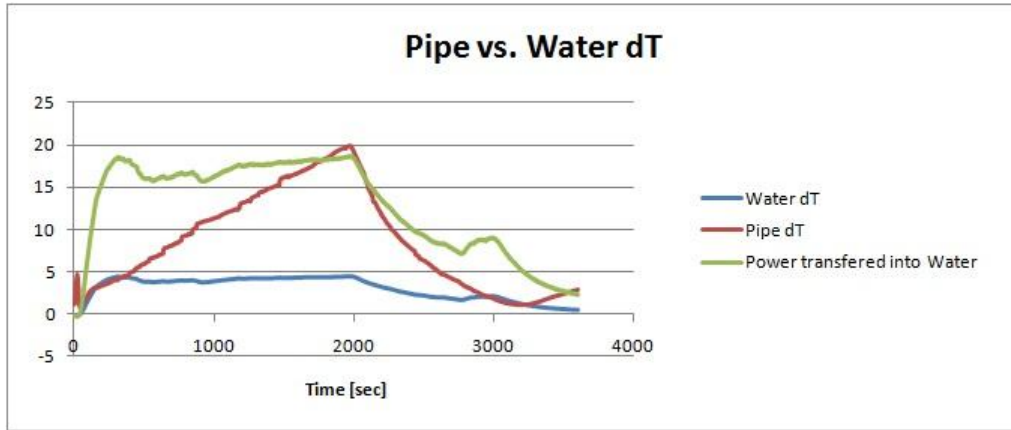


Figure A4-103: Analysed Results Heat Pipe 4 50W Run

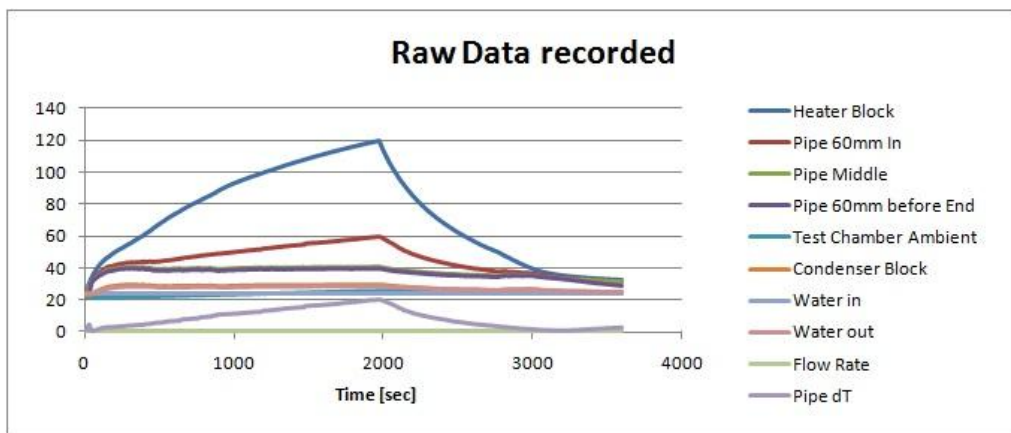


Figure A4-104: Recorded Results Heat Pipe 4 50W Run

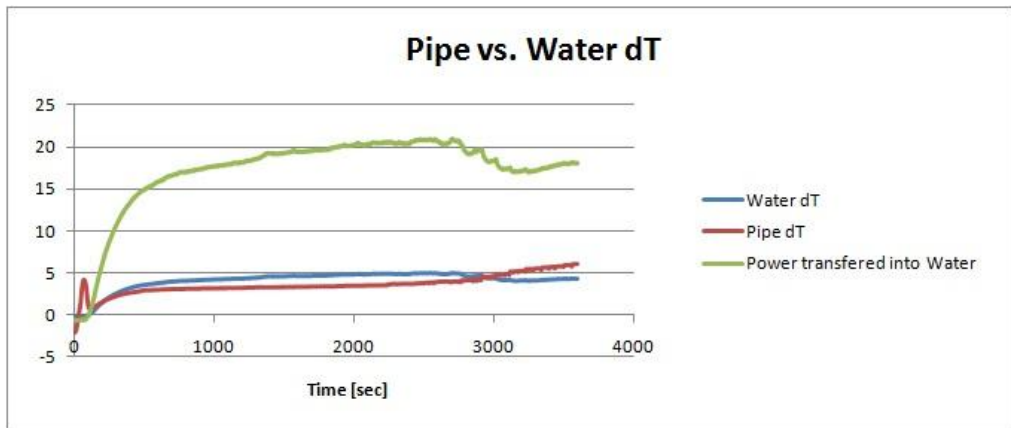


Figure A4-105: Analysed Results Heat Pipe 4 30W Ramp-Up Run

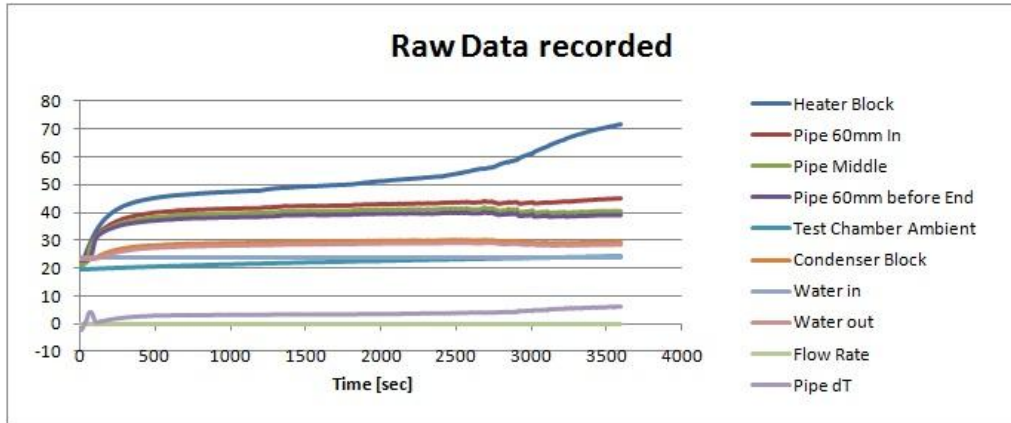


Figure A4-106: Recorded Results Heat Pipe 4 30W Ramp-Up Run

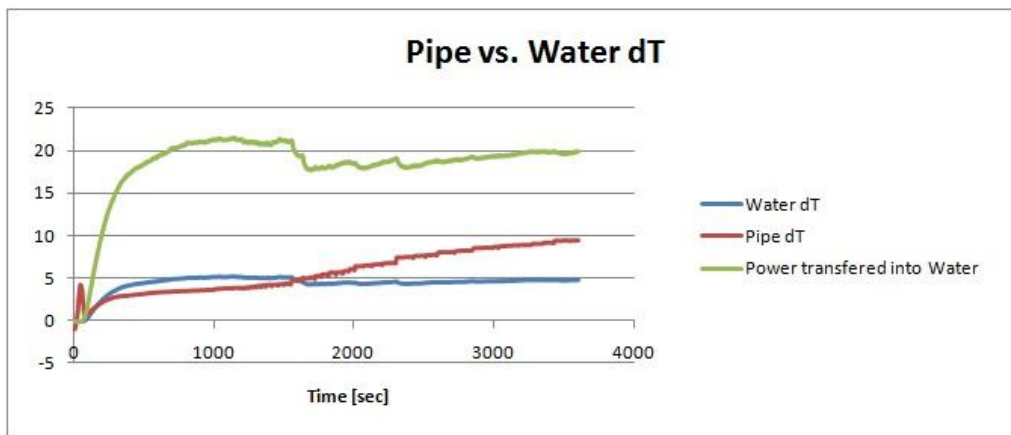


Figure A4-107: Analysed Results Heat Pipe 4 38W Ramp-Up Run

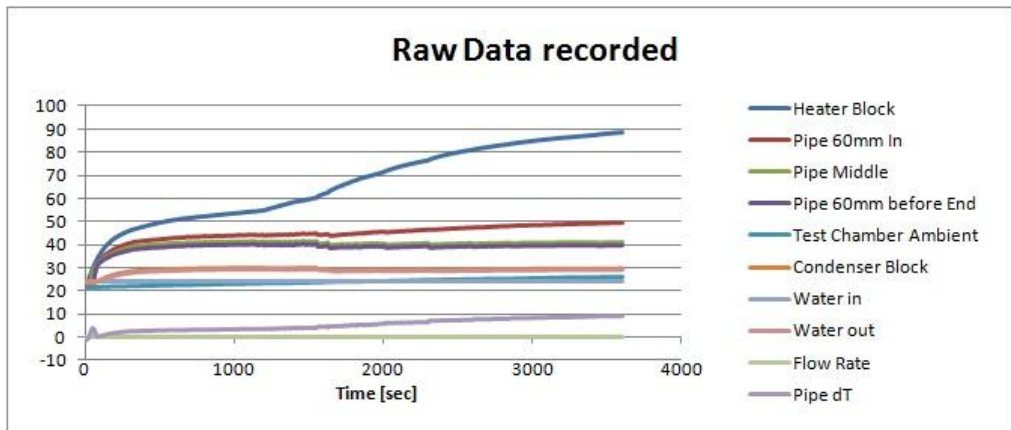


Figure A4-108: Recorded Results Heat Pipe 4 38W Ramp-Up Run

Heat Pipe 5:

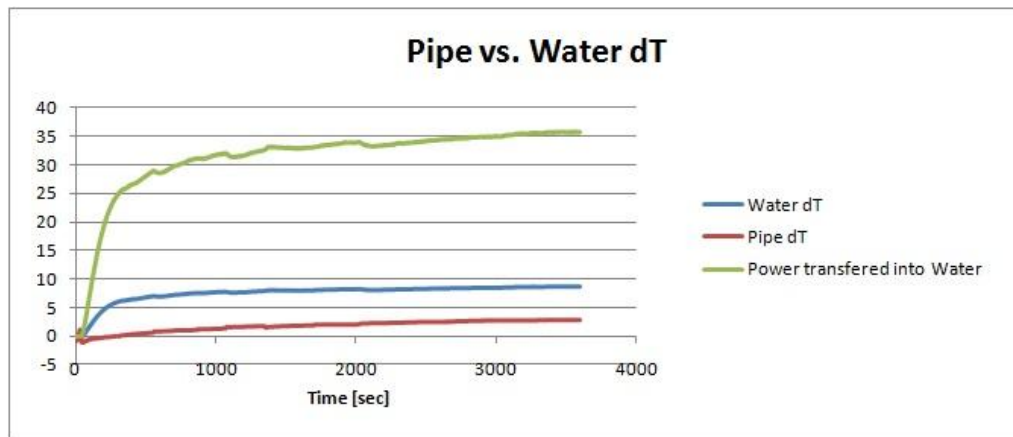


Figure A4-109: Analysed Results Heat Pipe 5 50W Run

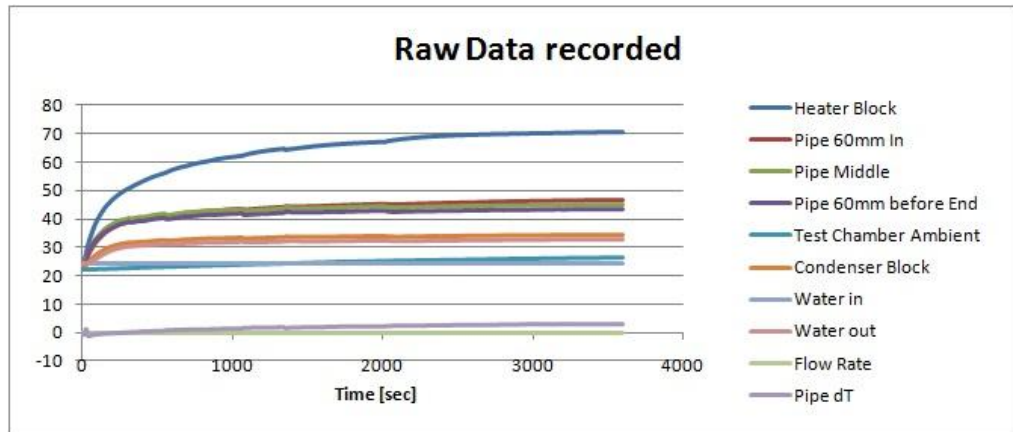


Figure A4-110: Recorded Results Heat Pipe 5 50W Run

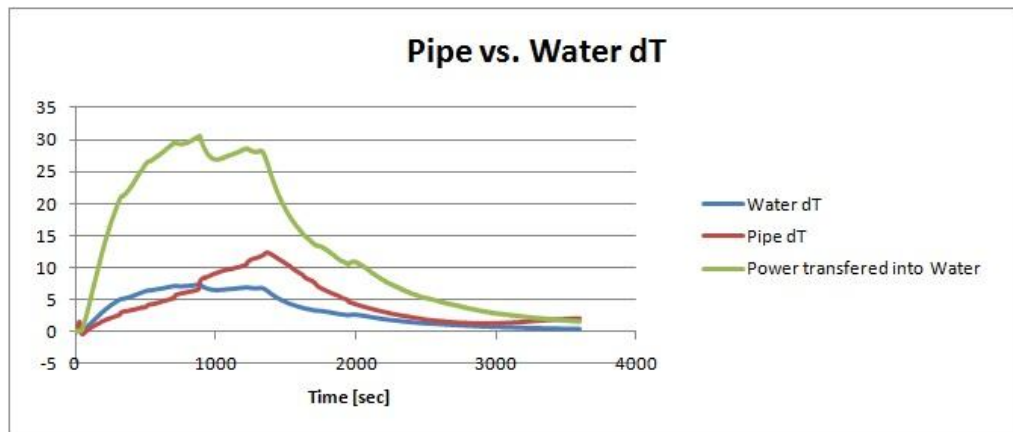


Figure A4-111: Analysed Results Heat Pipe 5 60W Run

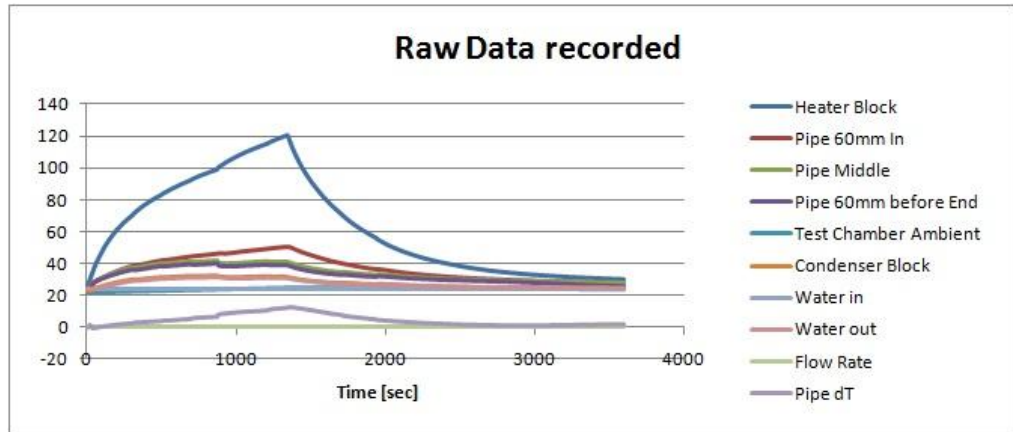


Figure A4-112: Recorded Results Heat Pipe 5 60W Run

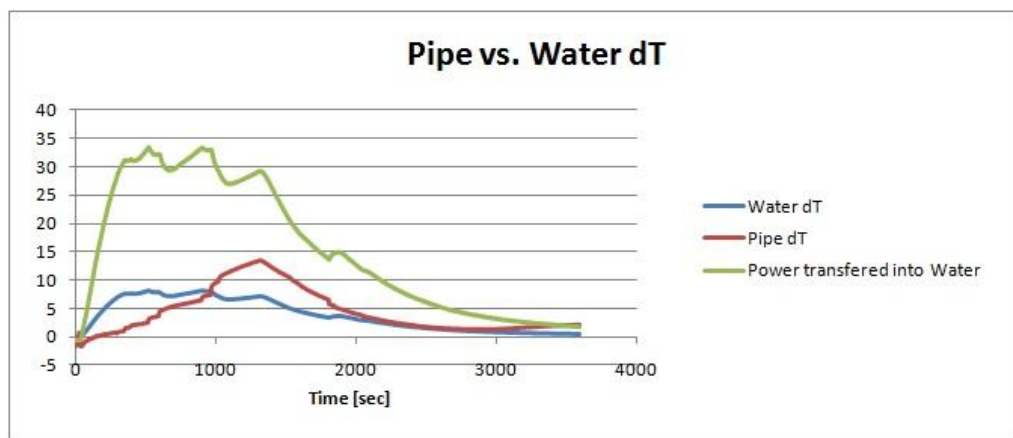


Figure A4-113: Analysed Results Heat Pipe 5 70W Run

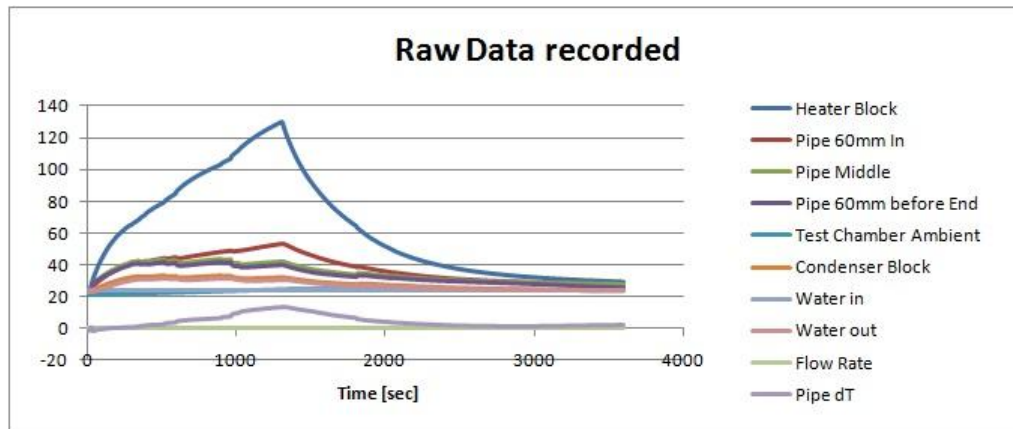


Figure A4-114: Recorded Results Heat Pipe 5 70W Run

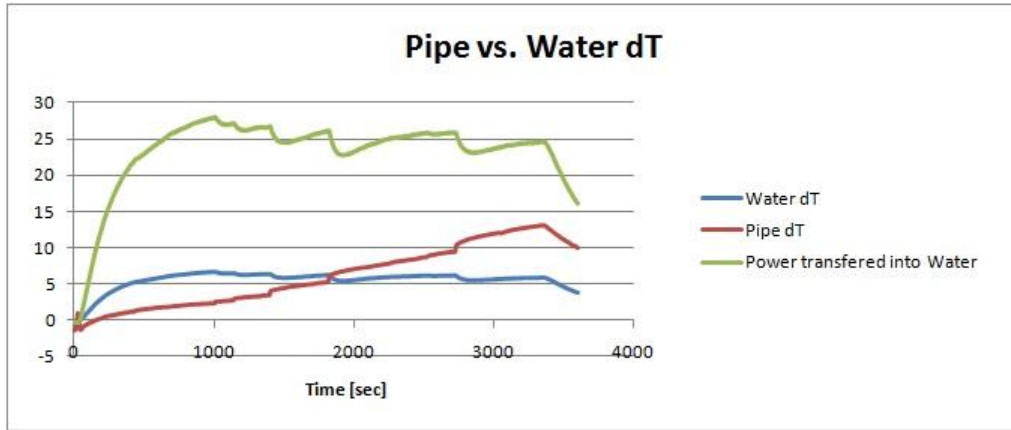


Figure A4-115: Analysed Results Heat Pipe 5 50W Ramp-Up Run

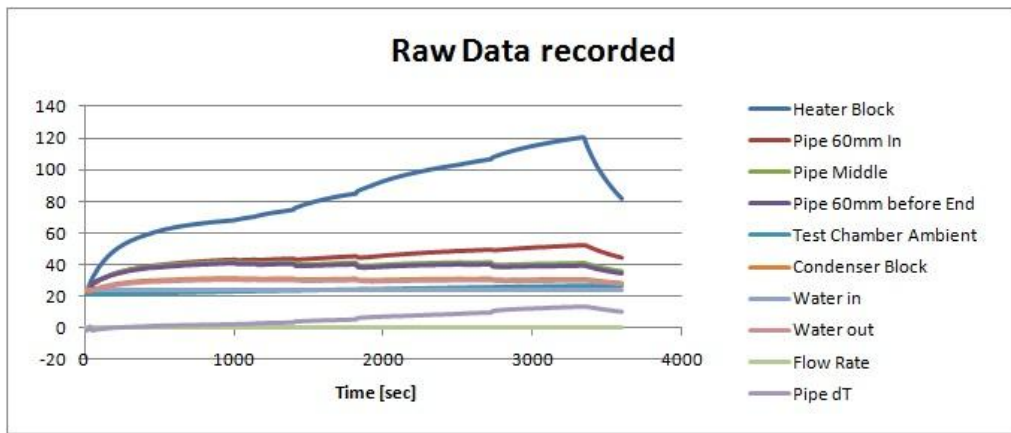


Figure A4-116: Recorded Results Heat Pipe 5 50W Ramp-Up Run

A4-4 135° Bent Heat Pipes:

Heat Pipe 1:

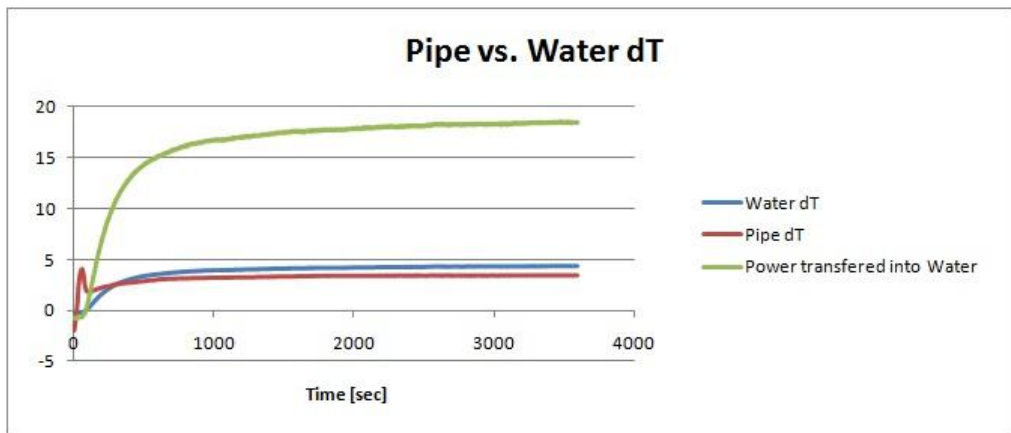


Figure A4-117: Analysed Results Heat Pipe 1 30W Run

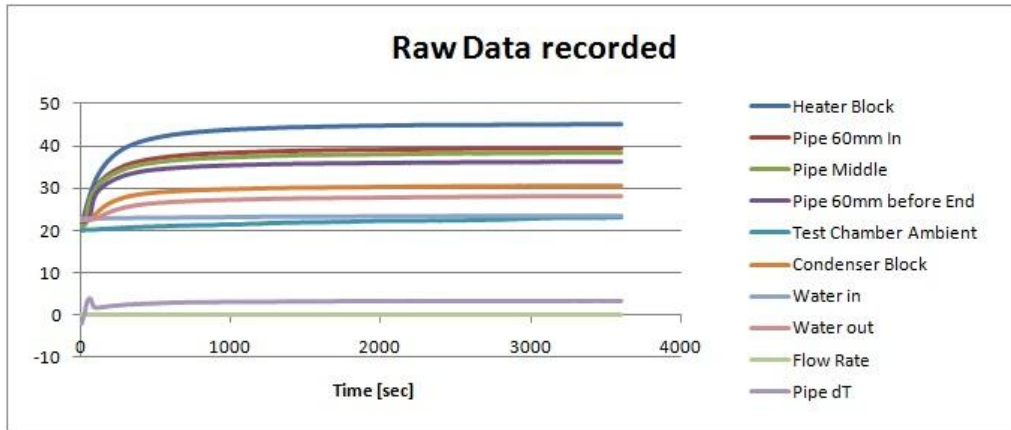


Figure A4-118: Recorded Results Heat Pipe 1 30W Run

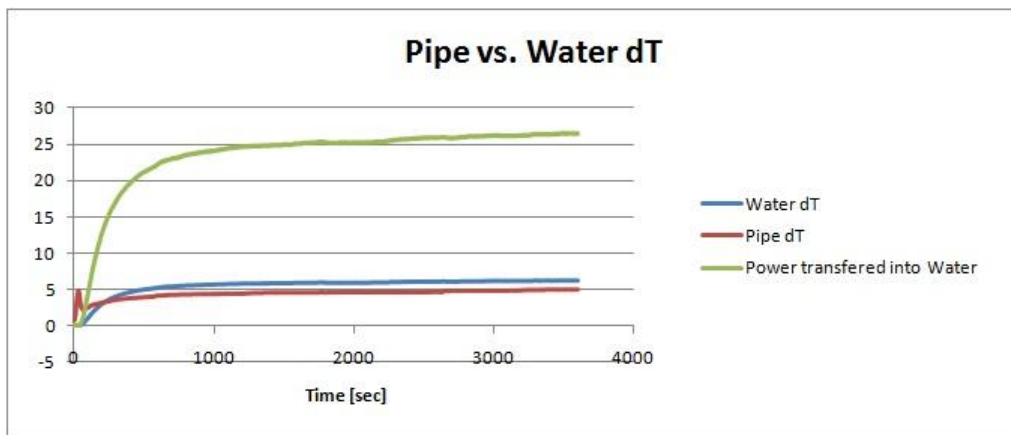


Figure A4-119: Analysed Results Heat Pipe 1 40W Run

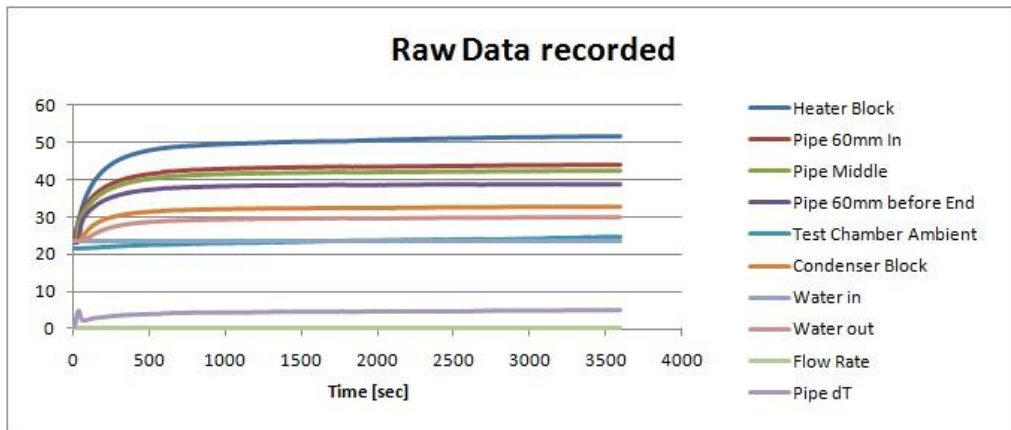


Figure A4-120: Recorded Results Heat Pipe 1 40W Run

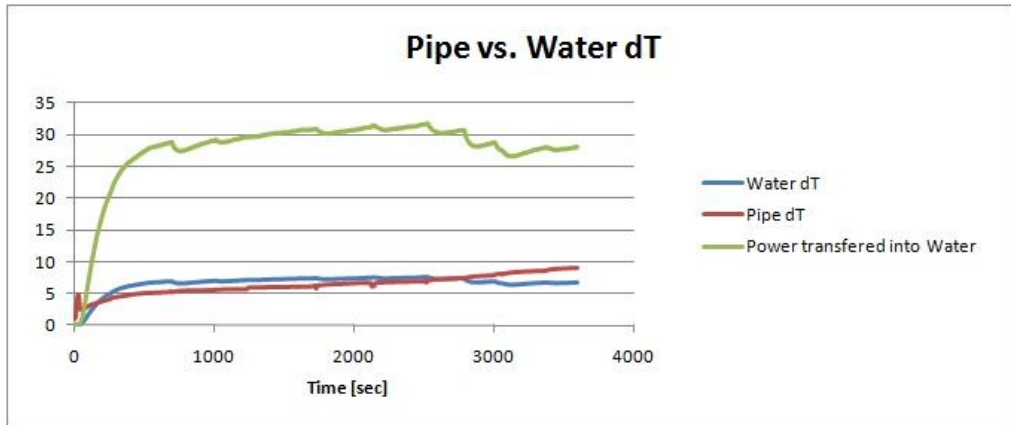


Figure A4-121: Analysed Results Heat Pipe 1 50W Run

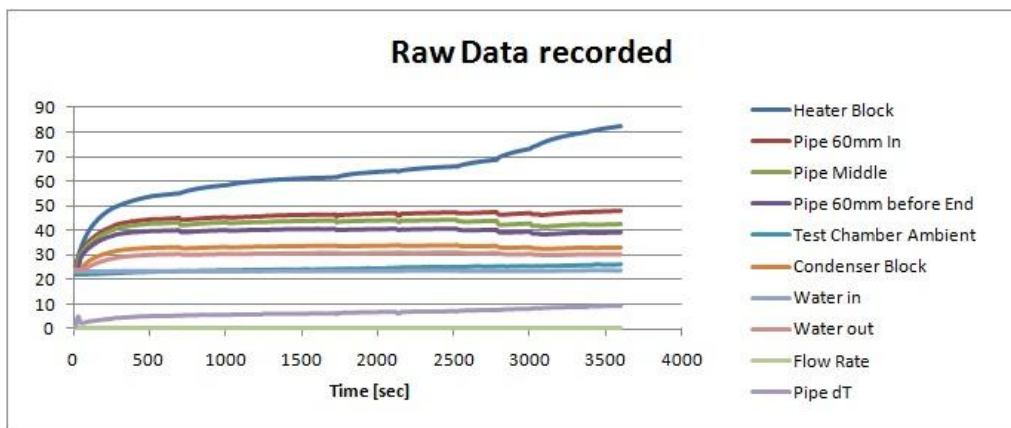


Figure A4-122: Recorded Results Heat Pipe 1 50W Run

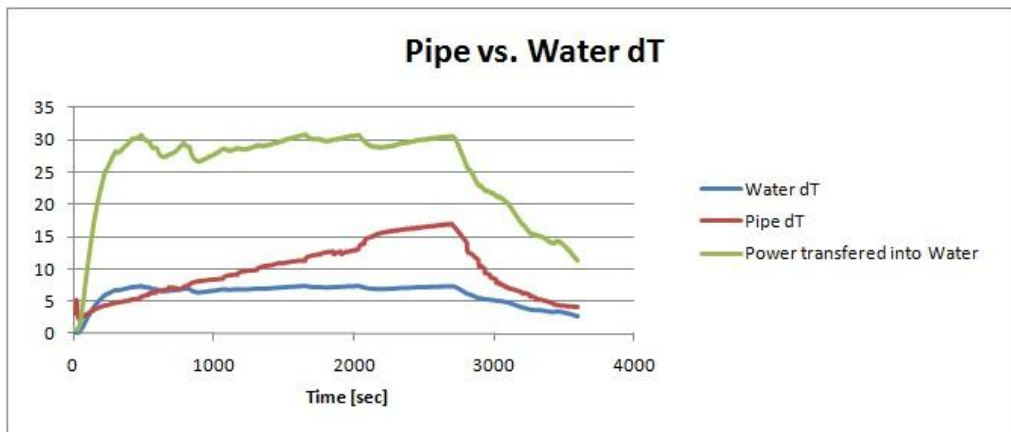


Figure A4-123: Analysed Results Heat Pipe 1 60W Run

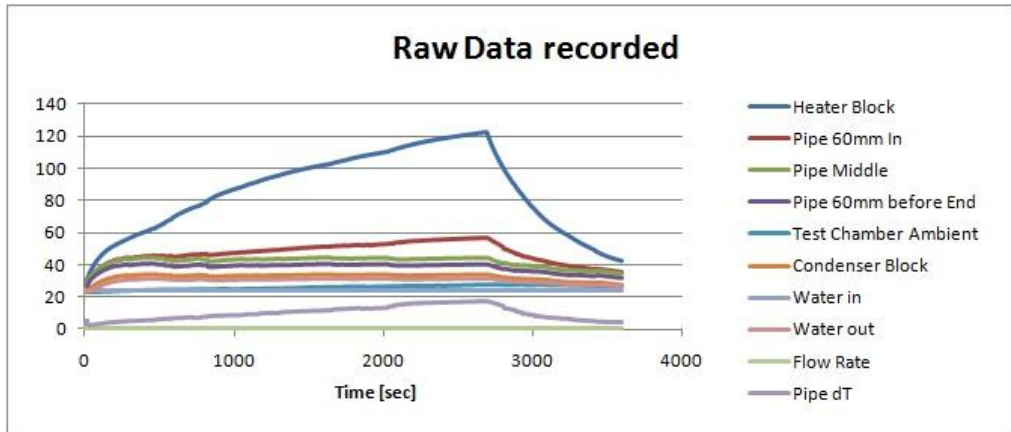


Figure A4-124: Recorded Results Heat Pipe 1 60W Run

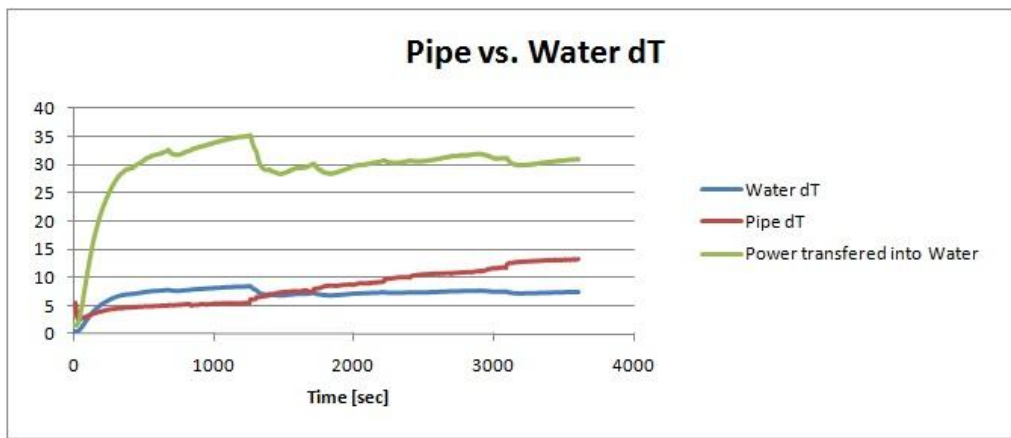


Figure A4-125: Analysed Results Heat Pipe 2 50W Ramp-Up Run

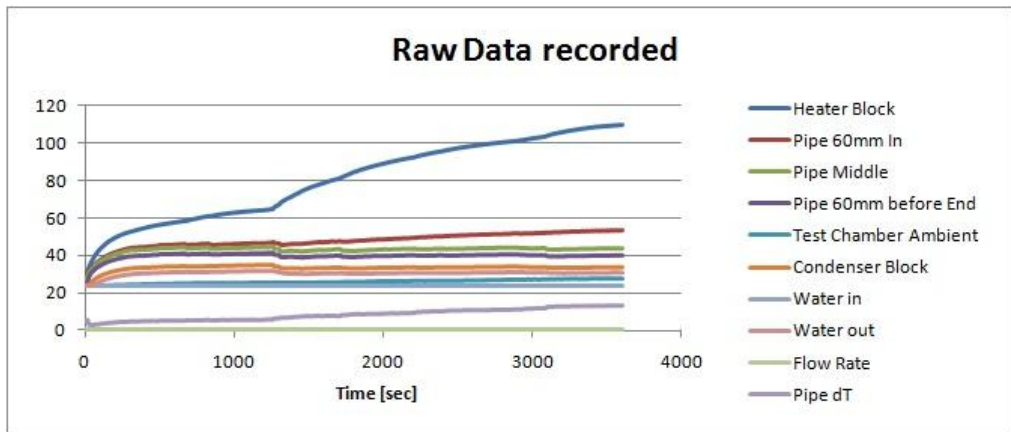


Figure A4-126: Recorded Results Heat Pipe 2 50W Ramp-Up Run

Heat Pipe 2:

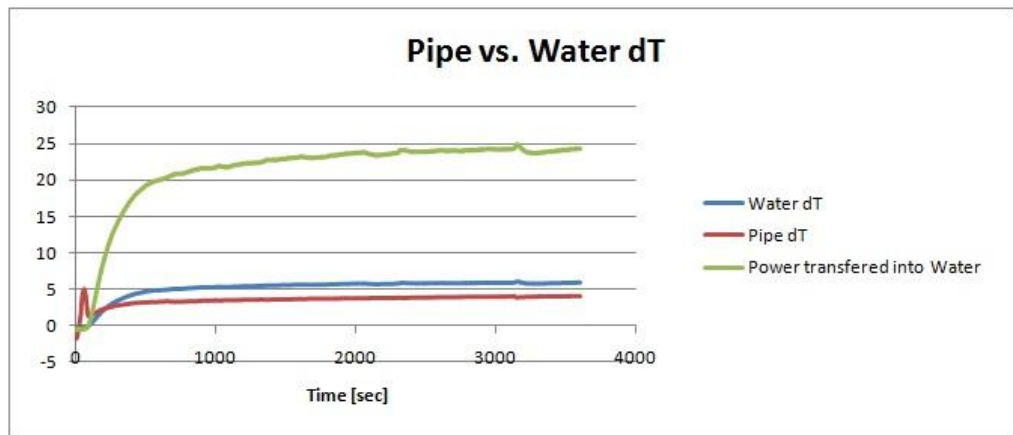


Figure A4-127: Analysed Results Heat Pipe 2 40W Run

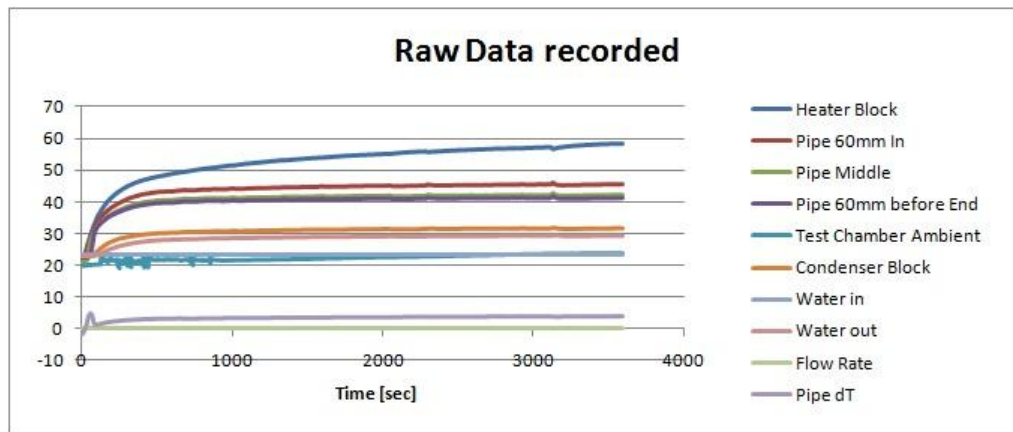


Figure A4-128: Recorded Results Heat Pipe 2 40W Run

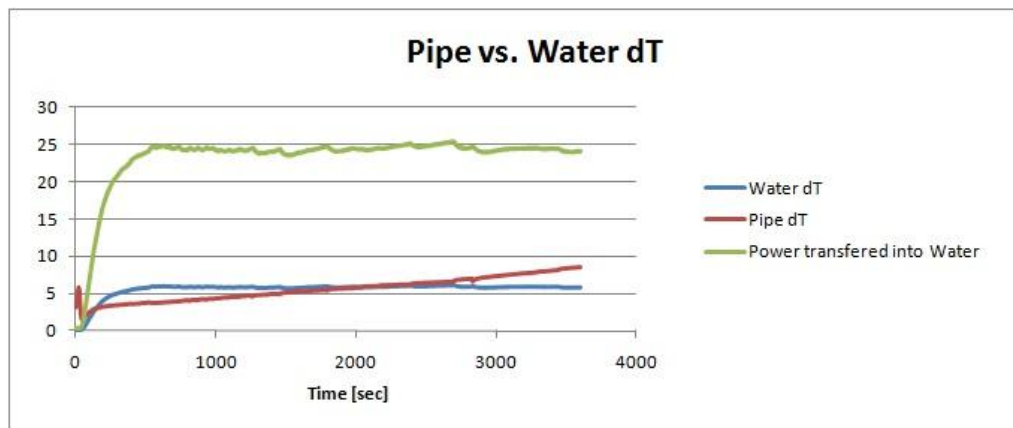


Figure A4-129: Analysed Results Heat Pipe 2 50W Run

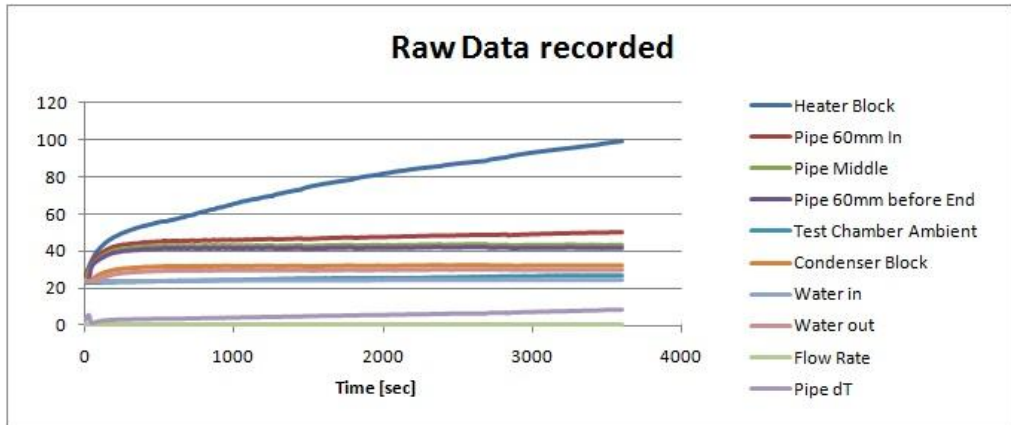


Figure A4-130: Recorded Results Heat Pipe 2 50W Run

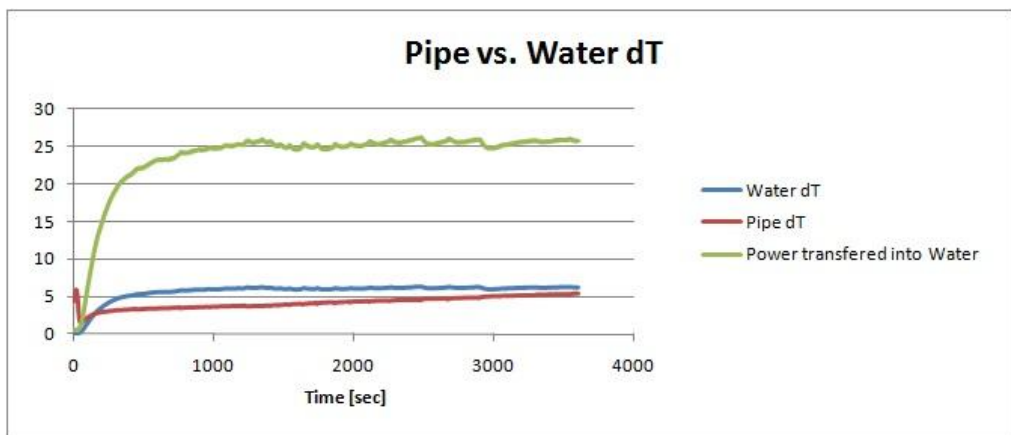


Figure A4-131: Analysed Results Heat Pipe 2 40W Ramp-Up Run

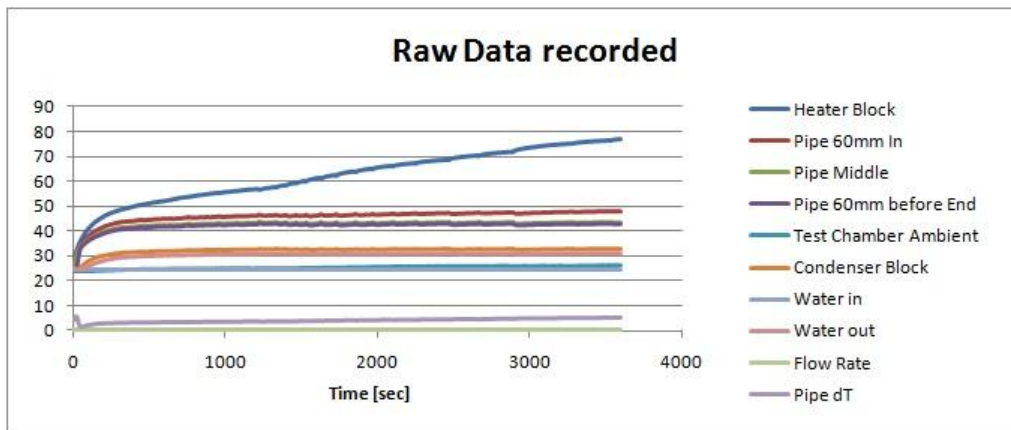


Figure A4-132: Recorded Results Heat Pipe 2 40W Ramp-Up Run

Heat Pipe 3:

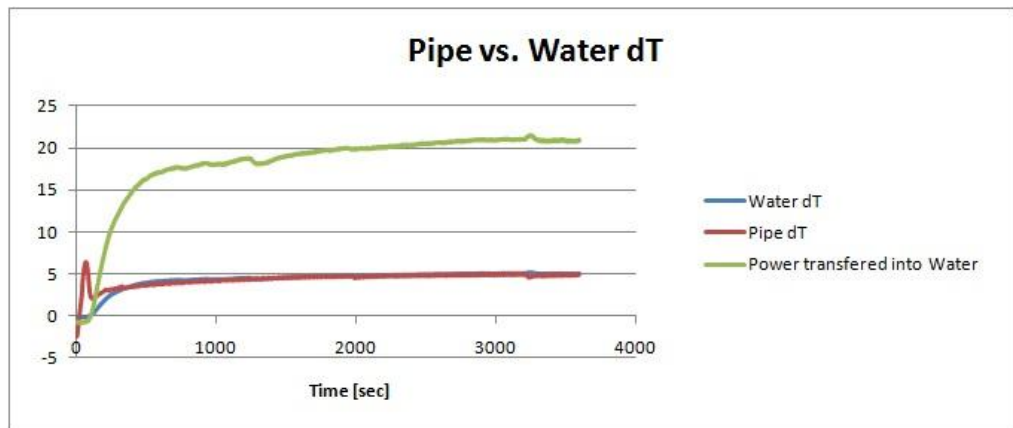


Figure A4-133: Analysed Results Heat Pipe 3 40W Run

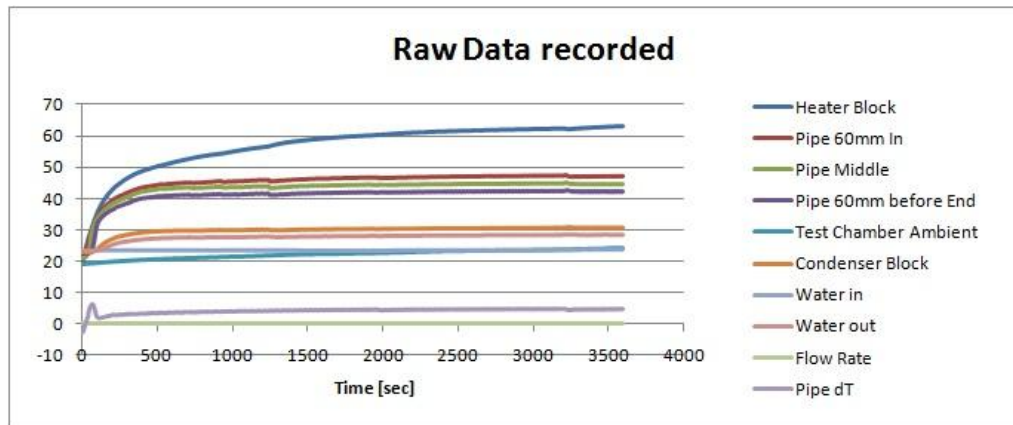


Figure A4-134: Recorded Results Heat Pipe 3 40W Run

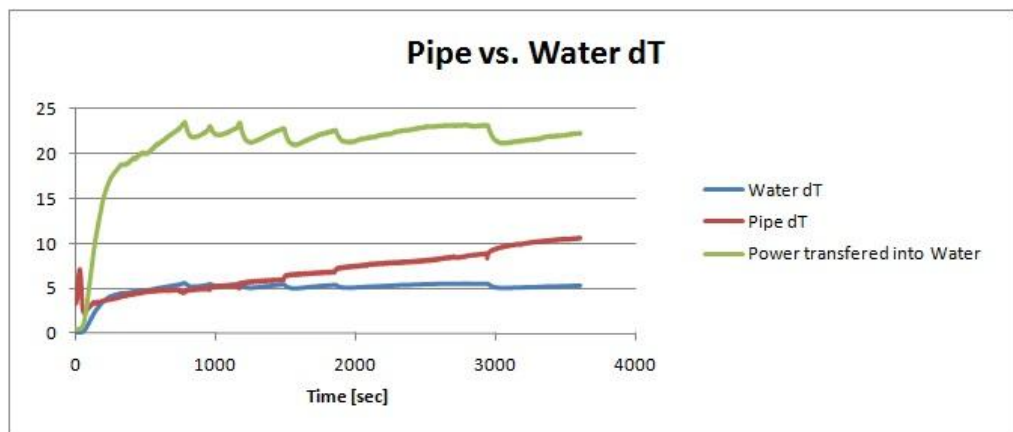


Figure A4-135: Analysed Results Heat Pipe 3 50W Run

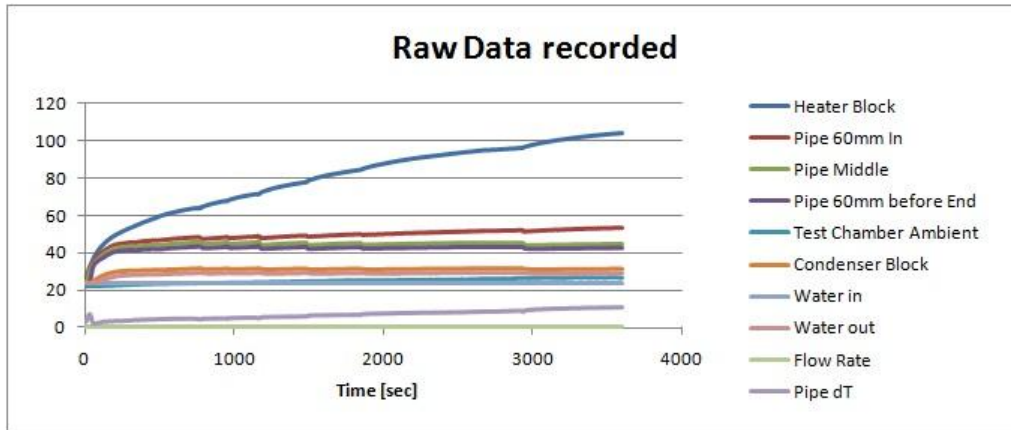


Figure A4-136: Recorded Results Heat Pipe 3 50W Run

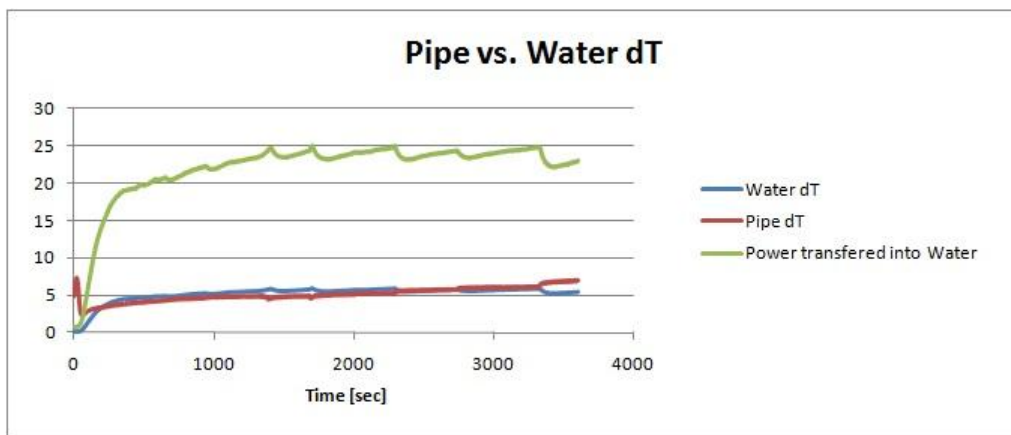


Figure A4-137: Analysed Results Heat Pipe 3 40W Ramp-Up Run

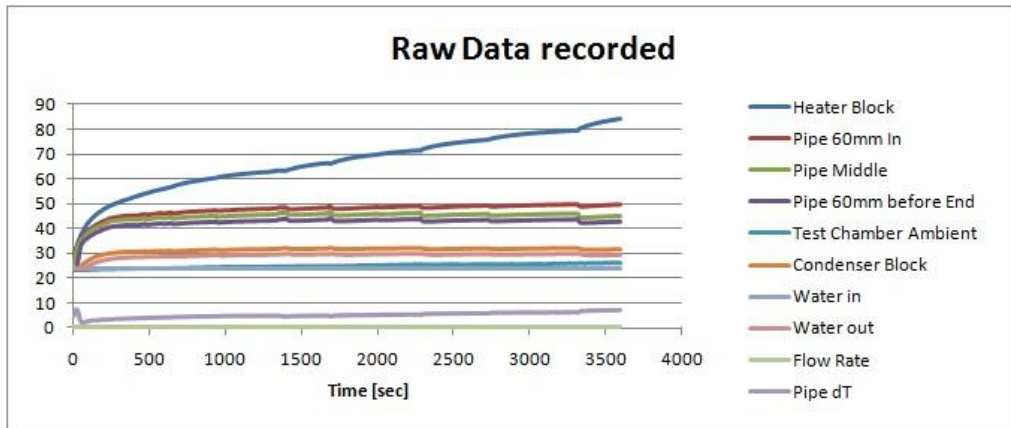


Figure A4-138: Recorded Results Heat Pipe 3 40W Ramp-Up Run

Heat Pipe 4:

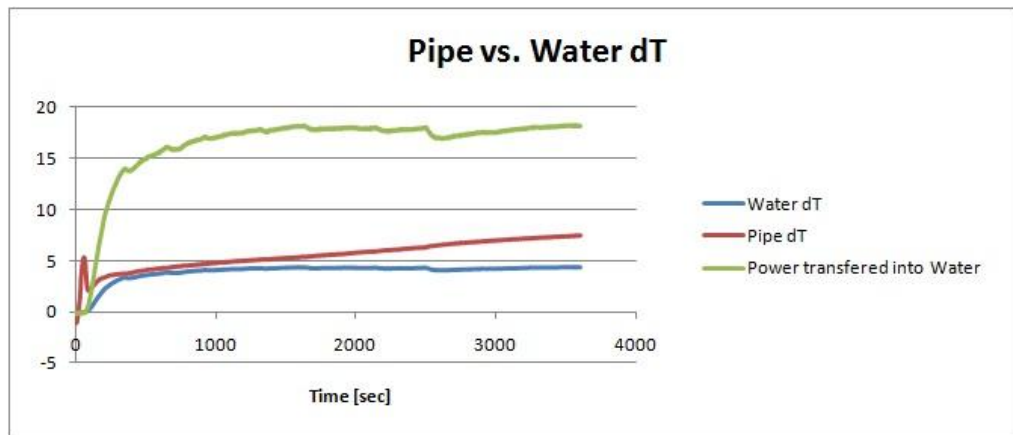


Figure A4-139: Analysed Results Heat Pipe 4 40W Run

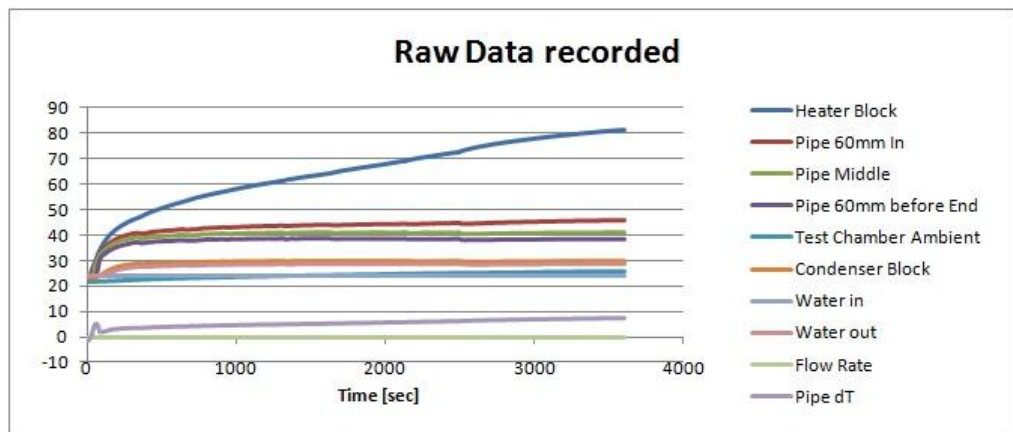


Figure A4-140: Recorded Results Heat Pipe 4 40W Run

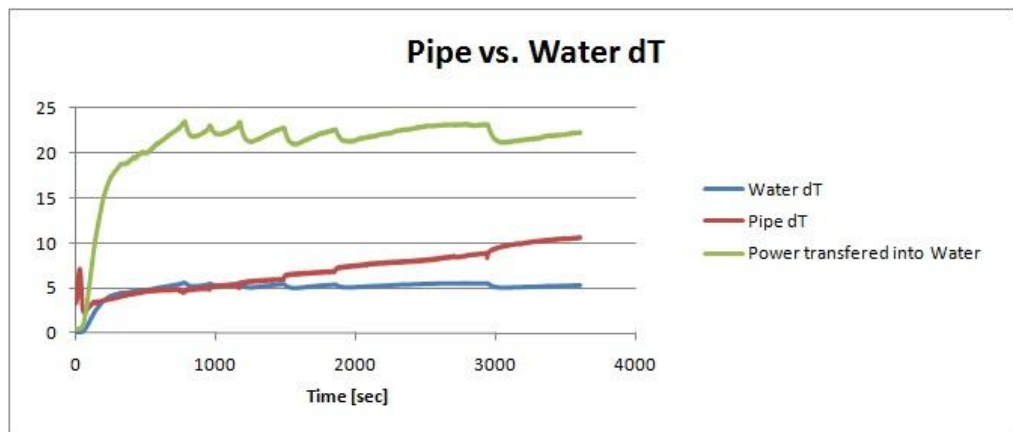


Figure A4-141: Analysed Results Heat Pipe 4 50W Run

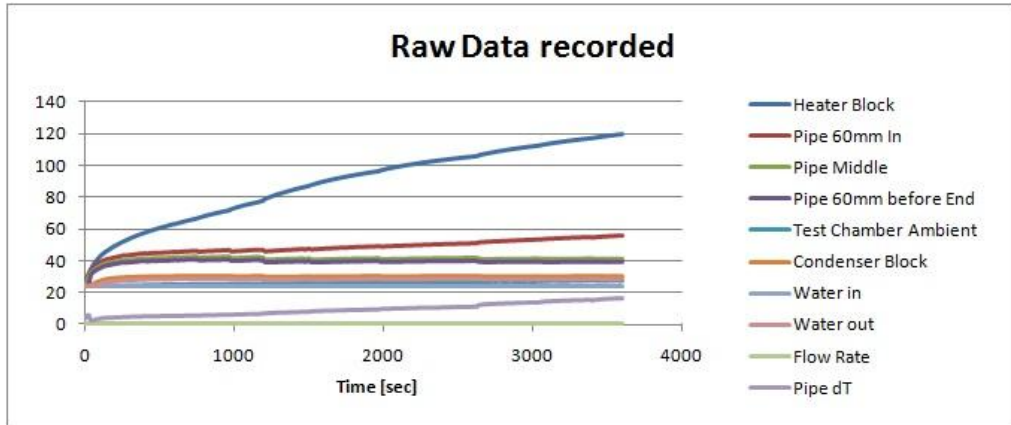


Figure A4-142: Recorded Results Heat Pipe 4 50W Run

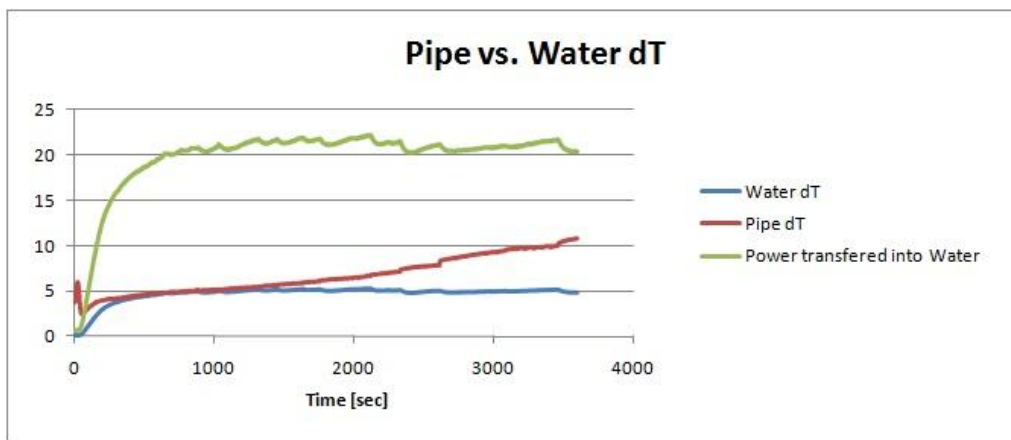


Figure A4-143: Analysed Results Heat Pipe 4 40W Ramp-Up Run

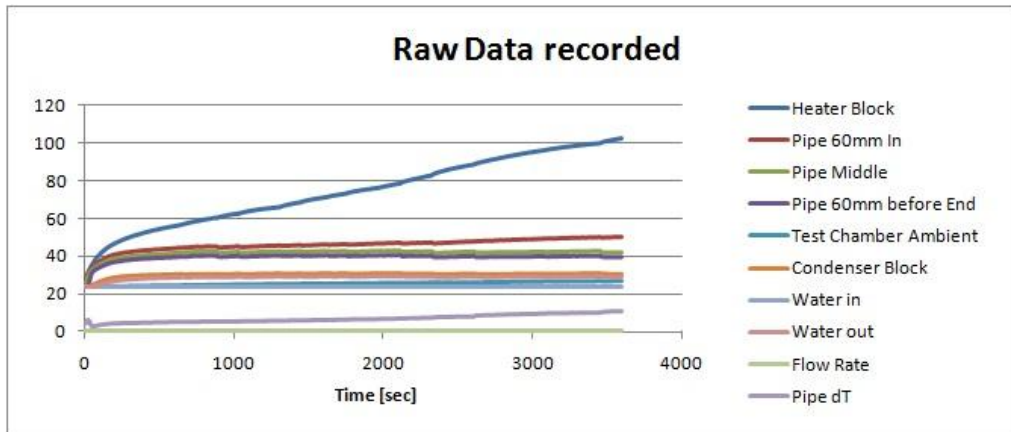


Figure A4-144: Recorded Results Heat Pipe 4 40W Ramp-Up Run

Heat Pipe 5:

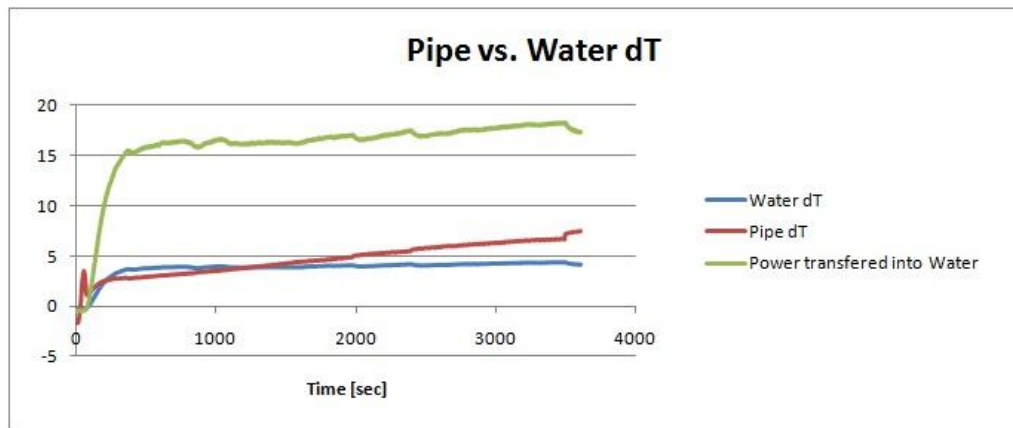


Figure A4-145: Analysed Results Heat Pipe 5 40W Run

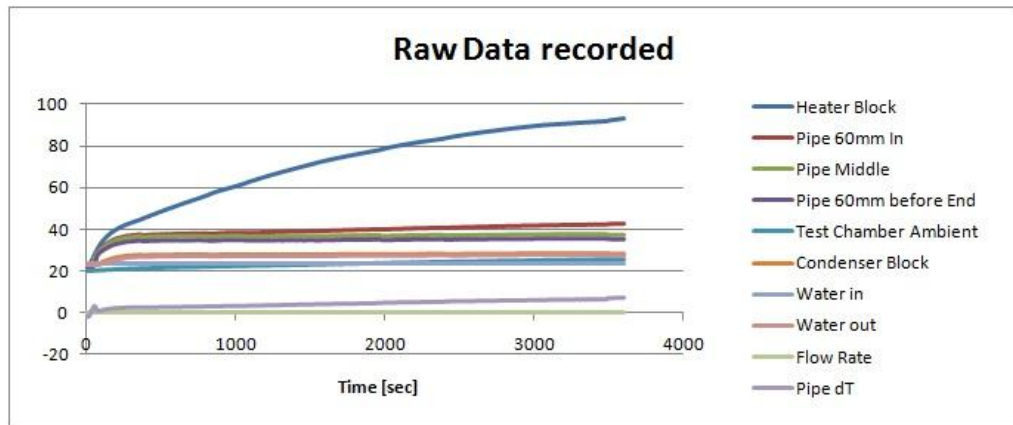


Figure A4-146: Recorded Results Heat Pipe 5 40W Run

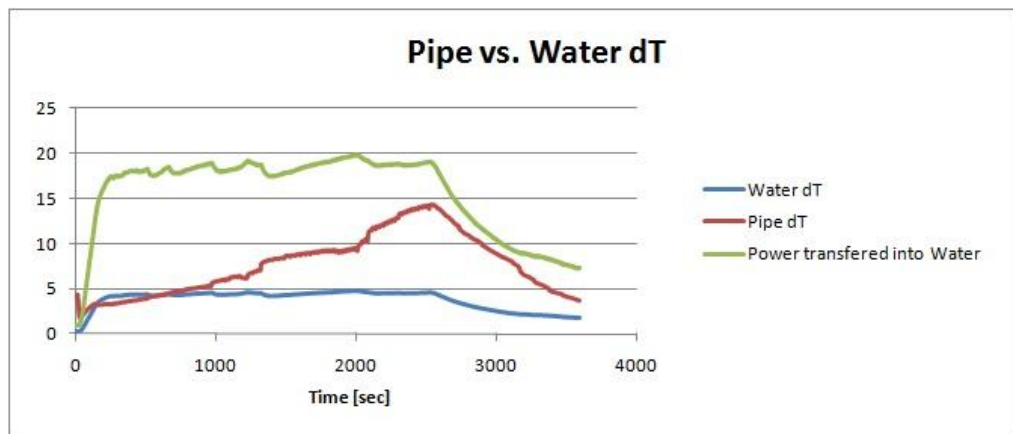


Figure A4-147: Analysed Results Heat Pipe 5 50W Run

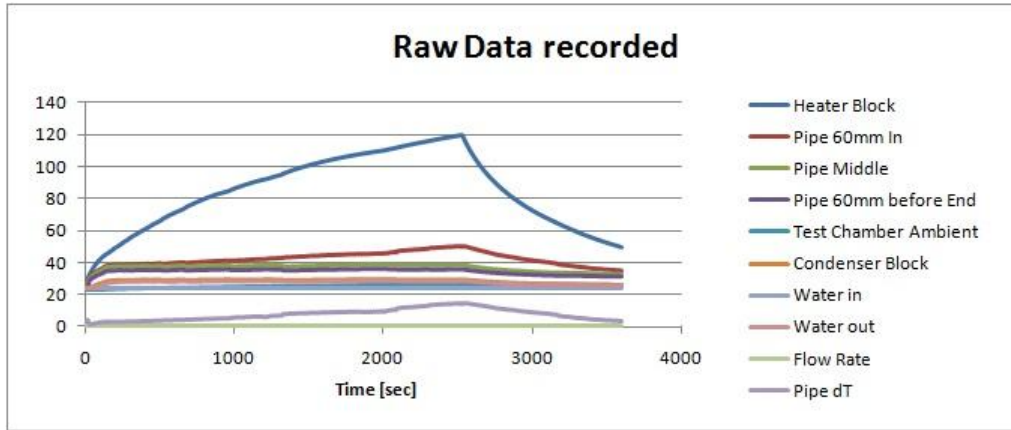


Figure A4-148: Recorded Results Heat Pipe 5 50W Run

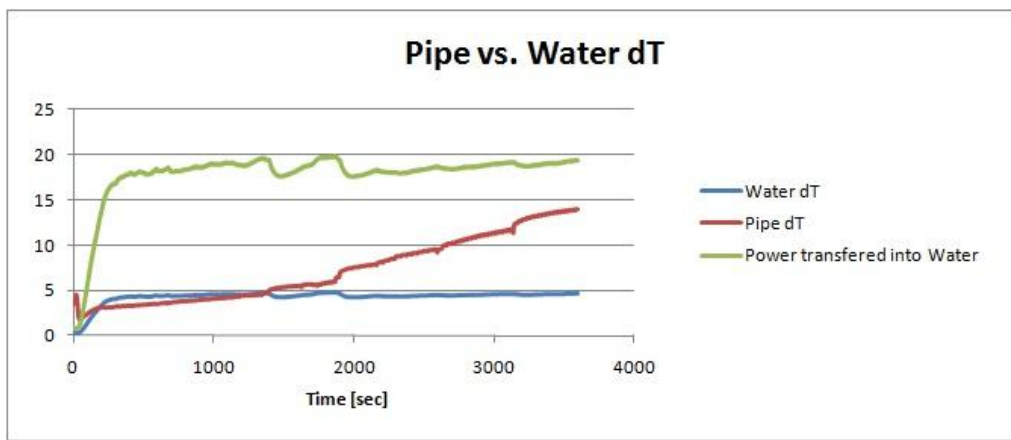


Figure A4-149: Analysed Results Heat Pipe 5 40W Ramp-Up Run

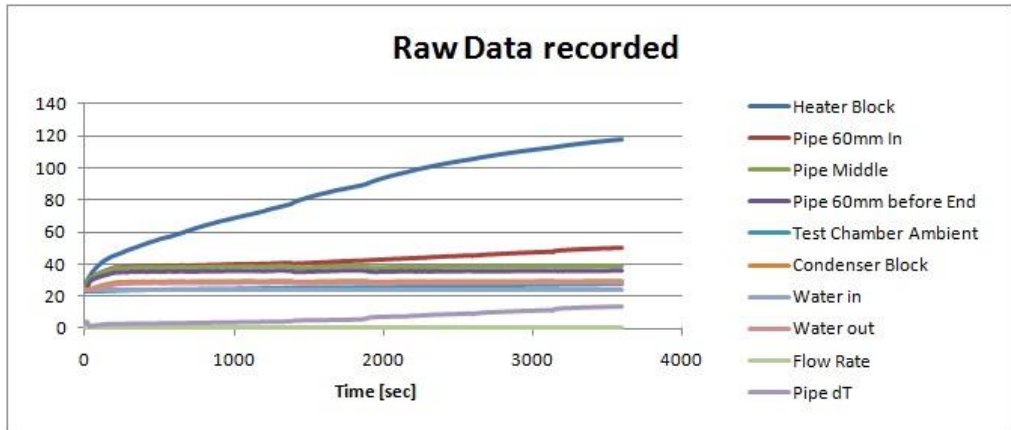


Figure A4-150: Recorded Results Heat Pipe 5 40W Ramp-Up Run

A4-5 180° Bent Heat Pipes:

Heat Pipe 1:

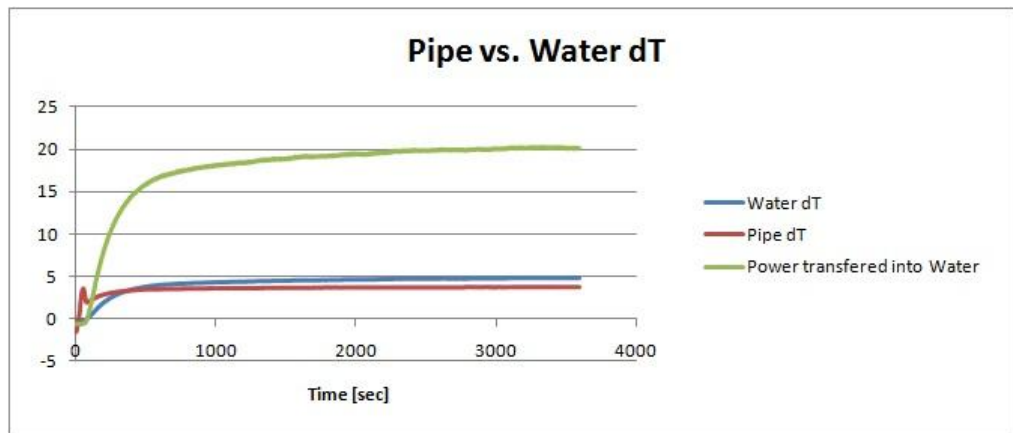


Figure A4-151: Analysed Results Heat Pipe 1 30W Run

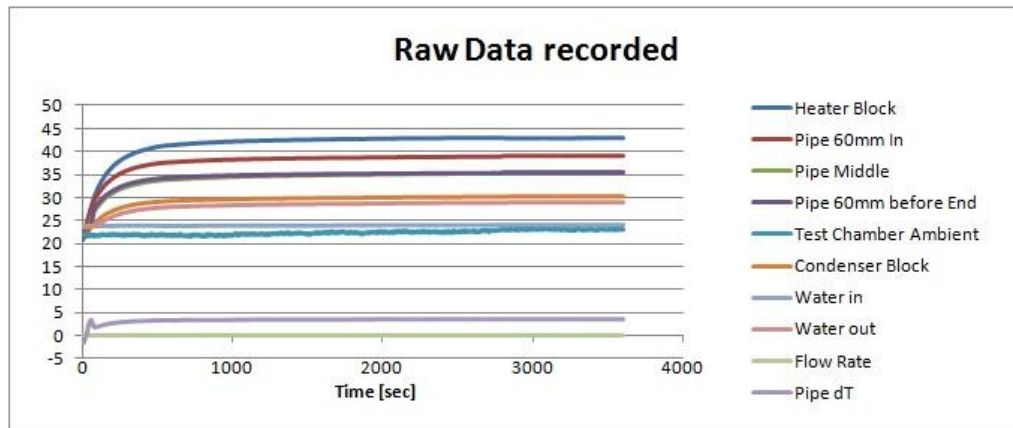


Figure A4-152: Recorded Results Heat Pipe 1 30W Run

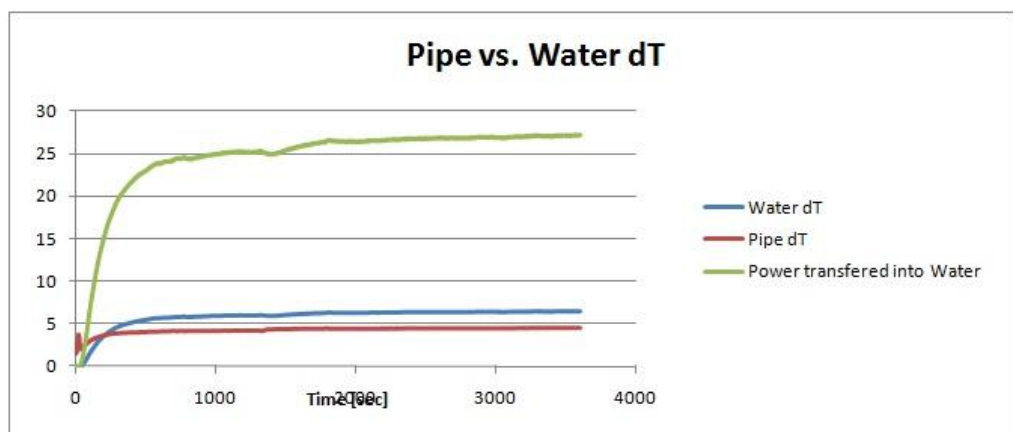


Figure A4-153: Analysed Results Heat Pipe 1 40W Run

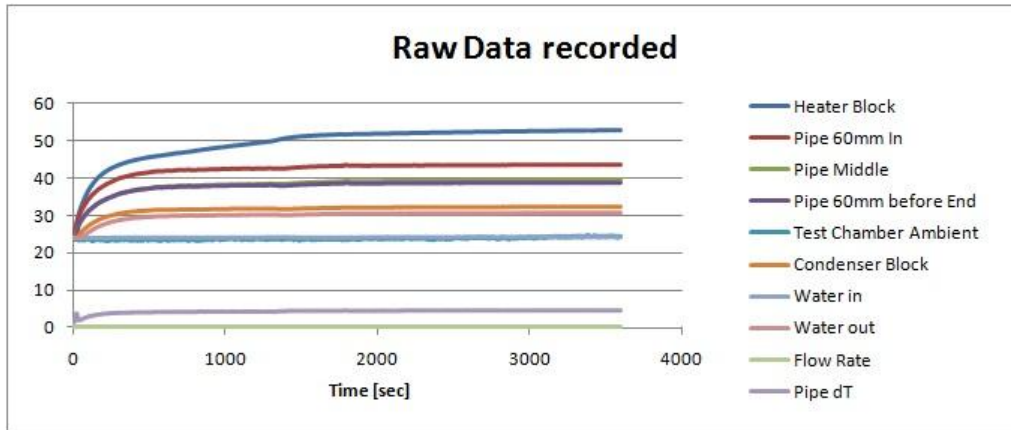


Figure A4-154: Recorded Results Heat Pipe 1 40W Run

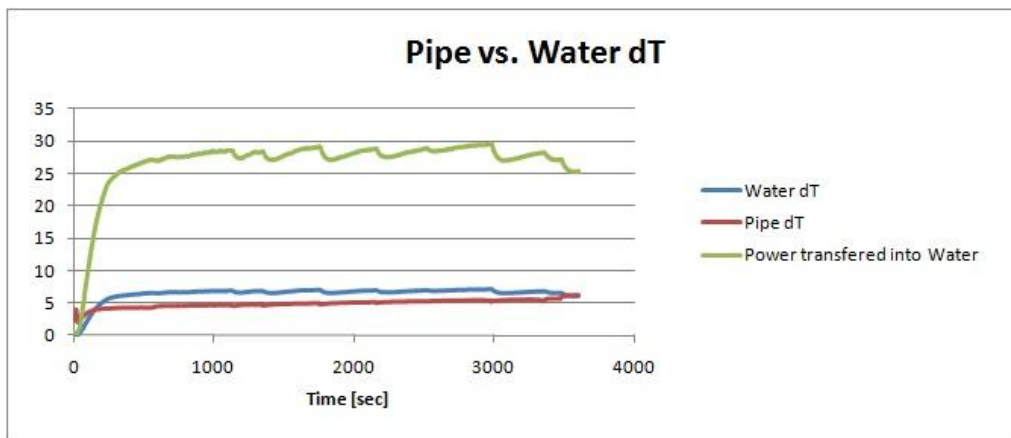


Figure A4-155: Analysed Results Heat Pipe 1 50W Run

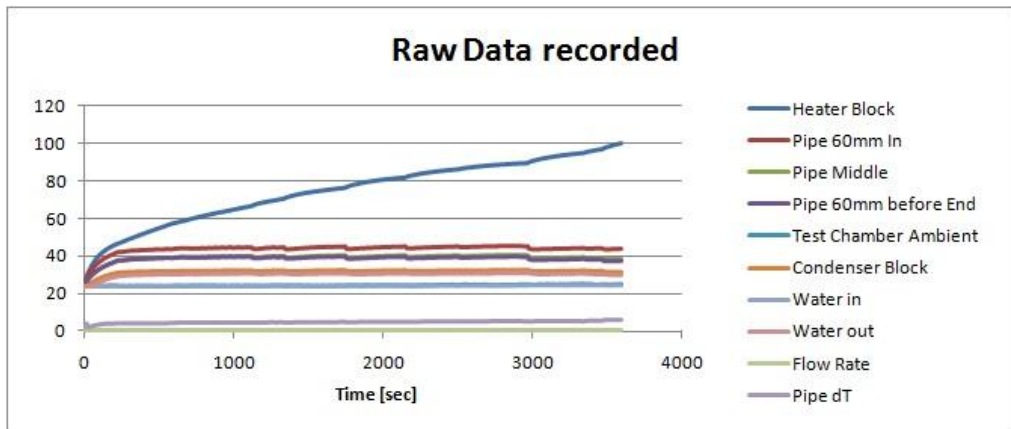


Figure A4-156: Recorded Results Heat Pipe 1 50W Run

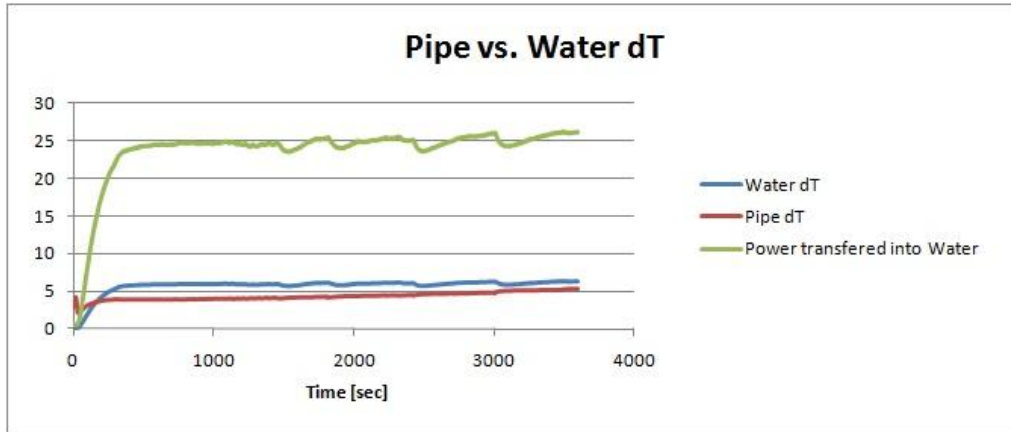


Figure A4-157: Analysed Results Heat Pipe 1 40W Ramp-Up Run

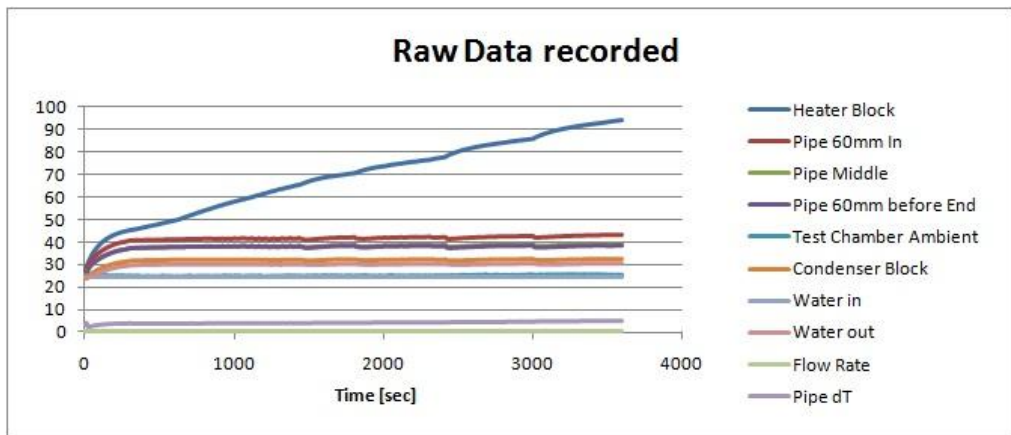


Figure A4-158: Recorded Results Heat Pipe 1 40W Ramp-Up Run

Heat Pipe 2:

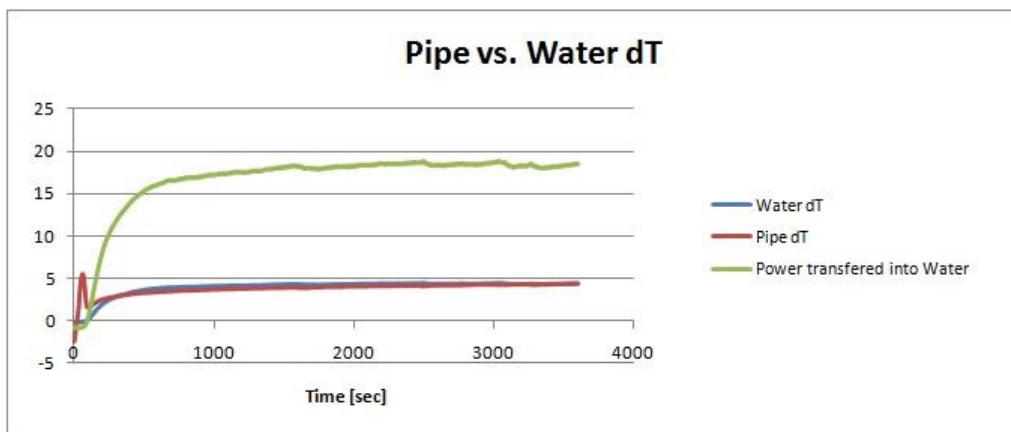


Figure A4-159: Analysed Results Heat Pipe 2 40W Run

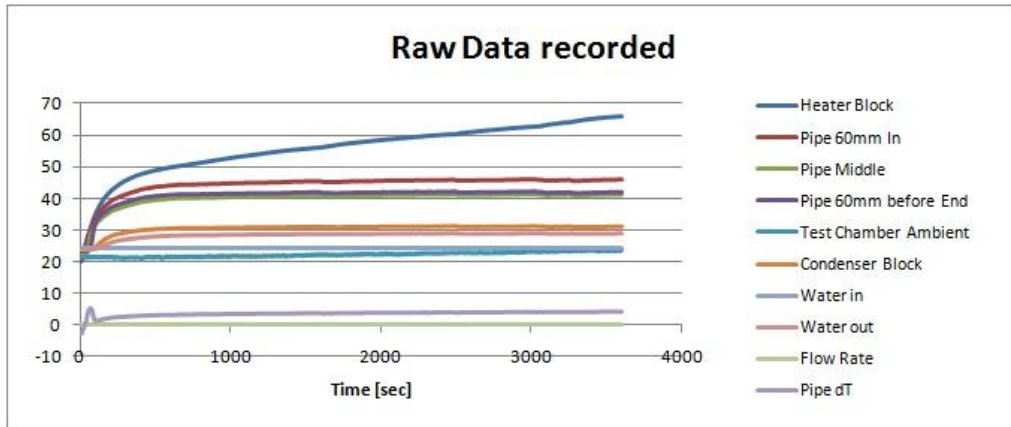


Figure A4-160: Recorded Results Heat Pipe 2 40W Run

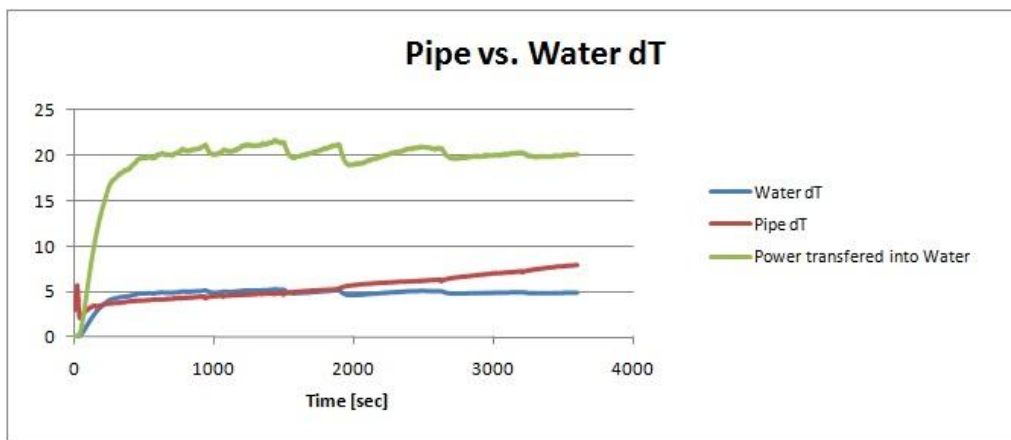


Figure A4-161: Analysed Results Heat Pipe 2 50W Run

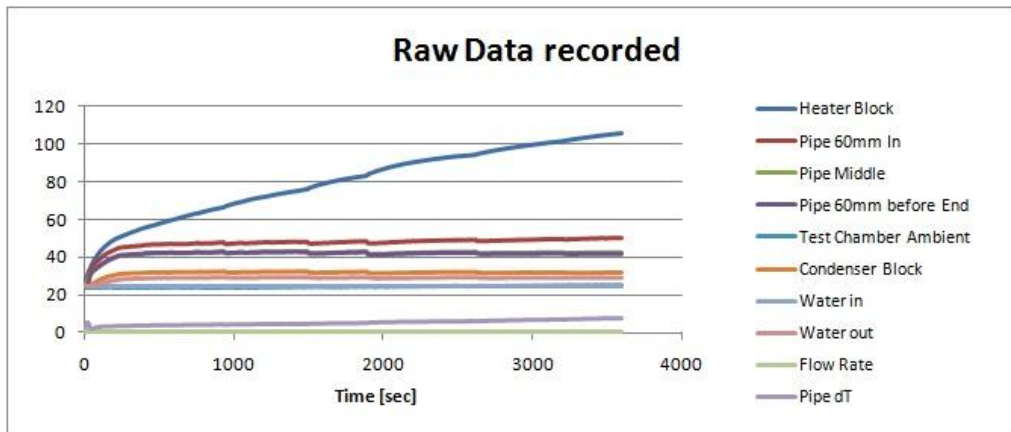


Figure A4-162: Recorded Results Heat Pipe 2 50W Run

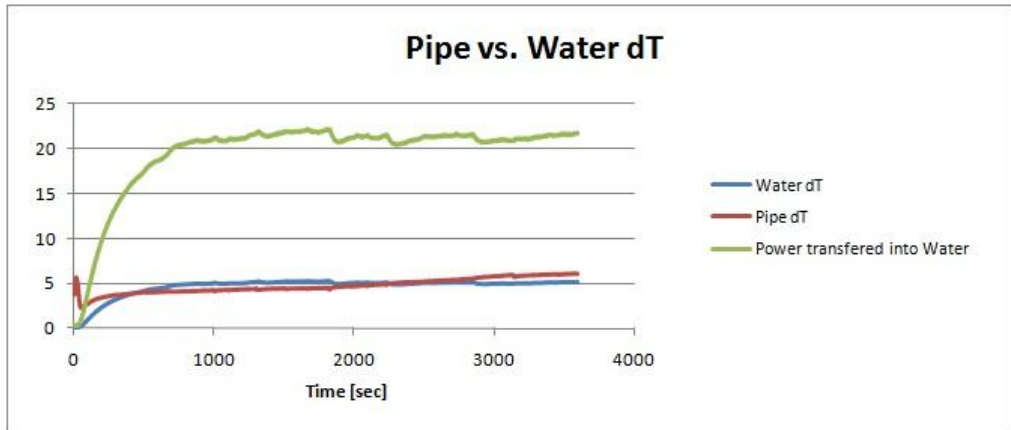


Figure A4-163: Analysed Results Heat Pipe 2 40W Ramp-Up Run

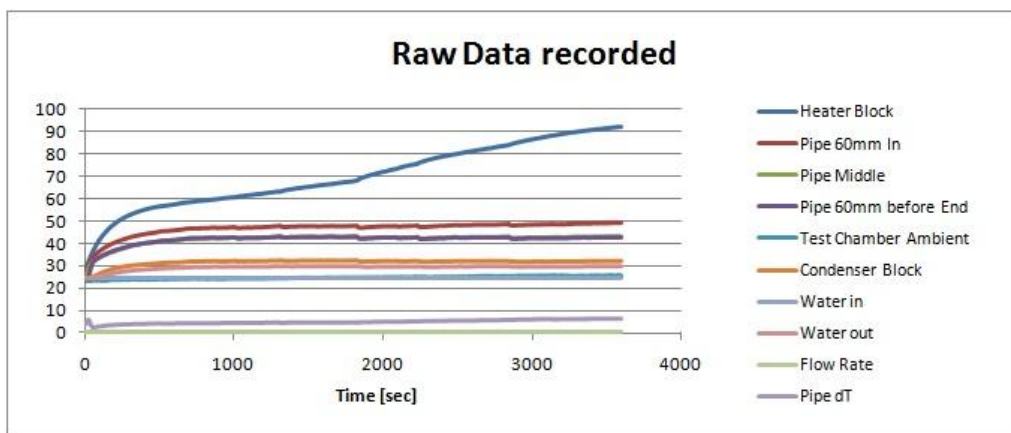


Figure A4-164: Recorded Results Heat Pipe 2 40W Ramp-Up Run

Heat Pipe 3:

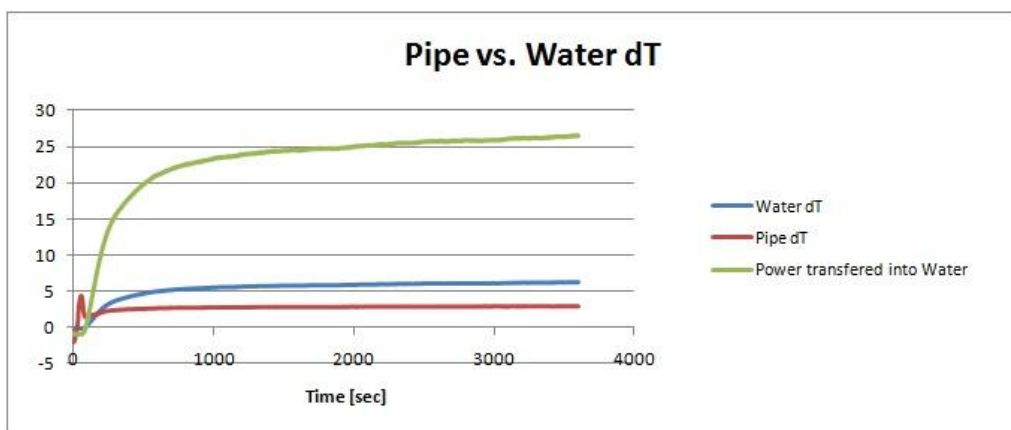


Figure A4-165: Analysed Results Heat Pipe 3 40W Run

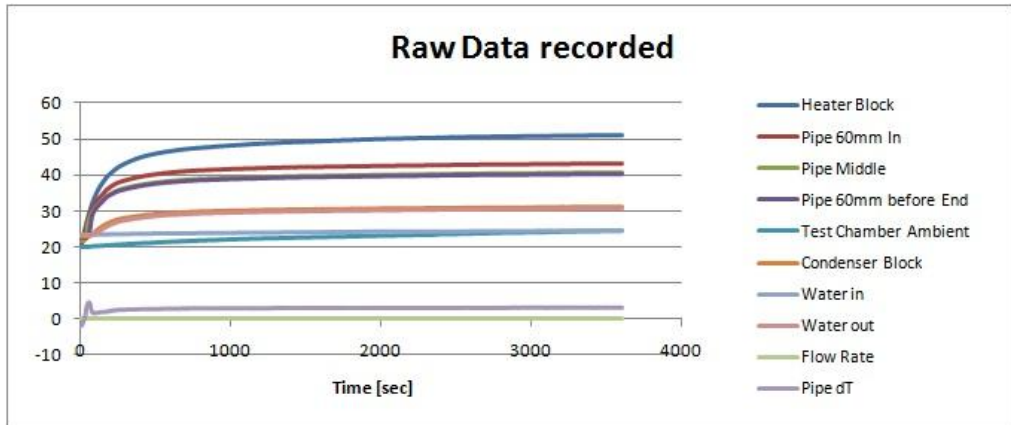


Figure A4-166: Recorded Results Heat Pipe 3 40W Run

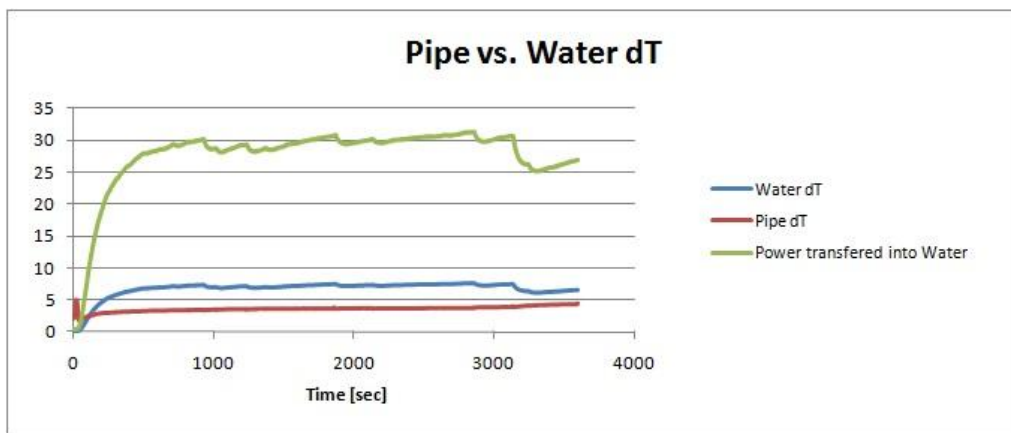


Figure A4-167: Analysed Results Heat Pipe 3 50W Run

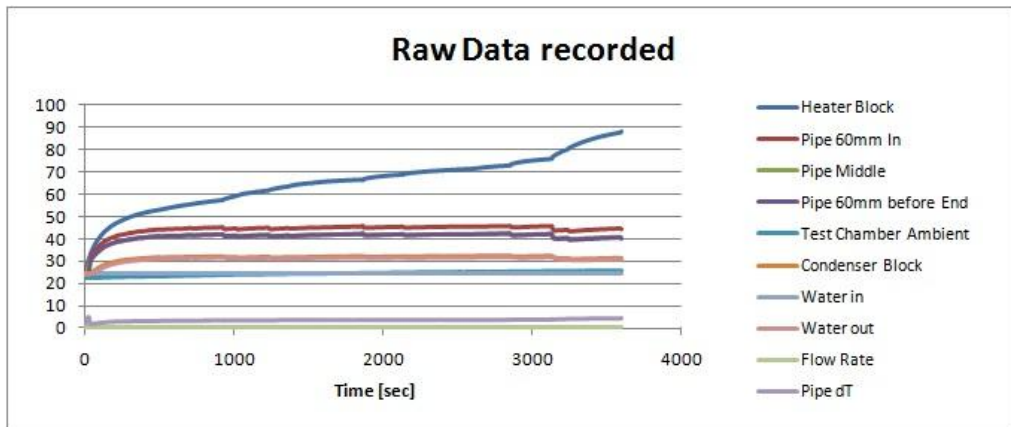


Figure A4-168: Recorded Results Heat Pipe 3 50W Run

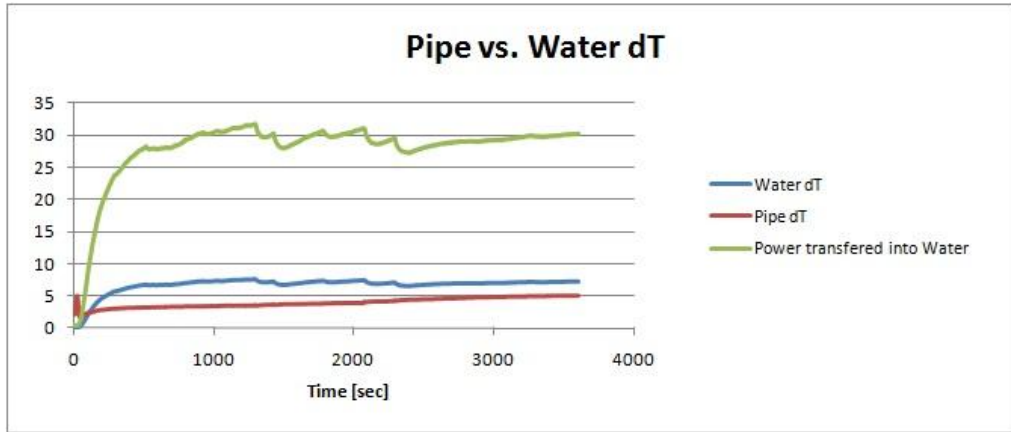


Figure A4-169: Analysed Results Heat Pipe 3 50W Ramp-Up Run

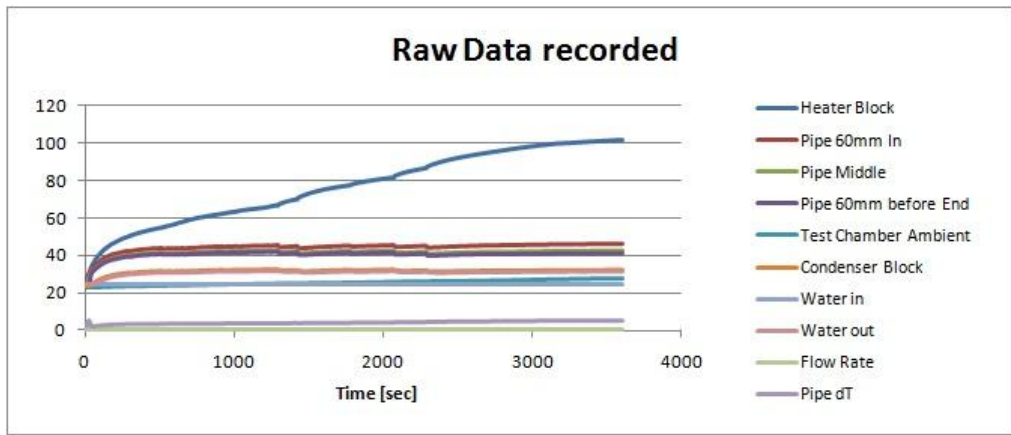


Figure A4-170: Recorded Results Heat Pipe 3 50W Ramp-Up Run

Heat Pipe 4:

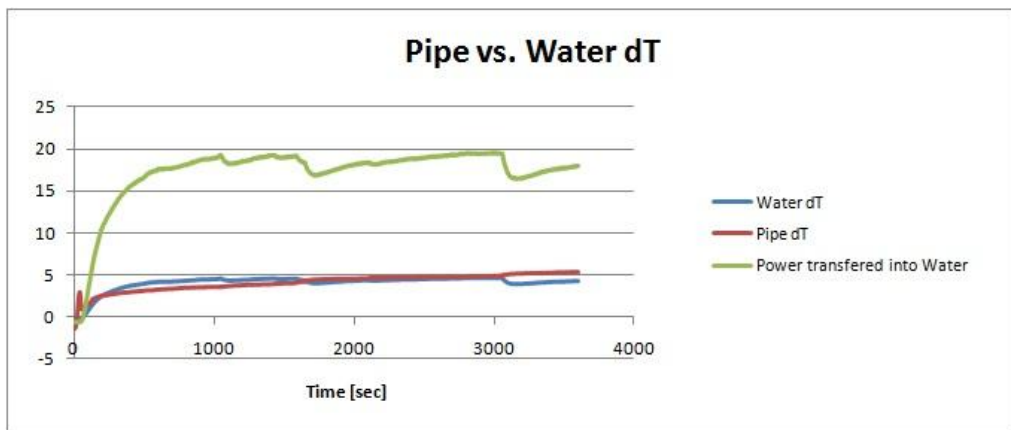


Figure A4-171: Analysed Results Heat Pipe 4 40W Run

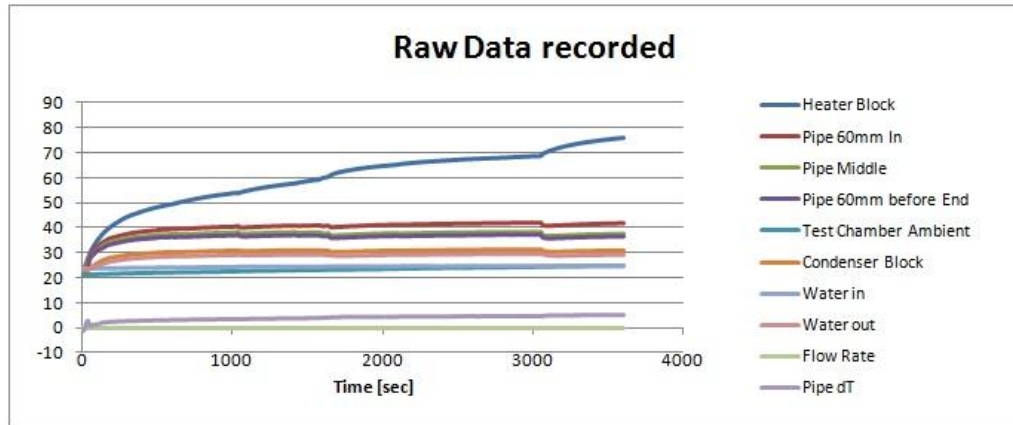


Figure A4-172: Recorded Results Heat Pipe 4 40W Run

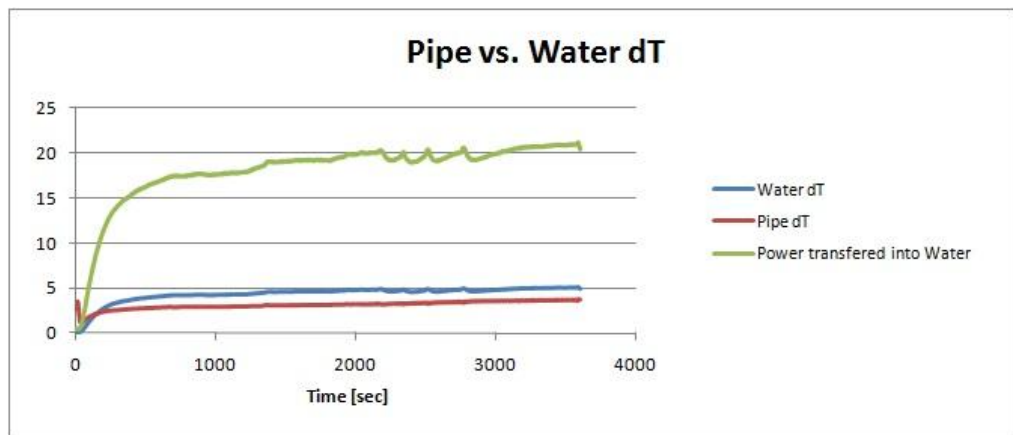


Figure A4-173: Analysed Results Heat Pipe 4 30W Ramp-Up Run 1

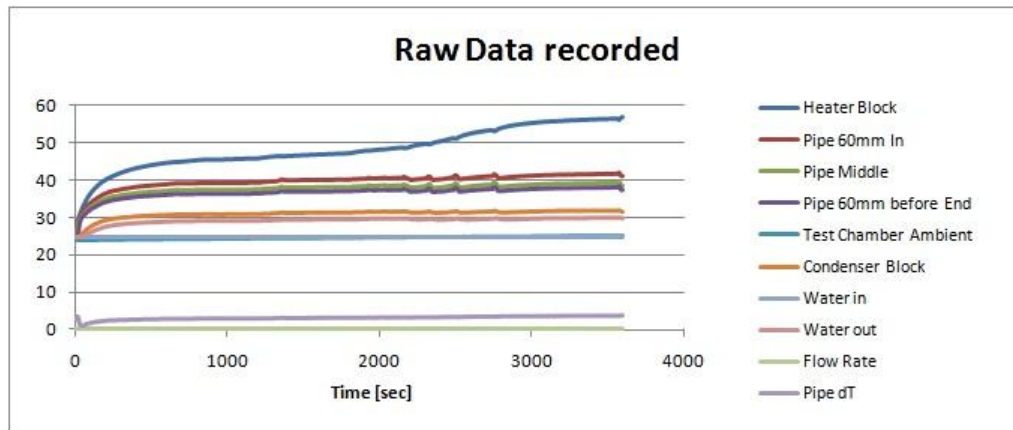


Figure A4-174: Recorded Results Heat Pipe 4 30W Ramp-Up Run 1

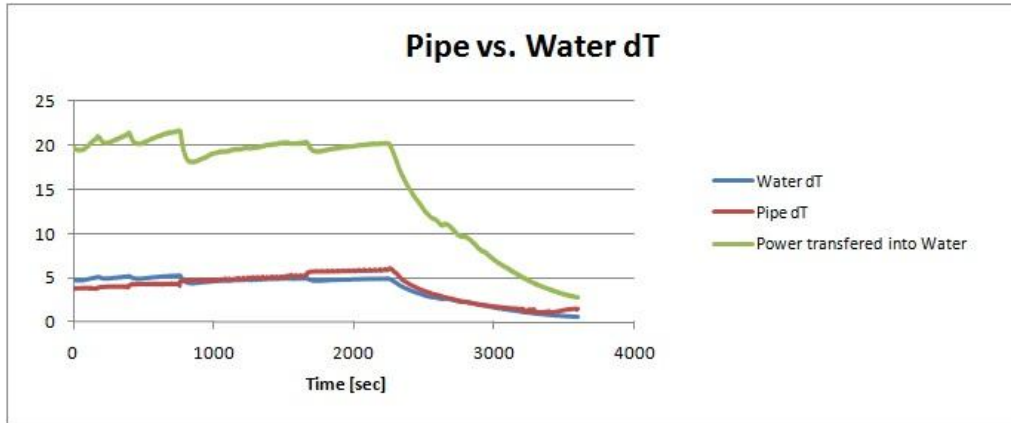


Figure A4-175: Analysed Results Heat Pipe 4 30W Ramp-Up Run 2

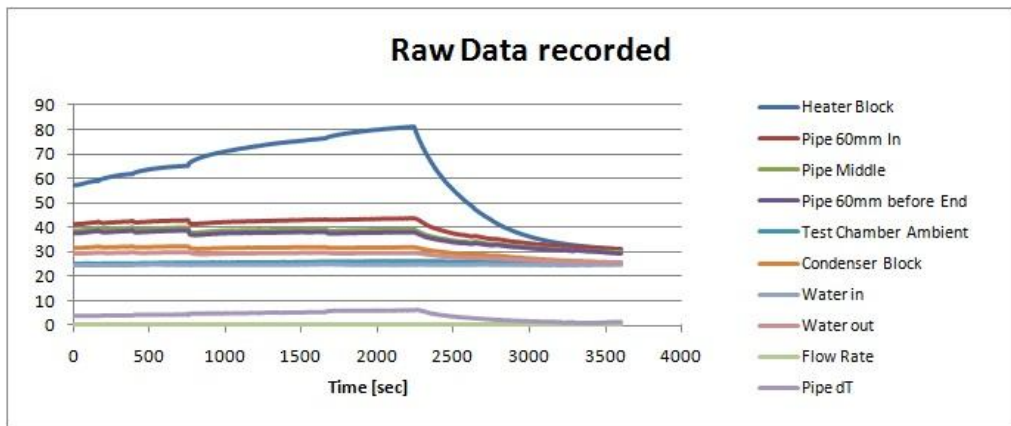


Figure A4-176: Recorded Results Heat Pipe 4 30W Ramp-Up Run 2

Heat Pipe 5:

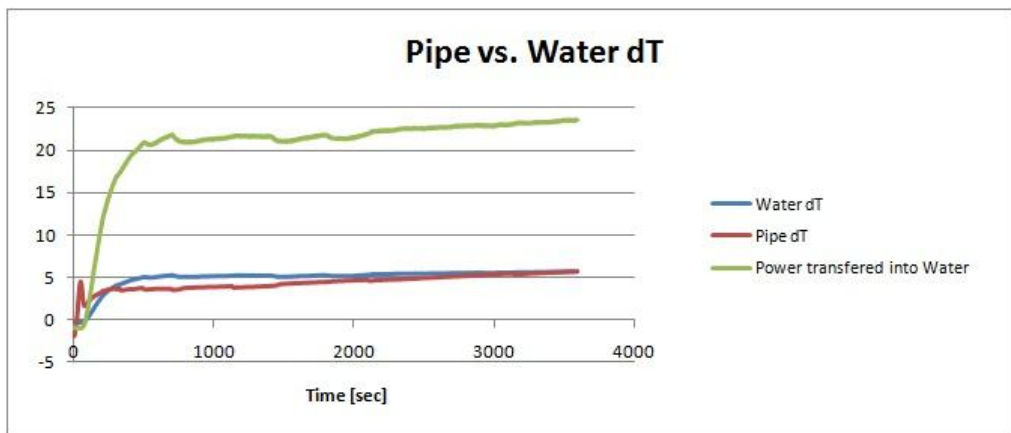


Figure A4-177: Analysed Results Heat Pipe 5 40W Run

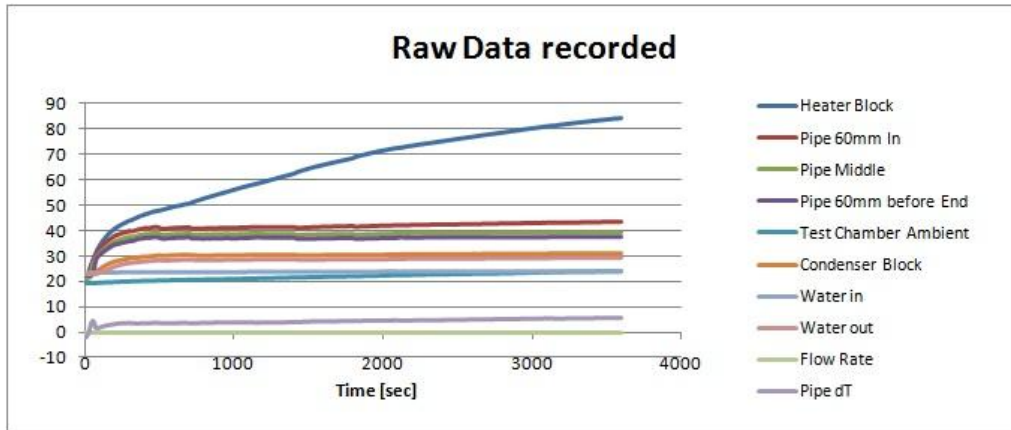


Figure A4-178: Recorded Results Heat Pipe 5 40W Run

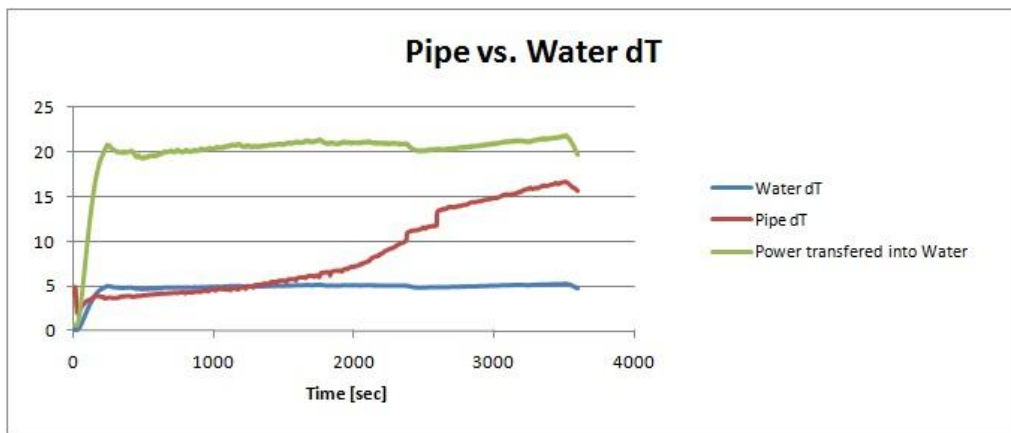


Figure A4-179: Analysed Results Heat Pipe 5 50W Run

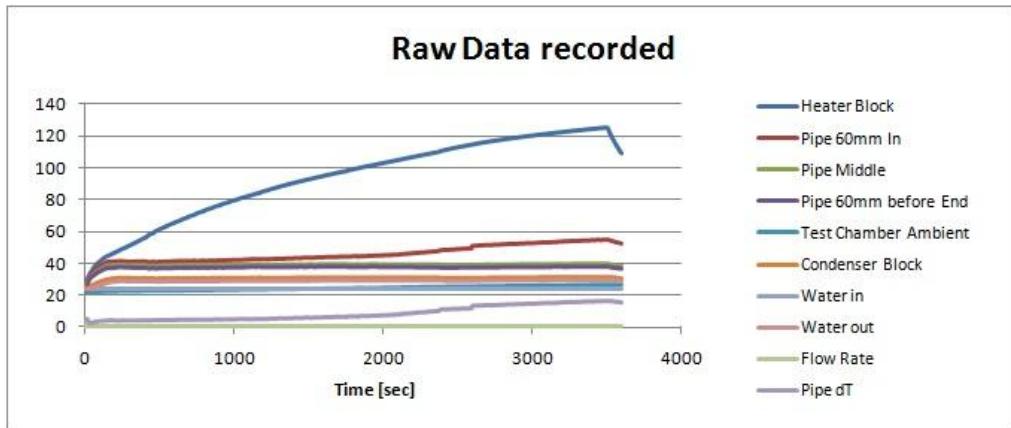


Figure A4-180: Recorded Results Heat Pipe 5 50W Run

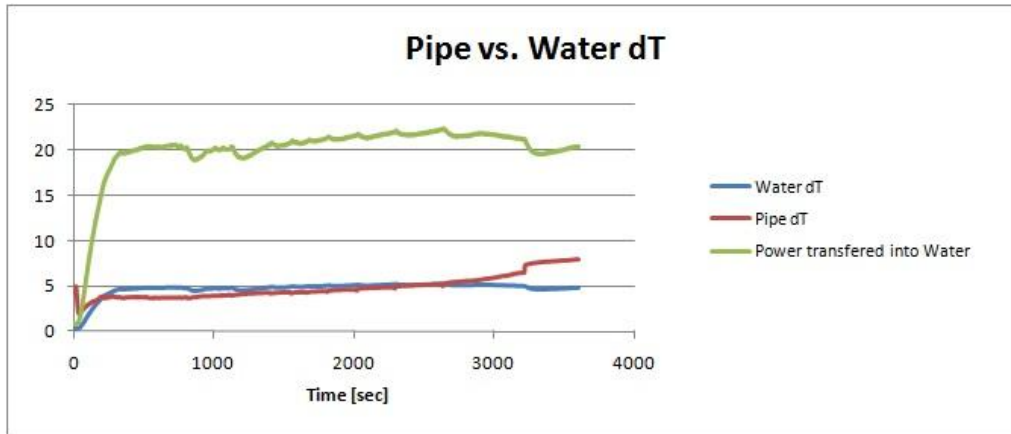


Figure A4-181: Analysed Results Heat Pipe 5 40W Ramp-Up Run

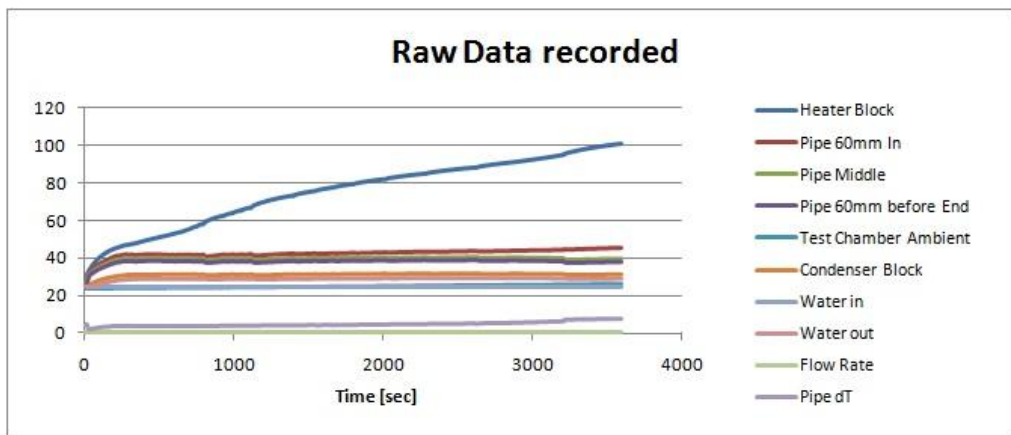


Figure A4-182: Recorded Results Heat Pipe 5 40W Ramp-Up Run

A4-6 100 Mesh at Wall Heat Pipes:

Heat Pipe 1:

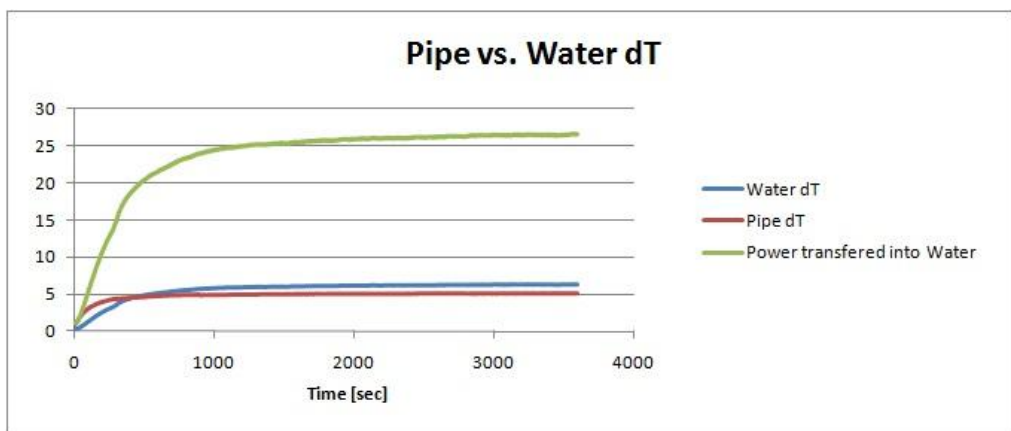


Figure A4-183: Analysed Results Heat Pipe 1 50W Run

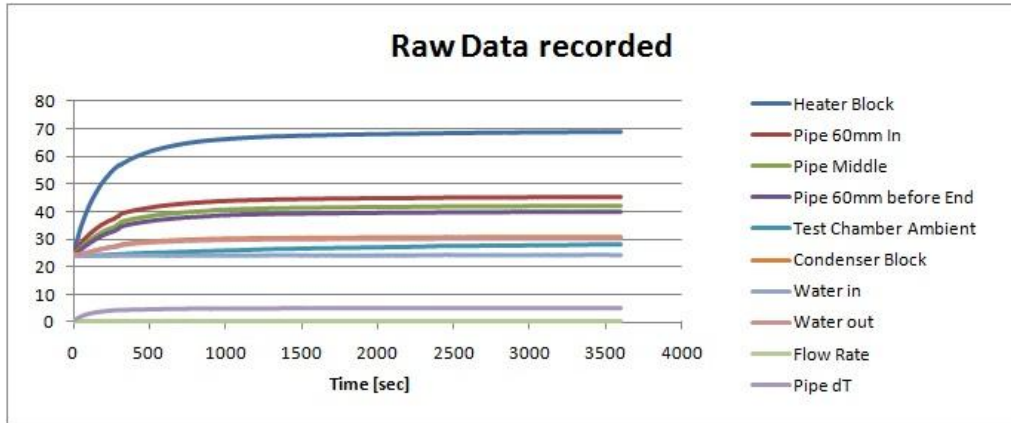


Figure A4-184: Recorded Results Heat Pipe 1 50W Run

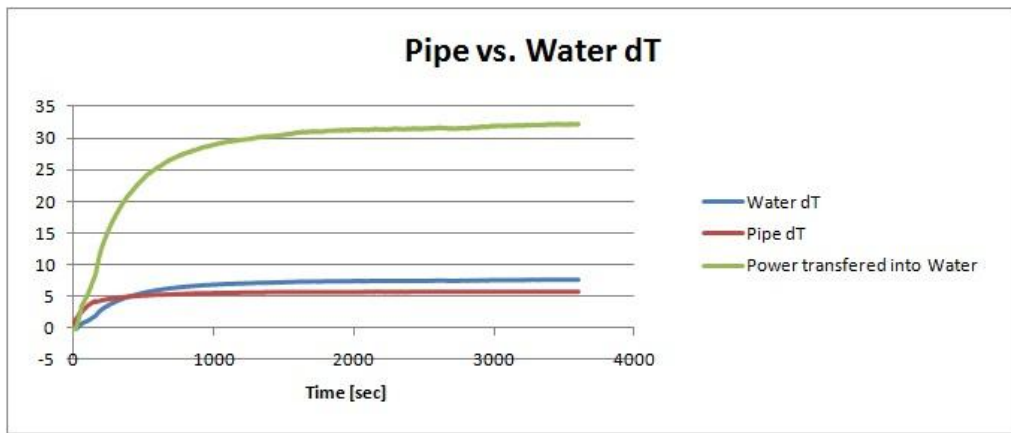


Figure A4-185: Analysed Results Heat Pipe 1 60W Run

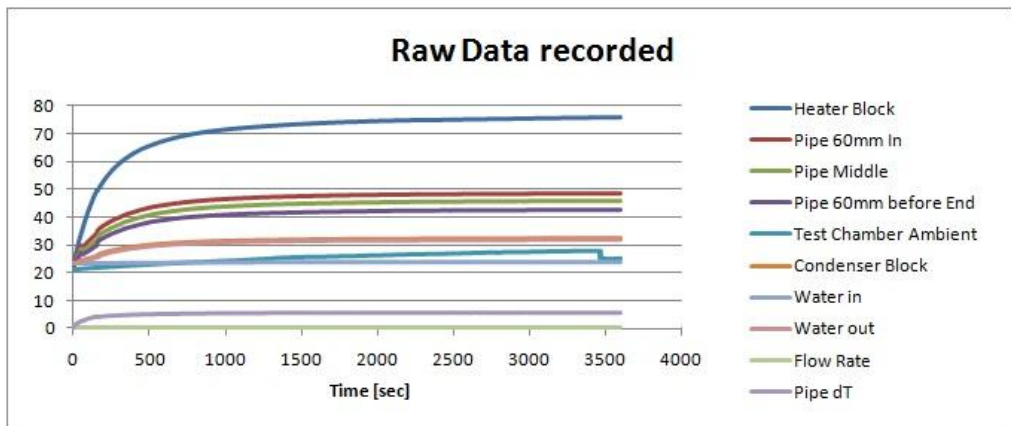


Figure A4-186: Recorded Results Heat Pipe 1 60W Run

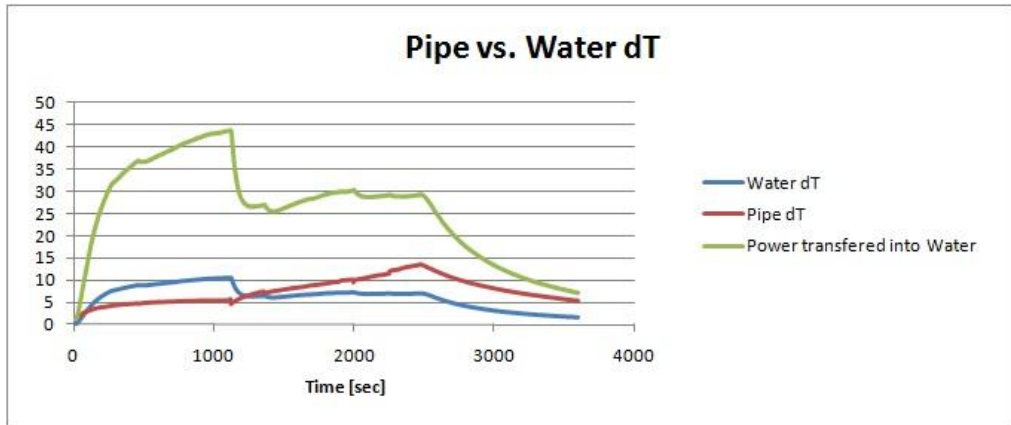


Figure A4-187: Analysed Results Heat Pipe 1 70W Run

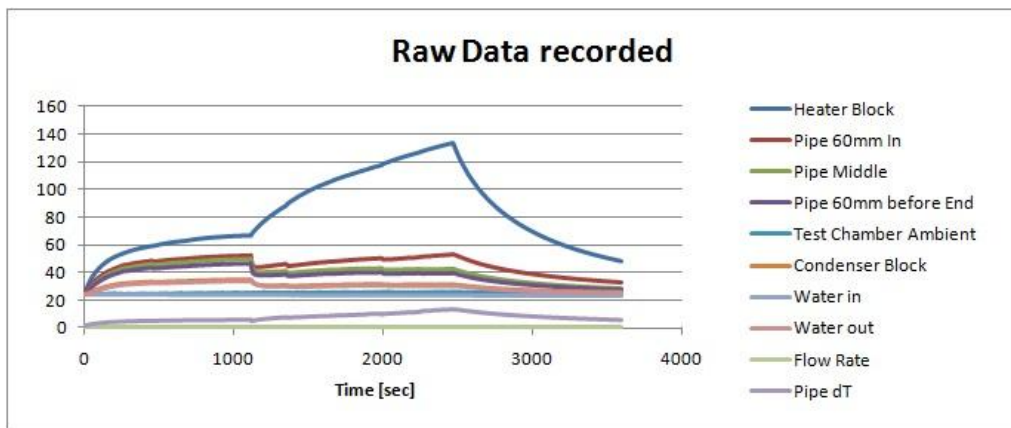


Figure A4-188: Recorded Results Heat Pipe 1 70W Run

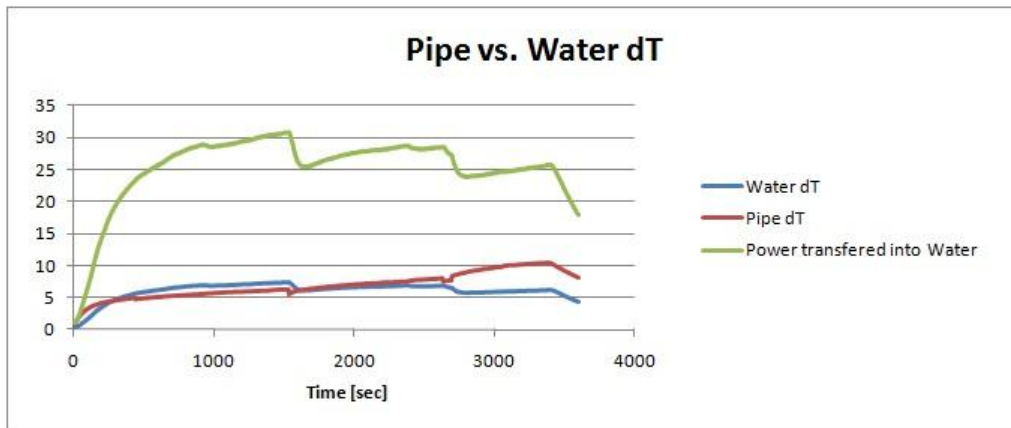


Figure A4-189: Analysed Results Heat Pipe 1 60W Ramp-Up Run

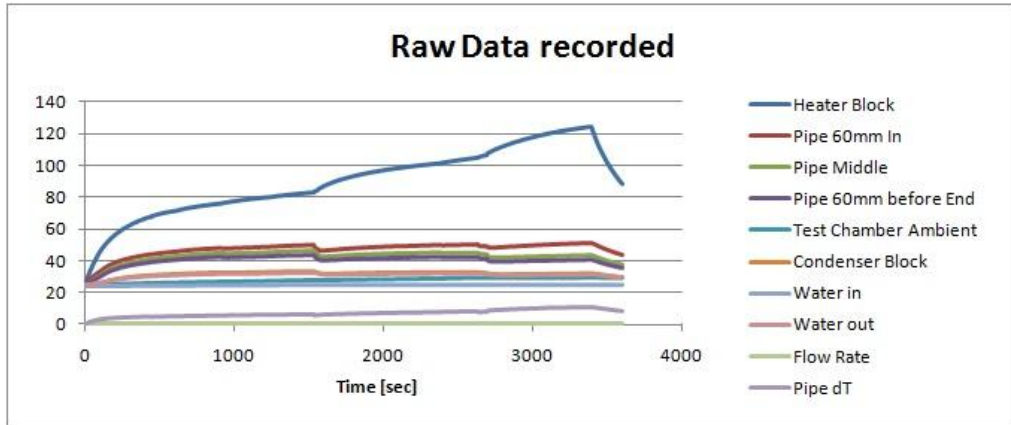


Figure A4-190: Recorded Results Heat Pipe 1 60W Ramp-Up Run

Heat Pipe 2:

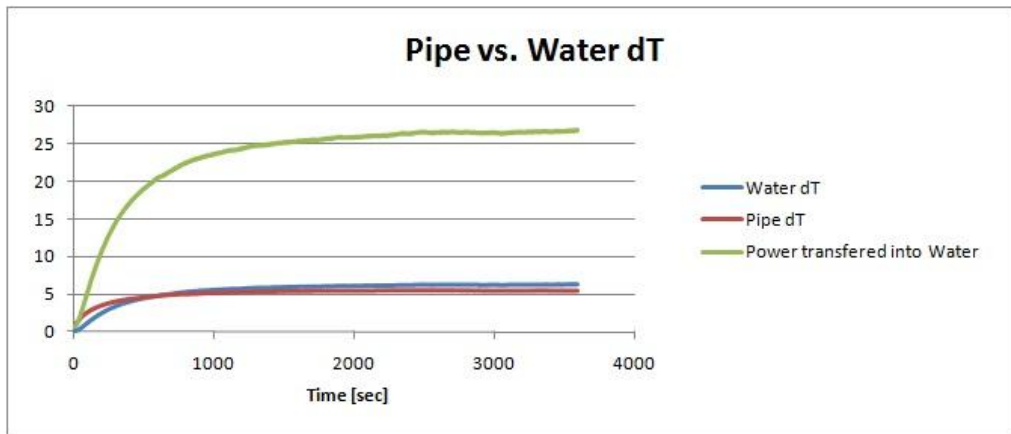


Figure A4-191: Analysed Results Heat Pipe 2 50W Run

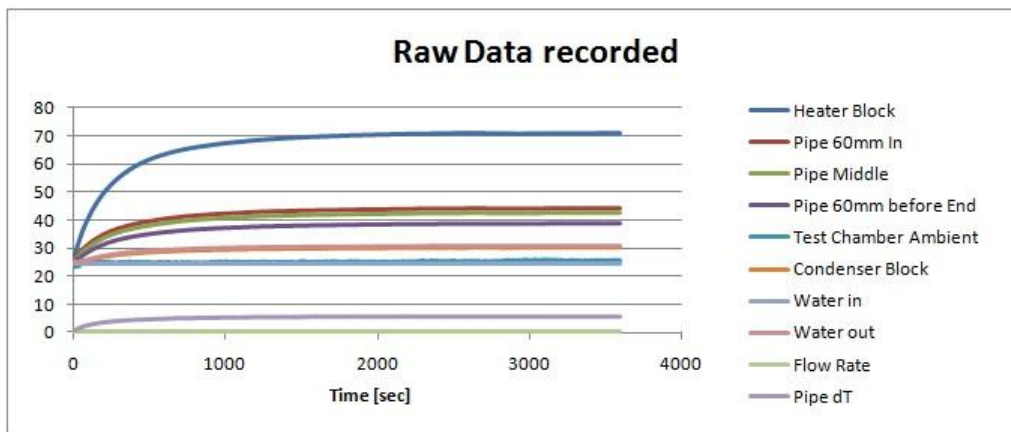


Figure A4-192: Recorded Results Heat Pipe 2 50W Run

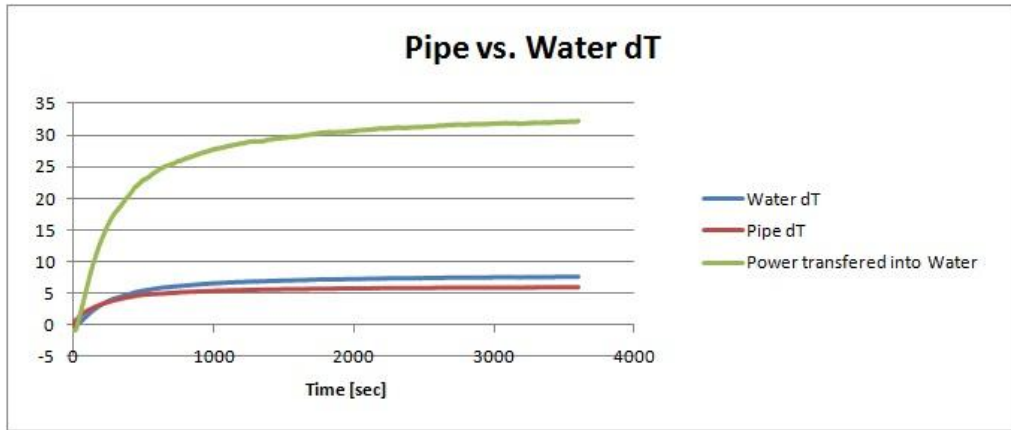


Figure A4-193: Analysed Results Heat Pipe 2 60W Run

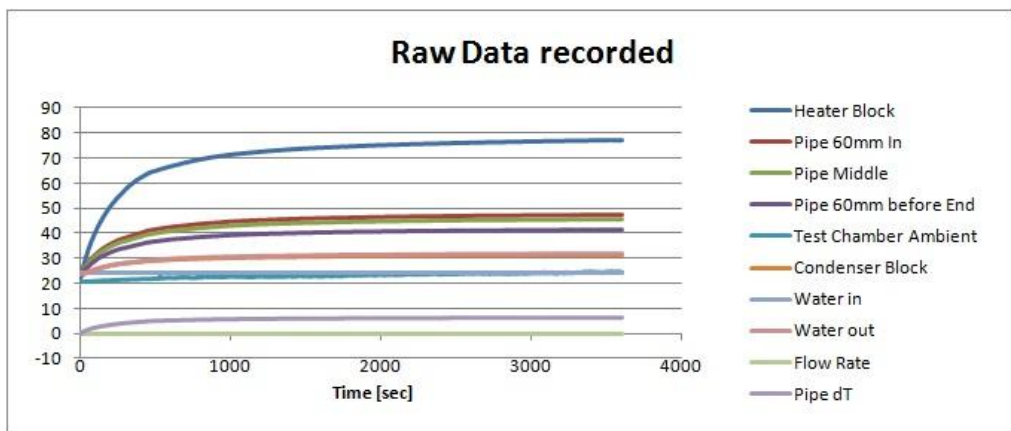


Figure A4-194: Recorded Results Heat Pipe 2 60W Run

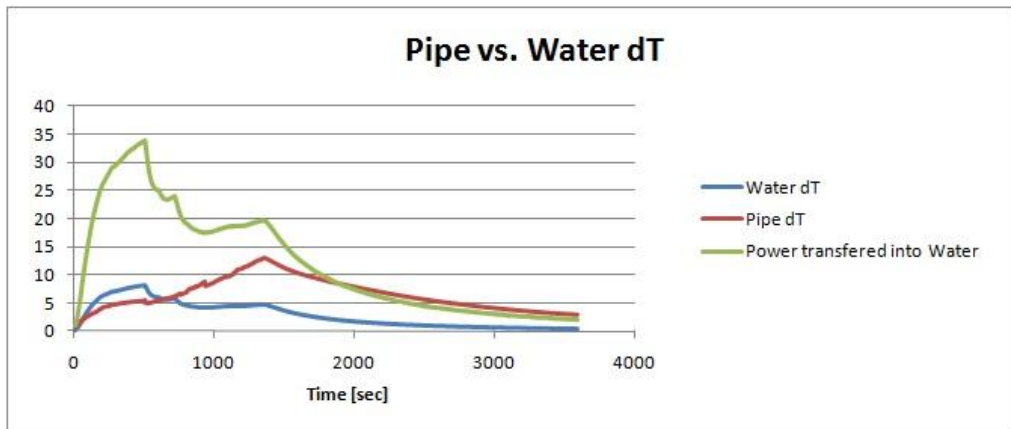


Figure A4-195: Analysed Results Heat Pipe 2 70W Run

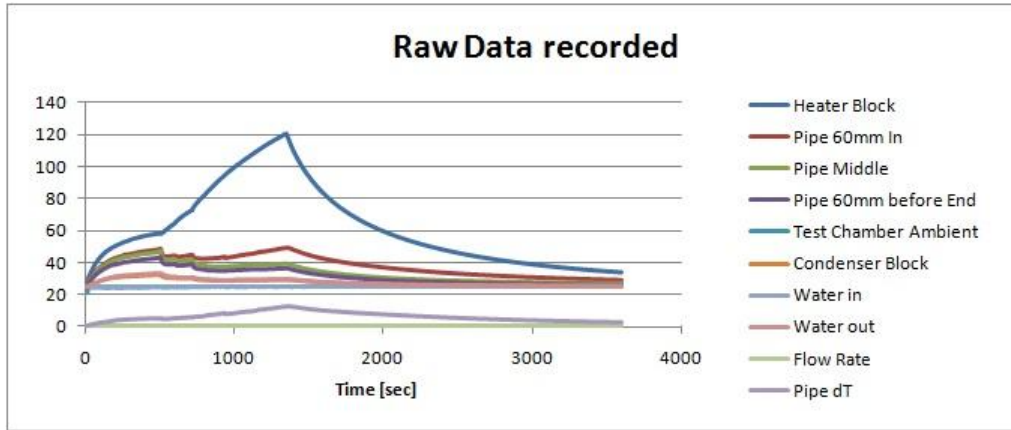


Figure A4-196: Recorded Results Heat Pipe 2 70W Run

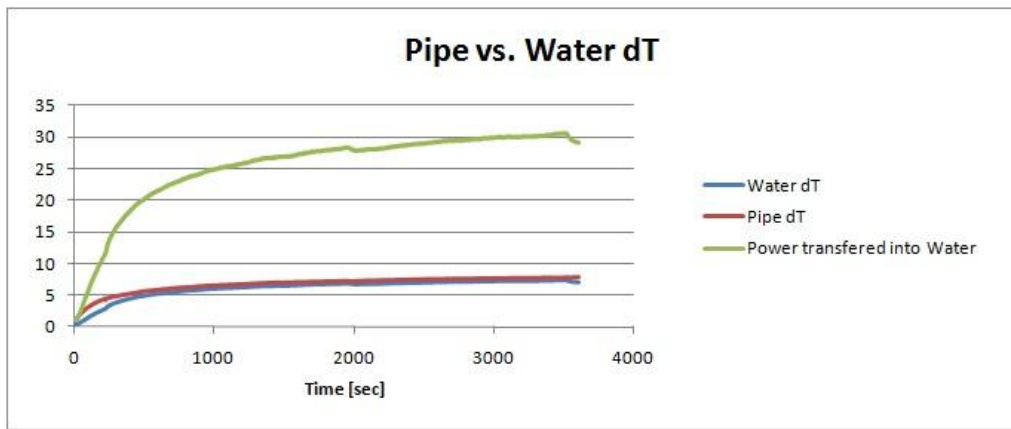


Figure A4-197: Analysed Results Heat Pipe 2 60W Ramp-Up Run 1

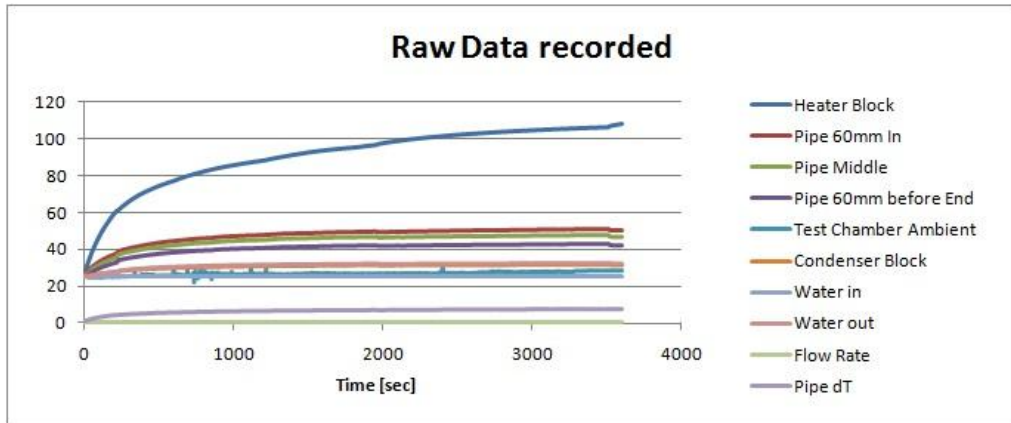


Figure A4-198: Recorded Results Heat Pipe 2 60W Ramp-Up Run 1

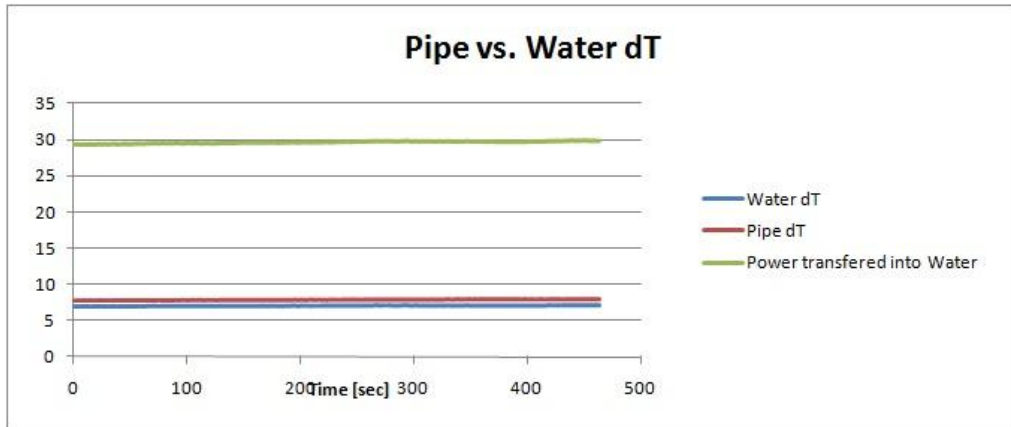


Figure A4-199: Analysed Results Heat Pipe 2 60W Ramp-Up Run 2

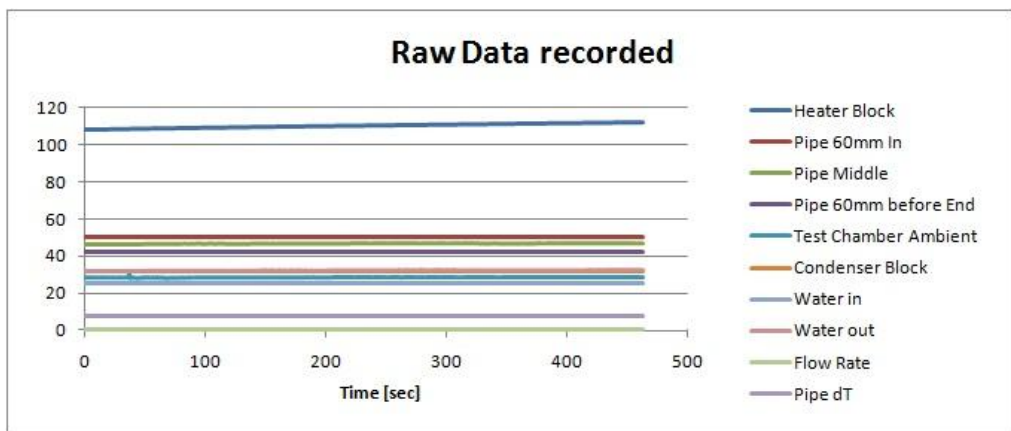


Figure A4-200: Recorded Results Heat Pipe 2 60W Ramp-Up Run 2

Heat Pipe 3:

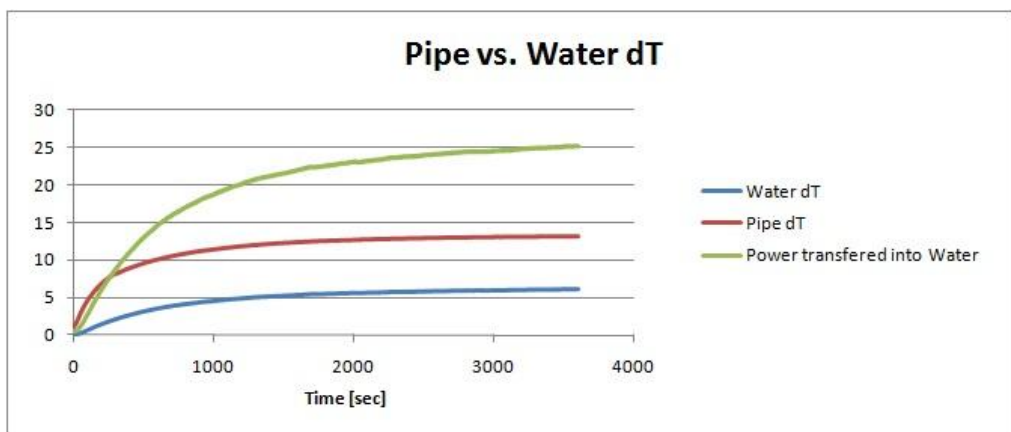


Figure A4-201: Analysed Results Heat Pipe 3 50W Run

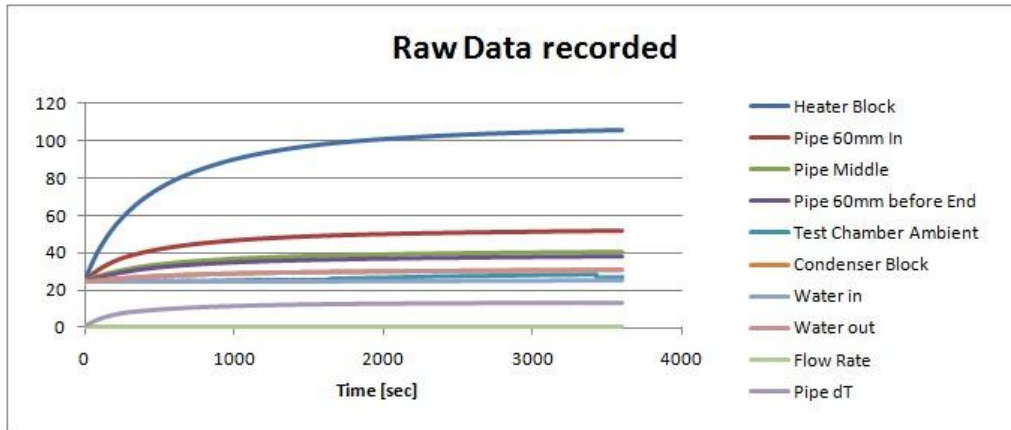


Figure A4-202: Recorded Results Heat Pipe 3 50W Run

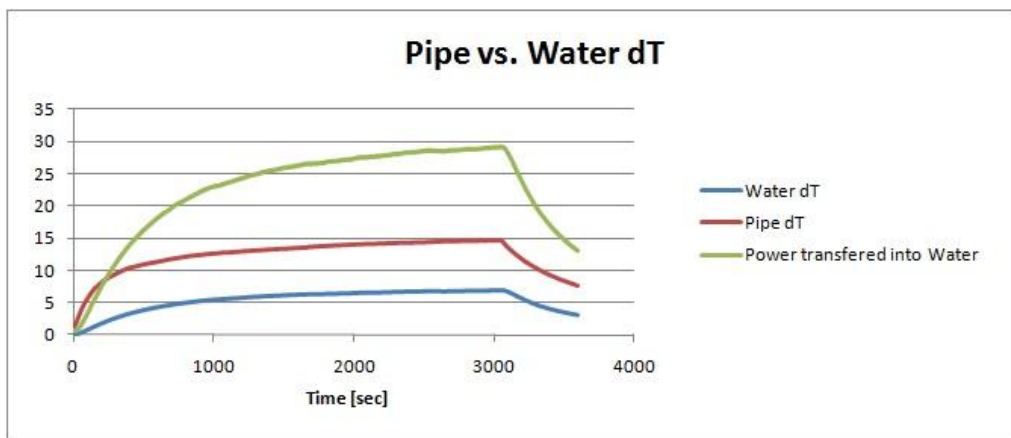


Figure A4-203: Analysed Results Heat Pipe 3 60W Run

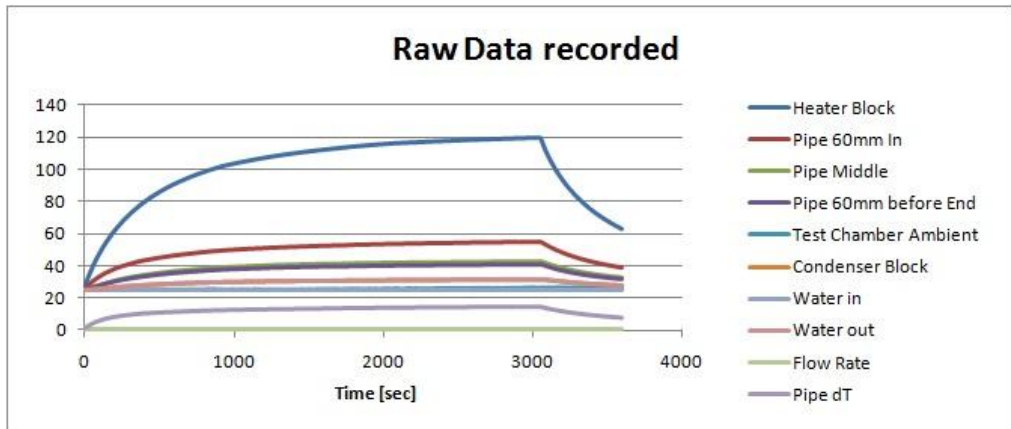


Figure A4-204: Recorded Results Heat Pipe 3 60W Run

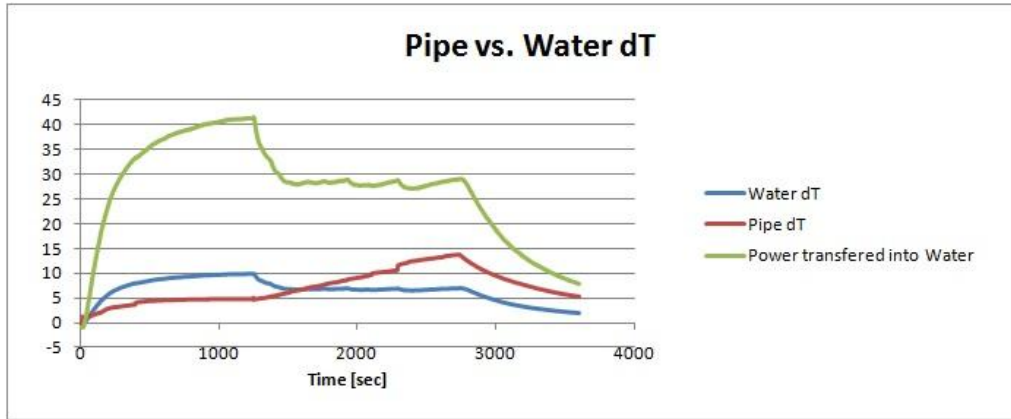


Figure A4-205: Analysed Results Heat Pipe 3 70W Run

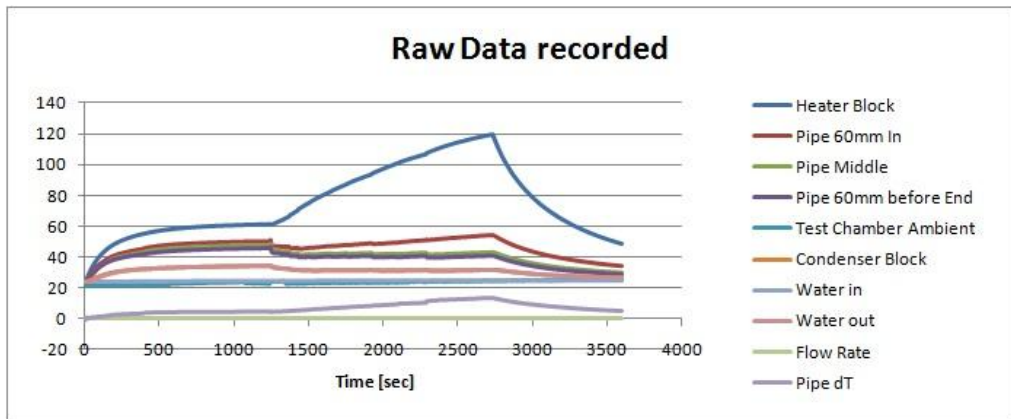


Figure A4-206: Recorded Results Heat Pipe 3 70W Run

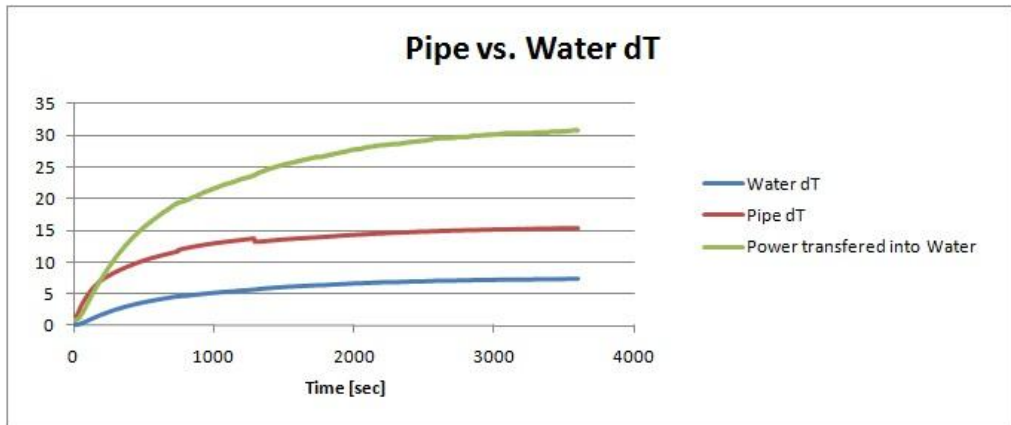


Figure A4-207: Analysed Results Heat Pipe 3 60W Ramp-Up Run

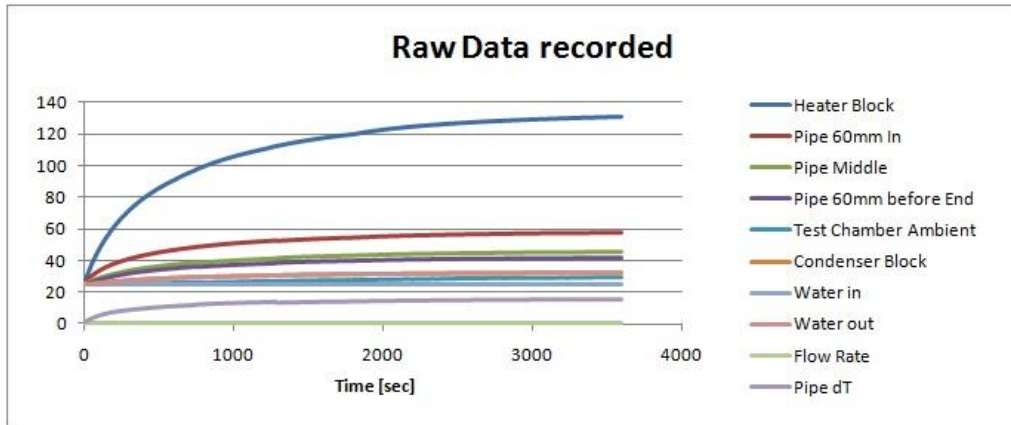


Figure A4-208: Recorded Results Heat Pipe 3 60W Ramp-Up Run

Heat Pipe 4:

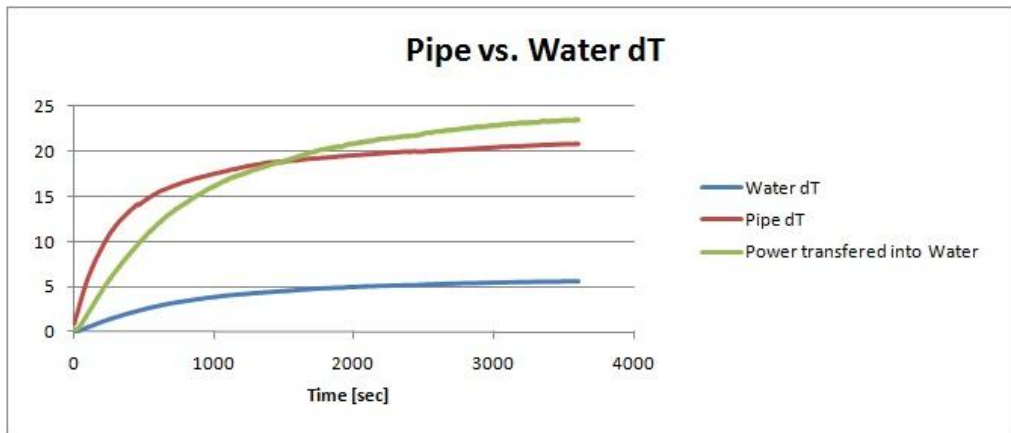


Figure A4-209: Analysed Results Heat Pipe 4 50W Run

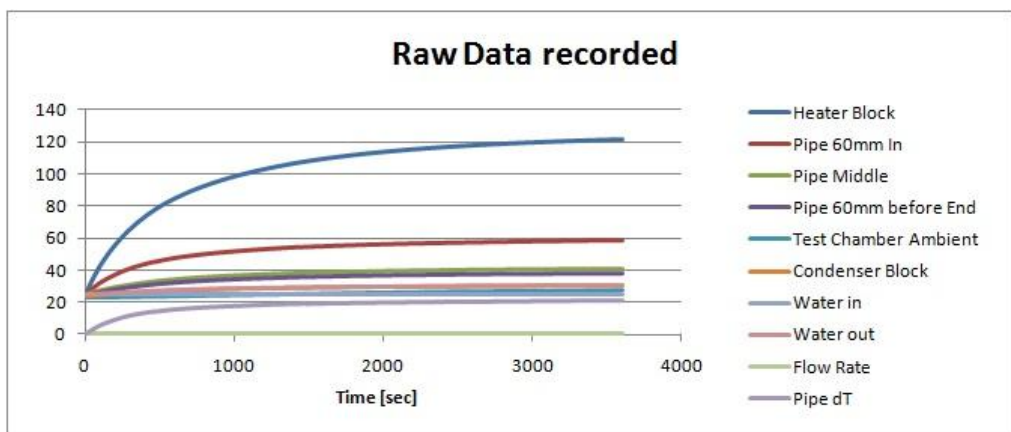


Figure A4-210: Recorded Results Heat Pipe 4 50W Run

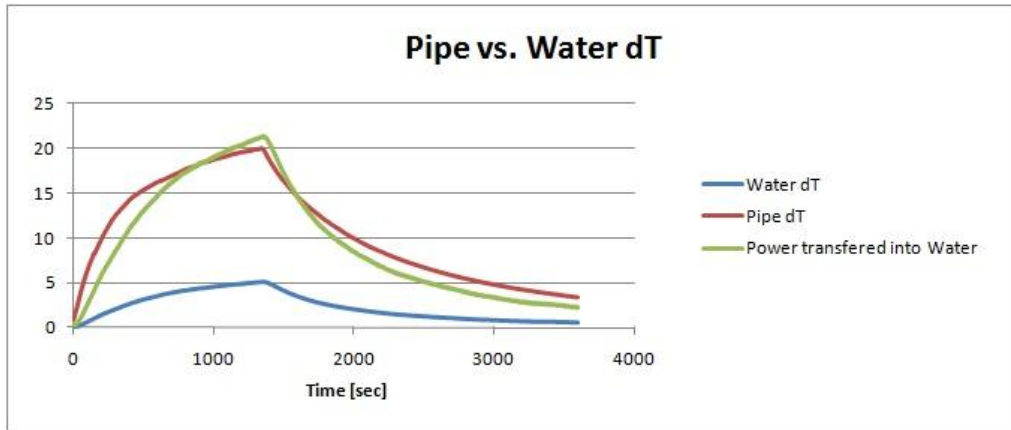


Figure A4-211: Analysed Results Heat Pipe 4 60W Run

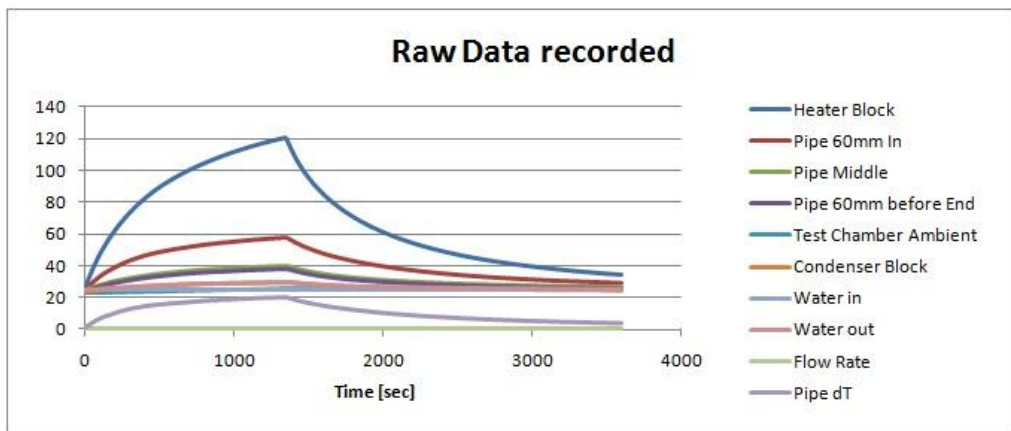


Figure A4-212: Recorded Results Heat Pipe 4 60W Run

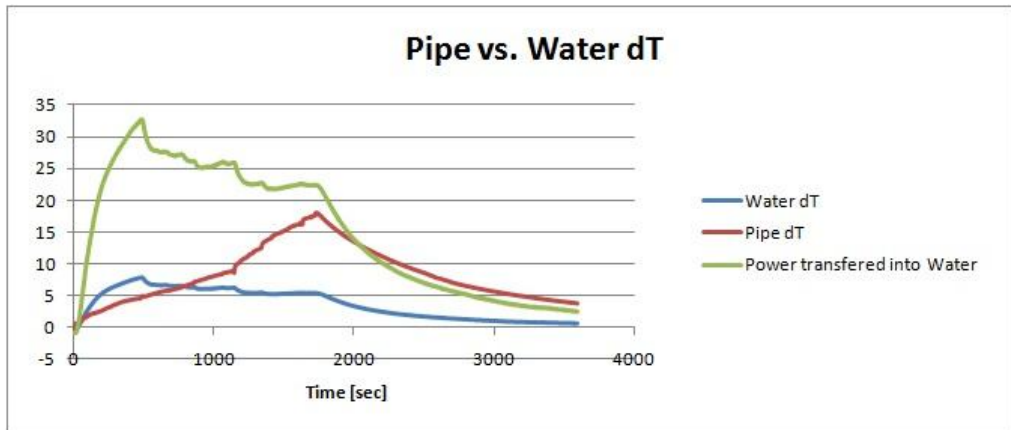


Figure A4-213: Analysed Results Heat Pipe 4 70W Run

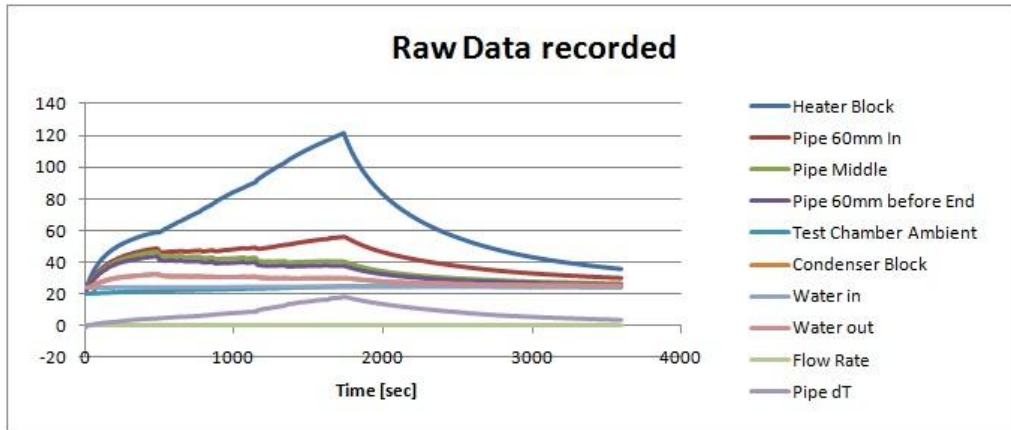


Figure A4-214: Recorded Results Heat Pipe 4 70W Run

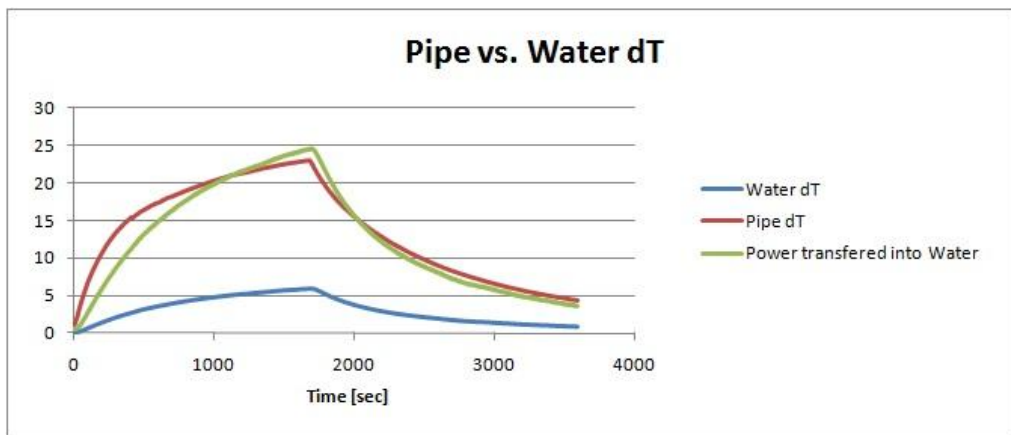


Figure A4-215: Analysed Results Heat Pipe 4 60W Ramp-Up Run

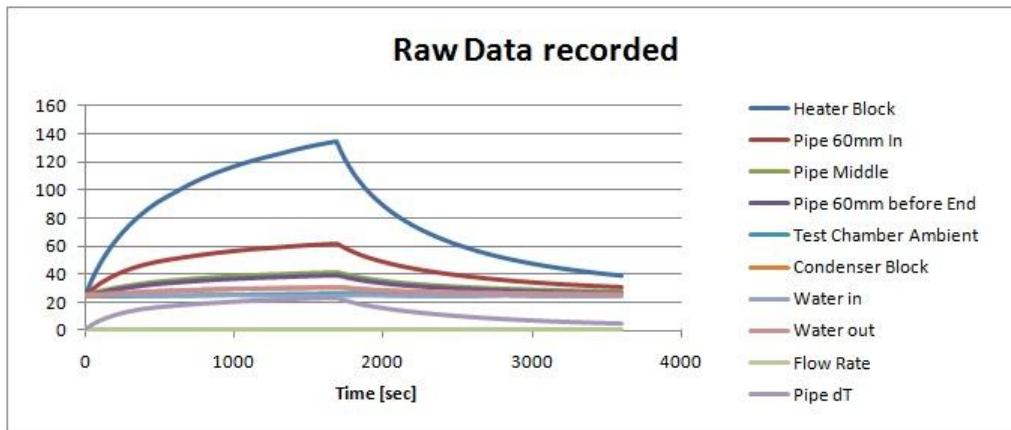


Figure A4-216: Recorded Results Heat Pipe 4 60W Ramp-Up Run

Heat Pipe 5:

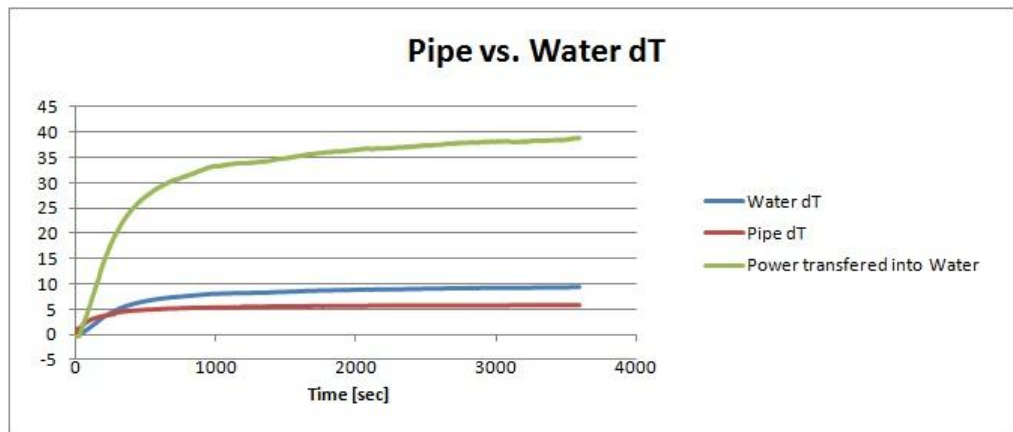


Figure A4-217: Analysed Results Heat Pipe 5 60W Run

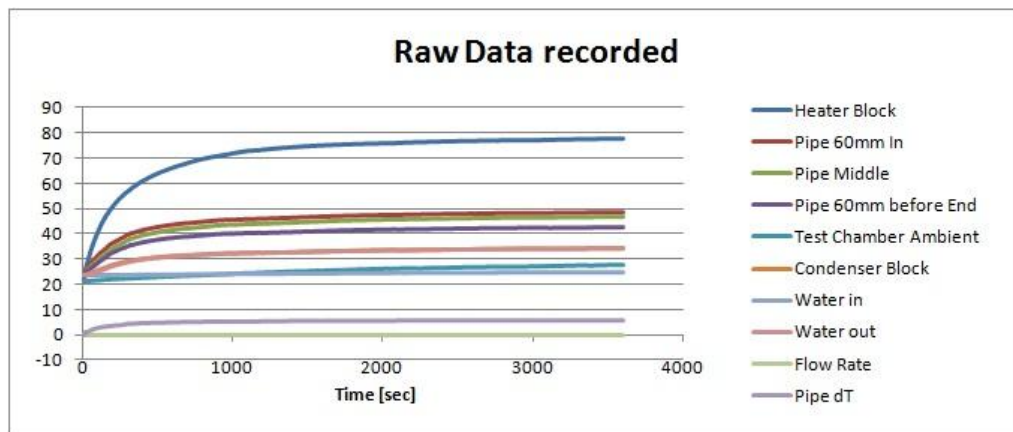


Figure A4-218: Recorded Results Heat Pipe 5 60W Run

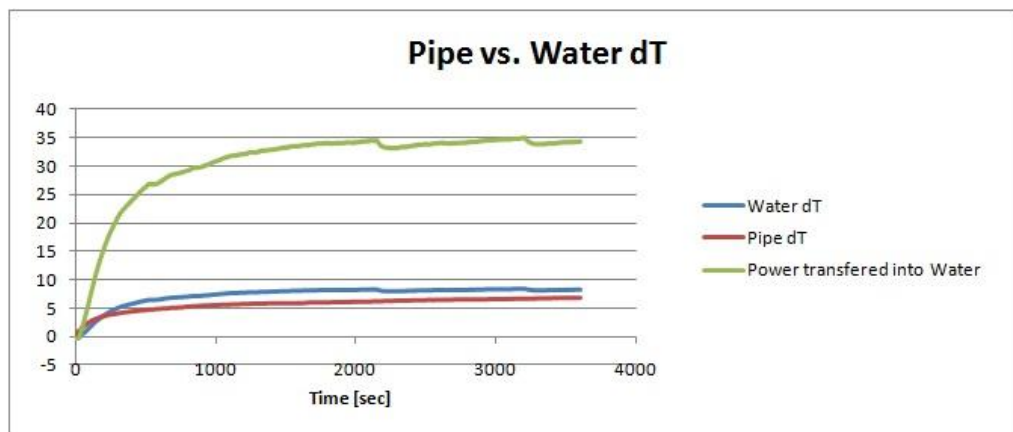


Figure A4-219: Analysed Results Heat Pipe 5 70W Run

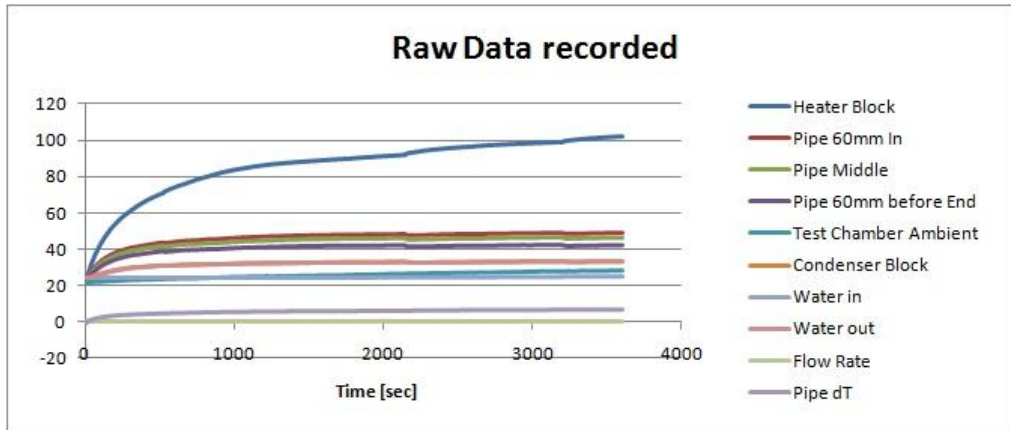


Figure A4-220: Recorded Results Heat Pipe 5 70W Run

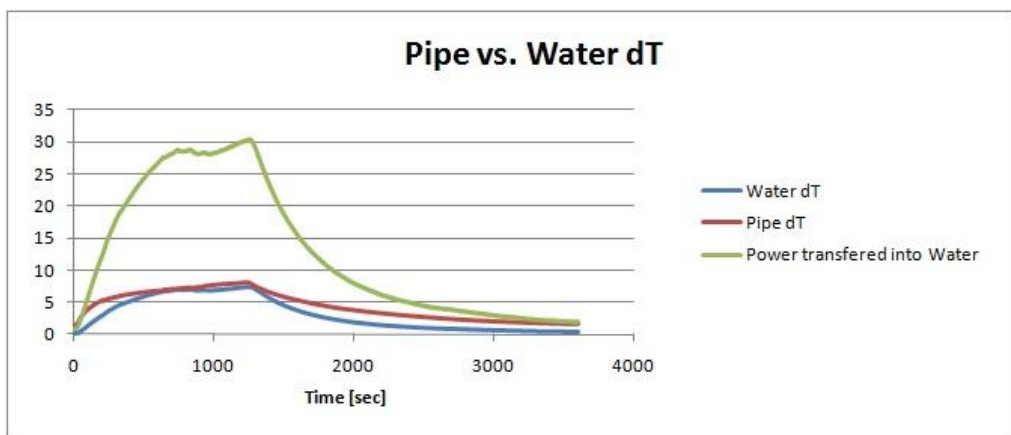


Figure A4-221: Analysed Results Heat Pipe 5 80W Run

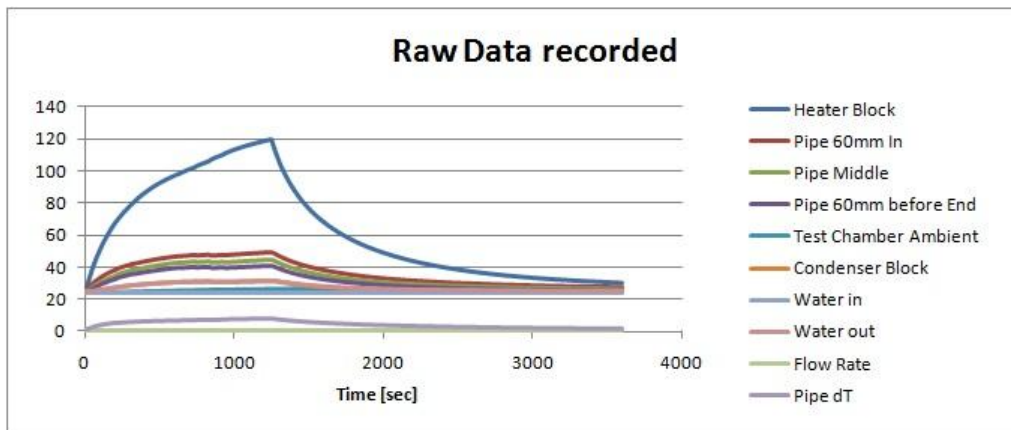


Figure A4-222: Recorded Results Heat Pipe 5 80W Run

A4-7 200 Mesh at Wall Heat Pipes:

Heat Pipe 1:

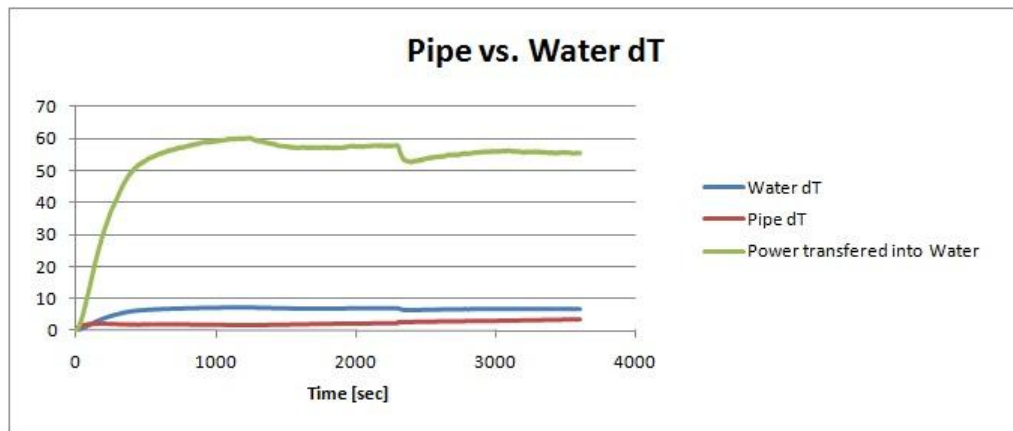


Figure A4-223: Analysed Results Heat Pipe 1 70W Run

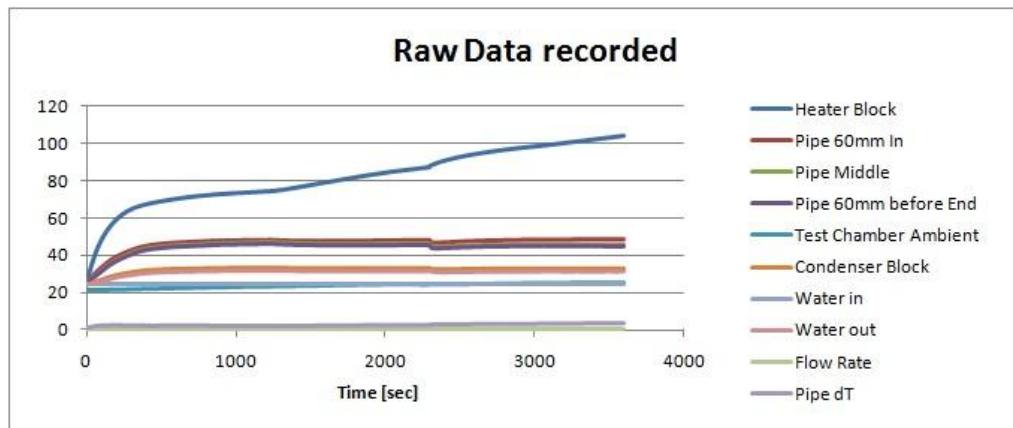


Figure A4-224: Recorded Results Heat Pipe 1 70W Run

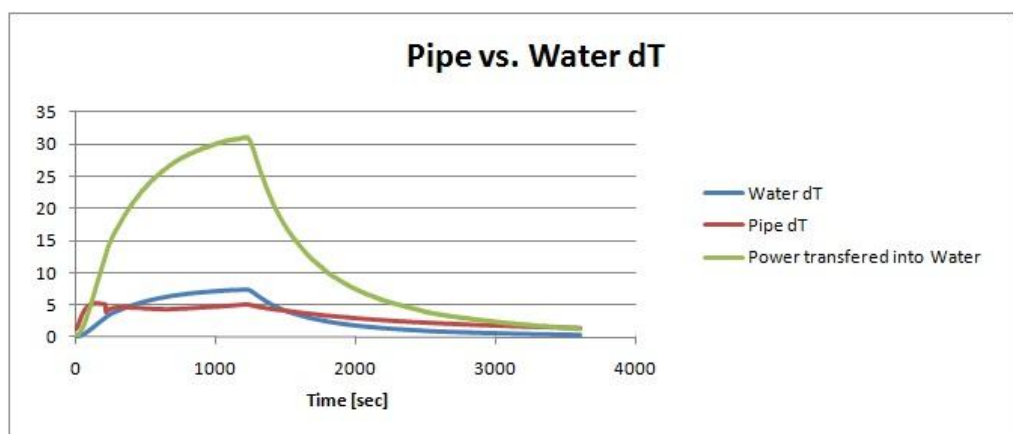


Figure A4-225: Analysed Results Heat Pipe 1 80W Run

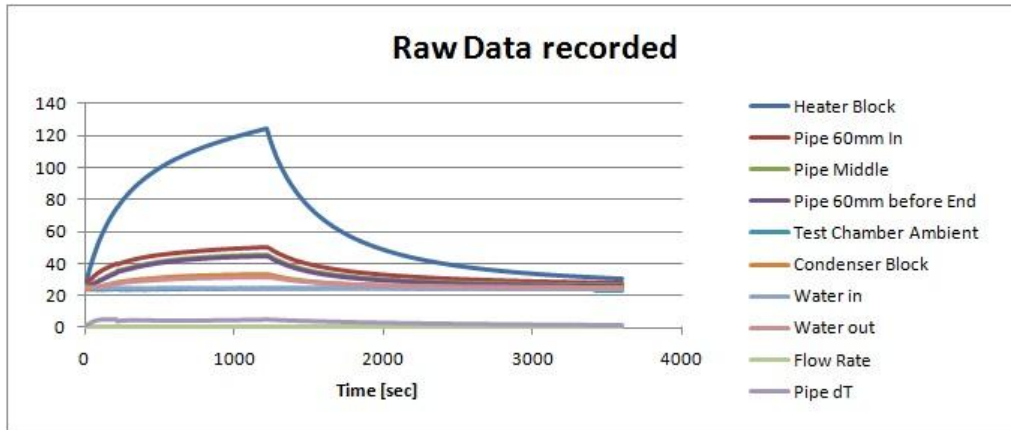


Figure A4-226: Recorded Results Heat Pipe 1 80W Run

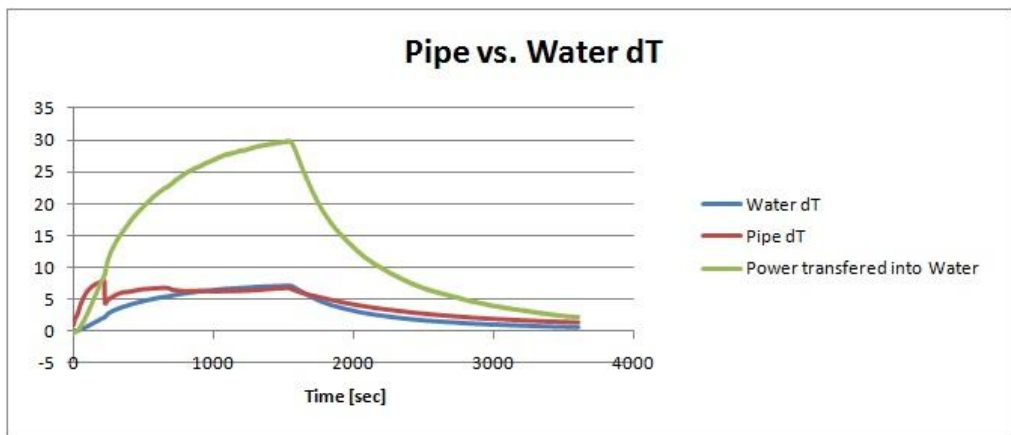


Figure A4-227: Analysed Results Heat Pipe 1 70W Ramp-Up Run

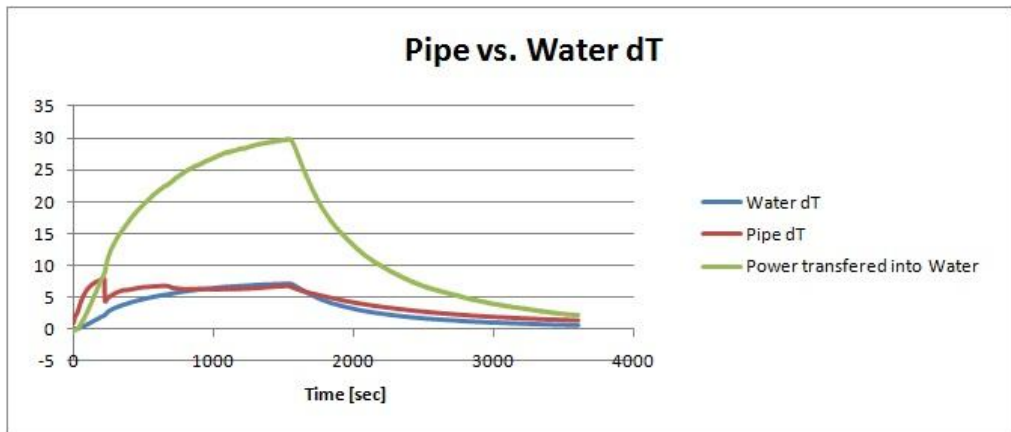


Figure A4-228: Recorded Results Heat Pipe 1 70W Ramp-Up Run

Heat Pipe 2:

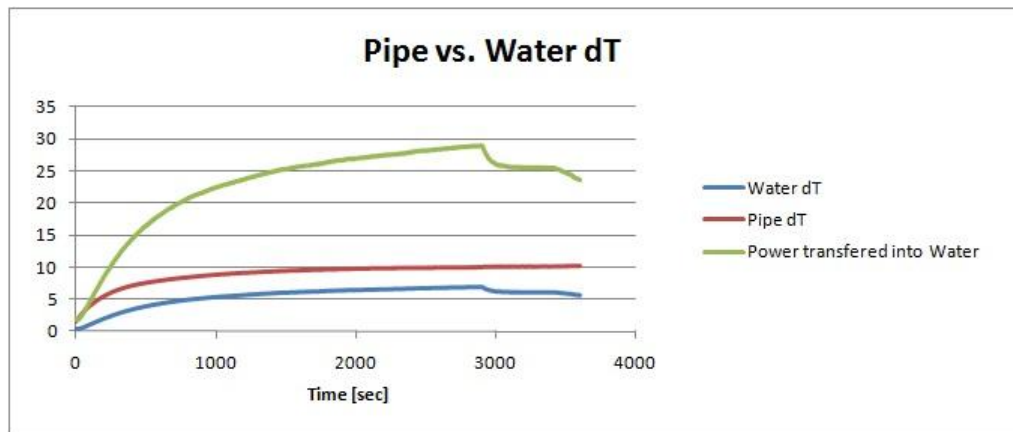


Figure A4-229: Analysed Results Heat Pipe 2 50W Run

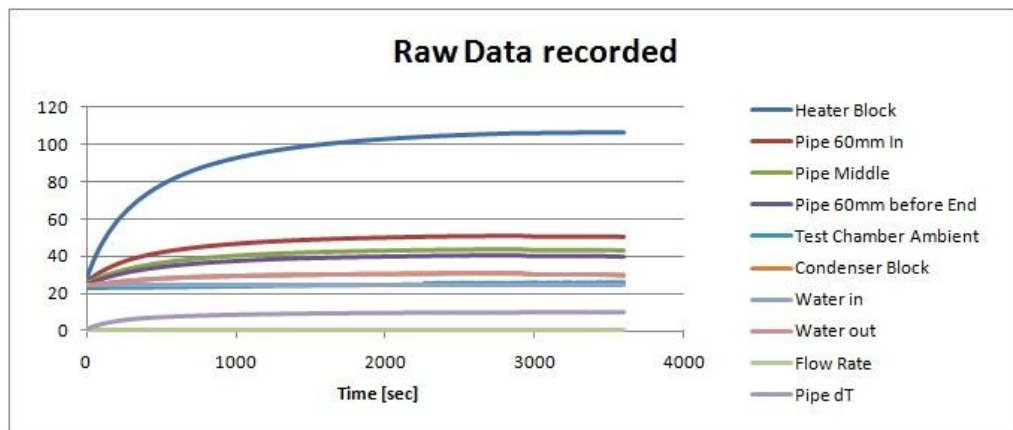


Figure A4-230: Recorded Results Heat Pipe 2 50W Run

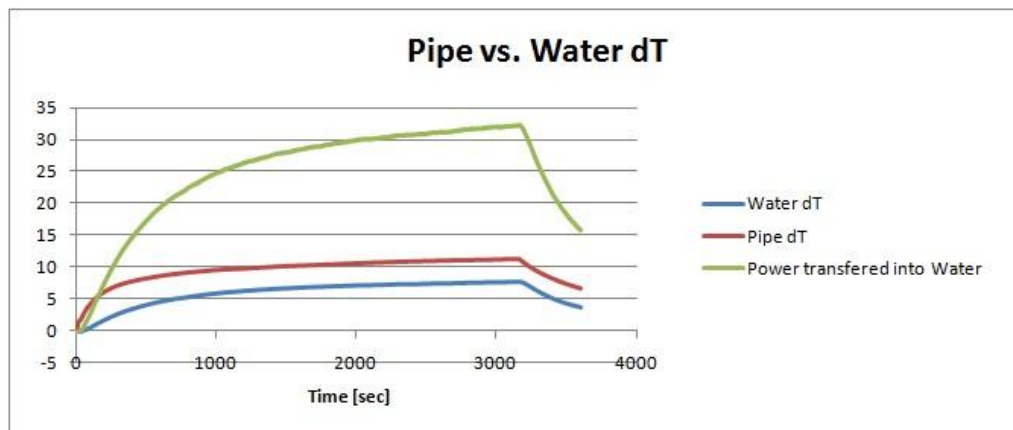


Figure A4-231: Analysed Results Heat Pipe 2 60W Run

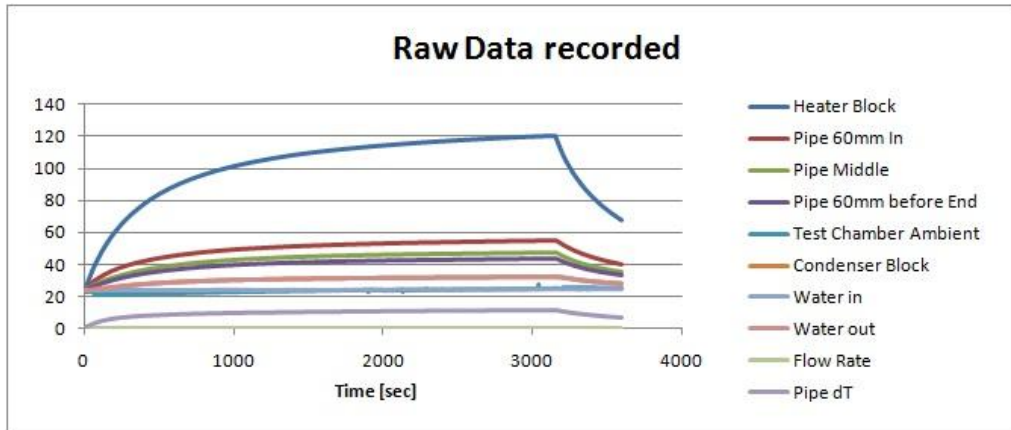


Figure A4-232: Recorded Results Heat Pipe 2 60W Run

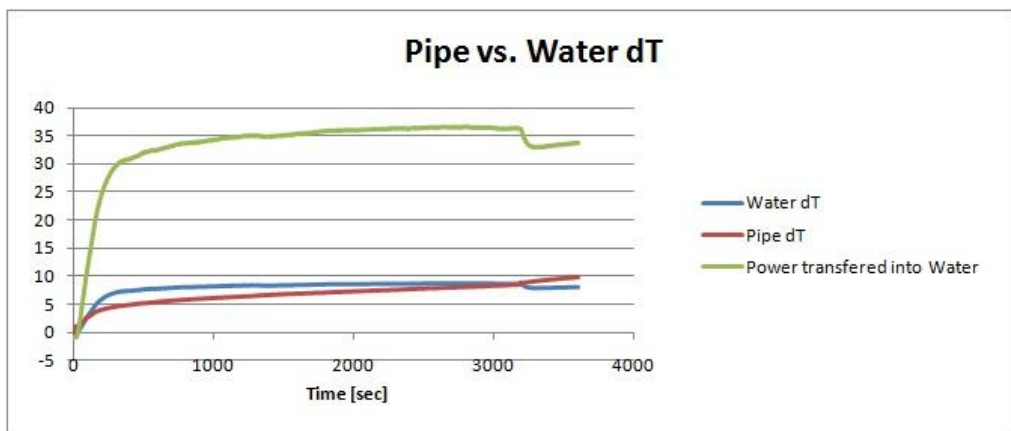


Figure A4-233: Analysed Results Heat Pipe 2 70W Run

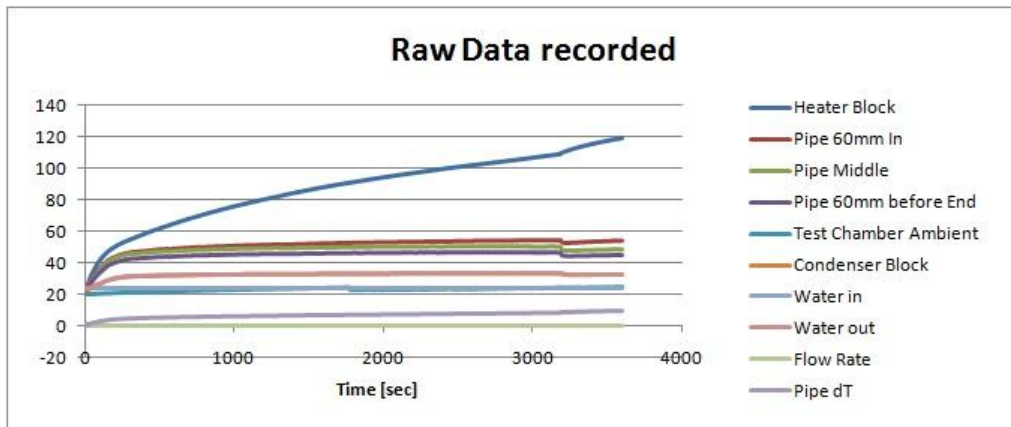


Figure A4-234: Recorded Results Heat Pipe 2 70W Run

Heat Pipe 3:

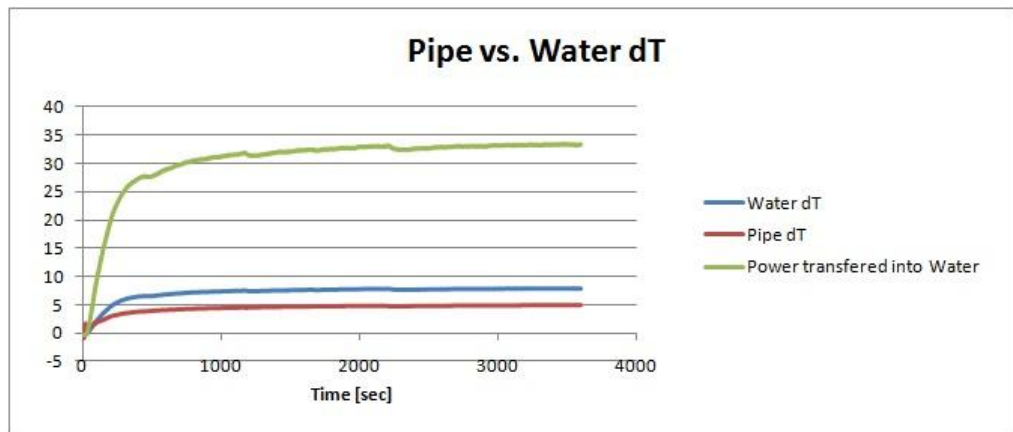


Figure A4-235: Analysed Results Heat Pipe 3 70W Run

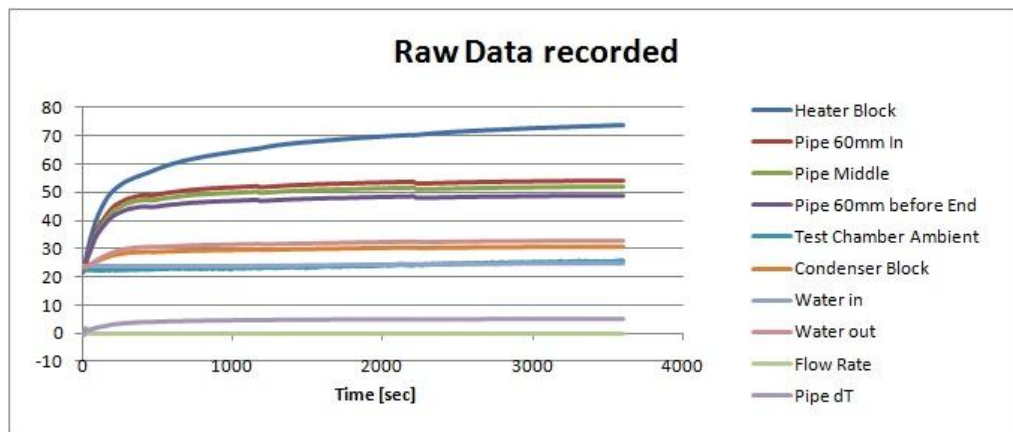


Figure A4-236: Recorded Results Heat Pipe 3 70W Run

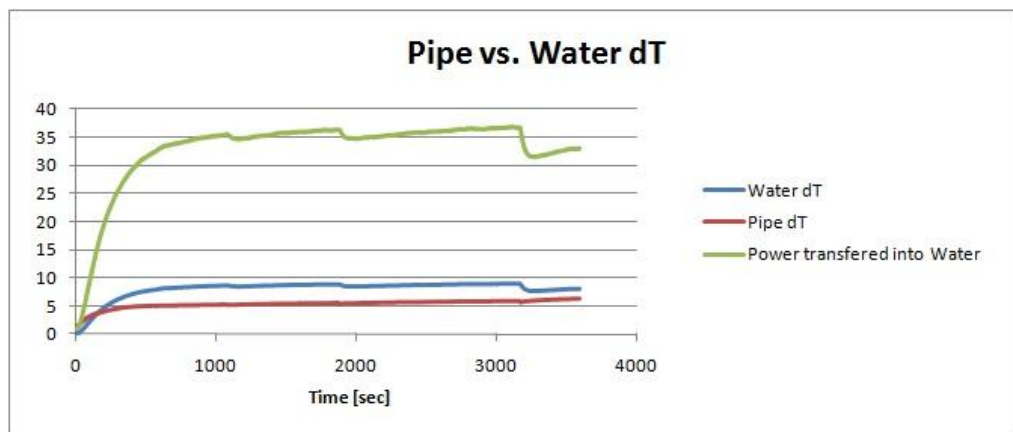


Figure A4-237: Analysed Results Heat Pipe 3 80W Run

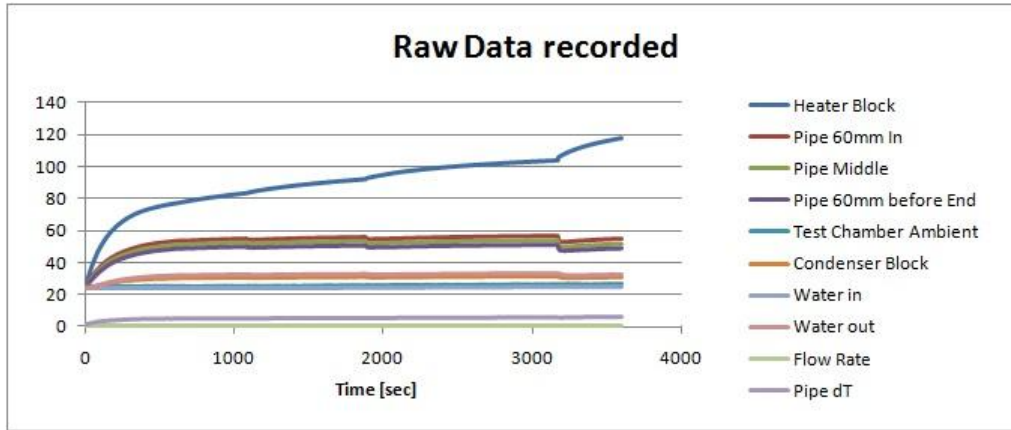


Figure A4-238: Recorded Results Heat Pipe 3 80W Run

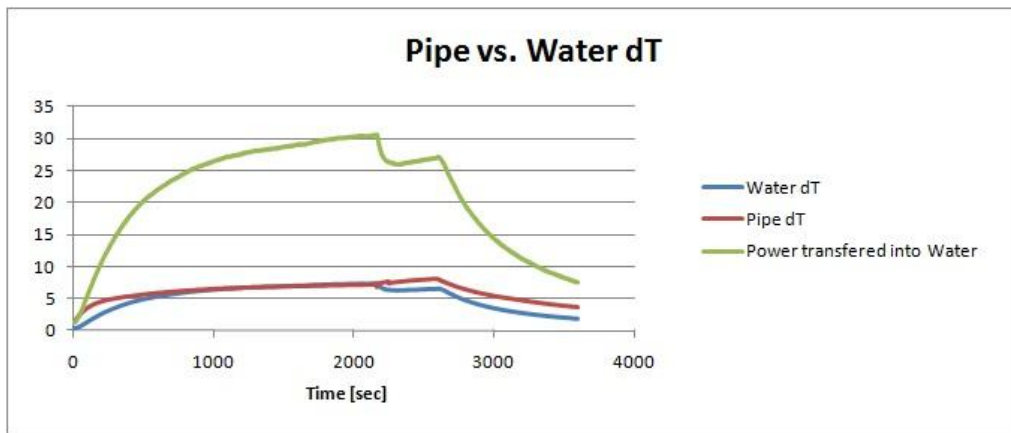


Figure A4-239: Analysed Results Heat Pipe 3 70W Ramp-Up Run

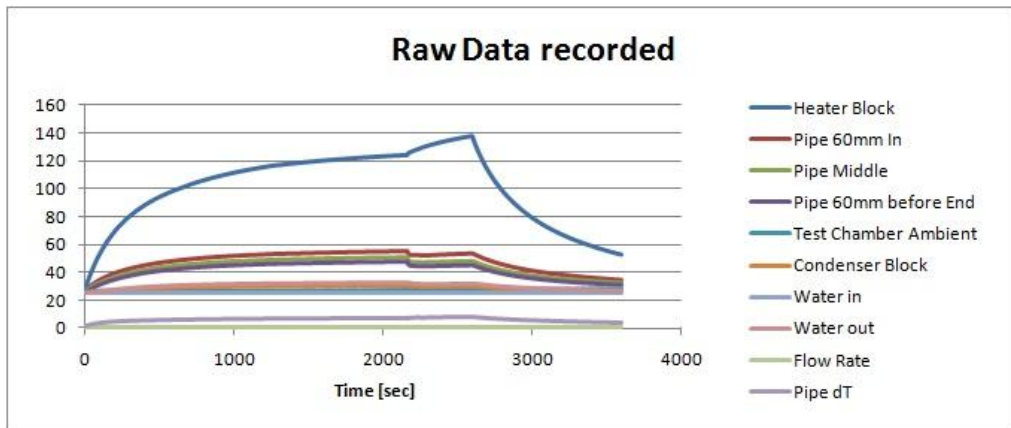


Figure A4-240: Recorded Results Heat Pipe 3 70W Ramp-Up Run

Heat Pipe 4:

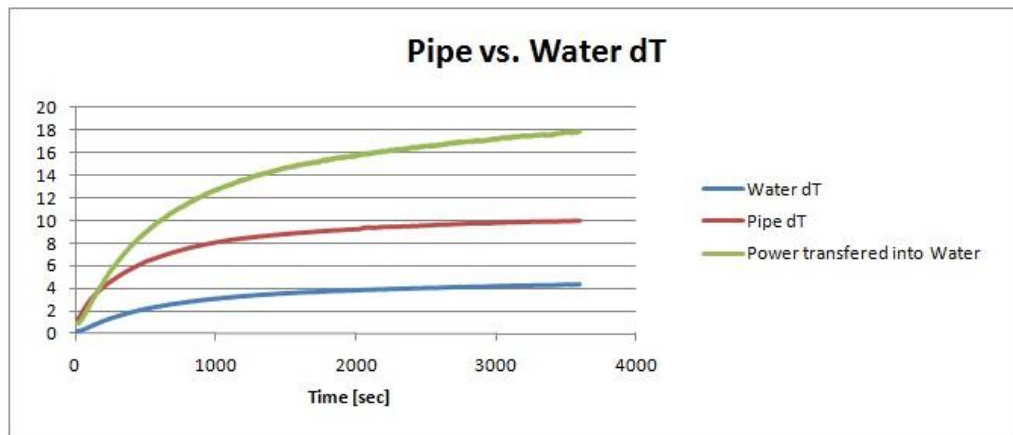


Figure A4-241: Analysed Results Heat Pipe 4 40W Run

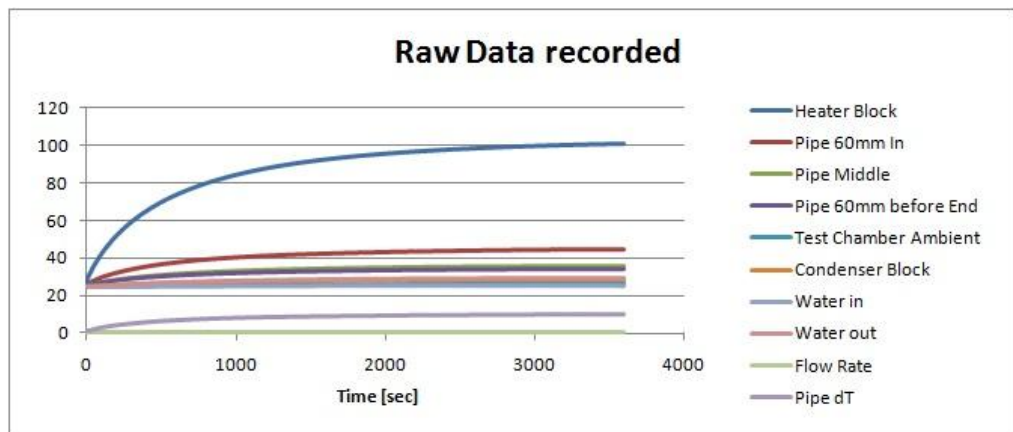


Figure A4-242: Recorded Results Heat Pipe 4 40W Run

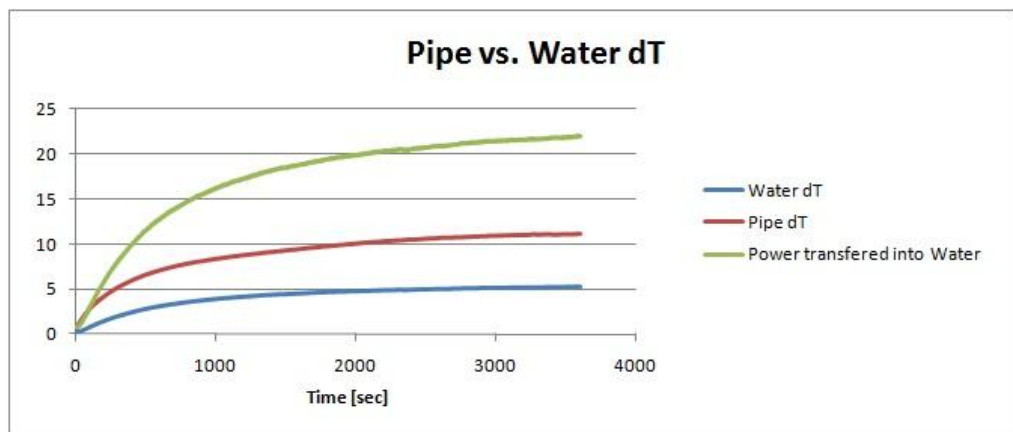


Figure A4-243: Analysed Results Heat Pipe 4 50W Run

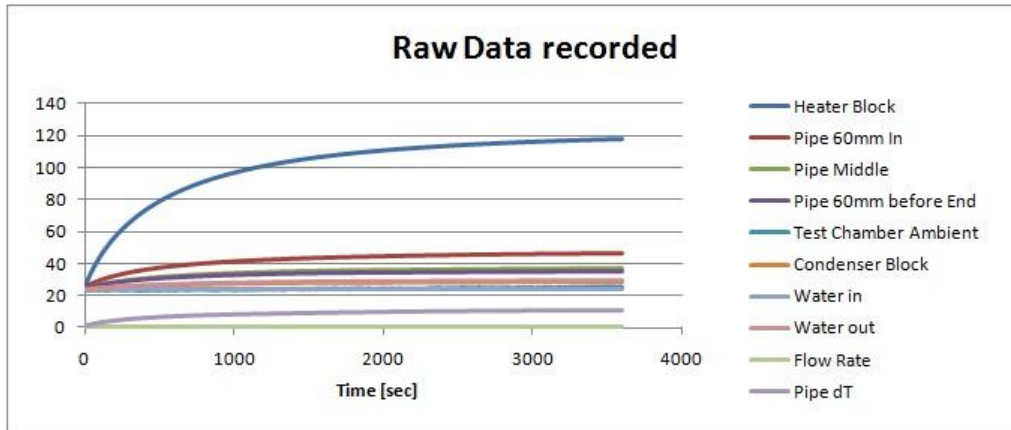


Figure A4-244: Recorded Results Heat Pipe 4 50W Run

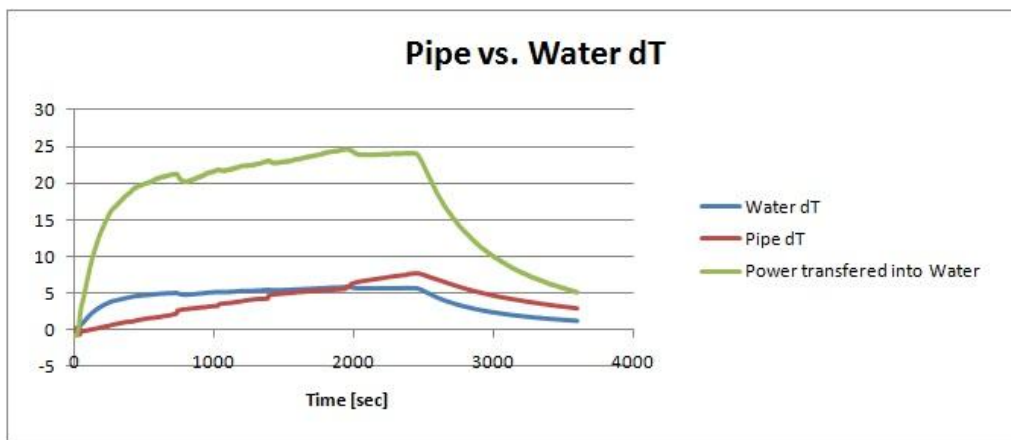


Figure A4-245: Analysed Results Heat Pipe 4 60W Run

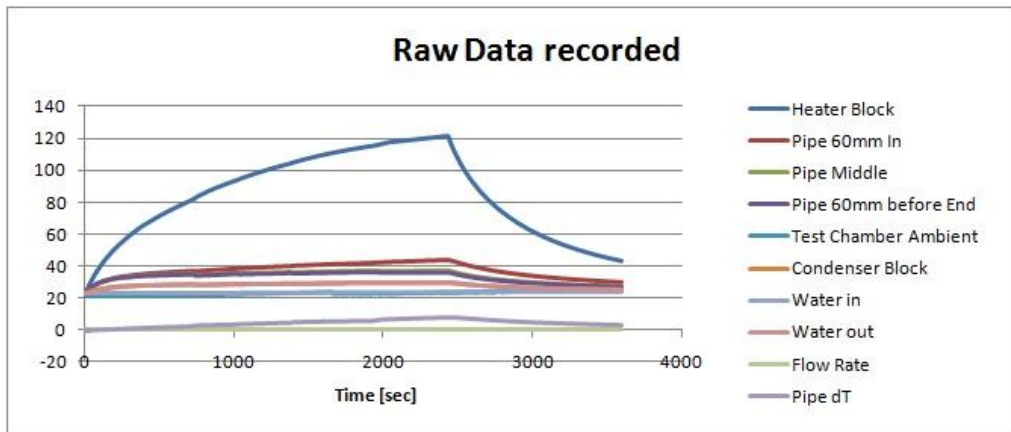


Figure A4-246: Recorded Results Heat Pipe 4 60W Run

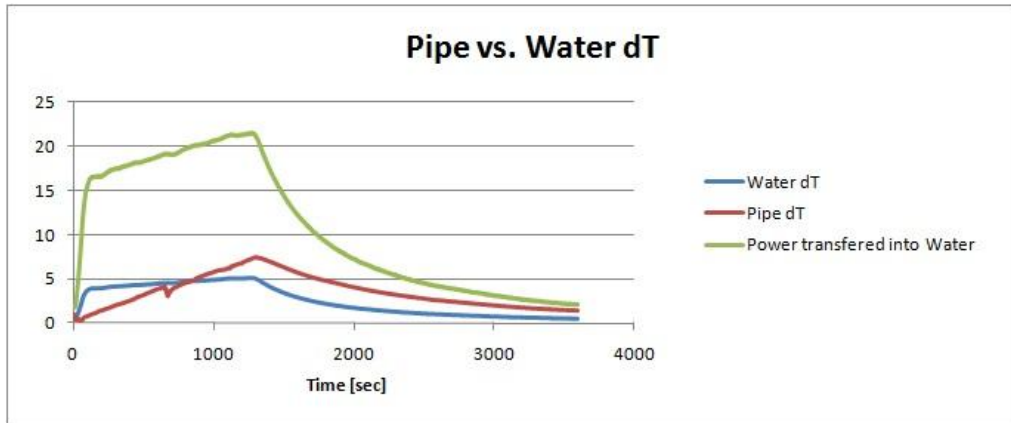


Figure A4-247: Analysed Results Heat Pipe 4 70W Run

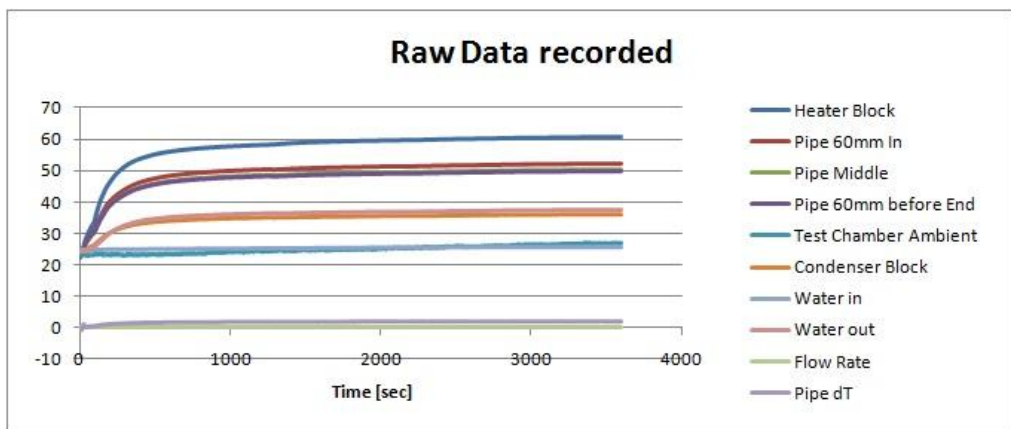


Figure A4-248: Recorded Results Heat Pipe 4 70W Run

Heat Pipe 5:

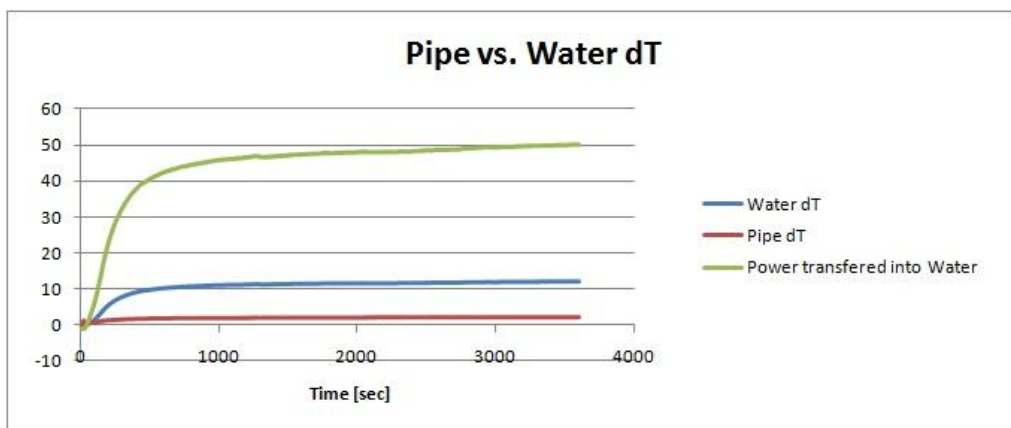


Figure A4-249: Analysed Results Heat Pipe 5 70W Run

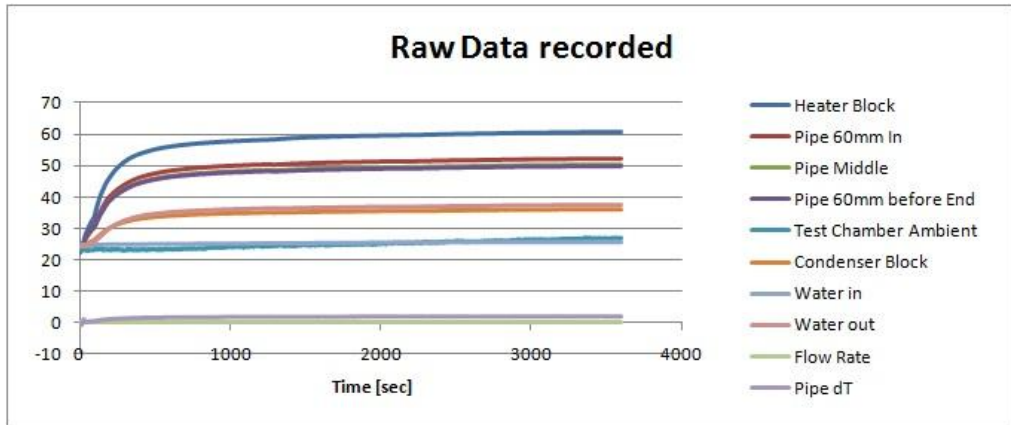


Figure A4-250: Recorded Results Heat Pipe 5 70W Run

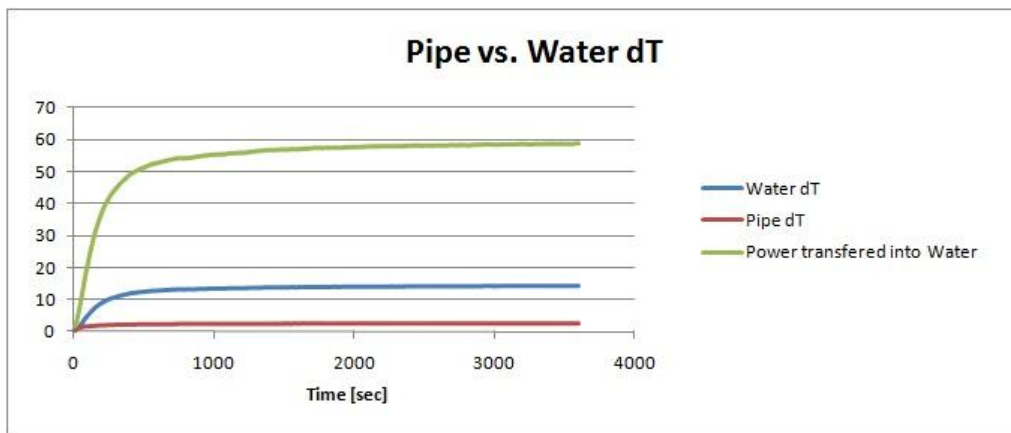


Figure A4-251: Analysed Results Heat Pipe 5 80W Run

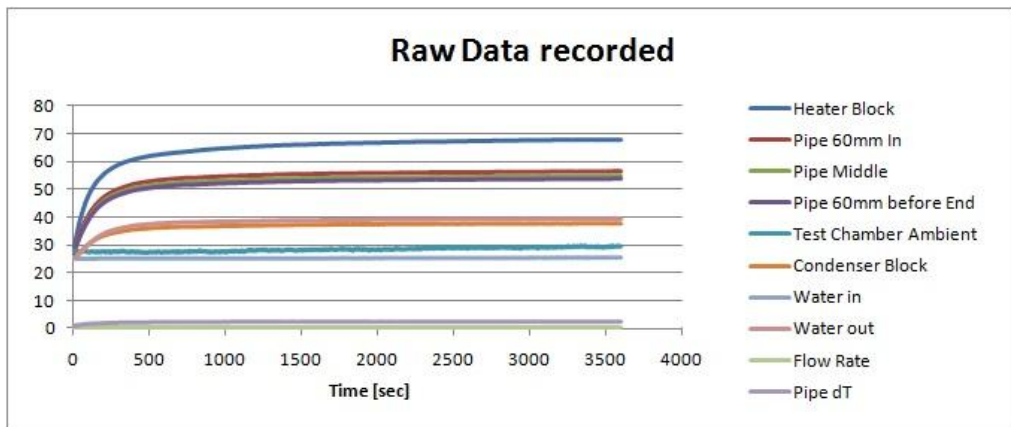


Figure A4-252: Recorded Results Heat Pipe 5 80W Run

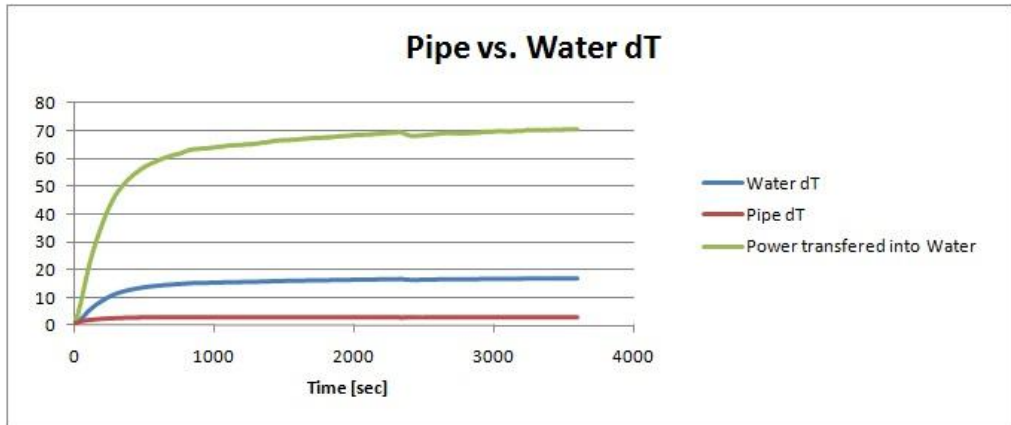


Figure A4-253: Analysed Results Heat Pipe 5 90W Run

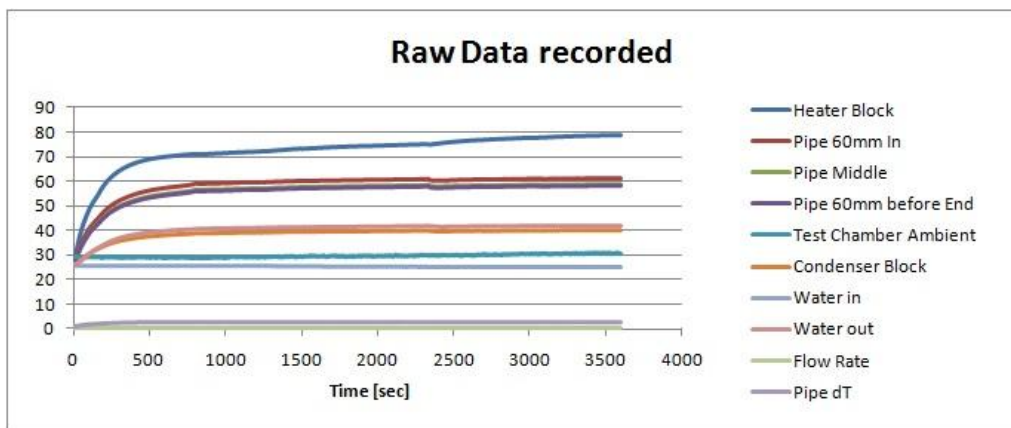


Figure A4-254: Recorded Results Heat Pipe 5 90W Run

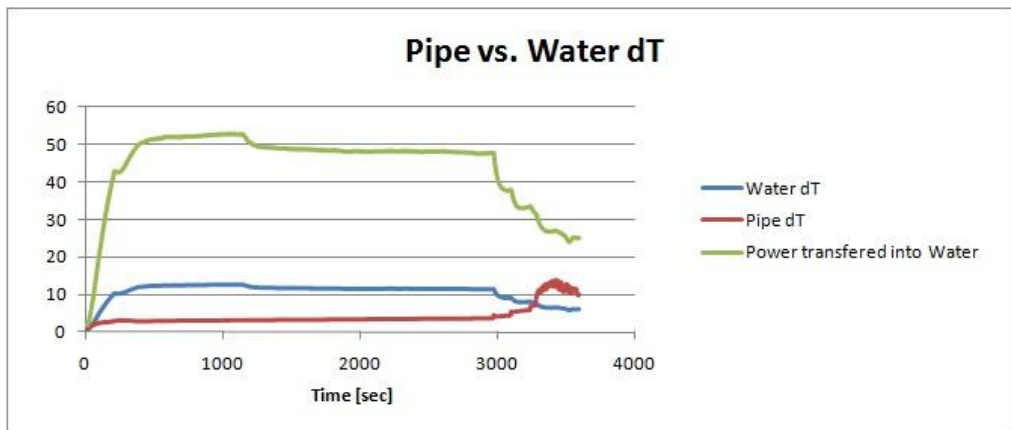


Figure A4-255: Analysed Results Heat Pipe 5 100W Run

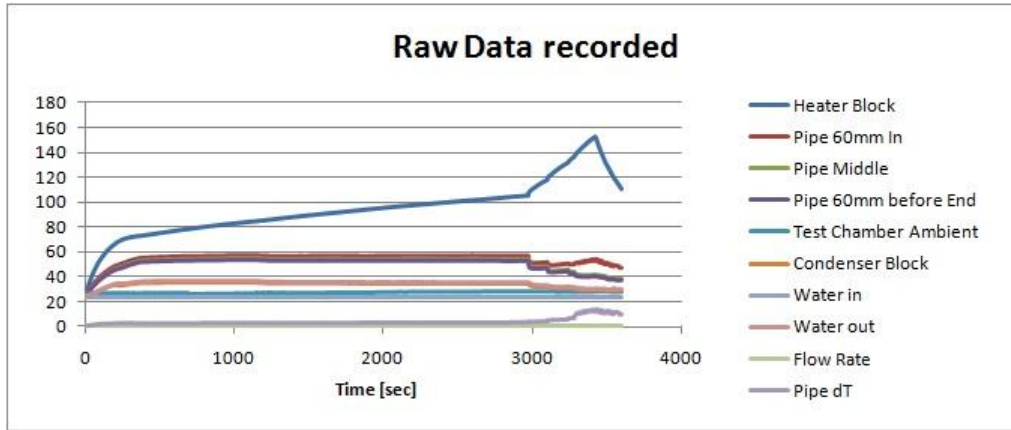


Figure A4-256: Recorded Results Heat Pipe 5 100W Run

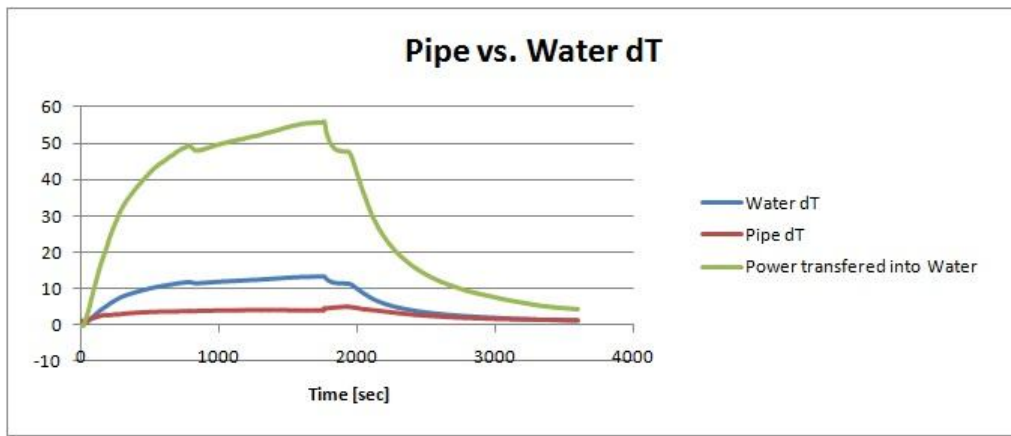


Figure A4-257: Analysed Results Heat Pipe 5 90W Ramp-Up Run

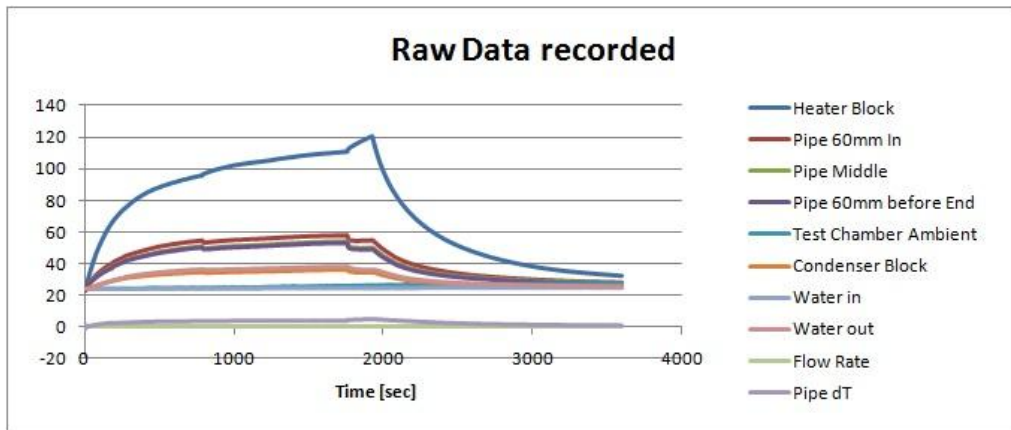


Figure A4-258: Recorded Results Heat Pipe 5 90W Ramp-Up Run